358

TERTIARY HIGH PRESSURE / LOW TEMPERATURE METAMORPHISM IN THE MESOZOIC COVER SERIES OF THE MENDERES MASSIF AND CORRELATION WITH THE CYCLADIC CRYSTALLINE COMPLEX

119682

A Thesis Submitted to the

Graduate School of Natural and Applied Science of

Dokuz Eylül University In Partial Fulfilment of the Requirements

for

The Doctor of Philosophy Degree

In Geology Engineering, Mineralogy-Petrography Program

T.C. YÜKSEKÖĞRETİM KURULU
DOKÜMANTASYON MERKEZİ

by

Mete Çetinkaplan

19687

August, 2002

İZMİR

Ph.D. THESIS EXAMINATON RESULT FORM

We certify that we have read this thesis, entitled "**TERTIARY HIGH PRESSURE / LOW TEMPERATURE METAMORPHISM IN THE MESOZOIC COVER SERIES OF THE MENDERES MASSIF AND CORRELATION WITH THE CYCLADIC CRYSTALLINE COMPLEX**" completed by Mete Çetinkaplan and supervision of Prof. Dr. Osman CANDAN and that our opinion it is fully adequate, in scope and in quality, as a thesis for the degree of Doctor of Philosophy.

Prof. Dr. Osman CANDAN
Supervisor

T.C. YÜKSEKÖĞRETİM KURULU
DOKÜMANTASYON MERKEZİ

Prof. Dr. Cemal GÖNCÜOĞLU
Committee Member

Prof. Dr. Özkan PİŞKİN
Committee Member

Approved for the
Graduate School of Natural and Applied Sciences

Prof. Dr. Cahit Helvacı
Director

ACKNOWLEDGMENTS

I would like to express my appreciation to Prof. Dr. Osman CANDAN for his kind supervision and insightful comments throughout the study. I special thank Prof. Dr.Roland Oberhaensli for critically reading the manuscript and laboratory supporting, and Julius Partzsch for help with microprobe work in Berlin. I also appreciate helpful suggestions of Prof. Dr. Özcan Dora. I gratefully acknowledge to Prof. Dr. Stefan Dürr who supplied the financial support for microprobe works in Mainz. I thank friends and the staff of Potsdam University for support while working in Germany during the six months. I am especially grateful to my wife Dilek Çetinkaplan for her patience and support and to my wife for her contributions to the writing.

ABSTRACT

In the western part of the Menderes Massif, in Dilek Peninsula –Selçuk – Torbalı – Tire and Gölmarmara area, the Mesozoic – Early Tertiary sequence is mainly represented by the Marble-schist series which made up of mica schist with metaconglomerate, minor metabasite/metapelite interlayers and metabauxite-bearing marble, and the Metaolistostrome unit. In this succession, the Tertiary high-pressure / low-temperature metamorphism is represented by blueschist metabasites, metaconglomerates with kyanite-chloritoid-phengite assemblage and high-pressure metamorphosed blocks embedded in a matrix of olistostrome of garnet-phengite schist / albite-phengite schist.

The mineral assemblage of the blueschist metabasites occurring in both Dilek Peninsula and Selçuk metaolistostrome, is "crossite / glaucophane - epidote - phengite (Si^{4+}= 3.37) – garnet - albite". The P-T conditions of the blueschist metabasites and metapelites from Dilek Peninsula were estimated as P=9.5 kbar T=450 °C and P=11 kbar T=445 °C, respectively. In Tire area, the temperature during the retrograde overprint reaches up to 487 ±10 °C. Whereas, this value is 433 ±12 °C in Dilek Peninsula. This indicates that the temperature during the retrograde overprint has increased from southwest to northeast. The metaconglomerates, most probably Lower Triassic in age, shows evidence for a high-pressure metamorphism which is characterized by the " kyanite + chloritoid (X_{Mg}= 0.35) + phengite" paragenesis. The Metaolistostrome which rests tectonically upon the metabauxite-bearing Upper Cretaceous marbles, contains high-pressure blocks such as eclogite, omphacite-epidotite, omphacite metagabbro, zoisite metagabbro, Ti-metagabbro and

metabasites with glaucophane relics. In addition, metaserpentinite and marble blocks are common in the metaolistostrome unit. The mineral assemblage of the eclogites which are converted to the garnet amphibolites along the marginal and internal shear zones, is " omphacite (max. Jd_{49}) – garnet (average Alm_{48}-Prp_6-Sps_{13}-Grs_{33}) – zoisite/epidote – rutile". The garnet porphyroblasts display growth zoning which is, in turn, formed during the eclogite (P=11.9 ±0.5 kbar T=491 ±24 °C) and retrograde stages (P=6 ±1 kbar and T=482 °C). The blueschist metabasites in the Metaolistostrome unit contain garnet (average Alm_{45}-Prp_6-Sps_{29}-Grs_{20}) with compositional zoning. The growth zoning in garnet was formed during blueschist stage (P=10 kbar T=457 °C) and the following diffusional retrograde zonation is related to the retrograde exhumation stage (P=6 ±1 kbar and T=490 ±7 °C). P-T estimations obtained from the omphacite metagabbros (Jd_{47}) are P=12.2 ±0.5 kbar - T=500 °C and P=6 ±1 kbar and T=480 ±10 °C for HP/LT metamorphism and greenschist overprint, respectively. The matrix of the Metaolistostrome unit is made up of garnet-phengite (Si^{4+}=3.42) schist and albite-phengite (Si^{4+}=3.40) schist. The garnets (average Alm_{56}-Prp_4-Sps_{09}-Grs_{31}) in the matrix display compositional zonation. The garnet growth in blueschist stage (P=10.6 kbar T=455 °C) is observed in the mantle part of garnet. The growth during the retrograde stage (P=6.8 kbar T=490 °C) is reflected by the rim composition of the garnet. Garnets in the garnet-phengite schist and blueschist metabasites of the Metaolistostrome unit do not show any evidence of eclogite stage indicating that the matrix of the Metaolistostrome and the Marble-schist series have not been subjected eclogite facies metamorphism.

Blueschist and eclogite relics from in the Selçuk-Torbalı-Tire-Gölmarmara and Dilek Peninsula reveal that a subduction-related high-pressure / low temperature metamorphism affected the Mesozoic – Early Tertiary series of the Menderes Massif under the epidote-blueschist facies condition during Eocene time. High-pressure assemblages were subsequently subjected to the re-equilibration during decompression under greenschist facies condition. The HP/LT metamorphism of Tertiary age in the western part of Menderes Massif is related with the closure of the Neo-Tethyan ocean along a northward-dipping intraoceonic subduction. In Anatolide-Tauride platform, the main tectonic zones from Tavşanlı Zone to

Menderes Massif are characterized by an imbrication of the metamorphosed thrust sheets which have been formed with subsequent tectonic development during subduction of Anatolide-Tauride platform. The relics of high-pressure metamorphism attest the common Tertiary high-pressure metamorphic evolution of the Menderes Massif and Cycladic Complex.

ÖZET

Menderes Masifi'nin batı kesiminde yer alan Selçuk, Torbalı, Tire, Gölmarmara bölgelerinde ve Dilek Yarımadasında, Mesozoik – Erken Tersiyer yaşlı istif metakonglomera, metabasit/metapelit arakatmanlı mika şist ve metaboksit içerikli mermerden oluşan mermer-şist serisi ve metaolistostrom biriminden oluşur. Bu istifte Tersiyer yaşlı yüksek basınç / düşük sıcaklık metamorfizması mavişist metabasitleri, disten-kloritoid-fengit topluluğuna sahip metakonglomeralar ve metaolistostromun granat-fengit şist / albit-fengit şist matriksi içindeki yüksek basınç metamorfik blokları ile temsil edilir.

Dilek Yarımadası ve Selçuk olistostromu'nda yer alan mavişist metabasitlerinin mineral bileşimi "krossit / glaukofan - epidot - fengit (Si^{4+}= 3.37) – granat - albit" dır. Dilek Yarımadası'ndaki mavişist metabasit ve metapelitlerinin P-T koşulları sırasıyla P=9.5 kbar T=450 °C and P=11 kbar T=445 °C olarak hesaplanmıştır. Tire bölgesinde retrograt evrede sıcaklık 487 ± 10 °C ye kadar ulaşır. Bu değer Dilek Yarımadasında 433 ± 12 °C dir. Bu güneybatıdan kuzeydoğuya dogru retrograt evrede sıcaklığın artması olarak yorumlanabilir. Olasılı olarak geç Triyas yaşlı metakonglomeralar yüksek basınç metamorfizmasını temsil eden "disten + kloritoid (X_{Mg}= 0.35) + fengit" parajenezine sahiptir. Metaboksit içerekli Üst Kretase mermerlerinin üstüne tektonik olarak gelen Metaolistostrom birimi eklojit, omfasit-epidotite, omfasit metagabro, zoisit metagabro, Ti-metagabro ve glaukofan kalıntıları içeren metabasit bloklarından oluşan yüksek basınç blokları içerir. Ayrıca matriks içinde bol miktarda metaserpantinit ve mermer blokları yer alır. Granatlı

amfibolitlere çepersel ve içsel makaslama zonları boyunca dönüşüm gösteren eklojitlerin mineral bileşimi "omfasit (maksimum Jd_{49}) – granat (ortalama Alm_{48}-Prp_6-Sps_{13}-Grs_{33}) – zoisit/epidot - rutil" dir. Granat porfiroblastları eklojitik (P=11.9 ±0.5 kbar T=491 ±24 °C) ve retrograd (P=6 ±1 kbar and T=482 °C) evrelerde gelişmiş büyüme zonlanması gösterirler. Metaolistostrom birimi içinde yer alan mavişist metabazitleri de bileşimsel zonlanma gösteren granat (ortalama Alm_{45}-Prp_6-Sps_{29}-Grs_{20}) içerirler. Mavişist metabazitlerinde, granatın büyüme zonlanması mavişist evresi (P=10 kbar T=457 °C) süresince gelişmiştir ve bunu izleyen exhumation ile ilişkili diffuzyonal retrograd zonlanma, retrograd evrede oluşmuştur (P=6 ±1 kbar and T=490 ±7 °C). Yüksek basınç / düşük sıcaklık metamorfizması ve yeşilşist metamorfizmaları için omfasit metagabrodan (Jd_{47}) elde edilen P-T tahminleri sırasıyla P=12.2 ±0.5 kbar - T=500 °C and P=6 ±1 kbar and T=480 ±10 °C dir. Metaolistostrom biriminin matriksi granat-fengit (Si^{4+}=3.42) şist / albit-fengit (Si^{4+}=3.40) şist den oluşur. Matrikste yer alan granatlar (ortalama Alm_{56}-Prp_4-Sps_{09}-Grs_{31}) bileşimsel olarak zonlu bir yapıya sahiptirler. Mavişist evresindeki (P=10.6 kbar T=455 °C) granat büyümesi, bu granatların çekirdekle kenar arasında yer alan manto bölümünde gözlenir. Retrograd evre (P=6.8 kbar T=490 °C) süresince gerçekleşen bu büyüme granatın kenar bileşimi ile temsil edilir. Metaolistostrome birimine ait mavişist metabasitlerinde ve granat-fengit şistler'deki granatlarda eklojitik evreye ait hiçbir veri yoktur. Mermer-şist serisi ve metaolistostromun matriksi eklojit fasiyesi metamorfizmasına maruz kalmamışlardır.

Selçuk-Torbalı-Tire-Gölmarmara ve Dilek Yarımadasında mavişist ve eklojit metamorfizması kalıntıları, Masifi'nin Mesozoik- Erken Tersiyer serisini etkileyen dalma-batma ile ilişkili Eosen yaşlı epidot-mavişist fasiyesi koşullarındaki yüksek basınç / düşük sıcaklık metamorfizmasının varlığını ortaya koyar. Yüksek basınç metamorfizması basınç azalımıyla birlikte yeniden dengelenmenin gerçekleştiği yeşilşist fasiyesi metamorfizması tarafından izlenir. Menderes Masifi'nin batı kesimindeki Tersiyer yaşlı yüksek basınç – düşük sıcaklık metamorfizması kuzeye dalımlı bir dalma-batma zonu boyunca gerçekleşen Neo-Tetis okyanusunun kapanımıyla ilişkilidir. Anatolid-Torid platformunda Tavşanlı zonundan Menderes Masifi'ne kadar uzanan ana tektonik zonlar Anatolid-Torid platformunun dalması

T.C. YÜKSEKÖĞRETİM KURULU
DOKÜMANTASYON MERKEZİ

sırasında ardıl tektonik süreçlerle oluşan birbiri üzerine bindirmiş metamorfik tektonik üniteler ile karakterize edilirler. Menderes Masifi'nin batı kesimindeki yüksek basınç metamorfizması kalıntıları Menderes Masifi ve Kikladik Kompleksin ortak Tersiyer yüksek-basınç metamorfik evrimi ortaya koymaktadır.

CONTENTS

Page

Acknowledgments.....ii
Abstract.....iv
Özet.....vii
List of tables.....xv
List of figures.....xix
Abbreviation list.....xxxv

CHAPTER ONE
INTRODUCTION

1.1. Location of the study area.....1
1.2. The aim of the study.....3
1.3. Previous studies.....3

CHAPTER TWO
LITOSTRATIGRAPHY

2.1. Litostratigraphy of rock assemblages.....7

CHAPTER THREE
GEOLOGY OF THE ROCK UNITS

3.1. Introduction.....10
3.2. Marble-schist series.....10
3.2.1. Dilek Peninsula.....11
3.2.2. Selçuk region.....18
3.2.2.1. Kuşadası-Selçuk area.....18
3.2.2.2. Selçuk-Ortaklar area.....20

Page

3.2.3. Akyurt and Hasançavuşlar area.....26
3.2.4. Tire area.....28
3.2.5. Gölmarmara area.....29
3.3. Metaolistostrome unit 32
3.3.1 Söke (Gümelez) area.....32
3.3.2. Kuşadası (Kirazlı) – Ortaklar (Gümüşyeniköy) area.....38
3.3.3. Selçuk (Şirince) area.....41
3.3.4. Hasançavuşlar – Akyurt area.....53
3.3.5. Torbalı area.....56
3.3.6. Tire area.....59
3.3.7. Gölmarmara area.....61
3.4. Lycian Nappes.....62
3.4.1. Söke (Gümelez) area.....63
3.4.2. Kuşadası (Kirazlı) area.....63

CHAPTER FOUR

PETROGRAPHY

4.1. Introduction.....65
4.2. Lower Triassic – Upper Cretaceous the Marble-schist series.....65
4.2.1. Quartz metaconglomerate.....65
4.2.2. Carbonate metaconglomerate.....68
4.2.3. Blueschist metabasite.....69
4.2.4. Blueschist metapelites.....70
4.2.4.1. Crossite-bearing calcareous schist.....70
4.2.4.2. Chloritoid phyllites.....72
4.2.5. Greenschist metabasites.....74
4.2.6. Phengite-quartz schist.....76
4.2.7. Garnet-mica schist.....78
4.2.8. Garnet phyllite.....81
4.2.9. Epidote amphibolite.....82
4.2.10. Garnet amphibolite.....82
4.2.11. Marble.....83
4.2.12. General evolution.....83

Page

4.3. Metaolistostrome unit.....83
4.3.1. Matrix of Metaolistostrome.....87
4.3.2. Blocks of Metaolistostrome.....88
4.3.2. Blocks of metaolistostrome.....87
4.3.2.1. Garnet metabasite.....88
4.3.2.2. Blueschist metabasites.....95
4.3.2.3. Eclogite.....100
4.3.2.4. Omphacite-epidotite.....106
4.3.2.5. Omphacite metagabbro.....108
4.3.2.6. Zoisite metagabbro.....111
4.3.2.7. Ti-metagabbro.....113
4.3.2.8. Fuchsite-albite schist.....113
4.3.2.9. Marble.....115
4.3.2.10. Metaserpentinite.....116
4.3.3. General evolution.....116
4.4. Lycian Nappes.....120

CHAPTER FIVE

MINERAL CHEMISTRY

5.1. Introduction.....122
5.2. Amphiboles.....122
5.2.1. Amphiboles in blueschist metabasites.....123
5.2.2. Amphiboles in eclogites.....130
5.2.3. Amphiboles in omphacite-epidotite, omphacite metagabbro and garnet amphibolite.....138
5.3. Clinopyroxene.....145
5.3.1. Clinopyroxene in eclogites.....145
5.3.2. Clinopyroxene in omphacite-epidotites and omphacite metagabbros.....156
5.4. Garnets.....167
5.4.1. Garnets in blocks and matrix of metaolistostrome.....167
5.4.1.1. Garnets in eclogite blocks.....167
5.4.1.2. Garnets in blueschist metabasite blocks.....194
5.4.1.3. Garnet in garnet amphibolite block.....202

Page

5.4.1.4. Garnets in garnet-phengite schist.....204

5.4.1.5. Garnets in marble/schist series.....218

5.5. Micas.....226

5.5.1. Dioctahedral micas.....226

5.5.1.1. White mica in eclogite block.....226

5.5.1.2. White mica from the matrix of the Metaolistostrome.....230

5.5.1.3. White mica in the Marble-schist series.....232

5.5.2. Trioctahedral micas.....236

5.5.2.1. Trioctahedral micas in the Metaolistostrome unit.....237

5.5.2.2. Trioctahedral mica in the Marble-schist series.....240

5.5.2.2.1. Trioctahedral mica in garnet-mica schists.....240

5.5.2.2.2. Trioctahedral mica in kyanite-chloritoid schists.....242

5.5.2.2.3. Trioctahedral mica in chloritoid phllites.....242

5.6. Chloritoids.....242

5.7. Epidotes.....245

5.8. Plagioclase.....250

CHAPTER SIX

P-T ESTIMATIONS

6.1. Introduction.....253

6.2. Marble-schist series.....253

6.2.1. Dilek Peninsula.....253

6.2.2. Selçuk-Tire area.....258

6.3. Metaolistostrome unit.....261

6.3.1. Matrix of metaolistostrome.....261

6.3.2. Eclogite blocks.....262

6.3.3. Omphacite metagabbro and omphacite-epidotite blocks.....267

6.3.4. Blueschist metabasite blocks.....275

CHAPTER SEVEN

DISCUSSION

.....282

CHAPTER EIGHT

CONCLUSIONS

.....306

References.....308

Plate I Geological map of Söke-Selçuk area.....inside the back cover

LIST OF TABLES

Page

CHAPTER FOUR

PETROGRAPHY

Table 4.1 X_{Mg} and Si^{4+} variations of chloritoid, chlorite and phengite-II in quartz metaconglomerate unit from Dilek Peninsula to Şirince Village.....68

Table 4.2 The general mineral assemblage of units belonging to marble-schist series from Dilek Peninsula, Selçuk, Tire and Gölmarmara.....84

Table 4.3 Graphical representation of the facies relationship of minerals in marble-schist series from Dilek Peninsula, Selçuk, Tire and Gölmarmara (Akhisar).....85

Table 4.4 Graphical representation of mineral distribution of the marble-schist series.....86

Table 4.5 The general mineral assemblage of matrix and blocks of the metaolistostrome.....117

Table 4.6 Graphical representation of the key minerals in metaolistostrome.....118

Table 4.7 Graphical representation of the key minerals of the metaolistostrome from different areas.....119

Table 4.8 The distribution of some minerals of metaolistostrome and marble-schist series.....120

Page

CHAPTER FIVE

MINERAL CHEMISTRY

Table 5.1 Representative amphibole analyses from blueschists in the Dilek Peninsula, Şirince and Çamlık areas.....124

Table 5.2 Structural formulae of representative amphiboles.....128

Table 5.3 Representative amphibole analyses from eclogites in Şirince and Gölmarmara areas.....131

Table 5.4 Representative amphibole analyses from omphacite-epidodite, omphacite metagabbro and garnet amphibolites in Şirince and Tire areas.....139

Table 5.5 Representative omphacite analyses from eclogite blocks in metaolistostrome unit.....146

Table 5.6 Average clinopyroxene compositions in eclogites.....151

Table 5.7 Representative clinopyroxene analyses from omphacite-epidotites and omphacite metagabro in Söke, Torbalı and Selçuk areas.....157

Table 5.8 Representative garnet analyses from eclogites in Şirince and Gölmarmara (r: rim, c: core).....168

Table 5.9 Representative garnet analyses from blueschist metabasites in Şirince and Çamlık (r: rim, c: core).....196

Table 5.10 Representative garnet analyses from garnet-amphibolite in Tire area.....205

Table 5.11 Representative garnet analyses from metaolistostrome matrix (garnet-phengite schist) in Şirince and Belevi (r: rim, c: core).....207

Table 5.12 Average end-member compositions of the garnet (61-77) belonging to core, mantle and rim.....214

Table 5.13 Representative garnet analyses from marble-schist series in Tire (Akkoyunlu) and Tire (Akyurt) (r: rim, c: core).....220

Table 5.14 Representative dioctahedral mica analyses from metaolistostrome unit.....227

Page

Table 5.15 Representative dioctahedral mica analyses from marble-schist series.....234

Table 5.16 Representative trioctahedral mica analyses from blueschist metabasite block (M98-52/2) and garnet-mica schist (M97-36 and M99-52/5).....238

Table 5.17 Representative chlorite analyses from metaolistostrome unit (M98-85/2) and marble-schist series.....241

Table 5.18 Representative chloritoid analyses from marble-schist series.....243

Table 5.19 Representative epidote and zoisite (clinozoisite) analyses from metaolistostrome and marble-schist series.....246

Table 5.20 Representative plagioclase analyses from metaolistostrome unit and marble-schist series.....251

CHAPTER SIX

P-T ESTIMATION

Table 6.1 Temperature estimations obtained by representative garnet-phengite (matrix) pairs after Green and Hellman (1982) geothermometer from sample M99-52/5.....259

Table 6.2 Garnet – phengite Fe / Mg exchange geothermometry for matrix of metaolistostrome.....262

Table 6.3 Temperature estimates obtained from Ellis & Green (1979) garnet clinopyroxene Fe/Mg exchange thermometry for eclogite blocks.....264

Table 6.4 Pressure estimations obtained from eclogite blocks by Holland (1980) calibration for high-pressure metamorphism.....266

Table 6.5 Temperature estimations obtained from eclogite blocks after Graham and Powell (1984) calibration for retrograde metamorphism.....266

Table 6.6 Pressure estimations obtained from omphacite-epidotites using Holland (1980) calibration.....271

Table 6.7 Estimation of P-T condition obtained from omphacite-epidotite samples for retrograde overprint based on different calibrations.....274

Table 6.8 Temperature estimations for HP/LT metamorphism for blueschist metabasites after Graham and Powell (1984) and Colombi (1989) geothermometric calibrations.....276

Table 6.9 Pressure estimations for blueschist metabasites based on Brown (1977) geobarometry.....277

Table 6.10 Peak temperature estimations for greenschist facies overprint on blueschist metabasites (P=6 kbar).....279

T.C. YÜKSEKÖĞRETİM KURULU
DOKÜMANTASYON MERKEZİ

LIST OF FIGURES

Page

CHAPTER ONE

INTRODUCTION

Figure 1.1 Tectonic map of the western Turkey and surrounding regions showing tectonic zones (Okay 2001).....1
Figure 1.2 The generalized geological map of the Menderes Massif and the locations of detailed mapped areas.....2
Figure 1.3 The set of 1/100.000 in scale maps in the western part of Menderes Massif.....3

CHAPTER TWO

LITOSTRATIGRAPHY

Figure 2.1 Generalized columnar section of the study area.....8

CHAPTER THREE

GEOLOGY OF THE ROCK UNITS

Figure 3.1 Geological map of the region occurring around Tuzburgazı and Doğanbey villages, SW of Söke, consisting of Early Triassic - Upper Cretaceous metaconglomerates, phyllite / mica schist and marble.....12
Figure 3.2 The cross section of the metaconglomerates and underlying metabauxite-bearing marble which is interpreted as overturned succession.....13
Figure 3.3 Repetition of the metaconglomerates in overturned succession in Dilek Peninsula. Section line is given in Figure 3.1.....13
Figure 3.4 Photo showing quartz pebbles in quartz metaconglomerate.....14

Page

Figure 3.5 Photo showing quartz metaconglomerate and quartz rich layers intercalations.....14
Figure 3.6 Kyanite (Ky) and chloritoid (Cld) crystals observed in phyllitic matrix of quartz metaconglomerate.....15
Figure 3.7 a) Carbonate pebbles in carbonate metaconglomerate show strong stretching. The length of carbonate pebbles can be reach up to 14-15 cm. b) The average size of carbonate pebbles is 5 - 6 cm. Carbonate pebbles are embedded in matrix which is composed of calcite, quartz and chlorite.....15
Figure 3.8 Isoclinal folding which is commonly observed in carbonate metaconglomerate and other units. 16
Figure 3.9a Increase in number and thickness of marble layers in close parts to marble-phyllite contact. 17
Figure 3.9b Photo showing increase in number of quartzite layers in stratigraphically lower levels of phyllites.....17
Figure 3.10 Photo of Na-amphibole crystals with epidote and calcite.....17
Figure 3.11 Geological map of the eastern part of Selçuk. Sample number and location of bulk rock analysed rocks are shown in the map.....19
Figure 3.12 Thin carbonate metaconglomerate levels in mica schist. Flattened carbonate pebbles are embedded in a matrix of quartz and carbonate groundmass.....21
Figure 3.13 The contact relationship between metabauxite bearing marble and metaconglomerate - schist intercalations. Section line is given in Figure 3.11.....21
Figure 3.14 The contact relationship between metabauxite bearing marble and metaconglomerate - schist intercalations.....22
Figure 3.15 The contact relationship between emery-bearing marble and mica schist in Selçuk - Çamlık road.....22
Figure 3.16 The measured columnar section showing the transitional contact between emery-bearing marble and mica schist in Top tepe.....23
Figure 3.17 Geological map of Şirince - Ortaklar and Selçuk.....24

Page

Figure 3.18 Muscovite-quartz schist and metaquartzite layers at around Selatin village.....25
Figure 3.19 Transitional contact relationship between mica schist and emery-bearing marble (02045:37750).....25
Figure 3.20 Cross section showing the tectonic contact relationship between the Metaolistostrome unit and underlying the Marble-schist series.....25
Figure 3.21 The geological map of Akyurt and Hasançavuşlar area.....27
Figure 3.22 The section of the Marble-schist series at around Akyurt and their intercalation.....28
Figure 3.23 The geological map of the Marble-schist series and Metaolistostrome unit around Karatekkeköy and Akkoyunlu villages in NW of Tire. 30
Figure 3.24 Intercalation of different lithologies in muscovite-quartz schist unit and the increase of amount of garnet amphibolite lenses in close parts to marble contact (18032;58966).....31
Figure 3.25 Tectonic contact between the Marble-schist series and the Metaolistostrome unit.....31
Figure 3.26 The geological map showing the relationship of the rocks belonging to İzmir-Ankara zone, the Metaolistostrome unit and the Marble-schist series in Ozanca and Kayaaltı villages, 3 km SW of Gölmarmara.....33
Figure 3.27 The cross section showing the tectonic contact relationship between the Marble-schist series and overlying the Metaolistostrome unit, SW of Ozanca village.....34
Figure 3.28 The geological map of area between Davutlar and Gümelez (Söke).....35
Figure 3.29 The tectonic contact relationships between platform type marble and the Metaolistostrome unit, and between the Metaolistostrome unit and Lycian Nappes.....36
Figure 3.30 Field view of klippe of Lycian nappes on the Marble-schist series in SW of Davutlar.....37
Figure 3.31 The highly deformed red phyllites are observed below the dolomite / limestone.....37

Page

Figure 3.32 The geological map of Kirazlı (Kuşadası) and surrounding area, and boundary relation among the Marble-schist series (emery-bearing marbles), the Metaolistostrome unit and Lycian Nappes.....39
Figure 3.33 The geological map of area among Gümüşyeniköy (Ortaklar), Kirazlı and Söke.....40
Figure 3.34 Field view showing the tectonic contact between metaolistostrome unit and Lycian nappes.....42
Figure 3.35 The section showing the contact relationships of emery-bearing marble (Marble schist series), garnet-phengite schist (Metaolistostrome unit) and Dolomite / limestone (Lycian Nappe).....42
Figure 3.36 Albite-phengite schists are distinguished from garnet-phengite schist by dark gray or blackish coloured and quartz nodules.....42
Figure 3.37 Metabauxite-bearing marble is tectonically overlain by the Metaolistostrome thrust sheet.....44
Figure 3.38 The field view of the Metaolistostrome unit thrusted over the metabauxite-bearing marble and muscovite-quartz schist.....44
Figure 3.39 albite-phengite schist containing quartz lenses which is typical feature for this schist.....44
Figure 3.40 Coarse albite porphyroblasts containing albite-phengite schist.....45
Figure 3.41 The field view of yellowish-brownish coloured garnet-phengite schists.....45
Figure 3.42 Isoclinal fold in matrix of metaolistostrome. This fold is cut by main foliation which is formed during the greenschist facies overprint.....45
Figure 3.43 The detailed map of eclogite body in metaserpentinite block in N of Şirince, Yılanlı Tepe.....47
Figure 3.44 A appearance from zoisite metagabbro which is made up of coarse green amphibole and whitish zoisite.....48
Figure 3.45 The general view from omphacite metagabbro.....48
Figure 3.46 The geologic map of eclogite body related to metaserpentinite block exposed on the Selçuk-Şirince road.....49
Figure 3.47 The general view from a) fresh eclogite and b) partly

retrograded eclogite (amphibolitized eclogite).....50
Figure 3.48 The general view of omphacite-epidotite which is made up of whitish zoisite / epidote and green omphacite crystals.....50
Figure 3.49 Pale green - yellowish epidote banded metabasite block.....52
Figure 3.50 The general view of zoisite metagabbro showing pronounced Foliation.....52
Figure 3.51 The general texture appearance from Ti-metagabbro which is characterized by yellowish sphene clusters in a groundmass which is composed of blackish coloured amphibole.....52
Figure 3.52 Cross section showing tectonic character of the contact between the Marble-schist series and the Metaolistostrome unit.....54
Figure 3.53 The cross section showing tectonic contact relationship between marble and the Metaolistostrome unit. Section line is given in Figure 3.21.....54
Figure 3.54 The contact relationship between marble and the Metaolistostrome unit from Halkapınar to Boğaziçi is defined by vertical fault.....55
Figure 3.55 Marble block showing isoclinal folding together with garnet-phengite schist.....57
Figure 3.56 The field view of marble blocks which are embedded in matrix of the Metaolistostrome.....57
Figure 3.57 Small marble block in garnet-phengite schist.....57
Figure 3.58 The geological map of the Metaolistostrome unit occurring between Çakallar and Korucuk villages, E of Torbalı.....58
Figure 3.59 The cross section showing contact relationship among marble, garnet-phengite schist and mica schist / muscovite-quartz schist between Çakallar and Korucuk villages. The section line is given in Figure 3.60.....59
Figure 3.60 Tectonic contact between the Marble-schist series and the Metaolistostrome unit.....60
Figure 3.61 The field view of the tectonic contact between marble (the Marble-schist series) and the Metaolistostrome unit.....60
Figure 3.62 The schists belonging to the Marble-schist series are directly overlain by the Metaolistostrome unit without platform type marble in the contact.

Limestone is tectonically underlain by the Metaolistostrome unit.....62
Figure 3.63 Small Lycian nappe klippe forming from highly deformed dolomite, on matrix of the Metaolistostrome.....64
Figure 3.64 The boundary relation among dolomitic limestone, red phyllite and garnet-phengite schist (the Metaolistostrome unit).....64

CHAPTER FOUR

PETROGRAPHY

Figure 4.1 a) photomicrograph showing prograde fabric (PF) (in chloritoid) and retrograde fabric (RF) (in matrix) foliations in quartz metaconglomerate with "kyanite-chloritoid-phengite" assemblage in Dilek Peninsula. b) strain caps and strain shadows around chloritoid which represent the growing of chloritoid during the earliest deformation.....67
Figure 4.2 Kyanite which is replaced by pyrophyllite (Ppy).....67
Figure 4.3 The general view of matrix of carbonate metaconglomerate.....71
Figure 4.4 Tabular and aligned Na-amphibole crystals in calc-schists.....71
Figure 4.5 Zoned crossite which is made up of core with zoisite inclusion.....71
Figure 4.6 Sub-euhedral crossite (Crs) crystals which are rimmed by retrograde barroisite. Width of view 1 mm. PPL.....73
Figure 4.7 Photomicrograph showing opaque mineral which includes crossite crystals. Width of view 1 mm. PPL.....73
Figure 4.8 Photomicrograph showing crossite partly replaced by chlorite.....73
Figure 4.9 Rosette-like chloritoid, developed during HP/LT metamorphism, cutting by retrograde fabric. Width of view 4 mm. CPL.....75
Figure 4.10 Photomicrograph showing the common secondary chlorite derived from Ca-amphibole. Light green minerals are chlorite.....75
Figure 4.11 Bluish zoisite as a phase of epidote-blueschist facies metamorphism is replaced by epidotes as a consequence of greenschist overprint.....75
Figure 4.12 Photomicrograph showing epidote bearing calcite.....77
Figure 4.13 Two phengite generation; coarse phengite-I crystals which is formed during epidote-blueschist facies metamorphism, are rich-in Si; Small phengite-II crystals defining the retrograde fabric, are poor-in Si.....77

Page

Figure 4.14 Coarse phengite-I crystals preserved in strain-free domains.....77
Figure 4.15 Textural zoning of albite porphyroblast which is defined by inclusion in the core (epidote-blueschist facies) and inclusion free rim (greenschist facies). Width of view 2.5 mm. CPL.....79
Figure 4.16 Phengite-II which are transected by C'-type shear band cleavage.....79
Figure 4.17 Subgrain migration in deformed quartz and typical fabric of dynamic recrystallization of quartz.....79
Figure 4.18 Photomicrograph showing syn-tectonic garnet crystal with respect to retrograde fabric. Width of view 4 mm. CPL.....80
Figure 4.19 Main cleavage cutting the phengite-II crystals belonging to older cleavage. Width of view 2.5 mm. CPL.....81
Figure 4.20 Inclusion fabric in albite which defines the early foliation, is almost perpendicular to main foliation. Width of view 2.5 mm. CPL.....89
Figure 4.21 Zoisite inclusions are dominantly observed in intermediate zone of garnet. Width of view 4 mm. CPL.....89
Figure 4.22 Photomicrograph showing quartz, albite and calcite crystals in skeletal garnet.....89
Figure 4.23 Garnet with S-shaped quartz, bluish zoisite and albite inclusion is pre-tectonic with respect to main foliation. Width of view 4 mm. CPL.....91
Figure 4.24 Biotite development which is parallel to main foliation of garnet-phengite schist.....91
Figure 4.25 Trapped zoisite inclusions in garnet define early foliation which is oblique to main foliation. Width of view 4 mm. CPL.....91
Figure 4.26 Microboudinage in garnet. Microboudinage necks are composed of chlorite. Width of view 2.5 mm. PPL.....92
Figure 4.27 The replacement of garnet by chlorite and albite assemblage.....92
Figure 4.28 a) zoisite inclusions are replaced by epidote in chloritized part of garnet. Whereas in the core, bluish zoisite inclusions are preserved from retrograde effect of greenschist overprint. Width of view 2.5 mm. CPL. b) view of (a) under PPL.....93

Page

Figure 4.29 The mesh-like structure composed of small albite and amphibole crystals which are probably derived from Na-pyroxene.....93
Figure 4.30 Ca-amphibole (Ca-amp) crystals perfectly aligned parallel to main foliation and smaller albite crystals derived from bigger albite crystals..... 94
Figure 4.31 a) Radial amphibole needles in albite corona resorbing the garnet. Width of view 2.5 mm. CPL. b) view of (a) under PPL.....94
Figure 4.32 Photomicrograph showing the general texture of relict Na-amphibole -bearing blueschist metabasites.....96
Figure 4.33 Na-amphibole (crossite) inclusions of garnet in blueschist metabasites. Width of view 2.5 mm. PPL.....96
Figure 4.34a Photomicrograph showing decompression texture around garnet.....97
Figure 4.34b Epidote crystals growing in albite corona during the decompression. Width of view 2.5 mm. CPL.....97
Figure 4.35 Garnet replaced by albite due to decompression. Garnet pseudomorp is denoted by dotted line. Width of view 2.5 mm. PPL.....97
Figure 4.36 Photomicrograph showing transition from crossite through barroisite to actinolite in blueschist metabasites. Width of view 1 mm. PPL.....98
Figure 4.37 a) mesh-like breakdown structure which is composed of amphibole and albite around crossite in the core of crystal. Width of view 2.5 mm. PPL. b) in later stage, crossite in the core is completely replaced by Na-Ca and/or Ca amphibole and albite fields are getting larger with greenschist overprint. Width of view 2.5 mm. PPL. c) in late stage, the large amount of Ca-amphibole is replaced by albite. The relict Ca-amphibole needles are observed in albit field after Ca-amphibole. Width of view 2.5 mm. PPL.....99
Figure 4.38 Photomicrograph showing albite, epidote and Ca amphibole (Ca-amp) assemblage after garnet. Width of view 2.5 mm. PPL.....101
Figure 4.39 Greenish omphacite (cprx-IIB) corroded by symplectitic intergrowth of cprx-III and albite. Maximum jadeite mol % of cprx-IIB is 27.....101
Figure 4.40 Photomicrograph showing the omphacite (cprx-IA) rimmed by symplectitic intergrowth of cprx-III and albite. Width of view 2.5 mm. CPL.....101

Page

Figure 4.41 Omphacite (cprx-IA) pseudomorph composed of omphacite aggregates (cprx-IIA) which are rimmed by symplectite (cprx-III and albite).....103
Figure 4.42 a) Photomicrograph showing garnet partly replaced from rim to core by epidote, albite and Ca-amphibole. Width of view 2.5 mm. CPL. b) view of (a) under PPL.....103
Figure 4.43 Photomicrograph showing the garnet partly replaced along the rim by epidote corona. Width of view 2.5 mm. PPL. Width of view 4 mm. PPL.....104
Figure 4.44 Partly replacement of garnet by albite.....104
Figure 4.45 a) euhedral and newly generated Ca-amphibole crystals growth in symplectite fields. Width of view 2.5 mm. CPL. b) symplectite field filled by needles and coarse crystals of Ca amphibole. 1: pseudosymplectite field, 2: amphibole needles, 3: coarse amphibole. Width of view 2.5 mm. PPL.....104
Figure 4.46 Photomicrograph showing zoned epidotes. Fe^{3+} content of these epidotes increase from core to rim. Width of view 2.5 mm. CPL.....105
Figure 4.47 Symplectites developed along albite-vein filling which cuts the omphacites (cprx-IA). Width of view 2.5 mm. PPL.....105
Figure 4.48 Photomicrograph showing Ca-amphibole and epidote crystals in albite vein. These crystals are aligned parallel to main foliation which is formed by greenschist overprint. Width of view 4 mm. PPL.....105
Figure 4.49 Photomicrograph showing omphacites (cprx-IA) which is in equilibrium with zoisite. There is no reaction texture between these minerals.....107
Figure 4.50 Photomicrograph showing multi-zoning structure in garnet. Inclusion in garnet are made up of zoisite and omphacite.....107
Figure 4.51 Photomicrograph showing the general texture of omphacite epidotites. Omphacites (cprx-IA) are replaced by fine-grained symplectitic intergrowth (cprx-III and albite). Width of view 4 mm. CPL.....107
Figure 4.52 Nematoblastic texture is observed in retrograde samples of omphacite epidotites. In these samples, symplectite fields are quite few.....109
Figure 4.53 Photomicrograph showing acicular amphibole crystals growth in fine-grained symplectite groundmass. Width of view 4 mm. PPL.....109
Figure 4.54 Photomicrograph showing the transformation stages from

coarse omphacite (cprx-IA) through omphacite aggregate (cprx-IIA) to symplectite (cprx-III and albite). Width of view 4 mm. CPL.....109
Figure 4.55 The breakdown of Ca amphibole belonging to HP metamorphism, to albite. Width of view 2.5 mm. CPL.....110
Figure 4.56 Ca amphibole belonging to HP metamorphism, and omphacite are equilibrium with each other. Width of view 2.5 mm. CPL.....110
Figure 4.57 Reaction texture developed between omphacite and Ca amphibole in retrograde overprint. Width of view 2.5 mm. CPL.....110
Figure 4.58 Rutile is rimmed by sphene which is interpreted as an evidence of greenschist facies overprint. Width of view 2.5 mm. CPL.....112
Figure 4.59 Main foliation cutting the Ca amphibole (1). The main foliation is defined by small zoisite and albite crystals. Width of view 2.5 mm. CPL.....112
Figure 4.60 Small prismatic amphibole crystals which are derived from coarse-grained amphibole, surround the earliest Ca-amphibole grain. Development of small amphibole crystals are related with deformation during the greenschist overprint. Width of view 4 mm. CPL.....112
Figure 4.61 Development of albite in microboudinage necks of Ca amphibole representing the greenschist facies overprint.....114
Figure 4.62 Photomicrograph showing the replacement of Ca amphibole by small albite crystals. Width of view 4 mm. CPL.....114
Figure 4.63 Coarse grained bluish coloured zoisites belonging to epidote-blueschist facies show grain-size reduction due to deformation during the greenschist overprint. Width of view 4 mm. CPL.....114
Figure 4.64 Cluster sphene crystals are commonly observed in Ti-metagabbros as clusters composed of small sphene crystals. Width of view 2.5 mm. PPL.....115
Figure 4.65 Photomicrograph showing fuchsite (Fhs) layer aligned parallel to main foliation. Width of view 4 mm. CPL.....116
Figure 4.66 Mylonitic texture observed in red phyllites.....121
Figure 4.67 Mylonitic texture and grain boundary migration in albites. Width of view 4 mm. CPL.....121

Page

CHAPTER FIVE

MINERAL CHEMISTRY

Figure 5.1 Composition of calcic (a). sodic-calcic (b) and sodic (c) amphiboles from the Metaolistostrome unit and the Marble - schist series plotted on Leake et al., (1978) diagram.....127

Figure 5.2 Zoning structure of a sodic amphibole (94-55/5) in blueschist Block.....129

Figure 5.3 Plot of NaM4 versus R(3+) diagram after Kryza et al. (1990) for amphiboles in blueschist metabasites (the Metaolistostrome unit and the Marble-schist series).....129

Figure 5.4 Aspects of the chemical variations of calcic amphiboles from eclogites. (a) sodium and calcium occupancy of M4+A structural positions; (b) plot of Al(VI) + Fe(3+) + Ti versus Al(IV).....133

Figure 5.5 Composition of calcic amphiboles (a, b and c) from eclogite blocks in metaolistostrome plotted on Leake et al., (1978) diagram.....134

Figure 5.6 Calcic amphibole zoning in M97-34/2 and element graphs monitoring the zonation. PPL: plane polarized light.....135

Figure 5.7 Pressure characteristic of Ca-amphiboles observed in eclogite blocks.....137

Figure 5.8 Pressure characteristic of Ca-amphiboles observed in eclogite blocks plotted on Raase (1974) diagram.....137

Figure 5.9 Composition of calcic amphiboles (a, b and c) and sodic-calcic amphibole (d) from omphacite-epidotite,omphacite metagabbro and garnet amphibolite plotted on Leake et al.,(1978) diagram.....141

Figure 5.10 Aspects of the chemical variations of calcic and sodic-calcic amphiboles from omphacite metagabbro, omphacite-epidotite and garnet amphibolite.(a) sodium and calcium occupancy of M4+A structural positions; (b) Plot of Al(VI) + Fe(3+) + (2*Ti) + (A-site) vs. Al(IV) diagram; (c) plot of Al(VI) + Fe(3+) + Ti vs. Al(IV) diagram.....142

Figure 5.11 Pressure characteristic of Ca-amphiboles from omphacite-epidotite, omphacite metagabbro and garnet amphibolite plotted on Laird

and Albee (1981) diagrams (a and b) and Raase (1974) diagram (c), respectively. High-pressure field is characterized by amphibole compositions from Sanbagawa and Franciscan terrains.....144

Figure 5.12 Clinopyroxene compositions from different type of eclogites (Smulikowski, 1972).....150

Figure 5.13 Classification of clinopyroxene analyses from eclogites on Q-J ternary diagram (Morimoto et al.1988).....150

Figure 5.14 Pyroxene composition in the eclogites of Şirince and Gölmarmara (M97-34/2).....152

Figure 5.15 Compositional profile across Na pyroxene grain; a) Jadeit (jd), Acmite (Ac)and Augite (Aug) end-members pattern belonging to profile line; b) element patterns belonging to profile line.....154

Figure 5.16 Proportions of six-coordinated cations p.f.u. in analyses of clinopyroxene from eclogites. The diagrams show the occupancy of M2 (a) and M1(b) structural positions.....155

Figure 5.17 Ternary atomic proportions of (Di+Hd)-Jd-Ac and of (Jd+Ac)-Hd-Di for clinopyroxenes (Ernst, 1976).....160

Figure 5.18 Classification of clinopyroxene analyses on Q-J ternary diagram (Morimoto et al.,1988).....160

Figure 5.19 Composition plots of clinopyroxenes from omphacite metagabbro and omphacite-epidotites of Şirince ,Söke and Torbalı areas.....162

Figure 5.20 Proportions of six-coordinated cations p.f.u. in analyses of clinopyroxene. The diagrams show the occupancy of M2 (a) and M1(b) structural positions.....164

Figure 5.21 Ternary atomic proportions of a) (Di+Hd)-Jd-Ac and of b) (Jd+Ac)-Hd-Di for clinopyroxenes in omphacite-epidotites (M96-92/4, M98-163/2, M97-151/3) and omphacite metagabbro (91-16).....165

Figure 5.22 a) garnet compositions plotted after Coleman et al. (1965). Garnet end-members are formed by almandine+spessartine (Alm+Sps), grossular (Grs) and pyrope (Prp), b) garnet composition compared to eclogite type (Smulikowski, 1972). K= nodular xenoliths in kimberlite; C= 'common'

eclogites (from high-grade gneisses and migmatites); O= 'ophiolitic' or 'alpine-type' eclogites (from high-P/low-T terranes).....174
Figure 5.23 Ternary atomic proportions of Alm+Prp-Sps-Grs (a) and Alm-Prp-Grs+Sps (b) for garnets from eclogite blocks in the Metaolistostrome.....175
Figure 5.24 Monitoring of compositional zoning in the garnet from 95-70/4; a) photo of analysed garnet in PPL, b) element distribution map of garnet (reddish colours indicate higher element content), c) compositional zoning profiles from rim to rim, d) line analyse along the A-A.....177
Figure 5.25 Monitoring of compositional zoning in the garnet from sample M97-34/2.....179
Figure 5.26 Monitoring of compositional zoning in the garnet (1-19) from sample SE-1.....181
Figure 5.27 Monitoring of compositional zoning in the garnet (35-50) from sample SE-1.....185
Figure 5.28 Compositional zoning in the garnet (145-154) from sample SE-1.....188
Figure 5.29 Photomicrograph in plane polarized light and composition of this garnet in M98-45C. Traverse is from rim to core.....189
Figure 5.30 Monitoring of compositional zoning in the garnet (M96-31).....191
Figure 5.31 Mn profiles from set of garnets of increasing diameter.....193
Figure 5.32 Photomicrograph in plane polarized light and element profiles of selected garnet grain (1-24) in 95-21/10. Traverse is from rim to rim.....193
Figure 5.33 In almandine+spessartine - grossular - pyrope ternary diagram, location of selected garnet grains from blueschist metabasites.....198
Figure 5.34 Ternary atomic proportions of Fe^{2+}-Mg-Ca+Mn (a) and of Fe^{2+}+Mg-Mn-Ca (b) for garnets from Şirince and Çamlık blueschist metabasites.....198
Figure 5.35 Compositional zoning in the garnet (5-15) from M98-52/2; a) microphoto of analysed garnet in PPL, b) element zoning profiles from rim to rim , c) A-A line analyse from rim to rim.....199
Figure 5.36 Monitoring of compositional zoning in the garnet (35-45) from

T.C. YÜKSEKÖĞRETİM KURULU DOKÜMANTASYON MERKEZİ

M98-52/2.....201
Figure 5.37 Monitoring of compositional zoning in the garnet (22-38) from 94-55/5.....203
Figure 5.38 Ternary atomic proportions of Alm+Prp-Sps-Grs (a) and Alm-Prp-Grs+Sps (b) for a garnet grain from garnet-amphibolite sample (M97-149/10) in the Metaolistostrome unit.....210
Figure 5.39 Garnet photomicrograph in plane polarized light and composition of selected garnet grain in M97-149/10. Traverse is from rim to rim.....210
Figure 5.40 In almandine+spessartine - grossular - pyrope ternary diagram, location of selected garnet grains from the Metaolistostrome matrix.....212
Figure 5.41 Ternary atomic proportions of Alm+Prp-Sps-Grs (a) and Alm-Prp-Grs+Sps (b) for garnet (10-32) from garnet-phengite schist (M98-99/2).....212
Figure 5.42 Monitoring of compositional zoning in the garnet (10-32) from M98-99/2.....213
Figure 5.43 Ternary atomic proportions of Alm+Prp-Sps-Grs (a) and Alm-Prp-Grs+Sps (b) for garnet (61-77) from garnet-phengite schist (M98-99/2).....215
Figure 5.44 Compositional zoning in the garnet (61-77) from M98-99/2.....216
Figure 5.45 Ternary atomic proportions of Alm - Prp - Gross + Spess and of Alm + Prp - Spess - Gross for garnet (36-46) from 94-30.....218
Figure 5.46 Compositional zoning in the garnet (36-46) from sample 94-30.....219
Figure 5.47 In almandine+spessartine - grossular - pyrope ternary diagram, location of selected garnet grains from garnet-mica schist belonging to the Marble-schist series.....222
Figure 5.48 Ternary atomic proportions of Alm+Prp-Sps-Grs (a) and Alm-Prp-Grs+Sps (b) for garnet (1-9) from garnet-mica schist (M97-36).....222
Figure 5.49 Compositional zoning in the garnet from sample M97-36.....223
Figure 5.50 Ternary atomic proportions of Alm+Prp-Sps-Grs (a) and Alm-Prp-Grs+Sps (b) for garnet (12-19) from garnet-mica schist (M99-52/5).....224
Figure 5.51 Compositional zoning in the garnet (12-19) from M99-52/5.....225
Figure 5.52 Phengite compositions from Metaolistostrome and the Marble-schist units shown in term of a) Si p.f.u. vs Al p.f.u; b) Na/(Na+K) vs Si p.f.u; c) Ms-

Pa-Cel triangle and d) Si vs (Fe^{2+}+Mg) per formula unit (p.f.u).....231
Figure 5.53 Compositional variation (Si, Na, T2Al, X_{Cel} and X_{Ms}) of individual phengite flake in 94-30.....233
Figure 5.54 Compositional difference of biotites from the Metaolistostrome unit and the Marble-schist series (Tosch and Lugmair, 1990).....237
Figure 5.55 Principal variations in mica compositions showing for each the number of octahedral sites filled (di-octahedral, 2; tri-octahedral,3), and Si Al and M2+ atoms per formula unit (Deer et al. 1992).....239
Figure 5.56 Fe^{2+}, Mg and Mn p.f.u variation in chloritoids from kyanite-chloritoid schist (94-85/1(a); M97-135/1 (b)).....244
Figure 5.57 Al(VI) vs. Fe(3+) plot for epidotes from the Metaolistostrome unit and the Marble-schist series.....248
Figure 5.58 Compositional variations, normal zoning (95-70/4) and reverse zoning (M97-151/3 and 91-16) in different epidote grains from core to rim.....249

CHAPTER SIX

P-T ESTIMATION

Figure 6.1 P-T conditions and apparent P-T path for blueschist metabasite and metapelites from Dilek Peninsula.....255
Figure 6.2 The relationship between the pressure of retrograde metamorphism and NaM4 content of barrosites in Dilek peninsula (Brown 1976).....257
Figure 6.3 Phengite compositions generated under greenschist and epidote-blueschist facies conditions.....257
Figure 6.4 PT- diagram showing the metamorphic evolution of the Marble – schist series in Selçuk - Tire area.....260
Figure 6.5 PT -diagram showing the metamorphic evolution of the matrix of the Metaolistostrome.....263
Figure 6.6 P-T estimations of prograde and retrograde eclogite crystallization.....265
Figure 6.7 Spear (1980) geothermometer based on plagioclase-amphibole exchange equilibria.....269
Figure 6.8 P-T path of the omphacite-metagabbro and omphacite-epidotites based on various geothermobarometric calibrations.....270

Page

Figure 6.9 According to Plyusnina (1982) calibration, pressure and temperature estimations of retrograde overprint in omphacite-metagabbro and omphacite - epidotites.....273

Figure 6.10 The relationship between pressure and Na_{M4} content of amphiboles in omphacite-epidotite samples.....273

Figure 6.11 The relationship between pressure and Na_{M4} vs Al^{IV} diagram after Brown (1977) from blueschist metabasites in the Metaolistostrome unit.....277

Figure 6.12 The possible P-T path of blueschist metabasites in the Metaolistostrome unit.....278

Figure 6.13 Comparative P-T paths from the Marble-schist series and the Metaolistostrome unit (blocks and matrix).....279

CHAPTER SEVEN

DISCUSSION

Figure 7.1 The correlation of the Dilek Peninsula - Selcuk area and Samos based on tectono-stratigraphy and the relics of Eocene HP/LT metamorphism (Candan et al., 1997).....285

Figure 7.2 Correlation of the Menderes Massif with the Cycladic Complex in terms of the main units and relic high-pressure rocks.....286

Figure 7.3 P-T paths obtained for Eocene high-pressure metamorphism in the Cyclades. The rocks exposed in the north-west part of the Cyclades have isothermal/cooling decompression paths whereas in the eastern part of the massif show broad clockwise P-T paths with significant heating (Avigad et al., 1992).....296

Figure 7.4 Schematic representation of tectonic evolution of the Eocene HP/LT Series of the Menderes Massif.....303

ABBREVIATION LIST

Act: Actinolite

Ann: Annite

Bar: Barroisite

Chl: Chlorite

Cel: Celadonite

East: Eastonite

Ep: Epidote

Gr: Garnet

Grap: Graphite

Ms: Muscovite

Pa: Paragonite

Phg: Phengite

Phl: Phlogopite

Pl: Plagioclase

Omp: Omphacite

Q: Quartz

Sym: Symplectite

Zo: Zoisite

BI: Backscattered image

CAB: Calc-alkaline basalt

IAT: Island-arc tholeiite

MORB: Mid-ocean ridge basalts

OIA: Ocean-island alkali basalt or seamount alkali basalt

OIT: Ocean-island tholeiite or seamount tholeiite

WPB: Within-plate basalt

CHAPTER ONE

INTRODUCTION

1.1. Location of the study area

Menderes Massif is located in western part of Turkey. Menderes Massif is bordered to the northwest by the İzmir – Ankara zone, to the north by the Afyon zone, to the west by the Cycladic metamorphic complex and to the south by the Lycian nappes (Figure 1.1). The evidence about Eocene high-pressure / low-temperature (HP/LT) metamorphism are recognised in western part of Menderes Massif, along a zone extending NE-SW direction of about 100 km. The main localities of HP relics, such as Dilek Peninsula, Söke, Selçuk, Torbalı, Tire and Gölmarmara, are located in the western part of Menderes Massif (Figure 1.2).

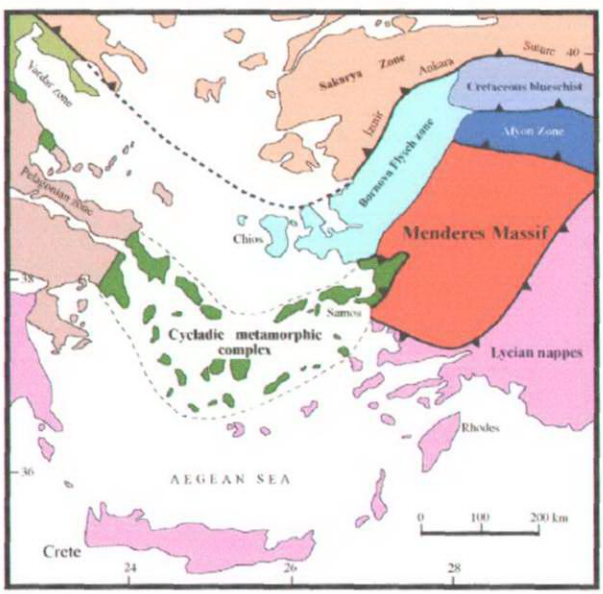


Figure 1.1 Main tectonic zones of the western Turkey (Okay 2001).

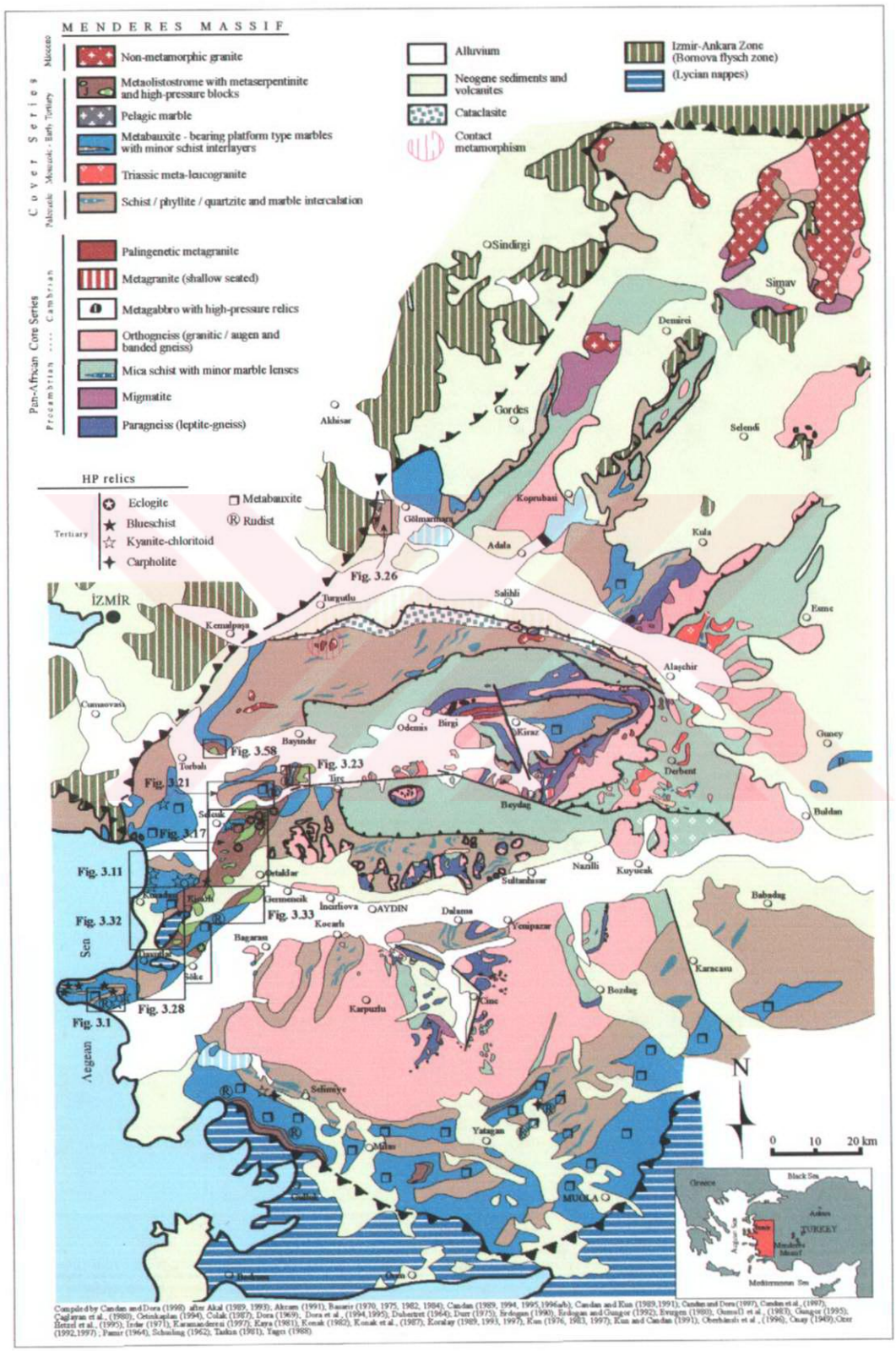


Figure 1.2 The generalized geological map of the Menderes Massif and the locations of mapped areas by this study (Candan and Dora 1998).

This study includes the 1/25.000 scaled sheets: M18d1, M18d2, M18c1, M18b1, M18b2, M18b3, M18b4, M19a1, L18c3, L19d4, L19d3, K19c2, K19c1 and L18c2 and covers an area of approximately 2000 km^2. Figure 1.3 shows the position of the sheets in 1/100.000 scale in the western part of Menderes Massif.

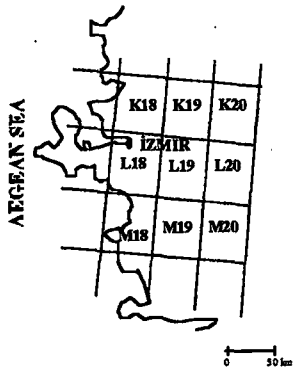


Figure 1.3 The set of 1/100.000 in scale maps in the western part of Menderes Massif.

1.2. The aim of the study

The aim of the study is to reveal the mineralogical and petrographical / petrological features of a subduction – related epidote-blueschist facies metamorphism which is recognised in the Mesozoic – Early Tertiary sequence (Marble-schist series and Metaolistostrome unit) from Dilek Peninsula, Söke, Selçuk, Torbalı, Tire and Gölmarmara areas and, to define the correlation between Mesozoic – Early Tertiary (?) series, in western part of Menderes Massif, and Cycladic Crystalline Complex in Aegean Sea in terms of the rock succession and poly-metamorphic evolution.

1.3. Previous studies

The Menderes Massif which is the western one of the large metamorphic culminations within the Turkish Alpine orogen, is bounded by the İzmir – Ankara Zone including the Bornova – Flysch zone, in the northwest, the Afyon zone in the north and the Lycian nappes comprising shales, carbonates and thick ophiolite slices in the south (Şengör and Yılmaz, 1981; Dora et al., 1995). The Menderes Massif is

considered to be linked to the Cycladic Crystalline Complex in the central Aegean Sea, as a part of Median Crystalline Belt (Dürr et al., 1978).

In recent years, the similarities between the Menderes Massif and Attic-Cycladic Crystalline Complex widely submerged below the Aegean Sea have been emphasized, and many attempts have been made to correlate these two crystalline regions (Dürr et al., 1978; Papanikolaou & Demirtaşlı 1987; Candan et al., 1997; Candan et al., 1999). The Menderes Massif is commonly interpreted as the eastward continuation of Attic-Cycladic Massif in the Aegean Sea (Jacobshagen, 1986; Oberhaensli et al., 1998). However, recently it has been suggested that two massifs are in all aspects not related (Ring et al., 1999b).

The metamorphic rocks exposing throughout the study area are included into the cover series of the Menderes Massif by Candan & Kun (1989). According to these authors, ophiolites are overlain by the thick platform type marbles and older than the Upper Creataceous emery-bearing carbonates. Based on this assumed stratigraphic position, this metaophiolitic belt has been interpreted as a paleo-melange zone and has been considered older than the İzmir-Ankara Zone.

Recent studies reveal that the Menderes Massif forms a complex nappe pile (Konak et al., 1994, Dora et al., 1995, Partzsch et al., 1998) rather than a simple onian-shaped structure which is built up by the Precambrian core and Paleozoic - Early Tertiary cover (Schuiling 1962, Başarır 1970, Konak et al., 1987, Dora et al., 1990). The Pan-African basement series is mainly composed of partly migmatizated Late Proterozoic metapelites (e.i. leptite-gneiss and micaschist) which were intruded by the Pan-African granitoids and gabbros (Candan et al., 1994, Dora et al., 1995, Hetzel & Reischmann 1996). The Paleozoic series is typified by a black coloured quartzite, marble and phyllite intercalation. This black series in Selçuk, Bayındır and Akhisar areas was named as Bayındır Formation by Erdoğan & Güngör (1992) and Güngör (1998).The Mesozoic sequence (Milas Formation) (Brinkman 1967), Triassic to Upper Cretaceous in age (Özer 1993), is characterized by the platform - type marbles with metabauxite lenses (Dürr 1975, Konak et al., 1987, Dora et al.,

1995, Özer 1998). This Mesozoic sequence is named as Kayaaltı Formation by Erdoğan & Güngör (1992) and Güngör (1998) in the Selçuk-Bayındır area. Kayaaltı Formation has similar lithologic and age relationships with Milas Formation. However the pelagic red marbles are not recognised at the boundary of marble and Metaolistostrome unit. According to these authors, Kayaaltı Formation is concordantly overlain by the Selçuk Formation made up of high-pressure blocks embedded in garnet-phengite schist / albite-phengite schist matrix of metaolistostrome. Metabauxites in the high-grade parts of marbles contain corundum whereas the same metabauxites in the lower-grade part of the marbles are dominated by diaspore (Yalçın 1987). Yalçın (1987) suggested that the age of the bauxite-bearing marbles is Jurassic or Early Cretaceous in age. The upper levels of the platform type marbles is characterized by the presence of well-preserved rudist fossils (Dürr 1975; Konak et al., 1987; Özer 1993). These metacarbonates are overlain by the Upper Paleocene – Lower Eosene pelagic marbles and metamorphosed olistostrome with ophiolite blocks (Dürr 1975; Gutnic et al., 1979; Çağlayan et al., 1980; Konak et al., 1987). The metaolistostrome is thought to have formed in front of advancing Lycian ophiolitic nappes (Erdoğan & Güngör, 1992). It has also been compared with the Cycladic olistostromes (Candan et al., 1997). HP/LT metamorphism in the Metaolistostrome unit has been documented by Dora et al., 1995; Candan et al., 1997; Candan & Dora 1998 and Çetinkaplan et al., 2000a, b.

Recent studies unambiguously reveal the complex tectonometamorphic evolution of the Menderes Massif. This may be outlined as i)Polyphase Pan-African metamorphism of the basement units under granulite, eclogite and amphibolite facies conditions (Candan et al., 1994, 1998, Çetinkaplan 1995, Oberhaensli et al., 1997, Oelsner et al., 1997, Candan & Dora 1998) and ii)Two subsequent Tertiary metamorphisms under epidote – blueschist to eclogite (?) and greenschist to amphibolite (?) facies conditions. These metamorphic events during the Tertiary time, similar to Cycladic Complex, have been recognised in the northwest part of the Menderes Massif (Candan et al., 1997, Oberhaensli et al.,1998, Candan & Dora 1998)

In Mesozoic – Early Tertiary series, blueschists and eclogites which are strongly overprinted by greenschist facies, have been documented by Candan et al., (1997), (1998) and Oberhaensli et al., (1997, 1998). These authors suggest a high-pressure / low-temperature metamorphism. Typical high-pressure minerals, such as glaucophane and phengite, in blueschist metabasites are determined in Dilek Peninsula (Candan et al., 1997; Oberhaensli et al., 1998). The same high-pressure minerals on Samos Island, 2km NW of Dilek Peninsula, in Cycladic Complex are documented by Okrush et al., (1985) and Chen et al., (1995). The phengites in the blueschist metabasites from Dilek Peninsula were dated at about 40-42 Ma by Ar^{39}/Ar^{40} method (Oberhaensli et al., 1998). This Upper Eocene age is well-consistent with the ages that were obtained for the HP/LT metamorphism in the Cycladic Complex (Andriessen et al., 1979; Altherr et al., 1979). This is attributed to a subduction-related HP metamorphism during the closure of Neotethys (Oberhaensli et al., 1998). The high-pressure unit of the Dilek Peninsula is interpreated as the eastward continuation of the HP unit of Samos Island (Candan et al., 1997; Oberhaensli et al., 1998). Okay (2001) suggested that this HP units should be excluded from the Menderes Massif and they belong to the Cycladic Complex Gessner et al., (2000) and Okay (2001) suggest that HP unit of the Dilek Peninsula as a part of Cycladic Complex was thrust onto the Menderes Massif during the Alpin orogeny. Ring et al., (1999b); Gessner et al. (2000); Okay (2001) and Bozkurt & Oberhaensli (2001) support that the Menderes and Cyclades can not be correlated. In contrast, the new discovery of high-pressure assemblage (Fe-Mg carpholite – kyanite) in cover series in southern flank of Menderes Massif supports the lateral continuation of both Menderes Massif and Cycladic Complex (Rimmele et al., 2002).

CHAPTER TWO

LITOSTRATIGRAPHY

2.1. Litostratigraphy of rock assemblages

In the western part of Menderes Massif, Dilek Peninsula, Söke, Selçuk, Torbalı, Tire and Gölmarmara, Paleozoic to Mesozoic – Early Tertiary sequence is mainly made up of, in ascending order, Marble-schist series (muscovite-quartz schist, metaquartzite, garnet-mica schist, mica schist, phyllite, metabasite lenses, metaconglomerates, metabauxite-bearing marble) and Metaolistostrome unit (Figure 2.1).

The Paleozoic (?) aged schist series is observed in Selçuk, Torbalı and Gölmarmara areas. This assemblage is represented by muscovite-quartz schist, metaquartzite (black), phyllite (black), mica schist /garnet-mica schist and minor metabasite lenses. The Paleozoic (?) aged assemblage is overlain by Mesozoic – Early Tertiary (?) assemblage. The lower levels of Mesozoic – Early Tertiary (?) assemblage begin with a sequence which is made up of mica schist containing glaucophane-bearing metabasite lenses, phyllite, muscovite-quartz schist, quartz metaconglomerate which includes "kyanite-chloritoid-phengite" mineral assemblage, carbonate metaconglomerate intercalation. The garnets appear with increasing metamorphic grade in mica schist and phyllites which occur in lower levels of Mesozoic – Early Tertiary assemblage. The yellowish dolomites in the uppermost levels of schist-dominant sequence gradually pass into platform type, thick marbles.

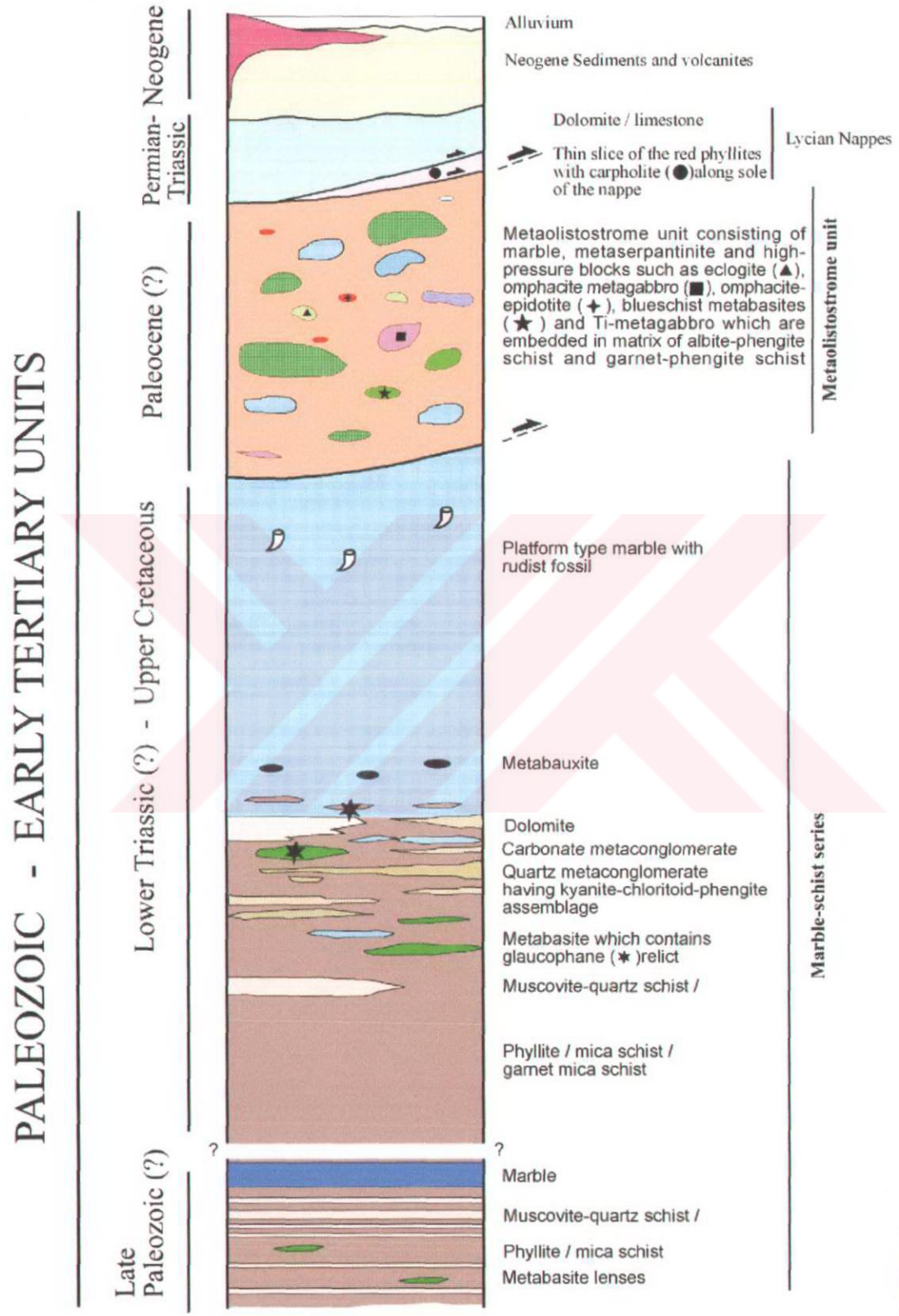


Figure 2.1 Generalized columnar section of the study area.

T.C. YÜKSEKÖĞRETİM KURULU
DOKÜMANTASYON MERKEZİ

The lower levels of the platform-type marbles contain metabauxite lenses. Upper Cretaceous rudist-bearing marbles occur in upper levels of platform type marble. Thick bedded platform type marbles are tectonically overlain by a thrust sheet of Metaolistostrome unit. The blocks in Metaolistostrome unit are made up of eclogite, omphacite metagabbro, zoisite metagabbro, Ti-metagabbro, omphacite-epidotite, metaserpentinite, blueschist metabasite and marble. These blocks are embedded in a matrix with garnet-phengite schist / albite-phengite schist. The Metaolistostrome unit is structurally overlain by the Lycian Nappes which are composed of red phyllites containing carpholite and Limestone/dolomite in low-grade crystallinity. In the study area, the Lycian Nappes are observed as small klippen lying on top of the Metaolistostrome unit. The sole of klippen are marked by brittle deformed red phyllites. In the study area, Neogene sediments disconformably cover all units.

CHAPTER THREE

GEOLOGY OF THE ROCK UNITS

3.1. Introduction

This chapter describes the geological characteristics of the rock units occurring in eight localities (Dilek Peninsula, Söke, Kuşadası (Kirazlı), Selçuk, Hasançavuşlar – Akyurt, Torbalı, Tire and Gölmarmara). They extend from west to northeast along the northwest border of the Menderes Massif (Figure 1.2). The metamorphic rocks in the areas mentioned can be divided into two main rock associations: ***Marble-schist series*** and ***Metaolistostrome unit***. Marble-schist series is composed of schists with different mineral compositions, phyllite, metaconglomerates, metabasic rocks and thick bedded platform type marble. The Metaolistostrome unit is made up of blocks embedded in a matrix of albite-phengite schist and garnet-phengite schist. Furthermore, ***Lycian Nappes*** occurring as klippen around Kuşadası and Söke areas rest tectonically over the Metaolistostrome unit and/or Marble-schist series.

3.2. Marble-schist series

Marble-schist series crops out in the Dilek Peninsula, Selçuk, Torbalı, Tire and Gölmarmara regions. The mica schists occur in the lower levels of the series. The pass gradually upward to the platform type marbles. The mica schists including metabasite rocks, quartzite, metaconglomerate intercalations, are quite thick. The general geologic features of Marble-schist series in different areas are given below.

3.2.1. Dilek Peninsula

The studied succession, located between Doğanbey and Tuzburgazı villages in Dilek Peninsula, is composed of platform-type marble, phyllite, metaconglomerates (quartz and carbonate) and quartz-mica schists (Figure 3.1). Due to the intense isoclinal folding, these rocks are repeated at different levels. The marble with diasporite lenses and preserved rudist fossils, occurs at the base of the rocks succession in this area (Figure 3.2). The marble is overlain by a thick succession of quartz metaconglomerate, carbonate metaconglomerate, phyllite and quartz-mica schist intercalations. This succession, dominated by phyllite, contains common metabasic lenses and layers. The repetition of quartz metaconglomerate and carbonate metaconglomerate is also observed in phyllites which are members of the overturned succession (Figure 3.3). The average length of pebbles is 2-3 cm (Figure 3.4). The quartz metaconglomerates are made of pebbles embedded in a quartz rich matrix. The pebbles are monogenic and composed only of quartzite. The length of the pebbles in quartz metaconglomerate can reach up to 7-8 cm due to stretching (Figure 3.4). Quartz metaconglomerates may contain pure quartzite layers (Figure 3.5). "Kyanite – chloritoid – phengite" assemblage in phyllitic layers is characteristic for quartz metaconglomerate (Figure 3.6). The maximum thickness of a quartz metaconglomerate layer is approximately 30-35 m. Quartz metaconglomerates are overlain by carbonate metaconglomerates (Figure 3.2 and 3.3). The length of carbonate pebbles in carbonate metaconglomerates can reach up to 14-15 cm (Figure 3.7a). The average size of carbonate pebbles is 5-6 cm (Figure 3.7b). On the other hand, quartzite and epidotite pebbles are rarely observed in the carbonate metaconglomerate unit. The matrix of the carbonate metaconglomerate consists of quartz, chlorite, amphibole and carbonate. The greenish colour of the matrix results from the presence of chlorite and amphiboles representing the existence of basic volcanism during the sedimentation of these conglomerates. The effects of deformation in carbonate metaconglomerate is represented by isoclinal folding (Figure 3.8), and strong stretching of the carbonate pebbles. The orientation of axes of isoclinal folding is average K35D. The thickness of carbonate metaconglomerate ranges from 2 - 3 to 40 m. The carbonate metaconglomerate is overlain by dark grey

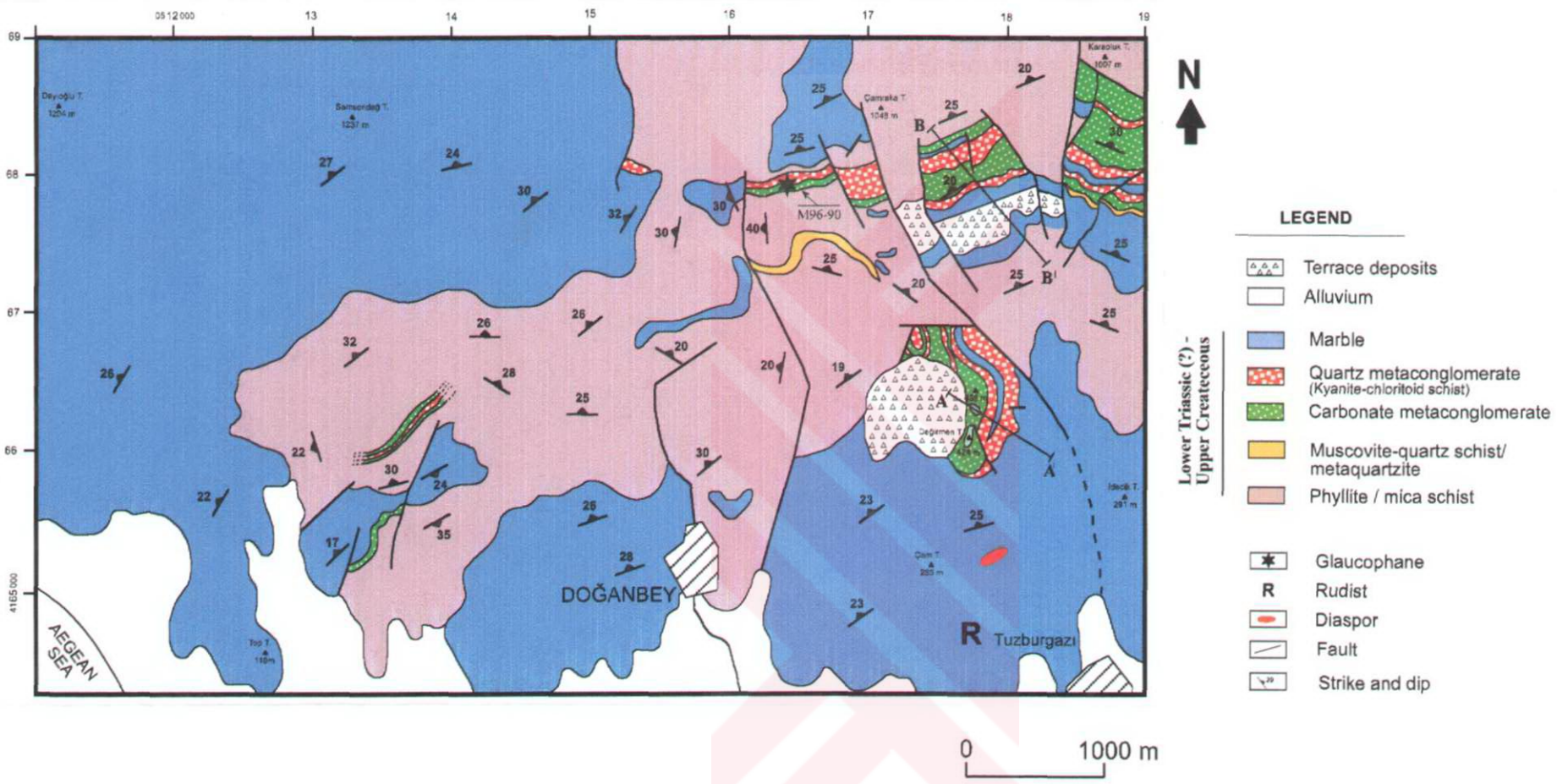


Figure 3.1 Geological map of the studied area in the Dilek Peninsula around Tuzburgazı and Doğanbey villages, SW of Söke. Sample number and location of analyzed rocks are shown in the map.

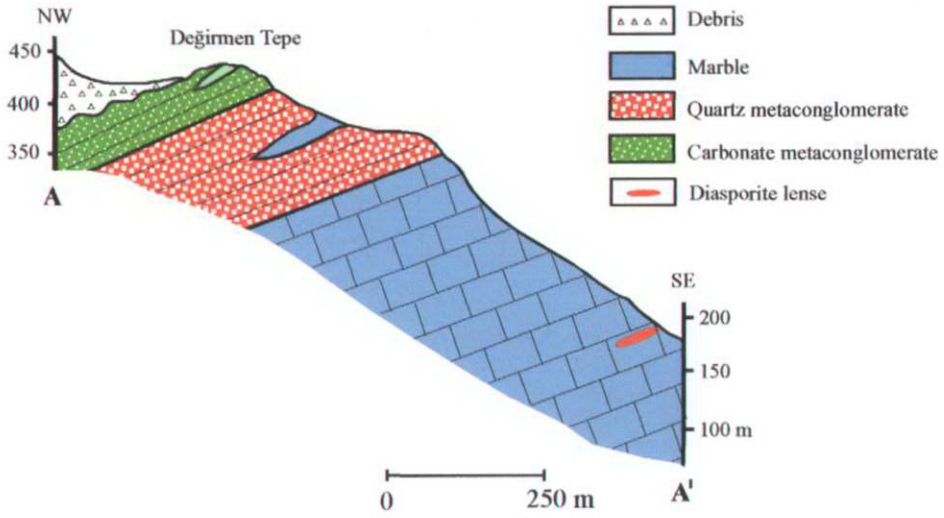


Figure 3.2 The cross section of the metaconglomerates and underlying metabauxite-bearing marble which is interpreted as overturned succession.

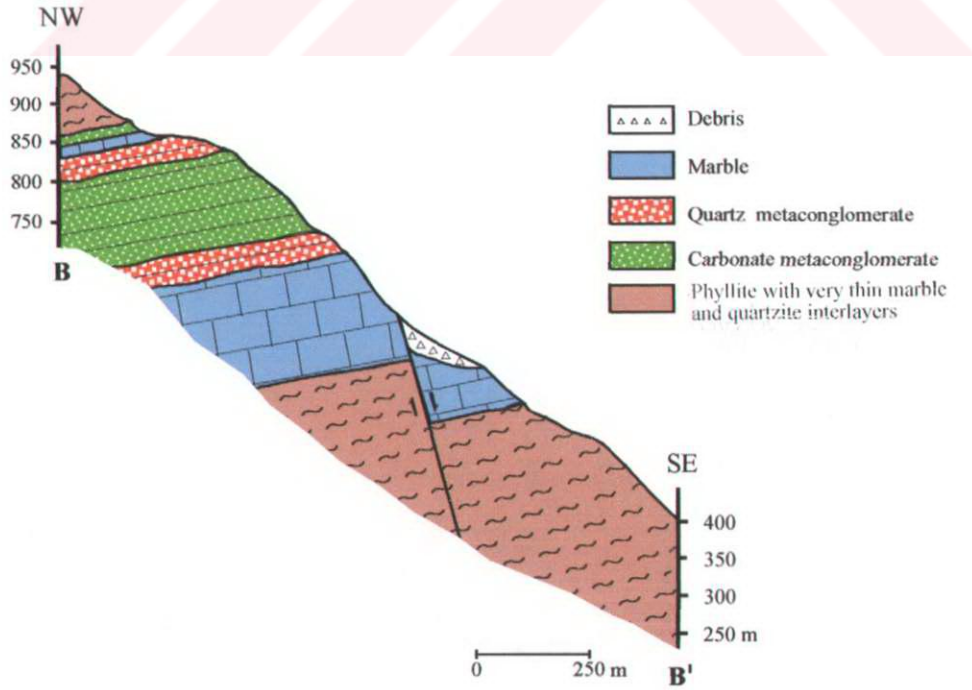


Figure 3.3 Repetition of the metaconglomerates in overturned succession in Dilek Peninsula. Section line is given in Figure 3.1.

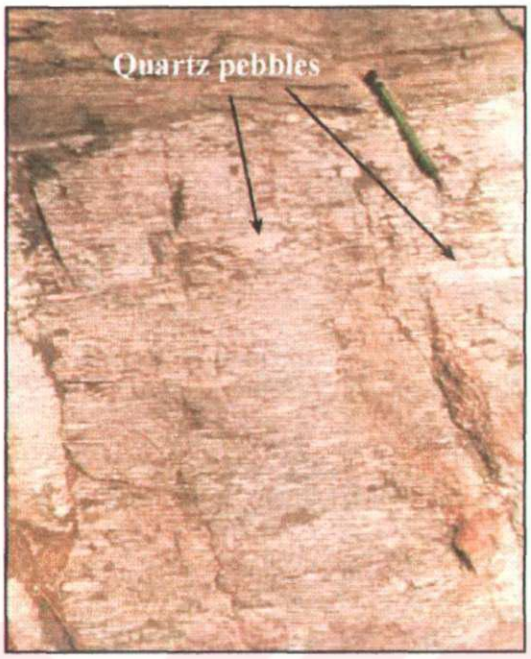


Figure 3.4 Photo showing quartz pebbles in quartz metaconglomerate.



Figure 3.5 Photo showing the interlayering quartz metaconglomerate and quartzites.

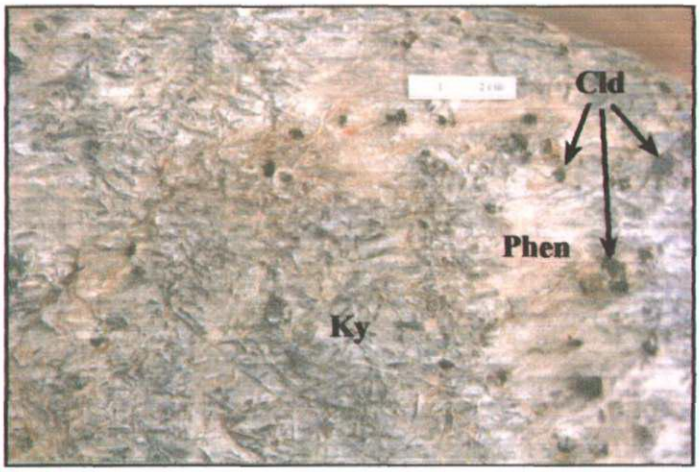


Figure 3.6 Kyanite (Ky) and chloritoid (Cld) crystals in the phyllitic matrix of quartz metaconglomerate.

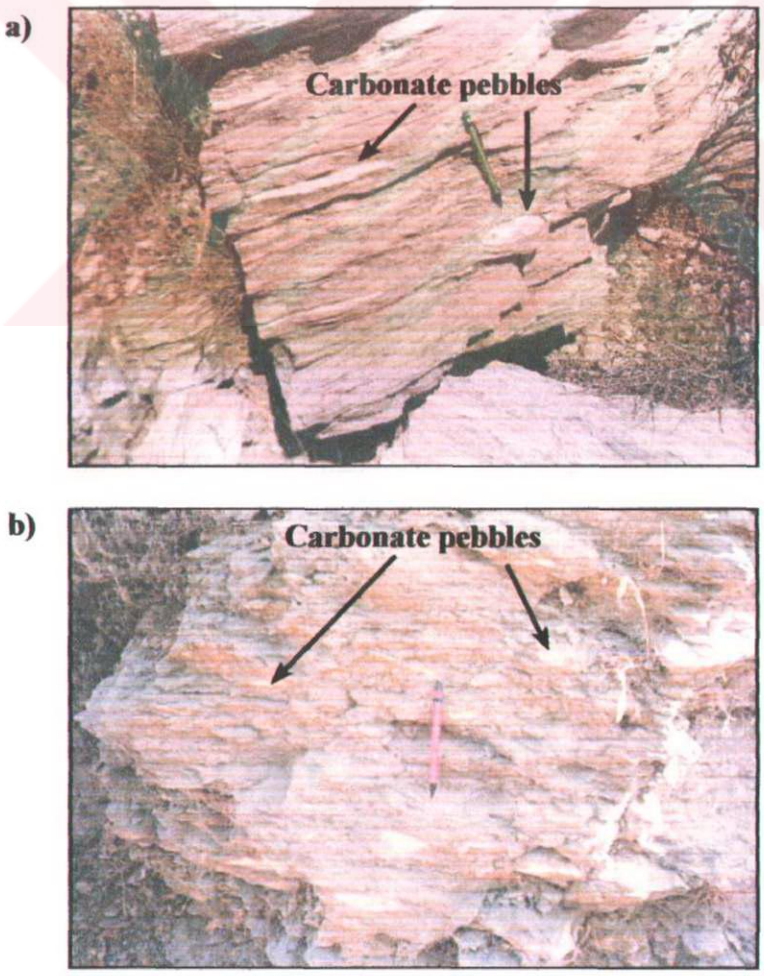


Figure 3.7 a) Carbonate pebbles in carbonate metaconglomerate show strong stretching. The length of carbonate pebbles can reach up to 14-15 cm. **b)** The average size of carbonate pebbles is 5 - 6 cm. Carbonate pebbles are embebdded in matrix composed of calcite, quartz and chlorite.

phyllite. The phyllites contain quartzite and marble layers. The number of marble layers in phyllites increase towards the marble contact (Figure 3.9a). In some levels the thickness of marble layers reaches up to 1-1.5 m. Whereas, quartzite increases away from the main phyllite-marble contact (Figure 3.9b). The marble levels, up to 2 – 3 cm in thickness, and thick quartzite layers occur at the stratigraphically lower levels of phyllites. The metabasic rocks occurring as layers and boudinaged lenses in the phyllites and quartz conglomerates contain well-preserved relict "Na-amphibole (crossite) – phengite – epidote" assemblage. Blue amphibole crystals up to 1 cm in size, can be easily recognisable in hand specimen (Figure 3.10). Phyllites are conformably overlain by thick marble. Thicknesses of marble layers gradually increase getting from the contact. The general strike and dip of foliation in marble and other units are SW – NE and NW, respectively.



Figure 3.8 Isoclinal folding commonly observed in carbonate metaconglomerate and other units.

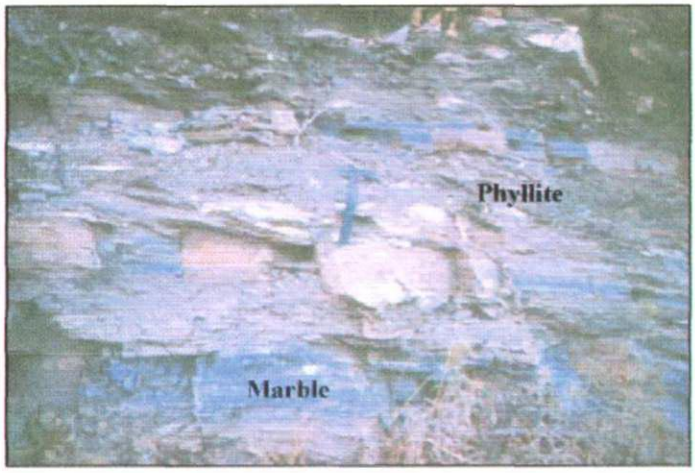


Figure 3.9a. Photo showing the increasing of the number and thickness of the marble layers towards marble-phyllite contact. This part represents the stratigraphically upper levels of the phyllites.

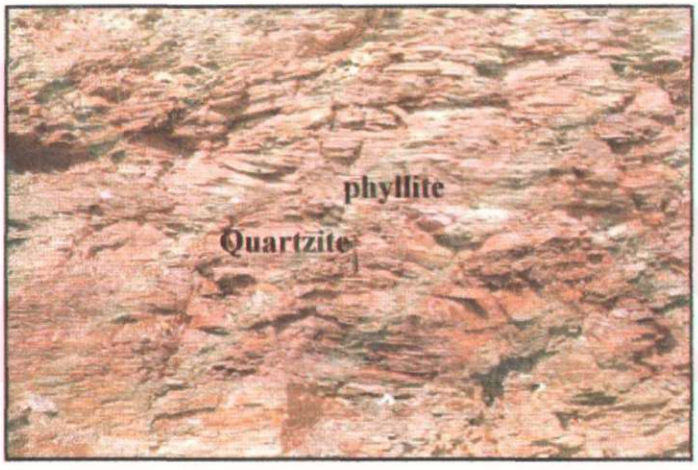


Figure 3.9b Photo showing the increase in number of the quartzite layers in the stratigraphically lower levels of the phyllites.

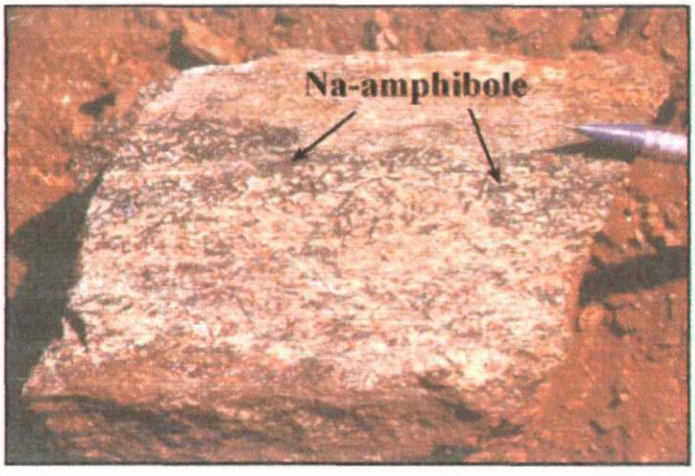


Figure 3.10 Photograph of Na-amphibole crystals in epidote and calcites.

3.2.2. Selçuk region

Two different areas, Kuşadası – Selçuk and Selçuk – Ortaklar, are studied in the region. Kuşadası-Selçuk area is made up of completely the Marble-schist series rocks. In Selçuk-Ortaklar area, the dominant rock unit is the the Metaolistostrome unit.

3.2.2.1. Kuşadası – Selçuk area

The general rock succession of the area between Kuşadası and Selçuk can be given in ascending order as follows: i) Marble / schist intercalations, Paleozoic (?) in age, ii) Lower Triassic schist with quartz and carbonate metaconglomerate layers, iii) Jurassic – Upper Cretaceous platform type thick marbles and iv) Metamorphic olistostrome, probably Paleocene (?) in age (Figure 3.11). In this area, mica schist, metaquartzites are overlain by marbles occur at the base of the metamorphic sequence and are Paleozoic (?) in age. This series can be distinguished from the Mesozoic Marble-schist series by the following features; i) these marbles do not contain metabauxite and are observed as interlayers within the schists, ii) there are no metabasic lenses and layers in this intercalations, iii) this marble / schist series do not contain metaconglomerate horizons. Based on these features, this marble-schist series which can be interpreated as the uppermost part of the Paleozoic (?) series, is separated as a different series from Lower Triassic - Upper Cretaceous sequence. The Marble - schist series Paleozoic (?) in age is conformably overlain by mica schist intercalated with lenses or layers of metaconglomerates, metabasites, metaquartzite and marbles (Figure 3.11). Quartz and carbonate metaconglomerates occur as lenses or layers showing lateral continuity (Figure 3.11). The quartz metaconglomerates with fine-grained phyllitic matrix are completely made up of strongly flattened and elongated quartz pebbles and have the characteristic "kyanite + chloritoid + phengite" paragenesis. Like in quartz metaconglomerate, carbonate metaconglomerate has got flattened carbonate pebbles embedded in matrix of quartz and carbonate (Figure 3.12). Some localities, green coloured mafic volcanic material can form the matrix of carbonate metaconglomerate. The thickness of quartz and carbonate metaconglomerates ranges from 0.2 m to 30-40 m.

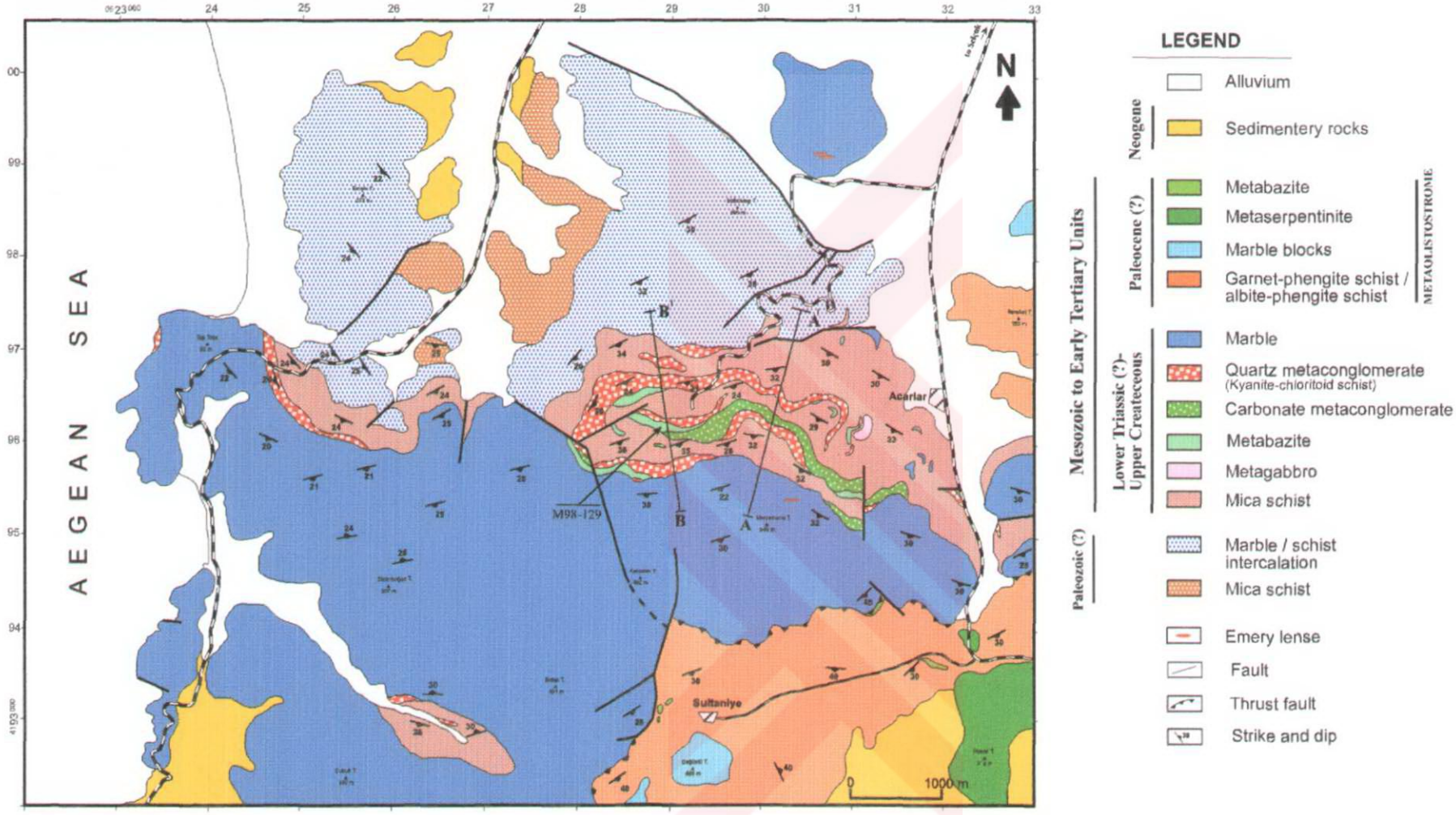


Figure 3.11 Geological map of the eastern part of Selçuk. Sample number and location of analyzed rocks are shown in the map.

Pale green coloured metabasites can reach up to 20 – 25 m in thickness and lateral continuity of them are approximately 1 km. Metabasites may contain thin epidote bands and clusters. The largest outcrop with 50 x 200 m in size occurs in the west of Acarlar village. No textural or mineralogical evidence related to the epidote-blueschist metamorphism is observed.

Metaconglomerate – schist intercalation is conformably overlain by platform type, metabauxite bearing, thick marbles (Figure 3.15). The contact relationships of these two units are given in Figure 3.13 and 3.14. Transitional contact relationship between metaconglomerate – schist intercalation and marble from Top Tepe, 6 km north of Kuşadası is given in Figure 3.16 In this columnar section, the contact is represented by the presence of yellowish dolomite horizons, probably upper Triassic in age (pers. comm. with O. Kaya). Metabauxite lenses in Meryemana Tepe occur 70 m above the lower contact of the marble. The marble has massive appearance in upper level of the unit or getting away from mica schist / marble contact. The Metaolistostrome unit around Sultaniye village tectonically overlies the greyish coloured massive marble.

3.2.2.2. Selçuk – Ortaklar area

In this area, Marble-schist series is composed of mica schist, muscovite-quartz schist, quartz metaconglomerate, metabasite lenses and emery-bearing marble (Figure 3.17). In NW and N of Şirince village, schists are rich-in mica. However, quartz-rich schists are observed at around Selatin village (Figure 3.18). In NW of Şirince village, mica schists are intercalated by muscovite-quartz schist layers 3-4 cm in thickness. Quartz metaconglomerate lenses and layers are seen in the upper levels of mica schist. Quartz metaconglomerates contain flattened quartz pebbles which are embedded in quartz-rich matrix. Kyanite - chloritoid – white mica assemblage occurs in greyish pelitic layers of quartz metaconglomerate. Chlorite-albite schist, albite schist, chlorite schist and muscovite-quartz layers are dominated in marble – schist contact.



Figure 3.12 Thin carbonate metaconglomerate levels in mica schist. Flattened carbonate pebbles are embedded in a matrix of quartz and carbonate groundmass.

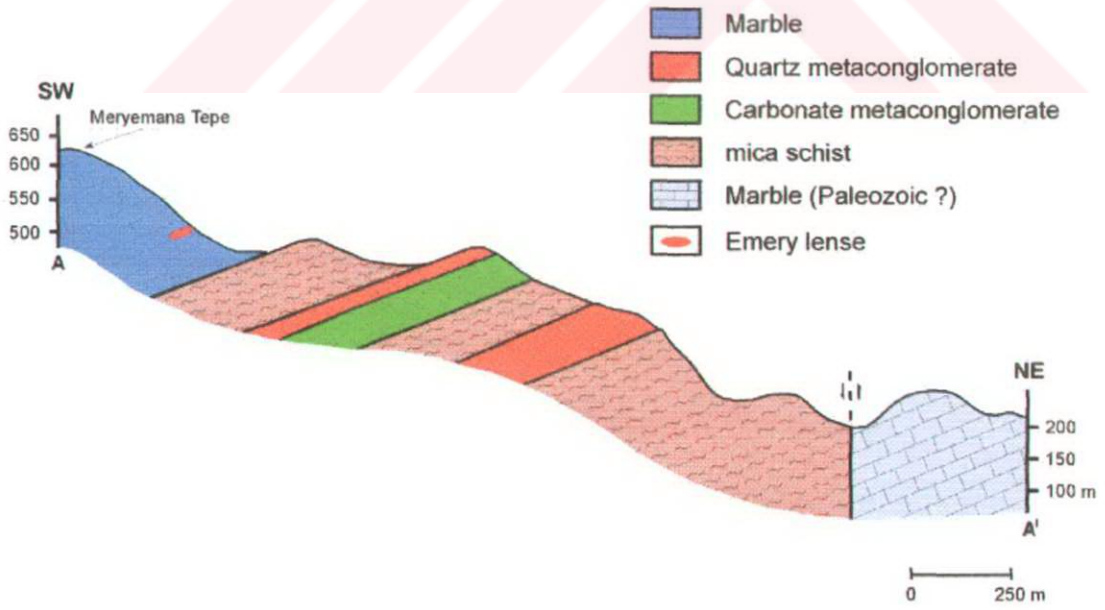


Figure 3.13 The contact relationship between metabauxite bearing marble and metaconglomerate - schist intercalations. Section line is given in Figure 3.11.

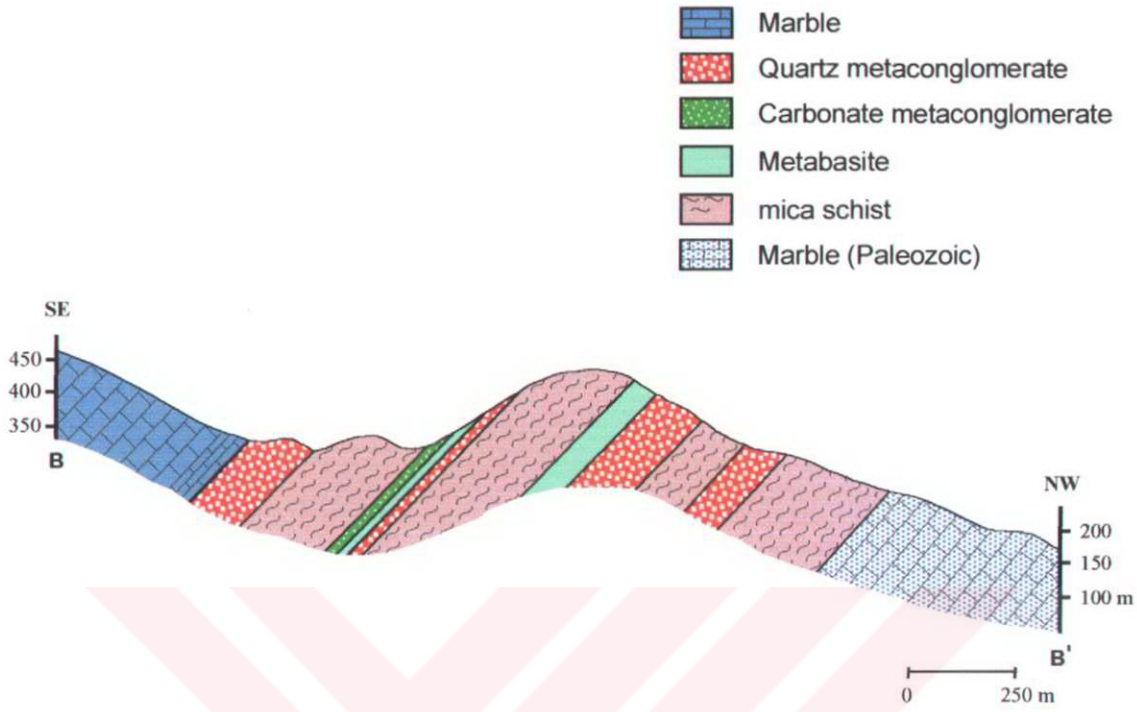


Figure 3.14 The contact relationship between metabauxite bearing marble and metaconglomerate - schist intercalations. Section line is given in Figure 3.11.

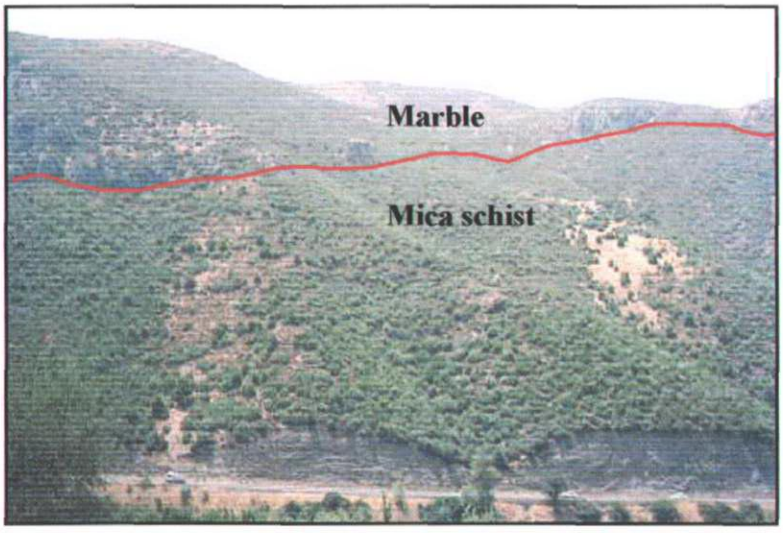


Figure 3.15 The contact relationship between emery-bearing marble and mica schist in Selçuk - Çamlık road.

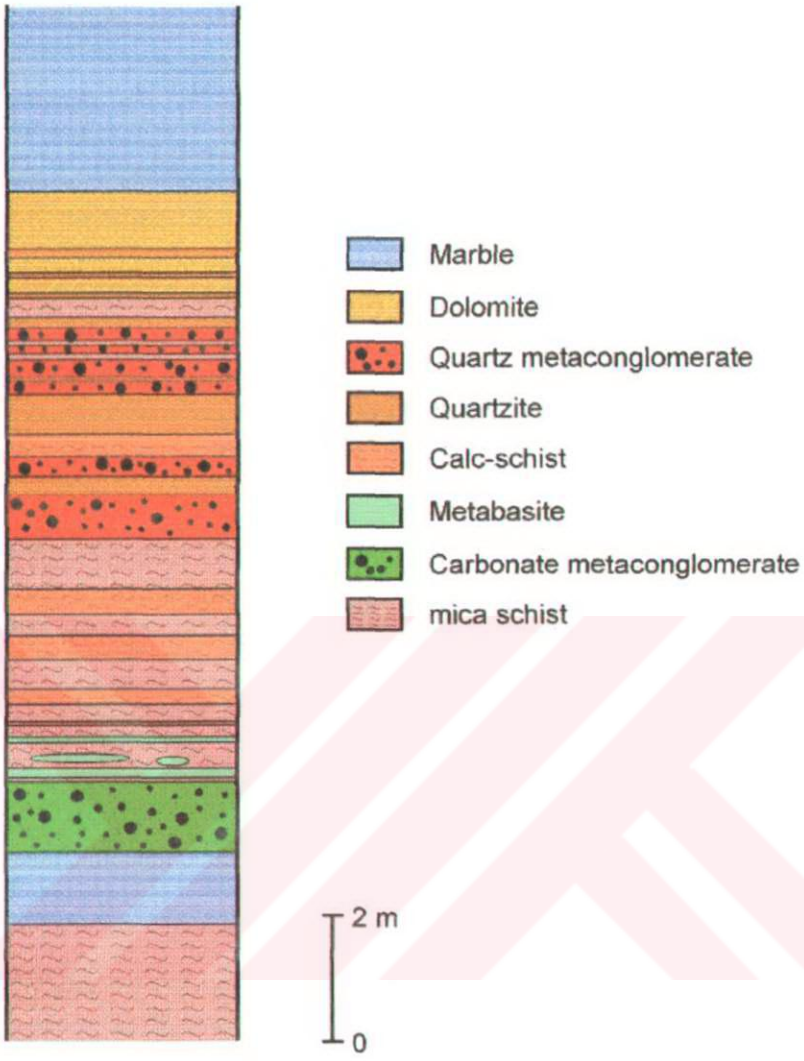


Figure 3.16 The measured columnar section showing the transitional contact between emery-bearing marble and mica schist in Top Tepe, 6 km north of Kuşadası.

In addition, metabasite lenses are commonly observed within this schist assemblage. The amphiboles in metabasites are Ca-amphiboles. No evidence related to the high-pressure metamorphism can be recognised by the naked eyes. The transition from mica schist to marble is transitional (Figure 3.19). Transition interval from schist to marble is 8-10 m. The emery lenses occur in lower levels of marble unit. The thickness of the original bedding in thick bedded marble increase towards to upper levels. The Metaolistostrome unit structurally overlies the metabauxite - bearing

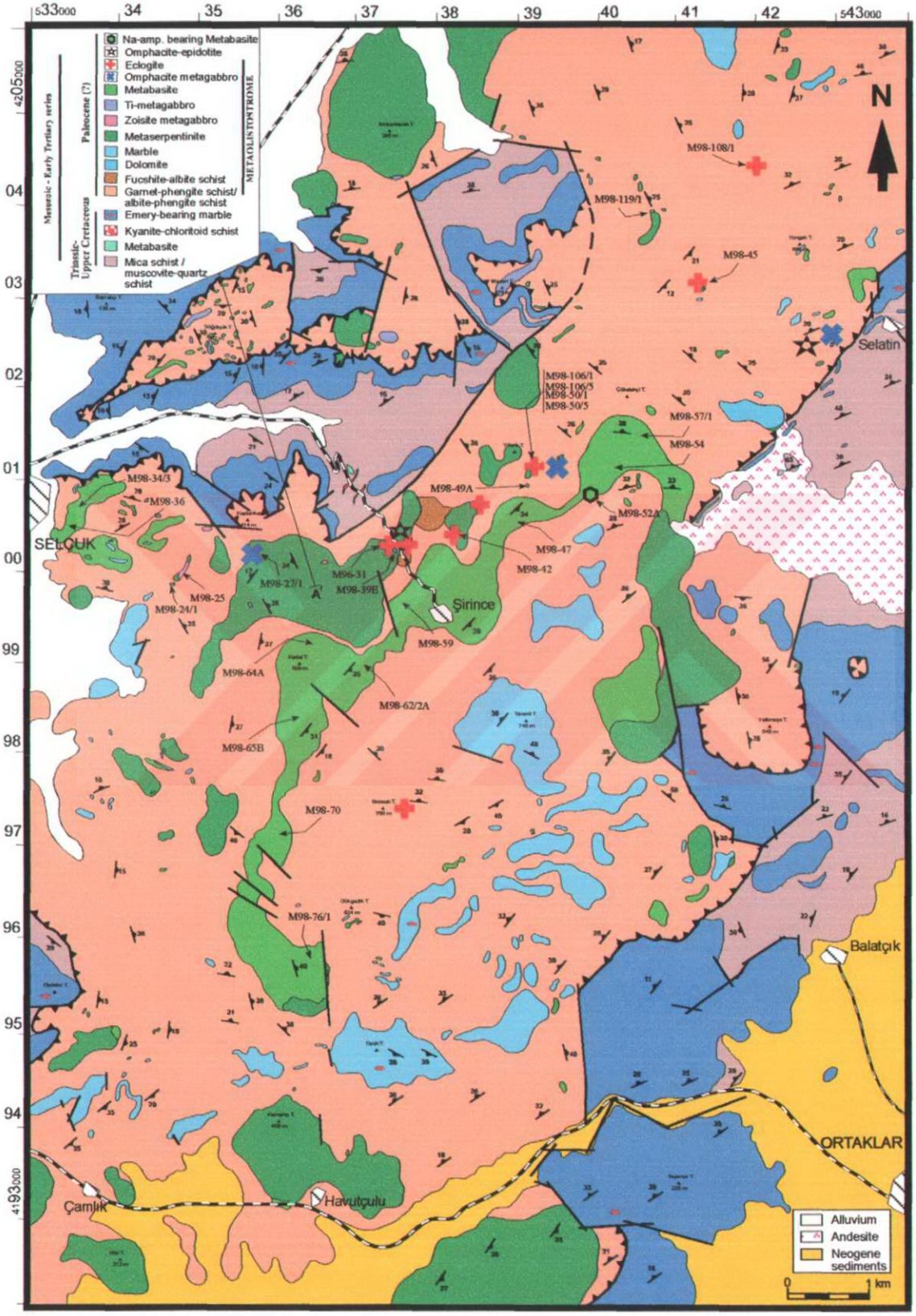


Figure 3.17 Geological map of Şirince - Ortaklar and Selçuk. Sample number and locations of analysed rocks are shown in the map.

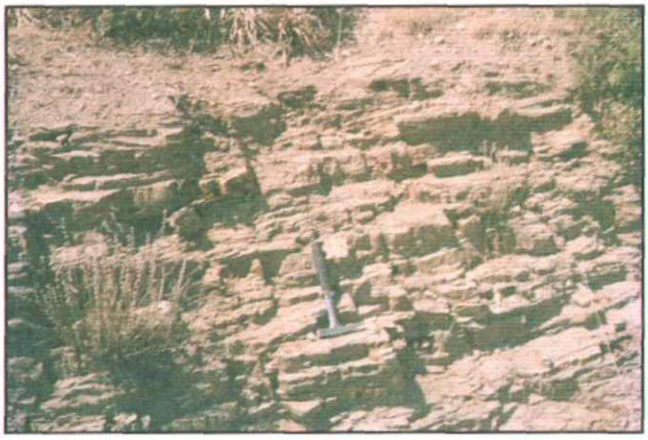


Figure 3.18 Muscovite-quartz schist and metaquartzite layers at around Selatin village.

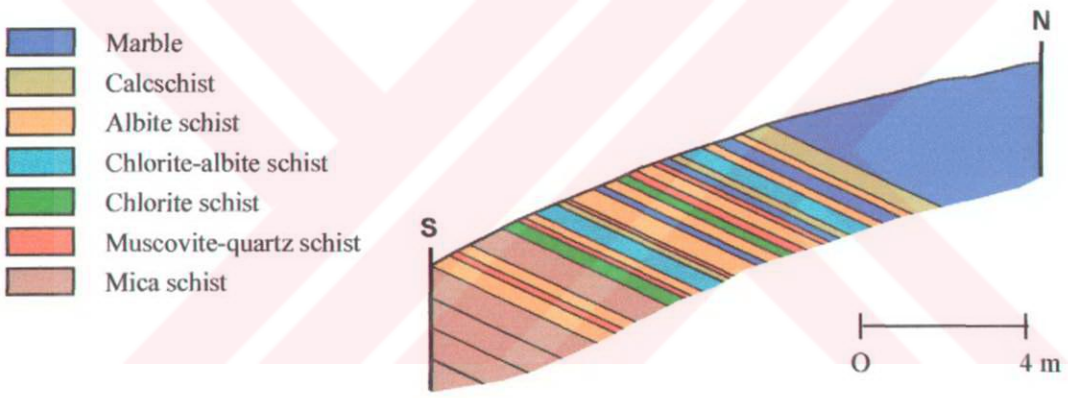
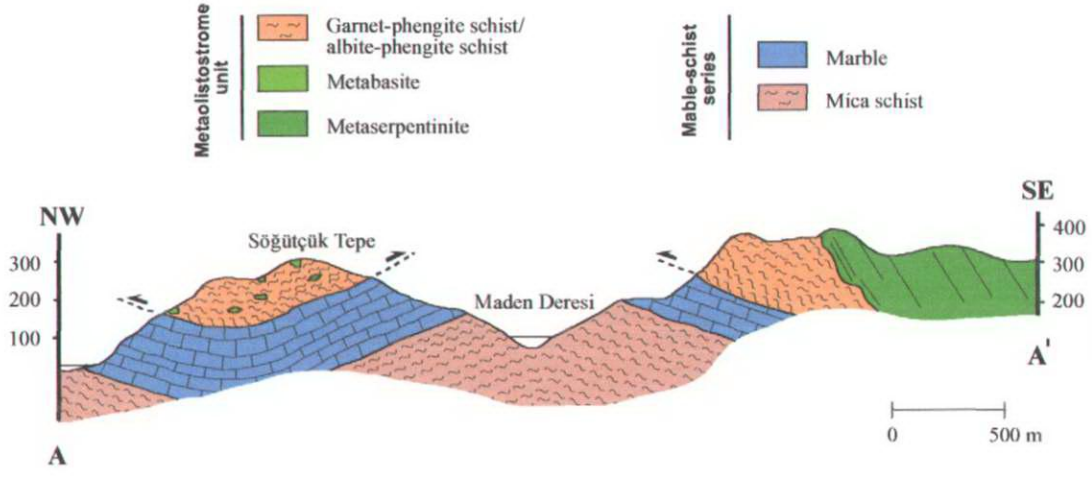


Figure 3.19 Transitional contact relationship between mica schist and emery-bearing marble (02045:37750).



3.20 Cross section showing the tectonic contact relationship between metaolistostrome unit and underlying marble-schist series.

T.C. YÜKSEKÖĞRETİM KURULU
DOKÜMANTASYON MERKEZİ

marble of the Marble-schist series (Figure 3.20). No evidence representing the foundering of platform and transition from neritic to pelagic environment which is characterized in the southern border of the Menderes Massif by the cherty marbles as noticed by Özer (1993, 1998), are observed along the boundary between massive marble and metaolistostrome. The contact between marble and the Metaolistostrome units is interpreated as thrust fault.

3.2.3. Akyurt and Hasançavuşlar area

The units of Marble-schist series are exposed over large areas at around Akyurt and Hasançavuşlar villages. These units are composed of mica schist, garnet mica schist, garnet phyllite, quartzite, muscovite-quartz schist, metabasite and marble (Figure 3.21). Alternation of schist, phyllite and quartzite are dominantly observed around Akyurt. In these series, thick marble layers can be followed more than 1 km along strike (Figure 3.21). The thickness of the schist, phyllite, marble and quartzite layers change from 1-2 cm up to 30-40 cm (Figure 3.22). This intercalation continues up to massive marbles which are overlain by the Metaolistostrome unit (Figure 3.21). Pale grey or cream coloured mica schist or garnet mica schists are more dominant. The prominent mica type is white mica. Black biotite crystals are also seen in these schists. In schist series, garnet phyllites which are of the same coloure with the schist, are characterized by the presence of garnet porphyroblasts which are partly altered into chlorite. In addition, garnet phyllites may contain irregular chlorite patches. Quartzite and muscovite-quartz schists of different thicknesses between schist and phyllites are strongly folded. The average trend of the fold axes is N30E. The amount of the marble lenses and bands increases towards the marble and schist contact (Figure 3.21). The series which made up of schist, phyllite and quartzite, is gradually overlain by emery-bearing thick marbles. In Hasançavuşlar village and the surrounding area, the main rock types of the Marble-schist series are mica schist, phyllite, garnet mica schist, muscovite-quartz schist, metabasite and emery-bearing marble (Figure 3.21). In some places, mica schists contain coarse albite porphyroblasts. Garnet mica schist and garnet metabasites occur 250 m to the north

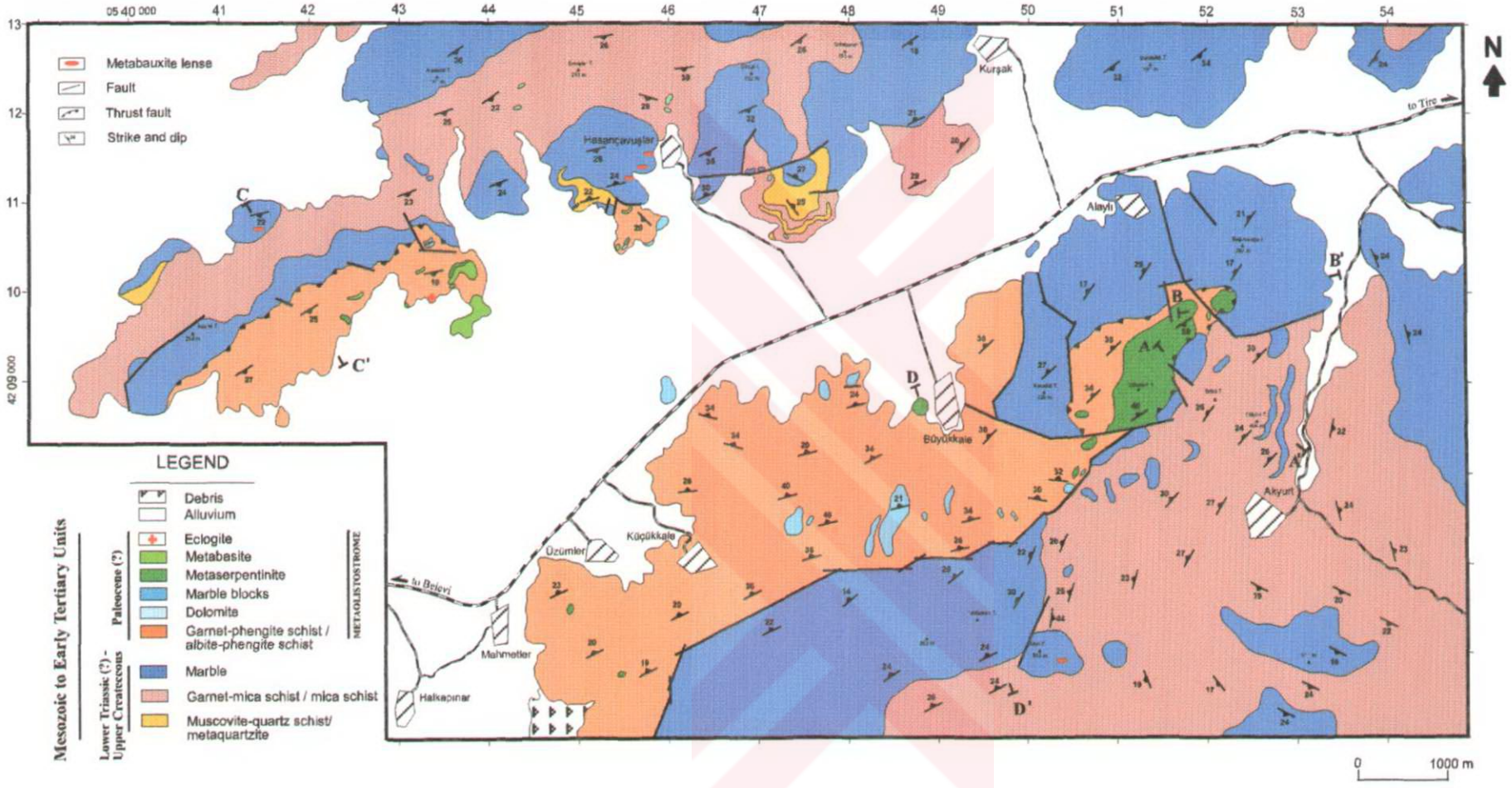


Figure 3.21 The geological map of Akyurt and Hasançavuşlar area. B-B', C-C'and D-D'sections are given in general map of the study area inside the back cover.

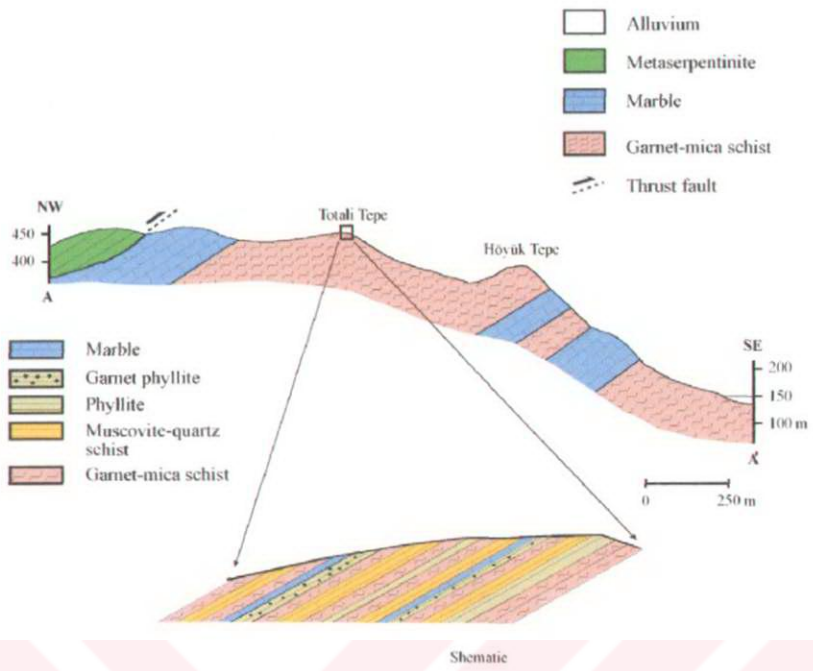


Figure 3.22 The section of the Marble-schist series at around Akyurt and their intercalation.

of Hasançavuşlar village. Metabasite lenses are highly altered and do not contain relict high-pressure minerals. In addition, metabasites are highly sheared and their contacts with schist are not always clear. In contrast to Akyurt, thick metaquarzite and muscovite-quartz schists occur close to marble – schist contact. Muscovite-quartz schists which are yellowish in colour, are observed as lenses and bands. The length of bands can reach up to 1 km. The pure metaquartzite are exposed in 750m west of İntepe (Figure 3.21). In Hasançavuşlar village and surrounding area, the average strike and dip of Marble-schist series is NE – SW and SE, respectively. Whereas they are NE – SW and NW in Akyurt which supports the existance of a synclinal. The axis of synclinal is parallel to Belevi – Tire road (Figure 3.21).

3.2.4. Tire area

The Marble-schist series in the Tire area is composed of garnet mica schist, garnet phyllite, muscovite – quartz schist, calcschist, emery-bearing marble and garnet amphibolite. The muscovite – quartz schist form the dominant lithology. The

muscovite – quartz schist are intercalated with garnet mica schist, mica schist and garnet phyllites. The thick mica schist (with or without garnet) layers occur between Karatekkeköy and Akkoyunlu villages (Figure 3.23). The garnet - mica schist with brownish – yellowish colours contain visible biotite flakes. In respect to garnet – mica schist in Akyurt, the colour of these garnet – mica schists is darker due to higher biotite content. Garnet amphibolite lenses occur in garnet mica schist / mica schist. These amphiboles are mainly dominated close to marble contact. Garnet amphibolites are highly shared and retrogressed. Therefore, they do not contain relict high-pressure minerals. The size of most garnet amphibolite lenses is less than 1 meter. Garnet phyllite, garnet – mica schist and mica schist layers and garnet amphibolite lenses occur in muscovite – quartz schist. The thickness of these layers changes from 2-3 cm up to several meters. Intercalation of muscovite – quartz schist is shown in Figure 3.24. In this cross section, the amount of garnet metabasites increase towards marble contact. The thin phyllites or garnet phyllite layers are observed in marble contact (Figure 3.24). The thick muscovite – quartz schists continues up to calcschist (Figure 3.25). The numerous thin mica schist layers occur within the muscovite – quartz schist. Brownish coloured calcschists are overlain by garnet phyllites which are 2-3 m in thickness. Garnet phyllites are concordantly overlain by emery-bearing marble. The thickness of marble is quite low in respect to other areas. In addition, these marbles contain ghost rudist fossils. The marble is overlain by a sharp contact by the Metaolistostrome unit. The rudist bearing levels of the marbles are directly overlain by the metaolistostrome. The contact relationship between massive marbles and the Metaolistostrome unit are given in Figure 3.25. The absence of the evidence related to the foundering of the platform, supports the tectonic character of the contact.

3.2.5. Gölmarmara area

Paleozoic (?) aged schist series in this area is composed of garnet-mica schist, mica schist, muscovite-quartz schist, metaquartzite and metabasite lenses (Figure 3.26). Garnet-mica schist and muscovite - quartz schists are dominantly observed

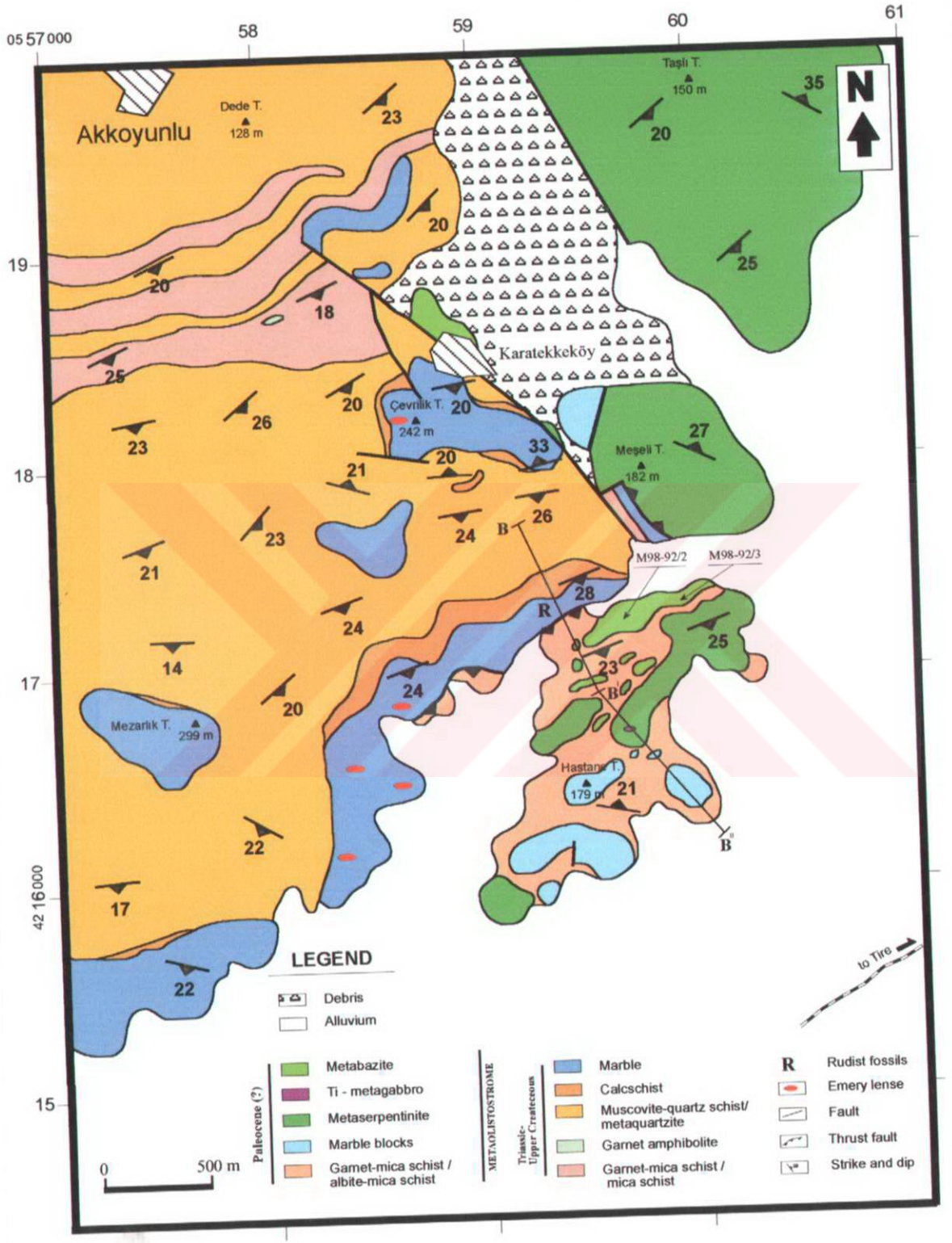


Figure 3.23 The geological map of the Marble-schist series and the Metaolistostrome unit around Karatekkeköy and Akkoyunlu villages in NW of Tire. Sample number and locations of analysed rocks are shown in the map.

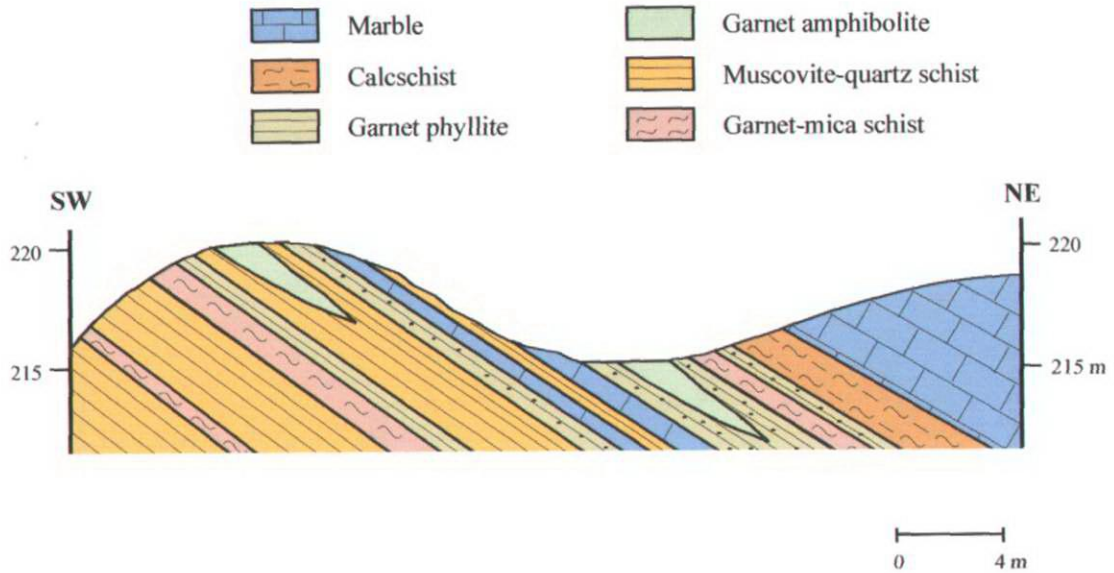


Figure 3.24 Intercalation of different lithologies in muscovite-quartz schist unit and the increase of amount of garnet amphibolite lenses in close parts to marble contact (18032;58966).

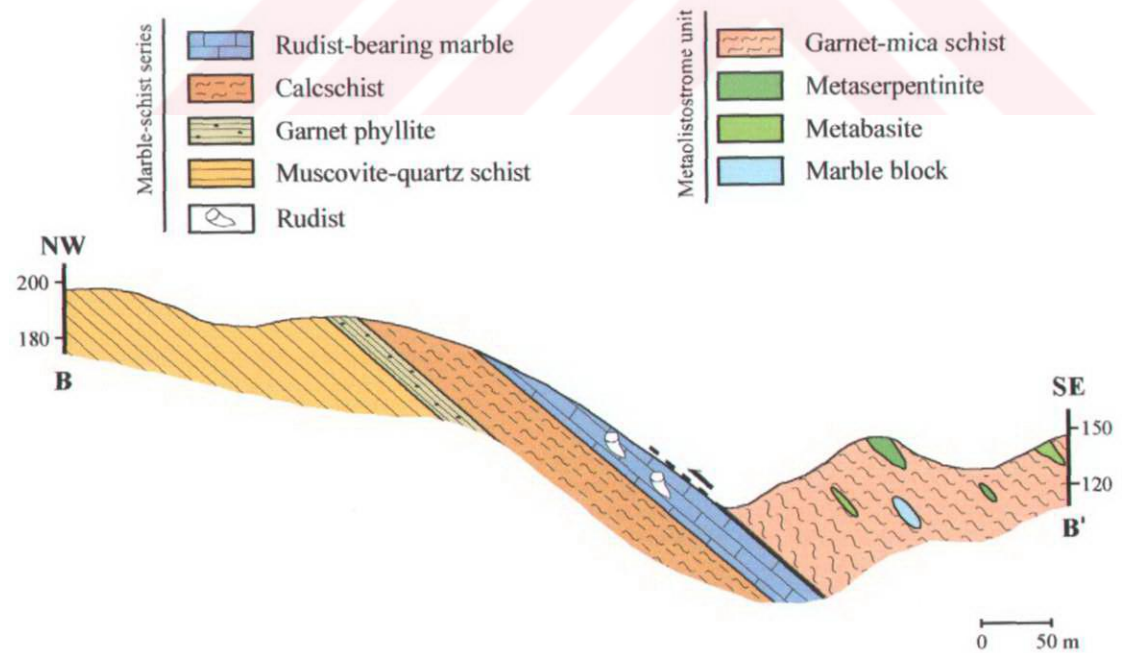


Figure 3.25 Tectonic contact between the Marble-schist series and the Metaolistostrome unit.

in the area. The dominant mica type in garnet mica schists is white mica. The amount of biotite flakes is quite low. Therefore, garnet-mica schists are grey in colour. Muscovite-quartz schists, the dominant schist type in this area, are easily distinguished with their yellowish colour and morphology from garnet-mica schist. Pure quartzite layers commonly occur in muscovite-quartz schists. Metabasites are lens shape bodies. The length of most metabasites are less than 2-3 m. Metabasite do not contain relict HP-related minerals and are composed of amphibole, epidote and plagioclase. The modal amount of epidotes is high in metabasites.

The rocks belonging to Paleozoic (?) schist series are tectonically overlain by the Metaolistostrome unit with a ductile thrust fault (Figure 3.26 and 3.27). Tectonic contact has completely ductile features. The absence of platform type Mesozoic marbles supports the tectonic character of the contact. The overthrusting limestone is a member of İzmir-Ankara Zone. The lower part of greyish limestone shows dolomitization. The limestone is gradually overlain by cherty limestone and minor spilite outside of mapped area.

3.3. Metaolistostrome unit

The general geologic features of the the Metaolistostrome unit with SW-NE aligning outcrops in Söke (Gümelez), Kuşadası (Kirazlı) – Ortaklar (Gümüşyeniköy), Selçuk (Şirince), Akyurt - Hasançavuşlar area, Torbalı (Çakallar), Tire (Karatekkeköy) and Gölmarmara (Ozanca) are given below.

3.3.1. Söke (Gümelez) area

This area is made up of the units of Marble-schist series, the Metaolistostrome unit and the Lycian Nappes (Figure 3.28). The Marble-schist series begins with mica schists containing quartzite layers. Thin marble bands and lenses occur in mica schists. The contacts between mica schist and emery-bearing thick-bedded marble are commonly modified by vertical faults (Figure 3.28). These marbles are tectonically overlain by the the Metaolistostrome unit (Figure 3.29).

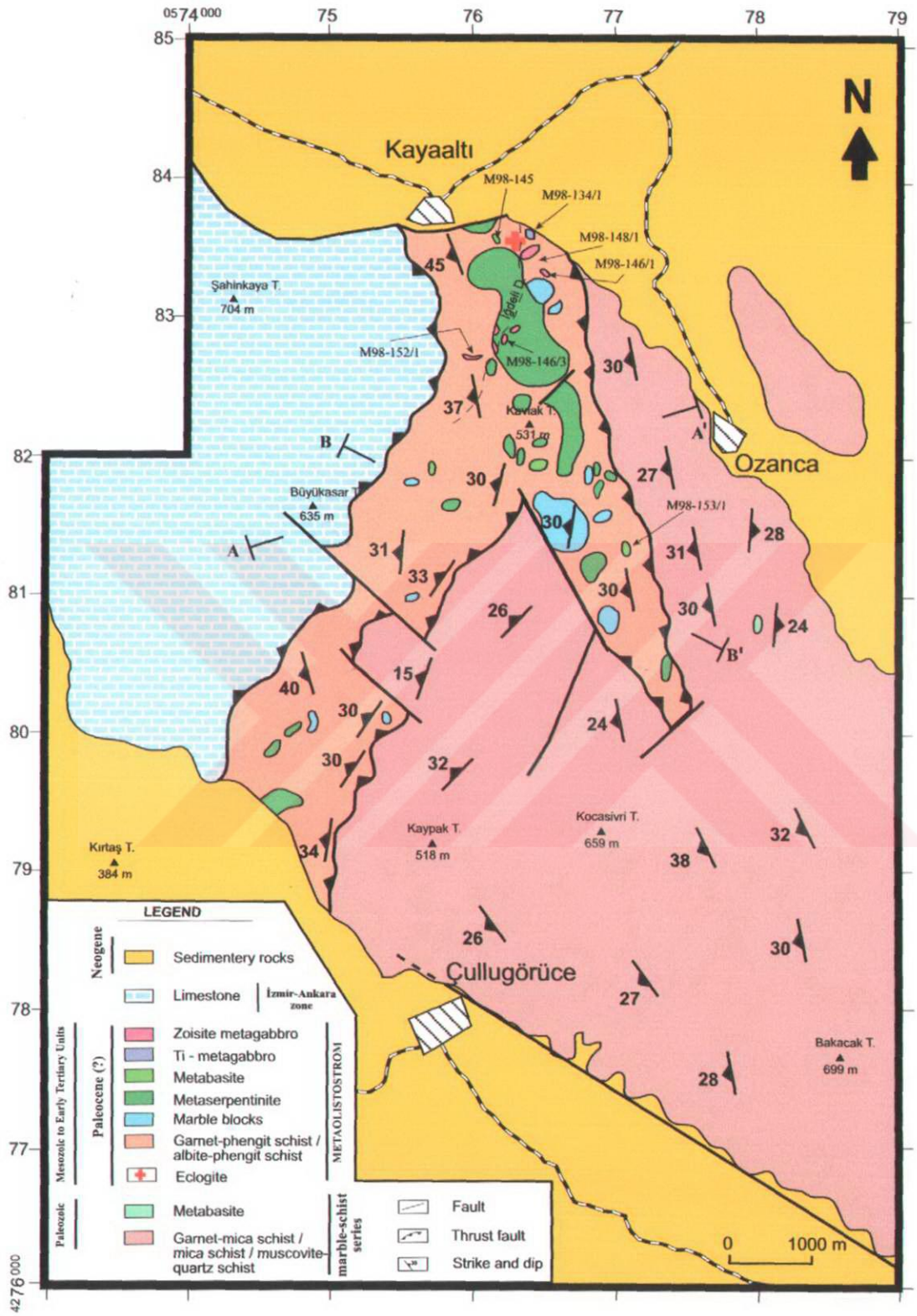


Figure 3.26 The geological map showing the relationship of the units belonging to İzmir-Ankara zone, the Metaolistostrome unit and schist series around Ozanca and Kayaaltı villages, 3 km SW of Gölmarmara. Numbers and locations of analysed samples are shown on the map.

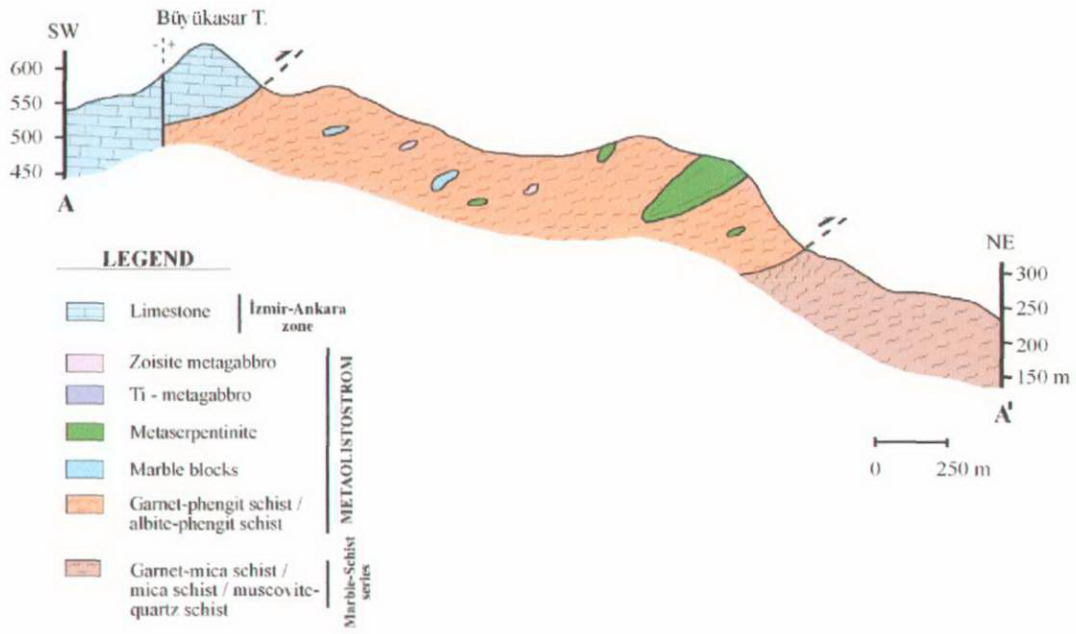


Figure 3.27 Cross section showing the tectonic contact relationship between the Marble-schist series and the overlying the Metaolistostrome unit, SW of Ozanca village.

In some places, Marble-schist series is thrusted by the Lycian Nappes. Out of the mapped area in Figure 3.28, this relation can be clearly observed in 5 km SW of Davutlar (Figure 3.30). The thrusted boundary between the Metaolistostrome unit and thick marble is quite short in this area.

The Metaolistostrome unit is made up of by different blocks embedded in a matrix of garnet-phengite schist. Omphacite-epidotite, omphacite-metagabbro, zoisite metagabbro, metabasite, metaserpentinite and marble form the blocks of the olistostrome. These blocks are embedded in a matrix which is composed of garnet-phengite schist. The great majority of the blocks are generally 4-5 m in length. However, especially, the marbles occur as big blocks in matrix. Due to intensive deformation, the original contact relationships between the matrix and basic blocks are mostly obliterated. Omphacite metagabbro blocks display mineralogical and structural zonation from core to rim. The core of the omphacite metagabbro blocks is dominated by zoisite and coarse omphacite crystals. Deformation and the amount of amphibole crystals in the core are limited. Omphacites are rarely seen in the rim. In the rim, zoisite and green amphiboles are dominant minerals. The thickness of this

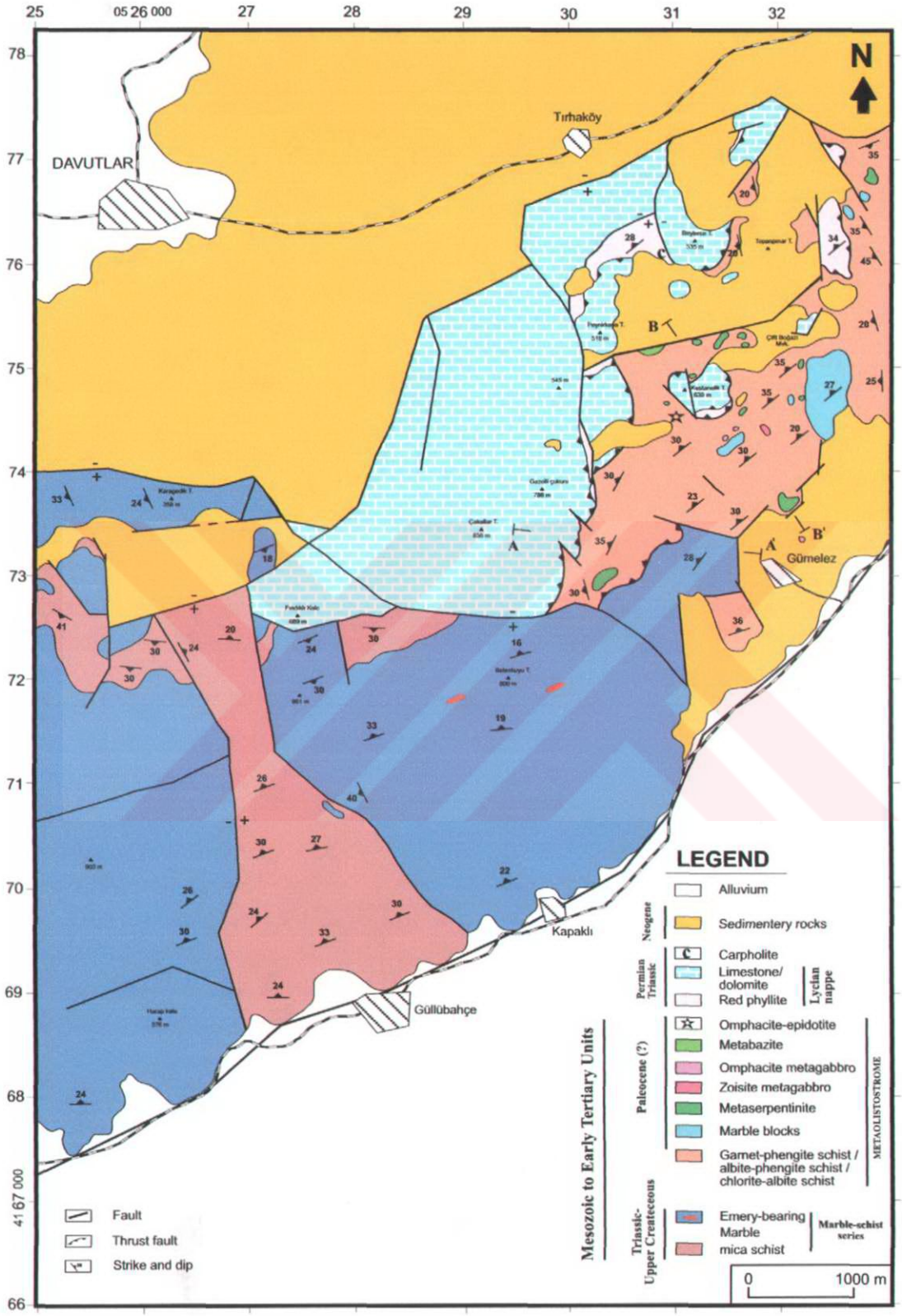


Figure 3.28 The geological map of the area between Davutlar and Gümelez (Söke).

zone is variable due to the deformation. Omphacite – epidote block is recognised in only one location. The length of this block is 1.5-2 m. The core of this block is massive and the high-pressure assemblages are well preserved, whereas, the rim is completely amphibolitized. The garnet-phengite schists are dark grey or black coloured, are rich-in quartz and may contain quartzite pebbles and quartzite nodules. The length of quartzite pebbles reach up to 1 cm. Quartzite nodules which are usually 35-40 cm in length, are quite common in the matrix of the the Metaolistostrome unit. The garnet-phengite schist is the dominant schist type within the mica schist. The Albite-phengite schist, chlorite-albite schist, phengite schist and phyllites are also observed in the matrix of the Metaolistostrome unit. Numerous small folds occur in the matrix. The matrix of the metaolistostrome shows mylonitic appearance close to the contact of the Lycian Nappes. The Metaolistostrome unit is tectonically overlain by the Lycian Nappes. Neogene sediments lie unconformably over the Metaolistostrome unit and The Lycian Nappes and the great majority of the contacts of Neogene sediments are tectonic and controlled by normal faults. Most of the contacts in the area are re-organized by normal faults related with an N-S extension (Figure 3.31).

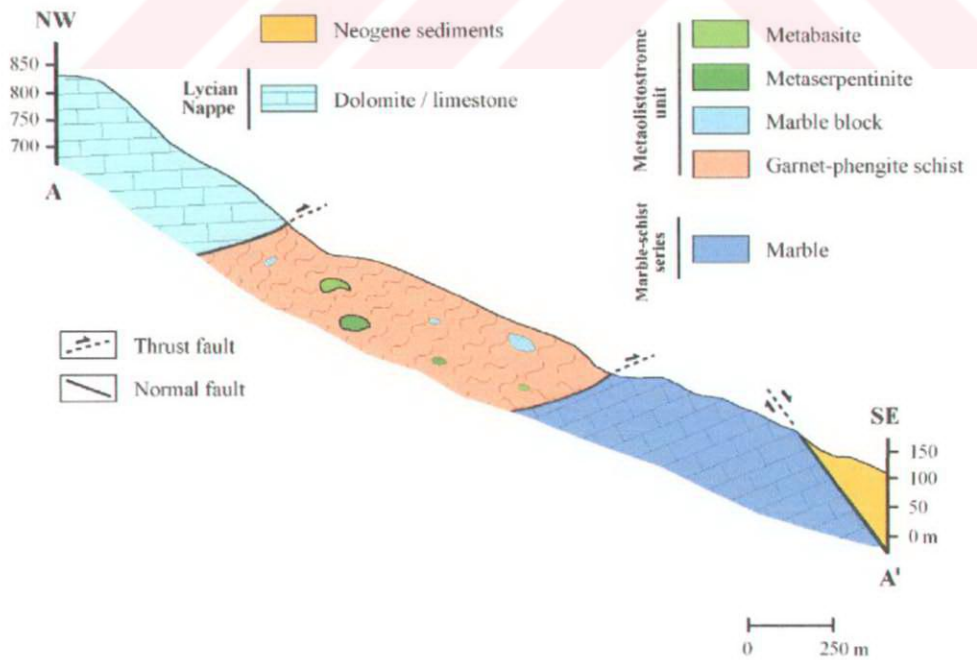


Figure 3.29 The tectonic contact relationships between platform type marble, the Metaolistostrome unit, and the Lycian Nappes in the Söke area.

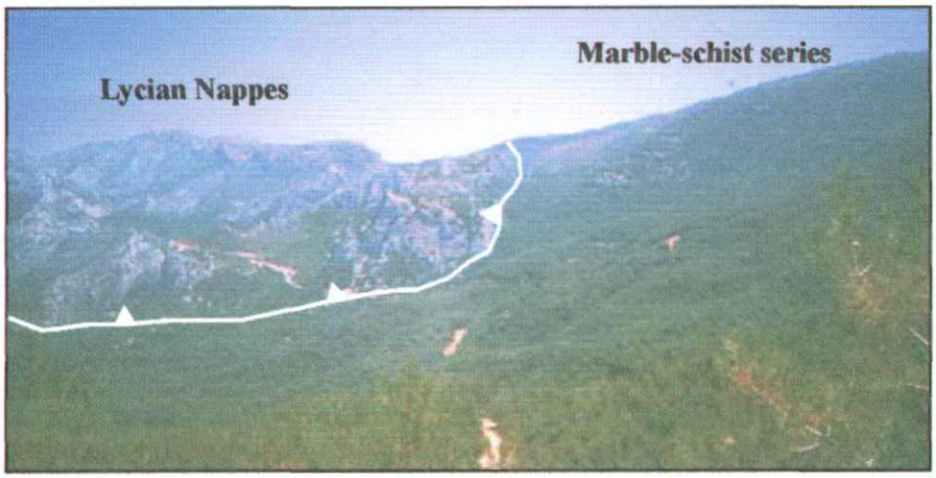


Figure 3.30 The contact relationship of a klippe of the Lycian Nappes on the Marble-schist series in SW of Davutlar.

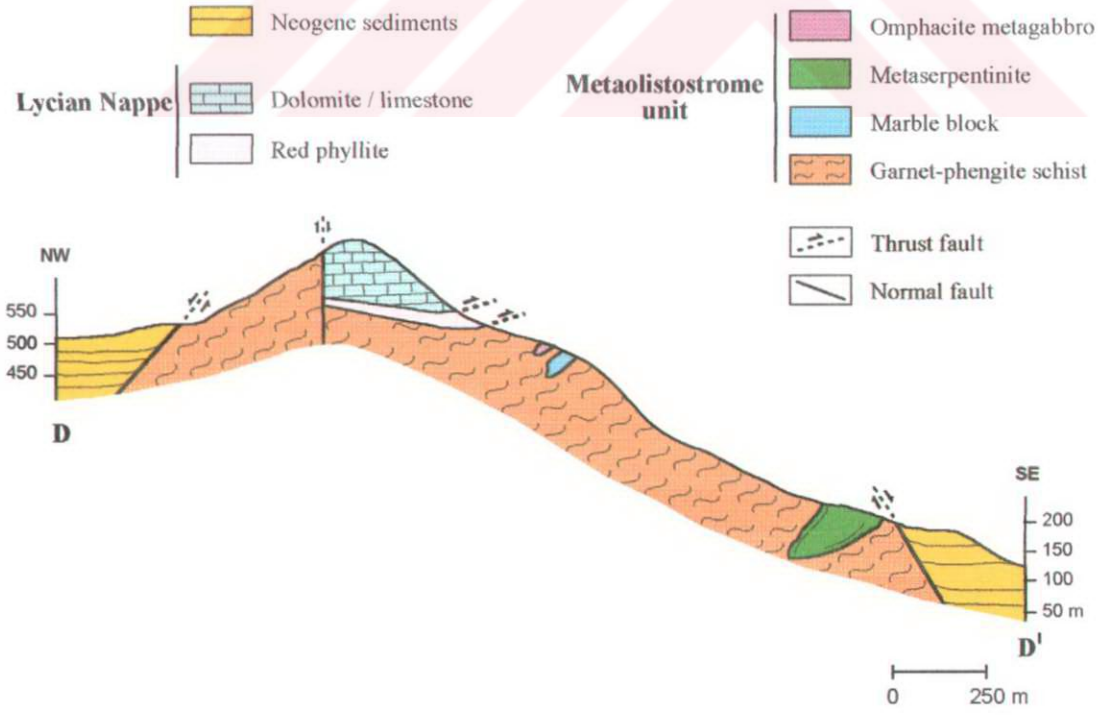


Figure 3.31 Highly deformed red phyllites are observed below the dolomite / limestone of the Lycian Nappes. The contact between these two rocks is tectonic.The contacts of the Neogene sediments are commonly controlled by normal faults.

3.3.2. Kuşadası (Kirazlı) – Ortaklar (Gümüşyeniköy) area

The litostratigraphic sequence in this area starts with Upper Cretaceous, metabauxite-bearing platform-type marbles. The marbles are tectonically overlain by the Metaolistostrome unit. The Metaolistostrome unit occurs as a thrust sheet over the Marble-schist series. This relation can be clearly observed in Kuşadası (Kirazlı) (Figure 3.32) and Ortaklar (Gümüşyeniköy) (Figure 3.33) areas. Red phyllites and dolomitic limestones belonging to Lycian Nappes are tectonically underlain by the Metaolistostrome unit (Figure 3.34). Neogene sediments lie unconformably over the Lycian Nappes and the Metaolistostrome unit. These sediments are cut by young volcanic rocks (Figure 3.32).

The Metaolistostrome unit which is tectonically underlain by thick, emery-bearing marble, contains blocks of metabasite, metaserpentinite, marble, omphacite metagabbro, Ti-metagabbro, omphacite-epidotite embedded in a matrix of garnet-phengite schist / albite-phengite schist (Figure 3.35). Omphacite metagabbro, omphacite-epidotite and metabasite blocks have relict HP/LT mineral assemblages. 2 km to the north of Kirazlı, Na-amphibole bearing garnet metabasite occur in metaserpentinite block (Figure 3.32). The metabasite and metaserpentinites are generally observed together. Another rock type showing high-pressure assemblages is omphacite metagabbro which occur in a metaserpentinite block in 1 km to the S of Kirazlı (Figure 3.32). Omphacite metagabbro which is 350 x 110 m in dimensions, show mineralogical zonation from core to rim. The core of omphacite metagabbro is composed of pale green omphacite porphyroblast and whitish zoisite crystals. The Ca-amphiboles are absent in the core. Close to the metaserpentinite contact, the omphacite metagabbro is transitional to zoisite metagabbro. Omphacite-epidotites also occur in a metaserpentinite block as small lenses 5 km to the NNB of Söke (Figure 3.33). These rocks have by pale green colours. In the Kirazlı and Gümüşyeniköy areas, the dominant block type is metaserpentinite. The number of metaserpentinite blocks is quite large. The length of these blocks may reach up to 2 km (Figure 3.32 and 3.33). In the Kirazlı area, the number of the marble blocks is

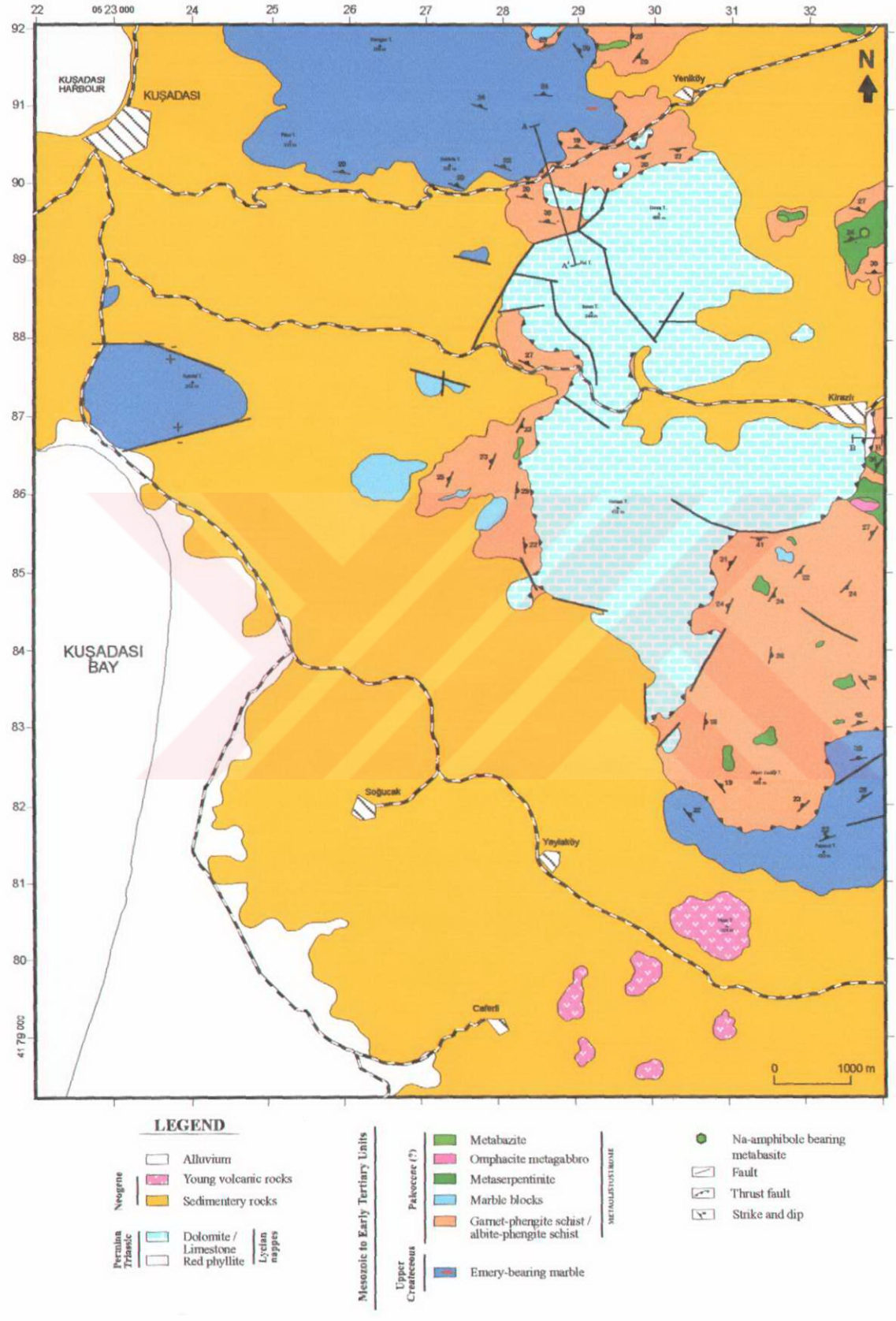


Figure 3.32 The geological map of Kirazlı (Kuşadası) and surrounding area, and the contact relations between the Marble-schist series (emery-bearing marbles), the Metaolistostrome unit and the Lycian Nappes

T.C. YÜKSEKÖĞRETİM KURULU
DOKÜMANTASYON MERKEZİ

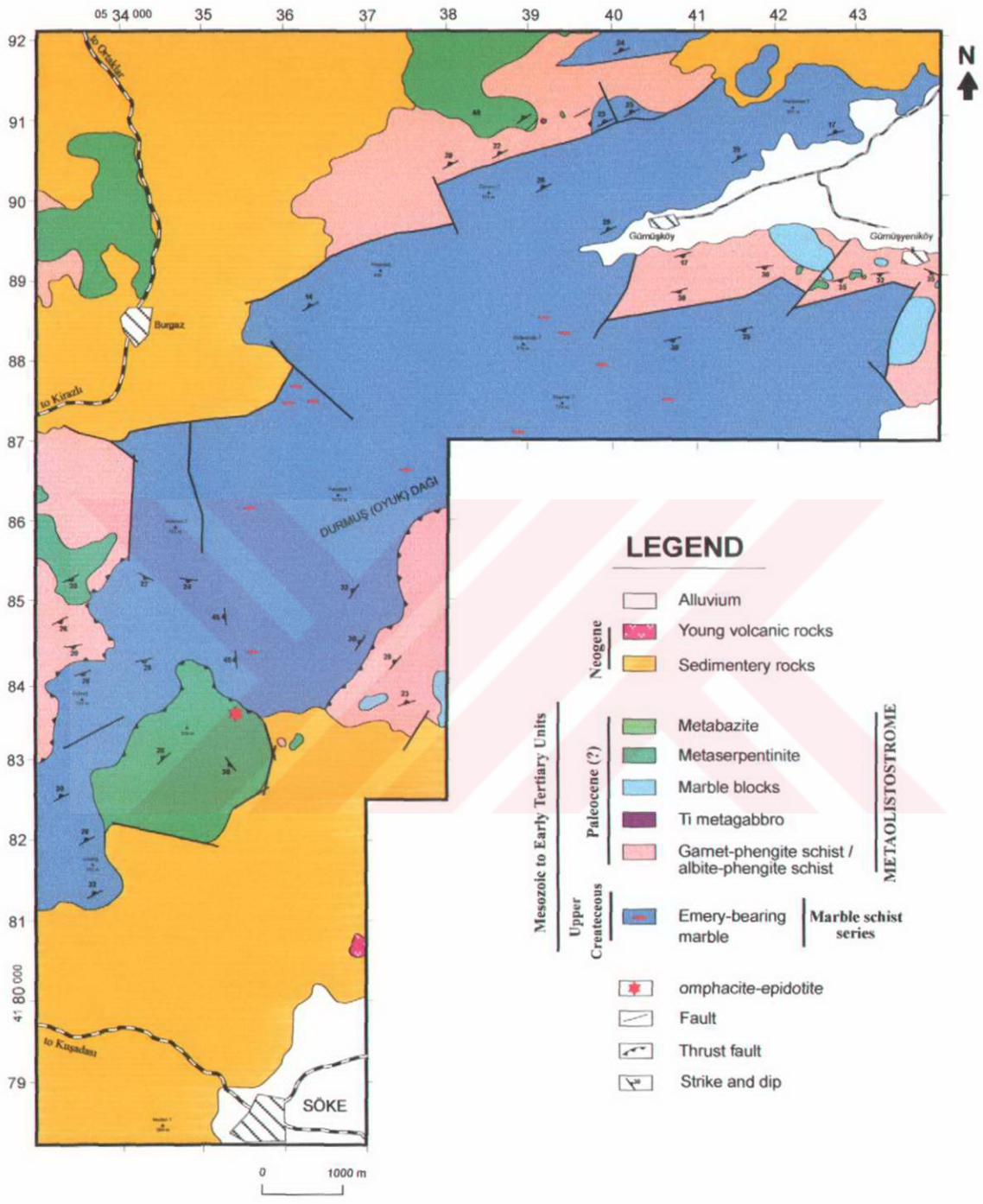


Figure 3.33 The geological map of area among Gümüşyeniköy (Ortaklar), Kirazlı and Söke.

low and their dimensions are generally small. Ti metagabbro blocks occur 1.5 – 2 km to the NW of Gümüşyeniköy. These blocks are quite small. The matrix of the Metaolistostrome is dominantly made up of garnet-phengite schist. Albite-phengite schists include numerous quartz nodules and are black in colour (Figure 3.36). Strike and dip of the foliation in the schists are variable. The Metaolistostrome unit is tectonically overlain by the Lycian Nappes (Figure 3.34). Neogene sediments unconformably cover all units. 2 km to the SE of Yaylaköy and 2 km NE of Söke, Neogene sediments are cut by young Neogene volcanic rocks (Figure 3.32 and 3.33).

3.3.3. Selçuk (Şirince) area

The widest outcrop of the Metaolistostrome unit is observed in Selçuk (Şirince) area (Figure 3.17). Litostratigraphic sequence of this area starts with Lower Triassic (?) – Upper Cretaceous rocks at the base. The uppermost level of the lower sequence is composed of metabauxite bearing, platform type marble. The marbles are tectonically overlain by the Metaolistostrome unit (Figure 3.37 and Figure 3.20). The evidence related to the tectonic character of the contact can be given as follows:

1) The uppermost levels of platform type marble contain rudist fossils in Kurşak (Özer, 1998) and Tire. This suggests a platform deposition for the marbles. But olistostrome is mostly represented by deep-sea setting. Between two units, there are no rocks representing transition from neritic to pelagic environment.
2) The contact relation between marble and the Metaolistostrome unit does not show any features of an unconformity.
3) Locally, the marbles are directly overlain by metaserpentinite blocks without having any matrix of the metaolistostrome at around Söğütçük Tepe, 3 km NE of Selçuk.
4) Muscovite-quartz schists belonging to the Marble-schist series, are directly overlain by the Metaolistostrome unit, 1-2 km to the SW of Selatin.
5) Garnet-phengite schists in the Metaolistostrome unit occur several meters above the muscovite-quartz schist of Marble-schist series, in the SW of Selatin.

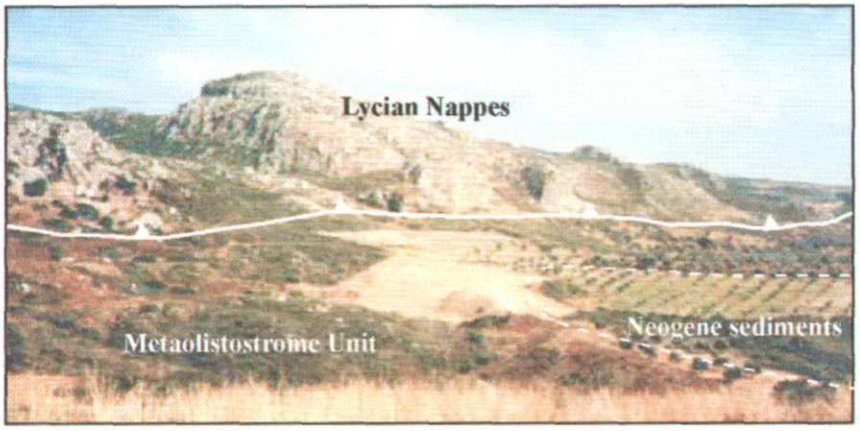


Figure 3.34 Field view showing the tectonic contact between the Metaolistostrome unit and the Lycian nappes.

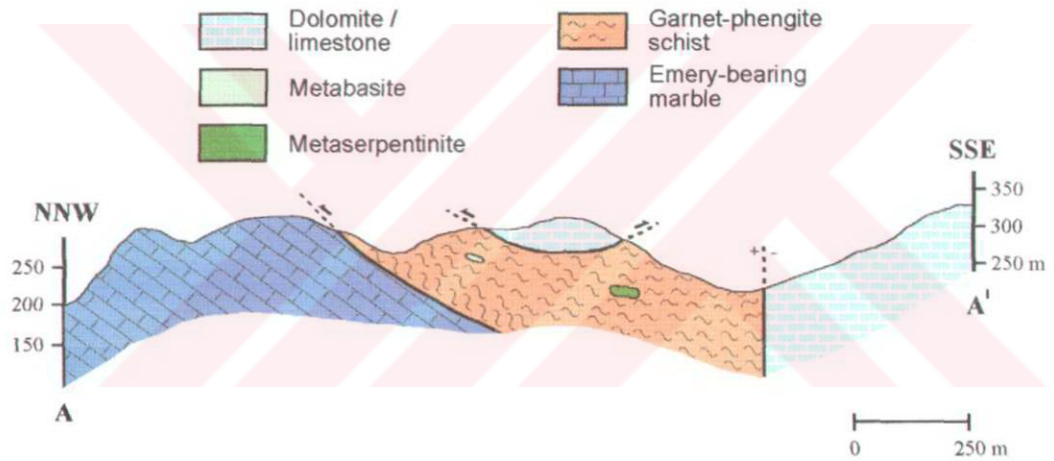


Figure 3.35 The section showing the contact relationships of emery-bearing marble (Marble schist series), garnet-phengite schist (Metaolistostrome unit) and dolomite / limestone (Lycian Nappe).



Figure 3.36 Albite-phengite schists are distinguished from garnet-phengite schist by dark gray or blackish colour and common quartzite nodules.

In the same Marble-schist series, garnet is observed at around Akyurt. This shows a break between the metamorphic grades of the matrix of the metaolistostrome (garnet-phengite schist) and schist of Marble-schist series (muscovite-quartz schist), SW of Selatin and 2 km N of Çamlık.

6) The Metaolistostrome unit thrusts over both the metabauxite-bearing marble and quartz metaconglomerate –bearing mica schist / muscovite quartz schist, 2 km N of Çamlık. Quartz metaconglomerate layer which does not exist in the Metaolistostrome unit, occurs at the upper levels of mica schist / muscovite-quartz schist (at 0532560 : 4195080 coordinate) (Figure 3.38)

The matrix of the metaolistostrome is composed of microfolded, strongly foliated garnet-phengite schist and albite-phengite schist. Especially garnet-phengite schists are more dominant in NE of Şirince. The matrix of the Metaolistostrome unit covers a large area between Selçuk and Ortaklar. The matrix contains numerous blocks of different rock types. These blocks consist of eclogite, omphacite metagabbro, omphacite-epidotite, zoisite metagabbro, Ti metagabbro, blueschist metabasite, metaserpentinite and marble. Dark grey or brownish albite-phengite schist contains numerous pure quartz lenses which are found only in the albite-phengite schist (Figure 3.39). Black albite porphyroblasts in the albite-phengite schists are easily recognised by the naked eyes and their length can reach up to 2-3 mm (Figure 3.40). Garnet-phengite schists are mainly observed at Boncuk Tepe and Görünmez Tepe. The colour of the garnet-phengite schists is yellow – pale brownish (Figure 3.41). Garnet crystals reach up to 5 mm in diameter. The matrix of the metaolistostrome is highly deformed. Isoclinal folding is commonly seen in the matrix (Figure 3.42). The folds which have been formed during HP/LT metamorphism, are cut by main foliation which is defined by greenschist facies overprint. The axis of the isoclinal folds trend in NNE direction and plunge NNE.

Typical HP/LT metamorphic rocks in the metaolistostrome are eclogite, omphacite metagabbro, omphacite-epidotite and blueschist metabasites. Eclogite blocks are determined in 8 locations (Figure 3.17). Five of them are directly

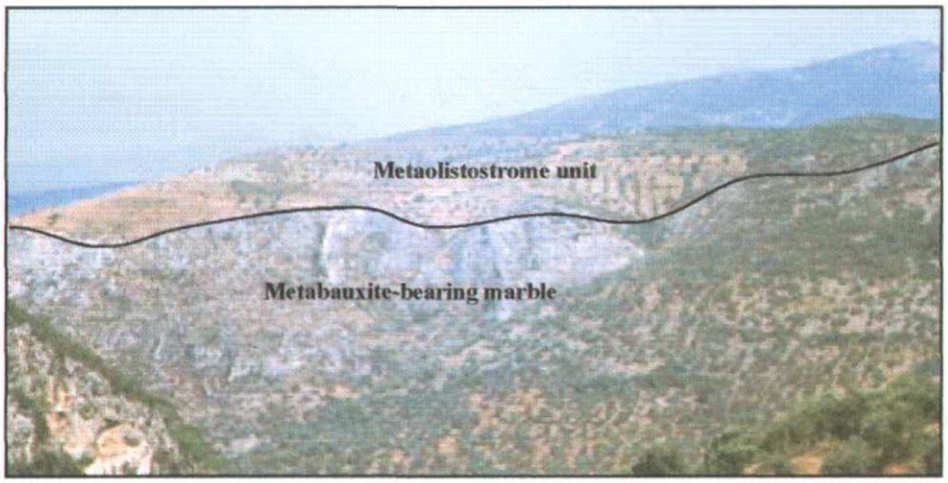


Figure 3.37 Metabauxite-bearing marble is tectonically overlain by the Metaolistostrome thrust sheet.

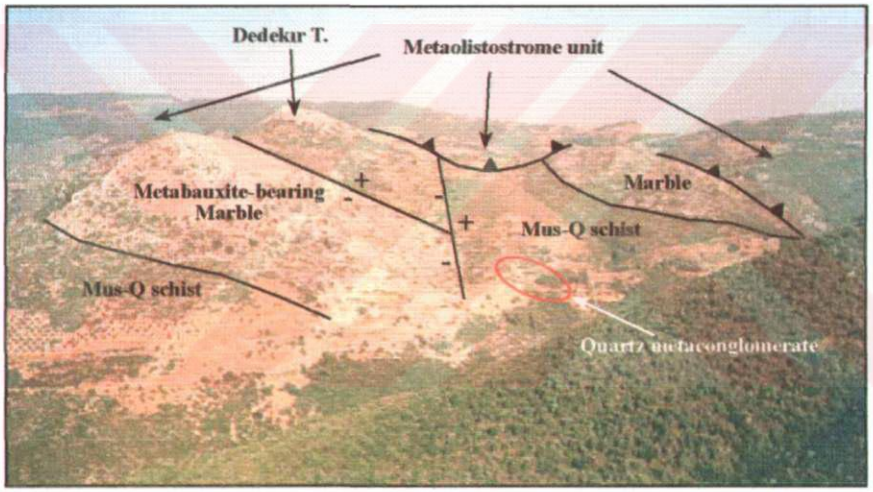


Figure 3.38 The field view of the Metaolistostrome unit thrusted over the metabauxite-bearing marble and the muscovite-quartz schist. Quartz metaconglomerate which forms one of the characteristic lithologies of the marble-schist series, occurs in the lower levels of muscovite-quartz schist.



Figure 3.39 Albite-phengite schist containing quartz lenses is one of the typical features of this schist.



Figure 3.40 Coarse albite porphyroblasts in the albite-phengite schist.

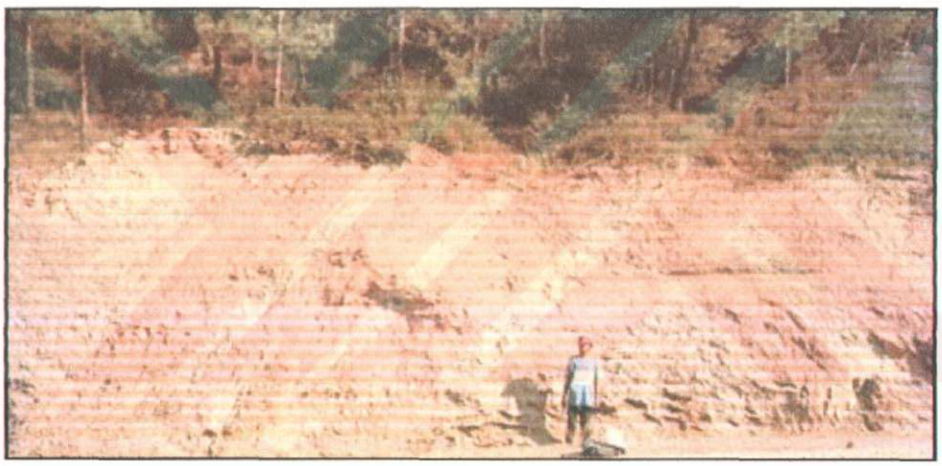


Figure 3.41 The field view of yellowish-brownish coloured garnet-phengite schists

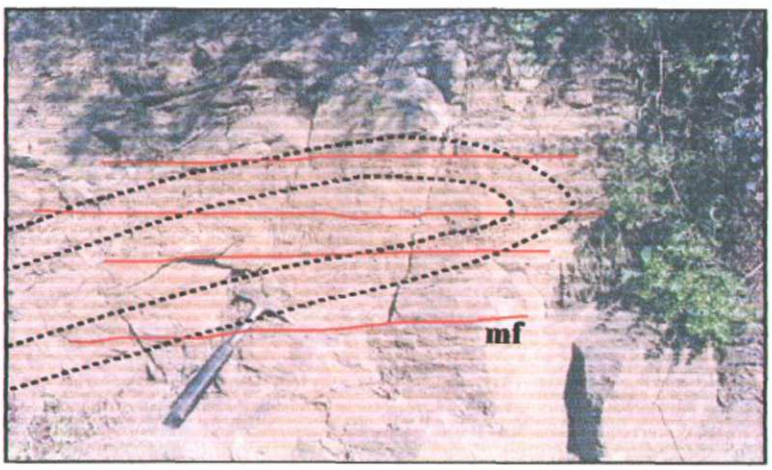


Figure 3.42 Isoclinal fold in the matrix of the metaolistostrome. This fold is cut by main foliation (mf) which is formed during the greenschist facies overprint.

associated with the metaserpentinites. These locations are in N of Şirince. To the NNE of Şirince the metaserpentinite block is 500 x 500 m in dimensions. In this location, an eclogite block, 2x3 m in size, is in contact with the metaserpentinite. This eclogite body can be divided into two zones, rim and core, based on mineralogical difference. The dark green coloured rim, 10-15 cm in thickness, is composed of amphibole and garnet. The core dominantly contains pale green omphacite and pinkish garnet. In the other location 1 km N of Şirince at Yılanlı Tepe, silicified eclogites are observed at the inner part of the metaserpentinite block which is 200x70 m in size (Figure 3.43). These eclogites are in contact with the coarse-grained gabbros and should have derived from this gabbroic body which is defined as zoisite metagabbro. The zoisite metagabbros are composed of green amphibole and zoisite crystals (Figure 3.44). It is partly enclosed by garnet amphibolites derived from the eclogites by the retrograde overprint (Figure 3.43). In addition, omphacite metagabbro bodies also exist in the metaserpentinite block. The original magmatic texture is well preserved in the omphacite metagabbros. In these rocks, plagioclase and clinopyroxene are replaced by zoisite and omphacite, respectively (Figure 3.45).

Another metaserpentinite block, approximately 5 km in length, is found in 1 km to the west of Şirince (Figure 3.17). Small eclogite and omphacite-epidotite bodies occur between the metaserpentinite block and the albite-phengite schist, NE part of this block (Figure 3.46). In this area, eclogites are made up of euhedral, pinkish garnet and green omphacite groundmass (Figure 3.47a). Partly retrograded eclogites also contain green amphibole (Figure 3.47b). Omphacite-epidotites are composed of pale green omphacite and whitish – greyish zoisite crystals (Figure 3.48). Another eclogite body closely related with the metaserpentinite blocks is found 4 km to the NE of Şirince. In this location, the eclogite body is 2x1 m in dimensions and has pale green colour. A garnet amphibolite zone, 10-15 cm thick, occur at the rim of the eclogite body. However, the eclogite block 3 km to the SE of Belevi is independent from the metaserpentinite (Figure 3.17). The size of this lens-shaped eclogite block is 2x3 m. From rim to core, four zones have been determined in this eclogite block:

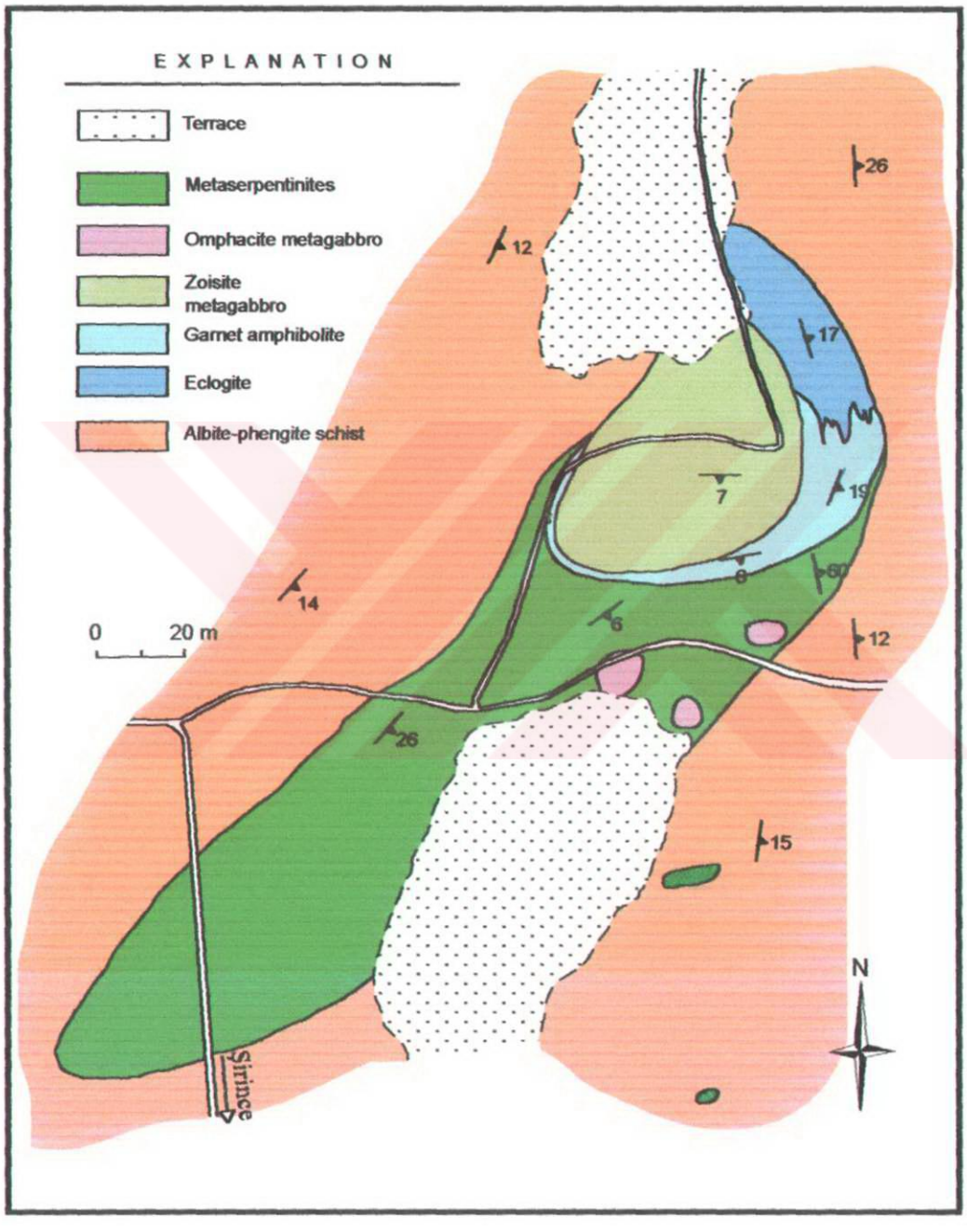


Figure 3.43 Detailed geological map of the eclogite body in the metaserpentinite block in Yılanlı Tepe, N of Şirince.



Figure 3.44 The general view of zoisite metagabbro which is made up of coarse green amphibole and whitish zoisite.

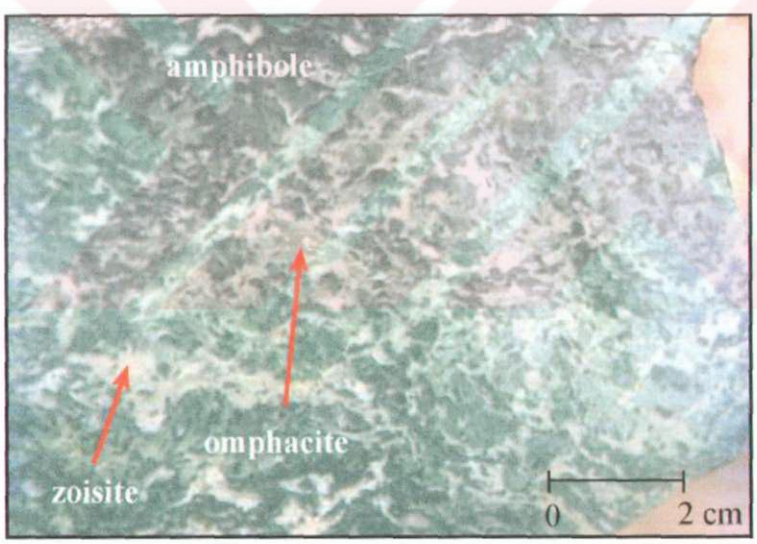


Figure 3.45 The general view of omphacite metagabbro. Plagioclase and clinopyroxenes of original gabbroic rock are replaced by whitish zoisite and pale green omphacite. Dark green minerals are amphiboles which are product of greenschist overprint.

- **Amphibolite zone:** this zone is completely composed of dark green amphibole crystals and does not contain any garnet. The thickness of this zone is approximately 10-15 cm.

- **Garnet amphibolite zone:** dark green amphiboles coexist with garnet in this zone. The thickness of zone is at about 10-15 cm.
- **Outer core zone:** In this zone, amphibole, omphacite and garnet are observed together. Amphiboles intensively developed along the veins or shear bands.
- **Inner core zone:** there is no amphibole in this zone which is composed of pinkish, euhedral garnet and pale green omphacite crystals. This zone can be defined as fresh eclogite.

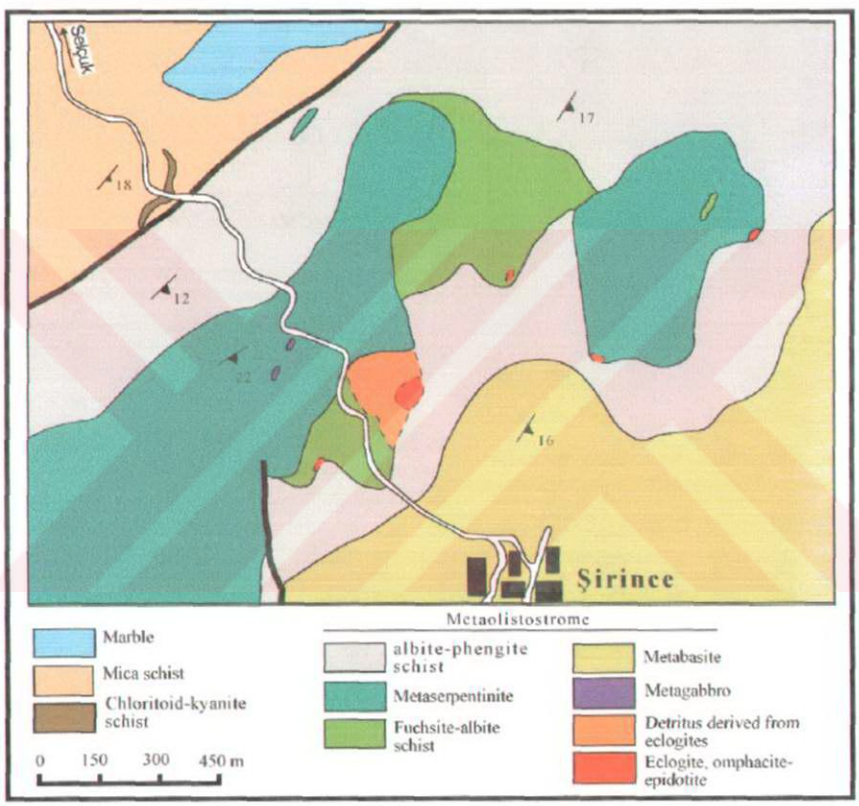
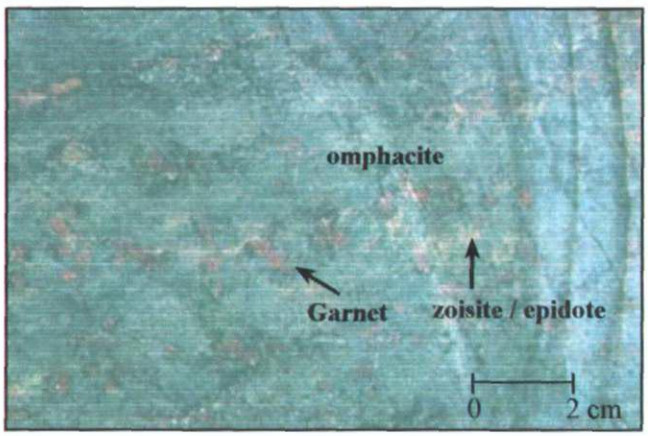


Figure 3.46 The geologic map of the eclogite body and the Metaserpentinite block exposed on the Selçuk-Şirince road.

In Boncuk Tepe, the eclogite block is highly retrograded. Omphacite, garnet, green amphibole and zoisite crystals are observed all over the block. The eclogite block is 3x5 m in size. The rim of the block is totally retrograded to garnet amphibolite. This block is surrounded by garnet-phengite schists of the matrix.

a)



b)

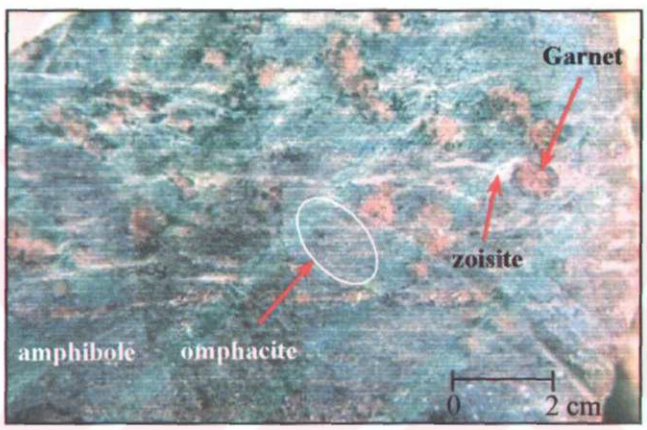


Figure 3.47 The general view from a) fresh eclogite and b) partly retrograded eclogite (amphibolitized eclogite).

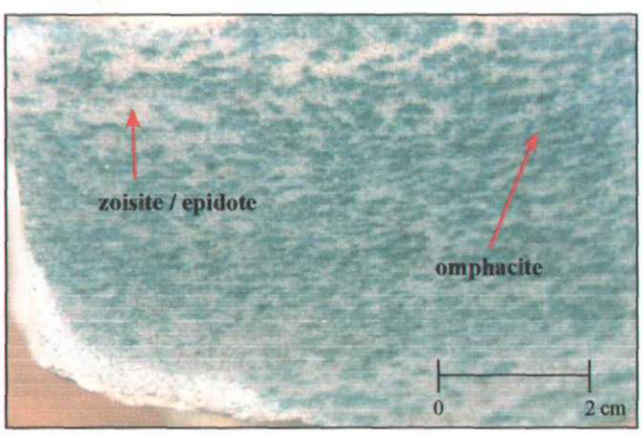


Figure 3.48 The general view of omphacite-epidotite which is made up of whitish zoisite / epidote and green omphacite crystals.

The metabasite blocks are less abundant than the metaserpentinite blocks. Metabasites can be observed as individual blocks or together with the metaserpentinites. The dimensions of metabasite blocks are quite variable. Metabasites have strong penetrative foliation parallel to that of the matrix and are fine grained and dark green in colour. The original contact relation between metabasite and matrix was obscured by penetrative foliation. Metabasite blocks commonly contain green amphibole, garnet and pale green coloured epidote. Epidotes are observed as nodules or irregular bands (Figure 3.49). Metabasite blocks are generally suffered by strong retrogression. In hand specimens, it is easy to recognize the garnets which are partly replaced by chlorite. Only in one location ($_{05}$40025:$_{42}$00920) Na-amphibole bearing metabasites (blueschist metabasite) are determined (Figure 3.17). In this location, Na-amphiboles commonly occur as inclusions in garnet porphyroblasts.

Beside the Yılanlı region ($_{05}$39200:$_{42}$01115), omphacite metagabbro blocks occur in two locations (Figure 3.17). The omphacite metagabbro, 2 km to the NW of Şirince, occurs in a metaserpentinite block. It is 40x20 m in dimensions and transformed into zoisite metagabbro along the rim and shear bands. Pale green omphacite and whitish zoisite crystals the omphacite metagabbro are replaced by coarse amphibole and smaller zoisite crystals along the shear zones. Another omphacite metagabbro block occur in 500 m SW of Selatin. In this location, omphacite metagabbro block is embedded in the matrix of the Metaolistostrome unit and independent from the metaserpentinite and is highly affected by retrograde overprint. This block which is 2x3 m in dimensions, is commonly retrogressed to zoisite metagabbro. The pure zoisite metagabbro blocks which are probably derived from omphacite metagabbro, are observed 1.2 km and 3 km NW of Şirince (Figure 3.50). Ti-metagabbro blocks commonly occur around Söğütçük and Maden tepe, NW and N of Şirince (Figure 3.17). Ti-metagabbro blocks with massif appearance and black colour are characterized by yellowish sphene crystals (Figure 3.51). The largest Ti-metagabbro block in the area is observed in Maden Tepe. The length of this block is approximately 650 m.

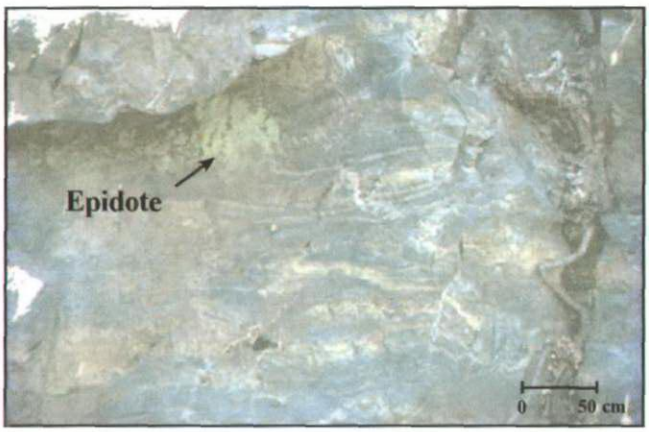


Figure 3.49 Pale green - yellowish epidote bands in metabasite block.

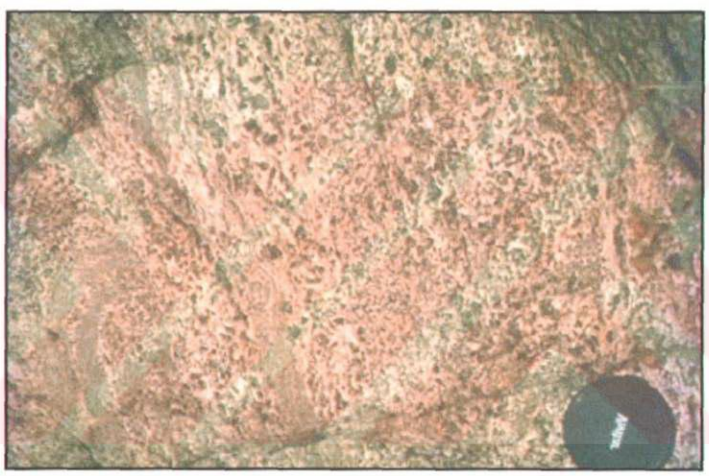


Figure 3.50 The general view of zoisite metagabbro showing pronounced foliation. Grain size reduction is observed in highly deformed zones. Coarse grained green and whitish minerals are amphibole and zoisite, respectively.



Figure 3.51 The general appearance of Ti-metagabbro which is characterized by yellowish sphene clusters in a groundmass which is composed of blackish coloured amphibole.

At around Selçuk (Şirince), numerous metaserpentinite blocks in different sizes are found in the matrix of the Metaolistostrome unit. These metaserpentinite blocks reach up to 3.5 km in size, and are found in different levels of the unit. These metaserpentinite blocks are generally massive. However, especially, the rim of some metaserpentinite blocks are strongly foliated. Metaserpentinites are olive green and yellowish green in colour, and do not contain relict texture of the original igneous rock.

The marble blocks of different sizes which are probably derived from Mesozoic platform type marble, occur in the matrix of the Metaolistostrome unit. The blocks of marble are mainly observed in S and SE of Şirince. Some of these marble blocks contain metabauxite lenses. Metabauxite-bearing marble blocks can reach up to 1.5 km in length in N of Havutçulu village. The block character of the marbles are recognised by their irregular boundary with the matrix of the metaolistostrome.

3.3.4. Hasançavuşlar – Akyurt area

Here, the Metaolistostrome unit is exposed on the W of Hasançavuşlar and NW-N of Akyurt villages (Figure 3.21). The Metaolistostrome unit tectonically overlies the metabauxite-bearing marble in these areas (Figure 3.52 and 3.53). The boundary between metabauxite-bearing marble and the Metaolistostrome unit, S and SW of Boğaziçi, is a vertical fault (Figure 3.54). In Çitlenbik Tepe, 2 km to the E of Boğaziçi, the Metaolistostrome unit thrusted over the marble. 1.3 km NE of Çitlenbik Tepe, the marbles are directly overlain by a metaserpentinite block of the Metaolistostrome unit (Figure 3.52). The cross section in Figure 3.52 shows the contact relation of these two units.

In Akyurt and Hasançavuşlar area, the matrix of the Metaolistostrome unit is dominantly composed of garnet-phengite schist. Metaserpentinite, metabasite, eclogite, omphacite-epidotite and marble blocks are embedded in garnet-phengite schist. Small scaled folds and strong foliation are commonly observed in garnet-

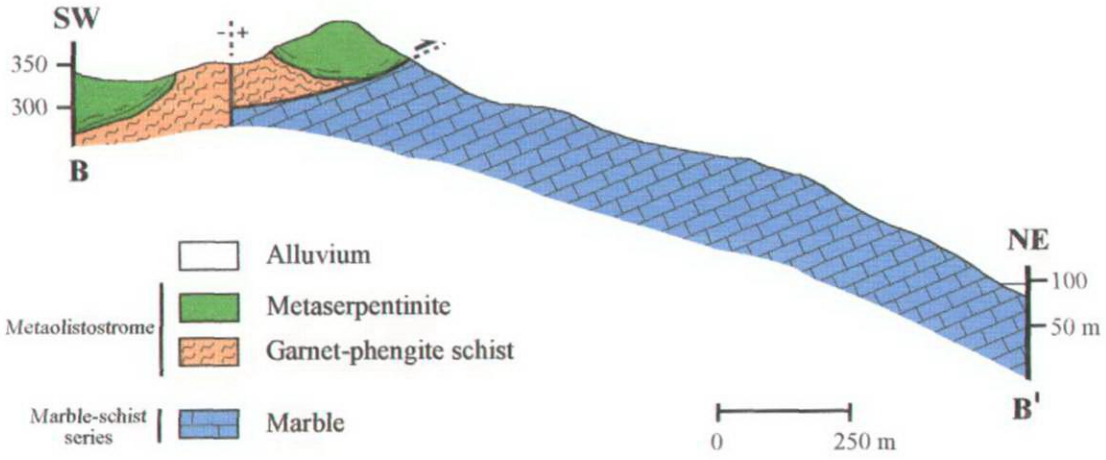


Figure 3.52 Cross section showing the tectonic character of the contact between the Marble-schist series and the Metaolistostrome unit. In some places, metaserpentinite directly overlies the thick platform type marble. Section line is given in Figure 3.21.

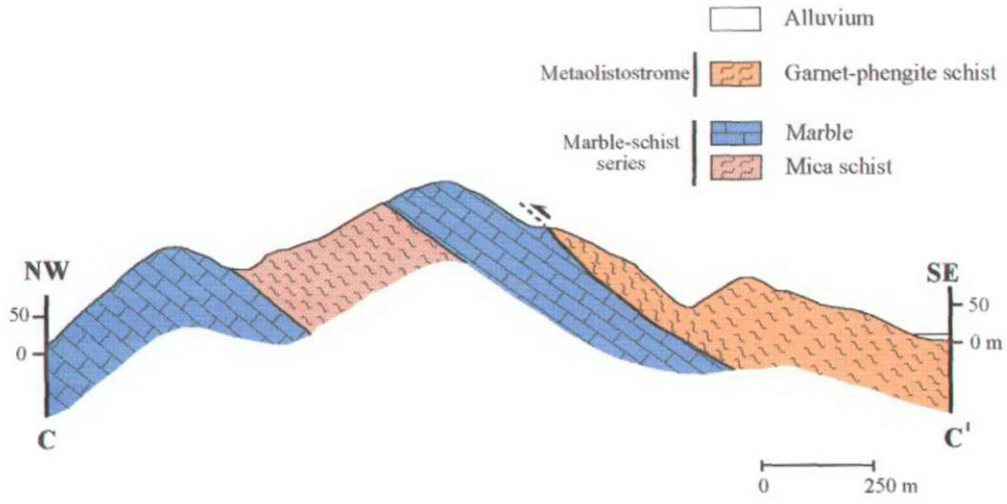


Figure 3.53 The cross section showing tectonic contact relationship between marble and the Metaolistostrome unit. Section line is given in Figure 3.21.

phengite schists. Marble blocks in the matrix shows isoclinal folding (Figure 3.55). The axis of these isoclinal folds in both matrix and blocks are NE.

Here the HP/LT blocks are represented by eclogite (Figure 3.21) and omphacite-epidotite (05 41750 : 42 06840). The eclogite block, 3 km to the SW of Hasançavuşlar, is 2x1 m in dimensions and is completely surrounded by garnet-phengite schists of tha matrix. Amphibolitization is dominant in the rim of the block. The thickness of the garnet amphibolite zone is approximately 20 cm. Green amphiboles are also seen in the core. The lens-shaped omphacite-epidotite block, 1.2 km to the NW of Halkapınar, is quite small, 2x1 m in dimensions. It is highly difficult to recognize the omphacite-epidotite block, due to retrograde overprint effects at the rim. Metabasite

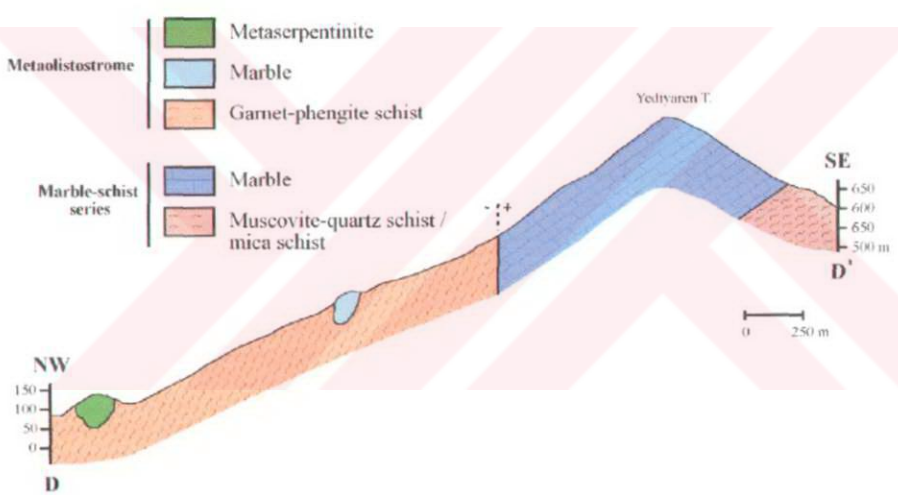


Figure 3.54 The contact relationship between marble and the Metaolistostrome unit in Boğaziçi is defined by vertical fault.

blocks of variable size occur 2 km to the SW of Hasançavuşlar. The length of the largest one is approximately 500 m. The small metabasite blocks are partly rimmed by metaserpentinite. The rims of these blocks are strongly foliated. These metabasite blocks are garnet-free. White albite porphyroblasts are observed especially at the rim of the block. The abundance of albite porphyroblasts decreases with decreasing of deformation or retrogression effects. Marble blocks commonly occur at around Büyükkale. They are surrounded by the matrix of the Metaolistostrome unit (Figure

3.56). Their dimensions change from 1.5 to 800 m. Figure 3.57 shows the block character of smaller marbles in the matrix of the metaolistostrome. The important evidence of this is, a) calcite vein-fillings in small marble block do not continue into the garnet-phengite schist, b) sharp and irregular contact relationship (Figure 3.57). Due to lithological contrast between matrix and marble blocks, marble blocks are clearly recognised by their irregular and sharp boundary with the matrix.

3.3.5. Torbalı area

The Paleozoic (?) schist series which is composed of blackish metaquartzite, phyllite, muscovite-quartz schist, metabasite lenses, marble, overlain by the Metaolistostrome unit and Neogene sediments, respectively are observed in Torbalı area (Figure 3.58). Dark grey coloured phyllites and mica schists form the dominant lithologies. The phyllites contain thin numerous muscovite-quartz schist and pure metaquartzite bands or layers. Metaquartzites are generally black in colour. Metabasite lenses are rarely observed at the upper levels of the mica schist. The phyllitic sequence is tectonically overlain by the Metaolistostrome unit (Figure 3.59).

The matrix of the Metaolistostrome unit is made up of garnet-phengite schist and albite-phengite schist. Metaserpentinite, Ti-metagabbro, omphacite-epidotite and metabasites form the blocks of the Metaolistostrome unit (Figure 3.58). The largest blocks in the area are metabasites. The length of metabasite blocks can reach up to 600 m. These blocks are strongly foliated and deformed. Green amphibole, epidote and albite form the main mineral assemblage of metabasites blocks. There is no relict mineral defining the HP/LT metamorphism. These minerals should have been replaced by minerals in greenschist facies. HP/LT metamorphism is represented by omphacite-epidotite blocks and garnet-phengite schist / albite-phengite schist in matrix. Lens-shaped omphacite-epidotite block of 2x1 m in size occurs to the SW of Çakallar (Figure 3.58). Dark green coloured amphiboles are homogeneous distributed in the rock. Ti-metagabbros which are characterized by coarse amphibole and yellowish sphene clusters, are determined in S of Çakallar. Four of six Ti - metagabbro outcrops occur in the metabasite block. The unique metaserpentinite

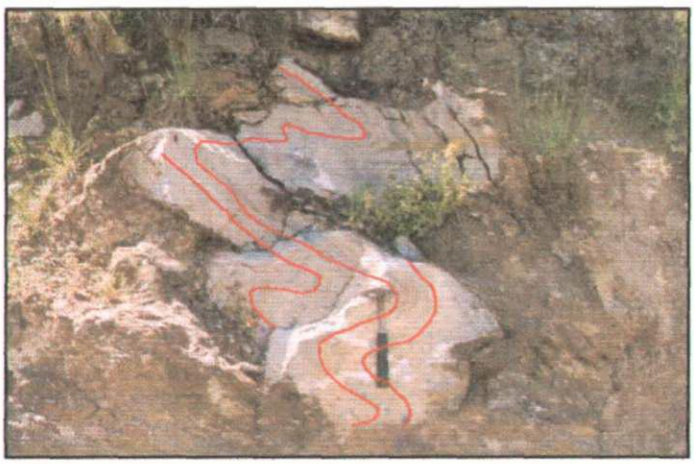


Figure 3.55 Marble block showing isoclinal folding together with garnet-phengite schist.

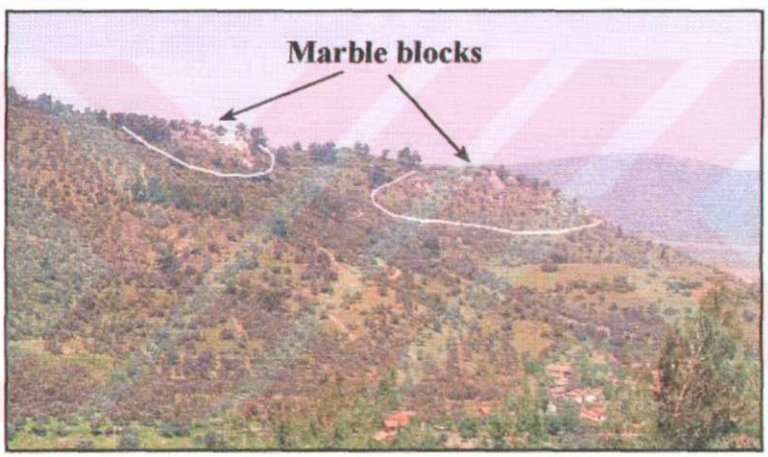


Figure 3.56 The field view of marble blocks which are embedded in the matrix of the metaolistostrome.



Figure 3.57 Small marble block in garnet-phengite schist. Calcite vein-filling which is culminated in garnet-phengite schist, and sharp - irregular contact relationship represent the block character of marble.

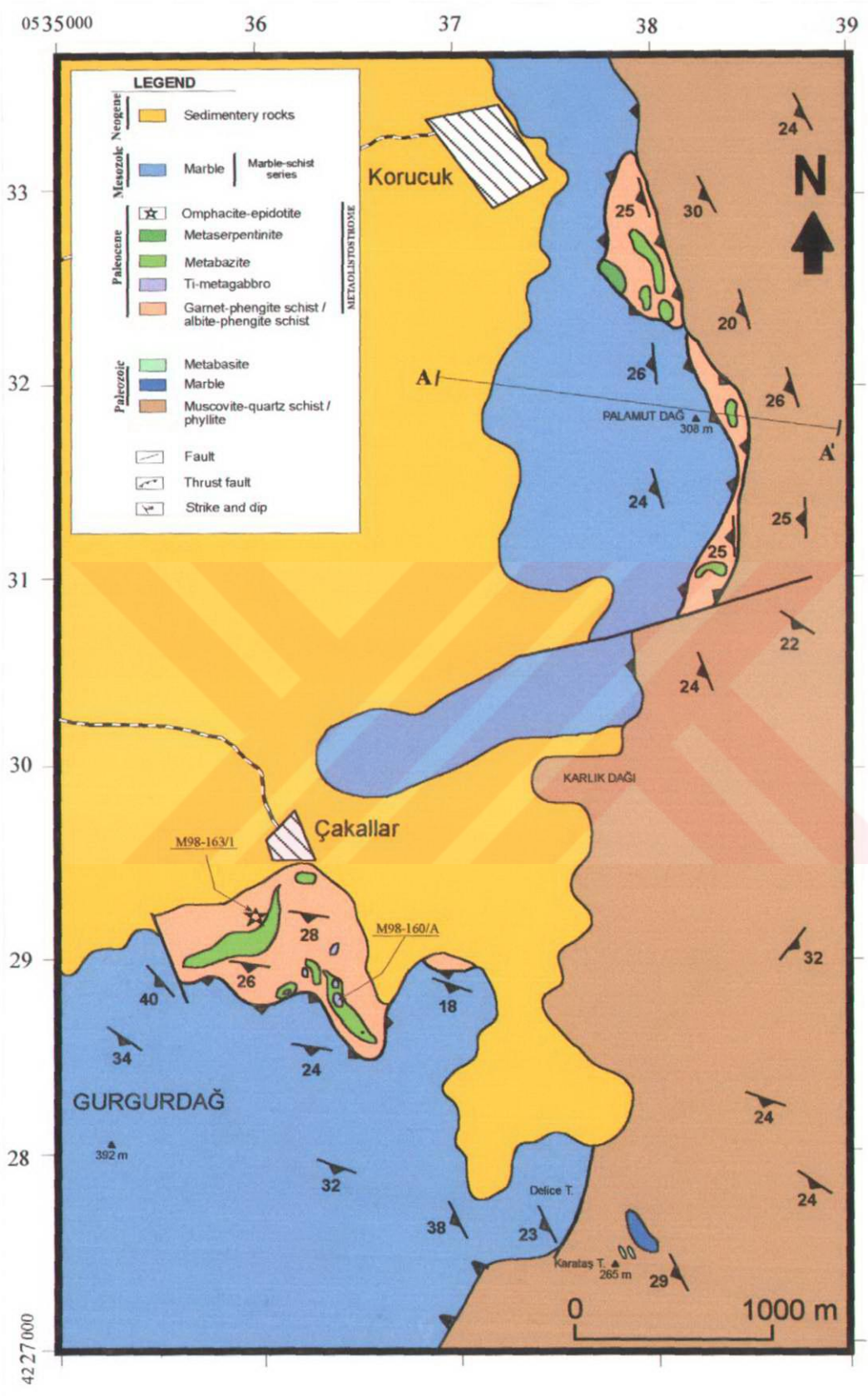


Figure 3.58 The geological map of the Metaolistostrome unit occurring between Çakallar and Korucuk villages, E of Torbalı. Sample number and location of analyzed rocks are shown in the map.

block which is founded, occur in SE of Korucak (Figure 3.58). This block is strongly deformed. The colour of the block is changed from dark green to pale green - greyish. The Metaolistostrome unit, as different from other studied areas, is tectonically overlain by grey coloured marble. These carbonates are probably the equivalents of the metabauxite-bearing Mesozoic marbles.

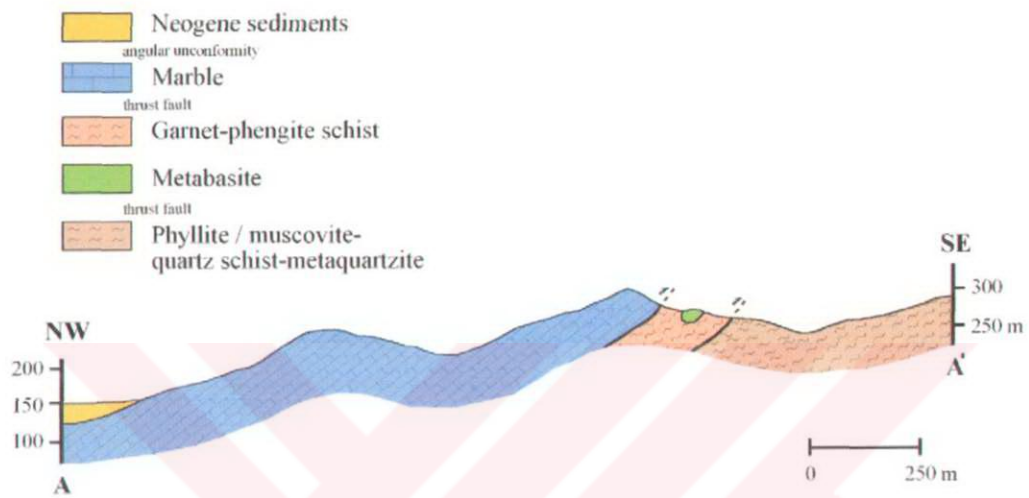


Figure 3.59 The cross section showing contact relationship among marble, garnet-phengite schist and mica schist / muscovite-quartz schist between Çakallar and Korucuk villages. The section line is given in Figure 3.58.

3.3.6. Tire area

The Marble-schist series and the Metaolistostrome unit are observed in this area, 5 km to the NW of Tire (Figure 3.23). Rudist-bearing marbles which represent the upper most levels of the Marble-schist series, are tectonically overlain by thrust contact by the Metaolistostrome unit (Figure 3.60 and 3.61). The evidence about tectonic contact are given in 3.2.4. The matrix of the Metaolistostrome unit is made up of garnet-mica schist and albite-mica schist. In garnet-mica schists, micas consist of white mica and biotite. Especially at around Hastane Tepe, the matrix is richer in biotite. Garnets are commonly rimmed by chlorite. Blocks in metaolistostrome are composed of marble, metaserpentinite, Ti-metagabbro and metabasite. The length of metaserpentinite blocks reach up to 2 km. Large metaserpentinite blocks occur at Meşeli Tepe and Taşlı Tepe. These blocks are largely covered by the alluvial plain.

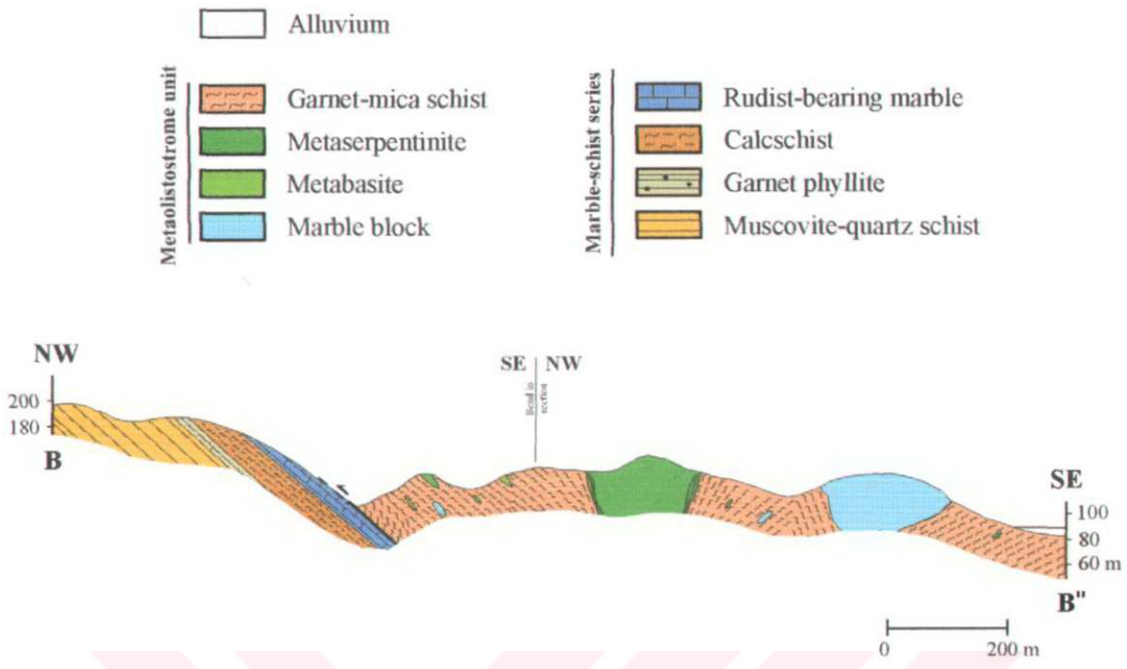


Figure 3.60 Tectonic contact between the Marble-schist series and the Metaolistostrome unit. The Metaolistostrome unit contains marble, metabasite, Ti-metagabbro and metaserpentinite blocks. Section line is given in Figure 3.23.

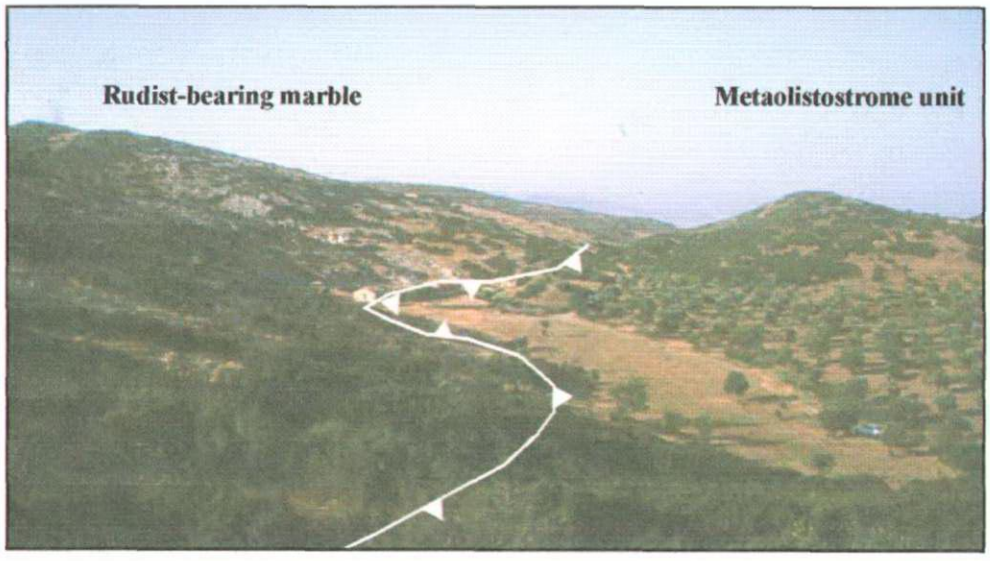


Figure 3.61 The field view of the tectonic contact between the marble (Marble-schist series) and the Metaolistostrome unit.

The largest metaserpentinite block in the matrix of the metaolistostrome is partly transformed into talc-schist. Ti-metagabbro body also occurs in this block. Metabasite blocks are dark green or blackish coloured. Numerous small metabasite blocks exist in the matrix. The mineral assemblage of metabasite blocks is garnet, green amphibole, albite and epidote. Metabasite blocks are completely transformed into garnet amphibolite, due to greenschist overprint. The evidence about HP/LT metamorphism in the Metaolistostrome unit are completely obscured in this area which has been strongly effected from greenschist overprint.

3.3.7. Gölmarmara area

Three tectonic sequences are determined in 3 km SW of Gölmarmara. These are in ascending order; a) probably Paleozoic aged schist and quartzite intercalation, b) metaolistostrome and c) limestone belonging to İzmir-Ankara zone (Figure 3.26). The Metaolistostrome unit among Kayaaltı, Ozanca and Çullugörüce is tectonically underlain by Paleozoic (?) schist series which is composed of garnet-mica schist, mica schist, muscovite-quartz schist and metaquartzite intercalation (Figure 3.27). The absence of platform type Mesozoic marbles supports the tectonic character of the contact (Figure 3.62).

The matrix of the Metaolistostrome unit is made up of garnet-phengite schist and albite-phengite schist. Garnet-phengite schists are more dominant in the area. Zoisite metagabbro, Ti-metagabbro, metaserpentinite, metabasite and marble blocks are embedded in the matrix of metaolistostrome (Figure 3.27). Metaserpentinite blocks reach up to 1 km in size occur in matrix. The largest metaserpentinite block contains boudinaged zoisite metagabbro dykes. The mineral assemblage of zoisite metagabbros are "green amphibole + zoisite + epidote". Coarse green amphiboles are anhedral in shape and are surrounded by whitish zoisite crystals. Zoisite metagabbros do not contain relict HP/LT minerals, such as omphacite, although they may have been derived from omphacite metagabbro, as in Yılanlı Tepe – Şirince. Ti-metagabbro block occur 500 m east of Kayaaltı village. Ti-metagabbro with massive appearance is blackish – bluish in colour. Yellowish sphene clusters are not seen in

the surface of the block. But, bulk rock analyse shows that Ti content of this block changes from 3 to 4 wt%, like those in the Selçuk area. Eclogite block and/or blocks have not been found in the Metaolistostrome unit in this area. Some eclogite pebbles are found in İğdeli Dere, 500 m SE of Kayaaltı village. The Metaolistostrome unit which is exposed along NE-SW direction, is tectonically overlain by limestone (Figure 3.62) belonging to İzmir-Ankara zone.

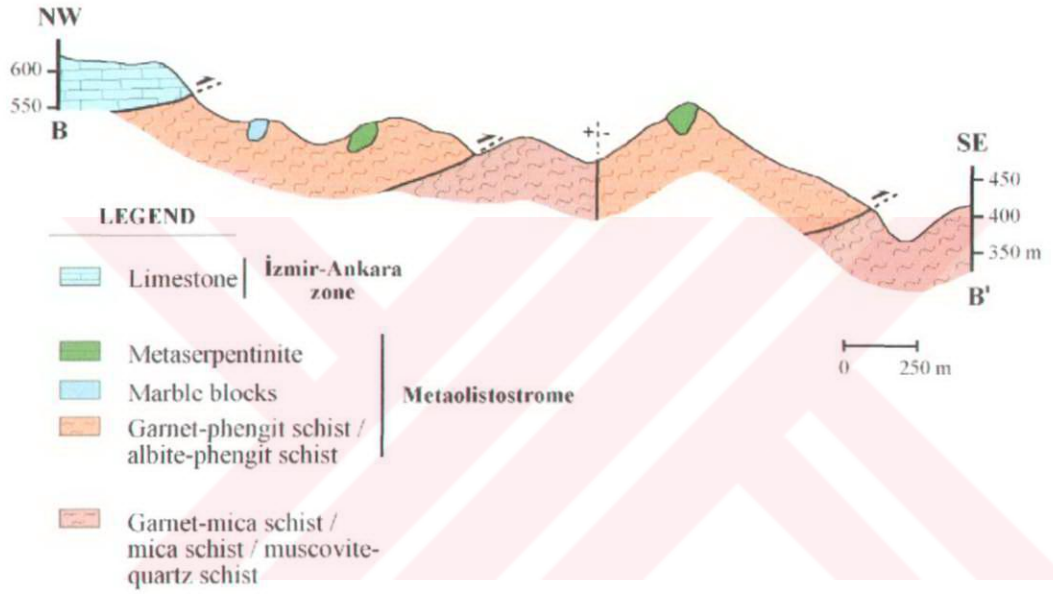


Figure 3.62 The schists of Paleozoic (?) series are directly overlain by the Metaolistostrome unit without platform type marble in the contact, which suggests a tectonic relationship. Limestone of the İzmir-Ankara Zone is tectonically overlying the Metaolistostrome unit. Section line is given in Figure 3.26.

3.4. Lycian Nappes

The Lycian Nappes are observed in Söke (Gümelez) and Kuşadası (Kirazlı). The Lycian Nappes are identified as small klippen lying on top of the Menderes metamorphics. Lycian Nappes are composed of thin red phyllite slices and dolomite/limestone (Figure 3.29). The red phyllites were first named as the Karaova formation by Brinkmann (1967).

3.4.1. Söke (Gümelez) area

A klippen of the Lycian Nappes cover approximately 10 km^2 area between Davutlar and Gümelez (Figure 3.28). In these area, Lycian Nappes is composed of dolomitic limestone and red phyllites and occur as a tectonic unit on top of the Metaolistostrome unit (Figure 3.29). A break between the metamorphic grades of the Lycian Nappes and the Metaolistostrome unit can be recognised easily in the field.

The matrix of the Metaolistostrome unit is represented by garnet-phengite schist and the red phyllites at the base of the overlaying Lycian Nappes rarely contain fibrous carpholite crystals representing a low grade HP/LT metamorphism (Figure 3.28). Fibrous carpholites occur in quartz segregations of the red phyllites. These phyllites are found as thin slice at the base of along klippen. The red phyllites show brittle deformation. The base of the thrust sheet in this area is defined by these phyllites (Figure 3.31). The boundary between dolomitic limestone and red phyllites is tectonic. (Figure 3.31).

3.4.2. Kuşadası (Kirazlı) area

In this area, Lycian Nappes consist of dolomitic limestone and red phyllites. Dolomitic limestone covers a large area between Kuşadası and Kirazlı - Yeniköy (Figure 3.32). A small dolomite klippe showing brittle deformation features occurs at Kuşadası – Yeniköy road (Figure 3.63). Tectonic character of the contact between the Metaolistostrome unit and Lycian Nappes is clearly observed on this outcrop. At he base of dolomitic limestone, the red phyllites showing brittle deformation are observed (Figure 3.64).

The contact between dolomitic limestone and red phyllites is also tectonic. The red phyllites are rarely seen in Kirazlı area. The widest outcrop of these rocks occurs in Kirazlı and is observed as a stripe of approximately 500 m in length.



Figure 3.63 Small Lycian Nappe klippe which is formed by highly deformed dolomite, on the matrix of the Metaolistostrome.

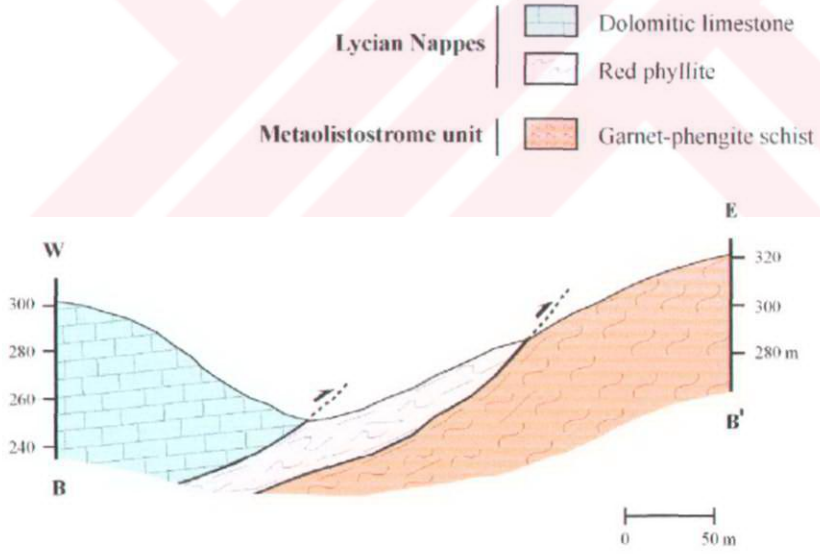


Figure 3.64 The contact relations of dolomitic limestone, red phyllite and garnet-phengite schist (Metaolistostrome unit).

CHAPTER FOUR

PETROGRAPHY

4.1. Introduction

The field observations of rock units from the Marble-schist series and the Metaolistostrome unit were given in the previous chapter. In this chapter, textural and mineralogical properties of concerning rock types in study area are presented. Petrographic properties of the rock units in Dilek Peninsula, Selçuk, Tire, Torbalı and Gölmarmara (Akhisar) are given as follows: a) Lower Triassic (?) – Upper Cretaceous Marble-schist series; b) Metaolistostrome unit; c) Lycian Nappe units.

4.2. Lower Triassic (?) – Upper Cretaceous Marble-schist series

The main lithologies of the Marble-schist series consist of quartz metaconglomerate, carbonate metaconglomerate, chloritoid phyllite, blueschist metabasites, blueschist metapelites, marble, phengite-quartz schist, epidote amphibolite, garnet phyllite, garnet amphibolite and garnet-phengite-biotite schist. Petrographic features in association with these units are given below.

4.2.1. Quartz metaconglomerate

Quartz metaconglomerates form one of the most typical lithologies which can be used as a key horizon in Mesozoic series of Menderes Massif. This unit is made up of well-rounded quartzite pebbles with white mica-rich matrix. The length of the

quartz pebbles can reach up to 7 cm. The matrix of quartz metaconglomerate consists of "kyanite – chloritoid – phengite – epidote – chlorite – quartz - pyrophyllite – tourmaline – magnetite". The amount of the quartz in matrix is always higher than 50 per cent. Kyanite-chloritoid-phengite assemblage is mostly restricted to Al-rich pelitic parts of this rock. Porphyroblasts in the matrix are commonly represented by chloritoids. Kyanite crystals are generally clouded by fine-grained opaque oxide inclusions. In addition, quartz inclusions are commonly observed in kyanite. In general, chloritoids show polysynthetic twining and are idioblastic porphyroblasts. The chloritoid porphyroblast with polysynthetic twining contains prograde fabric (PF) inclusion patterns, whereas the matrix shows retrograde fabric (RF), which is markedly perpendicular or oblique to the inclusion patterns in the chloritoid porphyroblast (Figure 4.1a). The existence of strain shadow especially around chloritoid and kyanite porphyroblasts indicates that these porphyroblasts are pretectonic with respect to retrograde fabric causing to the development of the matrix foliation (Figure 4.1b). The first phase of deformation produced prograde fabric which can be traced in the kyanite and chloritoid porphyroblasts. Whereas, greenschist facies overprint caused well-developed retrograde axial planar fabric defined by small Phengite-II crystals (poor-in Si), chlorite, stretched kyanite and pyrophyllite to be breakdown product of kyanite (Figure 4.2). Phengite-II and chlorite inclusions do not exist in chloritoid and kyanite. Phengite-II crystals have very low Si (average 3.126 p.f.u) content. Some chlorites are observed as secondary minerals which are altered from chloritoid. Quartz and magnetite are ubiquitous in the matrix and as inclusions in porphyroblasts. Mineral assemblages of the Epidote - blueschist facies (**EBF**) represented by S1 foliation and greenschist facies (**GS**) marked by S2 foliation, are given below.

- **EBF**: kyanite - chloritoid (rich-in Mg)- Phengite-I (Si^{4+}=3.40) - quartz - opaque oxide
- **GS**: Phengite-II (Si^{4+}=3.16) - chlorite - pyrophyllite - quartz - opaque oxide

High-pressure assemblage consisting of "kyanite – chloritoid – phengite" is observed from Dilek Peninsula through Kuşadası (Kapalıboğaz), Selçuk (Acarlar) to

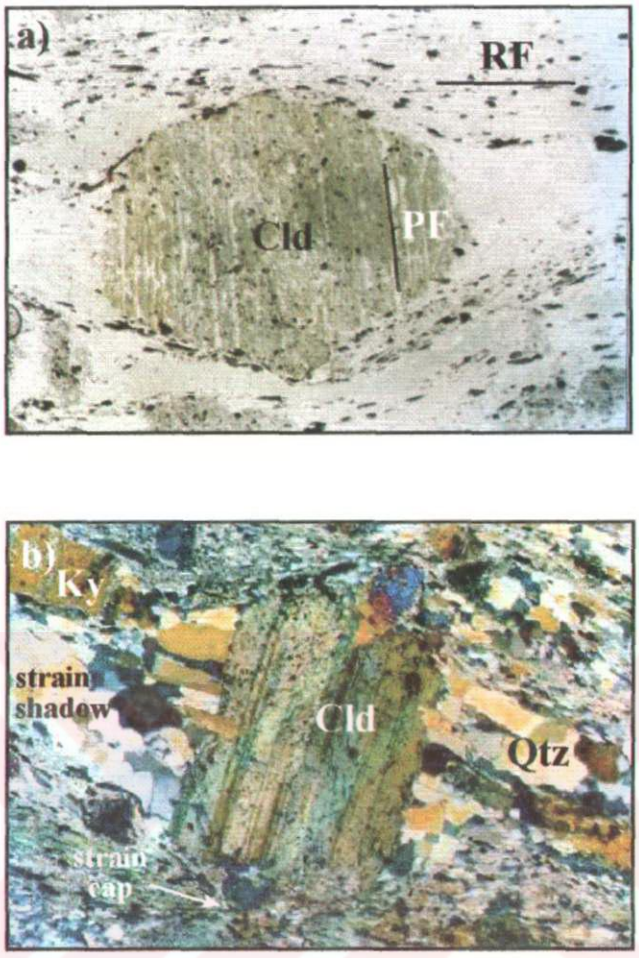


Figure 4.1 a) photomicrograph showing prograde fabric (PF) (in chloritoid) and retrograde fabric (RF) (in matrix) foliations in quartz metaconglomerate with "kyanite-chloritoid-phengite" assemblage in Dilek Peninsula. Width of view 4 mm. PPL. **b)** strain caps and strain shadows around chloritoid which represent the growing of chloritoid during the earliest deformation. Width of view 4 mm. CPL.

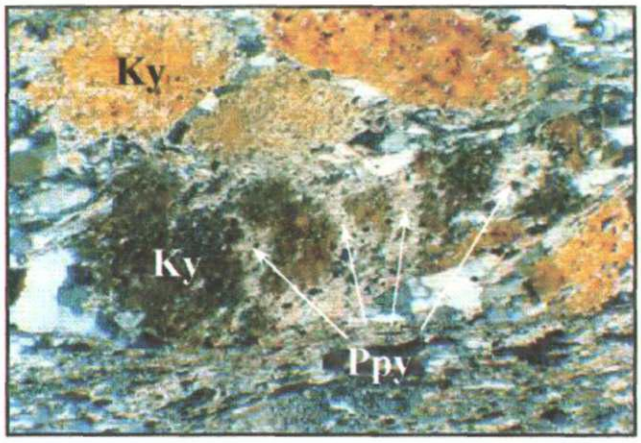


Figure 4.2 Photomicrograph of kyanites replaced by pyrophyllite (Ppy). Width of view 2.5 mm. CPL.

Selçuk (Şirince). The variations of the chemical composition of chloritoid, Phengite-II and chlorite from Dilek Peninsula to Şirince are given in Table 4.1.

Table 4.1 X_{Mg} and Si^{4+} variations of chloritoid, chlorite and Phengite-II in quartz metaconglomerate unit from Dilek Peninsula to Şirince Village.

	S1 foliation	S2 foliation	S2 foliation
Dilek Peninsula (Atburgazı)	Chloritoid (X_{Mg}=0.35)	Phengite-II (Si^{4+}= 3.16)	Chlorite (X_{Mg}=0.84)
Kuşadası (Kapalıboğaz)	Chloritoid (X_{Mg}=0.34)	Phengite-II (Si^{4+}= 3.14)	----
Selçuk (Acarlar)	Chloritoid (X_{Mg}=0.33)	Phengite-II (Si^{4+}= 3.18)	Chlorite (X_{Mg}=0.82)
Selçuk (Şirince)	Chloritoid (X_{Mg}=0.32)	Phengite-II (Si^{4+}= 3.12)	Chlorite (X_{Mg}=0.78)

The changes of the chemical composition of the minerals can be interpreted that the affect of greenschist facies overprint increases from west to east.

4.2.2. Carbonate metaconglomerate

The carbonate metaconglomerate consists of cream-coloured marble pebbles embedded in a matrix rich in quartz and calcite. Apart from marble pebbles, quartz and epidotite pebbles are also present in these rocks. The matrix of the carbonate metaconglomerate is composed of " calcite - phengite - epidote - zoisite - plagioclase - chlorite - ankerite - magnetite - quartz - sphene ". Lepidoblastic texture which is defined by the alignment of phengite and chlorite, is observed in the matrix (Figure 4.3). Mineral assemblage of carbonate metaconglomerate can be given as "*calcite - zoisite - Phengite-I (rich-in Si) - albite (An_2) - quartz*". This assemblage is characterized by the HP/LT metamorphism. The inclusion patterns in albite porphyroblasts and orientation of Phengite-I crystals are oblique to retrograde fabric. The retrograde assemblage is represented by "*epidote - Phengite-II (poor-in Si)-*

albite (An_5) - chlorite - magnetite - sphene - ankerite". The increase of the amount of chlorite and epidote in the matrix of the carbonate metaconglomerate may be related with the amount of the volcanoclastic material in the sediment. Phengite-II which is generally smaller than Phengite-I, is commonly replaced by chlorite. Epidotes with yellowish pleochroism occur as individual crystals in chlorite-rich domains. The carbonate pebbles are generally rimmed by a brownish coloured shell which is formed by ankerite. Magnetite is preferentially observed in chlorite-rich domains. Sphene which is a typical mineral of greenschist overprint, appears as randomly oriented individual crystals in the matrix.

4.2.3. Blueschist metabasites

Na-amphibole-bearing metabasites in the Marble-schist series are restricted to the Dilek Peninsula, western part of the Menderes Massif. The general mineral assemblage of blueschist metabasites is amphibole (Na, Na-Ca), epidote, phengite, clinozoisite, albite, chlorite, sphene, magnetite and calcite. They show well-developed nematoblastic texture (Figure 4.4). There is no any evidence about primary magmatic texture and mineralogy, due to penetrative deformations. Based on the textural relationship and chemical composition of the minerals, two metamorphic stages can be separated: ***prograde*** and ***retrograde*** stages.

Prograde stage; this can be divided into two stages:

- early assemblage;

Crossite (Al^{VI}= 1.243) - zoisite - phengite (Si^{4+}= 3.37) - albite (An_1)

- late assemblage;

Crossite (Al^{VI}= 0.855) - epidote (Ps_{17}) - phengite (Si^{4+}= 3.34) - albite (An_2)

Retrograde stage;

Barrosite (Al^{VI}= 0.319) - epidote (Ps_{24}) - phengite (Si^{4+}= 3.16) - chlorite (X_{Mg}= 0.7) - albite (An_{4-5}) - sphene - magnetite.

Zoisite as a phase of early assemblage of prograde stage (HP/LT) is rarely observed in the matrix. Zoisite and crossite are in textural equilibrium with phengite. Crossites appear as medium to large euhedral or sub-euhedral crystals characterized

by a strong violet or blue pleochroism. Crossites show textural zoning as core and rim. The core contain numerous zoisite inclusion which are partly replaced by epidotes. Whereas, the rim is almost devoid of inclusion (Figure 4.5). Epidotes occurring as small sub-euhedral and slightly zoned crystals are relatively abundant in late assemblage. Due to their low Fe^{3+} content, these minerals have pale yellow pleochroism. The anorthite contents of albites are at around 2 %. Late stage crossites are characterized by the absence of inclusions (Figure 4.5). Retrograde stage is represented by the development of barroisite. The crossite is rimmed by dark green barroisite (Figure 4.6). Epidotes have stronger yellow pleochroism. In this stage, phengites are partly replaced by chlorite. In addition, modal amount of chlorites steeply increases in matrix. The great majority of matrix is formed by albite including small epidote inclusions. Sphene is observed as tiny crystals surrounding the large epidote grains. Opaque oxides with irregular grain boundary contain numerous Na-amphibole inclusions. These type opaque oxides should have been formed during the late stage of HP/LT metamorphism (Figure 4.7). Opaque oxides formed during the greenschist facies, occur as euhedral crystals and do not contain Na-amphibole inclusions.

4.2.4. Blueschist metapelites

The general mineral assemblage of blueschist metapelites is "phengite - crossite - chloritoid - zoisite - epidote - albite - chlorite - stilpnomelane - calcite - sphene - quartz - tourmaline - opaque oxide". Blueschist metapelites consist of two lithologies; crossite-bearing calc-schist and chloritoid phyllites.

4.2.4.1. Crossite-bearing calcareous schist

Crosssite-bearing calcareous schist is composed of " crossite - phengite (Si=3.44) - epidote - chlorite - albite - calcite - sphene - opaque oxide". High-pressure metamorphism under epidote-blueschist facies conditions is represented by " crossite

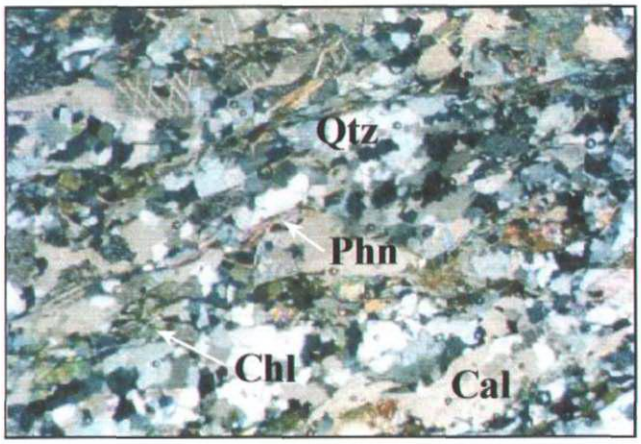


Figure 4.3 The general view of matrix of carbonate metaconglomerate. Lepidoblastic texture is defined by aligned parallel to foliation of phengite (phn) and chlorites. Width of view 4 mm. CPL.

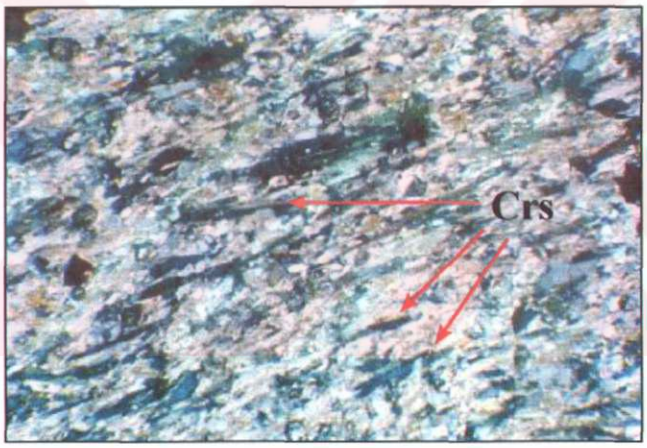


Figure 4.4 Tabular and aligned Na-amphibole crystals in calc-schists. Width of view 2.5 mm. CPL.

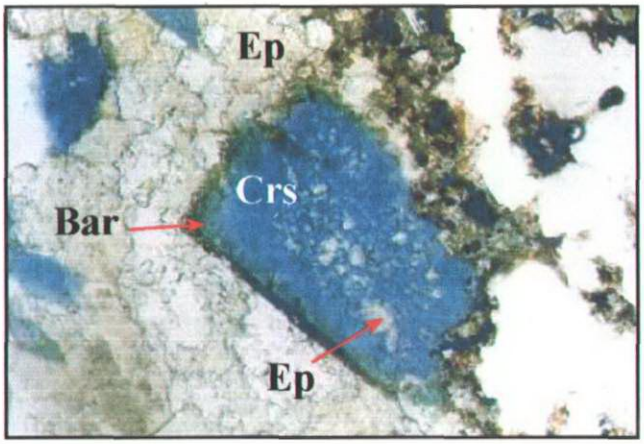


Figure 4.5 Zoned crossite which is made up of core with zoisite inclusion. In addition, crossite (Crs) is rimmed by a barroisite zone developed during the retrograde overprint. Width of view 1 mm. PPL.

+ phengite " assemblage in crossite-bearing calcareous schists. Schistosity defined by the alignment of tabular minerals and lineation is well-developed in these rocks. Crossites with purple to blue coloured pleochroism occur as subhedral prismatic crystals up to 2.5 mm in length. Although, they show irregular optical zonation, any chemical zoning are not observed in these minerals. Crossites appear in textural equilibrium with phengite with high Si content and albite. Albite with epidote inclusions forms subhedral crystals. In general, some albite crystals show carlsbad twining. Epidotes generally appear as inclusions in albite porphyroblasts. Crossite-bearing calcareous schist show a banded texture consisting of carbonate-rich and silica-rich layers (phengite, crossite and chlorite). The typical greenschist facies minerals in crossite-bearing calcareous schists are chlorite, epidote and sphene. The transformation from epidote-blueschist to greenschist facies is commonly observed with different stages in most of samples. Crossites and phengites are partly or completely replaced by chlorite (Figure 4.8). Opaque oxides are preferentially concentrated around chlorite rich domains. Epidotes developed under greenschist facies conditions are rich in Fe^{3+} typified by their yellowish pleochroism. Sphenes, clouded by tiny opaque oxide inclusions, are associated with chlorite and opaque oxides.

4.2.4.2. Chloritoid phyllites

The general mineral assemblage of these rocks is " phengite - chloritoid - chlorite - albite - zoisite - epidote - stilpnomelane - tourmaline - quartz - opaque oxide". High-pressure metamorphism in chloritoid phyllites is characterized by the coexistence of " chloritoid (rich–in Mg) + phengite ". Two deformation phases are recognized in chloritoid phyllites. Progressive deformation under epidote-blueschist facies conditions caused prograde fabric which is defined by chloritoid (rich-in Mg), Phengite-I (rich-in Si) and zoisite. Chloritoid and phengites form larger crystals than that of minerals formed during the retrograde deformation. The long axis of chloritoid and Phengite-I crystals which define prograde fabric, are approximately perpendicular to the retrograde fabric. Chloritoid phyllites are common in Dilek Peninsula. Chloritoids in phyllites occur as rosette-like crystals which are never

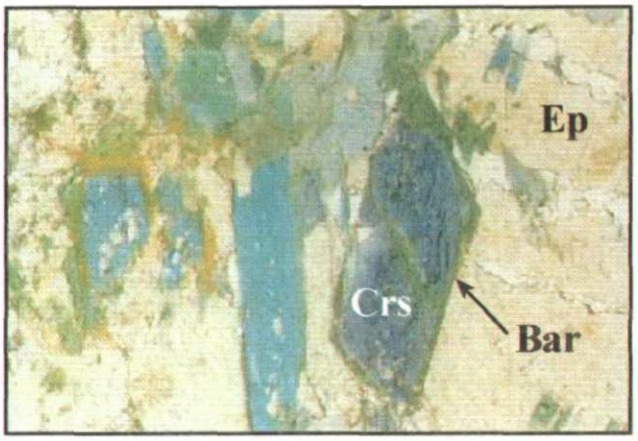


Figure 4.6 Sub-euhedral crossite (Crs) crystals which are rimmed by retrograde barroisite. Width of view 1 mm. PPL.

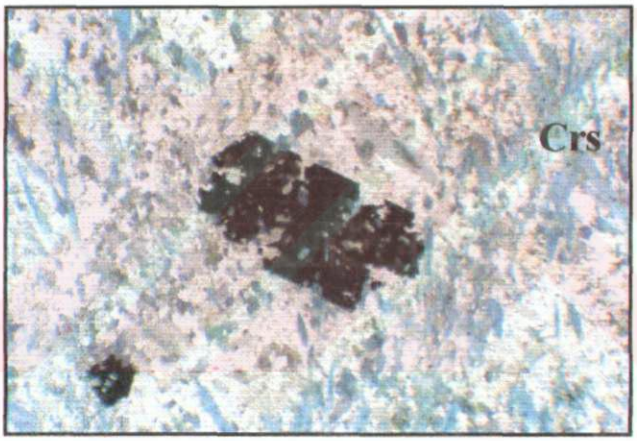


Figure 4.7 Photomicrograph showing opaque mineral which includes crossite crystals. Width of view 1 mm. PPL.

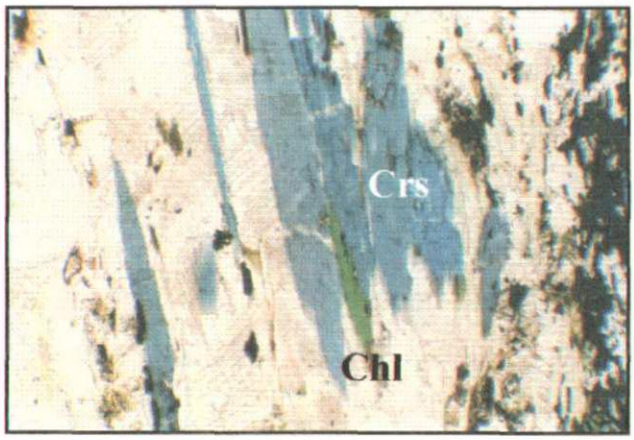


Figure 4.8 Photomicrograph showing crossite partly replaced by chlorite. Width of view 2.5 mm. PPL.

observed in quartz metaconglomerate. Rosette-like chloritoids (rich-in Mg) show a parallel alignment to prograde fabric. Prismatic chloritoid crystals are cut by retrograde fabric (Figure 4.9). Zoisites occur as rounded crystals, due to retrograde deformation. The retrograde overprint caused well-developed retrograde axial planar fabric defined by chloritoid (rich-in Fe), phengite (low-in Si), chlorite and stilpnomelane. Two types of chlorite are recognized; individual crystals with the parallel alignment to the foliation and at the rim of chloritoids. Stilpnomelane which is commonly intergrown with chlorites, developed during the retrograde stage and align parallel to retrograde fabric.

4.2.5. Greenschist metabasites

These rocks are commonly observed in Dilek Peninsula and at around Selçuk. The general mineral assemblage of these rocks is " epidote - phengite - albite - chlorite - calcite - Ca-amphibole - biotite - zoisite - quartz - sphene - ankerite - opaque oxide ". Two type metabasite rocks are distinguished. The first type is rich-in chlorite, coarse grained, massif appearance in macro-scale and calcite-free. They occur in Acarlar, SW of Selçuk. In these rocks, most of the calcic amphiboles produced by retrograde metamorphism are replaced by chlorite. There is no any sign about relict magmatic texture. These rocks have up to 35-40 % chlorite (Figure 4.10). In addition, they may contain minor biotite. Albites which have second important volume, are full of epidote and amphiboles inclusions. Epidote inclusions in albites are more prominent relative to amphiboles. Individual epidote-group minerals display zoisite-rich cores and epidote-rich rims (Figure 4.11). This zonation is very probably related with decompression which is developed during the exhumation. Euhedral or subhedral sphene crystals are randomly oriented and distributed in the matrix. The second type metabasites is described by calcite crystals together with mafic material and are rich-in epidotes. Sometimes this type metabasites may have more than 40 % (by volume) epidote and albite which are in unhedral crystal form. Chlorites occur as the most common retrograde phase in metabasites. Two types of calcite occurrences are recognized; individual crystals with epidote inclusions (Figure 4.12) and vein-filling

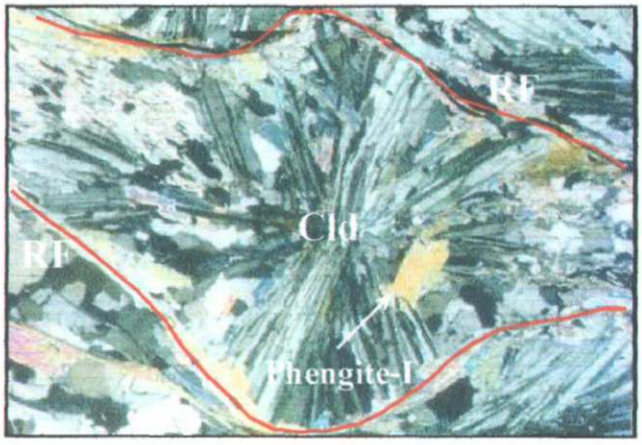


Figure 4.9 Rosette-like chloritoid, developed during HP/LT metamorphism, surrounding by retrograde fabric (RF). Width of view 4 mm. CPL.

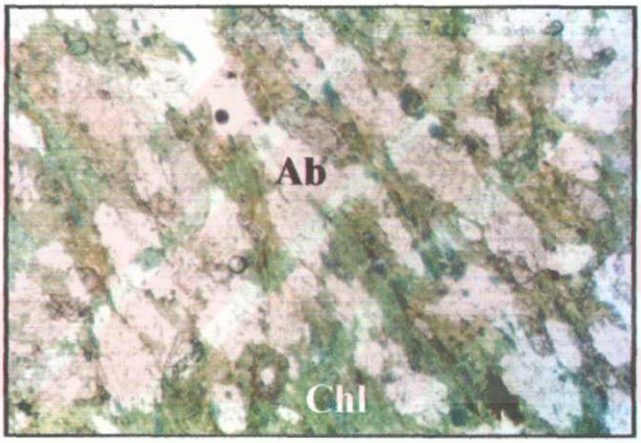


Figure 4.10 Photomicrograph showing the common secondary chlorite derived from Ca-amphibole. Light green minerals are chlorite. Width of view 4 mm. PPL.

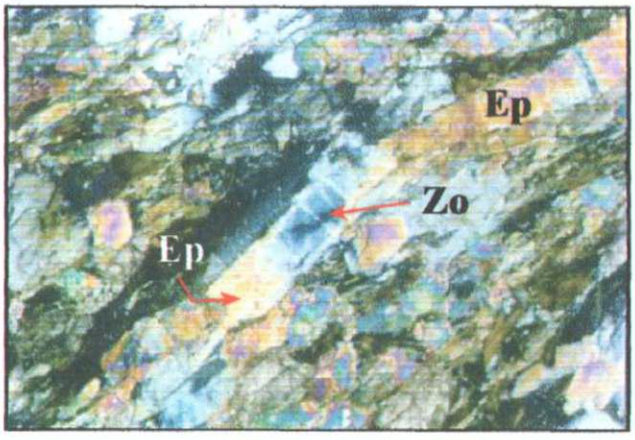


Figure 4.11 Bluish zoisite as a phase of epidote-blueschist facies metamorphism is replaced by epidotes as a consequence of greenschist overprint. Width of view 1 mm. CPL.

T.C. YÜKSEKÖĞRETİM KURULU
DOKÜMANTASYON MERKEZİ

calcites with no inclusions. The common presence of calcite in metabasic rocks represents the volcano-sedimentary origin of the second type greenschist metabasites. Most of calcites with epidote inclusions are partly transformed into ankerite. In sedimentary rocks ankerite occurs as a result of both hydrothermal and low temperature metasomatism (Deer et al. 1992).

4.2.6. Phengite-quartz schist

These rocks are exposed over large areas, in Dilek Peninsula and Selçuk, Tire, Torbalı and Gölmarmara regions. The general mineral assemblage of phengite-quartz schists is " phengite - quartz - albite - biotite - chlorite - tourmaline - opaque oxide ". These rocks show dominantly lepidoblastic texture. On the other hand, in albite-rich zones, porphyroblastic texture can be observed. Albite content of these schists is variable and can reach up to 15 %. Two phengite generations (Phengite-I and phengite II) are recognized in phengite-quartz schists. Phengite-I crystals which have been developed during the epidote-blueschist facies metamorphism, are rich-in Si and relatively larger in respect to the Phengite-I (Figure 4.13). The alignments of Phengite-I crystals are different from minerals which have been formed during the greenschist facies overprint (Figure 4.13). Small phengite–II crystals which are poor-in Si, are align parallel to greenschist facies foliation. Some Phengite-I crystals are preserved from retrograde deformation in strain-free domains (Figure 4.14). The graphite internal pattern in albite porphyroblasts are oblique to the greenschist facies foliation. Modal abundance of albites changes from 5 % to 15 % in phengite-quartz schist samples. Most of the albite crystals show zoning. The core of them has folded graphite inclusion pattern. Whereas, the rim is of inclusion-free (Figure 4.15). In the rim, inclusion-free albite zoning is most probably formed in late stage greenschist facies metamorphism. This case is supported by inclusion free, euhedral, nearly undeformed albite neoformations in the matrix. On the other hand, some albites contain quartz and bluish zoisite inclusions. This type of albites have been probably formed in epidote-blueschist facies conditions. Three types of albite are distinguished in these schists. Based on the common occurrence in Dilek Peninsula where the

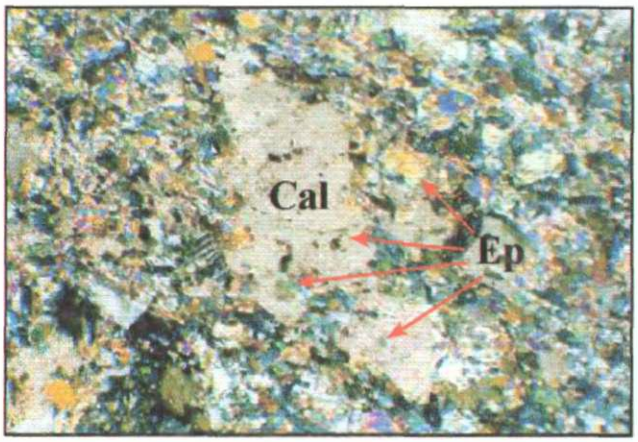


Figure 4.12 Photomicrograph showing epidote bearing calcite. This may show volcano-sedimentary origin of the greenschist metabasites. Width of view 2.5 mm. CPL.

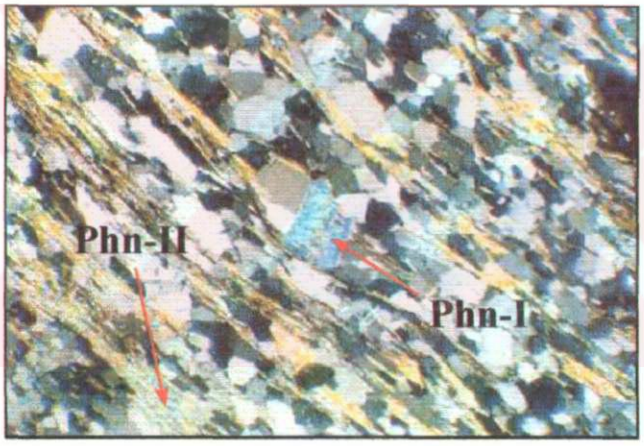


Figure 4.13 Two phengite generation; coarse Phengite-I crystals which are formed during the epidote-blueschist facies metamorphism, are rich-in Si; small Phengite-II crystals defining the retrograde fabric, are poor-in Si. Width of view 2.5 mm. CPL.

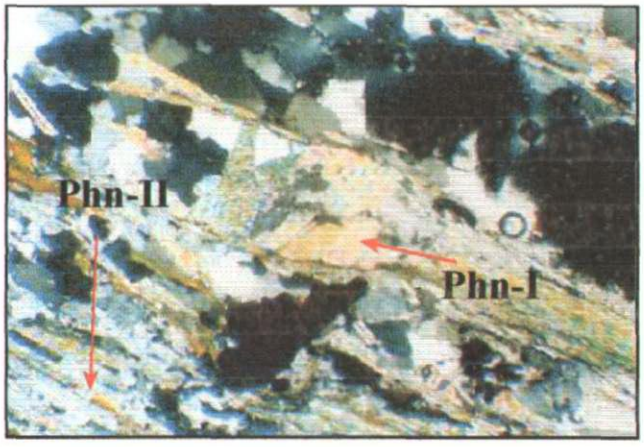


Figure 4.14 Coarse Phengite-I crystals preserved in strain-free domains. Width of view 2.5 mm. CPL.

blueschist assemblages are well-preserved, albites with especially zoisite inclusions could be interpreted to have been formed during the epidote-blueschist facies. The fabric which is developed during the greenschist overprint, is defined by the quartz and phengite (poor-in Si) dominated layers (Figure 4.13). Especially in Gölmarmara area, retrograde foliation dominated by Phengite-II is transacted with small angles by sets of subparallel minor shear bands which can be described as shear band cleavage (White 1979b; Gapais & White 1982) (Figure 4.16). Shear band cleavage observed in these schists is similar to C'-type shear band cleavage of Passchier and Trouw (1996) (Figure 4.16). Quartz crystals show pronounced undulose extinction as a result of crystal plastic deformation (Passchier & Trouw 1996) in Gölmarmara area. Elongated subgrains in deformed quartz crystals are probably formed by grain boundary migration. Figure 4.17 shows typical fabric of dynamic recrystallization of quartz. The relicts of large old quartz grain with undulose extinction and elongate subgrains pass laterally into domains of small dynamically recrystallized quartz grains (Figure 4.16). Especially in Tire, Gölmarmara areas and east of Hasançavuslar Village, biotites are observed as small crystals. Biotites are replaced by the small chlorite crystals.

4.2.7. Garnet-mica schist

Biotite and garnet assemblage occurs at 300 m west of Akyurt village in the Marble-schist series. In addition, garnet is observed at 250m north of Hasançavuşlar village. The garnets have been completely replaced by chlorite. The general mineral assemblage of these schists is "garnet - phengite - biotite - albite - chlorite - quartz - tourmaline - opaque oxide". Garnet-mica schists show lepidoblastic and porphyroblastic texture as a consequence of preferentially oriented phengites and garnet porphyroblasts, respectively. Two phengite generations are recognized in the schists. Phengites (Phengite-I) with high Si content (3.34 p.f.u) are products of the epidote-blueschist facies metamorphism and form larger crystals relative to phengite poor-in Si. The amount of Phengite-II crystals (Si=3.14 p.f.u) which are products of the greenschist facies overprint, reaches up to 35 % and align parallel to the retrograde fabric.

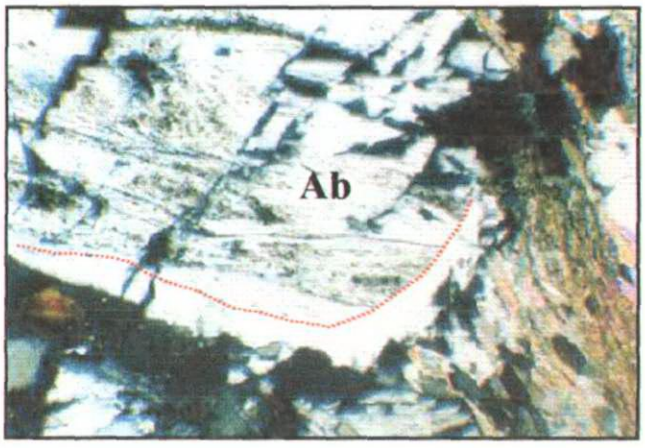


Figure 4.15 Textural zoning of albite porphyroblast which is defined by inclusions in the core (epidote-blueschist facies) and inclusion free rim (greenschist facies). Width of view 2.5 mm. CPL.

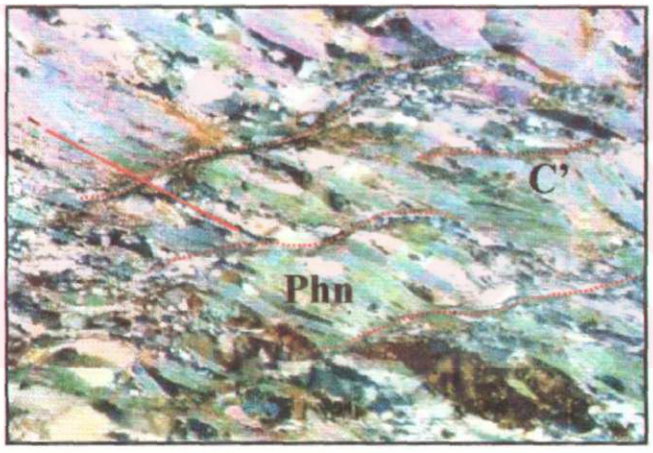


Figure 4.16 Phengite-II which are transected by C'-type shear band cleavage. Section parallel to the stretching lineation and normal to the foliation. Width of view 4 mm. CPL.

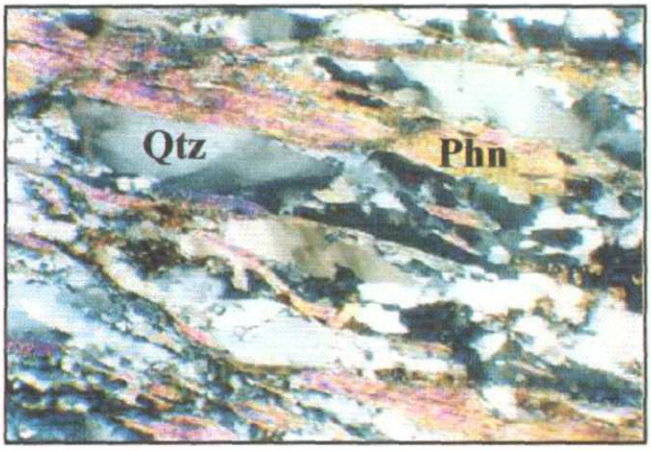


Figure 4.17 Subgrain migration in deformed quartz and typical fabric of dynamic recrystallization of quartz. Section parallel to the stretching lineation and normal to the foliation. Width of view 2.5 mm. CPL.

The main foliation is defined by compositional layering and the preferred orientation of small Phengite-II crystals. Albites with quartz, albite and zoisite / epidote inclusions, occur as porphyroblasts in Phengite-II dominated domains. Garnets are partly replaced by biotite and chlorite. Garnet crystals have been grown preferentially in quartz rich domains. They includes many quartz crystals. Such kind of garnet porphyroblasts show skeletal texture (Figure 4.18). Some relict Phengite-I inclusions are observed in garnet. Most of the garnet porphyroblasts have generally subhedral or anhedral crystal shape. Spiral internal fabric of syn-tectonic garnet shows 90° rotation with respect to external retrograde fabric (Figure 4.18). The central part of garnet has approximately straight inclusion bands whereas close to the rim, quartz inclusion trails indicate deflection. There is no continuation between inclusion pattern of garnet and retrograde fabric (Figure 4.18). This can be interpreted that garnet porphyroblast growth is pre-tectonic with respect to retrograde fabric.

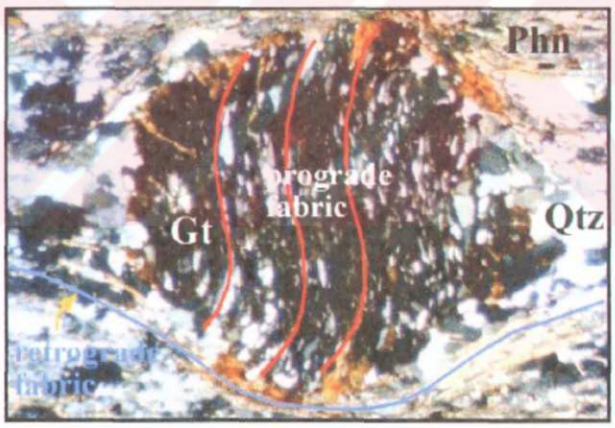


Figure 4.18 Photomicrograph showing syn-tectonic garnet crystal with respect to retrograde fabric. Width of view 4 mm. CPL.

Especially in Gölmarmara area, dynamic recrystallization which is developed after greenschist facies overprint, affected the Marble-schist series and the Metaolistostrome unit. Microtextural structures such as undulose extinction and subgrain boundaries in quartz crystals are commonly seen in the garnet-mica schists from the Marble-schist series. The trusting of the units belonging to İzmir-Ankara zone has probably caused this dynamic recrystallization on the Marble-schist series and the Metaolistostrome unit.

4.2.8. Garnet phyllite

The general mineral assemblage of this unit is " garnet - phengite - chlorite - quartz - opaque oxide ". Preferred orientation of small Phengite-II's (poor-in Si) form dominant compositional layering in the garnet phyllites. The relict Phengite-I's (rich-in Si) defining older cleavage are rarely observed in the matrix. Phengite-I crystals cutting by the main cleavage occur as independent crystals from matrix (Figure 4.19).

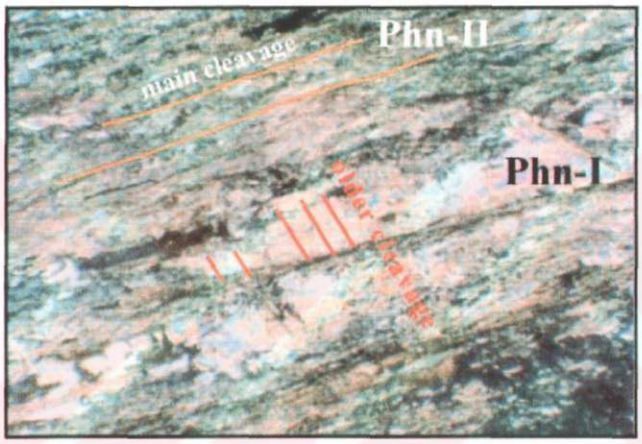


Figure 4.19 Main cleavage cutting the Phengite-II crystals belonging to older cleavage. Width of view 2.5 mm. CPL.

Elongated inclusions in garnet porphyroblasts are completely formed by quartz crystals in garnet phyllites. These inclusions form sigmoidal pattern in garnet. The asymmetry of the strain shadows indicates sinistral shear sense, which implies that the garnet rotated in anti-clockwise sense with respect to the kinematic frame during its growth. Pre-tectonic garnet shows nearly 30° of sinistral rotation with respect to main cleavage. Enclosed quartz fabric curves through garnet is not in line with external fabric. It is clear that garnet has pre-tectonic growth structure. Consequently, this garnet must have been formed during the blueschist facies metamorphism. Outside of the garnet poikiloblast, the quartz grains have a polygonal shape and are

strain-free. This indicates that static recrystallisation was developed after greenschist facies deformation.

4.2.9. Epidote amphibolite

Epidote amphibolites are observed at around Hasançavuşlar village and Gölmarmara area. The mineral assemblage of these rocks is "Ca-amphibole - garnet - epidote - albite - chlorite - sphene - rutile - calcite - quartz - ilmenite". Nematoblastic texture resulting from tabular amphibole crystals, is observed in epidote amphibolites. Kink-band structure, which is regarded to develop under low temperature and/or high strain rate (Biermann, 1981) cut the main schistosity. The epidote content of these rocks reaches up to 40 %. These minerals show a zoned structure with a inclusion-rich blue or green coloured core and a inclusion-free yellow or red coloured rim zone. The core of the epidotes contain abundant inclusions. The clinozoisite inclusions are randomly distributed in the core of epidote crystals. The older HP fabric was completely obliterated by a later fabric which is defined by green amphibole orientation. Albites cover 20 – 25 % volume of the rock and generally include epidote and amphibole inclusions. Rutils coexist with ilmenites. Chlorites are formed by the transformation from amphiboles.

4.2.10. Garnet amphibolite

The general mineral assemblage of the garnet amphibolites which are exposed in the west of Tire, is "garnet - Ca-amphibole - zoisite - epidote - albite - chlorite - rutile - sphene - calcite - quartz - opaque oxide". Ca-amphiboles cover 60 – 70 % volume of the rock. Two groups of Ca-amphiboles are distinguished. Ca-amphiboles which are assumed to be altered from Na-amphiboles, are aligned parallel to older foliation which is formed during the epidote blueschist facies conditions. Second group of Ca-amphibole are defined by dominant main foliation which has been formed during the greenschist facies. Albites with zoisite inclusions are in subordinate amounts. Sub-euhedral garnet crystals contain numerous zoisite inclusions. Zoisites which are in equilibrium with crossites in Dilek Peninsula, are

observed as inclusions in garnets. Therefore, garnet crystals must have been formed during epidote-blueschist facies metamorphism. Chlorites are secondary mineral derived from Ca-amphibole.

4.2.11. Marble

Marble is exposed over large areas in Dilek Peninsula, Selçuk and Tire. The general mineral assemblage of the marble is "calcite - albite - phengite - quartz". Calcite crystals are almost equal-in size and cover 90-95 % of mineral assemblage. Albite occurs in subordinate amounts in mineral assemblage of marble. Marble show granoblastic texture. The foliation is defined by alignment of thin and rare phengite crystals. Greenschist facies overprint is represented by alignment of thin phengite (poor-in Si) crystals.

4.2.12. General evaluation

The mineral assemblages of the main lithologies of the Marble-schist series are comparatively given in Table 4.2. Table 4.3 represents the appearance and disappearance of the minerals in the Marble-schist series. Distributions of minerals according to investigated fields (Dilek Peninsula, Selçuk, Torbalı, Tire and Gölmarmara) are shown in Table 4.4. Na-and Na-Ca amphiboles in Dilek Peninsula, chloritoids in Dilek Peninsula and Selçuk, and garnet and intensively biotites are observed in Tire and Torbalı areas. Through phengites exist in Dilek Peninsula, Selçuk and Gölmarmara. The first garnet being outcrops are seen at around Akyurt and Hasançavuşlar village, whereas, biotites mainly occurs at around Selçuk.

4.3. Metaolistostrome unit

The Metaolistostrome unit can be divided into two parts; blocks (eclogite, omphacite metagabbro, omphacite epidotite, zoisite metagabbro, Ti-metagabbro, garnet metabasite, blueschist metabasite, marble and metaserpantinite) and matrix (Garnet-phengite schist / albike phengite schist).

Table 4.2 The general mineral assemblage of units belonging to marble-schist series from Dilek Peninsula, Selçuk, Tire and Gölmarmara.

Minerals	Quartz metaconglomerate	Carbonate metaconglomerate	Blueschist metabasite	Blueschist metapelite	Chloritoid phyllite	Metabasite intrusion	Epidote metabasite	Phengite-quartz schist	Garnet-phengite-biotite schist	Garnet phyllite	Epidote amphibolite	Garnet amphibolite	Marble
Na amphibole			X	X									
Na-Ca amphibole			X										
Ca amphibole						X					X	X	
Kyanite	X												
Chloritoid	X			X	X								
Phengite	X	X	X	X	X		X	X	X	X			X
Garnet									X	X	X	X	
Biotite						X		X	X				
Albite		X	X	X		X	X	X	X	X	X	X	X
Epidote		X	X	X	X	X	X				X	X	
Zoisite		X		X	X	X	X					X	
Chlorite	X	X	X	X	X	X	X	X	X	X	X	X	
Pyrophyllite	X												
Stilpnomelane				X	X								
Sphene		X	X	X		X	X				X	X	
Ankerite							X						
Calcite		X	X	X			X				X	X	X
Quartz	X	X		X	X	X	X	X	X	X	X	X	X
Tourmaline	X			X	X			X	X				
Rutile											X	X	
Opaque mineral	X	X	X	X	X	X	X	X	X	X	X	X	

Table 4.3 Graphical representation of the facies relationship of minerals in the Marble-schist series from Dilek Peninsula, Selçuk, Tire and Gölmarmara (Akhisar).

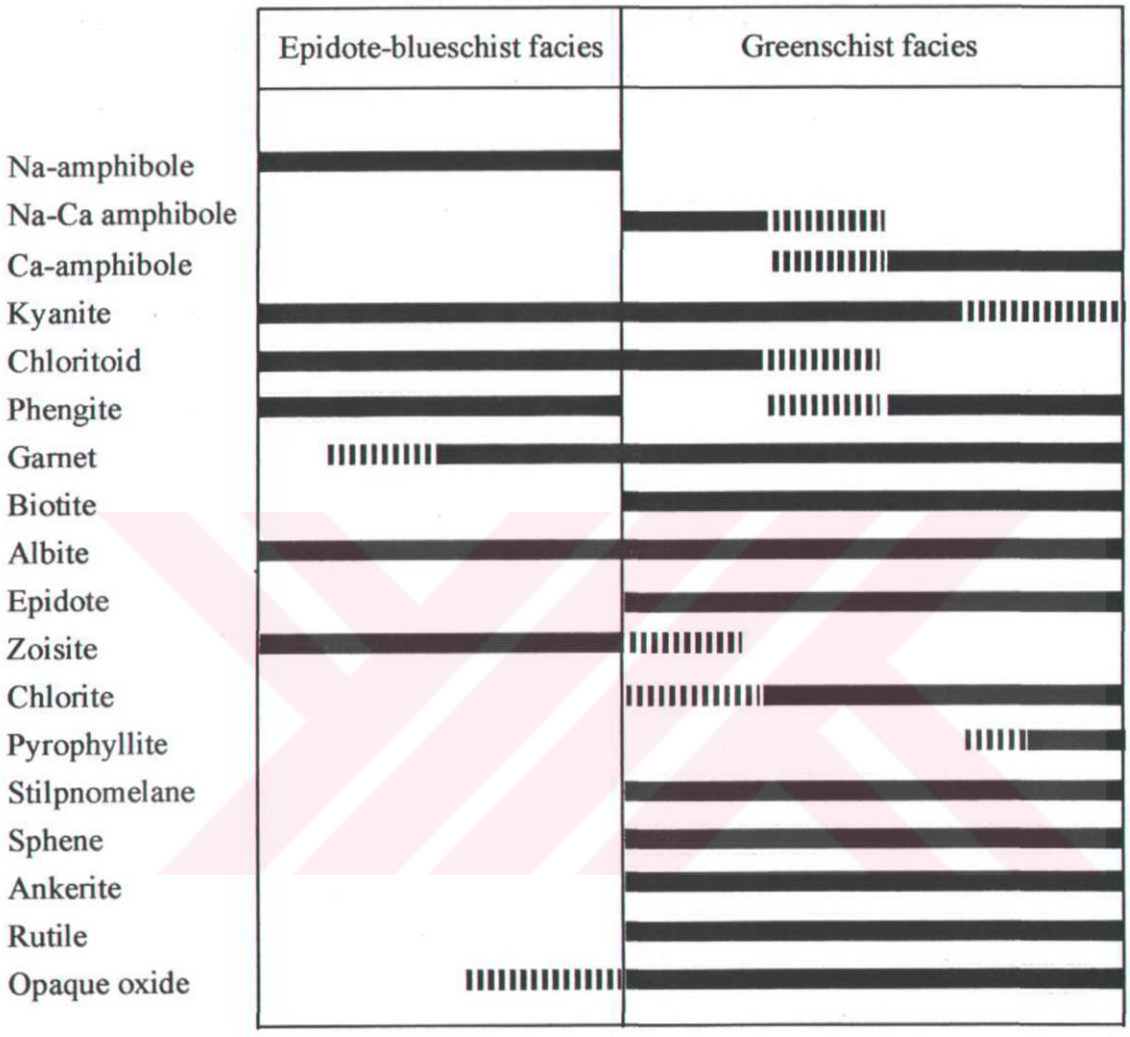
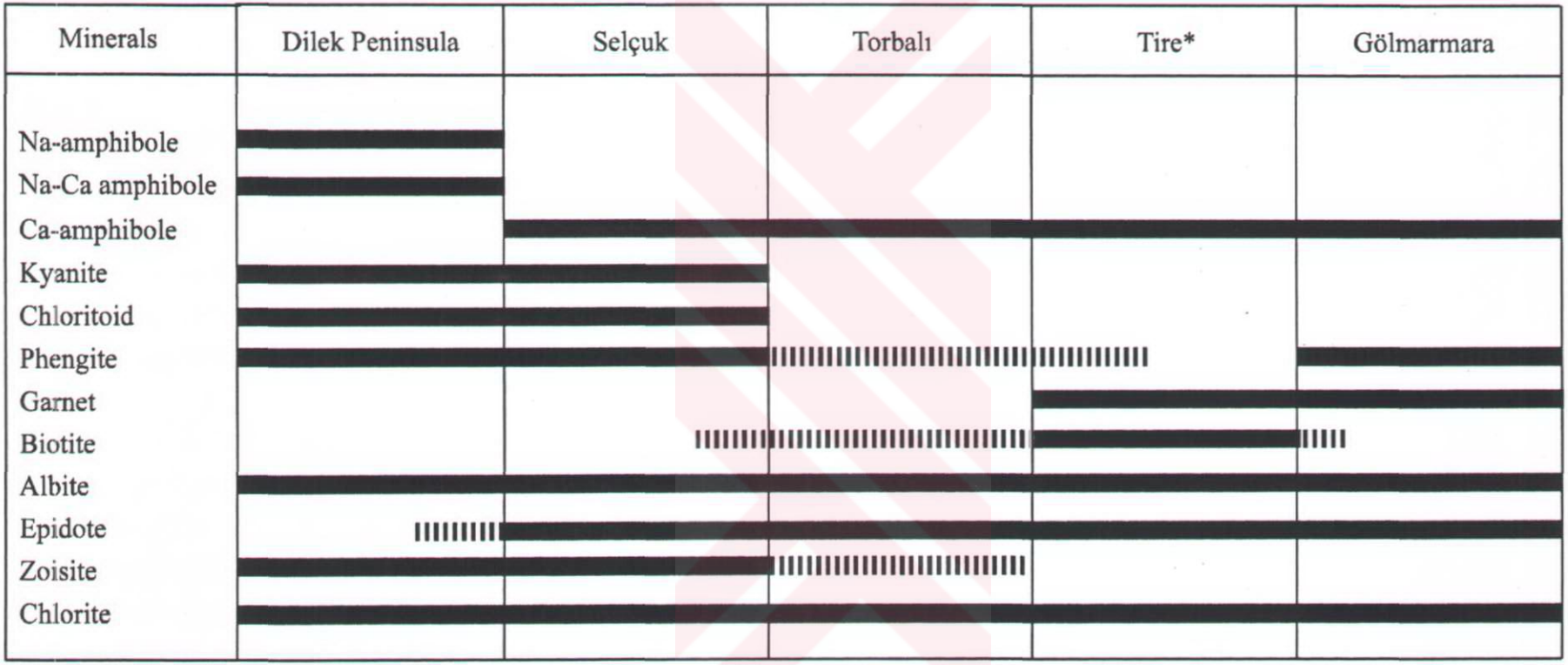


Table 4.4 Graphical representation of mineral distribution of the Marble-schist series.



* Akyurt, Hasançavuşlar and Karatekke Villages

T.C. YÜKSEKÖĞRETİM KURULU
DOKÜMANTASYON MERKEZİ

4.3.1. Matrix of the Metaolistostrome

The matrix of the metaolistostrome is mainly composed of two type schists; *albite – phengite schist and garnet – phengite schist.* The general mineral assemblage of **albite – phengite schist** is "albite - phengite - chlorite - quartz - biotite - sphene - calcite - opaque oxide". The main foliation of albite – phengite schist with lepidoblastic and porphyroblastic texture, is defined by the parallel alignment of phengites. Albites may contain epidote, quartz, albite and opaque oxide inclusions. Albite porphyroblasts include inclusion fabric which is oblique or perpendicular to the main foliation (Figure 4.20). These albites are most probably developed during the earliest deformation. Albites subjected to the rotation, have inclusion-free rims. The thickness of these rims increases with retrogression. Biotite which covers 2-3 % in mineral assemblage, is rarely accompanied by chlorite. The main foliation caused grain-size reduction in phengites. Phengites which are preserved from deformation in strain-free domains, are relatively bigger. The modal rate of biotite in albite-phengite schists is less than 3 %.

The general mineral assemblage of **garnet – phengite schists** is "garnet - phengite - zoisite - chlorite - sphene - biotite - albite - calcite - quartz - opaque oxide". Garnets can be divided into two types: zoned and skeletal garnet. Mineral inclusions cause textural zoning in garnets. These inclusions are zoisite, epidote, quartz and calcite. The zoisite does not exist in the matrix, but occur only in the garnets. Zoisite is poor-in Fe^{3+}. Euhedral zoisite inclusions with deep blue colour are intensively observed in the intermediate zone between the core and the rim of the garnets (Figure 4.21). This zone probably represents the peak P-T conditions of epidote-blueschist facies metamorphism. In both core and rim, the amount of zoisite inclusions decreases away from the intermediate zone. Syn-tectonic garnet with bluish zoisite inclusion must have been formed during epidote-blueschist facies. The second-type garnets which are relatively small-in size (<1mm), may contain intensive zoisite inclusions in the core. This type garnets must have been formed in peak P-T conditions of epidote-blueschist facies. Some garnets are skeletal in form and may contain individual quartz, albite and calcite inclusions. These crystals are

separated by thin garnet seams (Figure 4.22). Skeletal garnets having zoisite, quartz and calcite inclusions are pre-tectonic with respect to main foliation. This type of garnets have symmetric or asymmetric pressure shadows. The pre-tectonic garnet porphyroblast in respect to the main foliation shows an S-shaped inclusion fabric. These inclusions are made up of dominantly quartz, rarely albite and bluish zoisite crystals. The external foliation is not related to the internal fabric of garnet (Figure 4.23). The amount of biotite shows an increasing trend from Şirince to Tire. At around Tire, modal amount of biotite reaches up to 20% in schist (Figure 4.24). The matrix of the Metaolistostrome unit does not contain biotite in Söke, Torbalı and Gölmarmara. Some of the garnet – phengite schists are rich-in calcite. Static recrystallization exists in matrix quartz. Quartz inclusions in garnet porphyroblast are quite smaller than the matrix quartz. The opaque oxides occur preferentially along the main foliation. Formation of opaque oxide is related with greenschist facies overprint. Phengites which are product of epidote-blueschist facies metamorphism, are rich-in Fe, Mg and Si^{4+}. But these phengites are cut by oblique main foliation. In addition, these phengites are larger than Si-poor phengites which are formed in greenschist overprint. New generation and small size phengites are developed along this foliation. However these phengites are relatively poor-in Fe, Mg and Si^{4+}.

As a conclusion, mineral assemblage belonging to epidote – blueschist facies in garnet – phengite schists is " phengite (rich-in Si) + garnet (core and intermediate zone) + zoisite + albite". Whereas mineral assemblage related with greenschist facies overprint is "phengite (poor-in Si) + biotite + epidote + sphene + chlorite + quartz + opaque oxide".

4.3.2. Blocks of the Metaolistostrome

4.3.2.1 Garnet metabasite

The general mineral assemblage of this unit is " garnet - Ca-amphibole - zoisite - epidote - chlorite - albite - sphene - phengite - quartz - opaque oxide". Nematoblastic

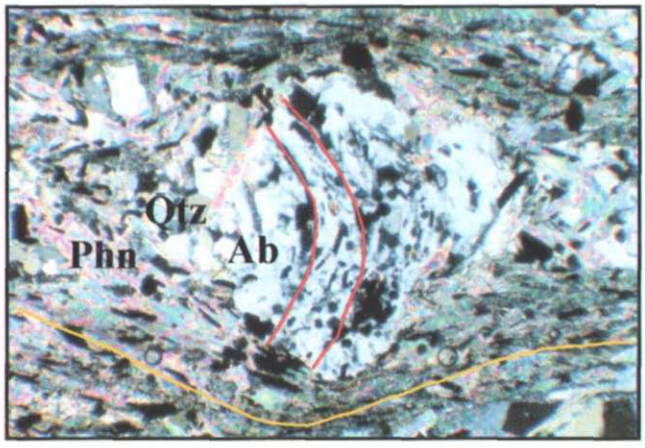


Figure 4.20 Inclusion fabric in albite which defines the early foliation, is almost perpendicular to main foliation. Width of view 2.5 mm. CPL.

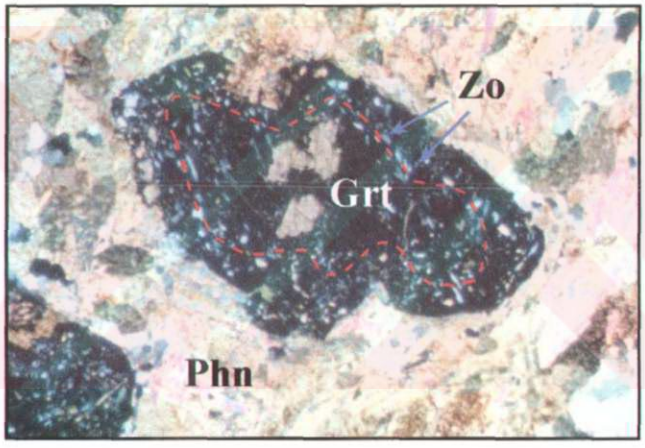


Figure 4.21 Zoisite inclusions are dominantly observed in intermediate zone of garnet. Width of view 4 mm. CPL.

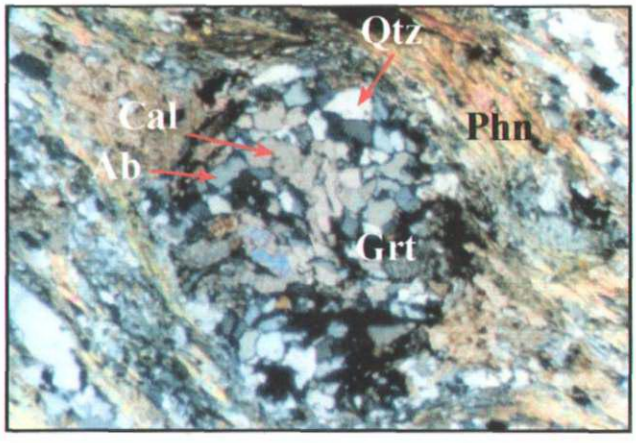


Figure 4.22 Photomicrograph showing quartz, albite and calcite crystals in skeletal garnet. These crystals are seperated by garnet seams. Width of view 4 mm. CPL.

and porphyroblastic textures are observed in garnet metabasites. Garnet porphyroblasts which cover 15-20 % in matrix, are enveloped by fine-grained Ca-amphibole, epidote, chlorite and sphene, which of all define greenschist overprint. Epidote-blueschist facies is defined by dominantly oriented inclusions of zoisite inclusion trails in garnet (Figure 4.25). Some garnet grains show pronounced systematic cracks which are perpendicular to main foliation and do not continue in the matrix. Microboudinage was developed along these cracks in garnet (Figure 4.26). Metamorphic conditions during boudinage can be estimated from mineral or mineral assemblage that grew in the boudins (Passchier and Throuw 1996). The mineral in the necks of the garnet boudins is chlorite which indicates the greenschist facies conditions. Garnet porphyroblasts contain numerous bluish coloured zoisite, albite and tiny sphene crystals. The density of inclusions gradually decreases from core to rim. The core of some zoisite crystals in garnet is red-in colour and have relatively yellowish pleochroism. This may suggest the existence of prograde greenschist facies before blueschist facies metamorphism. This case can be supported by tiny sphene crystals together with zoned zoisites in garnet porphyroblast. Garnet porphyroblasts which are developed during epidote-blueschist facies, are altered into chlorite and albite, due to greenschist facies overprint. Garnets in the early stage of greenschist overprint are replaced by chlorite and albite (Figure 4.27). In Tire area, garnet alteration starts with albite instead of chlorite. This can be attributed to the higher temperature conditions during retrograde overprint. The zoisite inclusions in altered part of garnet by chlorite are transformed into epidote (rich-in Fe^{3+}) during greenschist facies overprint (Figure 4.28). In contrast to inclusions in garnet, zoisite crystals are seen as anhedral crystal shape in groundmass. The amount of zoisite decreases together with increasing of retrogression state of the rock. The amount of epidote rich-in Fe^{3+} increases in highly retrograded rocks. In addition, epidotes can be observed as vein-fillings in the garnet metabasites. These veins are almost parallel to the main foliation. This shows that epidote–rich fluids intruded into these rocks during the greenschist facies overprint. Ca-amphiboles reaching up to 40 – 45 %, occur as small prismatic crystals. Amphibole crystals are generally aligned parallel to main foliation which is formed during greenschist overprint.

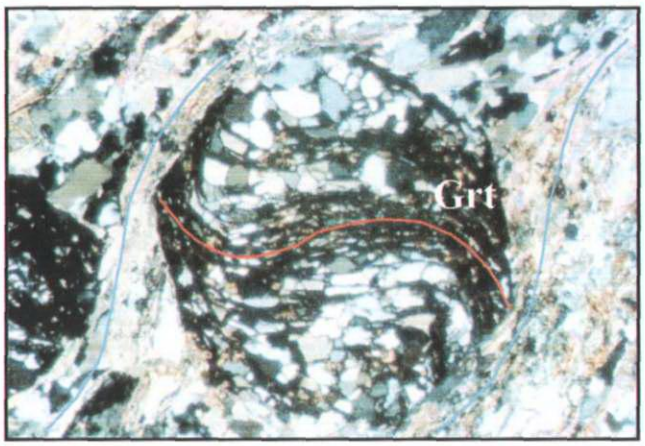


Figure 4.23 Garnet with S-shaped quartz, bluish zoisite and albite inclusions is pre-tectonic with respect to main foliation. Width of view 4 mm. CPL.



Figure 4.24 Biotite development which is parallel to main foliation of garnet-phengite schist. The amount of biotite increases with retrograde overprint. Width of view 4 mm. PPL.

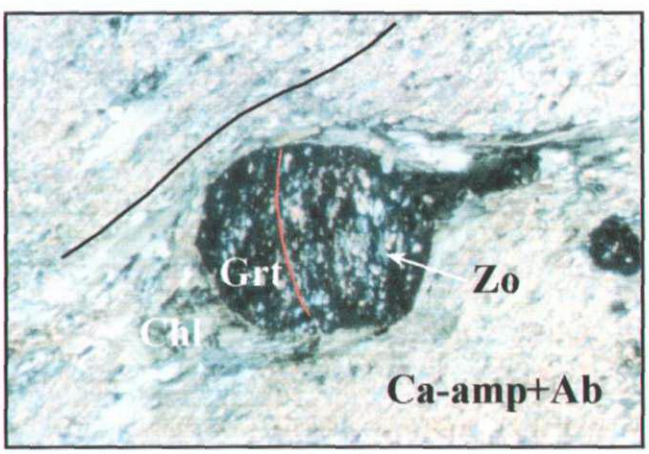


Figure 4.25 Trapped zoisite inclusions in garnet define early foliation which is oblique to main foliation. Width of view 4 mm. CPL.

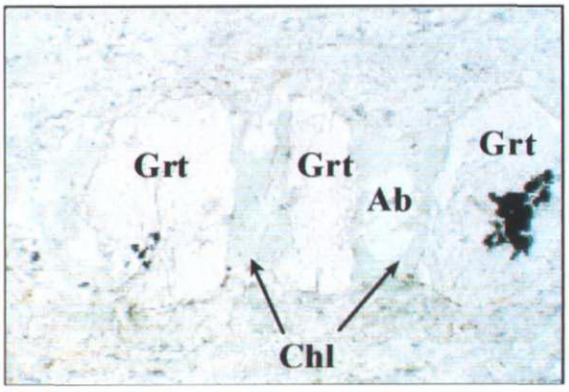


Figure 4.26 Microboudinage in garnet. Microboudinage necks are composed of chlorite. Width of view 2.5 mm. PPL.

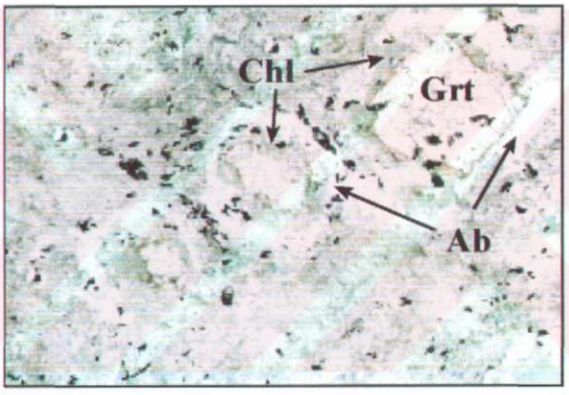
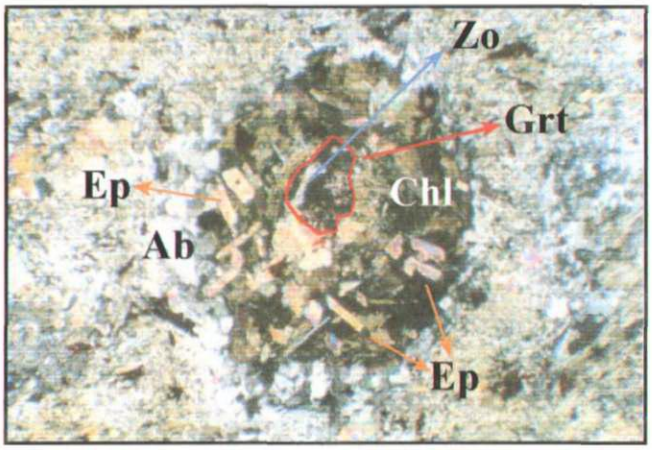


Figure 4.27 The replacement of garnet by chlorite and albite assemblage. Width of view 4 mm. PPL.

The most of these amphiboles have a mesh-like appearance composed of tiny amphibole and albite crystals (Figure 4.29). The breakdown of Na-amphibole to Ca-amphibole during the retrograde overprint leads to excess Na in these domains. The excess Na gave rise to the crystallization of the new albites among the mesh-like amphiboles. In Tire area, Ca-amphiboles are observed as perfectly aligned tabular crystals (Figure 4.30). Radial amphibole needles in albite corona developed as a result of the resorbtion of the garnet is a typically texture suggesting the decreasing of pressure (Figure 4.31a-b). Three different type of albites are found in garnet metabasites:

a)



b)

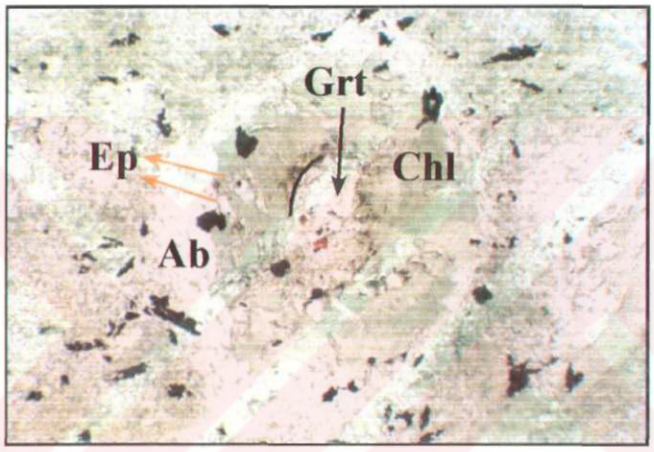


Figure 4.28 a) Zoisite inclusions are replaced by epidote in chloritized part of garnet. Whereas in the core, bluish zoisite inclusions are preserved from retrograde effect of greenschist overprint. Width of view 2.5 mm. CPL. **b)** view of (a) under PPL.

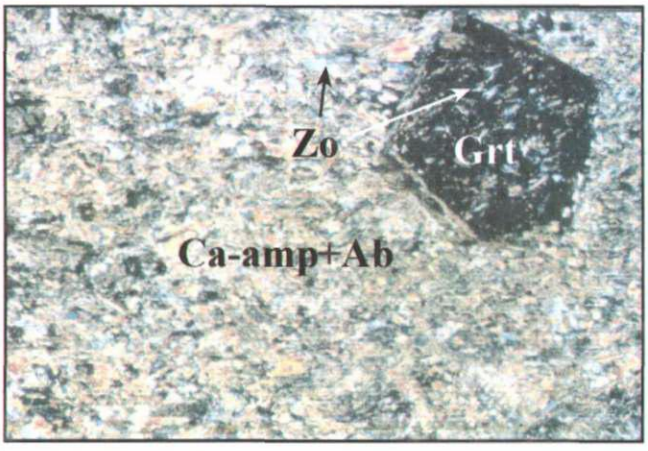


Figure 4.29 The mesh-like structure composed of small albite and amphibole crystals which are probably derived from Na-pyroxene. Width of view 4 mm. CPL.

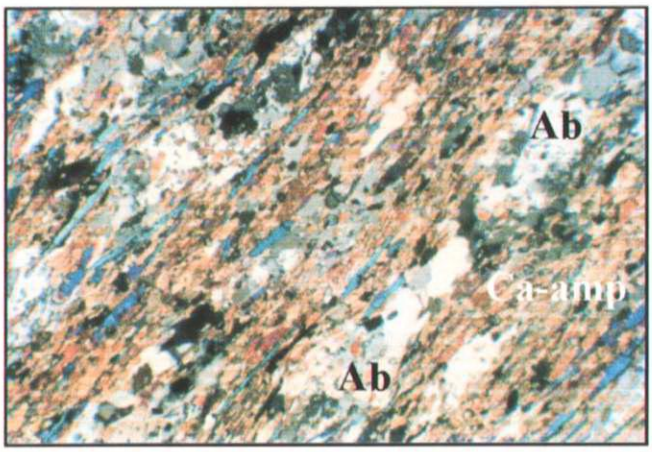
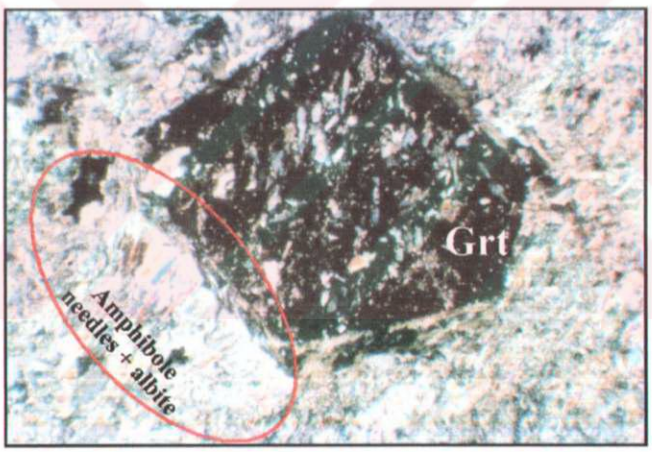


Figure 4.30 Ca-amphibole (Ca-amp) crystals are perfectly aligned parallel to main foliation and smaller albite crystals derived from bigger albite crystals. Width of view 2.5 mm. CPL.

a)



b)

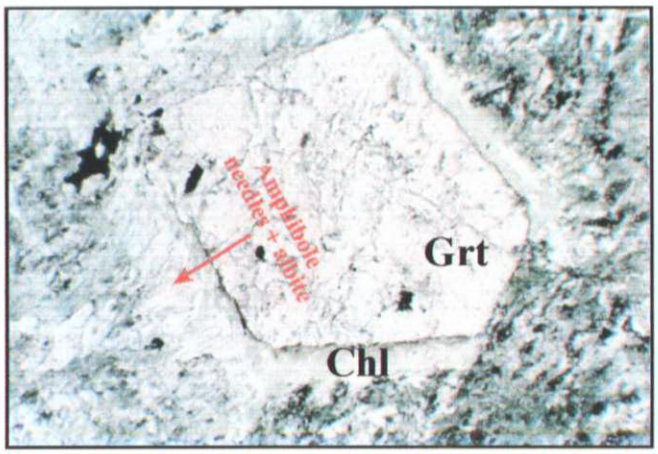


Figure 4.31 a) Radial amphibole needles in albite corona resorbing the garnet. Width of view 2.5 mm. CPL. **b)** view of (a) under PPL.

- inclusions in garnet: these albites are inclusion-free
- mesh-like crystals in matrix: these type albites are anhedral in shape and have numerous bluish zoisite and small amphibole inclusions which are consistent with the main foliation
- with chlorite as breakdown product of garnet (Figure 4.28)

The first type albite is related with epidote-blueschist facies metamorphism. The second type albite should have been formed during the initial stages of greenschist facies. In a later stage of greenschist facies, the crystal size of these albites gradually increases. In the last stage of retrograde overprint, albite crystals with inclusions are transformed into smaller crystals within previous borders of albite (Figure 4.30). This is especially observed in Tire area. The last type is also formed during greenschist facies overprint. Chlorites which cover 15 - 20 % in groundmass, are observed as secondary minerals after Ca-amphibole and garnet. In contrast to other areas studied, there is no primary or secondary chlorite in Tire area. Sphenes in groundmass occur aligned crystals parallel to main foliation and are relatively bigger than inclusions in garnet.

4.3.2.2. Blueschist metabasites

The general mineral assemblage of blueschist metabasites is " garnet - Na, Na-Ca, Ca amphibole - zoisite - epidote - albite - phengite - chlorite - calcite - quartz - opaque oxide". Although blueschist metabasites show great similarity to garnet metabasites in terms of mineral assemblage, the textural appearance and grain size of blueschist metabasites are quite different (Figure 4.32). The dominant texture type in these rocks is nematoblastic. Epidote vein-fillings are almost concordant with main foliation. Besides rare Na-amphibole inclusions, the subhedral garnet grains contain bluish zoisite and opaque oxide inclusions. Na-amphibole (crossite) inclusions in garnet are observed both in core and rim (Figure 4.33). These inclusions may show alteration to Na-Ca amphibole. Garnets with Na-amphibole and zoisite inclusions, should has been occurred during the epidote-blueschist facies conditions.

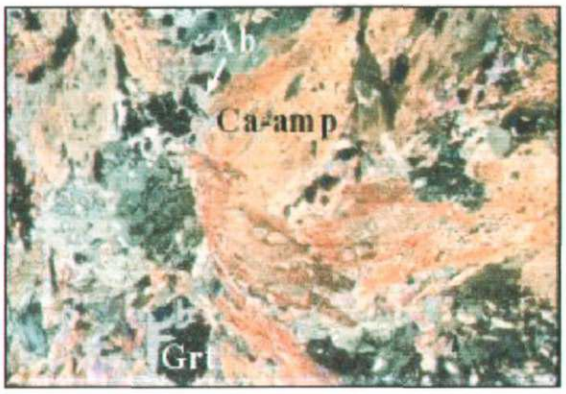


Figure 4.32 Photomicrograph showing the general texture of relict Na-amphibole - bearing blueschist metabasites. Na-amphiboles are commonly observed as a inclusion in garnet. Width of view 4 mm. CPL.

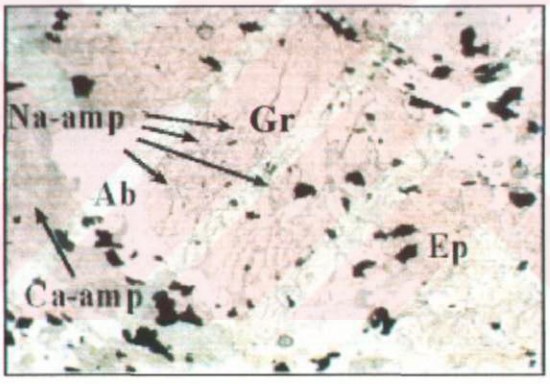


Figure 4.33 Na-amphibole (crossite) inclusions in garnets in blueschist metabasites. Width of view 2.5 mm. PPL.

The effects of retrograde overprint in garnet are represented by the development of albite, epidote and rarely chlorite along the rims (Figure 4.34a). Bluish coloured zoisite of epidote group minerals are trapped in garnet. Epidotes with reddish and yellowish birefringence which are product of greenschist facies overprint, replace the garnet along the rims (Figure 4.34b). In progressive stages of retrograde overprint, albite corona around garnet are getting larger (Figure 4.35). Amphibole needles which are radial to garnet, coexist with albite. This texture has been formed as a result of decreasing of pressure. The existence of epidote in albite fields around garnet is commonly observed in this type depressurization texture (Figure 4.34a).

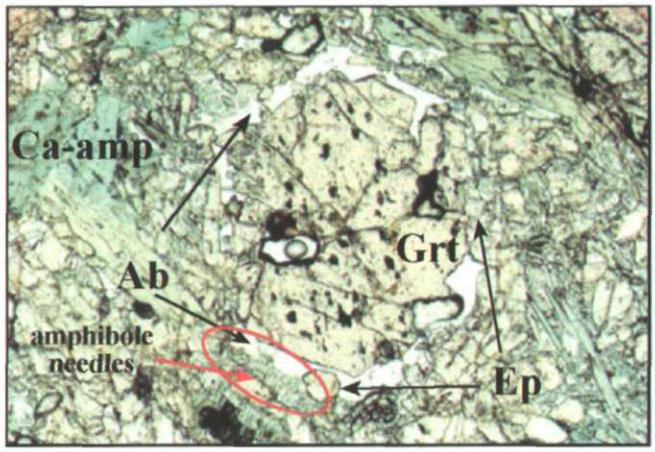


Figure 4.34a Photomicrograph showing decompression texture around garnet. Width of view 1.5 mm. PPL.

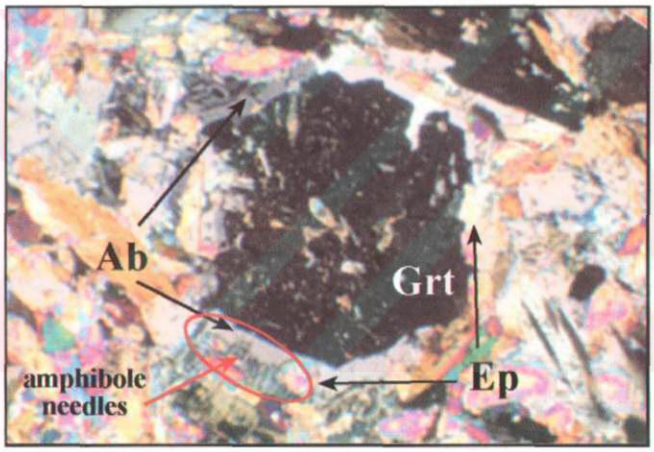


Figure 4.34b Epidote crystals growing in albite corona during the decompression. Width of view 2.5 mm. CPL.

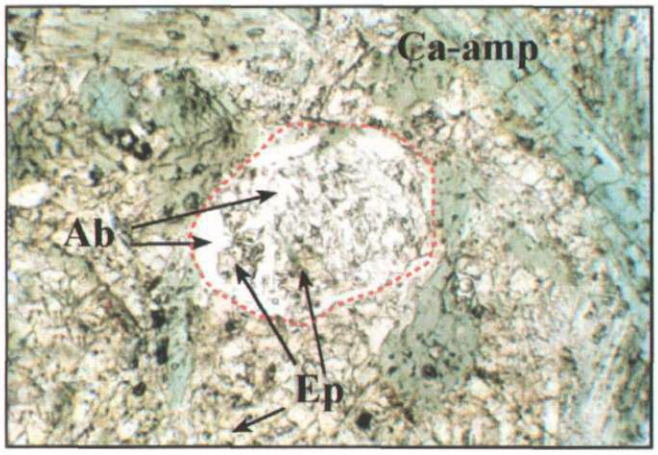


Figure 4.35 Garnet replaced by albite due to decompression. Garnet pseudomorp is denoted by dotted line. Width of view 2.5 mm. PPL.

Amphiboles which cover 30-40 % of the matrix, are dominantly Ca-amphiboles in composition. Na-and Na-Ca amphiboles are found in garnet as inclusions. Na-and Na-Ca amphiboles are rarely seen in matrix. Na-amphiboles in matrix are rimmed by green coloured barroisite and/or actinolite (Figure 4.36).

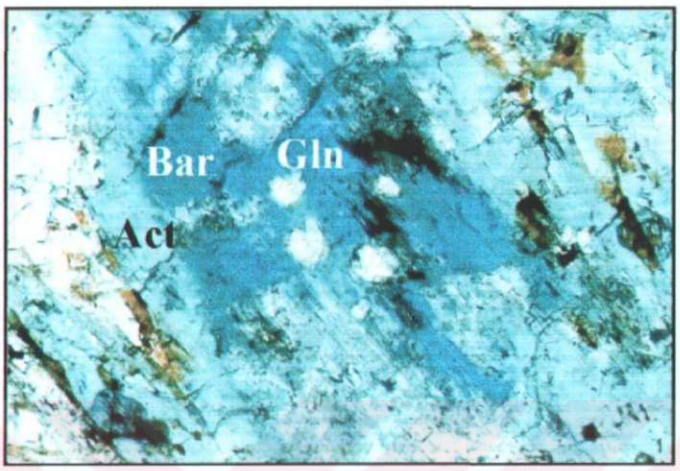


Figure 4.36 Photomicrograph showing transition from crossite through barroisite to actinolite in blueschist metabasites. Width of view 1 mm. PPL.

The epidote-rich parts of blueschist metabasites may contain over 70% epidote. Epidotes are observed as individual crystals, inclusions in albite or vein-filling. Most of the epidote crystals are zoned. The core of epidote is full of inclusions composed of opaque oxide, whereas, the rim is almost inclusion-free. Both the core and rim have the same pleochroism colour (yellowish) and should have been formed during greenschist facies overprint. Like in garnet metabasite, epidote-vein fillings which have been formed during retrograde overprint, enclose some Ca-amphiboles but not chlorites. Epidote crystals in vein-fillings are coarse grained when compared to epidotes in groundmass. Albite crystals, up to 1.5 mm in diameter, are generally anhedral, strongly poikiloblastic, and contain abundant inclusions of Ca-amphibole and epidote. There is a mesh-like breakdown structure which is composed of Na-Ca amphibole and albite, around Na-amphiboles (Figure 4.37a). The similar texture is also observed in garnet metabasites. In further stages, albite corona progress into Ca-amphibole grain (Figure 4.37b). In later stage, the relict Ca-amphibole needles are observed in albite corona (Figure 4.37c). Thus new albite crystals with small Ca-amphibole crystal are appeared in groundmass. To summarize, these results can be

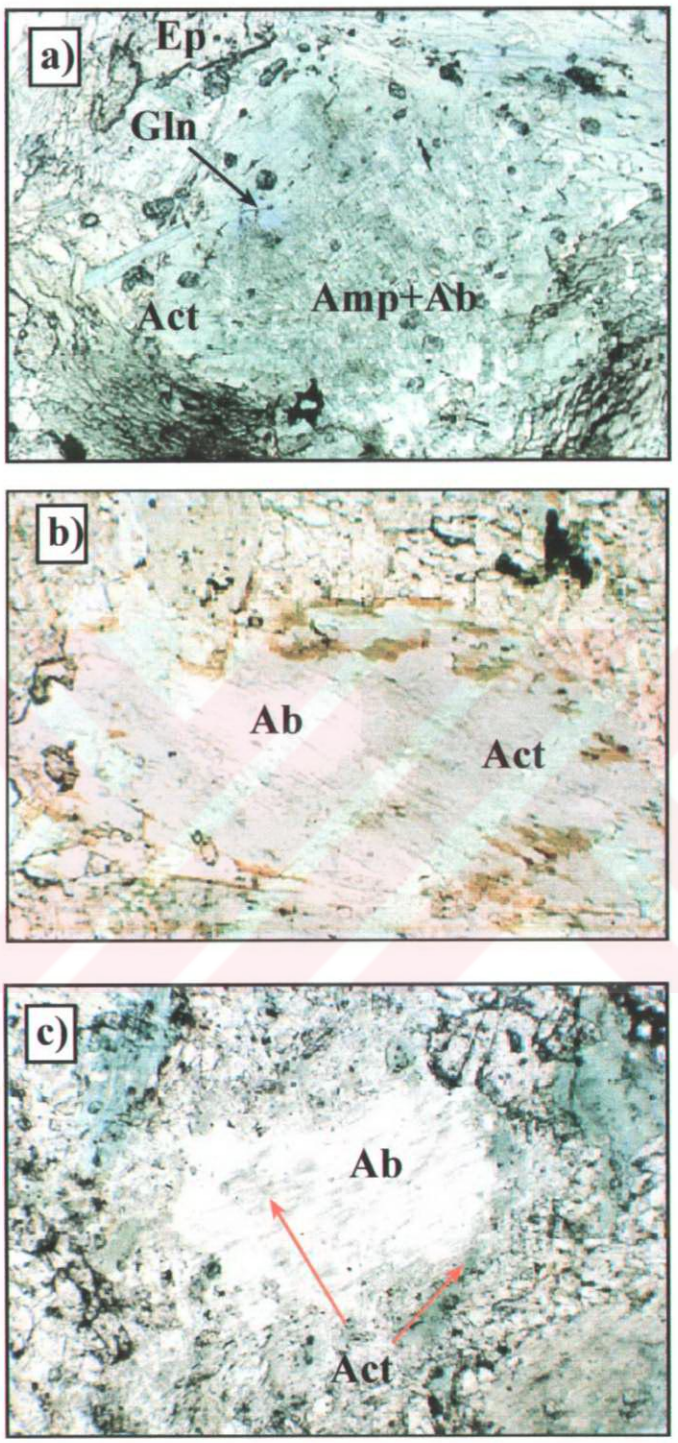


Figure 4.37 a) mesh-like breakdown structure which is composed of amphibole and albite around crossite in the core of crystal. Width of view 2.5 mm. PPL. **b)** in later stage, crossite in the core is completely replaced by Na-Ca and/or Ca amphibole and albite fields are getting larger with greenschist overprint. Width of view 2.5 mm. PPL. **c)** in late stage, the large amount of Ca-amphibole is replaced by albite. The relict Ca-amphibole needles are observed in albit field after Ca-amphibole. Width of view 2.5 mm. PPL.

excluded for albites: 1) albite crystals with inclusions of epidote and Ca-amphibole should have been transformed from garnet (Figure 4.38), but 2) albite without epidote inclusions is from Na-amphiboles (Figure 4.37c).

4.3.2.3. Eclogite

The general mineral assemblage of eclogites is " garnet - clinopyroxene - zoisite - epidote - Ca-amphibole - albite - sphene - apatite - phengite - quartz - opaque oxide". Clinopyroxenes in eclogites can be texturally divided into five groups (Cprx-IA, Cprx-IB, Cprx-IIA, Cprx-IIB and Cprx-III). Omphacites with pale green pleochroism and coarse grained crystals are named as Cprx-IA. Cprx-IA commonly has high Jd content (24 to 45 mol%). Omphacite inclusions especially in garnet are called as Cprx-IB. Their Jd contents are range from 30 to 36 mol%. Cprx-IIA is represented by omphacite aggregates. They have jadeite content ranging between 20 and 35 mol%. Omphacites with more greenish pleochroism are named as Cprx-IIB. Jd content of Cprx-IIB ranges from 12 to 29%. The symplectites (Cprx-III) are composed of vermicular and granular intergrowths of plagioclase (albite) and clinopyroxene. Symplectites are poor-in jadeite end-member (3 to12 mol%). The detailed information about clinopyroxenes in eclogite is given in mineral chemistry chapter. But in this part, only the textural characteristic of clinopyroxene IA, IIA, IIB and III are given. In Gölmarmara area, there is cprx-IIB, instead of cprx-IIA. Cprx-IIA has corroded rims and is enclosed by symplectite field (Figure 4.39)

In eclogites, each light-green patch in plane-polarized light (PPL) is seen a single coarse crystal (Cprx-IA) or composite grain of many small crystals (polygonal aggregate) of pale-green pleochroic clinopyroxene (Cprx-IIA). Boundaries of each crystal in Cprx-IIA patch are poorly defined. Garnets with S-shaped zoisite inclusion are syn-tectonic with respect to deformation in eclogite facies. Figure 4.40 – 4.45 gives stages of transformation from Cprx-IA through Cprx-III to amphibole crystals. Coarse- grained omphacite (cprx-IA) which is formed in eclogite facies, looses its stability due to retrograde overprint. As a result of this, all Cprx-IA is extensively altered. The Cprx - IA grain boundaries are not smooth and are corroded by

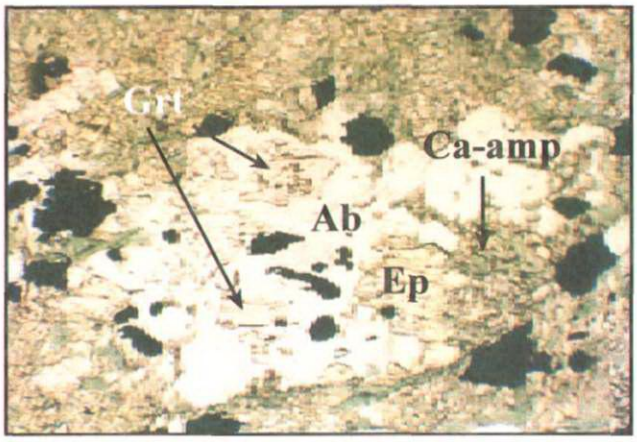


Figure 4.38 Photomicrograph showing albite, epidote and Ca amphibole (Ca-amp) assemblage after garnet. Width of view 2.5 mm. PPL.



Figure 4.39 Greenish omphacite (cprx-IIA) corroded by symplectitic intergrowth of Cprx-III and albite. Maximum jadeite mol % of Cprx-IIB is 27. Width of view 2.5 mm. PPL.

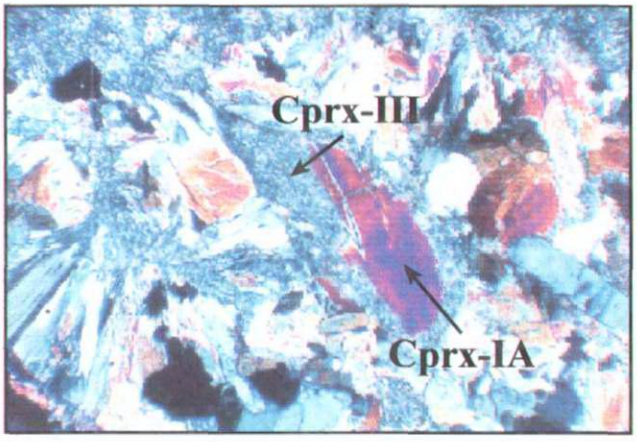


Figure 4.40 Photomicrograph showing the omphacite (Cprx-IA) rimmed by symplectitic intergrowth of Cprx-III and albite. Width of view 2.5 mm. CPL.

symplectites. Very fine-grained albite – Cprx-III symplectites occur as coronas in a mesh-like fashion around entire crystal (Figure 4.40). In the following stage, coarse-grained omphacite (Cprx-IA) altered into omphacite aggregates (Cprx-IIA) (Figure 4.41). By growing symplectite field in respect to omphacite or omphacite aggregates, garnet with zoisite inclusion can be corroded by

- epidote, albite and Ca-amphibole assemblage (Figure 4.42a-b)
- single epidote corona (Figure 4.43)
- single albite corona (Figure 4.44).

In this stage, a thin epidote zone is observed at the rim of bluish coloured zoisites. In later stages, euhedral amphibole crystals are seen in symplectite fields (Figure 4.45a). The number of amphibole crystals increase during the greenschist overprint. In addition, the fine-grained symplectite groundmass gradually changes into acicular amphibole crystals (Figure 4.45b). After this stage, symplectite fields are rarely seen. Ca-amphiboles meka up 50 – 60 % of the groundmass. Most of the zoisite crystals are transformed into pleochroic and iron-rich epidotes during the retrograde overprint. Some of these epidotes are zoned (Figure 4.46) and the amount of Fe^{3+} increases from core (0.40) to rim (0.45). This also suggests the existance of retrograde overprint. Garnets with zoisite inclusion include crack systems which are almost perpendicular to main foliation. Ca-amphibole and dominantly albite fill these cracks. The cracks should have been formed during the early stage of decompression. Zoisite inclusions in garnet are also transformed into epidote due to retrograde overprint. Some eclogite samples are cut by broad albite veins. Symplectization in omphacite is preferentially observed along these veins (Figure 4.47). Albite veins cut garnet, zoisite and omphacite but not Ca-amphibole and iron-rich epidotes. These veins should have been formed during the initial stage of retrograde overprint. Ca-amphibole and epidote crystals which are parallel to main foliation, formed during the greenschist overprint, occur on the albite veins (Figure 4.48). Bluish zoisites (iron-poor and non-pleochroic) are in equilibrium with omphacite (Figure 4.49) and are observed as inclusions in garnet. Some eclogites are rich-in epidote group minerals and contain garnet with dominant zoisite inclusion. The modal abundance of epidote group minerals in these eclogites can reach up to 40 %.

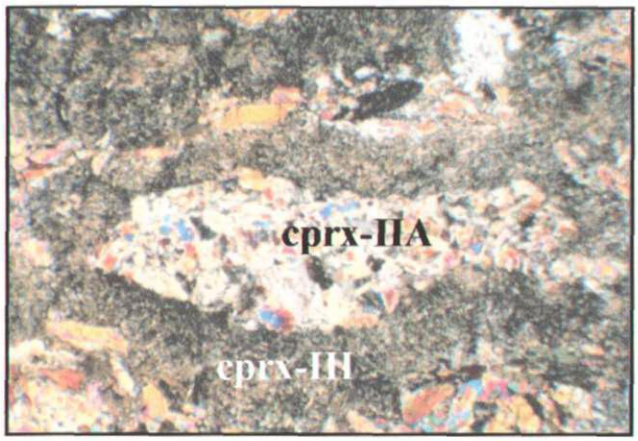


Figure 4.41 Omphacite (cprx-IA) pseudomorph composed of omphacite aggregates (cprx-IIA) which are rimmed by symplectite (cprx-III and albite). Width of view 2.5 mm. CPL.

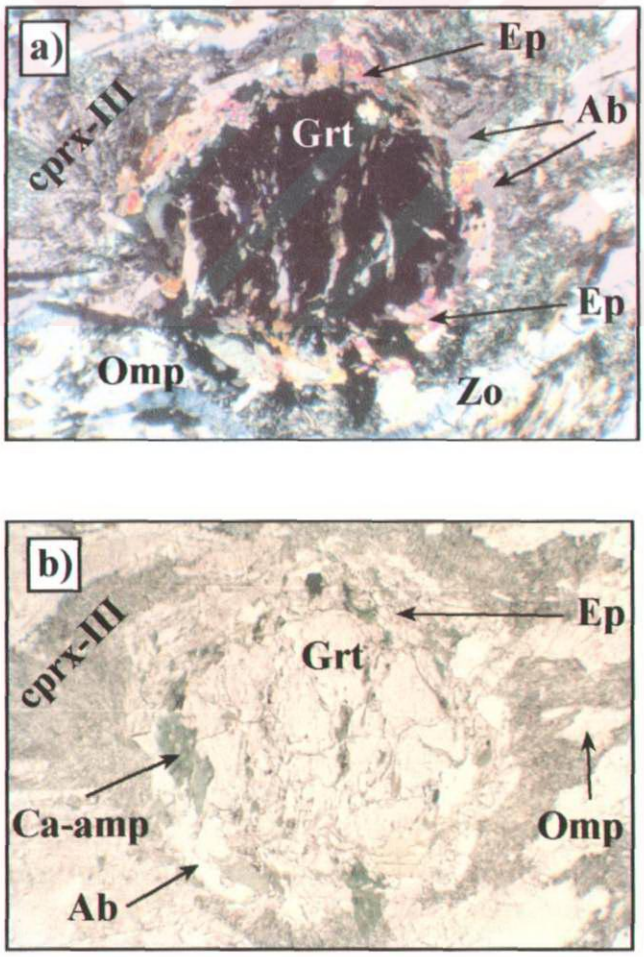


Figure 4.42 a) Photomicrograph showing garnet partly replaced from rim to core by epidote, albite and Ca-amphibole. Width of view 2.5 mm. CPL. **b)** view of (a) under PPL.

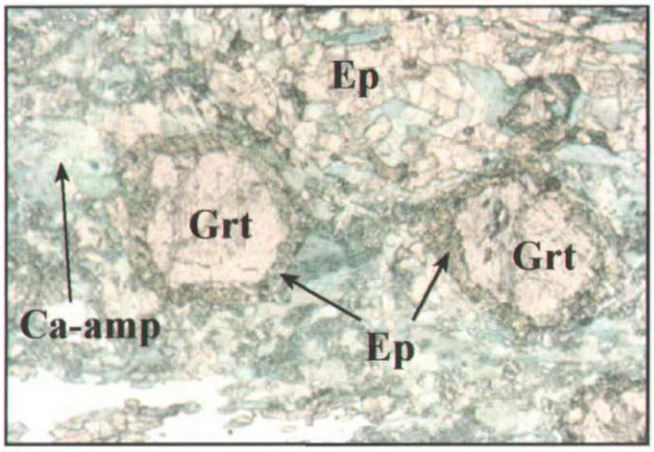


Figure 4.43 Photomicrograph showing the garnet partly replaced along the rim by epidote corona. Width of view 2.5 mm. PPL. Width of view 4 mm. PPL.

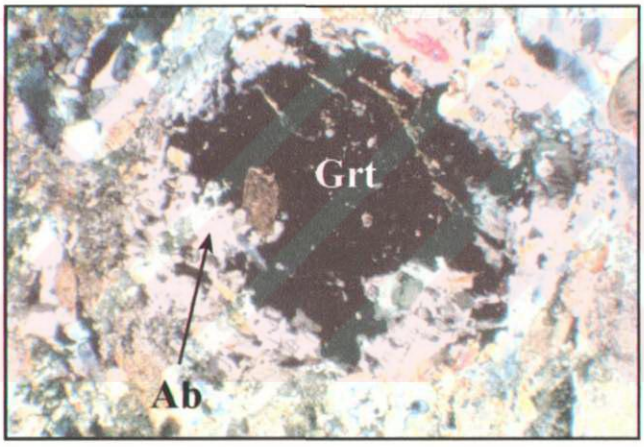


Figure 4.44 Partly replacement of garnet by albite. Width of view 2.5 mm. CPL.

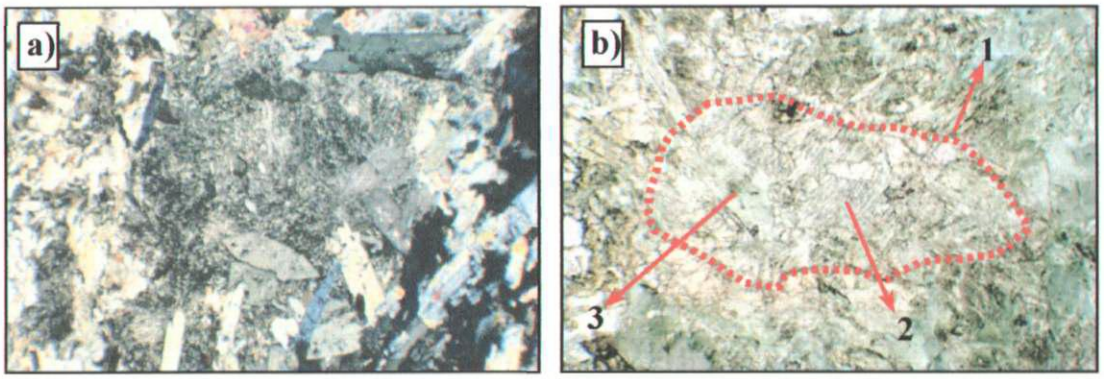


Figure 4.45 a) euhedral and newly generated Ca-amphibole crystals growth in symplectite fields. Width of view 2.5 mm. CPL. **b)** symplectite field filled by needles and coarse crystals of Ca amphibole. 1: pseudosymplectite field, 2: amphibole needles, 3: coarse amphibole. Width of view 2.5 mm. PPL.

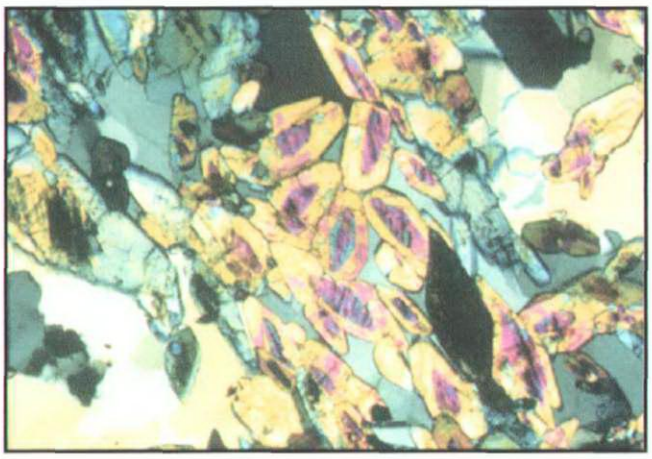


Figure 4.46 Photomicrograph showing zoned epidotes. Fe^{3+} content of these epidotes increase from core to rim. Width of view 2.5 mm. CPL.

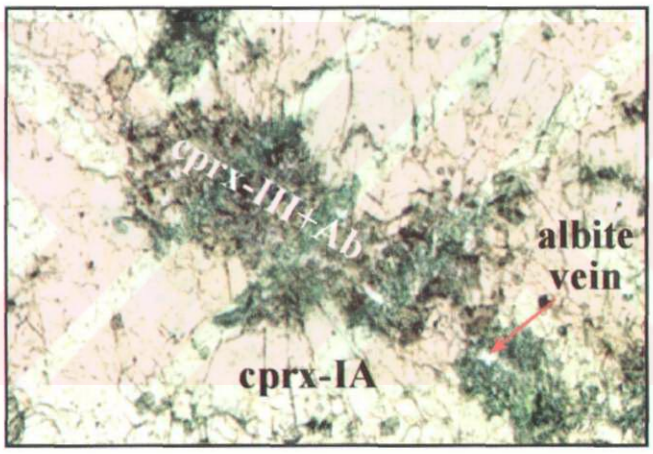


Figure 4.47 Symplectites developed along albite-vein filling which cuts the omphacites (cprx-IA). Width of view 2.5 mm. PPL.

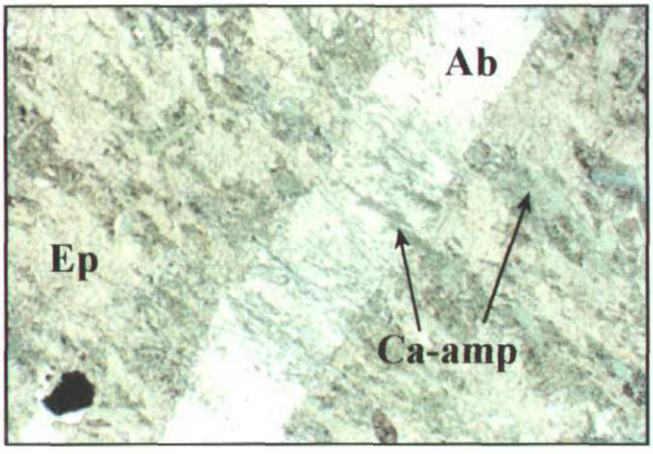


Figure 4.48 Photomicrograph showing Ca-amphibole and epidote crystals in albite vein. These crystals are aligned parallel to main foliation which is formed by greenschist overprint. Width of view 4 mm. PPL.

Multi-zoning structure in garnet is defined by zoisite and omphacite inclusions from core to rim (Figure 4.50). Except for two samples, this zoning is interpreated as growth zoning (see the mineral chemistry chapter).

4.3.2.4. Omphacite epidotite

The general mineral assemblage of the omphacite-epidotite is " clinopyroxene (IA, IIA and III) - zoisite - epidote - albite - Ca-amphibole - calcite - opaque oxide". These rocks display textural and compositional resemblances to eclogite. The only difference between these two rock types is the common occurrence of garnet in eclogite. The general view of texture from fresh omphacite-epidotite is given in Figure 4.51). The amount of epidote group minerals and omphacites reach up to 40 % and 35 %, respectively. In highly retrograded samples, alignment of tabular Ca-amphibole and epidote crystals causes to the development of the nematoblastic texture (Figure 4.52). Pale-green pleochroic omphacites (Cprx-IA) are unhedral in form and are replaced along the margins by fine-grained clinopyroxene (Cprx-III) and albite symplectitic intergrowth (Figure 4.51). Cprx-IA is in equilibrium with blue coloured zoisite. There is no reaction rim between these two minerals. Most of the omphacite grains show transformation to symplectite with different stages due to retrograde overprint under decompression conditions. The rim of coarse omphacite grains (Cprx-IA) are made up of small polygonal omphacite aggregates (Cprx-IIA). This zone is replaced by the fine-grained symplectitic intergrowths which are developed into aggregates. Newly generated and euhedral Ca-amphibole crystals have grown in the symplectitic zone during the retrograde overprint (Figure 4.53). In later stages, the amount of Ca-amphibole in the rock increase by the consumption of symplectites (Figure 4.52). The modal abundance of pleochroic and iron-rich epidote rises together with increasing amount of amphibole (Figure 4.52).

4.3.2.5. Omphacite metagabbro

The general mineral assemblage of the omphacite metagabbros is " clinopyroxene (IA, IIA and III) - Ca-amphibole - zoisite - epidote - albite - rutile - sphene – opaque

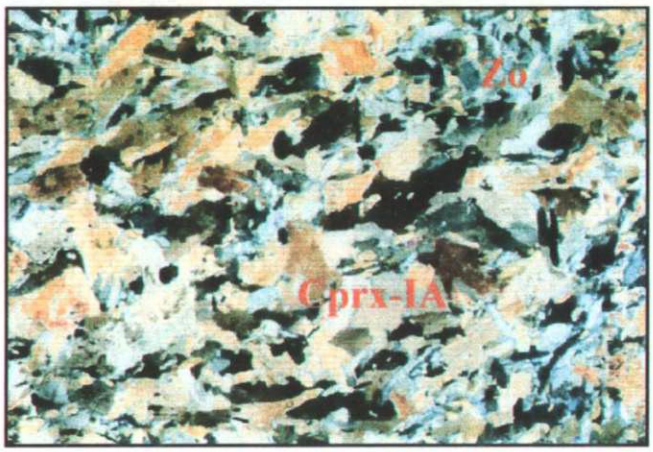


Figure 4.49 Photomicrograph showing omphacites (Cprx-IA) which are in equilibrium with zoisite. There is no reaction texture between these minerals. Width of view 4 mm. CPL.

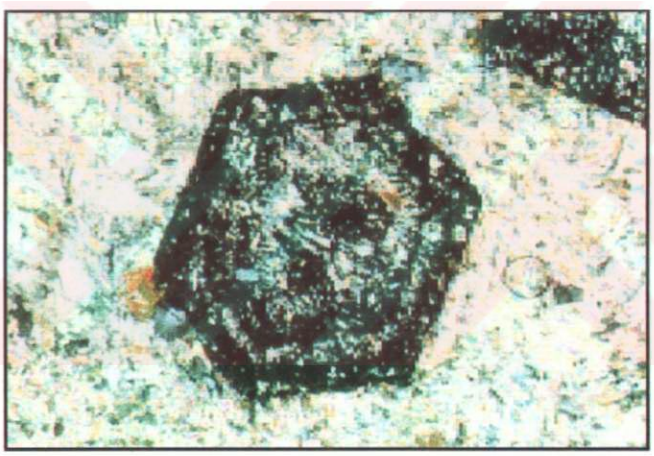


Figure 4.50 Photomicrograph showing multi-zoning structure in garnet. Inclusions in garnet are made up of zoisite and omphacite. Width of view 4 mm. CPL.

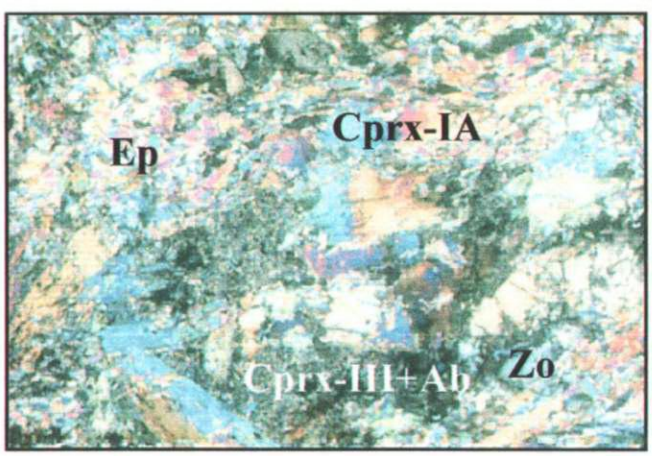


Figure 4.51 Photomicrograph showing the general texture of omphacite epidotites. Omphacites (Cprx-IA) are replaced by fine-grained symplectitic intergrowth (Cprx-III and albite). Width of view 4 mm. CPL.

oxide". Omphacites are unhedral in shape and are observed as coarse grains (Cprx-IA) or aggregates (Cprx-IIA) in groundmass. Coarse-grained omphacites are rimmed by polygonal omphacite aggregate and fine-grained symplectite which is composed of jadeite-poor clinopyroxene (Cprx-III) and albite (Figure 4.54). The development of aggregates continues up to complete consumption of omphacite crystal by the omphacite aggregates. There is two types amphibole in omphacite metagabbros. They are Ca-amphibole in composition (Leake et al., 1978). These can be easily discriminated from each other. The features belonging to the first type amphiboles (I) which is edenitic hornblende in composition, are:

- coarse grained
- numerous bluish coloured zoisite inclusions
- irregular boundary with symplectite
- alteration into albite (Figure 4.55)
- dominantly unhedral crystals

The features of the second group amphiboles (II) are :

- small size
- smooth boundary with symplectite
- euhedral crystals in symplectite fields
- no alteration and zoisite inclusion

The first type amphiboles in Laird and Albee (1981) diagrams are plotted into high-pressure amphibole field as shown in following chapter. In many samples, the boundaries between Ca-amphibole and omphacite (partly symplectized) are regular (Figure 4.56). The reaction texture which is occurred during the retrograde overprint, is observed between some Ca-amphiboles (I) and omphacite. The reaction rim is composed of small, euhedral Ca-amphiboles (II) and albite minerals (Figure 4.57). In addition, Ca-amphiboles (I) can be altered into albites during the retrograde overprint (Figure 4.55). The amount of epidote inclusions is quite low in Ca-amphiboles and commonly occur in the matrix. Rutile which is one of the eclogite facies minerals,

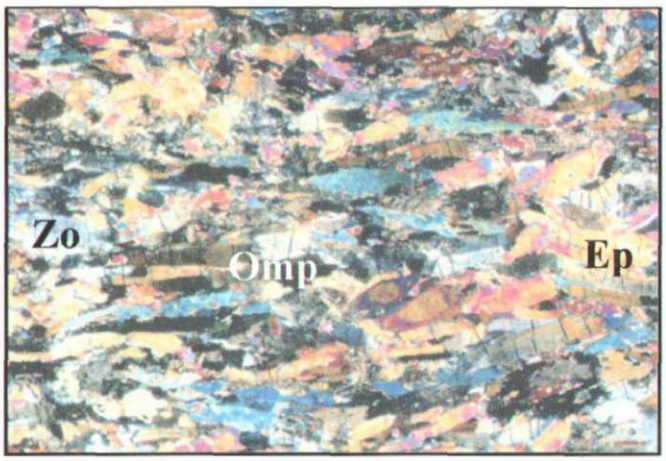


Figure 4.52 Nematoblastic texture is observed in retrograde samples of omphacite epidotites. In these samples, symplectite fields are quite few. Width of view 4 mm. CPL.

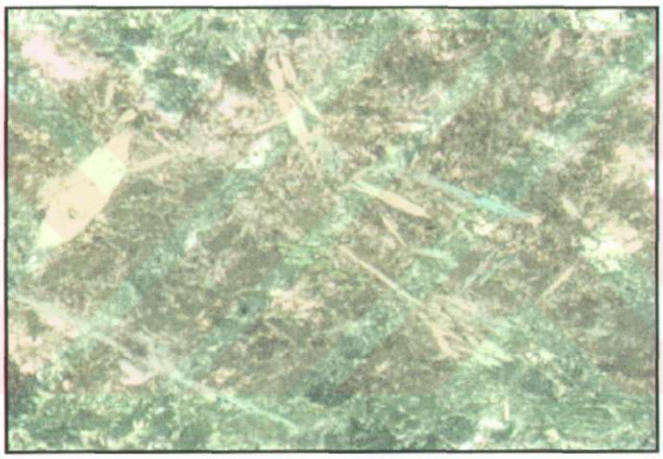


Figure 4.53 Photomicrograph showing acicular amphibole crystals growth in fine-grained symplectite groundmass. Width of view 4 mm. PPL.

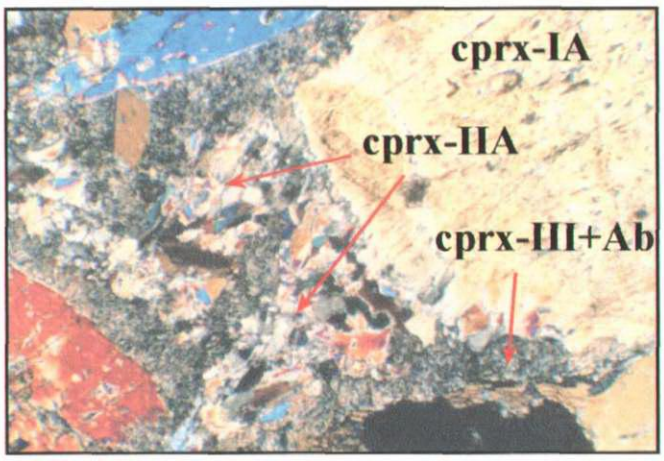


Figure 4.54 Photomicrograph showing the transformation stages from coarse omphacite (cprx-IA) through omphacite aggregate (cprx-IIA) to symplectite (cprx-III and albite). Width of view 4 mm. CPL.

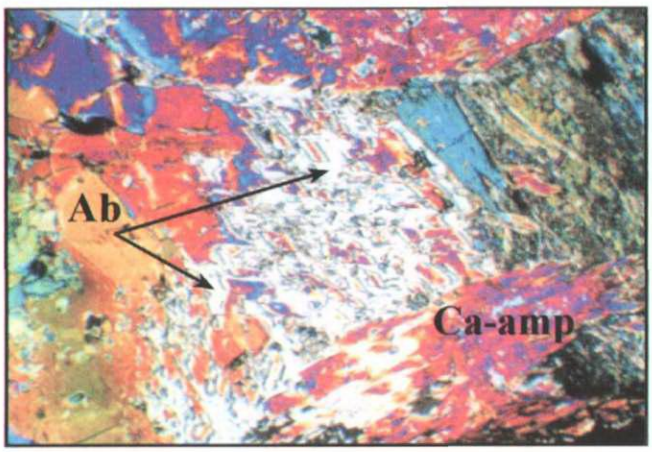


Figure 4.55 The breakdown of Ca amphibole belonging to HP metamorphism, to albite. Width of view 2.5 mm. CPL.

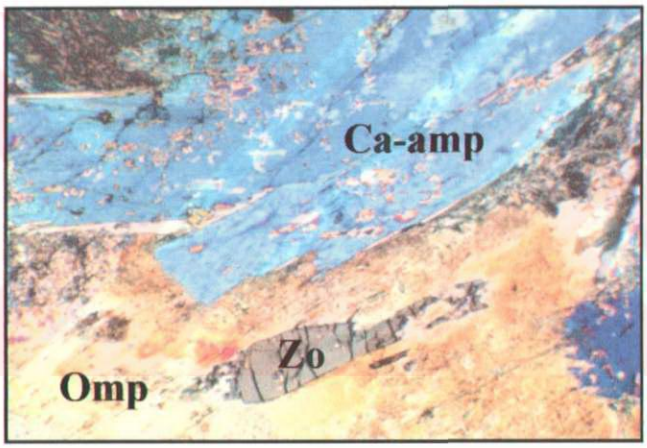


Figure 4.56 Ca amphibole belonging to HP metamorphism, and omphacite are equilibrium with each other. Width of view 2.5 mm. CPL.

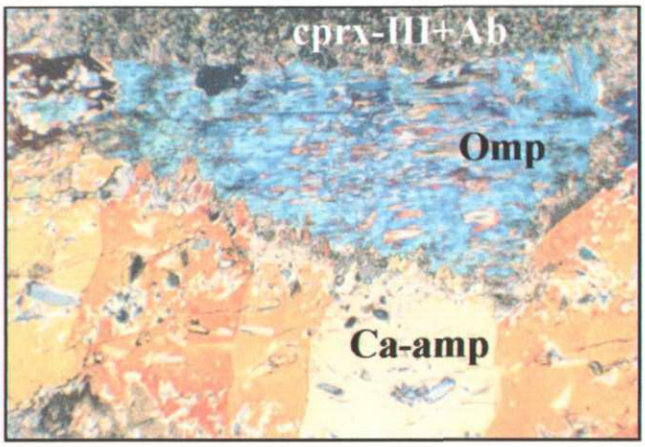


Figure 4.57 Reaction texture developed between omphacite and Ca amphibole in retrograde overprint. Width of view 2.5 mm. CPL.

is commonly rimmed by sphene which represents the effects of retrograde overprint (Figure 4.58).

4.3.2.6. Zoisite metagabbro

The general mineral assemblage of the zoisite metagabbros is " Ca-amphibole - zoisite - albite - sphene - epidote - opaque oxide". The modal amount of Ca-amphibole and zoisite crystals reach up to 80 % in matrix. Alignment of prismatic and newly generated Ca-amphibole crystals in matrix defines the main foliation. There are two groups of Ca-amphiboles in matrix. The features of the first and second groups are given below.

First group:

- coarse-grained
- perpendicular or oblique to main foliation (Figure 4.59)
- microboudinage structure

Second group:

- small-in size
- parallel to main foliation
- generation from first group amphiboles

The orientation of the coarse-grained Ca-amphibole crystals are parallel to earliest foliation. Deformation related with greenschist overprint gave rise to the grain size reduction on Ca-amphiboles (I). By this mechanism, new prismatic amphiboles are generated from Ca-amphibole (I) (Figure 4.60). Ca-amphibole (II) and albite occur along the microboudinage necks in Ca-amphibole (I) (Figure 4.61). Albite can be formed by breakdown of Ca-amphibole (I). Albites formed by this way, are very fine-grained (Figure 4.62) and are observed coexisting with small zoisite crystals in groundmass. Coarse, prismatic and bluish coloured zoisite crystals are seen in equilibrium with omphacite in eclogite and, omphacite and Ca-amphibole in omphacite metagabbro. In this unit, coarse zoisite crystals show grain size reduction due to penetrative deformation during the greenschist overprint (Figure 4.63). The existance of coarse grained and bluish coloured zoisite in matrix, the typical

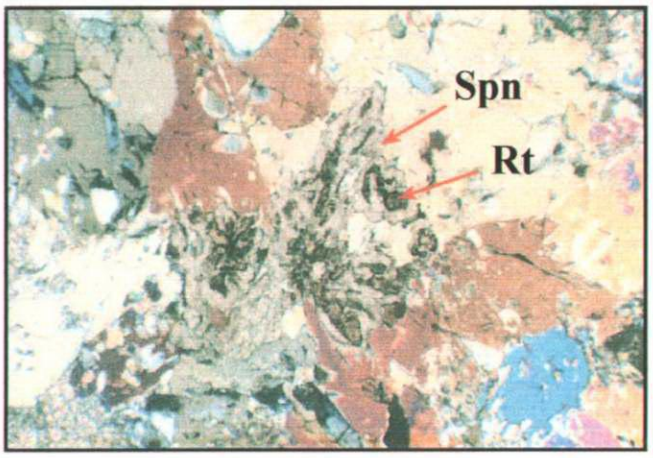


Figure 4.58 Rutile is rimmed by sphene which is interpreted as an evidence of greenschist facies overprint. Width of view 2.5 mm. CPL.

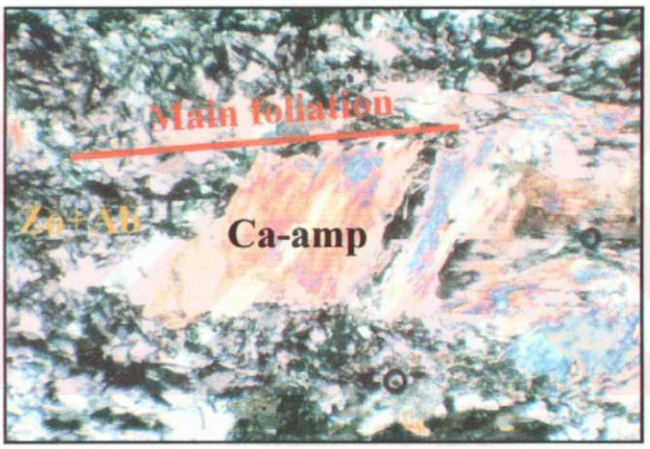


Figure 4.59 Main foliation cutting the Ca amphibole (I). The main foliation is defined by small zoisite and albite crystals. Width of view 2.5 mm. CPL.

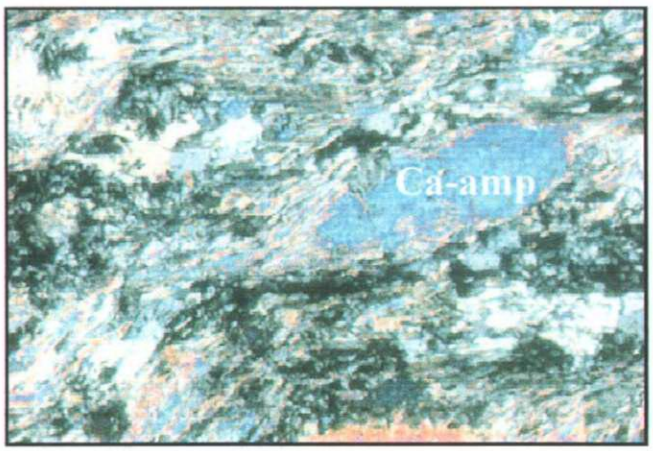


Figure 4.60 Small prismatic amphibole crystals which are derived from coarse-grained amphibole, surround the earliest Ca-amphibole (Ca-amp I) grain. Development of small amphibole (Ca-amp II) crystals are related with deformation during the greenschist overprint. Width of view 4 mm. CPL.

breakdown of Ca-amphibole (I) to albite, the equilibrium of Ca-amphibole (I) with coarse-grained zoisite suggest that Ca-amphibole (I) may have been formed during the eclogite facies.

4.3.2.7. Ti-metagabbro

The general mineral assemblage of Ti-metagabbros is "Ca-amphibole - albite - epidote - sphene - chlorite - apatite - opaque oxide". Nematoblastic texture defined by the orientation of Ca-amphibole crystals are observed. Ca-amphiboles are partly replaced by chlorites. Anhedral albite crystals reaching up to 20-25 %, occur among Ca-amphiboles. Albites include small zoisite and epidote inclusions. The size of albite crystals increase with retrograde overprint. In highly retrograded samples, albites with epidote inclusions form big porphyroblasts. The modal abundance of secondary chlorite reachs up to 40 % in these type of rocks. In Gölmarmara area, albite porphyroblasts contain epidote and euhedral amphibole crystals. Ca-amphibole show rosette shape crystal form. Sphene crystals with modal amount of about 10-15 %, can be observed as euhedral or small unhedral crystal mass among the Ca-amphiboles (Figure 4.64). Small and anhedral aggregates of sphene are almost parallel to main foliation. In Gölmarmara area, these crystals are randomly distributed in matrix. Apatite occurs as an accessory mineral in Ti-metagabbros, and in some may amount to as much as 5 %.

4.3.2.8. Fuchsite-albite schist

The general mineral assemblage of these rocks is " fuchsite - albite - zoisite - epidote - chlorite - Ca-amphibole - quartz - opaque oxide". Chromium is normally present in muscovites only in trace amounts, but chromian muscovites with as much as 6 per cent Cr_2O_3 are called as fuchsite (Deer et al. 1991). The presence of Cr in fuchsite leads to green colour. The modal percentage of fuchsite is about 20-25 in matrix. Albite and fuchsites form dominant minerals in these rocks. Fuchsites align parallel the main foliation which is formed during the greenschist overprint (Figure 4.65).

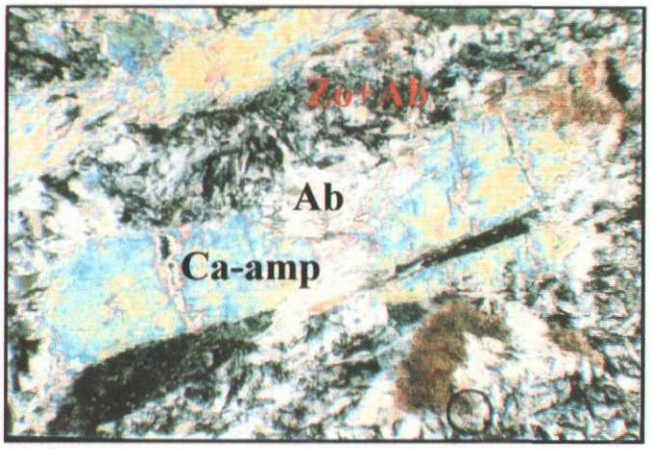


Figure 4.61 Development of albite in microboudinage necks of Ca amphibole (I) representing the greenschist facies overprint. Width of view 2.5 mm. CPL.

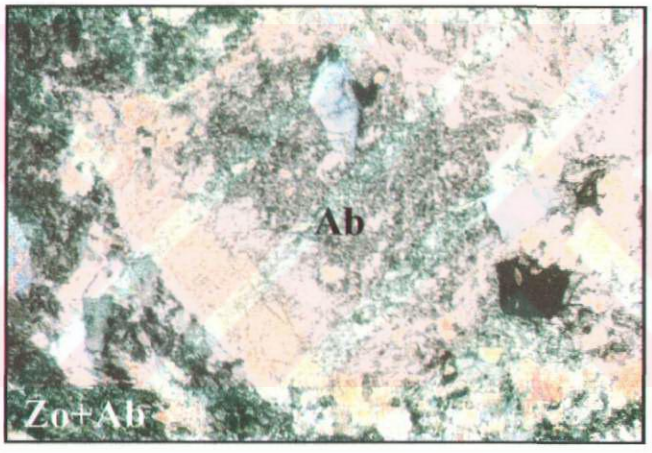


Figure 4.62 Photomicrograph showing the replacement of Ca amphibole (I) by small albite crystals. Width of view 4 mm. CPL.

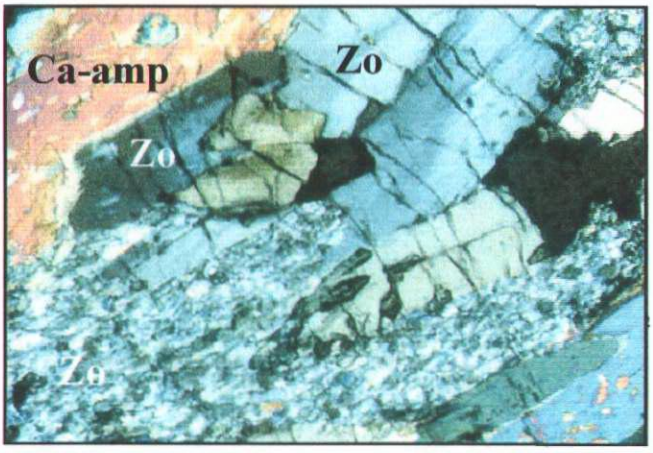


Figure 4.63 Coarse grained bluish coloured zoisites belonging to epidote-blueschist facies show grain-size reduction due to deformation during the greenschist overprint. Width of view 4 mm. CPL.

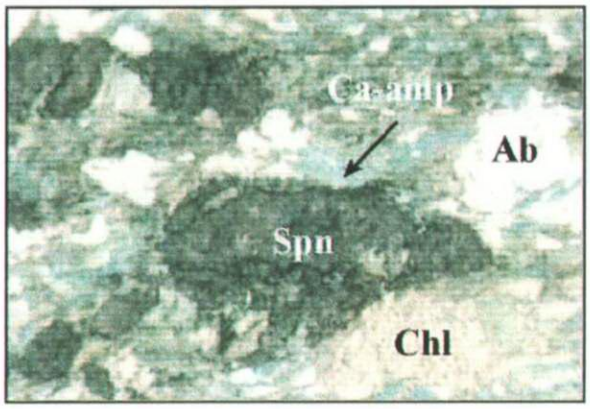


Figure 4.64 Sphene crystals are commonly observed in Ti-metagabbros as clusters composed of small sphene crystals. Width of view 2.5 mm. PPL.

Fuchsites are replaced by chlorite. The amount of secondary chlorite can reach up to 15-20 %. Subhedral albites, 25-30 % in matrix, contain small zoisite, epidote and fuchsite inclusions. Inclusion pattern in albite is consistent with main foliation. Bluish coloured zoisites which are parallel to main foliation, occur as small crystal aggregates. Modal abundance of epidote group minerals reachs up to 40 %. Ca-amphiboles are rarely seen in fuchsite-albite schist. All amphibole crystals are unhedral. Except for the presence of fuchsite, the mineral assemblage of this unit shows great resemblance to zoisite metagabbros. Fuchsite-albite schists may represent the highly deformed part of zoisite metagabbro.

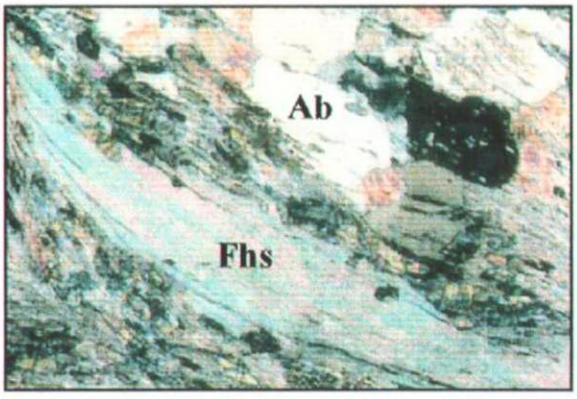


Figure 4.65 Photomicrograph showing fuchsite (Fhs) layer aligned parallel to main foliation. Width of view 4 mm. CPL.

4.3.2.9. Marble

The general mineral assemblage of marbles is " calcite + quartz + phengite ± epidote". Granoblastic texture is dominantly observed in these rocks. In highly deformed or phengite rich parts, lepidoblastic texture is also seen due to elongated calcite crystals and alignment of phengites which defines main foliation. The amount of calcite can reach up to 90 % by volume. The rest is made up of quartz, phengite and epidote. The quartz crystals show undulose extinction.

4.3.2.10. Metaserpentinite

The general mineral assemblage of metaserpentites is "serpentine (antigorite?) - relict pyroxene - opaque oxide". Metaserpentinites are almost entirely made up of serpentine together with opaque oxide. Fine grained metaserpentinites with low birefringence display a characteristic mesh texture. Some metaserpentinites contain relic pyroxene within the network of serpentine but not so such relic grains are present, except for pyroxene. Unhedral pyroxene crystals are rarely seen in metaserpentinites. The relict pyroxenes are surrounded by a brown zone which is possibly hematite stained.

4.3.3. General Evolution

The mineral contents of blocks and matrix in metaolistostrome, and the facies relationship of these minerals are given in Table 4.5 and 4.6, respectively. In addition, distributions of minerals from different areas are shown in Table 4.7. Table 4.8 shows the distribution of some important minerals from the Metaolistostrome unit and the Marble-schist series. The first occurrence of garnet in the Marble - schist series is recognized in Tire area (Akyurt and Hasançavuşlar villages). Whereas garnet in the Metaolistostrome unit is firstly seen in Söke area (Gümelez village).

Table 4.5 The general mineral assemblage of matrix and blocks of the Metaolistostrome.

Minerals	Matrix of the Metaolistostrome		Blocks in the Metaolistostrome									
	albite-phengite schist	garnet-phengite schist	Garnet metabasite	Blueschist metabasite	Eclogite	Omphacite epidotite	Omphacite metagabbro	Zoisite metagabbro	Ti metagabbro	Fuchsite-albite schist	Marble	Metaserpentinite
Clinopyroxene-IA					X	X	X					
Clinopyroxene-IIA					X	X	X					
Clinopyroxene-IIB					X							
Clinopyroxene-III					X	X	X					
Garnet		X	X	X	X							
Na-amphibole				X								
Na-Ca amphibole				X								
Ca-amphibole			X	X	X	X	X	X	X	X		
Phengite	X	X	X	X	X						X	
Biotite	X	X										
Zoisite		X	X	X	X	X	X	X		X		
Epidote			X	X	X	X	X	X	X	X	X	
Albite	X	X	X	X	X	X	X	X	X	X		
Chlorite	X	X	X	X					X	X		
Sphene	X	X	X		X		X	X	X			
Fuchsite										X		
Quartz	X	X	X	X	X					X	X	
Serpentine												X
Apatite					X				X			
Rutile							X	X				
Calcite	X	X		X		X					X	
Opaque mineral	X	X	X	X	X	X	X	X	X	X		X
Relict pyroxene												X

Table 4.6 Graphical representation of the key minerals in the Metaolistostrome.

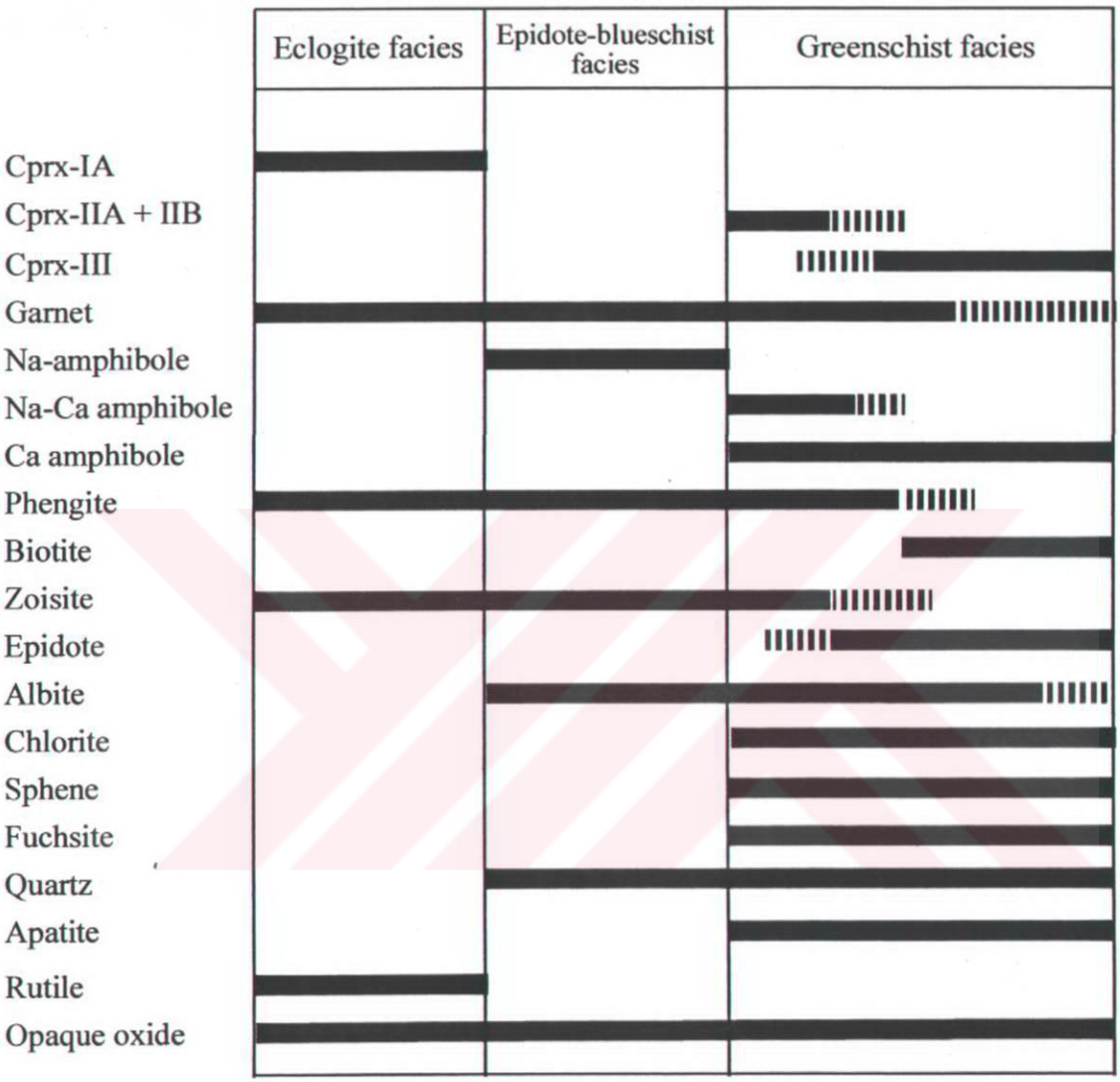


Table 4.7 Graphical representation of the key minerals of the Metaolistostrome from different areas

Minerals	Söke*	Selçuk	Torbalı	Tire**	Gölmarmara
Cprx-IA	■	■			
Cprx-IIA	■	■	■		
Cprx-IIB					■
Cprx-III	■	■	■	▮▮▮▮▮▮▮▮▮▮▮▮▮▮▮▮▮▮▮▮▮▮▮▮	■
Garnet	■	■	■	■	■
Na amphibole		■			
Na-Ca amphibole		■			
Ca amphibole	■	■	■	■	■
Phengite	■	■	■		■
Biotite				■	
Zoisite	■	■	■		■
Epidote	■	■	■	■	■
Chlorite	■	■	■	▮▮▮▮▮▮▮▮▮▮▮▮▮▮▮▮▮▮▮▮▮▮▮▮	■
Sphene	■	■	■	■	■

* Gümelez and Kayaş Villages
** Karatekke Village

Table 4.8 The distribution of some minerals of metaolistostrome and the Marble-schist series.

	Dilek Peninsula	Söke / Kuşadası	Selçuk	Tire	Gölmarmara
Marble-schist series	Na amphibole Phengite Chloritoid Zoisite -----	Ca amphibole Phengite Chloritoid Zoisite -----	Ca amphibole Phengite Chloritoid Zoisite -----	Ca amphibole Biotite ----- Epidote Garnet	Ca amphibole Phengite/Biotite ----- Epidote Garnet
Metaolistostrome unit	Not existing	Omphacite Garnet Phengite Zoisite -----	Omphacite Garnet Phengite Zoisite Na amphibole	----- Garnet Biotite Epidote Ca amphibole	Omphacite* Garnet Phengite Zoisite Ca amphibole

* (cprx-IIA)

4.4. Lycian Nappes

This unit is composed of red phyllites and dolomites. The general mineral assemblage of ***red phyllites*** is "albite - calcite - white mica - chlorite - quartz - carpholite - opaque oxide". Lepidoblastic and dominantly mylonitic texture (Figure 4.66) is observed. The deformation caused grain-size reduction in this unit. Albite porphyroblasts show grain boundary migration and mortar texture around porphyroblast due to deformation (Figure 4.67).



Figure 4.66 Mylonitic texture observed in red phyllites. Width of view 4 mm. CPL.

In strain free domains, it is possible to recognise the white mica and chlorite. In addition, carpholite which defines high-pressure and low-temperature metamorphism, is exist in this unit. Fibrous carpholite preferentially occurs in quartz-rich parts of rock. In many places, carpholite fibres have undergone chloritization. ***Dolomites*** are almost completely made up of dolomites. The effective deformation, like in red phyllites, is also observed in dolomite crystals. The boundaries of dolomite crystals is not clear. Dolomites have undergone grain-size reduction due to deformation. The dominant texture type is mylonitic texture.

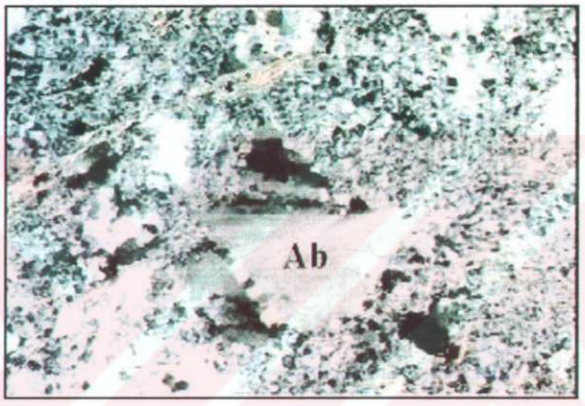


Figure 4.67 Mylonitic texture and grain boundary migration in albites. Width of view 4 mm. CPL.

CHAPTER FIVE

MINERAL CHEMISTRY

5.1. Introduction

Mineral analyses were performed on a JEOL JXA-8900 and JEOL JXA-8800 electron microprobes at the Institut für Geowissenschaften at the Johannes Guttenberg University of Mainz and at the Museum für Naturkunde at the University of Humbolt, Berlin, Germany, respectively. Natural and synthetic standards were used for most of major and minor elements. The instruments are equipped with 5 and 4 wavelength-dispersive automated spectrometers and operates with a beam current 20 nA, 15 kV accelerating voltage and a beam size of 2 μm, and 25 s counting time. Data were reduced by a ZAF correction program. Detailed features of selected amphibole, clinopyroxene, garnet, epidote, phengite, chloritoid, biotite, muscovite, chlorite and plagioclase analyses from metaolistostrome unit and marble-schist series are given below.

5.2. Amphiboles

Amphiboles from numerous samples of blueschist, eclogite, omphacite-epidotite, omphacite metagabbro and garnet amphibolite were analysed. All amphibole analyses have been calculated on the basis of 23 oxygens and 13 cations (comprising eight in tetrahedral and five in octahedral sites). The standard amphibole formula is taken as a $A_{(0-1)}$ (=Na,K) B_2 (=Na,Ca,Mg,Fe^{2+}) C_5 (=Mg,Fe^{2+},Al,Fe^{3+}) T_8 (=Si,Al)

O_{22} $(OH)_2$. M4 for B, M1+M2+M3 for C and T for tetrahedral site terms were used in expression of occupancies of sites. Leake et al., (1978) was used for the nomenclature and terminology.

5.2.1. Amphiboles in blueschist metabasites

A total of 5 samples were analysed from three different locations in Dilek Peninsula belonging to marble-schist series and Şirince and Çamlık blueschist locations in metaolistostrome (Table 5.1). Sodic, sodic-calcic and calcic amphiboles were determined in blueschist amphiboles. Cation proportions of sodic amphiboles based on one formula unit appear a minor amount higher than the ideal value. The range of total cations is between 15.004 - 15.142 with an average value of 15.047 which is close to the ideal value of 15.000. Ca and Na contents range from 0.086 to 0.345 and from 1.640 to 1.903, respectively, indicating an average of about five percent Ca occupancy of M4, the remaining 95 percent being Na. Mn contents of amphiboles are different in marble-schist series (average Mn: 0.004) and metaolistostrome unit (average Mn: 0.086). Amphibole bearing rocks in both units are of magmatic origin. This difference in Mn content is probably related with the bulk rock composition of the protoliths of these basic rocks. Based on one formula unit, the average contents of Ti (= 0.004), Cr (= 0.004), K (= 0.005) are negligible in the sodic amphiboles. $Mg/Mg+Fe^{2+}$ ratio of these amphiboles vary between 0.556 and 0.812 per formula unit and $Fe^{3+}/Fe^{3+} + Al^{VI}$ contents range from 0.262 to 0.560. Sodic amphiboles are glaucophane to crossite in composition (Figure 5.1a). Compositional variations in sodic amphiboles are largely restricted to the crossite field. Sodic amphiboles from marble-schist series and metaolistostrome are chemically and optically zoned (Figure 5.2). NaM4 slightly increases from core (1.771) to innerrim (1.903). But at the rim, NaM4 value dramatically decreases to 0.445 (Figure 5.2). $Mg/(Mg+Fe^{2+})$ slightly increases from core to rim. NaM4 ranges approximately from 1,90 to 1,64 (Figure 5.3). The sodic, sodic-calcic, calcic amphiboles exhibit a graditional and continuous transition from glaucophane to actinolite (Figure 5.3). The nearly 1:1 correlation of NaM4 (NaM4 = Na in B) and $R^{3+}(Al^{VI} + Fe^{3+} + 2.Ti)$ in Figure 5.3 suggests a glaucophane - barroisite-hornblende

Table 5.1 Representative amphibole analyses from blueschists in the Dilek Peninsula, Şirince and Çamlık areas.

	Dilek Peninsula												Şirince	
	Marble-schist series												Metaolistostrome	
	Na-Ca Amp	Na-Amp	Na-Amp	Ca Amp	Na-Ca Amp	Na Amp	Na-Ca-Amp	Na-Amp	Na-Amp	Na-Amp	Na-Amp	Na-Amp	Na-Amp	Na-Amp
Sample no	95-90-11	95-90-11	95-90-11	95-90-11	95-90-11	95-90-11	95-90-11	95-90-11	M96-80-1	M96-80-1	TAG	TAG	M98-52-2	M98-52-2
Analyse no	21	22	23	15	16	17	11	12	27	29	13	14	1	3
SiO2	50,79	56,97	56,31	51,72	52,27	57,24	49,68	55,67	55,73	55,47	56,37	56,83	55,52	55,46
TiO2	0,082	0,034	0	0,058	0,068	0,01	0,11	0,101	0,021	0	0	0,009	0,042	0,073
Al2O3	6,38	8,06	7,19	4,81	6,28	8,34	6,74	7,08	5,68	5,06	7,45	6,85	7,19	7,37
FeO	17,15	15,1	15,7	15,37	16,86	15,17	16,85	16,07	13,7	14,79	15,12	15,93	14,18	14,38
MnO	0	0,074	0	0,036	0,02	0,032	0,049	0,012	0,032	0,06	0,069	0,033	0,785	0,78
MgO	12,23	9,89	10,06	13,53	11,42	9,73	12,21	10,19	11,44	11,45	10,43	10,24	11,05	11,09
CaO	7,9	0,756	0,946	8,68	5,06	0,582	8,18	1,263	1,01	0,95	0,822	0,73	1,66	1,86
Na2O	3,52	6,88	6,88	2,84	5,06	7,14	3,23	6,73	7,03	7,19	7,25	7,12	6,12	6,08
K2O	0,196	0,025	0,01	0,162	0,15	0,027	0,257	0,021	0,009	0,019	0,027	0,008	0,026	0,035
Cr2O3	0	0,05	0,036	0,033	0,089	0,046	0,019	0,088	0,031	0,011	0	0,027	0	0,055
Total	98,25	97,84	97,13	97,24	97,28	98,32	97,33	97,23	94,69	95	97,54	97,78	96,573	97,183
Atoms per formula unit (23 oxygens)														
T: Si	7,260	7,882	7,877	7,429	7,473	7,889	7,172	7,799	7,962	7,931	7,846	7,898	7,759	7,714
Al(IV)	0,740	0,118	0,123	0,571	0,527	0,111	0,828	0,201	0,038	0,069	0,154	0,102	0,241	0,286
Fe3+	0,000	0,000	0,000	0,000	0,000	0,000	0,000	0,000	0,000	0,000	0,000	0,000	0,000	0,000
Ti	0,000	0,000	0,000	0,000	0,000	0,000	0,000	0,000	0,000	0,000	0,000	0,000	0,000	0,000
T-Sum	**8,000**	**8,000**	**8,000**	**8,000**	**8,000**	**8,000**	**8,000**	**8,000**	**8,000**	**8,000**	**8,000**	**8,000**	**8,000**	**8,000**
C: Al(VI)	0,335	1,196	1,062	0,243	0,531	1,243	0,319	0,968	0,918	0,783	1,068	1,020	0,944	0,923
Ti	0,009	0,004	0,000	0,006	0,007	0,001	0,012	0,011	0,002	0,000	0,000	0,001	0,004	0,008
Fe3+	0,956	0,836	0,906	0,820	0,991	0,777	1,002	0,991	0,855	0,997	0,879	0,940	1,128	1,142
Cr	0,000	0,005	0,004	0,004	0,010	0,005	0,002	0,010	0,004	0,001	0,000	0,003	0,000	0,006
Mg	2,606	2,039	2,097	2,896	2,433	1,999	2,627	2,128	2,436	2,440	2,164	2,121	2,302	2,299
Fe2+	1,094	0,911	0,930	1,026	1,024	0,972	1,032	0,891	0,782	0,771	0,880	0,911	0,529	0,531
Mn	0,000	0,009	0,000	0,004	0,002	0,004	0,006	0,001	0,004	0,007	0,008	0,004	0,093	0,092
Ca	0,000	0,000	0,000	0,000	0,000	0,000	0,000	0,000	0,000	0,000	0,000	0,000	0,000	0,000
C-Sum	**5,000**	**5,000**	**5,000**	**5,000**	**5,000**	**5,000**	**5,000**	**5,000**	**5,000**	**5,000**	**5,000**	**5,000**	**5,000**	**5,000**
B: Ca	1,210	0,112	0,142	1,336	0,775	0,086	1,265	0,190	0,155	0,146	0,123	0,109	0,249	0,277
Na	0,790	1,845	1,858	0,664	1,225	1,908	0,735	1,810	1,845	1,854	1,877	1,891	1,658	1,640
B-Sum	**2,000**	**1,957**	**2,000**	**2,000**	**2,000**	**1,994**	**2,000**	**2,000**	**2,000**	**2,000**	**2,000**	**2,000**	**1,907**	**1,917**
A: Ca	0,000	0,000	0,000	0,000	0,000	0,000	0,000	0,000	0,000	0,000	0,000	0,000	0,000	0,000
Na	0,185	0,000	0,007	0,126	0,177	0,000	0,169	0,017	0,102	0,138	0,079	0,027	0,000	0,000
K	0,036	0,004	0,002	0,030	0,027	0,005	0,047	0,004	0,002	0,003	0,005	0,001	0,005	0,006
A-Sum	**0,221**	**0,004**	**0,009**	**0,156**	**0,205**	**0,005**	**0,216**	**0,021**	**0,103**	**0,142**	**0,084**	**0,028**	**0,005**	**0,006**

Table 5.1 continued

	Şirince					Çamlık								
	Metaolistostrome unit													
	Na-Amp	Na-Ca Amp	Na-Ca Amp	Ca-Amp	Ca-Amp	Na-Amp	Na-Amp	Na-Amp	Na-Amp	Na-Amp	Na-Amp	Na-Amp	Na-Ca Amp	Na-Ca Amp
Sample no	M98-52-2	M98-52-2	M98-52-2	M98-52-2	M98-52-2	94-55-5	94-55-5	94-55-5	94-55-5	94-55-5	94-55-5	94-55-5	94-55-5	94-55-5
Analyse no	69	4	9	5	6	5	48	60	2	6	3	4	51	72
SiO2	56,6	53,26	50,53	53,03	51,82	56,05	56,03	55,8	56,82	56,64	56,29	56,37	50,75	53,14
TiO2	0	0,013	0,029	0,058	0	0,082	0,042	0,042	0,01	0,026	0,01	0,071	0,01	0,093
Al2O3	7,34	5,44	5,71	3,71	4,57	9,49	7,49	8,59	8,21	8,35	7,98	7,21	6,3	6,55
FeO	15,44	12,98	14,84	11,38	11,65	15,83	15,3	13,48	14,61	14,64	14,61	14,87	15,33	15
MnO	0,299	1,41	0,941	1,089	0,938	0,24	0,47	0,442	0,486	0,424	0,559	0,55	0,735	0,651
MgO	10,43	14,07	13,7	16,52	16,11	8,12	9,9	10,26	10,01	9,95	10,18	10,56	12,46	11,46
CaO	0,84	6,4	8,38	10,11	10,7	1,092	1,027	2,3	0,657	0,698	1,47	1,54	8,12	5,23
Na2O	6,7	3,89	2,59	1,5	1,52	6,91	6,97	6,44	7,17	7,29	6,86	6,77	2,8	5,14
K2O	0,015	0,108	0,188	0,092	0,099	0,077	0,024	0,041	0,027	0	0,015	0,032	0,213	0,126
Cr2O3	0,066	0,009	0,059	0	0,018	0,029	0,013	0,048	0	0,034	0,059	0,027	0,073	0,041
Total	97,73	97,579	96,967	97,489	97,426	97,92	97,27	97,44	98	98,05	98,03	98	96,79	97,43
Atoms per formula unit (23 oxygens)														
T: Si	7,827	7,468	7,222	7,452	7,341	7,846	7,845	7,806	7,854	7,837	7,817	7,831	7,310	7,580
Al(IV)	0,173	0,532	0,778	0,548	0,659	0,154	0,155	0,194	0,146	0,163	0,183	0,169	0,690	0,420
Fe3+	0,000	0,000	0,000	0,000	0,000	0,000	0,000	0,000	0,000	0,000	0,000	0,000	0,000	0,000
Ti	0,000	0,000	0,000	0,000	0,000	0,000	0,000	0,000	0,000	0,000	0,000	0,000	0,000	0,000
T-Sum	**8,000**	**8,000**	**8,000**	**8,000**	**8,000**	**8,000**	**8,000**	**8,000**	**8,000**	**8,000**	**8,000**	**8,000**	**8,000**	**8,000**
C: Al(VI)	1,023	0,368	0,184	0,067	0,104	1,412	1,081	1,222	1,191	1,198	1,123	1,011	0,380	0,681
Ti	0,000	0,001	0,003	0,006	0,000	0,009	0,004	0,004	0,001	0,003	0,001	0,007	0,001	0,010
Fe3+	1,096	1,161	1,262	0,999	0,870	0,504	0,859	0,515	0,832	0,794	0,764	0,853	0,973	0,671
Cr	0,007	0,001	0,007	0,000	0,002	0,003	0,001	0,005	0,000	0,004	0,006	0,003	0,008	0,005
Mg	2,150	2,941	2,918	3,460	3,401	1,694	2,066	2,139	2,062	2,052	2,107	2,186	2,675	2,436
Fe2+	0,690	0,361	0,511	0,338	0,510	1,349	0,932	1,062	0,856	0,900	0,932	0,874	0,873	1,118
Mn	0,035	0,167	0,114	0,130	0,113	0,028	0,056	0,052	0,057	0,050	0,066	0,065	0,090	0,079
Ca	0,000	0,000	0,000	0,000	0,000	0,000	0,000	0,000	0,000	0,000	0,000	0,000	0,000	0,000
C-Sum	**5,000**	**5,000**	**5,000**	**5,000**	**5,000**	**5,000**	**5,000**	**5,000**	**5,000**	**5,000**	**5,000**	**5,000**	**5,000**	**5,000**
B: Ca	0,124	0,961	1,283	1,522	1,624	0,164	0,154	0,345	0,097	0,103	0,219	0,229	1,253	0,799
Na	1,796	1,039	0,717	0,409	0,376	1,836	1,846	1,655	1,903	1,897	1,781	1,771	0,747	1,201
B-Sum	**1,921**	**2,000**	**2,000**	**1,931**	**2,000**	**2,000**	**2,000**	**2,000**	**2,000**	**2,000**	**2,000**	**2,000**	**2,000**	**2,000**
A: Ca	0,000	0,000	0,000	0,000	0,000	0,000	0,000	0,000	0,000	0,000	0,000	0,000	0,000	0,000
Na	0,000	0,019	0,001	0,000	0,041	0,039	0,046	0,091	0,019	0,059	0,066	0,052	0,035	0,221
K	0,003	0,019	0,034	0,016	0,018	0,014	0,004	0,007	0,005	0,000	0,003	0,006	0,039	0,023
A-Sum	**0,003**	**0,038**	**0,035**	**0,016**	**0,059**	**0,053**	**0,050**	**0,098**	**0,023**	**0,059**	**0,068**	**0,058**	**0,074**	**0,244**

Table 5.1 continued

	Çamlık	
	Metaolistostrome unit	
	Ca-Amp	Ca-Amp
Sample no	94-55-5	94-55-5
Analyse no	1	7
SiO2	54,05	53,53
TiO2	0,099	0,168
Al2O3	3,21	4,31
FeO	10,93	10,87
MnO	0,798	0,764
MgO	16,74	15,97
CaO	10,35	9,56
Na2O	1,8	2,53
K2O	0,159	0,175
Cr2O3	0,016	0,095
Total	98,15	97,97
Atoms per formula unit (23 oxygens)		
T: Si	7,581	7,535
Al(IV)	0,419	0,465
Fe3+	0,000	0,000
Ti	0,000	0,000
T-Sum	**8,000**	**8,000**
C: Al(VI)	0,112	0,250
Ti	0,010	0,018
Fe3+	0,656	0,563
Cr	0,002	0,011
Mg	3,499	3,351
Fe2+	0,625	0,717
Mn	0,095	0,091
Ca	0,000	0,000
C-Sum	**5,000**	**5,000**
B: Ca	1,555	1,442
Na	0,445	0,558
B-Sum	**2,000**	**2,000**
A: Ca	0,000	0,000
Na	0,045	0,132
K	0,028	0,031
A-Sum	**0,073**	**0,164**

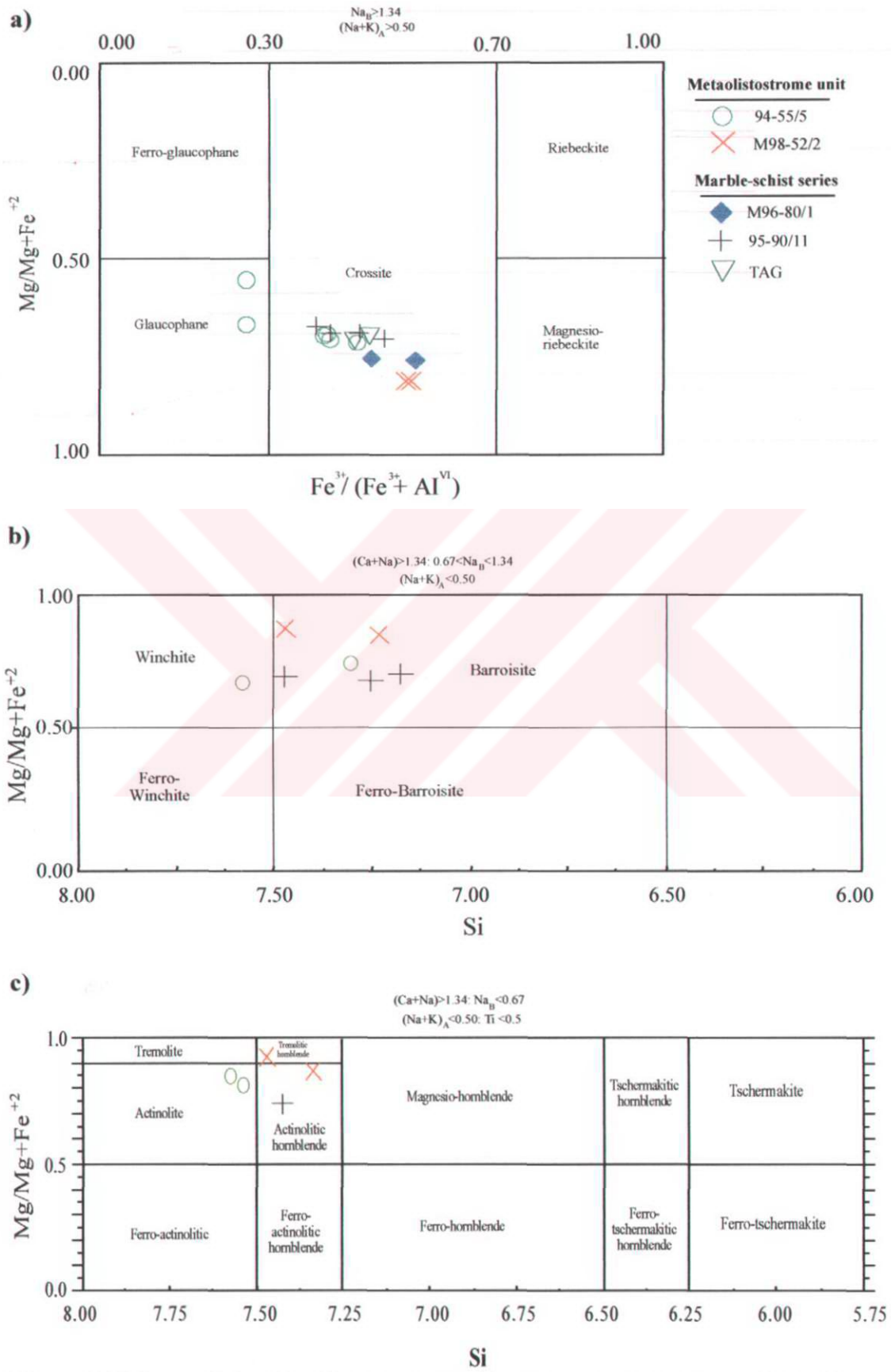


Figure 5.1 Composition of sodic (a) sodic-calcic (b) and calcic (c) amphiboles from metaolistostrome unit and marble-schist series plotted on Leake et al.,(1978) diagram.

substitution. Amphiboles belong to the Marble-schist series are dominantly sodic and sodic-calcic in composition. But, in amphiboles of metaolistostrome unit, it is possible to see a complete series of amphibole from sodic to calcic in composition.

Cation proportions based on one formula unit of sodic-calcic amphiboles appear higher than the ideal value. The range of total cations is between 15.035 and 15.216 with an average of 15.118, essentially within the ideal stoichiometric 15.000-16.000 range. The occupancy of M4 site by Na and Ca is between 0.717-1.225 and 0.775-1.283, respectively. Maximum Na percentage in M4 of sodic-calcic amphiboles is 61%. The sodic-calcic amphiboles are winchite and dominantly barroisite in composition (Figure 5.1b). Sodic-calcic amphiboles are in between winchite and barroisite compositional range (Figure 5.3). The total number of cations per formula unit of calcic amphiboles ranges from 15.016 to 15.164. Maximum Ca and Na occupancies in M4 structural position are 1.624 and 0.664, respectively. The calcic amphiboles are actinolite, tremolitic hornblende and actinolitic hornblende in composition (Figure 5.1c). NaM4 ranges from 0,66 to 0,37 (Figure 5.3). Representative sodic, sodic-calcic and calcic amphibole formulae in blueschists are given in Table 5.2.

Table 5.2 Structural formula of representative amphiboles.

	Amphibole	Formula
Metaolistostrome (94-55-5)	Glaucophane	$(K_{0.01}Na_{0.04})(Na_{1.84}Ca_{0.16})(Mn_{0.03}Fe^{2+}_{1.35}Mg_{1.70}Fe^{3+}_{0.50}Ti_{0.01}Al_{1.41})(Al_{0.15}Si_{7.85})O_{22}(OH)_2$
	Crossite	$(K_{0.00}Na_{0.02})(Na_{1.90}Ca_{0.10})(Mn_{0.06}Fe^{2+}_{0.86}Mg_{2.06}Fe^{3+}_{0.83}Ti_{0.00}Al_{1.19})(Al_{0.15}Si_{7.85})O_{22}(OH)_2$
	Barroisite	$(K_{0.04}Na_{0.03})(Na_{0.75}Ca_{1.25})(Mn_{0.09}Fe^{2+}_{0.88}Mg_{2.68}Fe^{3+}_{0.97}Ti_{0.00}Al_{0.38})(Al_{0.69}Si_{7.31})O_{22}(OH)_2$
	Actinolite	$(K_{0.03}Na_{0.04})(Na_{0.45}Ca_{1.55})(Mn_{0.10}Fe^{2+}_{0.63}Mg_{3.50}Fe^{3+}_{0.65}Ti_{0.01}Al_{0.11})(Al_{0.42}Si_{7.58})O_{22}(OH)_2$
Marble-schist series (93-90-11)	Crossite	$(K_{0.00}Na_{0.00})(Na_{1.86}Ca_{0.14})(Mn_{0.00}Fe^{2+}_{0.93}Mg_{2.10}Fe^{3+}_{0.91}Ti_{0.00}Al_{1.06})(Al_{0.12}Si_{7.88})O_{22}(OH)_2$
	Barroisite	$(K_{0.04}Na_{0.18})(Na_{0.80}Ca_{1.20})(Mn_{0.00}Fe^{2+}_{1.09}Mg_{2.60}Fe^{3+}_{0.96}Ti_{0.01}Al_{0.34})(Al_{0.74}Si_{7.26})O_{22}(OH)_2$
	Actinolite	$(K_{0.03}Na_{0.12})(Na_{0.66}Ca_{1.34})(Mn_{0.00}Fe^{2+}_{1.03}Mg_{2.90}Fe^{3+}_{0.82}Ti_{0.01}Al_{0.24})(Al_{0.57}Si_{7.43})O_{22}(OH)_2$

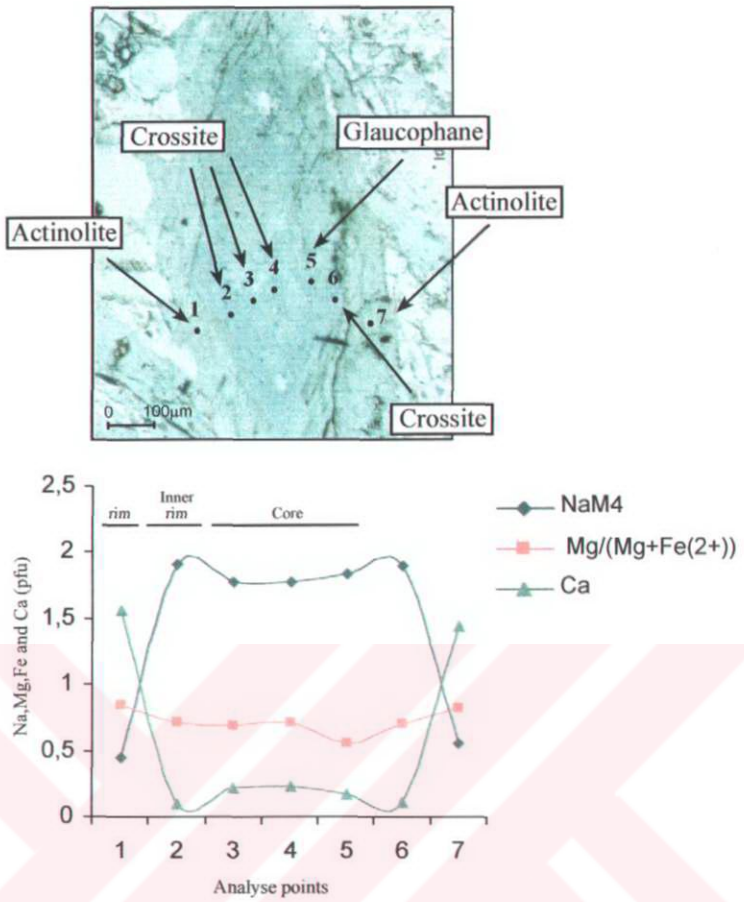


Figure 5.2 Zoning structure of a sodic amphibole (94-55/5) in blueschist block in the Mateolistostrome unit.

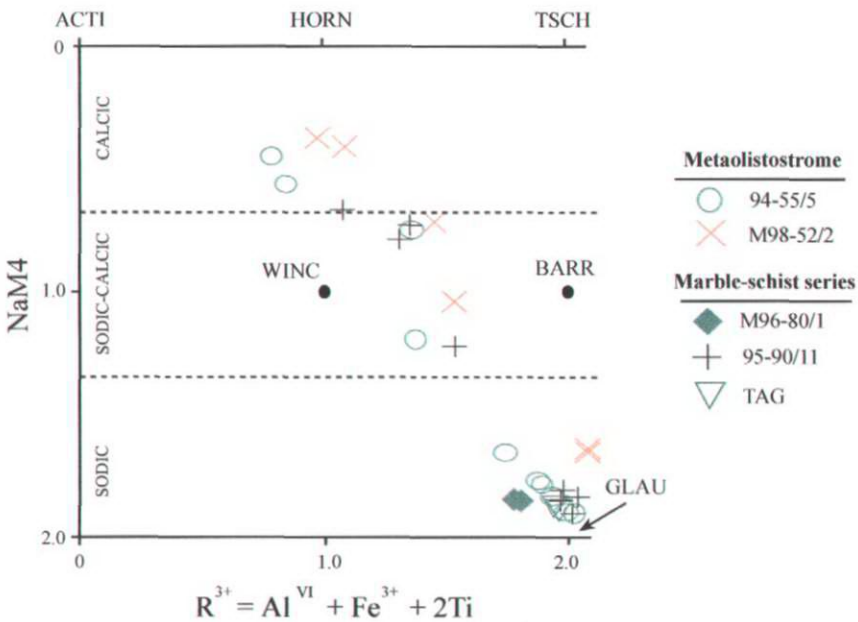


Figure 5.3 Plot of NaM4 versus R(3+) diagram after Kryza et al. (1990) for amphiboles in blueschist metabasites (metaolistostrome unit and marble-schist series). ACTI = actinolite, BARR =barroisite, GLAU = glaucophane, HORN = hornblende, TSCH = tschermakite, WINC = winchite.

5.2.2. Amphiboles in eclogites

Seven representative eclogite samples were analysed from Selçuk (Şirince) and Gölmarmara areas (Table 5.3). Amphiboles in eclogites are calcic amphiboles. There are three kind of calcic amphibole groups. These groups are separated according to their $(Na+K)_A$, Ti, Fe^{3+} and Al^{VI} contents. In analysed calcic amphiboles, the total number of cations per formula unit ranges from 15.023 to 15.891, with an average of 15.604, essentially within the ideal stoichiometric 15.000-16.000 range which is appropriate for actinolite-edenite+pargasite solid solutions (Figure 5.4a and 5.4b). Some cations present in these amphiboles are low but variable in amount, and their average concentrations are as follows: Ti = 0.018, Cr = 0.005, Mn = 0.073, and K = 0.072. These constitutes are less abundant in high-Si amphiboles compared to the edenitic-pargasitic amphiboles.

The proportions of Na and Ca are shown in Figure 5.4a, which fairly portrays the cation occupancy of M4+A sites in amphibole. Analysed calcic amphiboles appear to be members of the actinolite-edenite+pargasite series. Calcic amphiboles in Figure 5.4a dominantly take place near to edenite-pargasite corner. 95-21/10 constitutes transition term between 95-70/4, M99-5/4 and M97-34/2, M96-31, SE-1, M98-45C groups. Compositional variation in calcic amphiboles is quite pronounced (Figure 5.4b) and is observed in range of actinolite-hornblende+edenite-pargasite. M99-5/4, 95-70/4 and 95-21/10 samples dominantly plot into actinolite and actinolitic hornblende fields (Figure 5.5a). Si content of these amphiboles ranges from 7.294 to 7.831 (pfu). Their $Mg/(Mg+Fe^{2+})$ contents are almost constant and changes from 0,77 to 0,81 (pfu). M98-45C and SE-1 amphiboles are edenite and edenitic hornblende in composition, respectively (Figure 5.5b). Some amphiboles in M96-31 are ferroan-pargasitic hornblende and ferroan-pargasite in composition (Figure 5.5b). Calcic amphibole composition in Figure 5.5c changes from edenite to magnesian-hastingsite. All amphibole analyses belonging to M97-34/2 are plotted into Figure 5.5c. The point analyses with numbers 45-46-47-48 belonging to M97-34/2 display optically and chemically pronounced compositional (Ca-amphibole) zoning (Figure 5.6). Points 45 (dark green) and 46 (dark green) are magnesian - hastingsitic

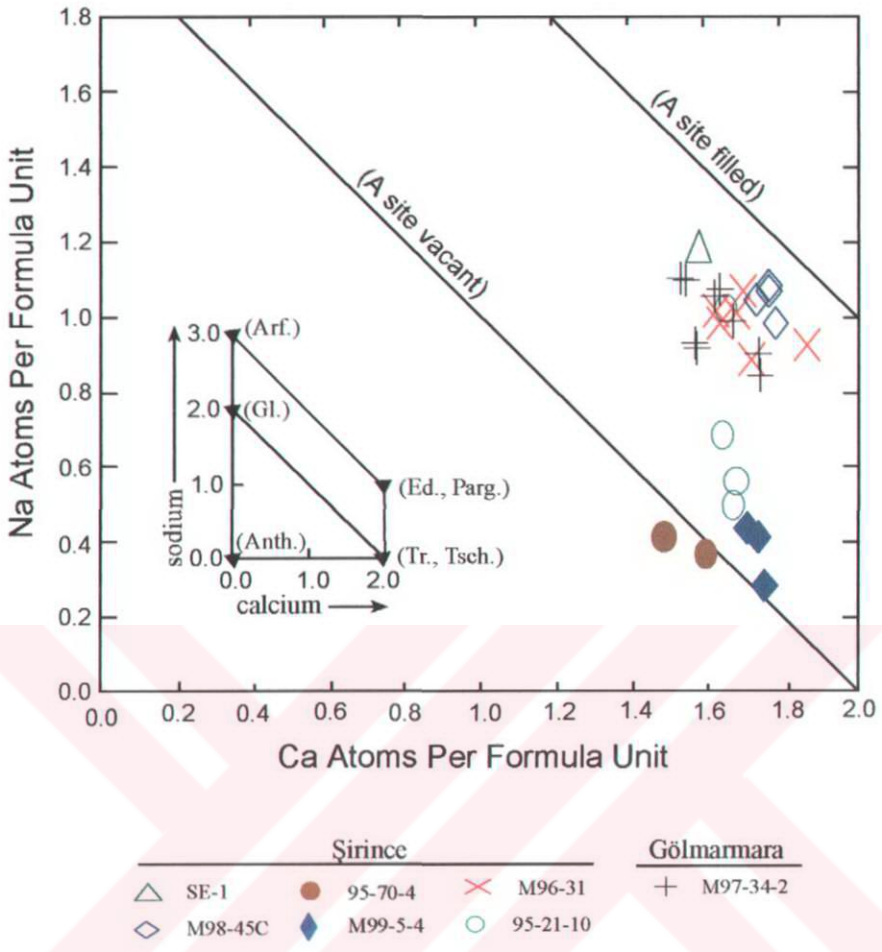
Table 5.3 Representative amphibole analyses from eclogites in Şirince and Gölmarmara areas.

	Şirince												Gölmarmara				
	Metaolistostrome																
Sample no	95-21/10	95-21/10	95-21/10	95-21/10	95-70/4	95-70/4	M96-31	M96-31	M96-31	M96-31	M96-31	M96-31	M97-34/2	M97-34/2	M97-34/2	M97-34/2	M97-34/2
Analyse no	m20-4	m20-5	m20-19	m20-20	m3-47	m3-48	m4-81	m4-82	m4-83	m4-84	m5-11	m5-12	m7-12	m7-26	m7-45	m7-46	m7-47
SiO2	51,18	44,15	52,76	50,66	53,12	53,02	44,7	47,53	46,62	45,31	50,01	48,25	41,71	44,74	42,69	43,42	48,78
TiO2	0,058	0,184	0,075	0,12	0,087	0,093	0,116	0,127	0,126	0,052	0,103	0,113	0,269	0,219	0,301	0,283	0,127
Al2O3	5,46	11,56	4,02	5,86	5,79	5,52	11	8,8	9,88	10,97	7,85	8,5	10,76	8,82	11,11	11,12	8,22
FeO	10,66	14,03	10,41	11,16	11,61	12,08	12,22	10,94	11,32	11,55	9,51	9,97	18,85	15,68	16,42	15,03	10,28
MnO	0,638	0,854	0,721	0,688	0,144	0,15	0,338	0,352	0,37	0,417	0,406	0,342	1,114	0,64	1,016	0,946	0,721
MgO	15,94	12,13	16,22	15,21	15,48	15,41	13,83	15,5	14,65	14,18	14,55	15,78	9,53	11,99	11,01	11,98	15,22
CaO	10,93	10,48	10,94	10,64	9,91	10,66	10,82	10,61	10,47	10,76	11,92	11,14	10,23	10,85	10,41	10,21	10,2
Na2O	2,03	3,58	1,79	2,43	1,55	1,338	3,77	3,54	3,65	3,58	3,29	3,19	3,36	2,92	3,43	3,69	3,29
K2O	0,284	0,491	0,163	0,261	0,165	0,13	0,449	0,383	0,316	0,398	0,223	0,379	0,777	0,554	0,824	0,837	0,354
Cr2O3	0,012	0,045	0,06	0,061	0,052	0,063	0,08	0,091	0,072	0,091	0,02	0,088	0,029	0,055	0,067	0	0
Total	**97,191**	**97,504**	**97,159**	**97,091**	**97,91**	**98,46**	**97,32**	**97,87**	**97,48**	**97,31**	**97,88**	**97,75**	**96,63**	**96,47**	**97,28**	**97,52**	**97,19**
Atoms per formula unit (23 oxygens)																	
T: Si	7,321	6,486	7,529	7,294	7,429	7,424	6,534	6,819	6,732	6,582	7,277	6,926	6,340	6,695	6,374	6,417	7,010
Al(IV)	0,679	1,514	0,471	0,706	0,571	0,576	1,466	1,181	1,268	1,418	0,723	1,074	1,660	1,305	1,626	1,583	0,990
Fe3+	0,000	0,000	0,000	0,000	0,000	0,000	0,000	0,000	0,000	0,000	0,000	0,000	0,000	0,000	0,000	0,000	0,000
Ti	0,000	0,000	0,000	0,000	0,000	0,000	0,000	0,000	0,000	0,000	0,000	0,000	0,000	0,000	0,000	0,000	0,000
T-Sum	**8,000**	**8,000**	**8,000**	**8,000**	**8,000**	**8,000**	**8,000**	**8,000**	**8,000**	**8,000**	**8,000**	**8,000**	**8,000**	**8,000**	**8,000**	**8,000**	**8,000**
C: Al(VI)	0,242	0,488	0,206	0,289	0,384	0,335	0,429	0,307	0,413	0,460	0,624	0,364	0,268	0,251	0,330	0,354	0,403
Ti	0,006	0,020	0,008	0,013	0,009	0,010	0,013	0,014	0,014	0,006	0,011	0,012	0,031	0,025	0,034	0,031	0,014
Fe3+	0,459	0,568	0,372	0,376	0,744	0,630	0,461	0,521	0,500	0,506	0,000	0,293	0,855	0,566	0,741	0,718	0,437
Cr	0,001	0,005	0,007	0,007	0,006	0,007	0,009	0,010	0,008	0,010	0,002	0,010	0,003	0,007	0,008	0,000	0,000
Mg	3,398	2,656	3,450	3,264	3,227	3,216	3,013	3,314	3,153	3,070	3,156	3,376	2,159	2,674	2,450	2,639	3,260
Fe2+	0,816	1,155	0,870	0,968	0,614	0,785	1,033	0,791	0,866	0,897	1,157	0,904	1,541	1,397	1,310	1,139	0,799
Mn	0,077	0,106	0,087	0,084	0,017	0,018	0,042	0,043	0,045	0,051	0,050	0,042	0,143	0,081	0,128	0,118	0,088
Ca	0,000	0,000	0,000	0,000	0,000	0,000	0,000	0,000	0,000	0,000	0,000	0,000	0,000	0,000	0,000	0,000	0,000
C-Sum	**5,000**	**5,000**	**5,000**	**5,000**	**5,000**	**5,000**	**5,000**	**5,000**	**5,000**	**5,000**	**5,000**	**5,000**	**5,000**	**5,000**	**5,000**	**5,000**	**5,000**
B: Ca	1,675	1,650	1,673	1,641	1,485	1,599	1,694	1,631	1,620	1,674	1,858	1,713	1,666	1,740	1,665	1,617	1,570
Na	0,325	0,350	0,327	0,359	0,420	0,363	0,306	0,369	0,380	0,326	0,142	0,287	0,334	0,260	0,335	0,383	0,430
B-Sum	**2,000**	**2,000**	**2,000**	**2,000**	**1,905**	**1,962**	**2,000**	**2,000**	**2,000**	**2,000**	**2,000**	**2,000**	**2,000**	**2,000**	**2,000**	**2,000**	**2,000**
A: Ca	0,000	0,000	0,000	0,000	0,000	0,000	0,000	0,000	0,000	0,000	0,000	0,000	0,000	0,000	0,000	0,000	0,000
Na	0,238	0,669	0,168	0,319	0,000	0,000	0,763	0,615	0,641	0,683	0,786	0,601	0,656	0,587	0,658	0,674	0,487
K	0,052	0,092	0,030	0,048	0,029	0,023	0,084	0,070	0,058	0,074	0,041	0,069	0,151	0,106	0,157	0,158	0,065
A-Sum	**0,290**	**0,761**	**0,198**	**0,367**	**0,029**	**0,023**	**0,847**	**0,685**	**0,700**	**0,756**	**0,828**	**0,670**	**0,807**	**0,692**	**0,815**	**0,832**	**0,552**

Table 5.3 continued

	Gölmarmara					Şirince								
	Metaolistostrome													
Sample no	M97-34/2	M97-34/2	M97-34/2	M97-34/2	M97-34/2	M98-45C	M98-45C	M98-45C	M98-45C	M99-5/4	M99-5/4	M99-5/4	M99-5/4	SE-1
Analyse no	m7-48	m7-64	m7-65	m7-66	m7-94	m4-34	m4-48	m4-49	m4-55	m19-7	m19-19	m19-20	m19-21	m8-160
SiO2	48,19	43,68	42,93	41,04	43,33	41,99	41,68	43,13	42,92	53,36	53,86	55,31	42,32	45,85
TiO2	0,09	0,279	0,326	0,376	0,255	0,126	0,272	0,234	0,206	0,033	0,065	0	0,256	0,183
Al2O3	8,39	10,03	10,53	11,42	9,99	13,98	14,47	13,35	12,55	3,33	3,14	1,796	13,41	10,26
FeO	10,9	15,99	17,17	19,05	16,51	16,3	14,9	13,28	16,31	10,16	10,12	9,2	14,6	13,31
MnO	0,721	0,939	1,09	1,177	1,043	0,437	0,402	0,373	0,422	0,155	0,143	0,091	0,206	0,775
MgO	15,1	11,36	10,33	9,38	11,09	10,08	10,47	11,91	10,43	16,86	16,87	17,84	11,05	12,73
CaO	10,14	9,62	9,44	10,04	10,75	10,85	11,03	11,16	11,18	11,32	11,17	11,54	11,01	10,04
Na2O	3,34	3,78	3,78	3,65	3,11	3,65	3,7	3,79	3,42	1,51	1,59	1,048	3,94	4,19
K2O	0,322	0,626	0,7	0,967	0,686	0,114	0,245	0,205	0,222	0,081	0,106	0,067	0,134	0,268
Cr2O3	0	0,023	0,03	0,035	0,038	0,028	0,069	0,021	0,26	0	0,045	0,042	0,058	0,02
Total	**97,19**	**96,33**	**96,33**	**97,14**	**96,8**	**97,56**	**97,24**	**97,45**	**97,92**	**96,81**	**97,109**	**96,934**	**96,984**	**97,63**
Atoms per formula unit (23 oxygens)														
T: Si	6,932	6,540	6,468	6,224	6,509	6,231	6,200	6,355	6,368	7,617	7,663	7,831	6,308	6,708
Al(IV)	1,068	1,460	1,532	1,776	1,491	1,769	1,800	1,645	1,632	0,383	0,337	0,169	1,692	1,292
Fe3+	0,000	0,000	0,000	0,000	0,000	0,000	0,000	0,000	0,000	0,000	0,000	0,000	0,000	0,000
Ti	0,000	0,000	0,000	0,000	0,000	0,000	0,000	0,000	0,000	0,000	0,000	0,000	0,000	0,000
T-Sum	**8,000**	**8,000**	**8,000**	**8,000**	**8,000**	**8,000**	**8,000**	**8,000**	**8,000**	**8,000**	**8,000**	**8,000**	**8,000**	**8,000**
C: Al(VI)	0,354	0,310	0,338	0,266	0,277	0,676	0,737	0,673	0,563	0,178	0,189	0,131	0,664	0,477
Ti	0,010	0,031	0,037	0,043	0,029	0,014	0,030	0,026	0,023	0,004	0,007	0,000	0,029	0,020
Fe3+	0,579	0,782	0,831	0,898	0,655	0,541	0,366	0,273	0,412	0,303	0,266	0,233	0,284	0,386
Cr	0,000	0,003	0,004	0,004	0,005	0,003	0,008	0,002	0,030	0,000	0,005	0,005	0,007	0,002
Mg	3,237	2,535	2,320	2,120	2,483	2,229	2,321	2,615	2,307	3,587	3,577	3,765	2,455	2,776
Fe2+	0,732	1,220	1,332	1,518	1,419	1,482	1,487	1,363	1,612	0,910	0,938	0,856	1,536	1,242
Mn	0,088	0,119	0,139	0,151	0,133	0,055	0,051	0,047	0,053	0,019	0,017	0,011	0,026	0,096
Ca	0,000	0,000	0,000	0,000	0,000	0,000	0,000	0,000	0,000	0,000	0,000	0,000	0,000	0,000
C-Sum	**5,000**	**5,000**	**5,000**	**5,000**	**5,000**	**5,000**	**5,000**	**5,000**	**5,000**	**5,000**	**5,000**	**5,000**	**5,000**	**5,000**
B: Ca	1,563	1,543	1,524	1,631	1,730	1,725	1,758	1,762	1,777	1,731	1,703	1,750	1,758	1,574
Na	0,437	0,457	0,476	0,369	0,270	0,275	0,242	0,238	0,223	0,269	0,297	0,250	0,242	0,426
B-Sum	**2,000**	**2,000**	**2,000**	**2,000**	**2,000**	**2,000**	**2,000**	**2,000**	**2,000**	**2,000**	**2,000**	**2,000**	**2,000**	**2,000**
A: Ca	0,000	0,000	0,000	0,000	0,000	0,000	0,000	0,000	0,000	0,000	0,000	0,000	0,000	0,000
Na	0,494	0,640	0,628	0,704	0,636	0,775	0,825	0,844	0,761	0,149	0,141	0,038	0,897	0,762
K	0,059	0,120	0,135	0,187	0,131	0,022	0,046	0,039	0,042	0,015	0,019	0,012	0,025	0,050
A-Sum	**0,553**	**0,760**	**0,762**	**0,891**	**0,767**	**0,796**	**0,871**	**0,883**	**0,803**	**0,164**	**0,160**	**0,050**	**0,922**	**0,812**

a)



b)

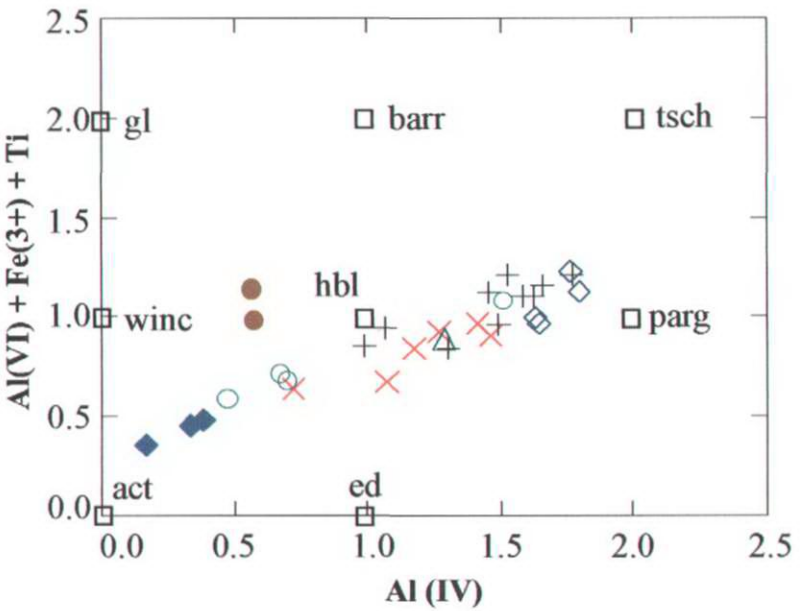


Figure 5.4 Aspects of the chemical variations of calcic amphiboles from eclogites .(a) sodium and calcium occupancy of M4+A structural positions; (b) plot of Al(VI) + Fe(3+) + Ti versus Al(IV)

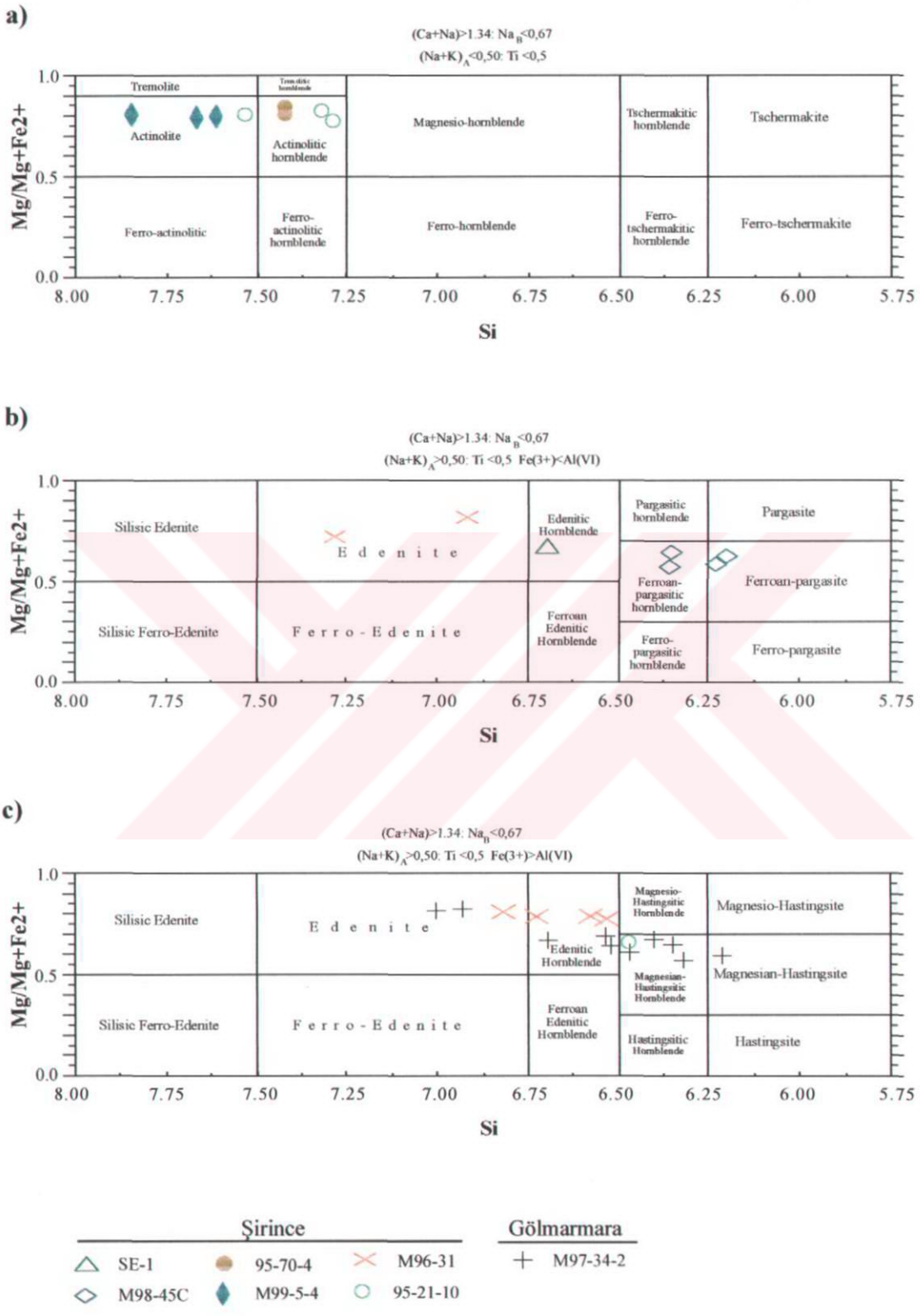


Figure 5.5 Composition of calcic amphiboles (a, b and c) from eclogite blocks in metalistostrome plotted on Leake et al.,(1978) diagram.

T.C. YÜKSEKÖĞRETİM KURULU
DOKÜMANTASYON MERKEZİ

hornblende in composition. Points 47 (pale green) and 48 (pale green) have higher Si content and fall into edenite composition field (Figure 5.5c). Zoning profiles of this calcic amphibole are given in Figure 5.6. Ti, Fe^{2+} and Ca content decrease from rim to core. The most pronounced zonation is observed in Ti. Ti content in rim is 2.5 times higher than the core. In calcic amphiboles, increases of Ti towards the rims display a cooling. Effective zoning in Ca is not observed. Ca slightly increases from core to rim (Figure 5.6). On the contrary, Si and Mg values decrease from core to rim. Decreasing in Si content of calcic amphibole can be interpreted to represent increasing in temperature. Mg profile, which is in consistent with Si profile, may represent decreasing in pressure from core to rim. Al^{VI} and NaM4 in amphiboles exhibit zoning pattern (Figure 5.6).

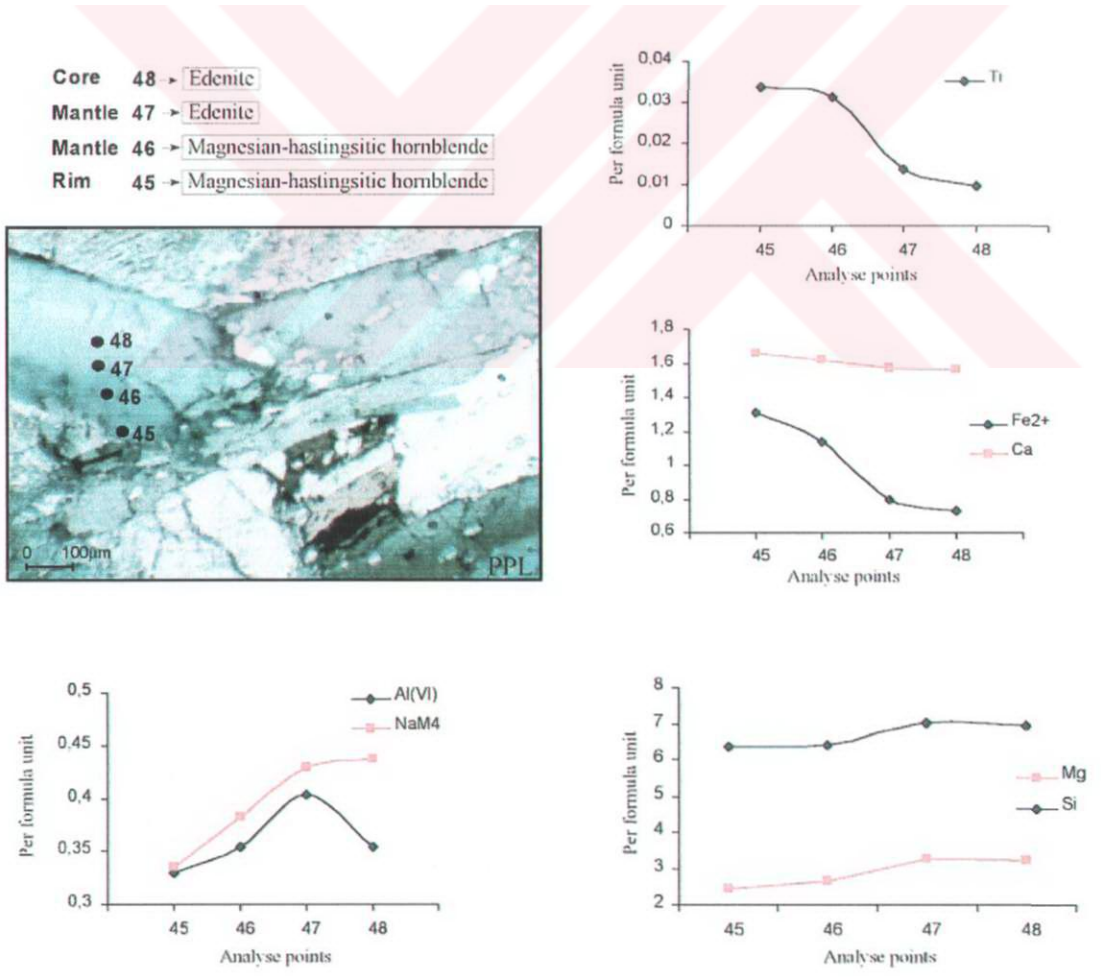


Figure 5.6 Calcic amphibole zoning in M97-34/2 and element graphs monitoring the zonation.

NaM4 decreases dramatically from core to rim. Decreasing in NaM4 value from core to rim is in consistent with Mg profile. Al^{VI} value display first an enrichment towards rim and than decreases. The analyses of numbers 64 (core) - 65 - 66 (rim) in M97-34/2 (Table 5.3) show calcic amphibole zonation. Edenetic-hornblende, magnesian-hastingsitic hornblende and magnesian-hastingsite series are observed from core to rim (Figure 5.5c). In this series, Si values decrease and Ti values increase in a composition interval between edenitic hornblende and magnesian-hastingsite. This zoning may reflect increasing in temperature from core to rim. In general, analysed calcic amphiboles tend to be richer in Ca, Ti and tend to be poorer in Na M4, and Al^{VI} during retrograde metamorphism.

Ca-amphiboles characterize commonly greenschist P-T conditions. However, Ca-amphiboles are also observed in rocks which suffered high and/or medium-pressure metamorphism. In the discrimination diagrams of Laird and Albee (1981), some of the Ca-amphiboles in eclogite blocks are clearly separated from post-eclogitic Ca-amphiboles and are concentrated in the field of intermediate- to high-pressure facies amphiboles (Figure 5.7). Ca-amphibole crystals from M97-34/2 have zoned structure consisting of pale and dark green coloured core and rim, respectively. Pale green coloured core section of Ca-amphiboles can be formed during late stage of high-pressure (prograde) or at the beginning of medium-pressure (retrograde) metamorphism. The dark green parts of the Ca-amphiboles are thin and occur at the rim of the crystal. Dark green amphiboles are probably formed in advanced stages of retrograde metamorphism. Due to the dark green cover of the Ca–amphiboles, it is hardly difficult to see the equilibration relationship between omphacite and Ca-amphiboles which are formed in high- or medium pressure condition. Ca-amphiboles from M98-45C are probably formed during retrograde metamorphism. These amphiboles are not equilibrated with omphacite and garnet (Figure 5.7). They are dark green in colour. Sample spots belonging to these amphiboles plot into low-pressure field in Figure 5.7. In Raase (1974) diagram, Ca-amphiboles which are plotted on intermediate- to high pressure facies field in Figure 5.7 occur above the 5 kbar line or on it (Figure 5.8). This result is consistent with Figure 5.7.

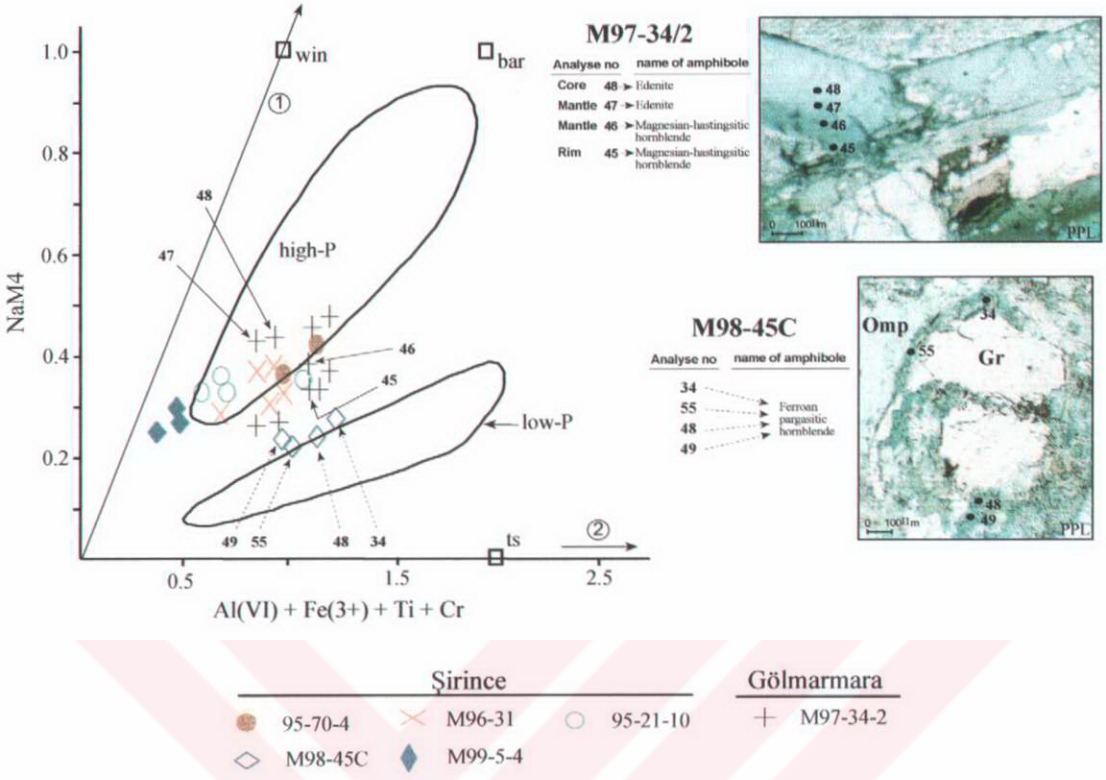


Figure 5.7 Pressure characteristics of the Ca-amphiboles observed in the eclogite blocks. Increasing pressure is generally represented by an increase in amphibole of the parameter (NaM4) plotted along the vertical axis and increasing temperature generally results in an increase in the parameter (Al(VI)+Fe(3+)+Ti+Cr)) plotted along the horizontal axis (Laird and Albee, 1981). The fields of high pressure and low pressure are from Laird and Albee (1981). Arrows 1 and 2 indicate the direction of glaucophane and tschermakite substitutions, respectively (win=winchite, bar=barroisite,

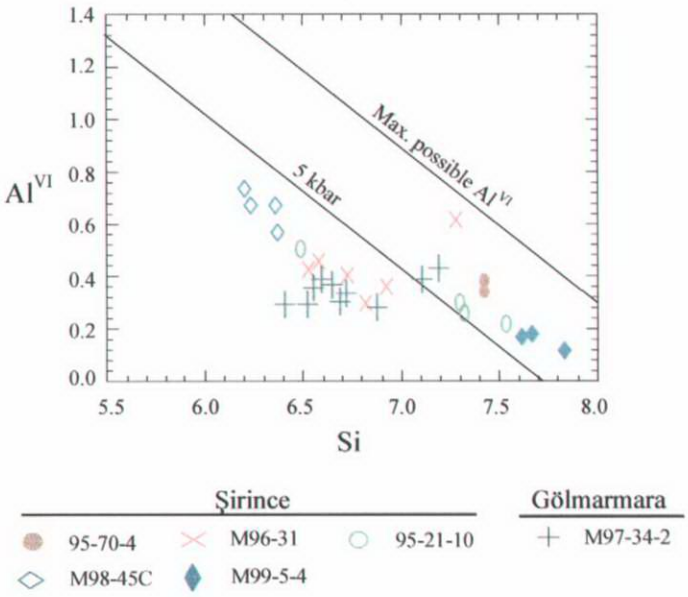


Figure 5.8 Pressure characteristic of Ca-amphiboles observed in eclogite blocks plotted on Raase (1974) diagram.

5.2.3. Amphiboles in omphacite-epidotite, omphacite metagabbro and garnet amphibolite

Three omphacite-epidotites (M98-163/2, M97-151/3, M96-92/4), one omphacite metagabbro and one garnet amphibolite sample were analysed from Şirince and Tire areas. Representative amphibole analyses belonging to these rocks are given in Table 5.4. All amphiboles related to these rocks exhibit calcic amphibole compositions. In omphacite-epidotites, total number of cations per formula unit ranges from 15.239 to 15.940, with an average of 15.538. These values are within the ideal stoichiometric value of 15.00-16.00. Calcic amphiboles in M98-163/2 are actinolitic hornblende and magnesio-hornblende in composition (Figure 5.9a). Although, in this amphibole, $Mg/(Mg+Fe^{2+})$ ratio is almost constant, Si values show variation. Calcic amphiboles in M97-151/3 and M96-92/4 are edenit / edenitic hornblende and magnesio-hastingsitic hornblende in compositions, respectively (Figure 5.9c).

Amphiboles in omphacite-epidotites are subcalcic in composition, containing between 1.465 and 1.684 calcium atoms with an average value of 1.564 per formula unit. Na in M4 site ranges from 0.316 to 0.535 with an average of 0.436 per formula unit. Amount of Na atoms in M4 site is close to 0.67 being minimum Na value in sodic-calcic amphiboles. The Na and Ca occupancy of M4+A are shown in Figure 5.10a. Positive correlation shown in Figure 5.10b indicates that combinations of actinolite – hornblende+edenite - tschermakite are exchanges in these amphiboles. Deviation from the actinolite – hornblende – pargasite tie-line indicates the existance of minor titanian, ferric or alkali-amphibole substitutions (e.g., glaucophane). Figure 5.10c depicts clear solid solution relationship between the minerals. Actinolite-hornblende and hornblende-tschermakite solid solutions are observed in Ca amphiboles belonging to omphacite-epidotites. In these solid solutions, effect of edenite end-member is lesser than hornblende end-member (Figure 5.10c). Omphacite metagabbro analyses fall into edenitic hornblende, edenite (calcic amphibole, Figure 5.9b) and magnesio-katophorite (sodic-calcic amphibole, Figure 5.9d) field. Total number of cations per formula unit ranges from 15.619 to 15.734. Compositional interval of analysed calcic amphiboles in omphacite metagabbro is

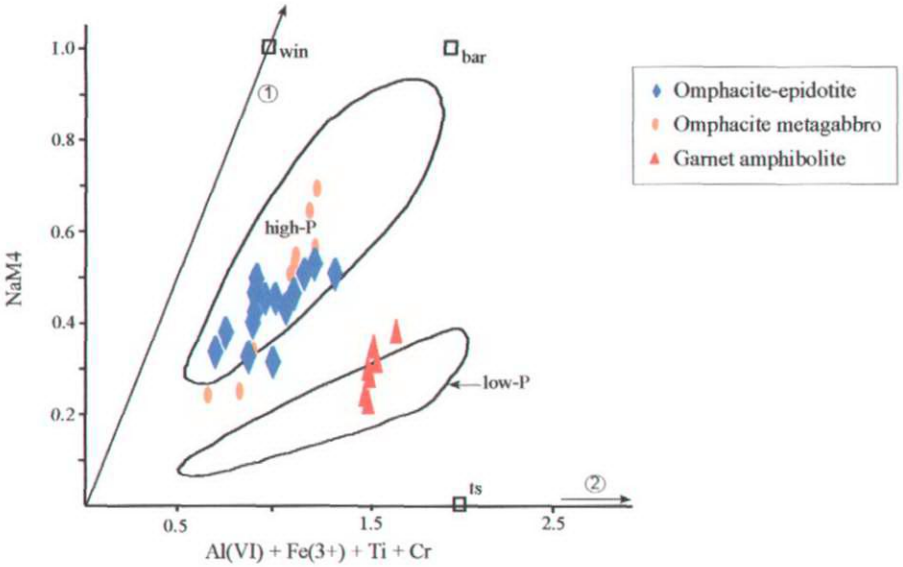
Table 5.4 Representative amphibole analyses from omphacite-epidodite, omphacite metagabbro and garnet amphibolites in Şirince and Tire areas.

	Şirince				Torbalı									Şirince					
	Metaolistostrome blocks																		
	Omphacite-epidotite															Omphacite metagabbro				
Sample no	M96-92/4	M96-92/4	M96-92/4	M96-92/4	M98-163/2	M98-163/2	M98-163/2	M98-163/2	M98-163/2	M98-163/2	M98-163/2	M98-163/2	M98-163/2	M97-151/3	M97-151/3	91-16	91-16	91-16	91-16	91-16
Analyse no	m13-14	m13-15	m13-16	m13-17	m12-1	m12-2	m12-3	m12-4	m12-12	m12-29	m12-40	m12-41	m12-49	m16-22	m16-28	m15-1	m15-2	m15-3	m15-29	m15-31
SiO2	44,09	43,74	43,78	43,39	48,5	49,24	50,61	48,48	50,02	50,28	51,12	50,35	51,78	44,57	48,08	47,56	47,42	47,47	47,19	47,89
TiO2	0,176	0,196	0,239	0,171	0,106	0,104	0,059	0,094	0,082	0,179	0,109	0,096	0,074	0,13	0,095	0,129	0,339	0,247	0,164	0,289
Al2O3	11,44	11,81	11,82	12,21	7,61	7,31	6,01	7,99	6,01	6,36	5,99	6,17	4,69	10,9	8,52	13,56	13,54	13,35	11,25	13,52
FeO	13,38	14,39	14,81	14,5	13,75	13,48	13,91	14,3	15,11	13,57	13,31	14,43	13,79	13,95	11,79	5,54	5,17	5,58	5,15	5,21
MnO	0,318	0,198	0,258	0,32	0,22	0,2	0,283	0,234	0,331	0,312	0,318	0,294	0,257	0,476	0,489	0,138	0,169	0,162	0,167	0,166
MgO	13,36	12,61	12,51	12,69	13,5	13,9	13,86	13,43	13,2	14,13	14,43	13,65	14,63	12,53	14,69	16,52	16,52	16,58	17,61	16,48
CaO	9,84	9,53	9,38	9,56	10,27	10,16	10,47	9,97	10,6	10,02	10,01	9,72	10,87	10,68	10,81	9,87	9,61	9,99	11,57	9,79
Na2O	4,63	4,73	4,83	4,51	2,8	2,81	2,44	3,04	2,15	2,47	2,52	2,85	1,95	3,42	2,99	4,62	4,38	4,54	3,25	4,49
K2O	0,322	0,418	0,4	0,419	0,281	0,326	0,233	0,351	0,264	0,229	0,216	0,285	0,19	0,436	0,235	0,037	0,051	0,037	0,275	0,074
Cr2O3	0,093	0,022	0,031	0,054	0,059	0,032	0,028	0,053	0,041	0,028	0	0,086	0,07	0,091	0,051	0,088	0,105	0,12	0,552	0,117
Total	**97,65**	**97,64**	**98,06**	**97,82**	**97,1**	**97,56**	**97,9**	**97,94**	**97,81**	**97,58**	**98,02**	**97,93**	**98,3**	**97,183**	**97,75**	**98,061**	**97,305**	**98,076**	**97,179**	**98,026**
Atoms per formula unit (23 oxygens)																				
T: Si	6,429	6,402	6,383	6,319	7,052	7,103	7,287	6,988	7,242	7,214	7,289	7,239	7,399	6,560	6,914	6,642	6,642	6,635	6,690	6,680
Al(IV)	1,571	1,598	1,617	1,681	0,948	0,897	0,713	1,012	0,758	0,786	0,711	0,761	0,601	1,440	1,086	1,358	1,358	1,365	1,310	1,320
Fe3+	0,000	0,000	0,000	0,000	0,000	0,000	0,000	0,000	0,000	0,000	0,000	0,000	0,000	0,000	0,000	0,000	0,000	0,000	0,000	0,000
Ti	0,000	0,000	0,000	0,000	0,000	0,000	0,000	0,000	0,000	0,000	0,000	0,000	0,000	0,000	0,000	0,000	0,000	0,000	0,000	0,000
T-Sum	**8,000**	**8,000**	**8,000**	**8,000**	**8,000**	**8,000**	**8,000**	**8,000**	**8,000**	**8,000**	**8,000**	**8,000**	**8,000**	**8,000**	**8,000**	**8,000**	**8,000**	**8,000**	**8,000**	**8,000**
C:Al(VI)	0,396	0,439	0,414	0,415	0,357	0,346	0,307	0,346	0,268	0,290	0,296	0,284	0,189	0,450	0,358	0,875	0,878	0,835	0,569	0,903
Ti	0,019	0,022	0,026	0,019	0,012	0,011	0,006	0,010	0,009	0,019	0,012	0,010	0,008	0,014	0,010	0,014	0,036	0,026	0,017	0,030
Fe3+	0,683	0,704	0,777	0,888	0,520	0,538	0,436	0,646	0,527	0,645	0,597	0,605	0,485	0,525	0,494	0,235	0,314	0,235	0,187	0,190
Cr	0,011	0,003	0,004	0,006	0,007	0,004	0,003	0,006	0,005	0,003	0,000	0,010	0,008	0,011	0,006	0,010	0,012	0,013	0,062	0,013
Mg	2,904	2,751	2,718	2,755	2,926	2,989	2,974	2,885	2,849	3,022	3,067	2,925	3,116	2,749	3,149	3,439	3,449	3,454	3,721	3,426
Fe2+	0,949	1,057	1,029	0,878	1,152	1,088	1,238	1,078	1,303	0,983	0,990	1,129	1,163	1,192	0,924	0,412	0,292	0,417	0,423	0,418
Mn	0,039	0,025	0,032	0,039	0,027	0,024	0,035	0,029	0,041	0,038	0,038	0,036	0,031	0,059	0,060	0,016	0,020	0,019	0,020	0,020
Ca	0,000	0,000	0,000	0,000	0,000	0,000	0,000	0,000	0,000	0,000	0,000	0,000	0,000	0,000	0,000	0,000	0,000	0,000	0,000	0,000
C-Sum	**5,000**	**5,000**	**5,000**	**5,000**	**5,000**	**5,000**	**5,000**	**5,000**	**5,000**	**5,000**	**5,000**	**5,000**	**5,000**	**5,000**	**5,000**	**5,000**	**5,000**	**5,000**	**5,000**	**5,000**
B: Ca	1,537	1,494	1,465	1,492	1,600	1,570	1,615	1,540	1,644	1,540	1,529	1,497	1,664	1,684	1,665	1,477	1,442	1,496	1,757	1,463
Na	0,463	0,506	0,535	0,508	0,400	0,430	0,385	0,460	0,356	0,460	0,471	0,503	0,336	0,316	0,335	0,523	0,558	0,504	0,243	0,537
B-Sum	**2,000**	**2,000**	**2,000**	**2,000**	**2,000**	**2,000**	**2,000**	**2,000**	**2,000**	**2,000**	**2,000**	**2,000**	**2,000**	**2,000**	**2,000**	**2,000**	**2,000**	**2,000**	**2,000**	**2,000**
A: Ca	0,000	0,000	0,000	0,000	0,000	0,000	0,000	0,000	0,000	0,000	0,000	0,000	0,000	0,000	0,000	0,000	0,000	0,000	0,000	0,000
Na	0,846	0,836	0,830	0,765	0,389	0,356	0,296	0,389	0,248	0,227	0,226	0,291	0,204	0,660	0,499	0,728	0,632	0,726	0,650	0,677
K	0,060	0,078	0,074	0,078	0,052	0,060	0,043	0,065	0,049	0,042	0,039	0,052	0,035	0,082	0,043	0,007	0,009	0,007	0,050	0,013
A-Sum	**0,906**	**0,914**	**0,905**	**0,843**	**0,441**	**0,416**	**0,339**	**0,454**	**0,296**	**0,269**	**0,265**	**0,344**	**0,239**	**0,742**	**0,542**	**0,734**	**0,641**	**0,733**	**0,700**	**0,690**

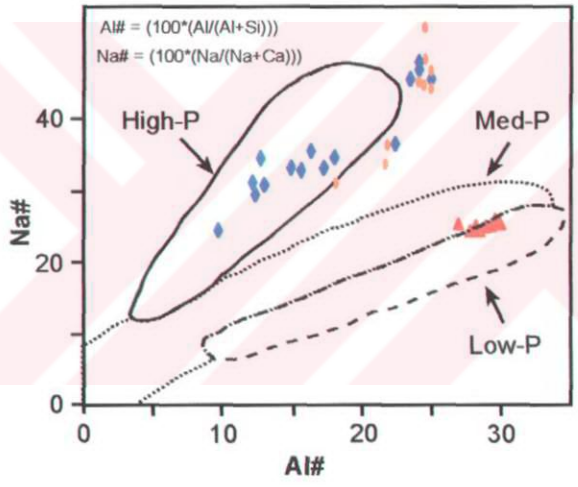
narrow (Figure 5.10). Calcic and sodic-calcic amphibole analyses belonging to omphacite metagabbro fall in the compositional range of edenite to barroisite, closer to edenite corner (Figure 5.10a). Deviation from hornblende+edenite-tschermakite tie-line indicates alkali-amphibole substitution in omphacite metagabbro (Figure 5.10b). Calcic amphiboles in omphacite metagabbro exhibit barroisite-edenite solid solution. In this solid solution, the effect of pargasite is less important (Figures 5.10c). Calcic amphiboles in garnet amphibolites are tschermakitic hornblende / tschermakite in composition (Figure 5.9a). Tschermakitic hornblende type amphiboles are more dominant in garnet amphibolite. Total of cation per formula unit in M97-149/10 (garnet amphibolite) is 15.362 in average. Based on one formula unit, the average contents of Ti (=0.049), Fe^{2+} (=1.324), and Na (A-site) (=0.288) are higher than the calcic amphiboles of omphacite-epidotites and omphacite metagabbro. Average NaM4 (=0.299) and Mg (=2.109) contents are low. Calcic amphiboles in garnet amphibolite take place near to tschermakite, tremolite corner in Figure 5.10a. Distribution of points belonging to garnet amphibolite is controlled by the combination of hornblende-tschermakite solid solutions in Figure 5.10b-5.10c.

Pressure characteristic of Ca-amphiboles from omphacite-epidotite, omphacite metagabbro and garnet amphibolites are given in Figure 5.11a-b-c. The most of Ca-amphiboles in omphacite metagabbro and omphacite-epidotite plot into high-pressure field of Laird and Albee (1981) diagram (Figure 5.11a). Ca-amphiboles from omphacite metagabbro plot outside of the high-pressure field, they are very near to high-pressure field and have same trend with high-pressure field (Figure 5.11b). Although, Ca-amphiboles from omphacite-epidotite in both diagrams of Laird and Albee (1981) display high-pressure character, they are not texturally equilibrium with high-pressure facies minerals such as omphacite and clinozoisite. But, Ca-amphiboles, which plot into high-pressure field in Figure 5.11a, in omphacite metagabbro are equilibrated with omphacite. Ca-amphiboles from garnet amphibole which are texturally and optically different from omphacite-epidotite and omphacite metagabbro, fall into low-pressure fields (Figure 5.11a - 5.11b). Textural interpretation of Ca-amphiboles from omphacite-epidotite, omphacite metagabbro and garnet amphibolite are consistent with results from the Raase (1974) diagram

a)



b)



c)

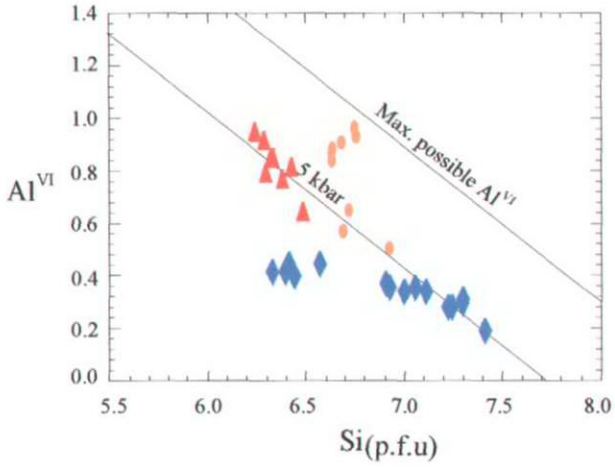


Figure 5.11 Pressure characteristic of Ca-amphiboles from omphacite-epidotite, omphacite metagabbro and garnet amphibolite plotted on Laird and Albee (1981) diagrams (a and b) and Raase (1974) diagram (c), respectively. High-pressure field is characterized by amphibole compositions from Sanbagawa and Franciscan terranes

based on the Al^{VI} vs Si contents of hornblende (Figure 5.11c). Ca-amphiboles in garnet amphibole and omphacite-epidotite occur on the 5 kbar line and below its in Figure 5.11c. The most of Ca-amphiboles from omphacite metagabbro are probably formed in higher pressure from 5 kbar. Based on this diagrams and textural relationship, the Ca-amphiboles in omphacite metagabbro can be interpreted to have been crystallized during the high-pressure metamorphism. Whereas, the Ca-amphiboles in garnet amphibolite and omphacite-epidotite characterise low-pressure metamorphism.

5.3. Clinopyroxenes

6 eclogite, 3 omphacite-epidotite and one omphacite metagabbro samples were analysed for clinopyroxene from Selçuk (Şirince), Akhisar (Gölmarmara), Söke (Nenemsuyu) and Torbalı. Representative clinopyroxene analyses are given in Table 5.5 and 5.7. The analyses of clinopyroxenes are calculated to atomic proportions on the basis of 6 oxygens. The reductions are fitted to the formula $M2M1T_2O_6$, where T, M1 and M2 represent the four-fold coordinated cations silicon and aluminum (IV), magnesium, ferric - ferrous iron and the larger coordination polyhedra containing calcium, sodium and potassium, respectively.

5.3.1. Clinopyroxenes in eclogites

Six eclogite samples were analysed from Şirince and Gölmarmara areas. All these eclogites blocks occur in metaolistostrome unit. 210 analyses were carried out from clinopyroxenes in eclogites. The representative analyses are given in Table 5.5 In Smulikowski's (1972) diagram based on the Na-Al-Ca atomic ratio, the great majority of the omphacitic clinopyroxenes are concentrated within or near to ophiolitic (low-temperature) eclogite field (Figure 5.12). Symplectitic clinopyroxenes in sodic augite and/or aegirine augite in composition generally fall near to O and C boundaries or outside of the fields. The cation sums per six oxygens range from 3.975 to 4 with an average of 3.990 which is in good agreement with the stoichiometric value of 4.000. The proportions of Si per formula unit range from

Table 5.5 Representative omphacite analyses from eclogite blocks in metaolistostrome unit.

	Şirince																				Gölmarmara				
sample no	95-21/10								M96-31												M97-34/2				
Analyse no	m20-3	m20-32	m20-33	m20-34	m20-21	m20-30	m20-31	m20-36	m5-26	m5-55	m5-61	m5-69	m4-93	m4-94	m4-95	m4-99	m4-96	m5-40	m5-47	m5-70	m7-25	m7-39	m7-40	m7-41	m7-42
	Cprx-IIB				Cprx-IA				Cprx-IA				Cprx-IB				Cprx-III				Cprx-IIB				
SiO2	52,99	53,13	53,13	53,07	54,68	54,31	54,21	54,59	56,02	56,19	56,45	55,84	55,64	54,95	55,52	54,25	54,63	54,00	55,18	54,05	53,34	54,48	54,34	54,38	53,24
TiO2	0,11	0,09	0,10	0,07	0,12	0,08	0,07	0,05	0,10	0,13	0,05	0,27	0,20	0,15	0,09	0,42	0,04	0,09	0,11	0,07	0,07	0,13	0,04	0,06	0,16
Al2O3	4,68	6,09	5,99	6,05	9,46	7,08	7,47	7,48	10,99	11,17	10,80	11,09	9,77	9,71	9,75	9,40	2,64	3,18	3,09	2,91	5,03	7,38	6,99	7,23	5,94
FeO	14,95	14,90	14,51	15,59	6,40	7,01	7,81	6,91	4,86	6,12	4,75	4,17	5,47	5,43	5,25	5,75	6,46	6,45	6,51	6,66	9,13	9,28	9,29	9,05	9,93
MnO	0,22	0,24	0,26	0,42	0,25	0,29	0,28	0,24	0,14	0,12	0,09	0,18	0,15	0,14	0,09	0,12	0,39	0,22	0,28	0,35	0,30	0,41	0,42	0,46	0,52
MgO	6,12	5,59	5,63	5,01	8,21	9,41	8,65	9,09	7,74	6,90	8,11	8,04	8,49	8,60	8,72	8,96	13,32	12,37	12,57	12,76	9,48	7,93	8,03	8,27	8,61
CaO	13,71	12,34	12,71	12,09	14,02	16,24	15,32	15,51	12,65	12,03	13,23	13,84	14,24	14,30	14,17	15,32	21,93	21,25	20,58	21,53	16,38	13,85	14,38	14,00	15,27
Na2O	6,26	7,13	6,87	7,08	6,49	5,06	5,65	5,37	7,50	8,18	7,45	7,05	6,81	6,78	6,93	6,01	2,15	2,37	2,32	2,45	5,28	6,61	6,44	6,33	5,65
K2O	0,00	0,02	0,02	0,01	0,00	0,00	0,04	0,01	0,00	0,01	0,00	0,02	0,02	0,02	0,00	0,01	0,00	0,01	0,01	0,00	0,02	0,01	0,01	0,02	0,00
Cr2O3	0,03	0,04	0,00	0,04	0,09	0,08	0,02	0,00	0,06	0,12	0,08	0,02	0,01	0,06	0,01	0,12	0,04	0,05	0,08	0,07	0,00	0,03	0,05	0,04	0,02
Total	99,06	99,58	99,22	99,44	99,72	99,55	99,52	99,24	100,06	100,97	101,01	100,52	100,81	100,15	100,53	100,36	101,61	99,99	100,72	100,84	99,03	100,12	99,99	99,84	99,34
normalized 6 oxygens																									
Si	1,977	1,959	1,968	1,968	1,964	1,973	1,968	1,985	1,985	1,975	1,980	1,972	1,967	1,953	1,962	1,936	1,968	1,977	2,008	1,960	1,955	1,965	1,965	1,968	1,949
Al(IV)	0,023	0,041	0,032	0,032	0,036	0,027	0,032	0,015	0,015	0,025	0,020	0,028	0,033	0,047	0,038	0,064	0,032	0,023	0,000	0,040	0,045	0,035	0,035	0,032	0,051
Sum	2,000	2,000	2,000	2,000	2,000	2,000	2,000	2,000	2,000	2,000	2,000	2,000	2,000	2,000	2,000	2,000	2,000	2,000	2,008	2,000	2,000	2,000	2,000	2,000	2,000
Al(VI)	0,182	0,224	0,230	0,233	0,364	0,276	0,288	0,306	0,444	0,438	0,427	0,434	0,374	0,360	0,369	0,332	0,080	0,114	0,133	0,085	0,172	0,279	0,262	0,276	0,205
Fe2+	0,175	0,135	0,157	0,178	0,071	0,108	0,098	0,123	0,060	0,039	0,041	0,053	0,041	0,012	0,014	0,035	0,093	0,123	0,170	0,077	0,033	0,065	0,058	0,075	0,062
Fe3+	0,291	0,324	0,292	0,306	0,121	0,105	0,139	0,087	0,084	0,141	0,099	0,070	0,121	0,150	0,141	0,137	0,102	0,074	0,028	0,125	0,246	0,215	0,223	0,199	0,242
Mg	0,340	0,307	0,311	0,277	0,438	0,507	0,468	0,483	0,408	0,361	0,424	0,423	0,447	0,456	0,459	0,477	0,715	0,675	0,664	0,690	0,518	0,426	0,433	0,446	0,470
Ti	0,003	0,002	0,003	0,002	0,003	0,002	0,002	0,001	0,003	0,003	0,001	0,007	0,005	0,004	0,002	0,011	0,001	0,003	0,003	0,002	0,002	0,004	0,001	0,002	0,004
Cr	0,001	0,001	0,000	0,001	0,003	0,002	0,001	0,000	0,002	0,003	0,002	0,001	0,000	0,002	0,000	0,003	0,001	0,001	0,002	0,002	0,000	0,001	0,001	0,001	0,001
Sum	0,993	0,994	0,993	0,997	1,000	1,000	0,996	1,000	1,000	0,986	0,993	0,988	0,988	0,983	0,986	0,994	0,992	0,991	1,000	0,980	0,972	0,990	0,978	0,998	0,984
Na	0,453	0,510	0,493	0,509	0,452	0,356	0,398	0,379	0,515	0,557	0,507	0,483	0,467	0,467	0,475	0,416	0,150	0,168	0,164	0,172	0,375	0,462	0,451	0,444	0,401
Ca	0,548	0,487	0,504	0,480	0,539	0,632	0,596	0,604	0,480	0,453	0,497	0,524	0,539	0,545	0,537	0,586	0,846	0,834	0,802	0,837	0,643	0,535	0,557	0,543	0,599
Mg	0,000	0,000	0,000	0,000	0,001	0,003	0,000	0,009	0,001	0,000	0,000	0,000	0,000	0,000	0,000	0,000	0,000	0,000	0,017	0,000	0,000	0,000	0,000	0,000	0,000
Sum	1,001	0,997	0,998	0,990	0,993	0,991	0,994	0,992	0,996	1,010	1,004	1,006	1,006	1,012	1,011	1,002	0,996	1,002	0,983	1,009	1,018	0,997	1,008	0,987	1,000
Jd	17,851	21,616	22,392	22,862	35,526	27,237	28,153	30,657	44,004	42,410	41,730	42,219	36,156	34,153	35,228	31,448	7,761	11,194	13,763	8,110	16,209	27,108	25,166	27,112	19,623
Ac	28,491	31,309	28,475	29,993	11,822	10,395	13,615	8,716	8,361	13,695	9,643	6,799	11,682	14,200	13,506	12,988	9,885	7,250	2,928	11,952	23,205	20,868	21,417	19,552	23,153
Au	53,658	47,075	49,133	47,145	52,652	62,369	58,232	60,627	47,635	43,895	48,627	50,982	52,162	51,647	51,267	55,563	82,354	81,556	83,309	79,937	60,586	52,023	53,417	53,336	57,224
Quad	1,063	0,930	0,972	0,935	1,050	1,249	1,162	1,220	0,948	0,853	0,962	1,000	1,027	1,012	1,010	1,097	1,654	1,632	1,654	1,603	1,194	1,027	1,047	1,063	1,130
Jd	0,905	1,019	0,987	1,018	0,904	0,713	0,795	0,757	1,030	1,115	1,013	0,965	0,933	0,934	0,950	0,832	0,300	0,336	0,327	0,345	0,750	0,924	0,903	0,888	0,802
Quad	54,016	47,705	49,634	47,878	53,743	63,672	59,361	61,708	47,936	43,349	48,701	50,885	52,400	51,989	51,532	56,880	84,638	82,908	83,479	82,312	61,420	52,622	53,704	54,497	58,497
Jd	17,713	21,358	22,171	22,545	34,707	26,294	27,392	29,815	43,752	42,823	41,670	42,302	35,976	33,911	35,036	30,516	6,757	10,374	13,623	7,151	15,866	26,770	25,011	26,438	19,039
Ae	28,270	30,937	28,195	29,577	11,550	10,035	13,247	8,477	8,313	13,828	9,629	6,813	11,623	14,099	13,432	12,603	8,605	6,719	2,898	10,538	22,714	20,608	21,285	19,066	22,464
Jd%	17,713	21,358	22,171	22,545	34,707	26,294	27,392	29,815	43,752	42,82324	41,670	42,302	35,976	33,911	35,036	30,516	6,757	10,374	13,623	7,151	15,866	26,770	25,011	26,438	19,039
Di%	35,643	33,127	32,969	29,153	46,261	52,569	49,103	49,361	41,826	39,17199	44,432	45,193	48,009	50,691	50,028	53,023	74,898	70,096	66,826	74,056	57,691	45,641	47,402	46,663	51,709
Hd%	18,374	14,578	16,665	18,725	7,482	11,102	10,258	12,348	6,110	4,176921	4,269	5,692	4,391	1,299	1,504	3,857	9,740	12,811	16,653	8,256	3,729	6,981	6,303	7,834	6,788
Ae%	28,270	30,937	28,195	29,577	11,550	10,035	13,247	8,477	8,313	13,82785	9,629	6,813	11,623	14,099	13,432	12,603	8,605	6,719	2,898	10,538	22,714	20,608	21,285	19,066	22,464

Cprx-IA: coarse grained clinopyroxene Cprx-IIA: omphacite aggregate Cprx-III: symplectite
Cprx-IB: omphacite inclusions in garnet Cprx-IIB: greenish colour clinopyroxene

Table 5.5 continued

	Gölmarmara					Şirince																		
	M97-34/2					M98-45C									M99-5/4				SE-1					
sample no	m7-27	m7-35	m7-36	m7-90	m7-91	m4-17	m4-22	m4-52	m4-53	m4-1	m4-2	m4-3	m4-20	m4-64	m19-4	m19-1	m19-2	m19-22	m8-28	m8-29	m8-30	m8-31	m8-33	m8-34	m8-179
Analyse no	Cprx-III					Cprx-IA				Cprx-IIB		Cprx-III			Cprx-IA				Cprx-IA					
SiO2	53,15	53,02	52,67	52,91	53,09	54,73	55,26	56,22	55,93	55,04	55,02	54,41	54,58	53,23	55,58	55,78	55,46	55,52	54,04	54,66	54,28	54,48	53,45	55,28	54,10
TiO2	0,04	0,08	0,04	0,00	0,09	0,15	0,22	0,06	0,08	0,08	0,05	0,00	0,11	0,10	0,03	0,07	0,08	0,00	0,25	0,08	0,02	0,11	0,03	0,11	0,05
Al2O3	3,95	2,25	2,60	2,85	2,56	9,50	9,78	11,60	11,24	6,91	7,43	3,01	2,68	2,74	11,61	11,97	10,45	8,38	7,75	7,63	5,65	7,63	5,27	7,89	5,07
FeO	9,28	9,28	9,73	10,78	10,23	5,24	5,60	5,27	5,53	6,37	6,17	6,75	7,29	6,98	6,75	6,64	7,00	5,46	7,26	7,12	8,06	6,83	7,71	6,89	8,93
MnO	0,60	0,66	0,68	0,46	0,54	0,11	0,16	0,05	0,03	0,11	0,10	0,17	0,22	0,17	0,00	0,04	0,01	0,14	0,51	0,32	0,18	0,27	0,26	0,32	0,24
MgO	10,26	11,50	11,16	10,14	10,83	8,45	8,46	7,12	7,25	9,97	9,72	12,73	12,13	12,64	6,18	5,92	6,75	9,17	8,61	9,04	10,15	9,28	10,20	8,87	10,06
CaO	18,16	20,34	19,87	18,65	19,29	14,10	14,33	12,40	12,93	16,63	16,42	20,72	21,88	22,24	11,19	10,65	12,37	15,52	14,87	15,52	17,79	15,23	17,89	14,77	17,59
Na2O	4,13	2,97	3,11	3,43	3,26	6,27	6,73	7,92	7,45	5,28	5,32	2,62	2,28	1,79	8,26	8,46	7,57	5,73	6,16	5,88	4,41	6,06	4,33	6,30	4,42
K2O	0,00	0,00	0,00	0,00	0,01	0,02	0,01	0,00	0,00	0,00	0,00	0,00	0,00	0,03	0,00	0,00	0,00	0,00	0,00	0,02	0,00	0,00	0,00	0,00	0,01
Cr2O3	0,07	0,05	0,05	0,10	0,01	0,15	0,27	0,08	0,05	0,16	0,01	0,03	0,40	0,18	0,01	0,03	0,00	0,01	0,06	0,04	0,04	0,07	0,00	0,00	0,01
Total	99,65	100,15	99,92	99,32	99,91	98,74	100,82	100,72	100,50	100,54	100,24	100,43	101,57	100,10	99,61	99,56	99,69	99,92	99,51	100,32	100,57	99,96	99,14	100,44	100,49
normalized 6 oxygens																									
Si	1,952	1,950	1,942	1,969	1,960	1,981	1,956	1,978	1,979	1,971	1,975	1,978	1,978	1,956	1,982	1,989	1,986	1,992	1,954	1,961	1,963	1,955	1,959	1,975	1,963
Al(IV)	0,048	0,050	0,058	0,031	0,040	0,019	0,044	0,022	0,021	0,029	0,025	0,022	0,022	0,044	0,018	0,011	0,014	0,008	0,046	0,039	0,037	0,045	0,041	0,025	0,037
Sum	2,000	2,000	2,000	2,000	2,000	2,000	2,000	2,000	2,000	2,000	2,000	2,000	2,000	2,000	2,000	2,000	2,000	2,000	2,000	2,000	2,000	2,000	2,000	2,000	2,000
Al(VI)	0,123	0,047	0,055	0,094	0,072	0,386	0,364	0,459	0,448	0,263	0,289	0,107	0,093	0,075	0,470	0,492	0,427	0,346	0,284	0,284	0,204	0,278	0,187	0,307	0,180
Fe2+	0,067	0,073	0,076	0,151	0,117	0,089	0,030	0,053	0,082	0,060	0,080	0,106	0,135	0,121	0,084	0,096	0,100	0,104	0,033	0,051	0,102	0,020	0,076	0,055	0,105
Fe3+	0,218	0,213	0,224	0,185	0,199	0,069	0,136	0,102	0,082	0,131	0,105	0,099	0,086	0,093	0,118	0,102	0,110	0,060	0,186	0,162	0,142	0,185	0,160	0,151	0,166
Mg	0,562	0,630	0,613	0,562	0,596	0,447	0,446	0,373	0,382	0,532	0,520	0,687	0,655	0,692	0,327	0,307	0,360	0,490	0,464	0,483	0,547	0,496	0,557	0,472	0,544
Ti	0,001	0,002	0,001	0,000	0,003	0,004	0,006	0,002	0,002	0,002	0,001	0,000	0,003	0,003	0,001	0,002	0,002	0,000	0,007	0,002	0,000	0,003	0,001	0,003	0,001
Cr	0,002	0,001	0,002	0,003	0,000	0,004	0,008	0,002	0,001	0,005	0,000	0,001	0,011	0,005	0,000	0,001	0,000	0,000	0,002	0,001	0,001	0,002	0,000	0,000	0,000
Sum	0,973	0,966	0,971	0,995	0,986	1,000	0,989	0,991	0,998	0,992	0,996	1,000	0,983	0,990	1,000	1,000	0,999	1,000	0,977	0,984	0,996	0,984	0,982	0,989	0,997
Na	0,294	0,212	0,222	0,247	0,233	0,440	0,462	0,540	0,511	0,367	0,370	0,185	0,160	0,128	0,571	0,585	0,526	0,399	0,432	0,409	0,309	0,422	0,308	0,436	0,311
Ca	0,714	0,801	0,785	0,744	0,763	0,547	0,543	0,467	0,490	0,638	0,631	0,807	0,850	0,876	0,428	0,407	0,475	0,597	0,576	0,596	0,689	0,586	0,703	0,565	0,684
Mg	0,000	0,000	0,000	0,000	0,000	0,009	0,000	0,000	0,000	0,000	0,000	0,003	0,000	0,000	0,001	0,007	0,000	0,001	0,000	0,000	0,000	0,000	0,000	0,000	0,000
Sum	1,009	1,013	1,007	0,991	0,996	0,995	1,005	1,007	1,001	1,005	1,001	0,995	1,010	1,003	1,000	0,999	1,000	0,996	1,008	1,005	0,998	1,007	1,010	1,002	0,995
Jd	11,642	4,442	5,199	9,190	6,937	38,524	34,887	44,631	43,936	25,471	28,163	10,585	9,022	7,201	46,319	49,143	42,236	34,529	27,167	27,199	19,697	26,521	17,827	30,024	17,499
Ac	20,663	20,046	21,013	18,062	19,234	6,904	13,032	9,909	7,998	12,670	10,275	9,779	8,383	8,928	11,580	10,213	10,856	6,002	17,812	15,583	13,709	17,652	15,265	14,745	16,114
Au	67,695	75,512	73,789	72,748	73,829	54,572	52,081	45,459	48,066	61,859	61,561	79,635	82,595	83,871	42,101	40,644	46,908	59,469	55,021	57,218	66,594	55,827	66,908	55,231	66,387
Quad	1,343	1,504	1,475	1,457	1,476	1,092	1,019	0,894	0,955	1,230	1,231	1,603	1,640	1,689	0,840	0,817	0,935	1,191	1,073	1,131	1,338	1,102	1,336	1,093	1,333
Jd	0,588	0,423	0,445	0,495	0,467	0,880	0,924	1,080	1,022	0,733	0,740	0,369	0,320	0,255	1,142	1,170	1,051	0,797	0,864	0,818	0,618	0,843	0,615	0,873	0,622
Quad	69,546	78,033	76,835	74,642	75,978	55,378	52,467	45,277	48,292	62,660	62,447	81,274	83,653	86,882	42,370	41,131	47,068	59,897	55,408	58,033	68,395	56,646	68,461	55,594	68,187
Jd	10,975	3,984	4,595	8,551	6,368	37,841	34,606	44,780	43,745	24,936	27,514	9,734	8,474	5,857	46,104	48,739	42,109	34,165	26,934	26,681	18,635	26,029	16,990	29,780	16,562
Ae	19,479	17,983	18,571	16,807	17,654	6,781	12,927	9,943	7,963	12,404	10,038	8,992	7,873	7,262	11,526	10,129	10,824	5,939	17,658	15,286	12,970	17,325	14,548	14,626	15,251
Jd%	10,975	3,984	4,595	8,551	6,368	37,841	34,606	44,780	43,745	24,936	27,514	9,734	8,474	5,857	46,104	48,739	42,109	34,165	26,934	26,681	18,635	26,029	16,990	29,780	16,562
Di%	62,145	69,970	68,316	58,857	63,505	46,296	49,185	39,634	39,759	56,304	54,140	70,440	69,388	73,931	33,767	31,534	36,860	49,450	51,726	52,481	57,662	54,472	60,241	49,804	57,158
Hd%	7,401	8,062	8,519	15,785	12,473	9,082	3,282	5,643	8,533	6,356	8,308	10,835	14,265	12,951	8,603	9,597	10,208	10,447	3,682	5,552	10,734	2,174	8,220	5,790	11,028
Ae%	19,479	17,983	18,571	16,807	17,654	6,781	12,927	9,943	7,963	12,404	10,038	8,992	7,873	7,262	11,526	10,129	10,824	5,939	17,658	15,286	12,970	17,325	14,548	14,626	15,251

Cprx-IA: coarse grained clinopyroxene
Cprx-IB: omphacite inclusions in garnet
Cprx-IIA: omphacite aggregate
Cprx-IIB: greenish colour clinopyroxene
Cprx-III: symplectite

Table 5.5 continued

	Şirince																					
	SE-1																					
sample no	m8-180	m8-181	m8-182	m8-183	m8-184	m8-185	m8-186	m8-187	m8-7	m8-20	m8-21	m8-22	m8-23	m8-24	m8-25	m8-27	m8-42	m8-51	m8-52	m8-84	m8-85	m8-126
Analyse no	Cprx-IA								Cprx-IB													
SiO2	54,83	54,32	54,87	54,73	54,22	54,65	54,47	54,03	54,14	54,29	54,55	54,12	53,84	54,68	54,06	54,39	55,22	54,61	54,90	54,56	54,20	54,93
TiO2	0,00	0,06	0,15	0,05	0,06	0,01	0,04	0,00	0,03	0,13	0,07	0,07	0,17	0,10	0,00	0,03	0,06	0,11	0,09	0,09	0,04	0,10
Al2O3	6,00	6,90	7,94	6,72	6,01	7,66	7,59	5,21	5,72	7,87	6,26	6,99	7,80	8,05	6,14	7,04	9,58	7,72	7,46	7,05	6,93	8,29
FeO	8,00	7,80	6,91	8,26	9,64	7,57	7,38	9,84	8,46	7,31	8,23	8,68	7,36	7,08	8,35	8,32	5,47	7,07	7,35	8,11	9,37	6,91
MnO	0,32	0,50	0,44	0,23	0,34	0,35	0,40	0,24	0,38	0,43	0,36	0,46	0,53	0,34	0,41	0,44	0,79	0,54	0,33	0,30	0,41	0,54
MgO	9,64	9,00	9,16	9,12	8,78	8,91	8,85	9,12	9,55	8,78	9,46	8,47	8,76	8,84	9,16	8,95	8,54	8,76	9,23	9,01	8,39	8,65
CaO	15,91	15,65	15,13	16,18	15,98	14,64	15,33	17,54	17,21	14,89	15,86	14,94	14,88	14,89	15,44	15,25	13,85	15,17	15,74	15,59	14,61	14,63
Na2O	5,56	5,24	5,95	5,56	5,23	5,96	5,65	4,50	4,76	6,17	5,75	5,84	6,07	6,02	5,45	6,05	6,74	5,90	5,60	5,81	6,15	6,03
K2O	0,00	0,00	0,01	0,01	0,00	0,01	0,00	0,00	0,01	0,01	0,00	0,00	0,00	0,01	0,00	0,00	0,03	0,00	0,00	0,00	0,02	0,00
Cr2O3	0,01	0,01	0,00	0,05	0,01	0,04	0,00	0,02	0,02	0,06	0,08	0,00	0,05	0,01	0,00	0,06	0,05	0,03	0,04	0,00	0,00	0,03
Total	100,27	99,49	100,56	100,91	100,26	99,79	99,72	100,49	100,28	99,93	100,62	99,57	99,45	100,03	99,01	100,53	100,33	99,91	100,74	100,52	100,12	100,10
normalized 6 oxygens																						
Si	1,975	1,979	1,961	1,963	1,971	1,972	1,971	1,970	1,965	1,953	1,958	1,968	1,948	1,966	1,977	1,951	1,963	1,969	1,966	1,960	1,959	1,974
Al(IV)	0,025	0,021	0,039	0,037	0,029	0,028	0,029	0,030	0,035	0,047	0,042	0,032	0,052	0,034	0,023	0,049	0,037	0,031	0,034	0,040	0,041	0,026
Sum	2,000	2,000	2,000	2,000	2,000	2,000	2,000	2,000	2,000	2,000	2,000	2,000	2,000	2,000	2,000	2,000	2,000	2,000	2,000	2,000	2,000	2,000
Al(VI)	0,229	0,275	0,296	0,247	0,228	0,297	0,295	0,194	0,209	0,287	0,222	0,267	0,280	0,307	0,242	0,249	0,365	0,297	0,281	0,258	0,254	0,326
Fe2+	0,057	0,123	0,056	0,072	0,125	0,081	0,094	0,145	0,097	0,033	0,029	0,089	0,030	0,068	0,087	0,030	0,027	0,070	0,081	0,059	0,066	0,090
Fe3+	0,184	0,114	0,151	0,176	0,168	0,147	0,129	0,155	0,160	0,187	0,218	0,175	0,193	0,144	0,168	0,220	0,135	0,143	0,139	0,184	0,217	0,117
Mg	0,517	0,485	0,488	0,487	0,476	0,473	0,477	0,496	0,517	0,471	0,506	0,459	0,472	0,474	0,499	0,479	0,453	0,471	0,493	0,482	0,452	0,463
Ti	0,000	0,002	0,004	0,001	0,002	0,000	0,001	0,000	0,001	0,004	0,002	0,002	0,005	0,003	0,000	0,001	0,002	0,003	0,002	0,002	0,001	0,003
Cr	0,000	0,000	0,000	0,001	0,000	0,001	0,000	0,000	0,001	0,002	0,002	0,000	0,001	0,000	0,000	0,002	0,001	0,001	0,001	0,000	0,000	0,001
Sum	0,988	1,000	0,995	0,984	0,999	1,000	0,997	0,990	0,984	0,983	0,979	0,992	0,981	0,996	0,996	0,980	0,983	0,985	0,997	0,987	0,990	1,000
Na	0,388	0,370	0,412	0,387	0,369	0,417	0,396	0,318	0,335	0,430	0,400	0,412	0,426	0,420	0,386	0,421	0,465	0,412	0,389	0,405	0,431	0,420
Ca	0,614	0,611	0,579	0,622	0,622	0,566	0,594	0,685	0,669	0,574	0,610	0,582	0,577	0,573	0,605	0,586	0,528	0,586	0,604	0,600	0,566	0,563
Mg	0,000	0,004	0,000	0,000	0,000	0,006	0,000	0,000	0,000	0,000	0,000	0,000	0,000	0,000	0,000	0,000	0,000	0,000	0,000	0,000	0,000	0,000
Sum	1,002	0,984	0,992	1,008	0,991	0,989	0,991	1,003	1,004	1,004	1,010	0,994	1,002	0,993	0,991	1,007	0,992	0,998	0,993	1,004	0,997	0,984
Jd	22,338	27,520	28,838	23,614	22,420	29,432	28,970	18,735	20,159	27,370	21,166	26,110	26,711	29,934	23,808	23,610	35,496	28,973	27,435	24,768	24,500	32,351
Ac	17,906	11,415	14,700	16,855	16,481	14,583	12,664	14,972	15,413	17,851	20,786	17,051	18,365	14,097	16,562	20,818	13,154	13,927	13,599	17,678	20,933	11,672
Au	59,756	61,065	56,462	59,531	61,099	55,986	58,365	66,293	64,428	54,779	58,048	56,839	54,924	55,969	59,630	55,572	51,349	57,100	58,966	57,554	54,567	55,977
Quad	1,188	1,223	1,123	1,181	1,223	1,126	1,166	1,326	1,282	1,077	1,144	1,130	1,079	1,115	1,191	1,095	1,008	1,127	1,177	1,142	1,084	1,117
Jd	0,776	0,740	0,825	0,773	0,737	0,834	0,793	0,636	0,670	0,861	0,800	0,823	0,851	0,839	0,773	0,842	0,929	0,825	0,778	0,809	0,862	0,840
Quad	60,483	62,296	57,662	60,433	62,397	57,456	59,528	67,579	65,690	55,596	58,854	57,857	55,891	57,071	60,659	56,537	52,025	57,741	60,225	58,521	55,705	57,070
Jd	21,934	26,650	28,043	23,087	21,672	28,448	28,161	18,020	19,444	26,876	20,760	25,494	26,138	29,185	23,201	23,097	35,003	28,540	26,593	24,204	23,886	31,553
Ae	17,583	11,054	14,295	16,480	15,931	14,095	12,311	14,401	14,866	17,528	20,387	16,649	17,971	13,744	16,140	20,366	12,971	13,719	13,182	17,275	20,408	11,383
Jd%	21,934	26,650	28,043	23,087	21,672	28,448	28,161	18,020	19,444	26,876	20,760	25,494	26,138	29,185	23,201	23,097	35,003	28,540	26,593	24,204	23,886	31,553
Di%	54,484	49,734	51,756	52,685	49,400	49,149	49,703	52,261	55,335	51,966	55,703	48,432	52,574	49,870	51,629	53,200	49,047	50,244	51,737	52,112	48,591	47,773
Hd%	5,998	12,562	5,906	7,748	12,997	8,307	9,825	15,318	10,355	3,630	3,150	9,425	3,317	7,201	9,030	3,337	2,978	7,496	8,488	6,409	7,114	9,302
Ae%	17,583	11,054	14,295	16,480	15,931	14,095	12,311	14,401	14,866	17,528	20,387	16,649	17,971	13,744	16,140	20,366	12,971	13,719	13,182	17,275	20,408	11,388

Cprx-IA: coarse grained clinopyroxene Cprx-IIA: omphacite aggregate Cprx-III: symplectite
Cprx-IB: omphacite inclusions in garnet Cprx-IIB: greenish colour clinopyroxene

1.936 to 2.007. Aluminum substitution for Si in the four-fold coordination site is very little. Maximum Al^{IV} and average Al^{IV} are 0.063 and 0.033, respectively. Average Ti content of analysed clinopyroxenes is 0.002. Average values in wt % for Cr2O3 and K2O are 0.049 and 0.006, respectively.

Clinopyroxenes in eclogites can be texturally divided into five groups (Cprx-IA, Cprx-IB, Cprx-IIA, Cprx-IIB and Cprx-III). Omphacites with pale green pleochroism and coarse grained crystals are named as a Cprx-IA. Cprx-IA commonly has high Jd content (24 to 45 mol%). Omphacite inclusions especially in garnet are called as a Cprx-IB. These omphacite inclusions are mainly observed in SE-1 and their Jd contents are range from 30 to 36 mol%. Cprx-IIA is represented by omphacite aggregates. They have jadeite content ranging between 20 and 35 mol%. Omphacites with more greenish pleochroism were named as a Cprx-IIB. Jd content of Cprx-IIB ranges from 12 to 29%. The symplectites (Cprx-III) are composed of vermicular and granular intergrowths of plagioclase and clinopyroxene. Symplectites are poor-in jadeite end-member (3 to12 mol%).

Clinopyroxene analyses are plotted in the Q-J diagram (Figure 5.13). The clinopyroxenes are included in the fields of Ca-Na and Quad pyroxene groups proposed by Morimoto et al. (1988). In the Q-J diagram, they plot very near to the line Q + J = 2 which represents the upper limit of Ca + Mg + Fe^{2+} + 2Na cations on M sites. Especially, symplectites with low jadeite content take place in Quad field.

In the diagram of Essene and Fyfe (1967), the clinopyroxenes in eclogites are omphacite, chloromelanite and sodic augite in composition (Figure 5.14) and their distribution along the omphacite – sodic augite probably reflects the existance of a miscibility gap between omphacite and sodic augite. Apart from minor chloromelanites, common sodic pyroxenes (Cprx-IA, Cprx-IB and Cprx-IIA) have lower acmite and hedenbergite contents and plot in the omphacite field (Figure 5.14). Cprx-IIB display a trend which is paralel to sodic augite – chloromelanite fields. All Cprx-III fall into sodic augite field. Locations of all clinopyroxene analyses in

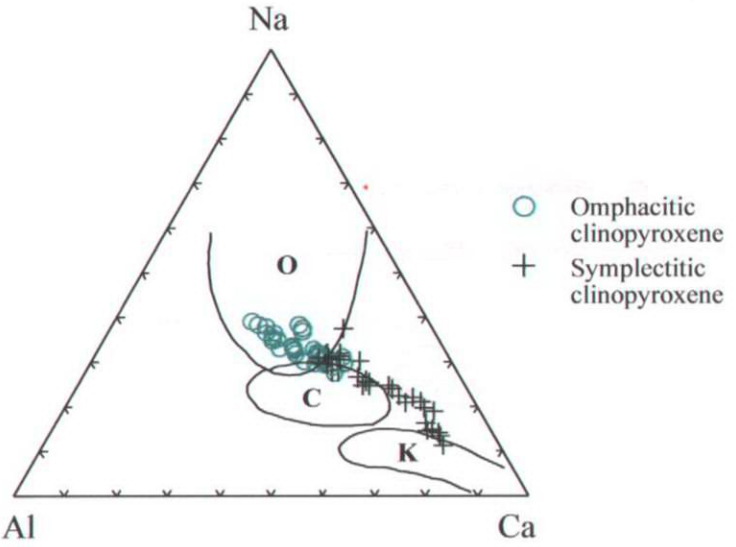


Figure 5.12 Clinopyroxene compositions from different type of eclogites (Smulikowski, 1972). K= nodular xenoliths in kimberlite; C= 'common' eclogites (from high-grade gneisses and migmatites); O='ophiolitic' or 'alpine-type' eclogites (from high-P/low-T terranes).

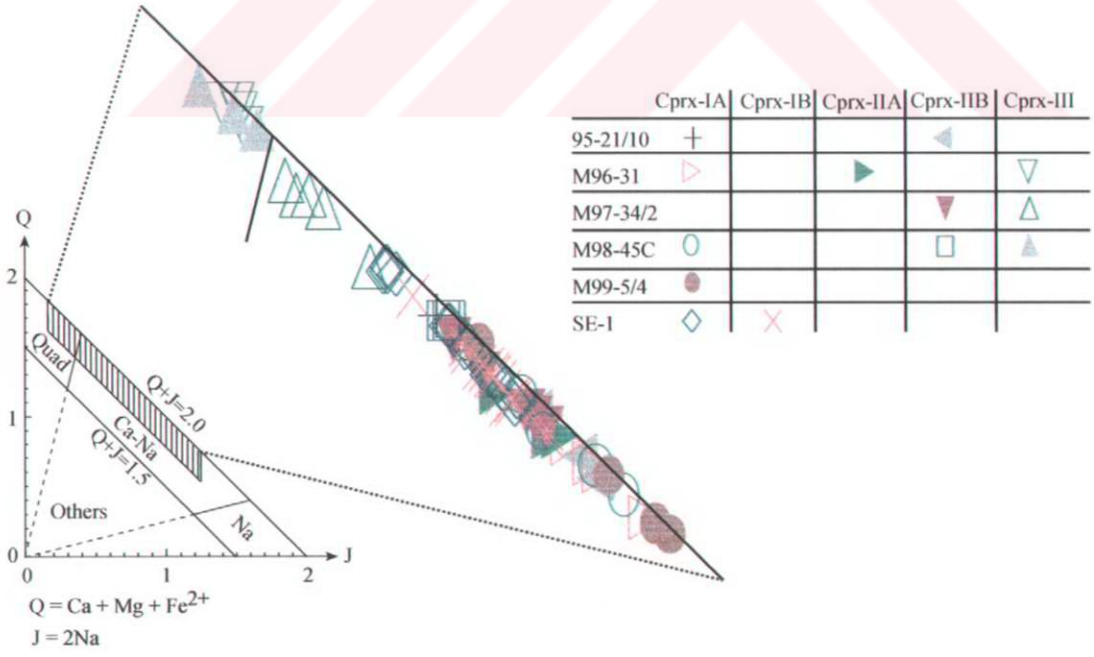


Figure 5.13 Classification of clinopyroxene analyses from eclogites on Q-J ternary diagram (Morimoto et al.1988).

Essene and Fyfe (1967) diagram are given in Figure 5.14g. Average composition of Cprx-IA, Cprx-IB, Cprx-IIA, Cprx-IIB, and Cprx-III are given in Table 5.6.

Table 5.6 Average clinopyroxene compositions in eclogites.

	Number of samples	Average composition
Cprx-IA	31	$Jd_{32}\ Ac_{12}\ Di_{48}\ Hd_{8}$
Crpx-IB	4	$Jd_{34}\ Ac_{13}\ Di_{50}\ Hd_{3}$
Cprx-IIA	14	$Jd_{26}\ Ac_{16}\ Di_{52}\ Hd_{6}$
Cprx-IIB	11	$Jd_{23}\ Ac_{22}\ Di_{45}\ Hd_{10}$
Cprx-III	12	$Jd_{8}\ Ac_{12}\ Di_{68}\ Hd_{12}$

The omphacite are essentially solid solution between diopside ($CaMgSi_2O_6$) and jadeite ($NaAlSi_2O_6$) with minor amount of hedenbergite ($CaFeSi_2O_6$) and acmite ($NaFe^{3+}Si_2O_6$) compenents. Compositional profiles across Na pyroxene grains show irregular zoning. However, in some specimens such as SE-1 where a regular variation has been found, Al^{VI} and Na decrease (Figure 5.15). Whereas both Mg and Ca slightly increase towards the rims (Figure 5.15). Fe is exchanged either by Na or Al (suggesting solid solution of aegirine in jadeite), or more commonly with Mg and Ca (suggesting diopside-hedenbergite solid solution in jadeite). The zonation (Figure 5.15) in coarse omphacite (core: Jd28, rim: Jd17) is indicative of retrograde P,T decrease due to exhumation processes.

Na vs Ca per six oxygens for the metamorphic clinopyroxenes are plotted in Figure 5.16a. Basically this diagram shows the occupancy of the large 6 fold structural site M2, in clinopyroxene. All analyses lie very close to the dashed line marking pyroxene composition, which satisfy the constraint $\sum Ca + Na = 1$. Departure of the points from the dashed line reflects analytical error, minor presence of additional cations such as Mn, Fe^{2+} and Mg (below line), or actual presence of minor Ca + Na (above line) in M1. The sum of Na + Ca ranges from 0.965 to 1.018 with an average 0.999, indicating that there is very minor solid solution. Figure 5.16a shows that the Na / Ca ratios of the clinopyroxenes are close to, but in most cases slightly exceed, 1/1 line. Figure 5.16b demonstrates that $(Al^{VI}+Fe^{3+}) / (Mg+Fe^{2+})$

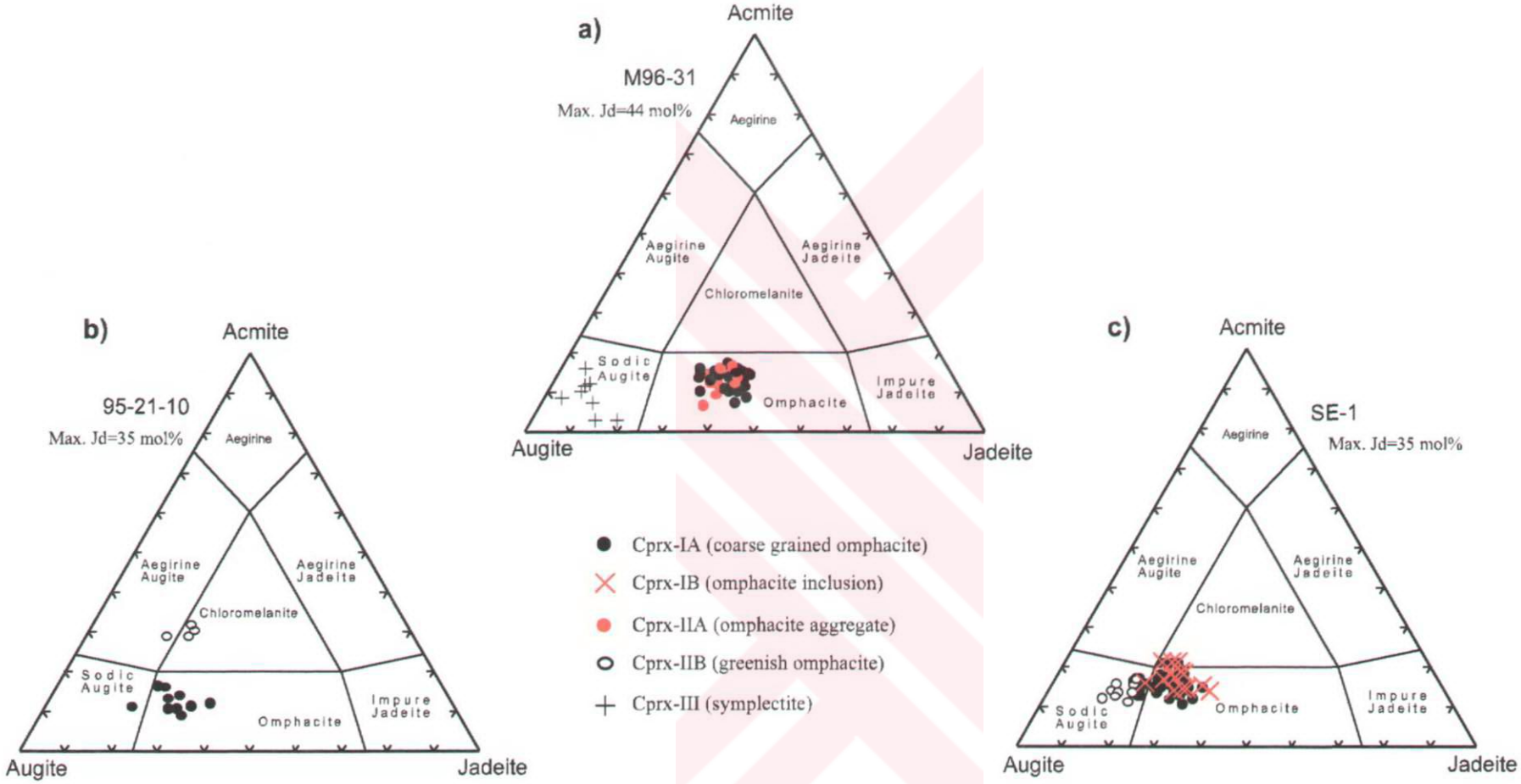


Figure 5.14 Pyroxene composition in the eclogites of Şirince and Gölmarmara (M97-34/2). Compositional fields and nomenclature are after Essene and Fyfe (1967).

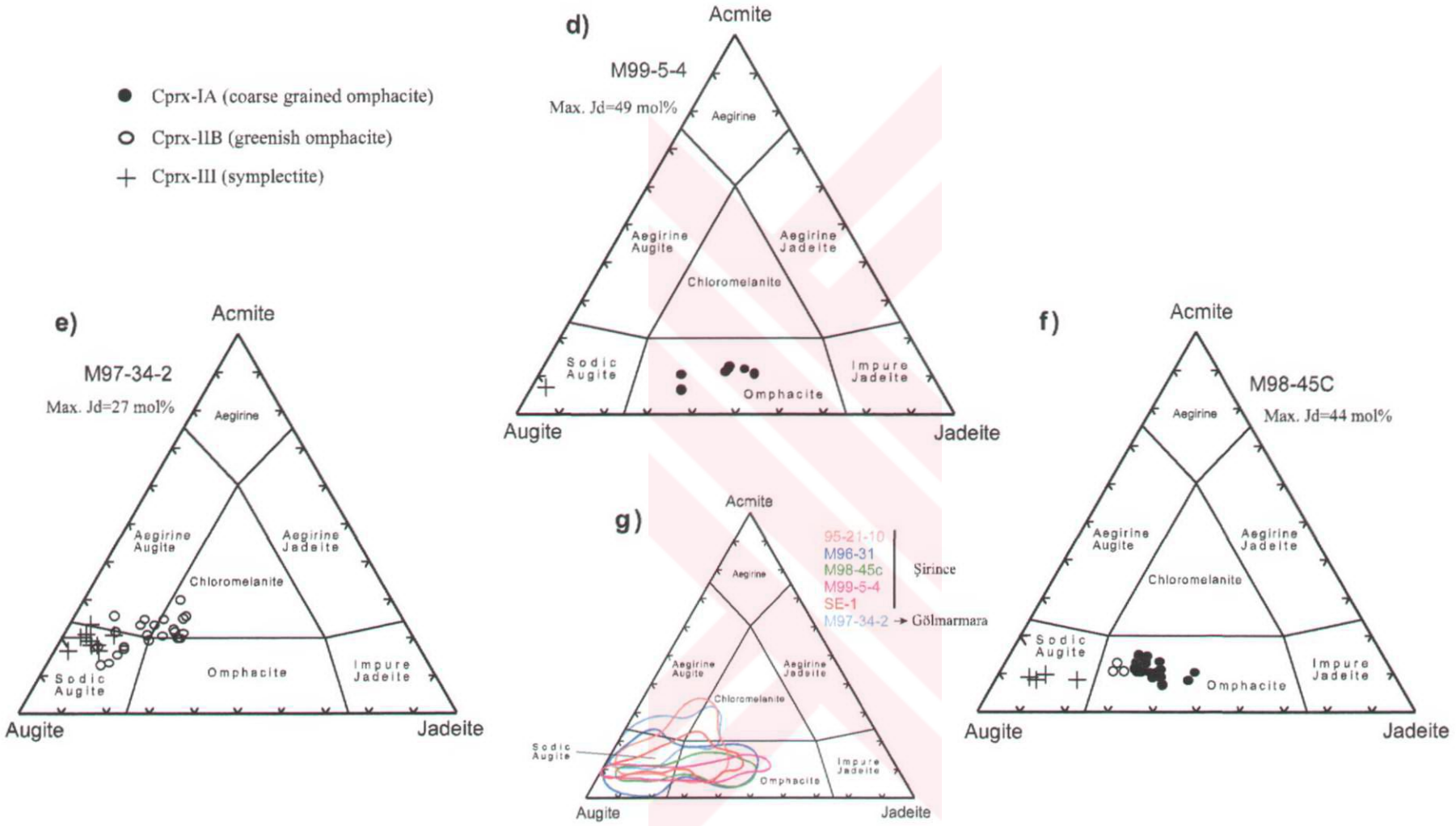


Figure 5.14 Continued

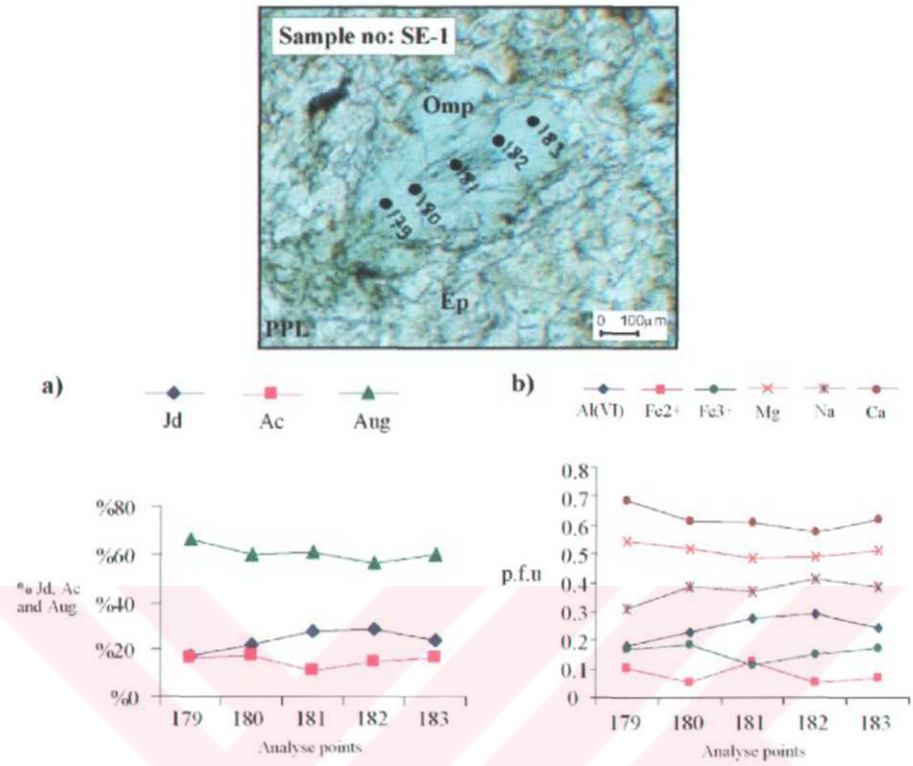


Figure 5.15 Compositional profile across Na pyroxene grain; a) Jadeite (jd), Acmite (Ac) and Augite (Aug) end-members pattern belonging to profile line; b) element patterns belonging to profile line.

ratios of clinopyroxenes in eclogites are close to but trifle larger and smaller than unity. Slight deviation from the dashed line reflects small proportions of $(Mg+Fe^{2+})$ residing in M2 (above line). The sum of $(Al^{VI}+Fe^{3+}) + (Mg+Fe^{2+})$ ranges from 0.966 to 1.017 with an average of 0.990. The sum of $Mg + Fe^{2+}$ and $Al^{VI} + Fe^{3+}$ are approximately equal to the Ca and the Na content, in each pyroxene respectively. Figure 5.17 depicts the ternary (Di + Hd) – Jd – Ac and (Jd + Ac) – Hd – Di compositional ranges, and provides indication of the chemical species occupying the small 6-fold coordinated M1 site in analysed clinopyroxenes. It is clear from this diagram:

- clinopyroxenes, except for Cprx-III, are rich in diopside (Mg) and jadeite (Al^{VI}) end-members
- symplectitic clinopyroxenes (Cprx-III) contain higher Mg and lesser Al^{VI}

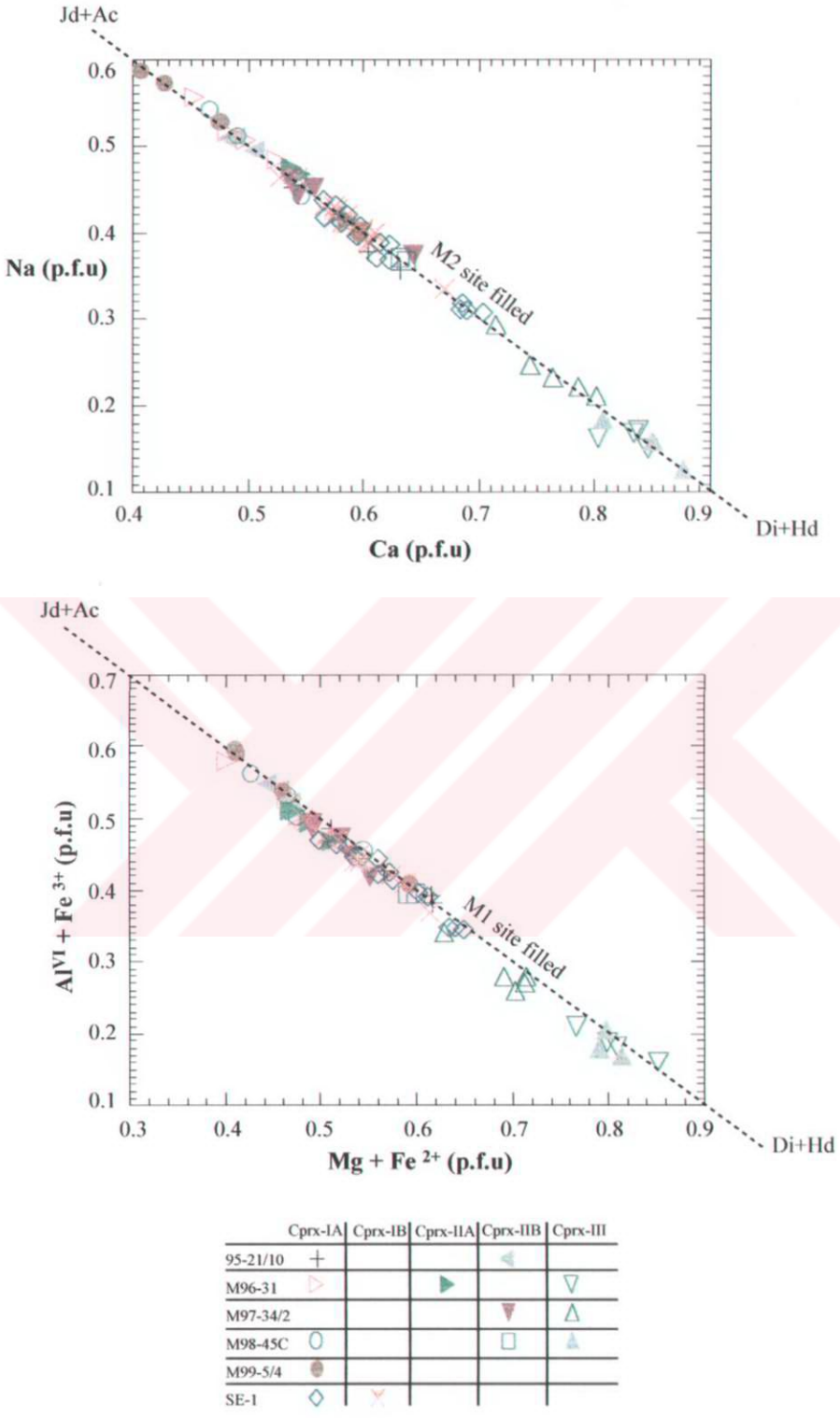


Figure 5.16 Proportions of six-coordinated cations p.f.u. in analyses of clinopyroxene from eclogites. The diagrams show the occupancy of M2 (a) and M1(b) structural positions. Diagrams are from Ernst (1976) and Ernst and Dal Piaz (1978), respectively.

- Cprx-IIB (greenish omphacite) is rich in acmite (Fe^{3+}) and poor-in hedenbergite (Fe^{2+}) end-members with respect to other type clinopyroxenes

5.3.2. Clinopyroxes in omphacite-epidotites and omphacite metagabbros

Three omphacite-epidotite and one omphacite metagabbro samples are analysed from Şirince, Torbalı and Söke areas. These omphacite metagabbro and omphacite-epidotite blocks occur in metaolistostrome unit. The representative analyses of clinopyroxene from omphacite-epidotites and omphacite metagabbro are given in Table 5.7. The same classification of clinopyroxenes based on the textural evidence (e.g., Cprx-IA, Cprx-IIA) used for eclogites is also valid for omphacite metagabbro and omphacite-epidotites. For omphacite-epidotite samples, the cation sums per six oxygens range from 3.979 to 4.018 with an average of 3.997 which is in good agreement with the stoichiometric value of 4.000. The proportions of Si per formula unit range from 1.934 to 2.009. Aluminum substitution for Si in the four-fold coordination site is very little. Maximum and average values of Al^{IV} are 0.066 and 0.019, respectively. On the other hand, average Ti, Cr_2O_3 and K_2O content of analysed clinopyroxenes in wt percent are 0.004, 0.05 and 0.01, respectively.

Clinopyroxene analyses belonging to omphacite-epidotites (M96-92/4, M98-163/2, M97-151/3) are plotted in the Q - J diagram (Figure 5.18). Clinopyroxene composition in Figure 5.18 shifts from Ca-Na pyroxene field to that of Quad. In general, symplectites take place close to Quad or in Quad field. All Cprx-IA and Cprx-IIA fall into Ca-Na field. Most of the analyses are fairly close to Q+J=2 line. This represents that M sites (M1+M2) are almost full.

The composition of clinopyroxene from omphacite-epidotites of Şirince, Söke (nenemsuyu) and Torbalı can be described in terms of the four components; jadeite (Jd), aegirine (Ae), diopside (Di) and hedenbergite (Hd) (Table 5.7). The Di and Hd components are combined as augite in the classic classification diagram of Essene and Fyfe (1967) which is given in Figure 5.19a-b-c. It can be seen on Figure 5.19a-b-c that, as a whole, the composition of the clinopyroxenes is interval of the omphacite, chloromelanite, and sodic augite fields.

Table 5.7 Representative clinopyroxene analyses from omphacite-epidotites and omphacite metagabro in Söke, Torbalı and Selçuk areas.

	Söke (nenemsuyu)												Torbalı											
sample no	M96-92/4 (omphacite-epidotite)												M98-163/2 (omphacite-epidotite)											
analyse no	m13-3	m13-4	m13-5	m13-11	m13-12	m13-13	m13-23	m13-24	m13-25	m13-26	m13-30	m13-31	m13-7	m13-8	m13-15	m13-32	m12-7	m12-8	m12-10	m12-17	m12-31	m12-46	m12-24	m12-30	m12-34
	Cprx-IA												Cprx-IIA				Cprx-IIA								
SiO2	55,33	55,55	55,90	55,66	55,27	55,86	55,95	56,31	55,69	56,24	56,02	55,94	56,29	56,28	51,68	56,36	53,56	53,38	54,22	55,38	54,30	52,23	53,66	54,19	54,24
TiO2	0,34	0,15	0,50	0,54	0,60	0,04	0,48	0,04	0,40	0,54	0,53	0,12	0,02	0,07	0,12	0,15	0,06	0,07	0,05	0,04	0,03	0,02	0,02	0,06	0,03
Al2O3	8,76	7,91	9,39	9,28	8,42	9,19	9,76	9,96	10,11	9,71	9,23	10,23	9,08	9,68	4,85	10,84	2,76	3,38	3,33	5,18	2,83	4,69	3,10	3,06	3,55
FeO	4,89	6,50	4,25	3,69	4,87	7,58	3,11	5,89	3,64	2,70	3,96	5,87	7,87	6,34	12,57	5,51	10,18	10,67	10,00	9,45	10,04	11,49	10,41	9,49	9,69
MnO	0,33	0,23	0,33	0,26	0,35	0,18	0,26	0,14	0,25	0,29	0,27	0,20	0,15	0,14	0,25	0,15	0,22	0,29	0,30	0,18	0,20	0,23	0,32	0,25	0,23
MgO	9,45	9,05	9,21	9,72	9,69	7,58	9,68	7,57	8,83	9,70	9,46	7,83	7,48	7,75	15,46	7,34	10,43	10,14	10,27	8,90	10,62	9,67	10,35	10,82	10,39
CaO	14,86	14,06	14,11	15,07	15,38	11,85	15,10	12,01	14,29	14,83	14,74	11,80	11,61	12,12	10,92	11,39	18,51	18,41	18,19	14,66	18,72	16,87	19,16	18,72	17,73
Na2O	6,39	6,88	6,80	6,13	5,84	8,18	6,39	8,01	6,72	6,44	6,54	8,07	8,26	7,95	1,91	8,31	3,72	3,44	4,02	6,49	3,38	4,04	3,40	3,85	4,22
K2O	0,00	0,00	0,00	0,04	0,02	0,01	0,01	0,00	0,01	0,00	0,00	0,00	0,00	0,03	0,24	0,02	0,01	0,01	0,00	0,00	0,00	0,07	0,00	0,01	0,02
Cr2O3	0,01	0,01	0,00	0,03	0,00	0,05	0,04	0,03	0,02	0,07	0,01	0,05	0,00	0,04	0,02	0,06	0,041	0,04	0,036	0,035	0,103	0,036	0,043	0,075	0,072
Total	100,36	100,34	100,49	100,42	100,43	100,52	100,78	99,96	99,96	100,52	100,76	100,12	100,75	100,40	98,01	100,13	99,49	99,83	100,41	100,31	100,22	99,35	100,46	100,52	100,17
normalized 6 oxygens																									
Si	1,964	1,975	1,975	1,972	1,969	1,975	1,969	1,996	1,977	1,982	1,976	1,977	1,987	1,989	1,933	1,990	1,980	1,975	1,982	1,993	1,997	1,934	1,971	1,976	1,982
Al(IV)	0,036	0,025	0,025	0,028	0,031	0,025	0,031	0,004	0,023	0,018	0,024	0,023	0,013	0,011	0,067	0,010	0,020	0,025	0,018	0,007	0,003	0,066	0,029	0,024	0,018
Sum	2,000	2,000	2,000	2,000	2,000	2,000	2,000	2,000	2,000	2,000	2,000	2,000	2,000	2,000	2,000	2,000	2,000	2,000	2,000	2,000	2,000	2,000	2,000	2,000	2,000
Al(VI)	0,331	0,306	0,366	0,360	0,323	0,358	0,374	0,413	0,400	0,386	0,360	0,403	0,365	0,392	0,146	0,441	0,101	0,122	0,126	0,213	0,120	0,139	0,106	0,107	0,134
Fe2+	0,009	0,004	0,015	0,034	0,050	0,001	0,011	0,034	0,033	0,022	0,019	0,005	0,020	0,026	0,337	0,028	0,131	0,182	0,130	0,038	0,186	0,140	0,155	0,102	0,114
Fe3+	0,136	0,189	0,111	0,075	0,095	0,225	0,081	0,140	0,075	0,058	0,098	0,169	0,213	0,161	0,056	0,134	0,184	0,148	0,176	0,246	0,123	0,216	0,165	0,187	0,182
Mg	0,500	0,480	0,485	0,513	0,515	0,400	0,508	0,400	0,467	0,510	0,497	0,412	0,394	0,408	0,457	0,386	0,575	0,545	0,560	0,477	0,567	0,504	0,567	0,588	0,566
Ti	0,009	0,004	0,013	0,014	0,016	0,001	0,013	0,001	0,011	0,014	0,014	0,003	0,000	0,002	0,003	0,004	0,002	0,002	0,001	0,001	0,001	0,001	0,001	0,002	0,001
Cr	0,000	0,000	0,000	0,001	0,000	0,001	0,001	0,001	0,001	0,002	0,000	0,002	0,000	0,001	0,001	0,002	0,001	0,001	0,001	0,001	0,003	0,001	0,001	0,002	0,002
Sum	0,985	0,983	0,990	0,997	0,998	0,985	0,987	0,989	0,986	0,991	0,988	0,994	0,991	0,991	1,000	0,995	0,993	1,000	0,993	0,977	1,000	1,000	0,994	0,988	0,999
Na	0,440	0,474	0,466	0,421	0,403	0,561	0,436	0,551	0,462	0,440	0,447	0,553	0,565	0,545	0,138	0,569	0,267	0,247	0,285	0,453	0,241	0,290	0,242	0,272	0,299
Ca	0,565	0,536	0,534	0,572	0,587	0,449	0,569	0,456	0,543	0,560	0,557	0,447	0,439	0,459	0,437	0,431	0,733	0,730	0,712	0,565	0,738	0,669	0,754	0,731	0,694
Mg	0,000	0,000	0,000	0,000	0,000	0,000	0,000	0,000	0,000	0,000	0,000	0,000	0,000	0,000	0,405	0,000	0,000	0,014	0,000	0,000	0,015	0,030	0,000	0,000	0,000
Sum	1,005	1,010	1,000	0,993	0,990	1,010	1,005	1,007	1,006	1,000	1,004	1,000	1,004	1,004	0,981	0,999	1,000	0,990	0,997	1,018	0,994	0,989	0,996	1,003	0,993
Jd	32,049	29,723	36,222	35,715	32,104	34,696	36,499	40,879	39,249	38,440	35,444	39,583	35,892	38,743	22,858	43,809	9,879	12,196	12,405	20,785	12,253	13,561	10,301	10,458	13,311
Ac	13,175	18,329	10,963	7,464	9,495	21,850	7,888	13,921	7,392	5,757	9,647	16,579	20,925	15,945	8,798	13,368	18,097	14,829	17,320	24,015	12,514	21,112	16,085	18,269	18,001
Au	54,777	51,948	52,815	56,820	58,402	43,453	55,613	45,200	53,360	55,804	54,909	43,838	43,182	45,312	68,344	42,823	72,025	72,975	70,276	55,200	75,233	65,327	73,614	71,273	68,688
Quad	1,074	1,019	1,034	1,119	1,151	0,847	1,088	0,890	1,043	1,091	1,073	0,864	0,852	0,893	1,636	0,845	1,438	1,470	1,402	1,081	1,506	1,343	1,476	1,421	1,374
Jd	0,879	0,948	0,932	0,842	0,807	1,122	0,872	1,101	0,925	0,880	0,894	1,106	1,131	1,089	0,277	1,137	0,533	0,493	0,570	0,906	0,482	0,580	0,484	0,544	0,598
Quad	54,986	51,803	52,601	57,071	58,798	43,022	55,508	44,708	53,010	55,358	54,545	43,854	42,980	45,047	85,522	42,629	72,954	74,876	71,104	54,417	75,753	69,829	75,293	72,307	69,681
Jd	31,900	29,812	36,386	35,509	31,798	34,961	36,585	41,246	39,543	38,827	35,730	39,571	36,020	38,931	10,454	43,958	9,551	11,338	12,059	21,149	11,996	11,801	9,646	10,082	12,889
Ae	13,114	18,385	11,013	7,421	9,404	22,017	7,907	14,046	7,447	5,815	9,725	16,575	21,000	16,022	4,024	13,413	17,496	13,786	16,837	24,435	12,251	18,371	15,062	17,611	17,430
Jd%	31,900	29,812	36,386	35,509	31,798	34,961	36,585	41,246	39,543	38,827	35,730	39,571	36,020	38,931	10,454	43,958	9,551	11,338	12,059	21,149	11,996	11,801	9,646	10,082	12,889
Di%	53,990	51,345	51,054	53,508	53,624	43,196	54,356	41,194	49,536	53,087	52,544	43,380	40,947	42,362	61,492	39,730	59,454	56,503	57,690	50,358	57,404	55,359	59,121	61,627	57,982
Hd%	0,996	0,458	1,547	3,563	5,174	0,174	1,153	3,514	3,474	2,272	2,001	0,474	2,033	2,685	24,031	2,899	13,50	18,37	13,41	4,06	18,35	14,47	16,17	10,68	11,70
Ae%	13,114	18,385	11,013	7,421	9,404	22,017	7,907	14,046	7,447	5,815	9,725	16,575	21,000	16,022	4,024	13,413	17,50	13,79	16,84	24,43	12,25	18,37	15,06	17,61	17,43

Cprx-IA: coarse grained clinopyroxene Cprx-IIA: aggregate clinopyroxene Cprx-III: symplectite

Table 5.7 continued

	Torbalı													Selçuk (Şirince)											
sample no	M98-163/2 (omphacite-epidotite)													M97-151/3 (omphacite-epidotite)									91-16		
analyse no	m12-35	m12-36	m12-44	m12-45	m12-18	m12-19	m12-20	m12-21	m12-22	m12-27	m12-37	m12-38	m12-39	m16-11	m16-12	m16-13	m16-14	m16-15	m16-23	m16-24	m16-25	m16-31	m15-13	m15-14	m15-16
	Cprx-IIA				Cprx-III									Cprx-IA					Cprx-IIA				Cprx-IA		
SiO2	53,54	53,39	54,54	53,89	54,22	53,87	53,01	54,49	53,83	53,46	53,99	53,96	53,84	56,05	56,00	55,31	56,10	55,76	55,68	55,55	55,58	55,53	57,08	56,79	55,98
TiO2	0,09	0,05	0,00	0,02	0,04	0,04	0,02	0,09	0,04	0,06	0,00	0,03	0,00	0,07	0,08	0,02	0,16	0,14	0,11	0,07	0,09	0,04	0,05	0,05	0,09
Al2O3	3,25	2,09	3,06	2,47	3,47	3,42	3,78	4,42	1,95	2,88	1,57	1,57	3,01	8,77	8,70	4,97	9,76	8,78	9,98	8,58	8,24	8,82	10,14	10,47	9,33
FeO	9,68	9,90	9,85	10,08	9,35	10,09	10,44	9,08	10,38	10,66	9,28	9,37	10,12	8,37	5,88	8,57	7,89	8,05	4,96	7,91	8,63	5,64	3,38	3,31	3,07
MnO	0,24	0,28	0,25	0,30	0,22	0,24	0,27	0,27	0,35	0,33	0,30	0,30	0,26	0,24	0,35	0,35	0,28	0,26	0,29	0,30	0,32	0,27	0,10	0,12	0,14
MgO	10,80	11,09	10,72	10,78	10,45	10,50	9,79	10,24	12,62	10,49	11,94	11,72	10,53	7,28	9,19	10,24	6,91	7,34	8,40	7,43	7,28	8,77	9,16	8,80	10,04
CaO	18,84	20,35	18,07	20,18	18,40	18,92	18,41	17,24	18,75	19,68	21,14	21,32	19,07	12,48	14,72	17,30	12,14	12,71	13,42	12,79	12,86	14,25	13,84	13,04	15,19
Na2O	3,29	2,54	4,06	3,09	4,07	3,36	3,50	4,79	1,57	3,06	2,13	2,12	3,62	7,60	6,20	4,44	7,66	7,08	6,87	7,17	7,25	6,31	7,00	7,44	6,27
K2O	0,03	0,00	0,00	0,00	0,00	0,01	0,00	0,03	0,01	0,00	0,00	0,00	0,01	0,00	0,03	0,00	0,02	0,00	0,00	0,00	0,00	0,00	0,00	0,02	0,00
Cr2O3	0,109	0,082	0,039	0,036	0,047	0,072	0,038	0,057	0,087	0,05	0,072	0,027	0,036	0,10	0,12	0,02	0,05	0,08	0,05	0,04	0,05	0,17	0,28	0,32	0,34
Total	99,86	99,77	100,59	100,84	100,27	100,53	99,26	100,71	99,59	100,66	100,42	100,42	100,50	100,96	101,28	101,22	100,97	100,20	99,76	99,85	100,29	99,80	101,03	100,35	100,45
normalized 6 oxygens																									
Si	1,974	1,982	1,986	1,974	1,980	1,975	1,971	1,969	2,009	1,966	1,991	1,992	1,971	1,990	1,980	1,992	1,990	2,000	1,985	1,996	1,993	1,990	1,998	1,996	1,975
Al(IV)	0,026	0,018	0,014	0,026	0,020	0,025	0,029	0,031	0,000	0,034	0,009	0,008	0,029	0,010	0,020	0,008	0,010	0,000	0,015	0,004	0,007	0,010	0,002	0,004	0,025
Sum	2,000	2,000	2,000	2,000	2,000	2,000	2,000	2,000	2,009	2,000	2,000	2,000	2,000	2,000	2,000	2,000	2,000	2,000	2,000	2,000	2,000	2,000	2,000	2,000	2,000
Al(VI)	0,115	0,074	0,118	0,081	0,129	0,123	0,137	0,157	0,086	0,091	0,059	0,060	0,101	0,357	0,342	0,203	0,398	0,371	0,405	0,360	0,341	0,363	0,417	0,430	0,363
Fe2+	0,154	0,182	0,117	0,144	0,107	0,170	0,181	0,068	0,297	0,168	0,183	0,190	0,125	0,074	0,073	0,144	0,099	0,124	0,066	0,096	0,091	0,085	0,041	0,017	0,002
Fe3+	0,144	0,125	0,183	0,164	0,178	0,139	0,144	0,207	0,027	0,160	0,103	0,099	0,185	0,175	0,101	0,115	0,135	0,117	0,082	0,141	0,168	0,084	0,058	0,080	0,089
Mg	0,581	0,614	0,581	0,589	0,569	0,564	0,537	0,552	0,586	0,575	0,653	0,645	0,575	0,385	0,478	0,538	0,363	0,381	0,443	0,398	0,389	0,462	0,475	0,461	0,528
Ti	0,002	0,001	0,000	0,001	0,001	0,001	0,001	0,002	0,001	0,002	0,000	0,001	0,000	0,002	0,002	0,000	0,004	0,004	0,003	0,002	0,002	0,001	0,001	0,001	0,002
Cr	0,003	0,002	0,001	0,001	0,001	0,002	0,001	0,002	0,003	0,001	0,002	0,001	0,001	0,003	0,003	0,000	0,001	0,002	0,002	0,001	0,001	0,005	0,008	0,009	0,010
Sum	1,000	0,999	1,000	0,979	0,985	1,000	1,000	0,987	1,000	0,996	1,000	0,996	0,987	0,995	1,000	1,000	1,000	1,000	1,000	0,999	0,992	1,000	1,000	0,998	0,993
Na	0,235	0,183	0,287	0,219	0,288	0,239	0,252	0,336	0,201	0,218	0,152	0,152	0,257	0,523	0,425	0,310	0,527	0,492	0,475	0,500	0,504	0,438	0,475	0,507	0,429
Ca	0,744	0,810	0,705	0,792	0,720	0,743	0,733	0,667	0,768	0,775	0,835	0,843	0,748	0,475	0,557	0,668	0,461	0,488	0,513	0,492	0,494	0,547	0,519	0,491	0,574
Mg	0,012	0,000	0,001	0,000	0,000	0,010	0,006	0,000	0,010	0,000	0,003	0,000	0,000	0,000	0,006	0,012	0,003	0,011	0,004	0,000	0,000	0,006	0,003	0,000	0,000
Sum	0,991	0,992	0,992	1,011	1,008	0,992	0,991	1,003	0,979	0,993	0,991	0,995	1,005	0,998	0,988	0,989	0,991	0,992	0,991	0,992	0,998	0,992	0,997	0,998	1,003
Jd	11,447	7,332	11,708	7,773	12,550	12,258	13,501	15,260	9,950	8,838	5,910	5,997	9,777	35,462	34,194	20,608	40,028	37,994	40,519	36,224	34,002	36,492	41,930	42,928	35,357
Ac	14,382	12,395	18,163	15,846	17,376	13,836	14,171	20,029	3,092	15,596	10,303	9,877	17,867	17,358	10,092	11,626	13,557	12,017	8,179	14,213	16,740	8,479	5,864	8,011	8,680
Au	74,171	80,272	70,129	76,381	70,074	73,907	72,328	64,711	86,958	75,566	83,787	84,126	72,356	47,180	55,714	67,766	46,415	49,989	51,302	49,563	49,257	55,029	52,206	49,060	55,963
Quad	1,491	1,606	1,404	1,525	1,395	1,487	1,457	1,287	1,749	1,518	1,675	1,678	1,448	0,934	1,115	1,361	0,926	1,005	1,025	0,987	0,974	1,100	1,038	0,969	1,103
Jd	0,470	0,366	0,573	0,439	0,576	0,478	0,505	0,671	0,227	0,436	0,305	0,303	0,514	1,046	0,850	0,620	1,053	0,985	0,950	0,999	1,008	0,877	0,950	1,014	0,858
Quad	76,030	81,450	71,010	77,652	70,776	75,690	74,274	65,721	88,504	77,676	84,614	84,688	73,803	47,161	56,738	68,699	46,778	50,508	51,910	49,694	49,142	55,652	52,201	48,871	56,269
Jd	10,623	6,895	11,363	7,355	12,255	11,420	12,551	14,823	8,771	8,075	5,609	5,785	9,265	35,475	33,403	20,012	39,757	37,600	40,013	36,130	34,080	35,987	41,934	43,088	35,111
Ae	13,347	11,655	17,627	14,993	16,969	12,890	13,175	19,456	2,726	14,249	9,777	9,527	16,932	17,364	9,859	11,290	13,465	11,892	8,077	14,176	16,778	8,362	5,864	8,041	8,619
Jd%	10,623	6,895	11,363	7,355	12,255	11,420	12,551	14,823	8,771	8,075	5,609	5,785	9,265	35,475	33,403	20,012	39,757	37,600	40,013	36,130	34,080	35,987	41,934	43,088	35,111
Di%	60,355	62,791	59,092	62,349	59,569	58,373	55,701	58,528	62,174	60,129	66,128	65,395	60,606	39,575	49,320	54,471	36,782	38,377	45,210	39,996	39,838	47,129	48,110	47,123	56,108
Hd%	15,68	18,66	11,92	15,30	11,21	17,32	18,57	7,19	26,33	17,55	18,49	19,29	13,20	7,586	7,418	14,227	9,996	12,131	6,700	9,697	9,304	8,523	4,091	1,748	0,161
Ae%	13,35	11,66	17,63	14,99	16,97	12,89	13,17	19,46	2,73	14,25	9,78	9,53	16,93	17,364	9,859	11,290	13,465	11,892	8,077	14,176	16,778	8,362	5,864	8,041	8,619

Cprx-IA: coarse grained clinopyroxene Cprx-IIA: aggregate clinopyroxene Cprx-III: symplectite

Table 5.7 continued

	Selçuk (Şirince)																		
sample no	91-16 (omphacite metagabbro)																		
analyse no	m15-17	m15-21	m15-51	m15-52	m15-53	m15-8	m15-10	m15-11	m15-18	m15-19	m15-20	m15-22	m15-27	m15-28	m15-54	m15-55	m15-59	m15-23	m15-39
	Cprx-IA					Cprx-IIA												Cprx-III	
SiO2	56,52	56,25	56,04	56,46	56,00	56,55	56,94	56,70	56,31	56,84	56,90	56,92	55,88	55,68	55,97	56,96	56,80	54,57	55,81
TiO2	0,07	0,03	0,08	0,15	0,03	0,05	0,01	0,00	0,02	0,03	0,03	0,05	0,06	0,05	0,00	0,05	0,00	0,08	0,00
Al2O3	9,94	9,38	9,27	10,80	9,28	10,74	11,38	9,06	8,84	9,80	10,64	10,15	7,61	7,76	9,47	11,70	11,43	2,39	3,17
FeO	2,94	2,77	3,02	3,07	3,59	3,78	3,78	3,22	4,11	3,88	3,63	3,99	3,24	3,47	4,02	3,14	2,99	3,62	3,40
MnO	0,08	0,07	0,10	0,08	0,09	0,01	0,12	0,15	0,10	0,12	0,12	0,14	0,21	0,18	0,21	0,06	0,12	0,14	0,19
MgO	9,44	9,95	10,14	8,42	9,23	8,43	8,23	10,08	9,78	9,05	8,72	8,76	10,87	10,73	9,16	8,42	8,21	14,71	14,36
CaO	13,81	14,97	15,14	12,43	14,33	12,79	12,08	15,21	14,72	13,54	12,86	13,56	15,99	15,82	13,77	12,28	12,22	22,87	21,46
Na2O	6,87	6,38	6,17	7,71	6,87	7,73	8,08	6,18	6,48	7,06	7,49	7,31	5,68	5,41	7,09	7,88	8,06	1,57	2,41
K2O	0,00	0,00	0,01	0,01	0,00	0,00	0,01	0,00	0,02	0,00	0,02	0,01	0,01	0,00	0,00	0,01	0,00	0,02	0,00
Cr2O3	0,83	0,92	0,28	1,09	0,80	0,03	0,05	0,21	0,11	0,04	0,01	0,03	0,84	0,89	0,28	0,12	0,53	0,08	0,21
Total	100,50	100,72	100,25	100,22	100,22	100,12	100,67	100,81	100,50	100,36	100,42	100,92	100,38	100,00	99,97	100,61	100,36	100,05	101,01
normalized 6 oxygens																			
Si	1,989	1,979	1,981	1,988	1,981	1,989	1,988	1,995	1,988	1,998	1,998	1,994	1,982	1,988	1,981	1,989	1,989	1,982	1,997
Al(IV)	0,011	0,021	0,019	0,012	0,019	0,011	0,012	0,005	0,012	0,002	0,002	0,006	0,018	0,012	0,019	0,011	0,011	0,018	0,003
Sum	2,000	2,000	2,000	2,000	2,000	2,000	2,000	2,000	2,000	2,000	2,000	2,000	2,000	2,000	2,000	2,000	2,000	2,000	2,000
Al(VI)	0,402	0,369	0,367	0,436	0,367	0,435	0,457	0,371	0,356	0,407	0,438	0,413	0,300	0,314	0,375	0,471	0,460	0,084	0,131
Fe2+	0,010	0,002	0,017	0,004	0,010	0,010	0,009	0,040	0,023	0,040	0,033	0,030	0,009	0,032	0,008	0,019	0,004	0,067	0,062
Fe3+	0,076	0,086	0,073	0,099	0,122	0,101	0,101	0,055	0,099	0,075	0,073	0,087	0,108	0,071	0,130	0,072	0,098	0,043	0,039
Mg	0,487	0,522	0,534	0,440	0,487	0,442	0,428	0,528	0,515	0,475	0,454	0,457	0,575	0,556	0,483	0,433	0,428	0,796	0,762
Ti	0,002	0,001	0,002	0,004	0,001	0,001	0,000	0,000	0,001	0,001	0,001	0,001	0,002	0,001	0,000	0,001	0,000	0,002	0,000
Cr	0,023	0,026	0,008	0,030	0,022	0,001	0,001	0,006	0,003	0,001	0,000	0,001	0,024	0,025	0,008	0,003	0,015	0,002	0,006
Sum	1,000	0,998	1,000	1,000	0,983	0,990	0,997	1,000	0,996	0,999	1,000	0,990	0,995	1,000	0,985	1,000	0,991	0,994	1,000
Na	0,469	0,435	0,423	0,526	0,471	0,527	0,547	0,422	0,444	0,482	0,510	0,497	0,390	0,374	0,486	0,533	0,547	0,111	0,167
Ca	0,521	0,564	0,573	0,469	0,543	0,482	0,452	0,573	0,557	0,511	0,484	0,509	0,607	0,605	0,522	0,459	0,458	0,890	0,823
Mg	0,008	0,000	0,001	0,002	0,000	0,000	0,000	0,000	0,000	0,000	0,002	0,000	0,000	0,015	0,000	0,005	0,000	0,000	0,004
Sum	0,998	1,000	0,997	0,997	1,014	1,009	0,999	0,996	1,000	0,994	0,996	1,006	0,998	0,995	1,008	0,998	1,005	1,000	0,994
Jd	40,219	36,155	36,237	43,427	35,576	42,702	45,222	37,130	35,194	41,004	44,027	40,945	29,541	31,713	36,531	46,950	45,281	8,251	13,175
Ac	7,623	8,483	7,172	9,853	11,846	9,961	10,041	5,508	9,768	7,507	7,363	8,651	10,596	7,200	12,683	7,227	9,637	4,226	3,957
Au	52,158	55,362	56,591	46,721	52,579	47,336	44,737	57,362	55,038	51,490	48,610	50,404	59,864	61,087	50,785	45,823	45,081	87,522	82,867
Quad	1,026	1,081	1,124	0,902	1,013	0,934	0,889	1,142	1,094	1,027	0,973	0,996	1,171	1,208	0,994	0,917	0,876	1,753	1,651
Jd	0,937	0,871	0,846	1,052	0,942	1,054	1,094	0,843	0,887	0,965	1,020	0,993	0,781	0,749	0,973	1,067	1,094	0,221	0,334
Quad	52,262	55,400	57,070	46,156	51,823	46,968	44,837	57,521	55,222	51,549	48,839	50,074	59,982	61,737	50,533	46,218	44,473	88,801	83,158
Jd	40,132	36,125	35,837	43,887	36,143	43,001	45,140	36,991	35,050	40,953	43,831	41,217	29,454	31,183	36,719	46,607	45,783	7,406	12,952
Ae	7,606	8,476	7,093	9,957	12,035	10,031	10,023	5,488	9,728	7,498	7,330	8,709	10,564	7,080	12,748	7,174	9,744	3,793	3,890
Jd%	40,132	36,125	35,837	43,887	36,143	43,001	45,140	36,991	35,050	40,953	43,831	41,217	29,454	31,183	36,719	46,607	45,783	7,406	12,952
Di%	51,185	55,932	55,350	47,060	53,603	45,954	43,920	53,505	52,906	47,566	45,517	47,037	61,201	58,434	51,756	44,275	45,585	81,912	76,889
Hd%	1,077	0,532	1,720	0,030	0,060	1,014	0,917	4,016	2,316	3,983	3,322	3,037	0,080	3,303	0,040	1,943	0,020	6,889	6,269
Ae%	7,606	8,476	7,093	9,957	12,035	10,031	10,023	5,488	9,728	7,498	7,330	8,709	10,564	7,080	12,748	7,174	9,744	3,793	3,890

Cprx-IA: coarse grained clinopyroxene Cprx-IIA: aggregate clinopyroxene Cprx-III: symplectite

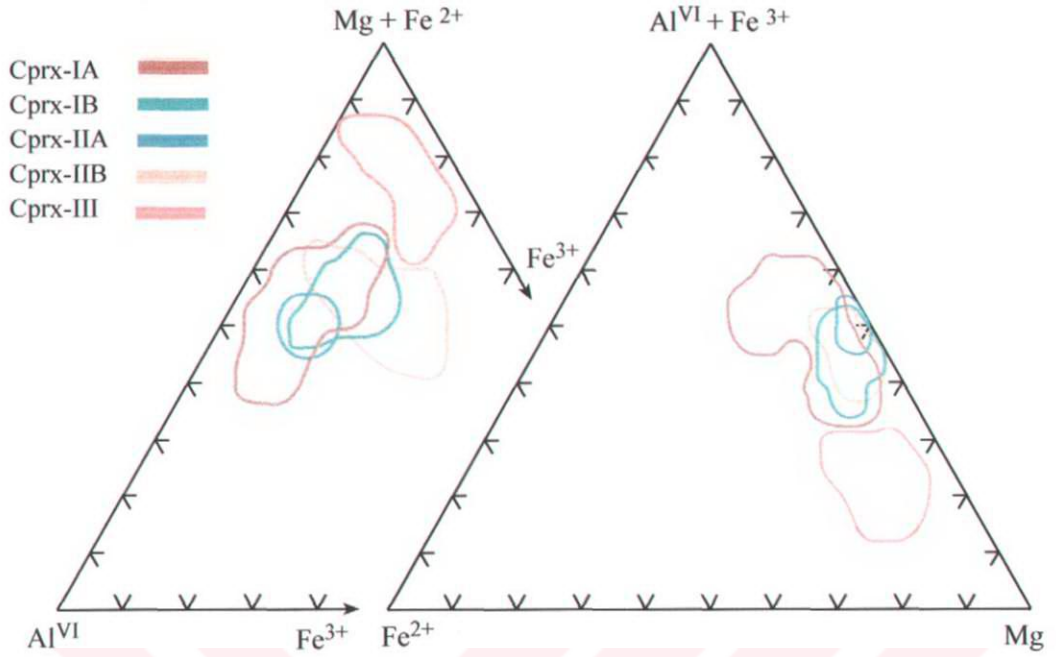


Figure 5.17 Ternary atomic proportions of (Di+Hd)-Jd-Ac and of (Jd+Ac)-Hd-Di for clinopyroxenes (Ernst, 1976).

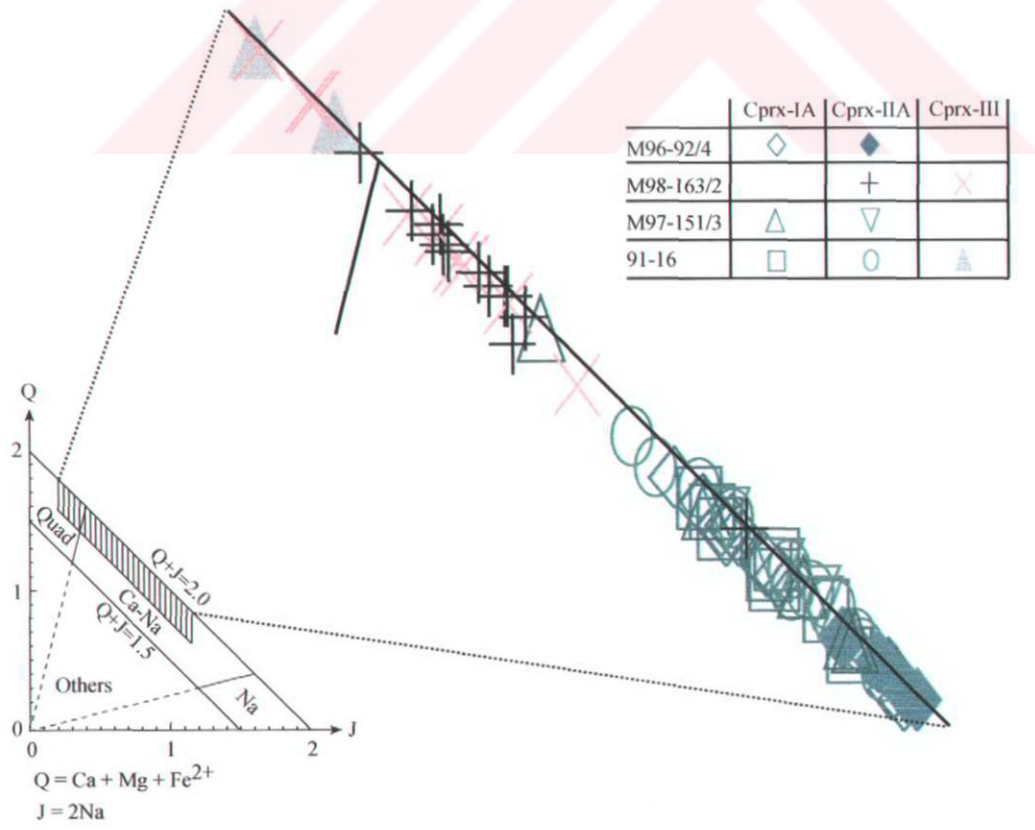


Figure 5.18 Classification of clinopyroxene analyses on Q-J ternary diagram (Morimoto et al. 1988).

.Jd content of clinopyroxenes (Cprx-IA and Cprx-IIA) in Nenemsuyu and Şirince are higher (average 36 mol%) and dominantly fall into omphacite field. In Torbalı, Cprx-IIA and Cprx-III have low Jd content (average 11 mol%). They, therefore, plot on sodic augite field.

The sum of Na + Ca ranges from 0.979 to 1.018 with an average of 0.996. This shows that there is minor solid solution (Figure 5.20a). In Figure 5.20a-b, the diagonal dashed lines indicate the locus of 100 percent filling of the M2 with respect to M1 sites by the plotted cations; therefore, deviations from the lines reflect limited proportions of the larger vs smaller cations located in the respective structural sites. Na, Ca, and Mg remaining from M1 site realize occupancy of the large M2 site. Minimum and maximum Mg content of M2 site are 0.00 and 0.030, respectively. Occupancy of the smaller M1 structural position is depicted in Figure 5.20b. Al^{VI} + Fe^{3+} + Mg + Fe^{2+} totals are quite close to the ideal formula value (1.000). These values change in range from 0.976 to 1.000.

Figure 5.21a-b depicts the ternary atomic proportions of (Di-Hd)-Jd-Ac and (Jd+Ac)-Hd-Di compositional ranges. Clinopyroxene analyses from omphacite-epidotites in Figure 5.21a take place close to edge between Al^{VI} and Mg+Fe^{2+} in triangle diagram. Aegerine content in clinopyroxenes does not access 21 mol%. Great compositional differences are not observed between Cprx-IA and Cprx-IIA, except for M98-163/2. Average composition for Cprx-IA and Cprx-IIA are "Jd_{35} Di_{48} Hd_5 Ae_{12} " and "Jd_{37} Di_{43} Hd_5 Ae_{15} ", respectively. Cprx-IA and Cprx-IIA are rich in Diopsite (46 mol%) and have minor hedenbergite. Hedenbergite content in Cprx-IA and Cprx-IIA (except for M98-163/2) is average 5 mol%. The Cprx-IIA in M98-163/2 exhibit similar chemical composition with Cprx-III. Hedenbergite content is high (average 14 mol%) in compared with other omphacite-epidotites. In Figure 5.21b, Cprx-IA and Cprx-IIA compositions from omphacite-epidotes and omphacite metagabbro are fairly close to each other. Therefore, they are shown in only a field. All clinopyroxene analyses take place near to edge between Al^{VI}+Fe^{3+} and Mg in triangle diagram (Figure 5.21b). Cprx-IIA analyses belonging to M98-163/2 are some more different in composition with respect to other Cprx-IIA, like in Figure

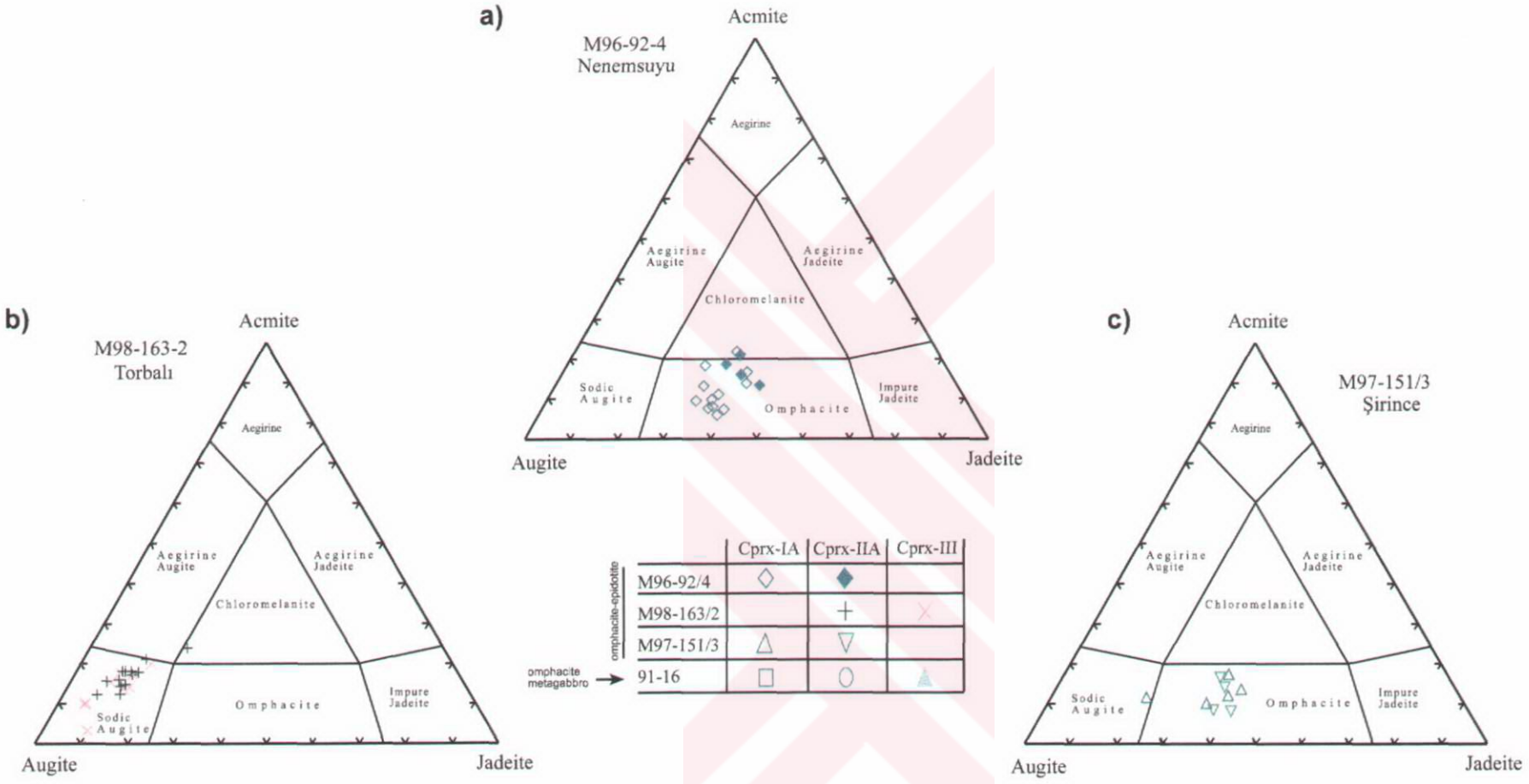
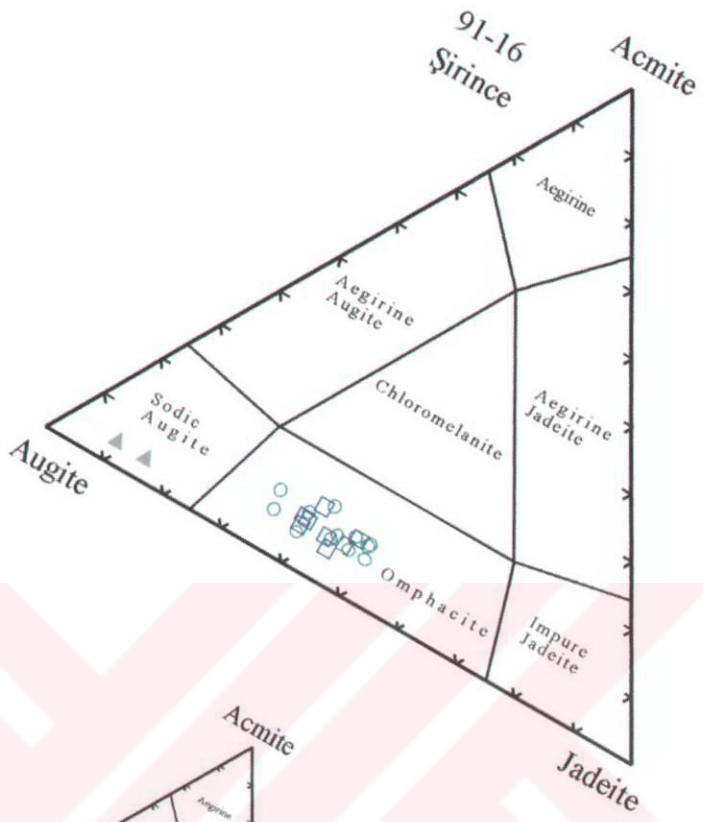


Figure 5.19 Composition plots of clinopyroxenes from omphacite metagabbro and omphacite-epidotites of Şirince ,Söke and Torbalı areas. Compositional fields and nomenclature are after Essene and Fyfe (1967).

d)



e)

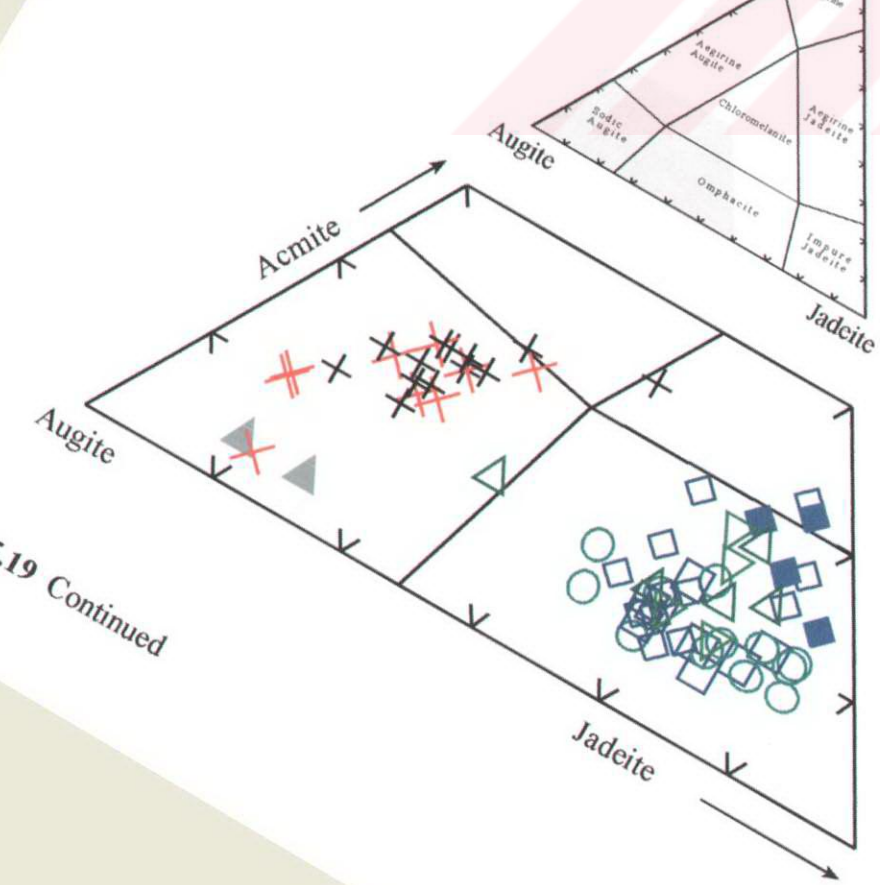


Figure 5.19 Continued

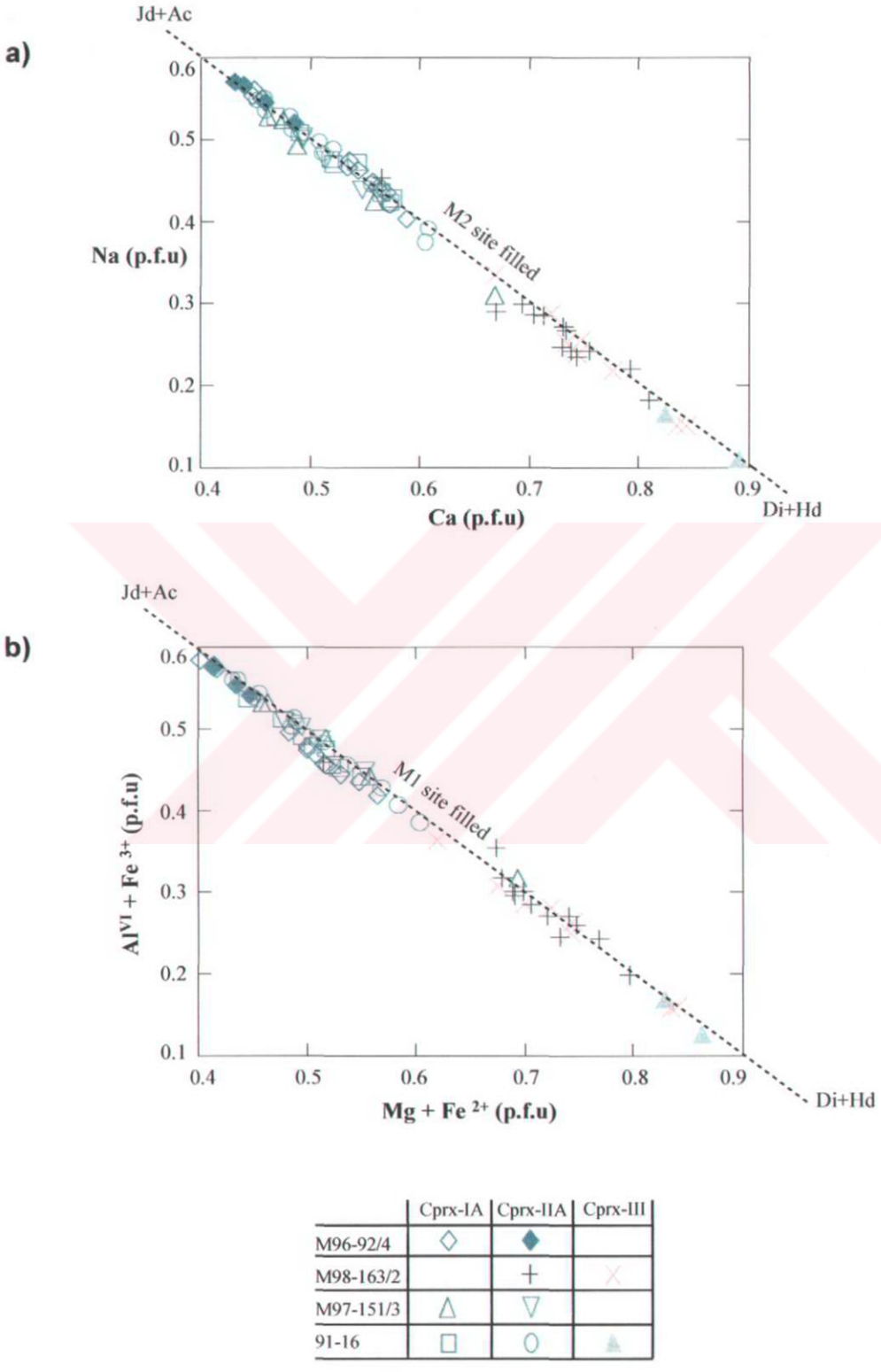


Figure 5.20 Proportions of six-coordinated cations p.f.u. in analyses of clinopyroxene. The diagrams show the occupancy of M2 (a) and M1(b) structural positions. Diagrams are from Ernst (1976) and Ernst and Dal Piaz (1978), respectively.

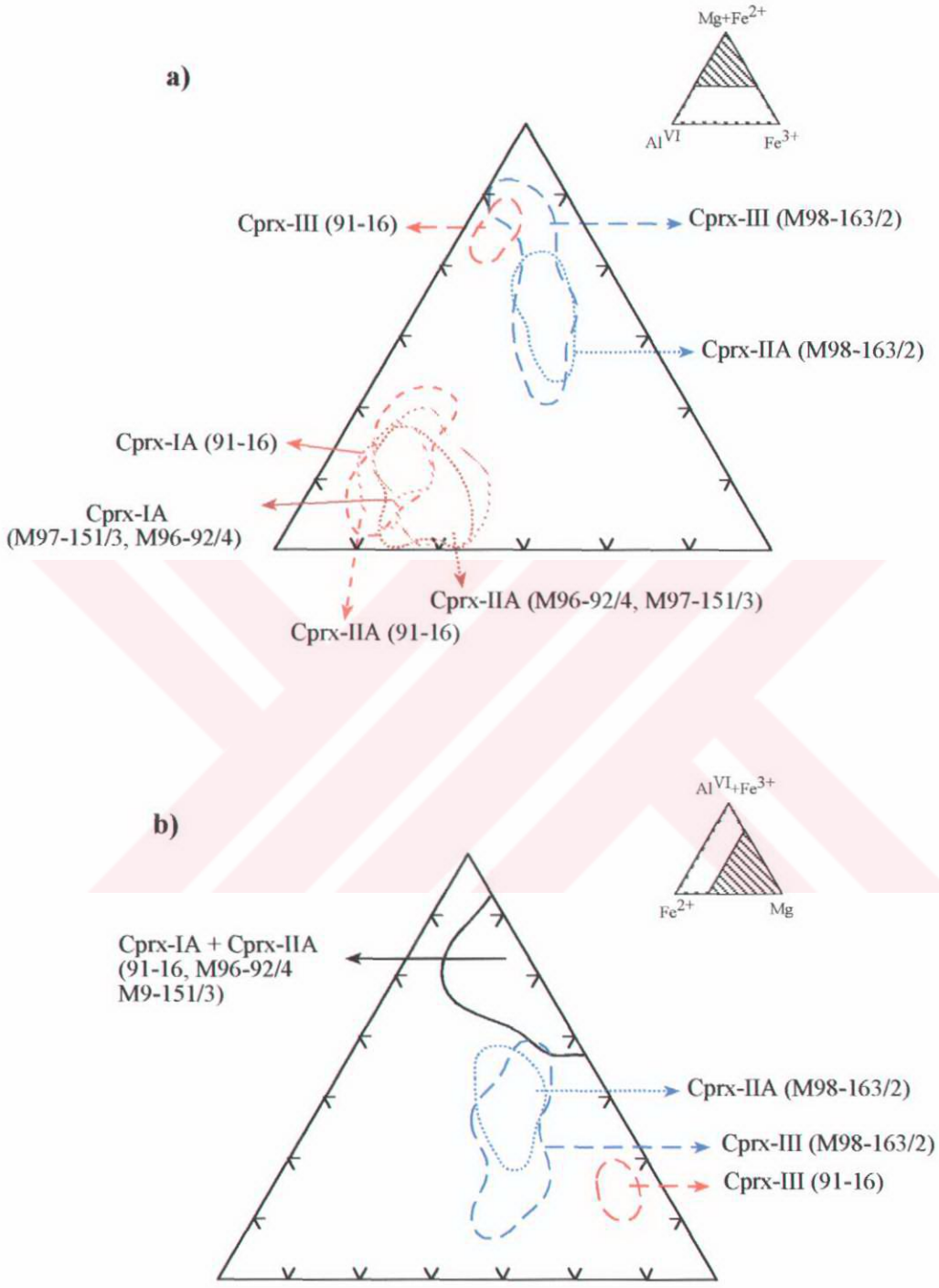


Figure 5.21 Ternary atomic proportions of a) (Di+Hd)-Jd-Ac and of b) (Jd+Ac)-Hd-Di for clinopyroxenes in omphacite-epidotites (M96-92/4, M98-163/2, M97-151/3) and omphacite metagabbro (91-16). Diagrams are from Ernst (1976).

5.21a. In omphacite-epidotites and omphacite metagabbro, graphically showing of sodic pyroxenes composed of four end-members are given in Figure 5.21a-b. The result obtained from these two diagrams are that Na-pyroxenes are rich-in jadeite and diopsite and solid solutions are quite limited.

The cation sums of clinopyroxenes from omphacite metagabbro based on six oxygens range between 3.994 and 4.023, very close to the stoichiometric value of 4.000. Minor amounts of aluminium are assigned to tetrahedral sites, averaging 0.016 based on one formula unit. Average value of Al^{VI} is 0.285. Clinopyroxene in omphacite metagabbro are Ca-Na and Quad in composition (Figure 5.18). Cprx-III falls into Quad field. The rest of clinopyroxenes plot on Ca-Na pyroxene field. Q+J in omphacite metagabbro ranges from 1.951 to 1.992. These values are quite close to Q+J=2 line in Figure 5.18. This shows that vacancy is very low in M sites. Clinopyroxenes in omphacite metagabbro are omphacite (Cprx-Ia and Cprx-IIA) and sodic augite (Cprx-III) in composition (Figure 5.19d). Omphacites are dominantly observed in compared with sodic augite. Average composition of Cprx-IA, Cprx-IIA and Cprx-III are Jd_{39} Ac Di_{52} Hd_1, Jd_{39} Ac_9 Di_{50} Hd_2 and Jd_{10} Ac_4 Di_{79} Hd_7, respectively. In Figure 5.19e, all analyses belonging to omphacite-epidotites and omphacite metagabbro are depicted in classification diagram of Essene and Fyfe (1967). The cation proportions in M2 site are illustrated in Figure 5.20a. Na+Ca sums closely approach 1.00 or sometimes slightly exceed 1.00. Maximum and minimum Na+Ca values are 0.994 and 1.014, averaging 1.000. Locations of these values in Na vs Ca diagram are close to Jd+Ac – Di+Hd dashed line (Figure 5.20a). This indicates filling of the M2 site in big ratio by the plotted cations. In Figure 5.20b, clinopyroxene analyses (omphacite metagabbro) are on dashed line or below it. Average occupancy of M1 site is 0.996. Excess Mg takes place in M2 site (Table 5.7). Cprx-IA and Cprx-IIA are nearer to Jd+Ac end-point of dashed line than Cprx-III. Inspection of Figure 5.21a-b provides an indication of cations occupying the 6-fold coordinated M1 site. Cprx-IA and Cprx-IIA have approximately similar chemical composition. Although Cprx-IIA are cover larger field than Cprx-IA in Figure 5.21a, both Cprx-IA, Cprx-IIA and Cprx-III are close to Al^{VI}-$Mg+Fe^{2+}$ edge of triangle diagram (Figure 5.21a). Cprx-IA and Cprx-IIA are rich-in diopside

(Mg=50-52 mol%) and jadeite (Al^{VI}=39 mol%) end-members. Maximum hedenbergite (Fe^{2+}) and acmite (Fe^{3+}) content in these type clinopyroxenes are 2 and 9 mol%, respectively. Cprx-III is characterized by high diopsite (79 mol%) and low jadeite (10 mol%) contents (Figure 5.21a-b). In Figure 5.21b, clinopyroxene analyses are close to $Al^{VI}+Fe^{3+}$ – Mg edge of triangle diagram. Acmite amount in jadeite (Al^{VI}) + acmite (Fe^{3+}) corner of triangle diagram does not excess 9 mol%. This shows that M1 site is commonly occupied by Al^{VI} and Mg.

5.4. Garnets

In this section, the garnets will be treated in two groups: 1) garnets in high-pressure blocks and matrix of metaolistostrome and 2) garnets in marble-schist series. Garnets are observed in eclogite, blueschist and garnet-amphibolite blocks surrounded by a matrix of garnet-phengite schist of metaolistostrome. In marble-schist series, they are observed in garnet-mica schists. Garnet zoning patterns are divided mainly into two groups as a prograde stage (P) that is composed of blueschist episode (PB) or eclogite episode (PE), and retrograde stage (R). Two or more growth episodes can be texturally and/or compositionally observed in some garnets during prograde stage. In this case, each growth episode is called as a PE1, PE2., etc

5.4.1. Garnets in blocks and matrix of metaolistostrome

First, garnets in eclogite, blueschist and garnet-amphibolite blocks will be investigated. Later the evidence obtained from high-pressure blocks will be compared with garnets in matrix of metaolistostrome.

5.4.1.1. Garnets in eclogite blocks

Garnets from six eclogite samples (95-21/10, 95-70/4, M96-31, SE-1, M98-45C, M97-34/2) were analysed. Representative garnet analyses from six eclogites are given in Table 5.8. Cation proportions were calculated based on 24 oxygens. In eclogites, garnet exhibits significant variation in Fe, Mn, Ca and Mg content. Garnet

Table 5.8 Representative garnet analyses from eclogites in Şirince and Gölmarmara (r: rim, c: core).

sample no	95-70/4 (Şirince)																			M97-34/2 (Gölmarmara)			
analyse no	m3-27 r	m3-28	m3-29	m3-30	m3-31	m3-32	m3-33	m3-34	m3-35	m3-36	m3-37 c	m3-38	m3-39	m39-40	m3-41	m3-42	m3-43	m3-44	m3-45	m3-46 r	m7-79 r	m7-80	m7-81	m7-82
SiO2	38,09	38,11	38,24	38,23	38,16	38,16	37,83	37,81	38,02	37,74	38,05	38,28	38,29	37,42	38,24	38,02	38,35	37,97	38,59	38,33	37,72	37,14	37,62	37,31
TiO2	0,09	0,08	0,13	0,20	0,17	0,19	0,23	0,23	0,16	0,30	0,24	0,17	0,22	0,18	0,18	0,16	0,15	0,16	0,11	0,13	0,06	0,21	0,07	0,06
Al2O3	21,25	21,26	21,21	21,39	21,31	20,99	21,06	21,06	21,06	20,94	21,33	21,01	21,07	20,88	21,37	21,28	21,21	21,14	21,50	21,62	20,64	20,31	20,17	20,71
FeO	26,09	26,92	27,14	24,27	23,50	23,82	22,39	22,17	21,62	20,14	20,73	21,00	21,81	22,39	22,18	23,59	24,94	26,34	27,06	26,49	28,85	28,24	28,26	18,95
MnO	0,62	0,87	1,23	4,55	6,10	6,81	7,90	7,97	9,06	10,09	10,22	9,54	8,69	8,41	8,29	7,24	4,62	1,91	0,69	0,74	3,02	4,28	6,24	15,19
MgO	1,84	1,60	1,33	1,17	1,03	1,01	0,78	0,84	0,73	0,63	0,62	0,74	0,79	0,85	0,83	1,02	1,11	1,26	1,55	1,58	1,79	1,26	1,24	1,79
CaO	12,98	12,05	11,95	12,00	11,37	10,73	11,07	10,97	11,17	11,00	10,91	10,79	10,70	10,47	10,87	10,58	11,07	12,16	12,51	12,82	8,80	9,48	7,76	7,10
Na2O	0,02	0,02	0,02	0,01	0,01	0,00	0,01	0,02	0,05	0,06	0,01	0,05	0,01	0,00	0,08	0,00	0,05	0,01	0,08	0,00	0,10	0,00	0,01	0,05
K2O	0,02	0,01	0,00	0,02	0,00	0,00	0,00	0,02	0,00	0,00	0,00	0,01	0,00	0,03	0,00	0,02	0,01	0,00	0,00	0,00	0,00	0,00	0,00	0,00
Cr2O3	0,12	0,00	0,09	0,04	0,00	0,08	0,06	0,05	0,03	0,03	0,09	0,00	0,04	0,08	0,04	0,04	0,00	0,07	0,00	0,08	0,01	0,02	0,05	0,03
Total	101,12	100,92	101,32	101,88	101,65	101,78	101,32	101,12	101,90	100,93	102,20	101,59	101,62	100,70	102,08	101,94	101,52	101,01	102,08	101,79	100,99	100,95	101,42	101,20
normalized oxygens 24																								
Si	5,973	5,998	6,006	5,981	5,994	6,006	5,983	5,987	5,987	5,992	5,973	6,032	6,028	5,969	5,994	5,977	6,025	5,988	6,000	5,972	5,999	5,950	6,013	5,954
Ti	0,011	0,009	0,015	0,024	0,020	0,022	0,027	0,027	0,019	0,035	0,028	0,020	0,026	0,021	0,021	0,018	0,018	0,019	0,013	0,015	0,008	0,026	0,008	0,007
Al	3,928	3,944	3,927	3,945	3,945	3,894	3,926	3,931	3,909	3,919	3,947	3,902	3,910	3,926	3,949	3,943	3,928	3,930	3,941	3,970	3,869	3,835	3,800	3,895
Fe	3,421	3,543	3,564	3,175	3,086	3,135	2,961	2,935	2,847	2,674	2,721	2,767	2,871	2,986	2,907	3,101	3,276	3,473	3,518	3,451	3,837	3,783	3,777	2,529
Mn	0,083	0,116	0,163	0,603	0,811	0,908	1,058	1,069	1,208	1,357	1,359	1,273	1,159	1,136	1,101	0,964	0,615	0,255	0,090	0,098	0,407	0,581	0,845	2,053
Mg	0,430	0,376	0,310	0,273	0,241	0,236	0,183	0,197	0,172	0,148	0,146	0,173	0,185	0,202	0,193	0,238	0,260	0,295	0,358	0,368	0,424	0,301	0,294	0,426
Ca	2,181	2,032	2,011	2,011	1,913	1,809	1,876	1,861	1,884	1,871	1,835	1,821	1,805	1,789	1,825	1,782	1,863	2,054	2,084	2,140	1,499	1,627	1,329	1,214
Na	0,007	0,005	0,005	0,004	0,004	0,000	0,003	0,005	0,014	0,020	0,003	0,015	0,003	0,000	0,024	0,000	0,016	0,004	0,023	0,000	0,030	0,000	0,004	0,016
K	0,003	0,002	0,000	0,003	0,000	0,000	0,000	0,003	0,000	0,000	0,000	0,002	0,000	0,005	0,000	0,004	0,002	0,000	0,000	0,000	0,000	0,000	0,000	0,000
Cr	0,015	0,000	0,011	0,005	0,000	0,010	0,007	0,006	0,004	0,004	0,011	0,000	0,005	0,010	0,005	0,005	0,000	0,008	0,000	0,010	0,001	0,003	0,007	0,004
Total	16,036	16,024	16,002	16,018	16,016	16,011	16,017	16,015	16,041	16,017	16,011	16,006	15,986	16,035	16,015	16,027	16,003	16,018	16,028	16,014	16,072	16,103	16,071	16,093
Mg	0,430	0,376	0,310	0,273	0,241	0,236	0,183	0,197	0,172	0,148	0,146	0,173	0,185	0,202	0,193	0,238	0,260	0,295	0,358	0,368	0,424	0,301	0,294	0,426
Mn	0,083	0,116	0,163	0,603	0,811	0,908	1,058	1,069	1,208	1,357	1,359	1,273	1,159	1,136	1,101	0,964	0,615	0,255	0,090	0,098	0,407	0,581	0,845	2,053
Ca	2,181	2,032	2,011	2,011	1,913	1,809	1,876	1,861	1,884	1,871	1,835	1,821	1,805	1,789	1,825	1,782	1,863	2,054	2,084	2,140	1,499	1,627	1,329	1,214
FeII	3,307	3,476	3,516	3,113	3,034	3,047	2,883	2,873	2,735	2,624	2,661	2,733	2,852	2,873	2,881	3,016	3,262	3,395	3,468	3,394	3,670	3,491	3,532	2,308
Summe X	6,000	6,000	6,000	6,000	6,000	6,000	6,000	6,000	6,000	6,000	6,000	6,000	6,000	6,000	6,000	6,000	6,000	6,000	6,000	6,000	6,000	6,000	6,000	6,000
rest Fe	0,114	0,067	0,049	0,062	0,052	0,088	0,078	0,062	0,112	0,050	0,060	0,034	0,019	0,113	0,026	0,085	0,014	0,078	0,051	0,057	0,167	0,292	0,245	0,221
Si	5,973	5,998	6,006	5,981	5,994	6,006	5,983	5,987	5,987	5,992	5,973	6,032	6,028	5,969	5,994	5,977	6,025	5,988	6,000	5,972	5,999	5,950	6,013	5,954
Aliv	0,027	0,002	0,000	0,019	0,006	0,000	0,017	0,013	0,013	0,008	0,027	0,000	0,000	0,031	0,006	0,023	0,000	0,012	0,000	0,028	0,001	0,050	0,000	0,046
Summe Z	6,000	6,000	6,006	6,000	6,000	6,006	6,000	6,000	6,000	6,000	6,000	6,032	6,028	6,000	6,000	6,000	6,025	6,000	6,000	6,000	6,000	6,000	6,013	6,000
Alvi	3,901	3,942	3,927	3,926	3,939	3,894	3,909	3,918	3,896	3,911	3,919	3,902	3,910	3,895	3,943	3,920	3,928	3,917	3,941	3,942	3,868	3,785	3,800	3,849
Cr	0,015	0,000	0,011	0,005	0,000	0,010	0,007	0,006	0,004	0,004	0,011	0,000	0,005	0,010	0,005	0,005	0,000	0,008	0,000	0,010	0,001	0,003	0,007	0,004
Ti	0,011	0,009	0,015	0,024	0,020	0,022	0,027	0,027	0,019	0,035	0,028	0,020	0,026	0,021	0,021	0,018	0,018	0,019	0,013	0,015	0,008	0,026	0,008	0,007
FeIII	0,114	0,067	0,049	0,062	0,052	0,088	0,078	0,062	0,112	0,050	0,060	0,034	0,019	0,113	0,026	0,085	0,014	0,078	0,051	0,057	0,167	0,292	0,245	0,221
Summe Y	4,040	4,018	4,001	4,017	4,012	4,014	4,022	4,013	4,031	4,001	4,019	3,957	3,960	4,039	3,995	4,029	3,959	4,023	4,004	4,023	4,043	4,105	4,060	4,081
Alm(%)	55,109	57,936	58,596	51,887	50,566	50,775	48,045	47,885	45,584	43,728	44,345	45,546	47,532	47,884	48,017	50,266	54,371	56,588	57,795	56,573	61,161	58,190	58,866	38,461
Prp(%)	7,167	6,271	5,170	4,543	4,023	3,941	3,057	3,284	2,871	2,473	2,433	2,881	3,082	3,360	3,216	3,971	4,332	4,920	5,968	6,127	7,071	5,014	4,908	7,095
Sps(%)	1,381	1,930	2,720	10,048	13,524	15,129	17,636	17,814	20,138	22,613	22,644	21,217	19,310	18,936	18,343	16,065	10,245	4,252	1,506	1,636	6,779	9,678	14,079	34,214
Grs(%)	35,087	33,224	32,892	32,761	31,312	29,254	30,387	30,279	30,360	30,486	29,821	29,938	29,698	28,754	30,024	28,896	30,803	33,345	34,179	34,946	23,903	25,003	20,730	19,078
And(%)	1,125	0,639	0,534	0,715	0,576	0,829	0,818	0,691	1,017	0,668	0,674	0,419	0,343	0,993	0,362	0,761	0,250	0,824	0,553	0,633	1,078	2,097	1,380	1,132
Uva(%)	0,130	0,000	0,088	0,045	0,000	0,072	0,056	0,046	0,030	0,031	0,083	0,000	0,035	0,074	0,039	0,040	0,000	0,071	0,000	0,085	0,008	0,018	0,037	0,020
Prp	7,167	6,271	5,170	4,543	4,023	3,941	3,057	3,284	2,871	2,473	2,433	2,881	3,082	3,360	3,216	3,971	4,332	4,920	5,968	6,127	7,071	5,014	4,908	7,095
Alm+Sps	56,490	59,867	61,317	61,935	64,090	65,904	65,682	65,699	65,722	66,342	66,989	66,763	66,842	66,820	66,359	66,332	64,616	60,840	59,301	58,209	67,940	67,868	72,945	72,675
Grs+And	36,212	33,862	33,425	33,476	31,887	30,083	31,205	30,970	31,377	31,154	30,495	30,356	30,041	29,747	30,386	29,657	31,052	34,169	34,732	35,579	24,981	27,100	22,110	20,209

Table 5.8 Continued

sample no	M97-34/2 (Gölmarmara)							SE-1 (Şirince)																
analyse no	m7-83	m7-84 c	m7-85	m7-86	m7-87	m7-88	m7-89 r	m8-1 r	m8-2	m8-3	m8-4	m8-5	m8-6	m8-8	m8-9	m8-10	m8-11	m8-12 c	m8-13	m8-14	m8-15	m8-16	m8-17	m8-18
SiO2	37,26	37,43	37,45	37,58	37,70	37,14	37,65	38,02	37,91	37,87	37,94	37,83	37,92	37,60	37,57	37,34	37,40	37,67	37,15	37,53	37,52	37,58	37,79	37,76
TiO2	0,07	0,08	0,10	0,13	0,17	0,12	0,07	0,06	0,06	0,01	0,10	0,15	0,06	0,16	0,14	0,24	0,21	0,13	0,18	0,12	0,25	0,13	0,09	0,04
Al2O3	20,48	20,65	20,31	20,20	20,29	20,59	20,98	21,29	21,16	21,00	21,03	20,93	21,09	21,03	21,05	20,92	20,65	21,20	20,88	20,62	20,87	21,13	21,11	21,20
FeO	17,37	17,15	24,92	28,85	28,49	27,67	28,67	22,56	20,73	19,87	20,33	18,23	20,07	17,92	21,56	22,10	20,66	20,91	21,60	21,47	21,19	19,10	19,13	19,23
MnO	17,22	17,25	9,55	5,69	3,88	3,79	3,43	3,48	5,66	6,68	5,93	7,27	7,16	9,25	6,17	6,72	8,41	7,89	7,05	5,94	6,67	7,95	7,06	7,60
MgO	1,89	1,91	1,47	1,20	1,17	1,41	1,81	1,62	1,67	2,10	2,06	1,51	2,09	1,52	1,72	1,64	1,56	1,58	1,67	1,79	1,63	1,83	2,01	1,91
CaO	7,12	6,77	7,97	8,07	9,64	9,47	8,61	14,16	13,80	12,34	13,13	14,76	12,51	13,21	12,11	11,39	11,18	11,52	11,30	12,00	12,24	12,92	13,27	13,14
Na2O	0,02	0,06	0,00	0,02	0,06	0,07	0,02	0,00	0,02	0,03	0,01	0,00	0,00	0,00	0,00	0,03	0,00	0,00	0,04	0,00	0,03	0,03	0,05	0,05
K2O	0,00	0,03	0,04	0,00	0,00	0,00	0,00	0,00	0,00	0,00	0,02	0,01	0,00	0,00	0,00	0,00	0,00	0,00	0,02	0,04	0,03	0,01	0,01	0,03
Cr2O3	0,06	0,02	0,00	0,00	0,04	0,09	0,06	0,11	0,11	0,07	0,00	0,04	0,03	0,04	0,06	0,05	0,00	0,03	0,07	0,05	0,06	0,11	0,02	0,03
Total	101,49	101,34	101,80	101,74	101,44	100,35	101,31	101,30	101,12	99,98	100,54	100,73	100,93	100,73	100,38	100,43	100,06	100,93	99,96	99,55	100,49	100,79	100,54	100,99
normalized oxygens 24																								
Si	5,943	5,964	5,967	5,994	5,999	5,957	5,968	5,952	5,952	5,994	5,975	5,957	5,963	5,941	5,954	5,938	5,971	5,951	5,934	5,993	5,950	5,928	5,955	5,939
Ti	0,009	0,009	0,012	0,016	0,020	0,015	0,008	0,007	0,007	0,001	0,012	0,018	0,007	0,019	0,017	0,029	0,025	0,015	0,022	0,015	0,030	0,015	0,011	0,004
Al	3,850	3,878	3,814	3,798	3,806	3,893	3,920	3,929	3,916	3,918	3,904	3,885	3,909	3,917	3,932	3,921	3,886	3,948	3,931	3,881	3,901	3,929	3,921	3,930
Fe	2,317	2,285	3,320	3,848	3,791	3,711	3,800	2,953	2,721	2,630	2,677	2,400	2,639	2,368	2,857	2,939	2,758	2,762	2,885	2,867	2,810	2,519	2,521	2,529
Mn	2,326	2,328	1,289	0,769	0,523	0,515	0,460	0,461	0,753	0,895	0,791	0,970	0,954	1,238	0,828	0,905	1,137	1,056	0,954	0,803	0,896	1,062	0,942	1,012
Mg	0,449	0,454	0,349	0,286	0,278	0,337	0,428	0,378	0,391	0,495	0,484	0,353	0,490	0,357	0,406	0,388	0,371	0,373	0,398	0,426	0,385	0,430	0,472	0,448
Ca	1,217	1,156	1,360	1,379	1,643	1,627	1,462	2,375	2,321	2,093	2,215	2,490	2,108	2,236	2,056	1,940	1,912	1,950	1,934	2,053	2,079	2,183	2,240	2,214
Na	0,005	0,019	0,000	0,006	0,019	0,021	0,007	0,000	0,007	0,010	0,003	0,000	0,000	0,000	0,000	0,010	0,000	0,000	0,013	0,000	0,009	0,008	0,014	0,016
K	0,000	0,006	0,007	0,000	0,000	0,000	0,000	0,000	0,000	0,000	0,003	0,002	0,000	0,000	0,000	0,000	0,000	0,000	0,003	0,008	0,005	0,002	0,001	0,006
Cr	0,007	0,002	0,000	0,000	0,005	0,011	0,008	0,013	0,014	0,009	0,000	0,005	0,004	0,004	0,007	0,006	0,000	0,004	0,009	0,006	0,008	0,014	0,002	0,003
Total	16,115	16,098	16,118	16,094	16,080	16,076	16,055	16,056	16,066	16,036	16,064	16,075	16,070	16,075	16,052	16,070	16,061	16,054	16,074	16,046	16,065	16,077	16,078	16,098
Mg	0,449	0,454	0,349	0,286	0,278	0,337	0,428	0,378	0,391	0,495	0,484	0,353	0,490	0,357	0,406	0,388	0,371	0,373	0,398	0,426	0,385	0,430	0,472	0,448
Mn	2,326	2,328	1,289	0,769	0,523	0,515	0,460	0,461	0,753	0,895	0,791	0,970	0,954	1,238	0,828	0,905	1,137	1,056	0,954	0,803	0,896	1,062	0,942	1,012
Ca	1,217	1,156	1,360	1,379	1,643	1,627	1,462	2,375	2,321	2,093	2,215	2,490	2,108	2,236	2,056	1,940	1,912	1,950	1,934	2,053	2,079	2,183	2,240	2,214
FeII	2,008	2,063	3,002	3,567	3,555	3,521	3,650	2,786	2,536	2,517	2,510	2,187	2,449	2,169	2,709	2,766	2,580	2,622	2,715	2,718	2,640	2,324	2,345	2,326
Summe X	6,000	6,000	6,000	6,000	6,000	6,000	6,000	6,000	6,000	6,000	6,000	6,000	6,000	6,000	6,000	6,000	6,000	6,000	6,000	6,000	6,000	6,000	6,000	6,000
rest Fe	0,308	0,222	0,318	0,281	0,235	0,190	0,151	0,168	0,186	0,113	0,167	0,213	0,190	0,198	0,148	0,172	0,178	0,140	0,170	0,149	0,170	0,195	0,175	0,203
Si	5,943	5,964	5,967	5,994	5,999	5,957	5,968	5,952	5,952	5,994	5,975	5,957	5,963	5,941	5,954	5,938	5,971	5,951	5,934	5,993	5,950	5,928	5,955	5,939
Aliv	0,057	0,036	0,033	0,006	0,001	0,043	0,032	0,048	0,048	0,006	0,025	0,043	0,037	0,059	0,046	0,062	0,029	0,049	0,066	0,007	0,050	0,072	0,045	0,061
Summe Z	6,000	6,000	6,000	6,000	6,000	6,000	6,000	6,000	6,000	6,000	6,000	6,000	6,000	6,000	6,000	6,000	6,000	6,000	6,000	6,000	6,000	6,000	6,000	6,000
Alvi	3,793	3,842	3,781	3,792	3,805	3,850	3,889	3,881	3,867	3,912	3,879	3,842	3,872	3,857	3,887	3,859	3,858	3,899	3,865	3,875	3,851	3,857	3,876	3,869
Cr	0,007	0,002	0,000	0,000	0,005	0,011	0,008	0,013	0,014	0,009	0,000	0,005	0,004	0,004	0,007	0,006	0,000	0,004	0,009	0,006	0,008	0,014	0,002	0,003
Ti	0,009	0,009	0,012	0,016	0,020	0,015	0,008	0,007	0,007	0,001	0,012	0,018	0,007	0,019	0,017	0,029	0,025	0,015	0,022	0,015	0,030	0,015	0,011	0,004
FeIII	0,308	0,222	0,318	0,281	0,235	0,190	0,151	0,168	0,186	0,113	0,167	0,213	0,190	0,198	0,148	0,172	0,178	0,140	0,170	0,149	0,170	0,195	0,175	0,203
Summe Y	4,117	4,075	4,111	4,089	4,066	4,066	4,056	4,069	4,074	4,036	4,058	4,079	4,073	4,079	4,059	4,065	4,061	4,058	4,066	4,045	4,058	4,081	4,065	4,079
Alm(%)	33,468	34,387	50,027	59,444	59,258	58,685	60,827	46,427	42,261	41,943	41,836	36,452	40,818	36,158	45,155	46,104	42,998	43,696	45,250	45,292	44,001	38,738	39,092	38,767
Prp(%)	7,488	7,559	5,822	4,762	4,637	5,614	7,128	6,300	6,513	8,257	8,059	5,887	8,164	5,946	6,772	6,474	6,175	6,216	6,626	7,101	6,413	7,171	7,868	7,462
Sps(%)	38,767	38,794	21,477	12,810	8,715	8,580	7,675	7,690	12,543	14,924	13,182	16,159	15,893	20,629	13,803	15,083	18,954	17,594	15,895	13,390	14,930	17,701	15,703	16,872
Grs(%)	18,679	18,159	20,854	21,314	25,635	25,680	23,368	37,751	36,726	33,805	35,295	39,093	33,392	35,239	32,819	30,695	30,279	31,218	30,638	32,781	32,882	34,393	35,605	34,994
And(%)	1,561	1,092	1,819	1,669	1,722	1,367	0,956	1,702	1,827	0,991	1,627	2,354	1,702	1,987	1,392	1,599	1,593	1,245	1,520	1,388	1,707	1,873	1,712	1,874
Uva(%)	0,036	0,009	0,000	0,000	0,034	0,074	0,047	0,129	0,131	0,079	0,000	0,054	0,031	0,041	0,059	0,045	0,000	0,032	0,070	0,048	0,067	0,125	0,021	0,031
Prp	7,488	7,559	5,822	4,762	4,637	5,614	7,128	6,300	6,513	8,257	8,059	5,887	8,164	5,946	6,772	6,474	6,175	6,216	6,626	7,101	6,413	7,171	7,868	7,462
Alm+Sps	72,235	73,181	71,505	72,255	67,973	67,266	68,502	54,117	54,803	56,868	55,019	52,612	56,710	56,787	58,958	61,187	61,952	61,289	61,145	58,682	58,931	56,439	54,795	55,638
Grs+And	20,241	19,251	22,674	22,983	27,357	27,046	24,324	39,454	38,553	34,797	36,922	41,447	35,094	37,226	34,211	32,294	31,873	32,463	32,158	34,169	34,589	36,265	37,317	36,868

Table 5.8 Continued

sample no	SE-1 (Şirince)																							
analyse no	m8-19 r	m8-32	m8-35 r	m8-36	m8-37	m8-38	m8-39	m8-40	m8-41	m8-43 c	m8-44	m8-45	m8-46	m8-47	m8-48	m8-49	m8-50 r	m8-145r	m8-146	m8-147	m8-148	m8-149c	m8-150	m8-151
SiO2	38,03	37,78	38,03	38,01	37,96	38,06	37,94	37,96	38,05	37,51	37,23	37,80	38,04	38,17	37,86	38,12	37,92	38,18	38,23	37,97	38,32	38,10	38,20	38,43
TiO2	0,11	0,05	0,07	0,05	0,10	0,16	0,14	0,11	0,20	0,10	0,12	0,16	0,20	0,12	0,14	0,02	0,07	0,04	0,10	0,11	0,19	0,08	0,17	0,11
Al2O3	21,36	21,11	21,29	20,98	21,09	20,63	20,93	20,77	20,97	20,99	20,78	20,58	20,95	21,15	21,01	21,28	21,07	21,20	21,00	20,87	21,23	21,17	21,14	21,01
FeO	22,08	21,69	22,32	20,18	20,63	21,77	22,75	21,56	19,74	19,78	19,57	19,54	21,37	22,35	21,34	18,49	21,08	23,20	20,53	20,86	21,27	20,45	21,37	18,11
MnO	2,96	3,51	4,18	5,99	5,99	5,37	5,74	6,81	10,68	10,74	10,50	10,60	7,09	5,89	6,23	7,83	5,06	3,17	6,38	6,58	6,20	6,28	6,13	8,51
MgO	1,69	1,65	1,53	1,50	1,97	1,61	1,46	1,40	1,48	1,39	1,41	1,46	1,49	1,77	1,97	1,74	1,49	1,45	1,62	2,18	1,70	1,64	2,03	1,77
CaO	14,48	14,16	13,68	13,99	13,29	13,49	12,30	12,11	10,39	10,18	10,44	10,75	11,88	11,98	12,08	13,27	14,53	14,56	12,95	12,24	13,16	13,18	12,58	13,11
Na2O	0,02	0,00	0,00	0,03	0,01	0,04	0,00	0,09	0,00	0,00	0,02	0,09	0,02	0,00	0,00	0,00	0,00	0,02	0,00	0,00	0,02	0,03	0,00	0,04
K2O	0,01	0,01	0,00	0,00	0,00	0,03	0,00	0,02	0,00	0,00	0,01	0,00	0,00	0,00	0,01	0,03	0,00	0,01	0,00	0,00	0,00	0,02	0,00	0,01
Cr2O3	0,02	0,00	0,03	0,12	0,04	0,05	0,00	0,09	0,06	0,05	0,02	0,06	0,08	0,00	0,02	0,09	0,01	0,05	0,04	0,06	0,02	0,05	0,03	0,01
Total	100,76	99,96	101,13	100,85	101,08	101,22	101,26	100,92	101,58	100,74	100,09	101,03	101,12	101,43	100,66	100,87	101,23	101,89	100,85	100,87	102,11	101,00	101,66	101,11
normalized oxygens 24																								
Si	5,964	5,977	5,966	5,981	5,958	5,987	5,977	5,999	5,990	5,964	5,958	5,993	5,992	5,985	5,974	5,983	5,952	5,956	6,011	5,978	5,965	5,983	5,967	6,018
Ti	0,013	0,006	0,008	0,006	0,012	0,019	0,017	0,014	0,024	0,011	0,015	0,019	0,024	0,015	0,017	0,002	0,008	0,005	0,012	0,013	0,022	0,010	0,020	0,012
Al	3,948	3,937	3,937	3,891	3,902	3,825	3,887	3,869	3,891	3,934	3,920	3,846	3,890	3,909	3,908	3,937	3,898	3,899	3,892	3,873	3,896	3,918	3,892	3,878
Fe	2,895	2,869	2,928	2,655	2,708	2,864	2,997	2,849	2,599	2,630	2,619	2,590	2,815	2,930	2,816	2,426	2,767	3,026	2,699	2,746	2,769	2,685	2,791	2,371
Mn	0,393	0,470	0,555	0,798	0,796	0,715	0,766	0,911	1,424	1,446	1,423	1,423	0,946	0,782	0,833	1,041	0,673	0,419	0,850	0,877	0,817	0,835	0,811	1,129
Mg	0,395	0,390	0,358	0,352	0,461	0,378	0,343	0,330	0,347	0,329	0,336	0,345	0,349	0,414	0,463	0,407	0,349	0,337	0,380	0,512	0,394	0,383	0,473	0,413
Ca	2,433	2,400	2,299	2,358	2,235	2,273	2,076	2,050	1,752	1,734	1,790	1,826	2,005	2,012	2,042	2,231	2,443	2,433	2,181	2,064	2,195	2,217	2,105	2,199
Na	0,006	0,000	0,000	0,009	0,004	0,013	0,000	0,026	0,000	0,000	0,005	0,027	0,006	0,000	0,000	0,000	0,000	0,006	0,000	0,000	0,006	0,008	0,000	0,012
K	0,002	0,002	0,000	0,000	0,000	0,006	0,000	0,004	0,000	0,000	0,001	0,000	0,000	0,000	0,002	0,006	0,000	0,003	0,000	0,000	0,000	0,003	0,000	0,002
Cr	0,002	0,000	0,004	0,015	0,004	0,006	0,000	0,011	0,008	0,006	0,003	0,007	0,010	0,000	0,002	0,011	0,001	0,007	0,005	0,008	0,002	0,007	0,004	0,002
Total	16,050	16,050	16,052	16,050	16,075	16,082	16,063	16,052	16,028	16,048	16,066	16,069	16,027	16,046	16,054	16,033	16,089	16,084	16,024	16,062	16,065	16,044	16,060	16,035
Mg	0,395	0,390	0,358	0,352	0,461	0,378	0,343	0,330	0,347	0,329	0,336	0,345	0,349	0,414	0,463	0,407	0,349	0,337	0,380	0,512	0,394	0,383	0,473	0,413
Mn	0,393	0,470	0,555	0,798	0,796	0,715	0,766	0,911	1,424	1,446	1,423	1,423	0,946	0,782	0,833	1,041	0,673	0,419	0,850	0,877	0,817	0,835	0,811	1,129
Ca	2,433	2,400	2,299	2,358	2,235	2,273	2,076	2,050	1,752	1,734	1,790	1,826	2,005	2,012	2,042	2,231	2,443	2,433	2,181	2,064	2,195	2,217	2,105	2,199
FeII	2,779	2,740	2,787	2,492	2,508	2,633	2,815	2,709	2,476	2,491	2,451	2,406	2,700	2,792	2,662	2,321	2,536	2,811	2,589	2,547	2,593	2,564	2,611	2,259
Summe X	6,000	6,000	6,000	6,000	6,000	6,000	6,000	6,000	6,000	6,000	6,000	6,000	6,000	6,000	6,000	6,000	6,000	6,000	6,000	6,000	6,000	6,000	6,000	6,000
rest Fe	0,116	0,129	0,141	0,164	0,199	0,231	0,182	0,140	0,122	0,139	0,167	0,184	0,115	0,138	0,153	0,105	0,231	0,216	0,110	0,199	0,175	0,121	0,180	0,113
Si	5,964	5,977	5,966	5,981	5,958	5,987	5,977	5,999	5,990	5,964	5,958	5,993	5,992	5,985	5,974	5,983	5,952	5,956	6,011	5,978	5,965	5,983	5,967	6,018
Aliv	0,036	0,023	0,034	0,019	0,042	0,013	0,023	0,001	0,010	0,036	0,042	0,007	0,008	0,015	0,026	0,017	0,048	0,044	0,000	0,022	0,035	0,017	0,033	0,000
Summe Z	6,000	6,000	6,000	6,000	6,000	6,000	6,000	6,000	6,000	6,000	6,000	6,000	6,000	6,000	6,000	6,000	6,000	6,000	6,011	6,000	6,000	6,000	6,000	6,018
Alvi	3,912	3,913	3,903	3,872	3,860	3,813	3,864	3,868	3,882	3,898	3,878	3,839	3,882	3,894	3,882	3,919	3,849	3,855	3,892	3,850	3,861	3,901	3,860	3,878
Cr	0,002	0,000	0,004	0,015	0,004	0,006	0,000	0,011	0,008	0,006	0,003	0,007	0,010	0,000	0,002	0,011	0,001	0,007	0,005	0,008	0,002	0,007	0,004	0,002
Ti	0,013	0,006	0,008	0,006	0,012	0,019	0,017	0,014	0,024	0,011	0,015	0,019	0,024	0,015	0,017	0,002	0,008	0,005	0,012	0,013	0,022	0,010	0,020	0,012
FeIII	0,116	0,129	0,141	0,164	0,199	0,231	0,182	0,140	0,122	0,139	0,167	0,184	0,115	0,138	0,153	0,105	0,231	0,216	0,110	0,199	0,175	0,121	0,180	0,113
Summe Y	4,044	4,048	4,055	4,056	4,075	4,068	4,063	4,033	4,036	4,055	4,063	4,049	4,031	4,046	4,054	4,038	4,090	4,082	4,019	4,070	4,060	4,039	4,064	4,005
Alm(%)	46,321	45,671	46,455	41,528	41,803	43,878	46,914	45,147	41,273	41,510	40,856	40,102	45,000	46,532	44,369	38,685	42,262	46,846	43,149	42,447	43,223	42,736	43,519	37,647
Prp(%)	6,583	6,492	5,970	5,863	7,681	6,307	5,722	5,492	5,788	5,486	5,593	5,746	5,822	6,894	7,722	6,783	5,809	5,615	6,339	8,525	6,574	6,389	7,877	6,885
Sps(%)	6,552	7,838	9,256	13,304	13,271	11,924	12,764	15,191	23,733	24,103	23,719	23,721	15,764	13,035	13,876	17,345	11,210	6,981	14,159	14,622	13,624	13,920	13,516	18,811
Grs(%)	39,225	38,667	36,876	37,524	35,276	35,508	32,907	32,775	28,090	27,782	28,475	28,854	32,179	32,272	32,589	36,092	38,322	38,302	35,205	32,551	34,783	35,695	33,322	35,498
And(%)	1,296	1,332	1,407	1,640	1,929	2,329	1,693	1,303	1,060	1,073	1,337	1,525	1,152	1,267	1,428	0,992	2,382	2,190	1,101	1,791	1,780	1,198	1,732	1,145
Uva(%)	0,024	0,000	0,035	0,142	0,041	0,054	0,000	0,093	0,057	0,046	0,020	0,053	0,083	0,000	0,017	0,102	0,015	0,066	0,047	0,064	0,017	0,061	0,034	0,015
Prp	6,583	6,492	5,970	5,863	7,681	6,307	5,722	5,492	5,788	5,486	5,593	5,746	5,822	6,894	7,722	6,783	5,809	5,615	6,339	8,525	6,574	6,389	7,877	6,885
Alm+Sps	52,872	53,509	55,711	54,831	55,074	55,802	59,679	60,337	65,006	65,614	64,574	63,823	60,764	59,567	58,244	56,031	53,472	53,826	57,308	57,069	56,846	56,656	57,035	56,458
Grs+And	40,521	39,999	38,284	39,163	37,204	37,837	34,600	34,078	29,150	28,855	29,812	30,378	33,331	33,539	34,017	37,084	40,704	40,492	36,307	34,342	36,563	36,893	35,054	36,642

Table 5.8 Continued

sample no	SE-1 (Şirince)			M98-45C (Şirince)									M96-31(Şirince)					95-21/10 (Şirince)						
analyse no	m8-152	m8-153	m8-154r	m4-5r	m4-6	m4-7	m4-8	m4-9	m4-10	m4-11	m4-12c	m4-13	m5-2c	m5-3	m5-4	m5-5	m5-6r	1r	2	3	4	5	6	7
SiO2	38,19	38,38	38,310	38,180	38,430	38,460	38,150	37,930	38,110	38,350	38,150	38,280	37,740	37,790	38,070	38,110	38,100	37,990	38,060	38,100	37,900	38,050	37,940	37,960
TiO2	0,09	0,11	0,108	0,155	0,124	0,119	0,126	0,154	0,196	0,111	0,161	0,154	0,159	0,277	0,108	0,136	0,129	0,159	0,188	0,195	0,304	0,257	0,268	0,321
Al2O3	20,58	21,14	21,300	21,310	21,320	21,150	21,230	21,170	21,340	21,100	21,220	21,370	21,190	21,280	21,250	21,280	21,520	21,810	21,330	21,370	21,140	20,910	21,150	20,670
FeO	20,16	21,43	22,910	27,580	27,850	28,000	24,430	22,950	21,220	20,200	20,490	20,010	18,430	18,540	18,720	19,380	22,620	17,550	24,980	24,280	25,550	26,160	26,130	26,640
MnO	6,14	2,77	3,510	0,757	0,969	1,970	4,800	6,980	9,010	9,890	10,310	10,140	12,650	12,100	12,520	11,350	6,780	8,790	1,204	1,330	1,720	1,530	1,690	1,740
MgO	1,65	0,96	1,720	1,970	1,830	1,750	1,321	1,091	0,930	0,962	0,959	0,917	0,717	0,787	0,738	0,788	1,003	1,438	1,930	1,720	1,499	1,386	1,377	1,325
CaO	13,56	16,05	13,440	10,730	10,520	9,950	10,830	10,930	11,020	10,710	10,370	10,910	10,260	10,770	10,200	10,740	11,680	13,580	12,610	13,450	13,320	12,550	12,560	13,090
Na2O	0,05	0,00	0,030	0,050	0,012	0,032	0,021	0,033	0,000	0,051	0,117	0,039	0,064	0,021	0,000	0,000	0,011	0,0	0,038	0,057	0,074	0,061	0,057	0,052
K2O	0,00	0,00	0,009	0,000	0,000	0,007	0,007	0,027	0,028	0,010	0,031	0,013	0,015	0,000	0,000	0,000	0,028	0,000	0,000	0,028	0,000	0,000	0,000	0,020
Cr2O3	0,07	0,00	0,000	0,082	0,061	0,082	0,067	0,080	0,067	0,163	0,039	0,133	0,115	0,010	0,138	0,057	0,016	0,00	0,07	0,03	0,02	0,05	0,00	0,00
Total	100,48	100,83	101,34	100,81	101,12	101,52	100,98	101,35	101,92	101,55	101,85	101,97	101,34	101,58	101,74	101,84	101,89	101,16	100,11	100,25	101,13	100,59	100,85	101,43
normalized oxygens 24																								
Si	6,028	6,013	5,987	6,007	6,031	6,034	6,016	5,985	5,982	6,032	5,998	5,999	5,976	5,962	5,998	5,993	5,970	5,936	5,989	5,985	5,943	5,998	5,970	5,964
Ti	0,011	0,012	0,013	0,018	0,015	0,014	0,015	0,018	0,023	0,013	0,019	0,018	0,019	0,033	0,013	0,016	0,015	0,019	0,022	0,023	0,036	0,030	0,032	0,038
Al	3,829	3,904	3,924	3,952	3,944	3,911	3,946	3,937	3,948	3,912	3,933	3,947	3,955	3,958	3,947	3,945	3,975	4,017	3,956	3,957	3,907	3,885	3,923	3,828
Fe	2,661	2,808	2,994	3,628	3,655	3,673	3,221	3,028	2,785	2,657	2,694	2,622	2,440	2,446	2,466	2,548	2,964	2,293	3,287	3,189	3,350	3,448	3,438	3,500
Mn	0,821	0,368	0,465	0,101	0,129	0,262	0,641	0,933	1,198	1,317	1,373	1,346	1,696	1,617	1,671	1,512	0,900	1,163	0,160	0,177	0,228	0,204	0,225	0,232
Mg	0,387	0,223	0,401	0,462	0,428	0,409	0,310	0,257	0,218	0,226	0,225	0,214	0,169	0,185	0,173	0,185	0,234	0,335	0,453	0,403	0,350	0,326	0,323	0,310
Ca	2,293	2,694	2,250	1,808	1,769	1,672	1,830	1,848	1,853	1,805	1,747	1,832	1,740	1,820	1,722	1,809	1,961	2,273	2,126	2,263	2,238	2,119	2,117	2,203
Na	0,014	0,000	0,009	0,015	0,004	0,010	0,006	0,010	0,000	0,016	0,036	0,012	0,020	0,006	0,000	0,000	0,003	0,000	0,012	0,017	0,022	0,019	0,017	0,016
K	0,000	0,000	0,002	0,000	0,000	0,001	0,001	0,005	0,006	0,002	0,006	0,003	0,003	0,000	0,000	0,000	0,006	0,000	0,000	0,006	0,000	0,000	0,000	0,004
Cr	0,008	0,000	0,000	0,010	0,008	0,010	0,008	0,010	0,008	0,020	0,005	0,016	0,014	0,001	0,017	0,007	0,002	0,000	0,009	0,004	0,003	0,006	0,000	0,000
Total	16,042	16,022	16,044	15,991	15,973	15,987	15,987	16,021	16,012	15,978	16,030	15,992	16,018	16,027	15,990	16,008	16,028	16,037	16,004	16,020	16,075	16,029	16,046	16,094
Mg	0,387	0,223	0,401	0,462	0,428	0,409	0,310	0,257	0,218	0,226	0,225	0,214	0,169	0,185	0,173	0,185	0,234	0,335	0,453	0,403	0,350	0,326	0,323	0,310
Mn	0,821	0,368	0,465	0,101	0,129	0,262	0,641	0,933	1,198	1,317	1,373	1,346	1,696	1,617	1,671	1,512	0,900	1,163	0,160	0,177	0,228	0,204	0,225	0,232
Ca	2,293	2,694	2,250	1,808	1,769	1,672	1,830	1,848	1,853	1,805	1,747	1,832	1,740	1,820	1,722	1,809	1,961	2,273	2,126	2,263	2,238	2,119	2,117	2,203
FeII	2,499	2,715	2,885	3,628	3,655	3,657	3,219	2,963	2,732	2,653	2,656	2,609	2,394	2,378	2,434	2,494	2,905	2,229	3,261	3,157	3,184	3,351	3,335	3,255
Summe X	6,000	6,000	6,000	5,999	5,980	6,000	6,000	6,000	6,000	6,000	6,000	6,000	6,000	6,000	6,000	6,000	6,000	6,000	6,000	6,000	6,000	6,000	6,000	6,000
rest Fe	0,161	0,092	0,109	0,000	0,000	0,017	0,002	0,065	0,053	0,004	0,038	0,013	0,046	0,068	0,032	0,054	0,059	0,065	0,025	0,032	0,166	0,097	0,104	0,245
Si	6,028	6,013	5,987	6,007	6,031	6,034	6,016	5,985	5,982	6,032	5,998	5,999	5,976	5,962	5,998	5,993	5,970	5,936	5,989	5,985	5,943	5,998	5,970	5,964
Aliv	0,000	0,000	0,013	0,000	0,000	0,000	0,000	0,015	0,018	0,000	0,002	0,001	0,024	0,038	0,002	0,007	0,030	0,064	0,011	0,015	0,057	0,002	0,030	0,036
Summe Z	6,028	6,013	6,000	6,007	6,031	6,034	6,016	6,000	6,000	6,032	6,000	6,000	6,000	6,000	6,000	6,000	6,000	6,000	6,000	6,000	6,000	6,000	6,000	6,000
Alvi	3,829	3,904	3,911	3,952	3,944	3,911	3,946	3,922	3,930	3,912	3,931	3,946	3,930	3,920	3,945	3,938	3,945	3,953	3,945	3,942	3,850	3,883	3,893	3,792
Cr	0,008	0,000	0,000	0,010	0,008	0,010	0,008	0,010	0,008	0,020	0,005	0,016	0,014	0,001	0,017	0,007	0,002	0,000	0,009	0,004	0,003	0,006	0,000	0,000
Ti	0,011	0,012	0,013	0,018	0,015	0,014	0,015	0,018	0,023	0,013	0,019	0,018	0,019	0,033	0,013	0,016	0,015	0,019	0,022	0,023	0,036	0,030	0,032	0,038
FeIII	0,161	0,092	0,109	0,000	0,000	0,017	0,002	0,065	0,053	0,004	0,038	0,013	0,046	0,068	0,032	0,054	0,059	0,065	0,025	0,032	0,166	0,097	0,104	0,245
Summe Y	4,009	4,009	4,033	3,980	3,966	3,952	3,972	4,015	4,014	3,949	3,993	3,994	4,010	4,022	4,007	4,015	4,021	4,037	4,001	4,000	4,055	4,017	4,028	4,074
Alm(%)	41,654	45,253	48,076	60,475	61,113	60,945	53,648	49,384	45,529	44,210	44,261	43,475	39,902	39,628	40,571	41,571	48,418	37,142	54,354	52,616	53,061	55,847	55,575	54,250
Prp(%)	6,453	3,721	6,677	7,700	7,158	6,820	5,175	4,276	3,626	3,758	3,746	3,570	2,820	3,084	2,888	3,078	3,904	5,582	7,544	6,711	5,839	5,427	5,382	5,171
Sps(%)	13,679	6,126	7,743	1,681	2,154	4,363	10,684	15,546	19,961	21,956	22,881	22,429	28,272	26,947	27,844	25,194	14,997	19,387	2,674	2,949	3,807	3,404	3,754	3,859
Grs(%)	36,496	43,727	36,369	29,928	29,411	27,585	30,296	30,079	30,232	29,792	28,660	30,159	28,433	29,568	28,251	29,576	32,063	37,108	34,930	37,168	35,408	34,143	34,103	34,173
And(%)	1,639	1,174	1,135	0,139	0,109	0,216	0,134	0,638	0,588	0,130	0,417	0,242	0,470	0,763	0,321	0,528	0,602	0,781	0,422	0,521	1,860	1,123	1,185	2,548
Uva(%)	0,079	0,000	0,000	0,077	0,056	0,072	0,064	0,077	0,064	0,154	0,035	0,126	0,104	0,009	0,123	0,053	0,016	0,000	0,076	0,035	0,025	0,056	0,000	0,000
Prp	6,453	3,721	6,677	7,700	7,158	6,820	5,175	4,276	3,626	3,758	3,746	3,570	2,820	3,084	2,888	3,078	3,904	5,582	7,544	6,711	5,839	5,427	5,382	5,171
Alm+Sps	55,333	51,379	55,819	62,156	63,266	65,307	64,332	64,930	65,490	66,165	67,142	65,904	68,174	66,575	68,416	66,765	63,415	56,529	57,028	55,565	56,868	59,251	59,329	58,108
Grs+And	38,135	44,901	37,504	30,067	29,520	27,801	30,430	30,717	30,820	29,922	29,077	30,401	28,902	30,331	28,573	30,104	32,665	37,889	35,352	37,689	37,268	35,266	35,289	36,721

Table 5.8 Continued

sample no	95-21/10 (Strince)																	M99-5/4 (Strince)			
analyse no	8	9	10	11	12	13	14c	15	16	17	18	19	20	21	22	23	24r	m19-10r	m19-11	m19-12	m19-13c
SiO2	38,010	38,050	37,630	37,720	37,760	37,740	37,920	37,440	38,040	37,800	37,480	37,780	38,260	37,640	38,140	38,150	37,480	38,260	38,090	37,950	37,910
TiO2	0,221	0,228	0,280	0,251	0,225	0,261	0,352	0,277	0,306	0,300	0,235	0,283	0,273	0,161	0,184	0,192	0,071	0,117	0,126	0,173	0,203
Al2O3	21,270	21,920	21,100	21,130	21,860	20,860	20,860	20,630	21,700	20,600	20,850	21,640	21,190	21,510	21,720	21,740	21,860	21,180	21,080	21,010	20,980
FeO	26,510	25,580	25,640	25,670	24,430	25,170	25,140	25,140	25,180	26,030	25,820	26,710	26,500	25,500	24,830	25,010	18,020	26,900	26,390	26,760	26,150
MnO	1,970	2,140	1,740	2,810	4,050	4,280	4,590	4,180	3,710	3,240	2,290	2,740	1,370	1,234	1,282	2,290	8,250	1,940	2,590	2,980	3,080
MgO	1,371	1,263	1,333	1,199	1,213	1,106	0,940	1,122	1,266	1,276	1,276	1,321	1,501	1,840	1,990	2,100	1,490	1,494	1,298	1,306	1,232
CaO	12,180	12,660	12,920	12,740	11,690	11,230	12,270	11,500	11,880	11,510	12,560	10,950	12,220	12,540	12,640	11,730	12,910	10,850	11,410	10,640	10,930
Na2O	0,049	0,018	0,051	0,031	0,000	0,012	0,057	0,042	0,045	0,038	0,000	0,038	0,044	0,041	0,024	0,060	0,011	0,013	0,000	0,000	0,022
K2O	0,025	0,000	0,000	0,019	0,000	0,015	0,000	0,007	0,012	0,000	0,000	0,000	0,014	0,000	0,000	0,000	0,007	0,032	0,000	0,000	0,000
Cr2O3	0,10	0,00	0,00	0,00	0,00	0,02	0,04	0,07	0,00	0,10	0,00	0,00	0,00	0,01	0,00	0,08	0,00	0,09	0,04	0,09	0,03
Total	101,31	101,61	100,36	101,27	101,00	100,39	100,78	100,01	101,78	100,46	100,28	101,14	101,04	100,26	100,60	101,02	100,01	100,88	101,03	100,91	100,54
normalized oxygens 24																					
Si	5,960	5,935	5,950	5,936	5,935	5,993	5,956	5,972	5,937	5,993	5,954	5,940	5,998	5,937	5,970	5,956	5,924	6,030	6,010	6,005	6,014
Ti	0,026	0,027	0,033	0,030	0,027	0,031	0,042	0,033	0,036	0,036	0,028	0,033	0,032	0,019	0,022	0,023	0,008	0,014	0,015	0,021	0,024
Al	3,931	4,030	3,933	3,920	4,050	3,904	3,862	3,879	3,992	3,850	3,905	4,011	3,916	3,999	4,007	4,001	4,073	3,935	3,920	3,919	3,923
Fe	3,476	3,336	3,390	3,378	3,211	3,342	3,302	3,353	3,286	3,451	3,430	3,512	3,474	3,363	3,250	3,265	2,382	3,545	3,482	3,541	3,469
Mn	0,262	0,283	0,233	0,375	0,539	0,576	0,611	0,565	0,490	0,435	0,308	0,365	0,182	0,165	0,170	0,303	1,104	0,259	0,346	0,399	0,414
Mg	0,320	0,294	0,314	0,281	0,284	0,262	0,220	0,267	0,295	0,302	0,302	0,310	0,351	0,433	0,464	0,489	0,351	0,351	0,305	0,308	0,291
Ca	2,046	2,116	2,189	2,148	1,968	1,910	2,065	1,965	1,986	1,955	2,138	1,845	2,052	2,119	2,119	1,962	2,186	1,832	1,929	1,804	1,857
Na	0,015	0,005	0,016	0,009	0,000	0,004	0,017	0,013	0,014	0,012	0,000	0,012	0,013	0,013	0,007	0,018	0,003	0,004	0,000	0,000	0,007
K	0,005	0,000	0,000	0,004	0,000	0,003	0,000	0,001	0,002	0,000	0,000	0,000	0,003	0,000	0,000	0,000	0,001	0,006	0,000	0,000	0,000
Cr	0,012	0,000	0,000	0,000	0,000	0,002	0,005	0,009	0,000	0,012	0,000	0,000	0,000	0,002	0,000	0,010	0,000	0,012	0,005	0,012	0,004
Total	16,041	16,026	16,058	16,081	16,014	16,024	16,073	16,049	16,039	16,033	16,065	16,027	16,020	16,048	16,009	16,015	16,033	15,976	16,007	15,997	15,998
Mg	0,320	0,294	0,314	0,281	0,284	0,262	0,220	0,267	0,295	0,302	0,302	0,310	0,351	0,433	0,464	0,489	0,351	0,351	0,305	0,308	0,291
Mn	0,262	0,283	0,233	0,375	0,539	0,576	0,611	0,565	0,490	0,435	0,308	0,365	0,182	0,165	0,170	0,303	1,104	0,259	0,346	0,399	0,414
Ca	2,046	2,116	2,189	2,148	1,968	1,910	2,065	1,965	1,986	1,955	2,138	1,845	2,052	2,119	2,119	1,962	2,186	1,832	1,929	1,804	1,857
FeII	3,372	3,308	3,264	3,196	3,208	3,252	3,105	3,203	3,229	3,308	3,252	3,481	3,415	3,284	3,246	3,247	2,358	3,545	3,420	3,489	3,437
Summe X	6,000	6,000	6,000	6,000	6,000	6,000	6,000	6,000	6,000	6,000	6,000	6,000	6,000	6,000	6,000	6,000	6,000	5,987	6,000	6,000	6,000
rest Fe	0,104	0,028	0,126	0,182	0,002	0,090	0,197	0,150	0,058	0,143	0,178	0,031	0,059	0,080	0,003	0,018	0,023	0,000	0,062	0,052	0,031
Si	5,960	5,935	5,950	5,936	5,935	5,993	5,956	5,972	5,937	5,993	5,954	5,940	5,998	5,937	5,970	5,956	5,924	6,030	6,010	6,005	6,014
Aliv	0,040	0,065	0,050	0,064	0,065	0,007	0,044	0,028	0,063	0,007	0,046	0,060	0,002	0,063	0,030	0,044	0,076	0,000	0,000	0,000	0,000
Summe Z	6,000	6,000	6,000	6,000	6,000	6,000	6,000	6,000	6,000	6,000	6,000	6,000	6,000	6,000	6,000	6,000	6,000	6,030	6,010	6,005	6,014
Alvi	3,891	3,965	3,883	3,856	3,985	3,897	3,818	3,851	3,929	3,843	3,859	3,951	3,913	3,936	3,977	3,956	3,997	3,935	3,920	3,919	3,923
Cr	0,012	0,000	0,000	0,000	0,000	0,002	0,005	0,009	0,000	0,012	0,000	0,000	0,000	0,002	0,000	0,010	0,000	0,012	0,005	0,012	0,004
Ti	0,026	0,027	0,033	0,030	0,027	0,031	0,042	0,033	0,036	0,036	0,028	0,033	0,032	0,019	0,022	0,023	0,008	0,014	0,015	0,021	0,024
FeIII	0,104	0,028	0,126	0,182	0,002	0,090	0,197	0,150	0,058	0,143	0,178	0,031	0,059	0,080	0,003	0,018	0,023	0,000	0,062	0,052	0,031
Summe Y	4,033	4,020	4,042	4,068	4,014	4,020	4,061	4,043	4,023	4,034	4,065	4,015	4,004	4,037	4,002	4,007	4,029	3,960	4,003	4,003	3,982
Alm(%)	56,200	55,135	54,402	53,271	53,473	54,206	51,747	53,388	53,811	55,139	54,200	58,017	56,918	54,725	54,106	54,112	39,308	59,213	57,000	58,146	57,292
Prp(%)	5,340	4,894	5,236	4,687	4,736	4,362	3,667	4,446	4,908	5,026	5,036	5,160	5,845	7,210	7,737	8,144	5,850	5,862	5,087	5,134	4,855
Sps(%)	4,360	4,712	3,884	6,242	8,985	9,593	10,176	9,412	8,173	7,251	5,135	6,081	3,031	2,747	2,832	5,046	18,406	4,325	5,768	6,656	6,896
Grs(%)	32,903	34,777	35,040	33,938	32,570	30,866	32,350	31,197	32,338	31,043	33,822	30,251	33,429	34,437	35,104	32,284	36,149	30,402	31,485	29,430	30,497
And(%)	1,098	0,483	1,438	1,862	0,237	0,956	2,021	1,484	0,769	1,442	1,807	0,491	0,776	0,865	0,220	0,332	0,286	0,107	0,615	0,546	0,430
Uva(%)	0,100	0,000	0,000	0,000	0,000	0,017	0,039	0,074	0,000	0,100	0,000	0,000	0,000	0,015	0,000	0,082	0,000	0,090	0,044	0,087	0,030
Prp	5,340	4,894	5,236	4,687	4,736	4,362	3,667	4,446	4,908	5,026	5,036	5,160	5,845	7,210	7,737	8,144	5,850	5,862	5,087	5,134	4,855
Alm+Sps	60,560	59,847	58,286	59,513	62,458	63,798	61,923	62,800	61,984	62,390	59,335	64,099	59,950	57,473	56,938	59,158	57,714	63,539	62,768	64,803	64,188
Grs+And	34,001	35,260	36,478	35,800	32,807	31,822	34,371	32,681	33,107	32,485	35,629	30,742	34,205	35,302	35,325	32,616	36,435	30,509	32,100	29,976	30,927

compositions show the following ranges of end-members: almandine 33.4 – 61.1 mol %, pyrope 2.4 – 8.5 mol %, grossular 18.1 – 43.7 mol %, spessartine 1.3 – 38.8 mol % and andradite 0.2 – 2.3 mol %. In the pyrope – (almandine + spessartine) – grossular ternary diagram (Figure 5.22a), garnets plot within the group C eclogite field of Coleman et al. (1965). Group C represents eclogites associated with blueschists. Most garnets are rich in Fe+Mn+Ca with pyrope end-members less than 30 mol % (C type; Coleman et al. 1965) showing a prograde core to rim zonation with decreasing Mn and increasing Mg content (Hollister 1966). In addition, garnets are all typical of ophiolitic, low temperature eclogites (Figure 5.22b). The zoning profiles of garnet from 95-70/4, 95-21/10, M96-31, SE-1, M98-45C and M97-34/2 samples are given below.

Sample one: In sample **95-70/4**, cation sums range between 15.986 and 16.041, very close to the stoichiometric value of 16.00. Minor amounts of aliminum are assigned to tetrahedral sites, averaging 0.011 based on one formula unit. Alkalis, Cr and Ti are present in insignificant proportions. Al(VI) averages 3.919 per 24 oxygens and, the amount of ferric iron ranges from 0.014 to 0.114 (Table 5.8). The ferric iron is of negligible amount. Andradite content of garnet ranges from 0.2 to 1.1 mol %. Hence compositional variation of this garnet can be shown adequately in terms of the Ca (grossular), Fe (almandine), Mg (pyrope) and Mn (spessartine) proportions. In Figure 5.23, the Fe(2+)/Mg/Ca/Mn ratios for a single garnet crystal are presented. This illustration basically shows the proportions of atoms occupying the large eightfold coordinated site in garnet. As seen from Figure 5.23, this garnet is calcium-, mangenese- and magnesium-bearing almandine. The proportion of the almandine and spessartine end member ranging from 43.7 to 59.4 and from 1.4 to 22.6 mole percent, respectively. Garnet rim and core compositions are near the value Alm_{56} Prp_7 $Gross_{35}$ $Spess_2$ and Alm_{44} Prp_3 $Gross_{30}$ $Spess_{23}$.

Selected garnet grain in eclogite sample 95-70/4 exhibit complicated chemical zoning pattern. Detailed micropyrobe analyses indicate that these zonations are nearly symmetrical. Figure 5.24 shows that both the direction and magnitude of the concentration gradients of Ca, Mg, Fe, Mn and Al cations change from core to rim

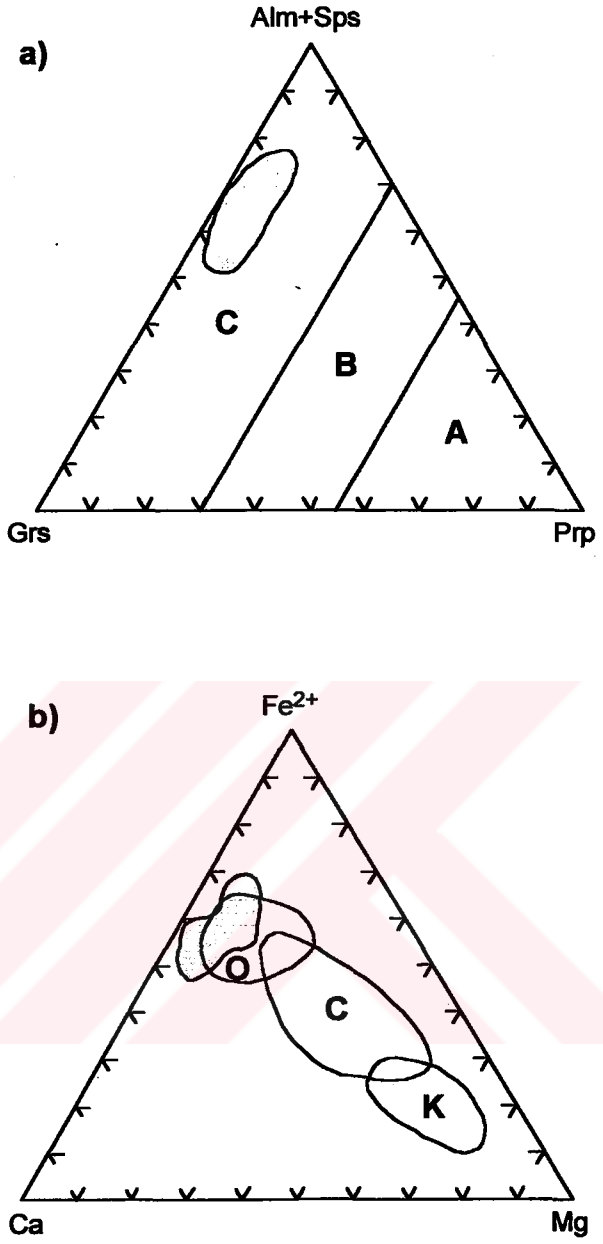


Figure 5.22 a) Garnet compositions plotted after Coleman et al. (1965). Garnet end-members are formed by almandine+spessartine (Alm+Sps), grossular (Grs) and pyrope (Prp). A, B and C fields represent compositions of garnets in eclogites associated with kimberlites and peridotites (A), with gneisses (B)and with blueschists (C). **b)** garnet composition compared to eclogite type (Smulikowski, 1972). K= nodular xenoliths in kimberlite; C= 'common' eclogites (from high-grade gneisses and migmatites); O= 'ophiolitic' or 'alpine-type' eclogites (from HP/LT terranes). Shaded fields represent all garnet analyses of eclogites from the Metaolistostrome unit.

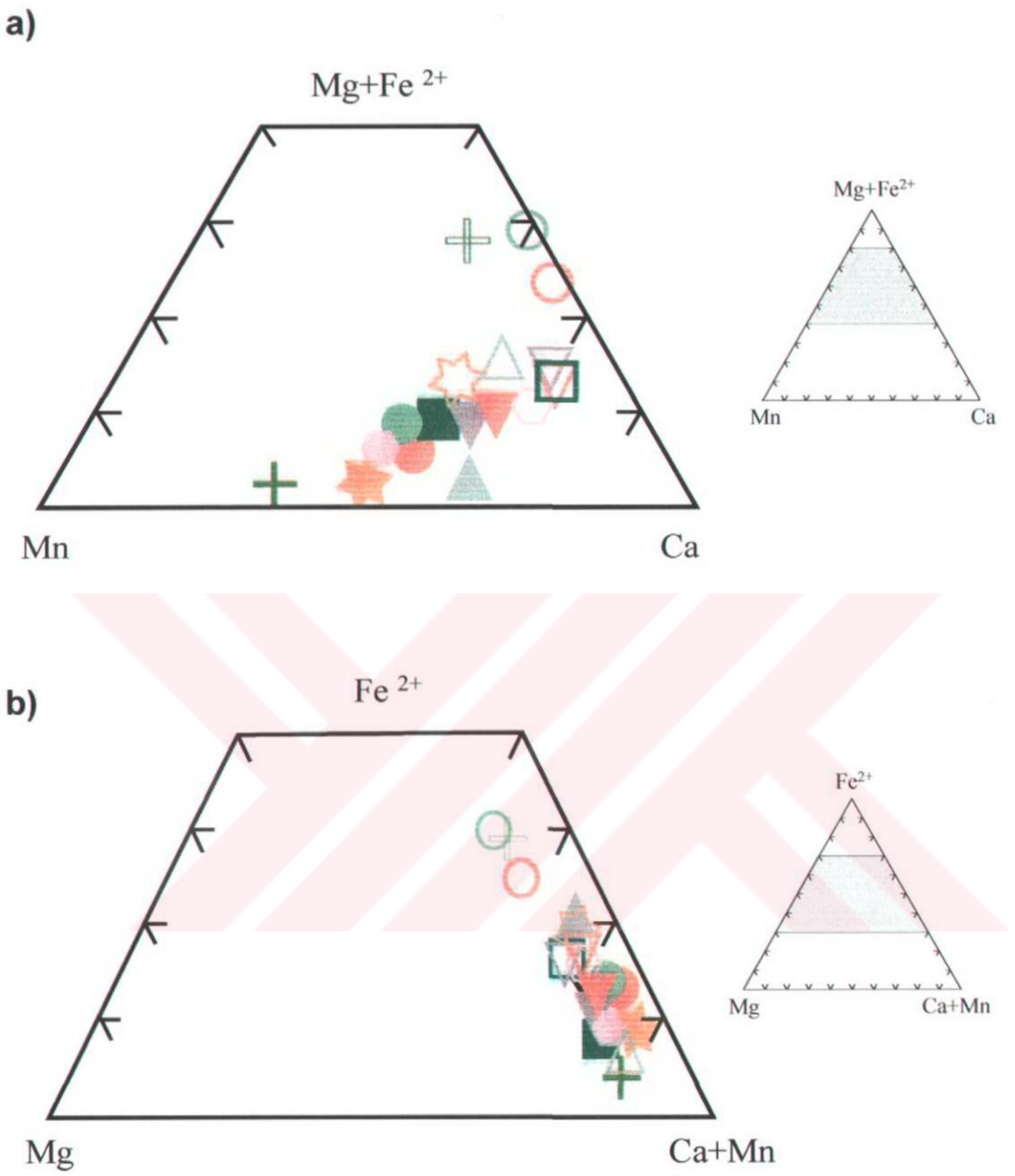


Figure 5.23 Ternary atomic proportions of Alm+Prp-Sps-Grs (a) and Alm-Prp-Grs+Sps (b) for garnets from eclogite blocks in the Metaolistostrome.

(Figure 5.24 and Table 5.8). Si and Al show no zoning since there are no major substitutions at their sites. Minor irregularities in the zoning profiles generally occur in the proximity of inclusions (Figure 5.24b-d). Ca, Mg, Fe and Mn exhibit typically zoning pattern in different magnitude from core to rim. In the core, X_{Alm} (= Fe^{2+}/ (Fe^{2+}+Ca+Mg+Mn)) content is about 44 mol %. Whereas, X_{Prp} (= Mg / (Fe^{2+}+Ca+Mg+Mn)) content is at about 2 mol %. Around the inner rim, X_{Alm} reaches up to maximum value of 56 mol % and X_{Prp} increases greatly from about 5 at the inner rim to 7.2 mol % at the outer rim (Figure 5.24b-c-d)). In the interval between inner and outer rim, X_{Alm} displays generally decrease trend. X_{Grs} (= Ca / (Fe^{2+}+Ca+Mg+Mn)) shows slight zoning pattern, with a flat core (about 30 mol %) and a gradual increasing up to 35 mol % at the outer rim (Figure 5.24b-c-d). Whereas, X_{Sps} (= Mn / (Fe^{2+}+Ca+Mg+Mn)) exhibits a typical bell-shaped zoning pattern. X_{Sps} content is at about 22 mol % in the core and decreases gradually to 4 mol % in the inner rim and to 1.4 mol % at the outer rim (Figure 5.24b-c-d). The bell-shaped zoning profiles are regarded to result from the increasing stabilization of Fe and Mg in the garnet structure with rising temperature and represent decrease of the average Mn content of garnet with increasing temperature (Müller and Schneider 1971). With increasing metamorphic grade and garnet diameter, the Mn profiles have lower maxima and broader shapes (Edmunds and Atherton 1971; Kretz 1973). In the core portion, the decrease of the X_{Sps} content is compensated by an increase in X_{Alm} and X_{Prp} (Figure 5.24c). Garnet compositions change at the inner rim. Both X_{Alm} and X_{Sps} contents decrease from inner to outer rim. On the other hand the Fe^{2+}/($Mg+Fe^{2+}$) ratio for garnet shows a regular decrease from 0.95 in the core to 0.92 in the inner and to 0.89 in the outer rim.

The zoning pattern of this garnet can be summarized as follows: i) a rimwards increase in X_{Prp} content and decrease of Fe^{2+}/($Mg+Fe^{2+}$) ratios, ii) essentially uniform X_{Grs} contents in the core, which show marked increase at the rim (300 μm or less), and iii) decrease in X_{Sps} content from core to outerrim (Figure 5.24b-c). According to mol % fraction pattern of end-member, garnet may be divided into two stages as a prograde (eclogite episode) stage (compression) and retrograde stage (decompression). In the prograde stage, the rimward (inner rim) increase in X_{Prp}, and

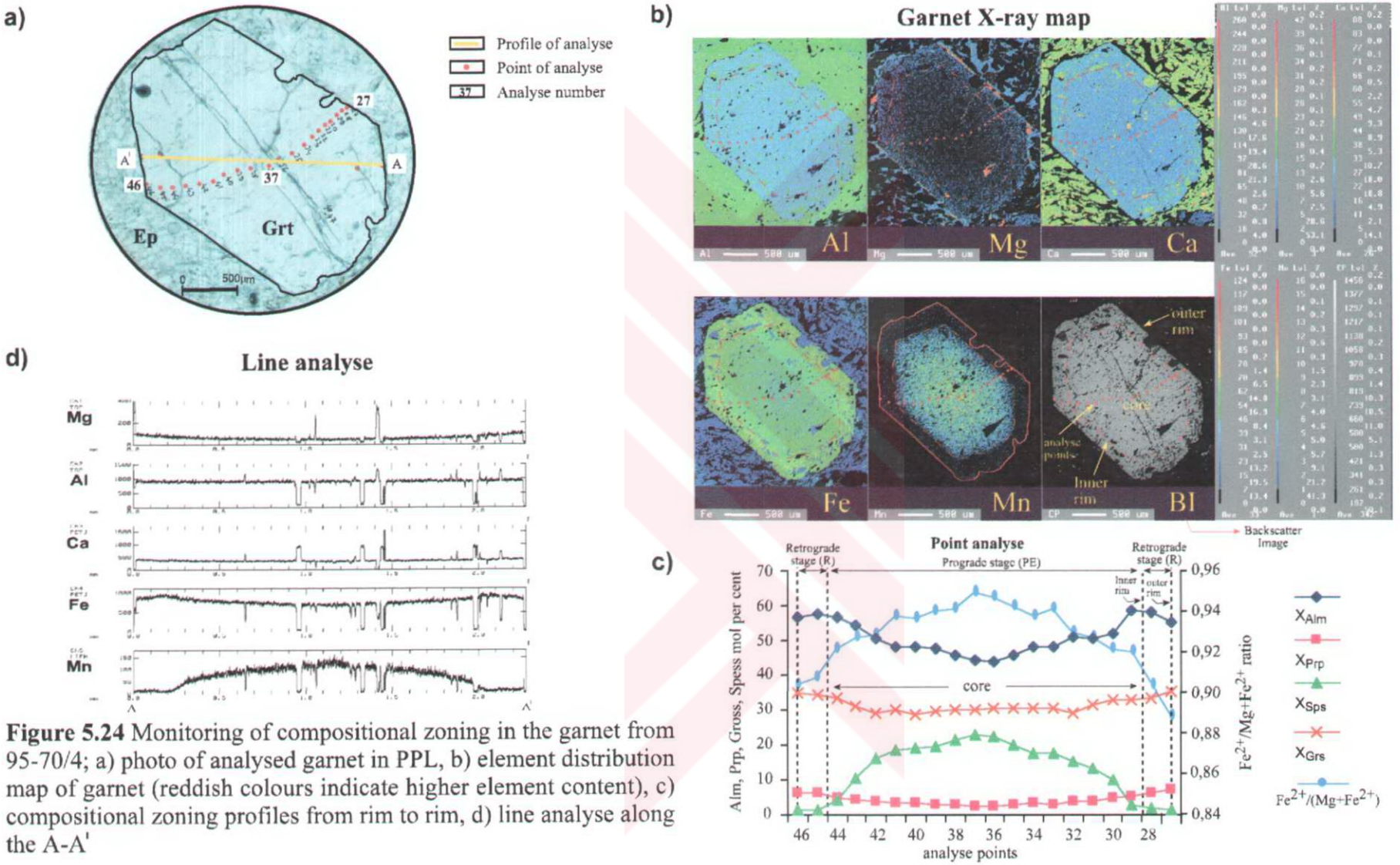


Figure 5.24 Monitoring of compositional zoning in the garnet from 95-70/4; a) photo of analysed garnet in PPL, b) element distribution map of garnet (reddish colours indicate higher element content), c) compositional zoning profiles from rim to rim, d) line analyse along the A-A'

decrease X_{Sps} and $Fe^{2+}/(Mg+Fe^{2+})$ ratios suggest the growth of garnet during the increasing temperature and compression (Möller, 1998). Garnets have at least two stages of growth as a prograde and retrograde. The retrograde stage is observed between the inner and outer rim in garnet (Figure 5.24c). Retrograde garnet growth is represented by abundant epidote inclusions between inner and outer rim, preserved well-defined idiomorphic growth faces of garnet and retrograde stage end-member mol % fraction patterns (Figure 5.24b-c-d). Optical zoning remarks are not observed in this garnet.

Sample two: Cation totals per formula unit of garnet which are chosen in **M97-34/2** range from 16.055 to 16.118, somewhat higher than the ideal value of 16.00. The ranges of the main cations can be given as follow: Si (5.943 – 6.013), octahedrally coordinated aluminium (3.781 –3.889), Ti (0.007 – 0.026) and Na (0.0 – 0.03), Al(VI) averages 3.823, and the amount of ferric iron (0.151 - 0.318). Andradite content of the garnet is very low and ranges from 0.956 to 2.097 mol %. Therefore, compositional variations of this garnet may be shown in quaternary solid solution system composed of almandine, pyrope, grossular and spessartine. In Figure 5.23, the Fe(2+)/Mg/Ca/Mn values for a single garnet crystal are shown; this illustration basically represents the proportions of atoms occupying the large eightfold coordinated site in garnet. As shown by Figure 5.23, analysed garnet which belongs to pyralspite series is rich-in almandine. The average core and rim compositions of this garnet are "Alm_{35} Prp_8 Grs_{18} Sps_{39}" and "Alm_{61} Prp_7 Grs_{24} Sps_8", respectively. The chemical zonation measured in garnet is from a manganese-rich core to an iron + magnesium-rich rim (Figure 5.25b-c-d).

The garnet profile is shown in Figure 5.25c. X_{Sps} content of garnet from M97-34/2 shows typical bell-shaped zoning profile, which is characterized by the decrease in Mn content from core to rim (Figure 5.25b-c-d). In the central part of the core, X_{Sps} exhibits almost flat pattern and drastically decreases towards the rim. Similar to X_{Sps} in the central part of the core, X_{Alm} represents relatively flat profile and abruptly increases towards the inner rim. But before arriving to the rim, X_{Alm} pattern becomes smooth and than upturns in the rim (Figure 5.25c). X_{Grs} increases gradually

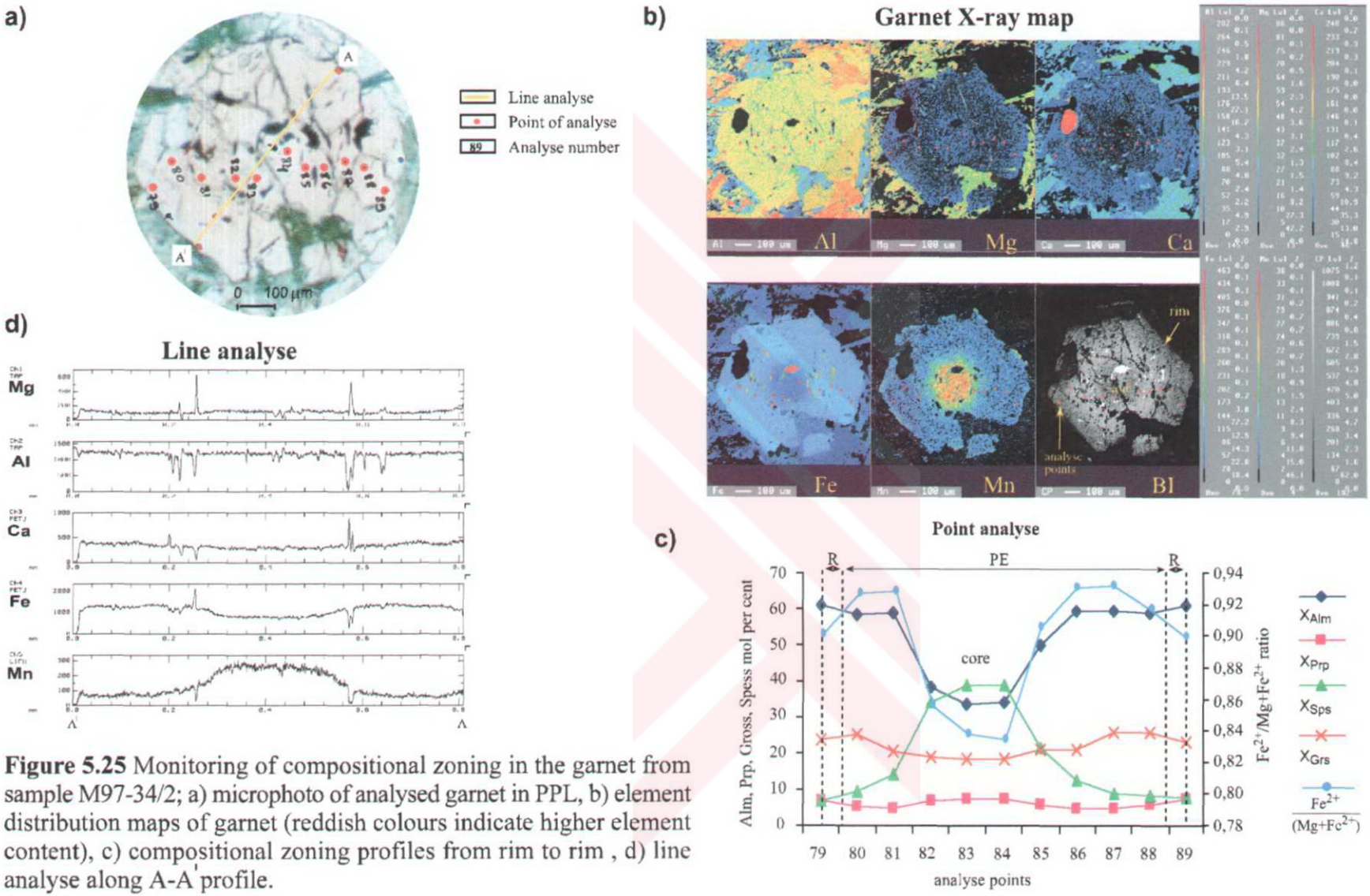


Figure 5.25 Monitoring of compositional zoning in the garnet from sample M97-34/2; a) microphoto of analysed garnet in PPL, b) element distribution maps of garnet (reddish colours indicate higher element content), c) compositional zoning profiles from rim to rim , d) line analyse along A-A' profile.

outwards and reaches a maximum at an intermediate position between core and rim (Figure 5.25c-d). The decrease and increase in X_{Grs} content is compensated by X_{Prp} and X_{Sps}. $Fe^{2+}/(Mg+Fe^{2+})$ ratios show a pattern similar to X_{Alm}, except for rim, from core (0.83), through (0.93) to 0.90 at the rim (Figure 5.25c). X_{Prp} slightly decreases outwards and than reaches a minimum at the intermediate position between core and rim.

The garnet has got two growth stages composed of eclogite stage (RE) and retrograde stage (R). This chemically zoning can be also observed under the microscope (Figure 5.25a). Textural zonation belonging to growth stages may be investigated in two parts such pink coloured section with abundance ilmenite (FeTiO3) inclusions at about three-fourths of the distance from core to rim and pale pink coloured with free ilmenite inclusions rim section having approximately 80 – 100 μm wide from rim to core (Figure 5.25b). Ilmenite inclusion part of garnet was growth during the eclogite stage. In the second growth stage, garnet growing had continued without interrupting to higher temperature conditions. Garnet growing in second stage may have stopped for a while and after that diffusion had started due to effect of high temperature. Diffusion effect is characterized by the flat of X_{Alm}, X_{Sps} and X_{Prp} patterns from mantle to rim. The degree of modification of garnet profiles during the post eclogite stage is restricted to 200 μm interval from outer rim towards core.

Sample three: Three garnet grains were chosen from sample SE-1; 1-19 (Figure 5.26), 35-50 (Figure 5.27) and 145-154 (Figure 5.28) which the numbers represent analyse numbers range for each garnet crystal (Table 5.8). The individual chemical characteristics of these garnets are given below.

- In the garnet **(1-19)** from sample **SE-1**, totals of cation for per formula unit range from 16.036 to 16.098, somewhat higher from the ideal stoichiometric value of 16.00. Minor amounts of aluminium are assigned to tetrahedral sites, averaging 0.044 based on one formula unit. The average value of Al(VI) for per 24 oxygens is 3.873 p.f.u. (Table 5.8). The ferric iron which ranges from 0.113 to 0.213 is of negligible

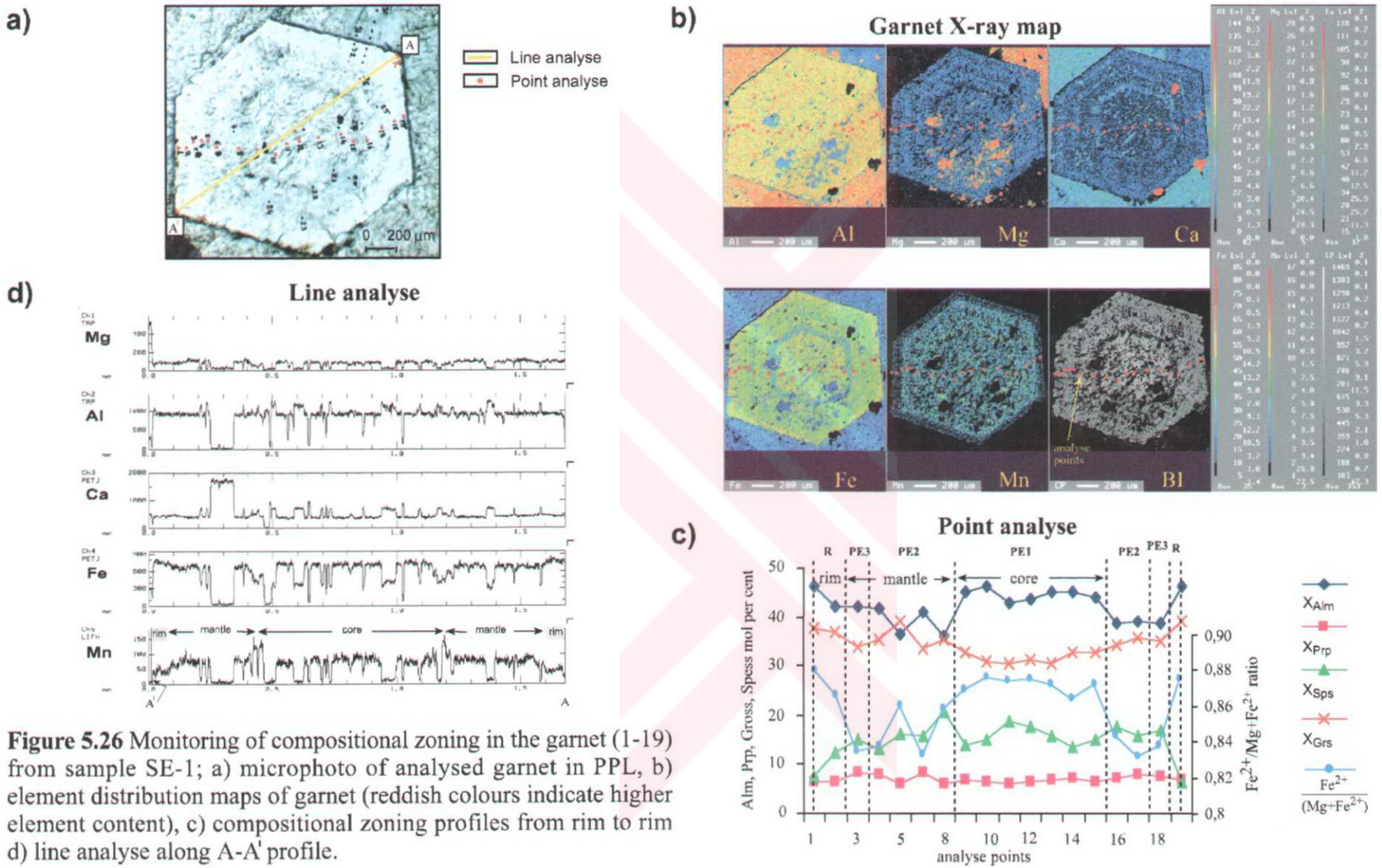


Figure 5.26 Monitoring of compositional zoning in the garnet (1-19) from sample SE-1; a) microphoto of analysed garnet in PPL, b) element distribution maps of garnet (reddish colours indicate higher element content), c) compositional zoning profiles from rim to rim d) line analyse along A-A' profile.

amount. Andradite content of garnet ranges from 0.991 to 2.354 mol %. The proportions of Ca, Fe(2+), Mg and Mn for this garnet are illustrated in Figure 5.23. Garnet which is composed of average 64 percent pyralspite and 36 percent ugrandite series is rich-in almandine (average 42 mol %) and grossular (average 34 mol %) (Figure 5.23). Core and rim composition of the garnet is "Alm_{44} Prp_6 Grs_{32} Sps_{18}" and "Alm_{48} Prp_6 Grs_{38} Sps_8", respectively.

The chemical analyses of this garnet are given in Table 5.8. On the other hand, the compositional maps of five elements (Al, Mg, Ca, Fe and Mn) and the profiles (point and line) are depicted in Figure 5.26b and Figure 5.26c-d, respectively. This garnet crystal displays very complex chemical zoning (Figure 5.26). Successor growing zones can be also easily recognized under microscope (Figure 5.26a). Garnet is made up of mainly resorbed core (PE1), partial resorbed mantle (PE2 and PE3) and rim (R). The discontinuous nature of the zonation patterns in this garnet can be interpreted to have been resisted from the resorbtion during the polyphase growing history. The core is characterized by the numerous inclusions of epidotes and omphacite. Epidotites are observed in light blue colour in Ca-map of garnet while omphacites have red colour in Mg-map of garnet (Figure 5.26b). Internal fabric defined by epidote inclusions does not pass from core to mantle. In addition, border between core and mantle is not smooth and edges of core are composed of epidote and omphacite inclusions (Figure 5.26a-b). Zoning profiles of point analyses is given in Figure 5.26c. According to this graphic, X_{Alm} is rich in core and shows almost flat profile. This profile drastically decreases close to core – mantle border (Figure 5.26c-d). X_{Grs} displays regular bowl-shape profile in core of the garnet. Whereas X_{Sps} display a bell-shaped profile in the middle of the core, but it starts to increase again near to core-mantle border (Figure 5.26c-d). $Fe^{2+}/(Mg+Fe^{2+})$ ratio is higher in core than that of mantle. X_{Prp} shows flat profile in core. On the core-mantle border, increase of X_{Sps} and X_{Grs} and decreases of X_{Alm} may represent resorbtion of garnet. Free Mn ions that formed from decomposing garnet during resorbtion diffuse into the garnet (Bethune et al., 1975), creating an enrichment in Mn on the core-mantle border. Releasing some Mn from garnet could not be taken up by any other mineral phase. The increasing of Mn is compensated by a decrease dominantly in Fe and

slightly Mg contents (Figure 5.26b-c-d). Thus, releasing of Mn due to dissolution of garnet had to re-enter into the garnet, diffusing through the structure along a front advancing inwards from the receding border of the corroding garnet (Bethune et al., 1975). Development of Mn-enriched rims during corrosion of garnet requires at least limited diffusion (Bethune et al., 1975; Loomis 1975). Ca is the slowest cation of the R(2+) site to diffuse into garnet, because the garnet crystal was able to preserve the original grossular growth zoning which is, on the contrary, developed some other eclogite samples during resorbtion. Diffusion of cations in garnet may take place in all temperatures, especially at low temperatures, diffusion rates and diffusion distances may not be detected (Dodson 1976). Petrakakis (1986) emphasizes the varying degrees of diffusion of the R(2+) cations in garnets, with an increasing order of Ca, Mn, Fe, Mg; which is connected by the decreasing ionic radius. This order is in consistent with the zoning profiles given in Figure 5.26c.

Two growths zoning in mantle can be optically recognized in mantle of garnet. The mantle is represented by presence of epidote and omphacite inclusions. Inclusions are mostly dominated along growth zoning and mantle / rim boundaries (Figure 5.26a-b). Inclusion density in garnet gradually decreases from core to rim. The fact that the garnet core is clouded by the numerous inclusions can be interpreted that this part of the garnet, probably, grew faster than that of mantle. In mantle part of garnet, X_{Alm} profile is nearly flat (Figure 5.26c). X_{Prp} display peak values in mantle. Omphacite inclusions which have maximum jadeite content (Jd= 30 mol%) occur in mantle. This part probably reflects peak pressure conditions. X_{Grs} shows fluctuated pattern in mantle. Deviations from general departure in X_{Grs} pattern related with epidote inclusions. In mantle part of garnet, these nearly flat profiles can not be explained homogenisation during greenschist – epidote/amphibolite facies metamorphism. Mn content is preferentially enriched along growth zoning in mantle and mantle/rim boundaries. Flat profiles that suggest growth over a limited range of pressure and temperature can also be originated by fast growing. This type zoning can be clarified with successor fast growing and partial or minor resorbtion. Diffusional effects of retrograde metamorphism modified the growth profiles at the

rim (Figure 5.26c). Diffusion of R(2+) cations have apparently been effective about 60 – 25 microns in rim, representing the re-equilibration of rim with the matrix.

- Cation totals per formula unit range from 16.027 to 16.089 in selected garnet grain_**(35-50)** from sample **SE-1**. These values are close to the ideal stoichiometric value of 16.00. Minor amounts of aluminium are assigned to tetrahedral sites, averaging 0.023 based on one formula unit. Al(VI) averages 3.873 per 24 oxygens, the amount of ferric iron ranges from 0.105 to 0.231. (Table 5.8). The ferric iron is of negligible amount. The proportions of Ca, Fe(2+), Mg and Mn for this garnet are illustrated in Figure 5.23. Garnet which is composed of average 65 percent pyralspite and 35 percent ugrandite series is rich in almandine (average 43 mol %) and grossular (average 33 mol %) (Figure 20/2). Core and rim compositions of the garnet are "Alm_{42} Prp_6 Grs_{28} Sps_{24} "and "Alm_{47} Prp_6 Grs_{37} Sps_{10} ", respectively (Figure 5.23).

Compositional maps and profiles of selected five elements in garnet are given in Figure 5.27. Zoning profile of this grain in Figure 5.27 may be divided in to three parts; resorbed core (PE1), mantle (PE2-PE3) and rim (R) (Figure 5.27c). Growth zones are situated one in core and two in mantle. Each zone of them can be called as overgrowth (Figure 5.27a-b). The repeated resorbtion processes can be recognised in all boundaries among zones with different degrees. X_{Alm}, X_{Sps} and X_{Grs} display almost flat profile in core (Figure 5.27c-d). The reason of that cutting line of garnet grain in thin section may be passed along resorbed rim of the garnet core or garnet core was growth very fast. The core contains omphacite (Jd=35.49 mol %) and many epidote inclusions. The boundary between core and mantle is designated by epidote inclusions. Due to epidote inclusions, this boundary has been obscured. X_{Alm} and X_{Grs} momentarily increase from core to mantle. Increasing in X_{Prp} is not too pronounce. X_{Prp} gradually increases and reaches to 7.68 mol % in the mantle and than decrease to 6.61 mol % at the rim, while average 5.65 mol % in the core. (Figure 5.27c). X_{Sps} showing plateau structure in core steeply decreases in beginning of mantle. X_{Sps} increases again at mantle-rim boundary. Corroded growth zones in mantle are designated by epidote inclusions. In mantle part of garnet, X_{Alm} displays

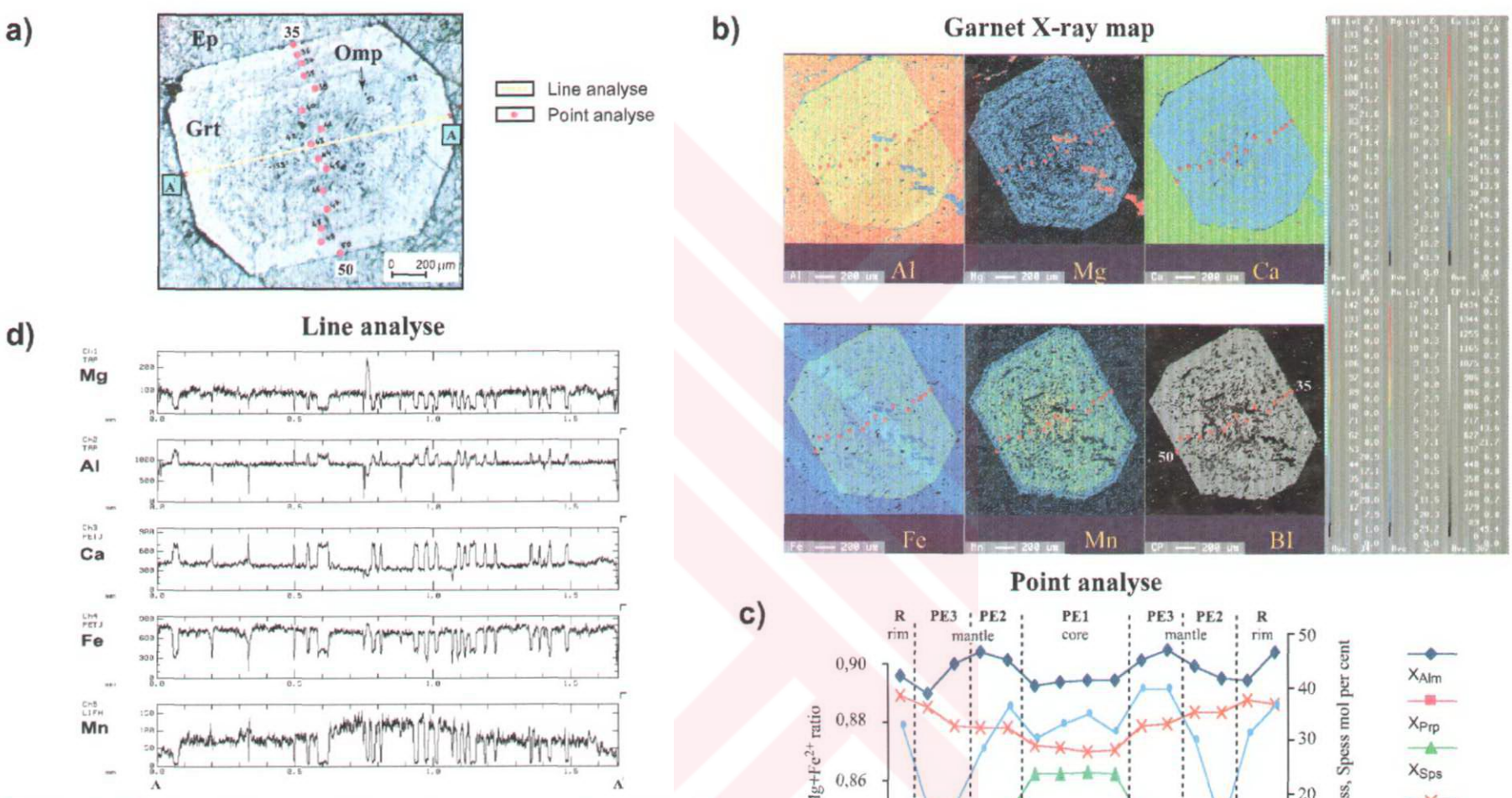


Figure 5.27 Monitoring of compositional zoning in the garnet (35-50) from sample SE-1; a) microphoto of analysed garnet in PPL, b) element distribution maps of garnet (reddish colours indicate higher element content), c) compositional zoning profiles from rim to rim d) line analyse along A-A' profile .

bell-shaped pattern. $Fe^{2+}/(Fe^{2+}+Mg)$ ratio decreases towards core-mantle boundary in the core and than displays importantly increase in the beginning of mantle. $Fe^{2+}/(Fe^{2+}+Mg)$ ratio decreases again and reaches to its lowest ratio at mantle – rim boundary. Retrograde diffusional zoning is detected at the rim. The reversal of X_{Alm}, X_{Prp}, X_{Sps}, X_{Grs} and $Fe^{2+}/(Fe^{2+}+Mg)$ zoning trends can be seen in the rims of garnet (20-30 microns from rim to core). All patterns in the rims have been resulted from variable degrees of diffusional modification of pre-existing growth zoning pattern. The outermost garnet rims in contact with epidote and clinopyroxene (omphacite) show increasing $Fe^{2+}/(Fe^{2+}+Mg)$ ratios, suggesting resetting by Fe-Mg diffusion (minor in Mg) and/or net-transfer reactions during cooling.

- Cation totals per formula unit of garnet **(145-154)** which are chosen in **SE-1** range from 16.022 to 16.084, somewhat higher than the ideal value of 16.00. Si (5.956 – 6.028) per formula unit of octahedrally coordinated aluminium (3.829 – 3.911), Ti (0.005 – 0.022) and Cr (0.00 – 0.008) atoms per garnet formula unit are observed in these ranges. Al(VI) averages 3.874 per 24 oxygens, the amount of ferric iron ranges from 0.092 to 0.216. Andradite content of the garnet ranges from 1.101 to 2.190 mol %. Therefore, compositional variations of this garnet can be shown in quaternary solid solution system that is composed of almandine (Fe^{2+}), pyrope (Mg), grossular (Ca) and spessartine (Mn). The proportions of Ca, Fe^{2+}, Mg and Mn for this garnet are illustrated in Figure 20/2. Garnet composed of average 63 percent pyralspite and 37 percent ugrandite series is rich-in almandine (average 43 mol %) and grossular (average 36 mol %) (Figure 5.23). Core and rim compositions of the garnet are "Alm_{43} Prp_7 Grs_{36} Sps_{14} " and "Alm_{48} Prp_6 Grs_{39} Sps_7 ", respectively (Figure 5.23).

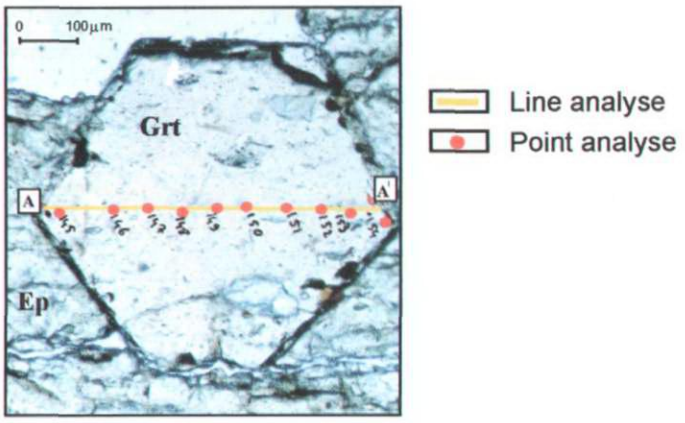
Analysed garnet grain, which has 623 microns in diameter, is euhedral in-shape and does not display optical zonation (Figure 5.28a). However, point and line analyses clearly reveal that this garnet is chemically zoned (Figure 5.28b-c). Zonation can be divided into two sections; core and rim. The bowl-shape of X_{Sps} from core to rim core is not pronounced in Figure 5.28b, however it is possible to recognize the bowl-shape zoning profile in line analyse (Figure 5.28c).

$Fe^{2+}/(Fe^{2+}+Mg)$ ratio and X_{Grs} decrease towards core-rim boundary and than reaches to maximum values at the rims. X_{Alm} reveals flat profile in the core. However, reversal of X_{Alm} pattern is observed in the rim. X_{Prp} value is 6.39 mol % in the core. This value reaches to 8.52 mol % at core – rim boundary. Minimum value of X_{Prp} in the rims is 5.61 mol % (Figure 5.28b). Garnet grain (145-154) is relatively small when compared to garnet grain 1-19 (Figure 5.26) and 35-50 (Figure 5.27) in SE1. In addition, garnet core pattern which is observed in 1-19 and 35-50 is not present in the core of garnet grain (145-154). The mantle pattern of garnet grain 1-19 and 35-50 is situated in the core of this garnet (145-154). The rim is characterized by tiny and rare epidote inclusions. Orientations of these inclusions are parallel to the schistosity of matrix. Increasing of X_{Alm}, X_{Grs} and $Fe^{2+}/(Fe^{2+}+Mg)$ ratios and decrease of X_{Sps} are observed in the rim. These patterns are probably related with cooling stage. Original pattern is modified by retrograde diffusion. In Figure 5.28b, analyse point of number 153 is near to epidote inclusion. Therefore, this analyse causes deviation from symmetrical zonation patterns.

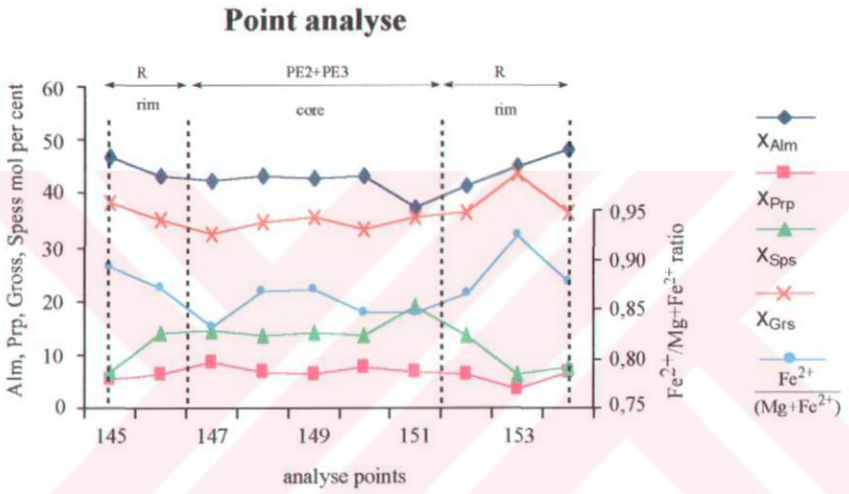
Sample four: Cation sums of this garnet **(M98-45C)** range between 15.973 and 16.030, very close to the stoichiometric value of 16.00. Minor amounts of aliminum are assigned to tetrahedral sites, with an average value of 0.004 based on one formula unit. Al(VI) averages 3.933 per 24 oxygens. The amount of ferric iron ranges from 0.000 to 0.065 (Table 5.8) and is of negligible amount. Andradite content of garnet ranges from 0.109 to 0.638 mol %. Hence compositional variation of this garnet can be shown adequately in terms of the Ca (grossular), Fe (almandine), Mg (pyrope) and Mn (spessartine) proportions. In Figure 5.23, the Fe^{2+}/Mg/Ca/Mn ratios for a single garnet crystal in M98-45C are illustrated. This Figure displays proportion of atoms occupying the large eightfold coordinated site in garnet. This garnet is rich-in almandine (average 52 mol%) and grossular (average 29 mol%). Core and rim compositions of the garnet are "Alm_{44} Prp_4 Grs_{29} Sps_{23} " and "Alm_{60} Prp_8 Grs_{30} Sps_2 ", respectively (Figure 5.23).

Zoning patterns from core to rim of selected garnet grain in M98-45C are given in Figure 5.29. X_{Alm} and X_{Prp} display a regular increasing from core through mantle to

a)



b)



c)

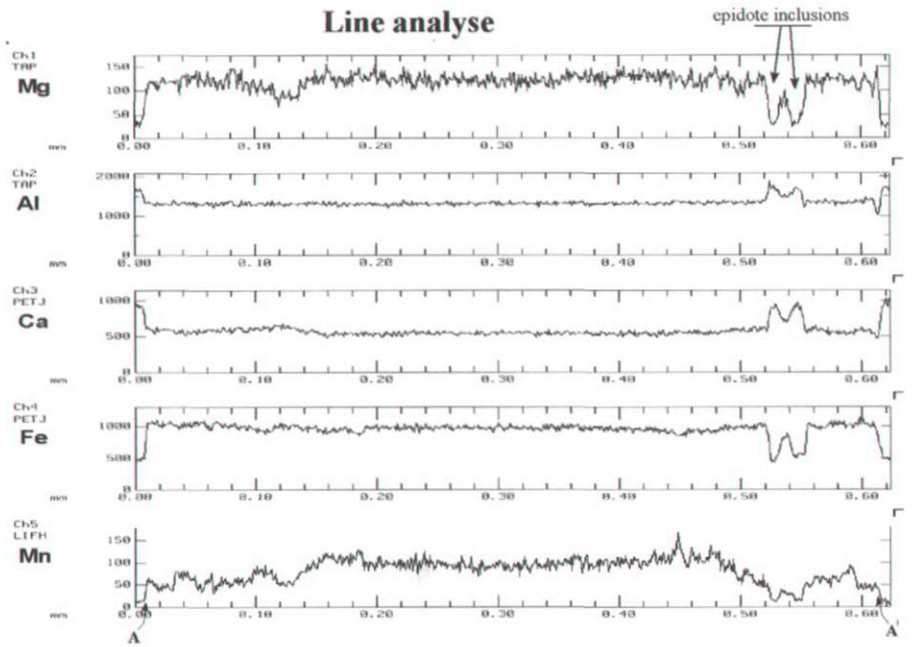


Figure 5.28 Compositional zoning in the garnet (145-154) from sample SE-1; a) microphoto of analysed garnet in PPL, b) element zoning profiles from rim to rim , c) A-A' line analyse from rim to rim.

rim. The regular increase in X_{Prp} contents may reflect garnet growth during increasing temperature conditions. X_{Alm} also shows flat profile across about 50-60 microns from outermost rim. X_{Sps} has got typical bell-shaped profile (Figure 5.29). $Fe^{2+}/(Fe^{2+}+Mg)$ ratio displaying bowl-shape pattern in core and X_{Sps} decrease towards the rim. X_{Alm} profile is almost the reverse of that for X_{Sps}. X_{Grs} shows an homogeneous distribution with a flat profile from core to rim (Figure 5.29). Ca content is not sensitive to variations in abundance of other divalent cations in garnet (Crawford 1974, de Bethune et al. 1975, Linthout and Westra 1968). The rimward decrease of X_{Sps} and $Fe^{2+}/(Fe^{2+}+Mg)$, and the increasing of X_{Alm} and X_{Prp}, favour the typical growth zoning character of garnet (Spear, 1989, 1993). Although, X_{Grs} profile of this garnet is in conflict with general garnet growth trend.

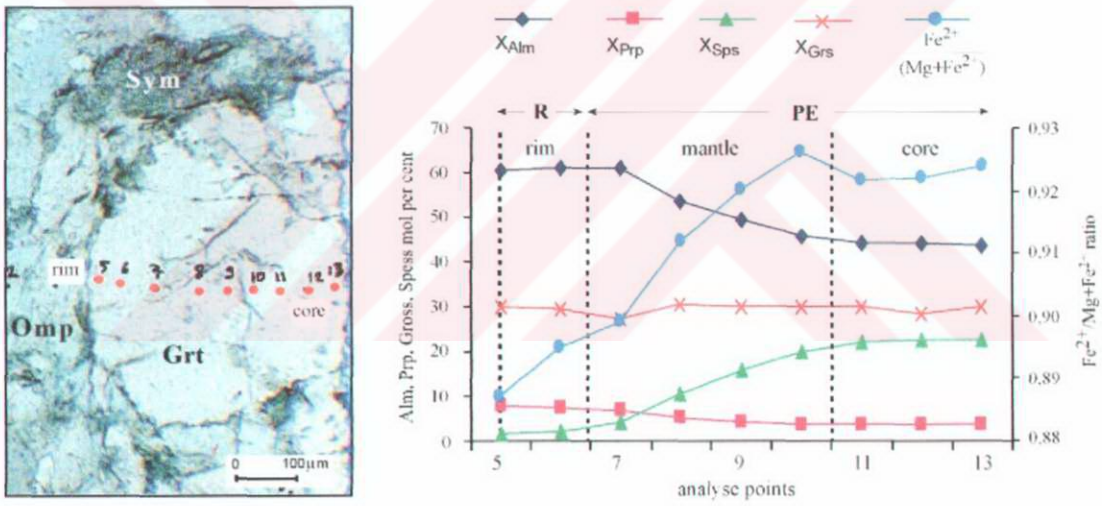


Figure 5.29 Photomicrograph in plane polarized light and composition of this garnet in M98-45C. Traverse is from rim to core.

Garnet grain can be divided into three parts; core, mantle and rim. Prograde garnet growth zoning is recognized along the core and mantle sections (Figure 5.29). Garnet growth zoning was re-constructed in the rim by retrograde diffusional effects with increasing temperature. In the rim rim, flat profile up to 50-60 microns wide of X_{Alm}, slight increase in X_{Grs} and less steep of $Fe^{2+}/(Fe^{2+}+Mg)$ profile represent increasing of temperature during retrograde metamorphism (Figure 5.29).

Sample five: Cation totals per formula unit of garnet (**M96-31**) range from 15.990 to 16.028, close to the ideal value of 16.00. Si (5.962 – 5.998), octahedrally coordinated aluminium (3.920 –3.945), Ti (0.013 – 0.033) and Cr (0.001 – 0.014) atoms per garnet formula unit are observed in these ranges (Table 5.8). Al(VI) averages 3.936 per 24 oxygens. The amount of ferric iron ranges from 0.032 to 0.068. Andradite content of the garnet ranges from 0.321 to 0.763 mol %. Andradite content of the garnet is in negligible amount. The proportion of Ca, Fe^{2+}, Mg and Mn for this garnet is illustrated in Figure 5.23. Garnet which is composed of average 70 percent pyralspite and 30 percent ugrandite series is rich in almandine (average 42 mol %) and grossular (average 30 mol %) (Figure 20/2). Core and rim composition of the garnet are "Alm_{40} Prp_3 Grs_{29} Sps_{29} " and "Alm_{49} Prp_4 Grs_{32} Sps_{15} ", respectively (Figure 5.23).

The chemical analyses of the garnet (**M96-31**) are given in Table 5.8 and are depicted in Figure 5.30. Core of unhedral garnet grain is compositionally homogeneous with almost completely flat profiles (Figure 5.30b-c). Whereas, in the outer zone of 160 microns in wide, the pattern of end-members display converse relationship. X_{Grs} increases slightly towards the rim, a prominent decrease of $Fe^{2+}/(Fe^{2+}+ Mg)$ ratios and X_{Sps} contents are observed in the rim. Element profiles described above characterize a slight growth zoning which is probably generated during high-pressure / low-temperature metamorphism. Epidotes that are in equilibrium with omphacite in matrix are observed in garnet as inclusions. Dimensions of analysed garnet are 900x600 microns and may be regarded as a small garnet (<1mm in diameter) (Figure 5.30a). Fractionation of Mn in small garnets nucleated at lower temperatures is stronger (Anderson and Olimpio, 1977). In addition, concentration of Mn at the core of the small garnets is higher than the bigger garnets (Figure 5.31) (Anderson and Olimpio, 1977). The analysed garnet is relatively small in size and it might be expected to have high concentration of X_{Sps} at the core of the garnet. But this prediction does not match with X_{Sps} profile in Figure 5.30b-c. This can be interpreted that X_{Sps} and other element profiles were partially re-constructed by retrograde metamorphism. Diffusion is more effective in almandine garnets (Yardley, 1977). Garnet has an unhedral crystal shape and is

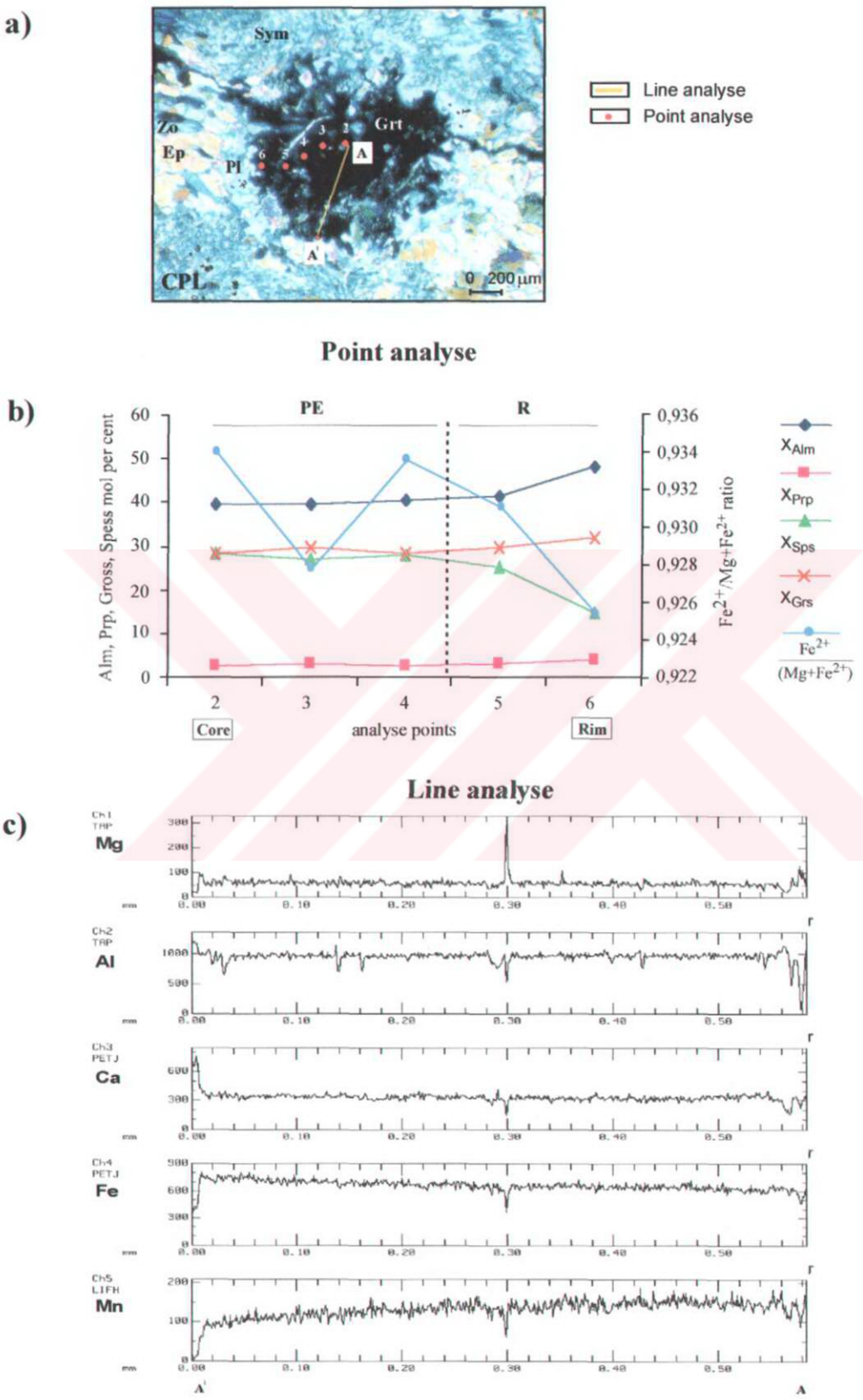


Figure 5.30 Monitoring of compositional zoning in the garnet (M96-31); a) Photomicrograph of analysed garnet (resorbed), b) compositional zoning profiles from core to rim , c) line analyse along A-A' profile.

resorbed along the rim (Figure 5.30a). Resorbtion is generally represented by Mn-rich rims (Bethune et al. 1975). X_{Sps} profile in Figure 5.30b-c does not indicate any enrichment in the rim. Released Mn ions by decomposition of garnet during corrosion must not have diffused into garnet to create enrichment in Mn rim. Because of the lack of chlorite in the matrix, free Mn ions are most probably trapped by the symplectitic clinopyroxene generated after omphacite. The average MnO % content of the large omphacite crystals is at about 0.147 while this value reaches up to 0.328 wt % in symplectitic clinopyroxene. Garnet is also rimmed by discontinuous plagioclase corona which is related to decompression of eclogite. As a result, it can be suggested that this garnet had formed during high-pressure / low-temperature metamorphism and than have been overprinted by medium-pressure / medium-high temperature metamorphism.

Sample six: Selected garnet grain (**1-24**) from sample **95-21/10** was examined. Numbers **1-24** represent analyse range of the garnet grain (Table 5.8). In garnet grain (**1-24**), cation totals per formula unit range from 16.004 to 16.094, which are close to the ideal stoichiometric value of 16.00. Si (5.924 – 5.988), octahedrally coordinated aluminium (3.792 –3.997), Ti (0.008 – 0.042) and Cr (0.000 – 0.012) atoms per garnet formula unit are observed in these ranges (Table 5.8). Al(VI) averages 3.907 per 24 oxygens. The amount of ferric iron ranges from 0.002 to 0.245. Andradite content of the garnet ranges from 0.220 to 2.548 mol %. Andradite content of the garnet is not so important. Therefore, compositional variations of this garnet may be shown in quaternary solid solution system composed of almandine, pyrope, grossular and spessartine. In Figure 5.23, the Fe^{2+}/Mg/Ca/Mn ratios for a single garnet crystal are presented. As shown by Figure 5.23, analysed garnet which belongs to pyralspite series is rich in almandine and core and rim composition are "Alm_{52} Prp_4 Grs_{11} Sps_{33} " and "Alm_{37} Prp_6 Grs_{20} Sps_{37} ", respectively.

Garnet grain and zoning profiles are shown in Figure 5.32. Garnet grain (**1-24**) selected from **95-21/10** can be divided into three sections (core, mantle and rim). The general growth zoning profile of the core and mantle can be given as follows: (a) an outward bell – shaped decrease in the X_{Sps} content; (b) slight increasing of X_{Alm}

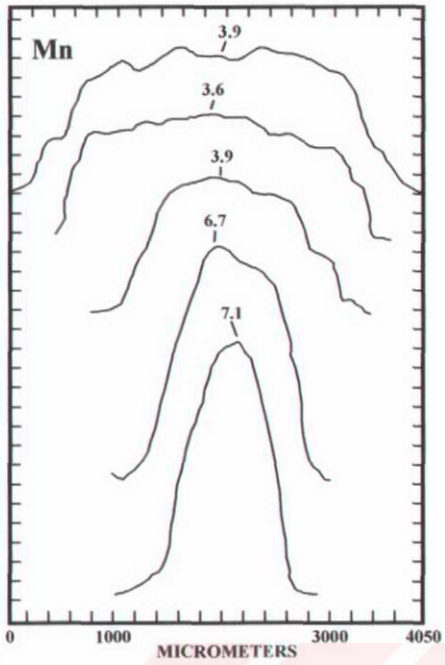


Figure 5.31 Mn profiles from set of garnets of increasing diameter. The contcentration of Mn (element wt. %) at the center of each garnet is shown on the profiles (Anderson and Olimpio, 1977).

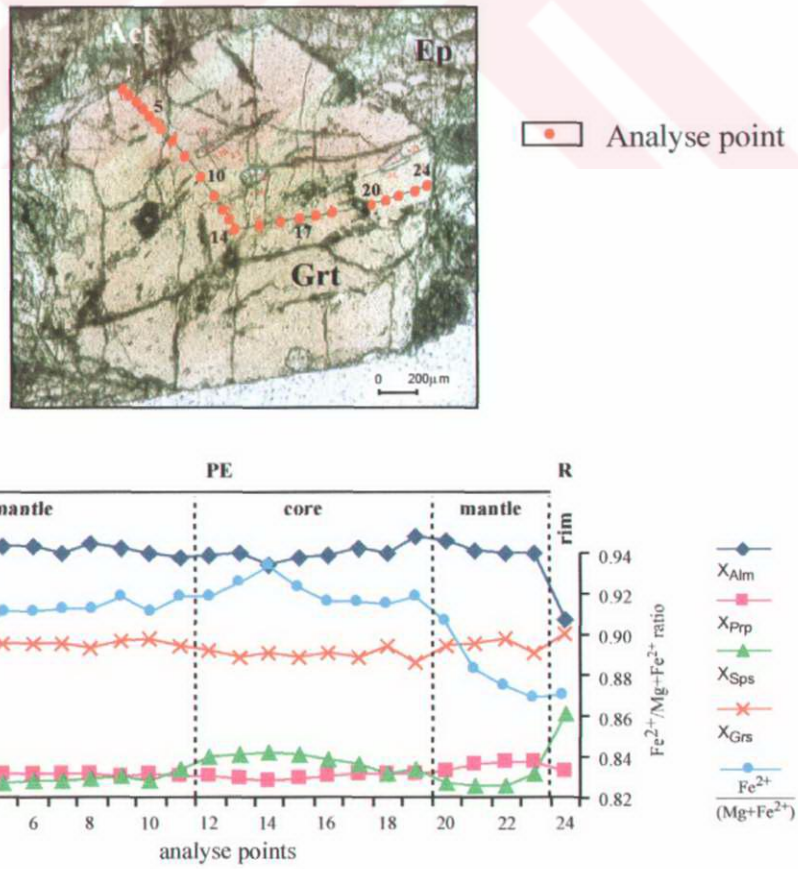


Figure 5.32 Photomicrograph in plane polarized light and element profiles of selected garnet grain (1-24) in 95-21/10. Traverse is from rim to rim.

towards mantle and than decreasing to rimward; (c) outward steadily increasing of X_{Prp}. X_{Grs} gradually increases from core to rim without being important deviations from general trend (Figure 5.32). The growth zoning between core and mantle is interpreted that this pattern is developed during prograde eclogite stage (PE). X_{Grs} hardly reflects diffusional affects. Therefore, retrograde zoning (R) in X_{Sps} and X_{Alm} profiles are more pronounced with respect to X_{Grs} in the rim. The outward (core to rim) increasing of X_{Grs} content represent the increasing of temperature. X_{Alm} profile in near parts to rim – mantle boundary display decreasing trend and than X_{Alm} rapidly decreases a few ten microns in the rim. This profile is probably related with high diffusion rate in almandine-rich garnets. Between analyse points of number 2 and 10, Fe^{2+}/Fe^{2+}+Mg ratio firstly stay constant and than rapidly decreases towards the rim. This decrease is caused by increase in X_{Prp} towards mantle-rim boundary (Figure 5.32). Rising of X_{Prp} profile close to mantle-rim boundary represents increase in temperature. Element profiles belonging to high-pressure metamorphism were re-constructed in the a few ten microns by diffusional retrograde zoning (R). X_{Sps}, X_{Alm}, X_{Prp} and X_{Grs} patterns of garnet in this part represent reversals pattern.

5.4.1.2. Garnets in blueschist metabasite blocks

Three garnets grain from two blueschist metabasite samples (M98-52/2 and 94-55/5) were examined. These samples contain partly reserved Na-amphiboles (crossite and glaucophane). Analyses belonging to garnet grains are given in Table 5.9. Cation proportions were calculated based on 24 oxygens. In blueschist metabasites, garnets display variation in Fe, Mn, Ca and Mg content. Garnet compositions show the following ranges: almandine 26-59 mol %, pyrope 2-9 mol%, grossular 16-23 mol%, spessartine 11-52 mol% and andradite 0,4-1,3 mol%. In the pyrope – (almandine + spessartine) – grossular ternary diagram, all garnets plot near to almandine + spessartine corner (Figure 5.33).

Sample one: Two garnet crystals (**5-15** and **35-45**) are examined from sample **M98-52/2**. The features belonging to these garnets are given below.

Cation totals per formula unit of garnet (**5-15**) in **M98-52/2** range from 16.015 to 16.053, somewhat higher than the ideal value of 16.00. Si (6.000 – 6.059), octahedrally coordinated aluminium (3.799 –3.893), Ti (0.005 – 0.029) and Cr (0.000 – 0.011) atoms per garnet formula unit are observed in these ranges (Table 5.9). Al(VI) averages 3.848 per 24 oxygens. The amount of ferric iron ranges from 0.103 to 0.170. Andradite content of the garnet ranges from 0.546 to 1.115 mol %. The proportions of Ca, Fe^{2+}, Mg and Mn for this garnet are illustrated in Figure 5.34. Garnet composed of average 78 percent pyralspite and 22 percent ugrandite series is rich in almandine (average 53 mol %) and grossular (average 21 mol %). Core and rim compositions of the garnet are "Alm_{45} Prp_5 Grs_{23} Sps_{27} " and "Alm_{55} Prp_9 Grs_{20} Sps_{14} ", respectively.

No chemical zoning of these garnets can be recognized in thin section (Figure 5.35a). In the core, X_{Sps} substitutes X_{Alm} and small amounts of X_{Prp}. The zoning profile of X_{Sps} (Figure 5.35b,c) represents a growth zonation. X_{Sps} content show a regular decrease from core to rim. At the left side of the graph (Figure 5.35b), X_{Sps} profile displays minor increase at the rim (Figure 5.35b,c). This is related to retrograde zoning. The general trend of X_{Grs} decreases from core to rim. But, X_{Grs} displays a slightly concave form in mantle. X_{Grs} is substituted partly by X_{Prp}, which regular increases from core to rim. In the mantle part of garnet, X_{Alm} shows a partly flat profile (the left side of the graph-Figure 5.35b) towards to rim. $Fe^{2+}/(Fe^{2+}+Mg)$ ratio is almost flat in the core (0,89) and variably drops through mantle to rim (0.84). The rimward decrease of X_{Grs}, X_{Sps} and $Fe^{2+}/(Fe^{2+}+Mg)$, and the increase of X_{Alm} and X_{Prp}, are typical characteristic of growth zoning (Spear, 1993). The same zoning profiles are observed in the garnets described above. Important reversals in element patterns are not detected in the uncorroded parts of the rim (Figure 5.35c). Diffusional retrograde zoning effects are not so strong and are restricted to 30-40 microns from rim to core. Garnet has been partly corroded along the rim by chlorite (Figure 5.35a). In general, in the corroded margins of garnet by secondary chlorite, thin Ca-Mn-rich margins have been described by de Bethune et al., (1975). They interpreted this as the result of garnet re-equilibration under lower temperatures than

Table 5.9 Representative garnet analyses from blueschist metabasites in Şirince and Çamlık (r: rim, c: core).

sample no	M98-52/2 (Şirince)																						94-55/5 (Çamlık)	
analyse no	m11-5r	m11-6	m11-7	m11-8	m11-9	m11-10c	m11-11	m11-12	m11-13	m11-14	m11-15r	m11-35r	m11-36	m11-37	m11-38	m11-39	m11-40c	m11-41	m11-42	m11-43	m11-44	m11-45r	m10-22r	m10-23
SiO2	38,02	38,07	37,96	38,02	37,85	38,11	38,08	37,93	38,20	38,07	38,27	38,17	37,92	37,86	37,94	38,03	37,82	37,98	37,97	38,23	38,05	38,09	37,81	37,98
TiO2	0,11	0,15	0,08	0,17	0,18	0,16	0,25	0,13	0,11	0,09	0,05	0,07	0,06	0,07	0,09	0,06	0,13	0,04	0,08	0,15	0,06	0,09	0,07	0,12
Al2O3	20,77	20,93	20,53	20,72	20,38	20,27	20,39	20,66	20,41	20,78	21,00	20,84	20,87	20,76	20,51	20,85	20,66	20,85	20,50	20,83	20,56	20,72	20,66	20,73
FeO	26,27	26,57	25,90	25,59	22,41	21,13	22,66	23,76	25,16	26,36	26,71	26,77	27,12	27,05	27,52	26,61	25,67	25,64	26,15	27,59	26,97	26,91	19,32	17,69
MnO	6,35	5,85	6,24	7,67	9,97	11,77	10,89	8,84	7,29	6,45	6,06	5,66	5,28	5,47	5,47	5,98	7,60	7,01	6,69	5,46	5,07	5,12	16,15	18,03
MgO	2,49	2,19	2,09	1,84	1,44	1,37	1,43	1,69	1,87	2,06	2,43	2,30	2,19	1,86	1,80	1,73	1,58	1,54	1,52	1,82	1,87	2,23	1,21	1,06
CaO	7,49	7,81	7,83	7,43	8,77	8,23	8,00	8,25	8,27	7,56	7,20	7,45	7,56	7,88	8,04	7,88	7,68	8,44	7,98	7,62	8,29	7,58	6,32	6,32
Na2O	0,01	0,01	0,05	0,00	0,06	0,04	0,09	0,03	0,07	0,07	0,02	0,00	0,05	0,02	0,00	0,04	0,05	0,05	0,05	0,00	0,00	0,00	0,00	0,01
K2O	0,00	0,01	0,00	0,00	0,03	0,02	0,00	0,00	0,01	0,01	0,02	0,00	0,01	0,02	0,00	0,02	0,01	0,02	0,03	0,01	0,00	0,00	0,00	0,00
Cr2O3	0,00	0,08	0,06	0,05	0,08	0,09	0,01	0,03	0,05	0,00	0,02	0,00	0,00	0,04	0,00	0,00	0,03	0,04	0,03	0,04	0,00	0,00	0,09	0,09
Total	101,51	101,66	100,74	101,49	101,18	101,19	101,80	101,32	101,44	101,44	101,77	101,26	101,06	101,03	101,37	101,20	101,23	101,60	101,00	101,75	100,87	100,74	101,63	102,03
normalized oxygens 24																								
Si	6,002	6,000	6,037	6,020	6,020	6,059	6,030	6,014	6,046	6,021	6,019	6,032	6,011	6,015	6,022	6,028	6,014	6,009	6,044	6,031	6,046	6,045	6,019	6,024
Ti	0,013	0,017	0,009	0,020	0,022	0,019	0,029	0,016	0,012	0,011	0,005	0,008	0,007	0,008	0,010	0,007	0,015	0,005	0,010	0,017	0,007	0,011	0,008	0,015
Al	3,865	3,888	3,849	3,867	3,821	3,799	3,806	3,861	3,808	3,874	3,893	3,882	3,900	3,888	3,837	3,896	3,872	3,888	3,847	3,873	3,851	3,876	3,877	3,875
Fe	3,468	3,502	3,444	3,388	2,980	2,809	3,001	3,150	3,330	3,486	3,513	3,537	3,595	3,593	3,652	3,527	3,413	3,392	3,481	3,639	3,583	3,571	2,572	2,346
Mn	0,849	0,781	0,841	1,028	1,343	1,585	1,461	1,187	0,977	0,864	0,807	0,757	0,709	0,736	0,735	0,803	1,023	0,939	0,902	0,729	0,682	0,688	2,177	2,422
Mg	0,586	0,514	0,495	0,434	0,340	0,323	0,338	0,399	0,441	0,486	0,570	0,542	0,517	0,440	0,426	0,409	0,374	0,363	0,361	0,428	0,443	0,527	0,287	0,251
Ca	1,267	1,319	1,334	1,260	1,494	1,402	1,357	1,401	1,402	1,281	1,213	1,261	1,284	1,341	1,367	1,338	1,308	1,431	1,361	1,288	1,411	1,289	1,078	1,074
Na	0,003	0,003	0,016	0,000	0,020	0,014	0,026	0,010	0,022	0,021	0,007	0,000	0,016	0,005	0,000	0,012	0,016	0,015	0,016	0,000	0,000	0,000	0,000	0,003
K	0,000	0,001	0,000	0,000	0,007	0,005	0,000	0,000	0,002	0,001	0,003	0,000	0,003	0,004	0,000	0,003	0,001	0,004	0,005	0,002	0,000	0,000	0,000	0,000
Cr	0,000	0,010	0,008	0,006	0,010	0,011	0,001	0,004	0,006	0,000	0,002	0,000	0,000	0,005	0,000	0,000	0,004	0,005	0,004	0,005	0,000	0,000	0,011	0,011
Total	16,053	16,026	16,026	16,018	16,046	16,015	16,049	16,040	16,041	16,043	16,031	16,019	16,041	16,030	16,049	16,024	16,037	16,045	16,027	16,008	16,022	16,007	16,018	16,009
Mg	0,586	0,514	0,495	0,434	0,340	0,323	0,338	0,399	0,441	0,486	0,570	0,542	0,517	0,440	0,426	0,409	0,374	0,363	0,361	0,428	0,443	0,527	0,287	0,251
Mn	0,849	0,781	0,841	1,028	1,343	1,585	1,461	1,187	0,977	0,864	0,807	0,757	0,709	0,736	0,735	0,803	1,023	0,939	0,902	0,729	0,682	0,688	2,177	2,422
Ca	1,267	1,319	1,334	1,260	1,494	1,402	1,357	1,401	1,402	1,281	1,213	1,261	1,284	1,341	1,367	1,338	1,308	1,431	1,361	1,288	1,411	1,289	1,078	1,074
FeII	3,298	3,386	3,330	3,277	2,823	2,690	2,844	3,012	3,179	3,370	3,410	3,440	3,490	3,482	3,472	3,450	3,295	3,268	3,376	3,555	3,464	3,496	2,458	2,253
Summe X	6,000	6,000	6,000	6,000	6,000	6,000	6,000	6,000	6,000	6,000	6,000	6,000	6,000	6,000	6,000	6,000	6,000	6,000	6,000	6,000	6,000	6,000	6,000	6,000
rest Fe	0,170	0,116	0,115	0,111	0,158	0,119	0,157	0,138	0,150	0,116	0,103	0,098	0,105	0,111	0,180	0,077	0,118	0,124	0,105	0,085	0,119	0,075	0,114	0,093
Si	6,002	6,000	6,037	6,020	6,020	6,059	6,030	6,014	6,046	6,021	6,019	6,032	6,011	6,015	6,022	6,028	6,014	6,009	6,044	6,031	6,046	6,045	6,019	6,024
Aliv	0,000	0,000	0,000	0,000	0,000	0,000	0,000	0,000	0,000	0,000	0,000	0,000	0,000	0,000	0,000	0,000	0,000	0,000	0,000	0,000	0,000	0,000	0,000	0,000
Summe Z	6,002	6,000	6,037	6,020	6,020	6,059	6,030	6,014	6,046	6,021	6,019	6,032	6,011	6,015	6,022	6,028	6,014	6,009	6,044	6,031	6,046	6,045	6,019	6,024
Alvi	3,865	3,888	3,849	3,867	3,821	3,799	3,806	3,861	3,808	3,874	3,893	3,882	3,900	3,888	3,837	3,896	3,872	3,888	3,847	3,873	3,851	3,876	3,877	3,875
Cr	0,000	0,010	0,008	0,006	0,010	0,011	0,001	0,004	0,006	0,000	0,002	0,000	0,000	0,005	0,000	0,000	0,004	0,005	0,004	0,005	0,000	0,000	0,011	0,011
Ti	0,013	0,017	0,009	0,020	0,022	0,019	0,029	0,016	0,012	0,011	0,005	0,008	0,007	0,008	0,010	0,007	0,015	0,005	0,010	0,017	0,007	0,011	0,008	0,015
FeIII	0,170	0,116	0,115	0,111	0,158	0,119	0,157	0,138	0,150	0,116	0,103	0,098	0,105	0,111	0,180	0,077	0,118	0,124	0,105	0,085	0,119	0,075	0,114	0,093
Summe Y	4,048	4,031	3,980	4,004	4,010	3,948	3,993	4,019	3,976	4,000	4,004	3,988	4,012	4,012	4,028	3,980	4,010	4,022	3,966	3,981	3,977	3,962	4,010	3,993
Alm(%)	54,971	56,432	55,498	54,617	47,045	44,830	47,397	50,202	52,990	56,162	56,833	57,327	58,163	58,041	57,864	57,504	54,912	54,459	56,263	59,246	57,730	58,261	40,970	37,558
Prp(%)	9,765	8,574	8,257	7,237	5,669	5,391	5,641	6,656	7,352	8,093	9,494	9,028	8,624	7,340	7,097	6,812	6,225	6,044	6,023	7,132	7,381	8,791	4,777	4,180
Sps(%)	14,150	13,015	14,009	17,141	22,381	26,415	24,342	19,785	16,286	14,398	13,453	12,625	11,814	12,266	12,254	13,380	17,058	15,654	15,032	12,158	11,371	11,469	36,289	40,364
Grs(%)	20,160	21,202	21,503	20,286	23,727	22,480	21,559	22,443	22,379	20,671	19,662	20,462	20,801	21,660	21,705	21,831	21,056	23,049	22,002	20,886	22,773	21,013	17,368	17,369
And(%)	0,954	0,725	0,690	0,688	1,115	0,821	1,054	0,893	0,957	0,677	0,546	0,558	0,597	0,662	1,079	0,473	0,727	0,765	0,658	0,550	0,746	0,466	0,546	0,480
Uva(%)	0,000	0,052	0,042	0,031	0,062	0,063	0,007	0,020	0,035	0,000	0,011	0,000	0,000	0,030	0,000	0,000	0,023	0,027	0,022	0,028	0,000	0,000	0,050	0,048
Prp	9,765	8,574	8,257	7,237	5,669	5,391	5,641	6,656	7,352	8,093	9,494	9,028	8,624	7,340	7,097	6,812	6,225	6,044	6,023	7,132	7,381	8,791	4,777	4,180
Alm+Sps	69,121	69,447	69,507	71,759	69,426	71,244	71,739	69,987	69,277	70,560	70,286	69,951	69,978	70,307	70,119	70,884	71,970	70,113	71,295	71,404	69,101	69,730	77,259	77,922
Grs+And	21,114	21,927	22,194	20,974	24,842	23,301	22,613	23,336	23,337	21,347	20,208	21,020	21,398	22,322	22,785	22,304	21,783	23,815	22,660	21,436	23,519	21,479	17,914	17,849

T.C. YÜKSEKÖĞRETİM KURULU
DOKÜMANTASYON MERKEZİ

Table 5.9 continue

sample no	94-55/5 (Çamlık)														
analyse no	m10-24	m10-25	m10-26	m10-27	m10-28	m10-29	m10-30	m10-31c	m10-32	m10-33	m10-34	m10-35	m10-36	m10-37	m10-38r
SiO2	37,22	37,44	37,56	37,41	37,60	37,41	37,50	37,52	37,12	37,68	37,79	37,60	37,45	37,59	37,74
TiO2	0,19	0,15	0,14	0,13	0,20	0,24	0,23	0,13	0,28	0,18	0,27	0,24	0,16	0,15	0,08
Al2O3	20,25	20,45	20,49	20,45	20,31	20,30	20,27	20,38	20,08	20,44	20,29	20,27	20,40	20,48	20,61
FeO	16,62	16,22	14,77	14,58	14,07	14,32	13,77	13,61	13,76	14,26	14,64	14,94	16,29	17,42	19,52
MnO	19,52	20,36	21,64	21,93	22,53	22,84	23,03	22,71	22,77	22,55	21,75	21,39	20,16	18,03	15,61
MgO	0,94	0,91	0,87	0,76	0,77	0,75	0,71	0,71	0,70	0,74	0,78	0,81	0,88	1,07	1,22
CaO	6,32	6,06	6,31	6,19	6,05	5,97	6,70	5,95	6,09	6,03	6,42	6,15	6,50	6,69	6,49
Na2O	0,06	0,02	0,00	0,01	0,00	0,02	0,08	0,06	0,00	0,00	0,02	0,03	0,11	0,01	0,00
K2O	0,00	0,00	0,00	0,01	0,00	0,00	0,02	0,01	0,01	0,04	0,00	0,01	0,00	0,00	0,00
Cr2O3	0,05	0,03	0,02	0,05	0,08	0,06	0,03	0,06	0,07	0,05	0,04	0,05	0,00	0,02	0,06
Total	101,18	101,64	101,80	101,51	101,61	101,90	102,34	101,15	100,87	101,96	101,99	101,49	101,96	101,46	101,33
normalized oxygens 24															
Si	5,985	5,991	5,997	5,995	6,017	5,986	5,977	6,025	5,995	6,011	6,021	6,020	5,980	6,004	6,021
Ti	0,023	0,019	0,017	0,015	0,024	0,028	0,027	0,016	0,034	0,021	0,033	0,029	0,020	0,018	0,010
Al	3,838	3,857	3,856	3,863	3,831	3,829	3,808	3,857	3,823	3,844	3,811	3,825	3,840	3,856	3,876
Fe	2,235	2,170	1,972	1,954	1,883	1,916	1,835	1,827	1,858	1,902	1,951	2,000	2,175	2,327	2,604
Mn	2,658	2,759	2,926	2,976	3,053	3,095	3,109	3,088	3,115	3,047	2,935	2,900	2,726	2,439	2,109
Mg	0,226	0,218	0,207	0,182	0,184	0,179	0,169	0,171	0,167	0,176	0,185	0,193	0,210	0,255	0,289
Ca	1,089	1,039	1,079	1,063	1,037	1,023	1,144	1,024	1,054	1,031	1,096	1,055	1,112	1,145	1,109
Na	0,018	0,007	0,000	0,002	0,000	0,005	0,026	0,019	0,000	0,000	0,005	0,009	0,034	0,004	0,000
K	0,000	0,000	0,000	0,002	0,000	0,000	0,004	0,001	0,003	0,008	0,000	0,002	0,000	0,000	0,000
Cr	0,006	0,003	0,002	0,006	0,010	0,008	0,004	0,008	0,008	0,006	0,005	0,007	0,000	0,003	0,008
Total	16,072	16,060	16,054	16,052	16,029	16,062	16,100	16,029	16,048	16,040	16,036	16,034	16,097	16,048	16,019
Mg	0,226	0,218	0,207	0,182	0,184	0,179	0,169	0,171	0,167	0,176	0,185	0,193	0,210	0,255	0,289
Mn	2,658	2,759	2,926	2,976	3,053	3,095	3,109	3,088	3,115	3,047	2,935	2,900	2,726	2,439	2,109
Ca	1,089	1,039	1,079	1,063	1,037	1,023	1,144	1,024	1,054	1,031	1,096	1,055	1,112	1,145	1,109
FeII	2,027	1,984	1,787	1,779	1,726	1,702	1,578	1,717	1,664	1,746	1,784	1,852	1,951	2,161	2,492
Summe X	6,000	6,000	6,000	6,000	6,000	6,000	6,000	6,000	6,000	6,000	6,000	6,000	6,000	6,000	6,000
rest Fe	0,208	0,187	0,184	0,174	0,157	0,214	0,258	0,110	0,194	0,156	0,167	0,148	0,224	0,166	0,112
Si	5,985	5,991	5,997	5,995	6,017	5,986	5,977	6,025	5,995	6,011	6,021	6,020	5,980	6,004	6,021
Aliv	0,015	0,009	0,003	0,005	0,000	0,014	0,023	0,000	0,005	0,000	0,000	0,000	0,020	0,000	0,000
Summe Z	6,000	6,000	6,000	6,000	6,017	6,000	6,000	6,025	6,000	6,011	6,021	6,020	6,000	6,004	6,021
Alvi	3,823	3,849	3,853	3,858	3,831	3,815	3,786	3,857	3,818	3,844	3,811	3,825	3,820	3,856	3,876
Cr	0,006	0,003	0,002	0,006	0,010	0,008	0,004	0,008	0,008	0,006	0,005	0,007	0,000	0,003	0,008
Ti	0,023	0,019	0,017	0,015	0,024	0,028	0,027	0,016	0,034	0,021	0,033	0,029	0,020	0,018	0,010
FeIII	0,208	0,187	0,184	0,174	0,157	0,214	0,258	0,110	0,194	0,156	0,167	0,148	0,224	0,166	0,112
Summe Y	4,060	4,057	4,057	4,053	4,022	4,065	4,074	3,992	4,054	4,027	4,015	4,010	4,063	4,042	4,006
Alm(%)	33,784	33,064	29,790	29,656	28,759	28,372	26,294	28,619	27,739	29,105	29,731	30,861	32,524	36,021	41,534
Prp(%)	3,767	3,633	3,454	3,029	3,065	2,985	2,823	2,848	2,788	2,937	3,087	3,218	3,503	4,246	4,823
Sps(%)	44,304	45,988	48,767	49,603	50,890	51,586	51,815	51,473	51,910	50,781	48,917	48,340	45,440	40,652	35,154
Grs(%)	17,085	16,426	17,083	16,856	16,466	16,008	17,717	16,486	16,540	16,395	17,337	16,774	17,423	18,203	17,890
And(%)	1,032	0,875	0,894	0,829	0,778	1,016	1,333	0,539	0,987	0,755	0,907	0,777	1,110	0,866	0,564
Uva(%)	0,028	0,013	0,011	0,026	0,042	0,033	0,018	0,034	0,036	0,027	0,022	0,030	0,000	0,012	0,035
Prp	3,767	3,633	3,454	3,029	3,065	2,985	2,823	2,848	2,788	2,937	3,087	3,218	3,503	4,246	4,823
Alm+Sps	78,088	79,052	78,558	79,260	79,649	79,958	78,108	80,092	79,649	79,886	78,648	79,201	77,964	76,673	76,688
Grs+And	18,117	17,301	17,977	17,685	17,244	17,024	19,050	17,025	17,527	17,150	18,243	17,551	18,533	19,069	18,453

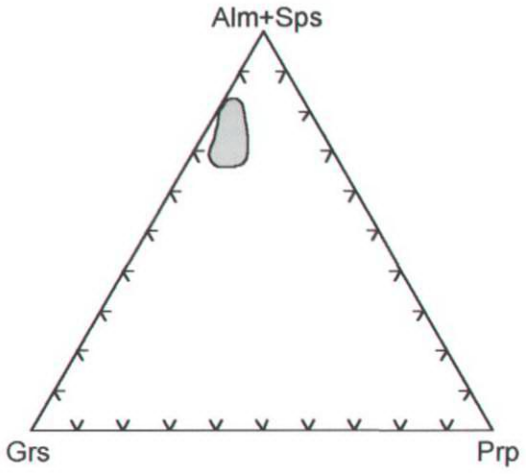


Figure 5.33 In almandine+spessartine - grossular - pyrope ternary diagram, location of selected garnet grains from blueschist metabasites

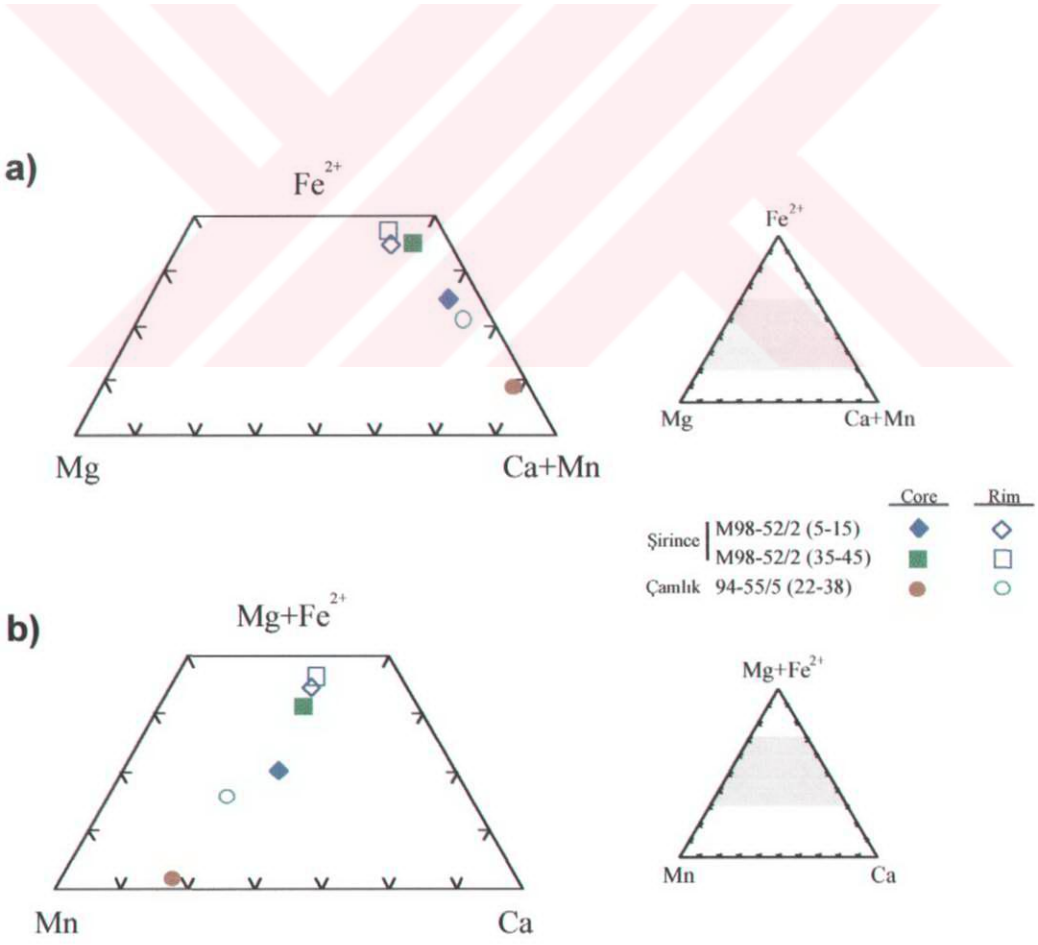
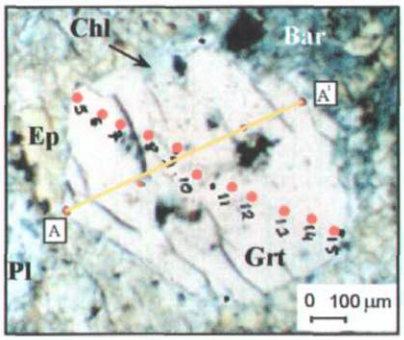
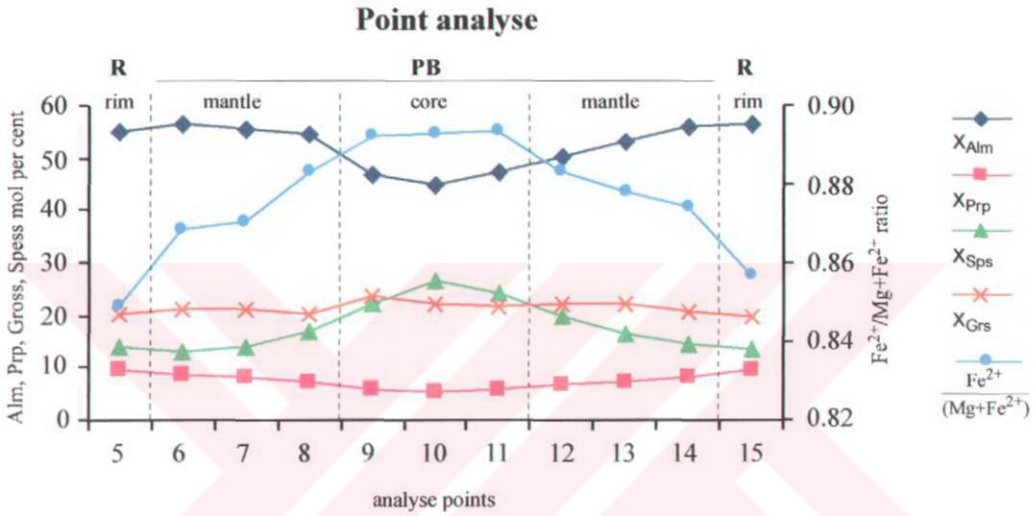


Figure 5.34 Ternary atomic proportions of Fe^{2+}-Mg-Ca+Mn (a) and of Fe^{2+}+Mg-Mn-Ca (b) for garnets from Şirince and Çamlık blueschist metabasites.

a)



b)



c)

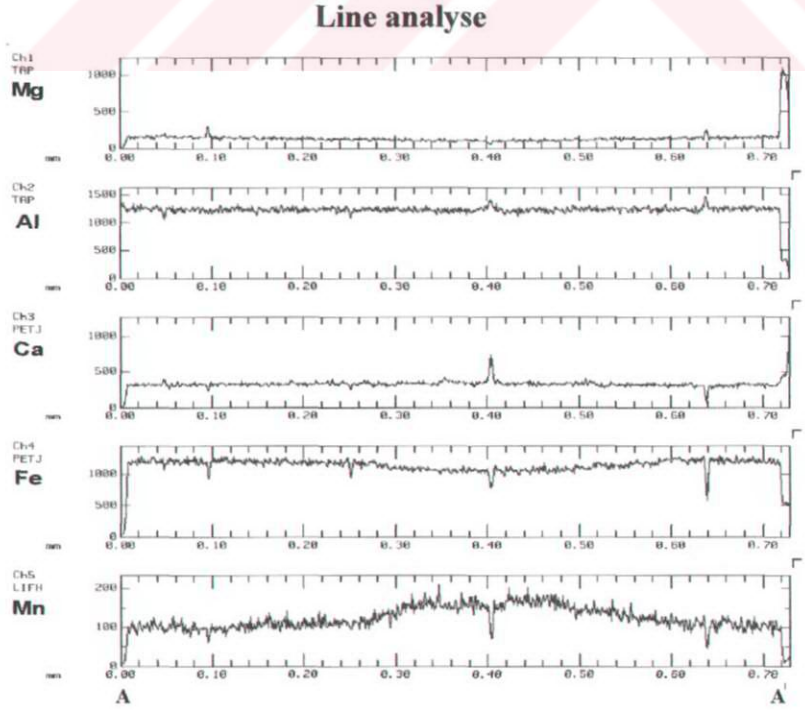


Figure 5.35 Compositional zoning in the garnet (5-15) from M98-52/2; a) microphoto of analysed garnet in PPL, b) element zoning profiles from rim to rim , c) A-A' line analyse from rim to rim.

those prevailing during the primary crystallization. But, controversial results are obtained from geothermometric estimates.

In garnet grain (**35-45**) from sample **M98-52/2**, cation totals per formula unit range from 16.007 to 16.049, somewhat higher than the ideal stoichiometric value of 16.00. Al(VI) averages 3.874 per 24 oxygens. The amount of ferric iron ranges from 0.075 to 0.180 p.f.u. (Table 5.9). The ferric iron is of negligible amount. Andradite content of garnet ranges from 0.466 to 1.079 mol %. The proportions of Ca, Fe(2+), Mg and Mn for this garnet are illustrated in Figure 5.34. Garnet which is composed of average 78 percent pyralspite and 22 percent ugrandite series is rich-in almandine (average 57 mol %) and grossular (average 21 mol %) (Figure 5.34). Core and rim compositions of the garnet are "Alm_{56} Prp_6 Grs_{21} Sps_{17} " and "Alm_{57} Prp_9 Grs_{21} Sps_{13} ", respectively.

Garnet (**35-45**) with subhedral crystal form is corroded by secondary chlorite and epidote (Figure 5.36a). Garnet is poor-in pyrope (X_{Prp}= 6.024 mol%) in the core. X_{Prp} content gradually increases rimward and reaches up to 9.02 mol%. On the contrary, the X_{Sps} content in the centre of the garnet crystal ,as in Hollister 1966, is particularly high (17 mol%) when compared with rim (11 mol%) (Figure 5.36b, c, d). $Fe^{2+}/(Fe^{2+}+Mg)$ ratio which is at about 0.90 in the core, variably decreases to 0.86 at the rim (Figure 5.36c). X_{Grs} displays minor changing from core (23 mol%) to rim (20 mol%). X_{Alm} pattern has a bowl-shape in the core and then shows flattening through the mantle to the rim. Element patterns mentioned above show typical compositional trends which characterize the growth zoning. But these trends were partially reset by retrograde effects which are represented by secondary chlorite occurences in the rim. The rim sections of garnet have re-equilibrated with the matrix during retrograde overprint.

Sample two: Cation totals per formula unit of garnet (**22-38**) in **94-55/5** range from 16.009 to 16.100, somewhat higher than the ideal value of 16.00. Si (5.977 – 6.025), octahedrally coordinated aluminium (3.786 –3.877), Ti (0.008 – 0.034) and Cr (0.000 – 0.011) atoms per garnet formula unit are observed in these ranges (Table

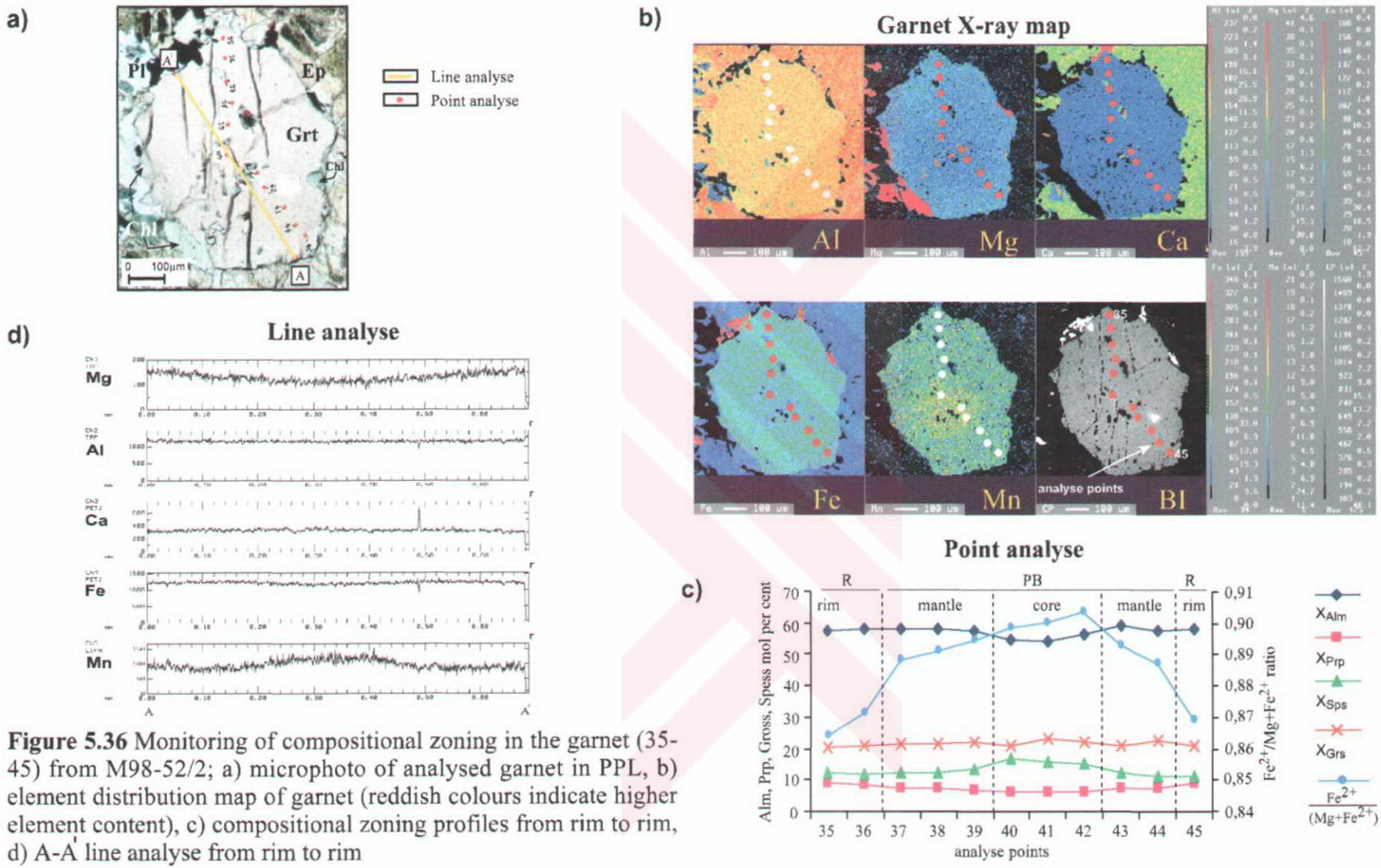


Figure 5.36 Monitoring of compositional zoning in the garnet (35-45) from M98-52/2; a) microphoto of analysed garnet in PPL, b) element distribution map of garnet (reddish colours indicate higher element content), c) compositional zoning profiles from rim to rim, d) A-A' line analyse from rim to rim

5.9). Al(VI) averages 3.840 per 24 oxygens. The amount of ferric iron ranges from 0.093 to 0.258. Andradite content of the garnet ranges from 0.840 to 1.333 mol %. Andradite content of the garnet is negligible amount. The proportion of Ca, Fe^{2+}, Mg and Mn for this garnet is illustrated in Figure 5.34. Garnet which is composed of average 82 percent pyralspite and 18 percent ugrandite series is rich in spessartine (average 47 mol%) and almandine (average 32 mol%). Core and rim compositions of the garnet are "Alm_{29} Prp_3 Grs_{17} Sps_{51} " and "Alm_{41} Prp_5 Grs_{17} Sps_{36}", respectively.

Garnet grain which is 730 microns in diameter is subhedral and does not show optical zonation. Garnet is surrounded by a plagioclase corona (Figure 5.37a). Upper right corner in Figure 5.37a, radial amphibole needles which are perpendicular to garnet are also exist in plagioclase corona. Chemical zonation in garnet is given in Figure 5.37b, c, d. X_{Sps} is substituted by X_{Alm} and small amounts of X_{Prp}. X_{Sps} zonation displays a growth zoning with X_{Sps} content gradually decreasing from core to rim (Figure 5.37c). X_{Alm} and X_{Prp} regularly increase rimward. The increase of X_{Alm} from core to rim is higher than X_{Prp}. X_{Grs} displays an almost flat profile from core to rim. $Fe^{2+}/(Fe^{2+}+Mg)$ ratio is 0.909 in the core and irregularly drops to 0.896 at the rim. The patterns of increasing X_{Alm}, X_{Prp} and decreasing X_{Sps} and $Fe^{2+}/(Fe^{2+}+Mg)$ ratio are usually indicative of garnet growth zoning (Spear, 1989).

Growth zoning has been modified in a limited range by a retrograde overprint under low-pressure / medium temperature conditions. As result of diffusional retrograde re-equilibration, especially $Fe^{2+}/(Fe^{2+}+Mg)$ profile displays a reversal at the rim (Figure 5.37c). Plagioclase corona and partly developed radial amphibole needles demonstrate an isothermal decompression during the retrograde overprint of the high-pressure blocks.

5.4.1.3. Garnet in garnet-amphibolite block

A garnet grain from garnet-amphibolite sample (**M97-149/10**) was examined. Analyses of this garnet are given in Table 5.10. Cation proportions were calculated based on 24 oxygens. Garnet composition shows the following ranges: almandine

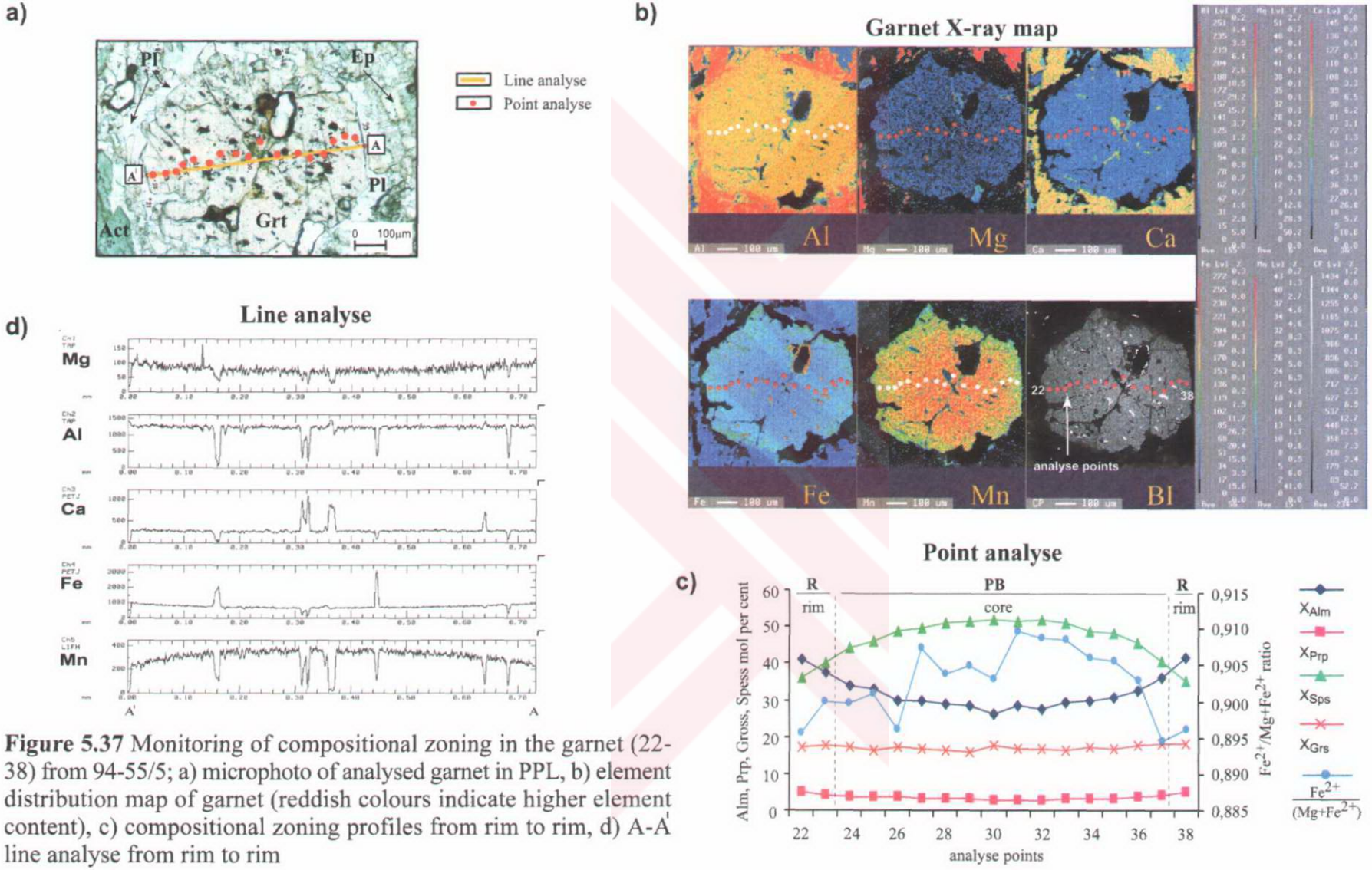


Figure 5.37 Monitoring of compositional zoning in the garnet (22-38) from 94-55/5; a) microphoto of analysed garnet in PPL, b) element distribution map of garnet (reddish colours indicate higher element content), c) compositional zoning profiles from rim to rim, d) A-A' line analyse from rim to rim

36-48 mol%, pyrope 2-6 mol%, grossular 29-35 mol%, spessartine 15-24 mol% and andradite 0.9-1.9 mol%. Amphiboles are tschermakitic hornblende in composition. Cation totals per formula unit of garnet (1-7) in M97-149/10 range from 16.025 to 16.080 somewhat higher than the ideal value of 16.00. Si (5.97 1- 6.007), octahedrally coordinated aluminum (3.820 – 3.889), Ti (0.013 – 0.020) and Cr (0.002 – 0.010) atoms per garnet formula unit are observed in these ranges (Table 5.10). Al(VI) averages 3.863 per 24 oxygens. The amount of ferric iron ranges from 0.107 – 0.234. Andradite content of the garnet ranges from 0.965 – 1.909 mol%. The proportions of Ca, Fe^{2+}, Mg and Mn for this garnet are illustrated in Figure 5.38. Garnet which is composed of average 67 percent pyralspite and 33 percent ugrandite series is rich-in almandine (average 41 mol%) and grossular (average 32 mol%). Core and rim compositions of the garnet are "Alm_{40} Prp_3 Grs_{32} Sps_{25} " and "Alm_{40} Prp_2 Grs_{36} Sps_{22} ", respectively.

The garnet grain that is 700 microns in diameter has an anhedral shape (Figure 5.39). There is no textural zonation in garnet which is consistent with slight chemical zonation determined by the point analyses (Figure 5.39). X_{Sps} and X_{Prp} patterns are almost flat. In analyse point 5 (Figure 5.39), Mn-Fe-Mg display deviation from the general trend. The reason of this deviation result from the close proximity of the crack. X_{Alm} and X_{Prp} decrease towards rim whereas X_{Grs} and X_{Sps} display an increasing trend. Decrease in X_{Alm} and increase in X_{Grs} from core to rim can be regarded to indicate the increasing of temperature (Loomis and Nimick, 1982). On the other hand, Zoning patterns can be considered as having been significantly flattened by post-growth diffusion. This garnet which has bluish zoisite inclusions from core to rim should have been formed during the epidote-blueschist facies in conditions.

5.4.1.4. Garnets in garnet-phengite schist (the matrix of the Metaolistostrome)

Three garnet grains from two samples (**94-30** and **M98-99/2**) belonging to the matrix of the metaolistostrome were selected to operate on the zoning profiles. These samples contain phengitic white mica with an average value of 3,38 Si^{4+} p.f.u.

Table 5.10 Representative garnet analyses from garnet-amphibolite in Tire area.

	m2-1(rim)	m2-2	m2-3	m2-4 (core)	m2-5	m2-6	m2-7 (rim)
SiO2	37,49	37,18	37,19	37,46	37,27	37,14	37,13
TiO2	0,11	0,15	0,15	0,12	0,17	0,15	0,11
Al2O3	20,63	20,52	20,41	20,41	20,49	20,31	20,33
FeO	18,75	18,95	19,90	18,73	22,18	20,36	17,36
MnO	9,70	10,55	9,77	10,85	6,84	10,40	10,83
MgO	0,70	0,71	0,76	0,71	1,56	0,96	0,53
CaO	12,91	11,40	11,25	11,64	10,51	10,75	12,85
Na2O	0,01	0,04	0,00	0,00	0,02	0,02	0,05
K2O	0,01	0,00	0,00	0,00	0,00	0,00	0,01
Cr2O3	0,07	0,01	0,03	0,08	0,05	0,05	0,07
Summe	100,375	99,509	99,465	99,995	99,087	100,134	99,271
normalized oxygens 24							
Si	5,979	5,990	5,997	6,007	6,002	5,972	5,991
Ti	0,013	0,018	0,018	0,014	0,021	0,018	0,014
Al	3,878	3,897	3,879	3,858	3,890	3,849	3,866
Fe	2,501	2,553	2,683	2,512	2,987	2,737	2,342
Mn	1,310	1,440	1,334	1,474	0,933	1,416	1,480
Mg	0,166	0,170	0,184	0,169	0,374	0,229	0,127
Ca	2,206	1,968	1,943	2,000	1,813	1,852	2,221
Na	0,004	0,012	0,000	0,000	0,005	0,007	0,016
K	0,002	0,000	0,000	0,000	0,000	0,000	0,003
Cr	0,008	0,002	0,004	0,010	0,006	0,006	0,008
TOTAL	16,059	16,047	16,039	16,034	16,025	16,081	16,059
Mg	0,166	0,170	0,184	0,169	0,374	0,229	0,127
Mn	1,310	1,440	1,334	1,474	0,933	1,416	1,480
Ca	2,206	1,968	1,943	2,000	1,813	1,852	2,221
FeII	2,318	2,423	2,539	2,357	2,879	2,503	2,172
Total X	6,000	6,000	6,000	6,000	6,000	6,000	6,000
rest Fe	0,183	0,130	0,145	0,154	0,108	0,234	0,170
Si	5,979	5,990	5,997	6,007	6,002	5,972	5,991
Aliv	0,021	0,010	0,003	0,000	0,000	0,028	0,009
Total Z	6,000	6,000	6,000	6,007	6,002	6,000	6,000
Alvi	3,858	3,887	3,876	3,858	3,890	3,821	3,857
Cr	0,008	0,002	0,004	0,010	0,006	0,006	0,008
Ti	0,013	0,018	0,018	0,014	0,021	0,018	0,014
FeIII	0,183	0,130	0,145	0,154	0,108	0,234	0,170
Total Y	4,061	4,037	4,043	4,037	4,024	4,079	4,049
Alm(%)	38,633	40,376	42,311	39,288	47,988	41,720	36,193
Prp(%)	2,765	2,837	3,060	2,820	6,241	3,814	2,124
Sps(%)	21,837	23,992	22,237	24,561	15,549	23,603	24,664
Grs(%)	34,918	31,577	31,055	31,856	29,212	28,910	35,260
And(%)	1,771	1,203	1,306	1,394	0,966	1,909	1,683
Uva(%)	0,075	0,013	0,031	0,081	0,045	0,043	0,076
TOTAL	100	100	100	100	100	100	100
Prp	2,765	2,837	3,060	2,820	6,241	3,814	2,124
Alm+Sps	60,470	64,368	64,549	63,849	63,537	65,323	60,857
Grs+And	36,689	32,781	32,360	33,250	30,177	30,819	36,943
TOTAL	99,925	99,987	99,969	99,919	99,955	99,957	99,924

Analyses of the garnet grains are given in Table 5.11. In garnet-phengite schists, garnets exhibit significant variation in Fe, Mn, Ca and Mg contents. Garnet compositions can be given by the following ranges; almandine 42 – 68 mol%, pyrope 2 – 7 mol%, grossular 24 – 37 mol%, spessartine 0.6 – 28 mol% and andradite 0.3 – 1.8 mol%. In the pyrope – (almandine + spessartine) – grossular ternary diagram (Figure 5.40), garnets concentrate close to almandine + spessartine corner.

Sample one: Two garnet grains (**10-32** and **61-77**) were chosen from sample **M98-99/2**. 10-32 and 61-77 represent analyse range of each garnet grain (Table 5.11). In garnet grain (**10-32**) from sample M98-99/2, cation sums are range from 15.990 to 16.067. Minor amounts of aluminium are assigned to tetrahedral sites, averaging 0.012 based on one formula unit; Al(VI) averages 3.901 which is slightly lower than the ideal value of 4.00. Na, K, Cr and Ti are present in insignificant proportions. Amount of ferric iron ranges from 0.023 to 0.167. Andradite content of the garnet ranges from 0.351 mol% to 1.430 mol% and is negligible. Therefore, compositional variations of this garnet may be shown adequately in terms of the Ca (grossular), Fe^{2+} (almandine), Mg (pyrope) and Mn (spessartine) proportions. Fe^{2+} / Mg / Ca / Mn ratios for the garnet are given in Figure 5.41; this ternary diagram displays the proportions of atoms occupying the large eightfold coordinated site in garnet. According to Figure 5.41, the garnet is calcuim-, mangenese- and magnesium-bearing almandine. The garnets composed of average 69 percent pyralspite and 31 percent ugrandite series are rich-in almandine (average 54 mol%) and grossular (average 30 mol%). Core and rim compositions of garnets are "Alm_{44} Prp_2 Grs_{27} Sps_{27} " and "Alm_{57} Prp_6 Grs_{35} Sps_2 ", respectively. As is clear from Figure 5.41, relict core (core) and overgrowth (mantle) - rim that have got different compositional trends can be easily separated from each other.

Garnet (**10-32**) is 1180 microns in diameter and shows a subhedral shape. This garnet porphyroblast shows textural zonation (Figure 5.42a) by a clear, inclusion-free, relict core, zoisite inclusions-bearing mantle which is expression of an blueschist stage (PB) and a rim which is rich-in tiny inclusions and represents the retrograde stage (R). Zoisite inclusions are observed especially in Fe rich zone of

Table 5.11 Representative garnet analyses from the matrix of the Metaolistostrome (garnet-phengite schist) in Şirince and Belevi (r: rim, c: core).

sample no	94-30 (Şirince)											M98-99/2 (Belevi)											
analyse no	36 r	37	38	39	40	41 c	42	43	44	45	46 r	m1-10 r	m1-11	m1-12	m1-13	m1-14	m1-15	m1-16	m1-17	m1-18	m1-19	m1-20	m1-21	m1-22
SiO2	37,12	36,69	36,54	36,80	36,36	37,09	36,66	36,89	36,57	36,95	37,41	37,55	37,08	37,25	37,34	37,42	37,35	37,24	37,28	37,57	36,83	37,36	36,91	37,03
TiO2	0,14	0,08	0,08	0,14	0,20	0,11	0,14	0,12	0,14	0,09	0,15	0,09	0,07	0,12	0,10	0,11	0,08	0,17	0,19	0,09	0,10	0,13	0,14	0,14
Al2O3	20,99	20,55	20,57	20,68	20,36	20,75	20,52	20,71	20,61	20,98	20,91	20,79	20,59	20,80	20,49	20,73	20,68	20,72	20,61	20,57	20,39	20,76	20,49	20,64
FeO	28,65	28,55	28,47	29,38	30,66	31,64	29,46	28,75	28,42	28,21	28,57	26,27	27,61	29,78	29,14	29,28	28,57	25,02	23,67	22,73	21,71	20,84	19,91	19,71
MnO	0,36	0,32	0,35	0,62	0,72	0,80	0,81	0,51	0,42	0,35	0,29	0,62	0,83	0,38	0,30	0,47	1,49	5,40	6,53	8,72	9,80	10,95	11,65	12,18
MgO	1,64	1,41	1,19	1,22	1,16	1,31	1,12	1,20	1,30	1,51	1,59	1,57	1,22	1,22	1,07	1,13	0,98	0,80	0,65	0,65	0,59	0,54	0,50	0,52
CaO	10,83	11,39	11,32	10,59	9,11	8,67	10,59	11,49	11,16	11,51	11,21	12,86	11,60	10,20	11,06	10,87	10,59	10,24	10,29	9,85	9,96	9,71	9,82	9,27
Na2O	0,04	0,04	0,02	0,00	0,04	0,11	0,06	0,01	0,10	0,01	0,07	0,09	0,03	0,05	0,00	0,09	0,00	0,02	0,00	0,02	0,01	0,00	0,02	0,00
K2O	0,02	0,01	0,00	0,00	0,01	0,00	0,01	0,01	0,03	0,00	0,00	0,00	0,02	0,01	0,01	0,01	0,00	0,01	0,01	0,00	0,01	0,00	0,00	0,00
Cr2O3	0,07	0,05	0,04	0,07	0,04	0,00	0,03	0,09	0,07	0,07	0,00	0,03	0,07	0,04	0,06	0,05	0,06	0,05	0,05	0,10	0,05	0,07	0,06	0,10
Total	99,85	99,09	98,57	99,49	98,65	100,47	99,40	99,78	98,81	99,68	100,20	99,86	99,11	99,84	99,57	100,16	99,80	99,67	99,28	100,30	99,46	100,36	99,50	99,59
normalized oxygens 24																								
Si	5,939	5,934	5,940	5,939	5,943	5,954	5,935	5,932	5,930	5,924	5,962	5,979	5,980	5,979	6,007	5,986	6,000	5,994	6,018	6,023	5,975	5,993	5,980	5,989
Ti	0,017	0,009	0,010	0,017	0,024	0,013	0,017	0,014	0,017	0,011	0,018	0,010	0,008	0,015	0,012	0,013	0,009	0,020	0,024	0,011	0,012	0,016	0,017	0,017
Al	3,959	3,918	3,942	3,934	3,922	3,926	3,916	3,925	3,940	3,965	3,928	3,902	3,914	3,935	3,885	3,909	3,916	3,931	3,922	3,887	3,899	3,926	3,913	3,935
Fe	3,833	3,861	3,870	3,965	4,190	4,247	3,988	3,865	3,854	3,782	3,807	3,498	3,723	3,997	3,920	3,917	3,838	3,367	3,195	3,047	2,945	2,796	2,697	2,666
Mn	0,049	0,044	0,048	0,084	0,099	0,109	0,111	0,070	0,057	0,047	0,039	0,084	0,113	0,051	0,040	0,063	0,203	0,736	0,893	1,184	1,346	1,488	1,599	1,668
Mg	0,390	0,340	0,288	0,293	0,282	0,312	0,270	0,287	0,315	0,361	0,378	0,372	0,293	0,291	0,257	0,269	0,233	0,192	0,156	0,155	0,143	0,128	0,121	0,126
Ca	1,856	1,974	1,972	1,831	1,595	1,491	1,837	1,979	1,939	1,977	1,914	2,194	2,004	1,754	1,906	1,863	1,822	1,766	1,780	1,692	1,731	1,669	1,705	1,606
Na	0,011	0,012	0,005	0,000	0,013	0,033	0,019	0,004	0,031	0,002	0,021	0,027	0,008	0,015	0,000	0,029	0,000	0,006	0,000	0,007	0,004	0,000	0,007	0,000
K	0,003	0,002	0,000	0,000	0,001	0,000	0,003	0,002	0,005	0,000	0,000	0,000	0,003	0,002	0,002	0,002	0,000	0,002	0,002	0,000	0,003	0,000	0,000	0,000
Cr	0,009	0,007	0,005	0,009	0,006	0,000	0,004	0,011	0,009	0,009	0,000	0,004	0,009	0,006	0,007	0,007	0,008	0,007	0,006	0,013	0,006	0,009	0,008	0,013
Total	16,058	16,094	16,074	16,064	16,071	16,086	16,095	16,078	16,088	16,069	16,067	16,067	16,047	16,039	16,029	16,051	16,021	16,015	15,990	16,006	16,058	16,015	16,038	16,007
Mg	0,390	0,340	0,288	0,293	0,282	0,312	0,270	0,287	0,315	0,361	0,378	0,372	0,293	0,291	0,257	0,269	0,233	0,192	0,156	0,155	0,143	0,128	0,121	0,126
Mn	0,049	0,044	0,048	0,084	0,099	0,109	0,111	0,070	0,057	0,047	0,039	0,084	0,113	0,051	0,040	0,063	0,203	0,736	0,893	1,184	1,346	1,488	1,599	1,668
Ca	1,856	1,974	1,972	1,831	1,595	1,491	1,837	1,979	1,939	1,977	1,914	2,194	2,004	1,754	1,906	1,863	1,822	1,766	1,780	1,692	1,731	1,669	1,705	1,606
FeII	3,705	3,642	3,692	3,791	4,024	4,088	3,782	3,664	3,689	3,615	3,669	3,350	3,590	3,904	3,796	3,805	3,741	3,307	3,172	2,970	2,780	2,715	2,576	2,600
Total X	6,000	6,000	6,000	6,000	6,000	6,000	6,000	6,000	6,000	6,000	6,000	6,000	6,000	6,000	6,000	6,000	6,000	6,000	6,000	6,000	6,000	6,000	6,000	6,000
rest Fe	0,129	0,219	0,178	0,174	0,167	0,159	0,206	0,201	0,165	0,167	0,138	0,148	0,133	0,093	0,124	0,112	0,096	0,061	0,023	0,078	0,165	0,080	0,121	0,066
Si	5,939	5,934	5,940	5,939	5,943	5,954	5,935	5,932	5,930	5,924	5,962	5,979	5,980	5,979	6,007	5,986	6,000	5,994	6,018	6,023	5,975	5,993	5,980	5,989
Aliv	0,061	0,066	0,060	0,061	0,057	0,046	0,065	0,068	0,070	0,076	0,038	0,021	0,020	0,021	0,000	0,014	0,000	0,006	0,000	0,000	0,025	0,007	0,020	0,011
Total Z	6,000	6,000	6,000	6,000	6,000	6,000	6,000	6,000	6,000	6,000	6,000	6,000	6,000	6,000	6,007	6,000	6,000	6,000	6,018	6,023	6,000	6,000	6,000	6,000
Alvi	3,898	3,852	3,882	3,873	3,865	3,880	3,851	3,857	3,870	3,889	3,890	3,882	3,894	3,914	3,885	3,895	3,915	3,925	3,922	3,887	3,874	3,919	3,894	3,924
Cr	0,009	0,007	0,005	0,009	0,006	0,000	0,004	0,011	0,009	0,009	0,000	0,004	0,009	0,006	0,007	0,007	0,008	0,007	0,006	0,013	0,006	0,009	0,008	0,013
Ti	0,017	0,009	0,010	0,017	0,024	0,013	0,017	0,014	0,017	0,011	0,018	0,010	0,008	0,015	0,012	0,013	0,009	0,020	0,024	0,011	0,012	0,016	0,017	0,017
FeIII	0,129	0,219	0,178	0,174	0,167	0,159	0,206	0,201	0,165	0,167	0,138	0,148	0,133	0,093	0,124	0,112	0,096	0,061	0,023	0,078	0,165	0,080	0,121	0,066
Total Y	4,053	4,087	4,074	4,072	4,062	4,053	4,077	4,083	4,061	4,076	4,046	4,044	4,044	4,028	4,028	4,027	4,029	4,013	3,975	3,989	4,057	4,024	4,039	4,020
Alm(%)	61,743	60,701	61,538	63,191	67,059	68,132	63,040	61,069	61,478	60,256	61,157	55,835	59,832	65,066	63,267	63,410	62,357	55,109	52,864	49,493	46,331	45,252	42,934	43,326
Prp(%)	6,506	5,665	4,802	4,883	4,706	5,204	4,492	4,777	5,253	6,010	6,294	6,202	4,883	4,848	4,292	4,490	3,891	3,195	2,595	2,577	2,378	2,140	2,012	2,097
Sps(%)	0,811	0,740	0,801	1,408	1,650	1,813	1,856	1,167	0,955	0,783	0,650	1,398	1,883	0,852	0,674	1,050	3,378	12,268	14,880	19,733	22,441	24,795	26,644	27,806
Grs(%)	29,759	31,002	31,308	29,027	25,300	23,793	28,912	31,157	30,798	31,439	30,670	35,099	32,159	28,412	30,642	30,031	29,518	28,785	29,268	27,480	27,547	27,089	27,386	26,131
And(%)	1,111	1,840	1,513	1,427	1,250	1,058	1,670	1,739	1,447	1,438	1,228	1,430	1,171	0,781	1,068	0,966	0,796	0,594	0,351	0,627	1,259	0,664	0,971	0,554
Uva(%)	0,070	0,052	0,037	0,064	0,036	0,000	0,031	0,091	0,069	0,074	0,000	0,035	0,073	0,041	0,057	0,053	0,060	0,049	0,043	0,090	0,045	0,060	0,053	0,085
Prp	6,506	5,665	4,802	4,883	4,706	5,204	4,492	4,777	5,253	6,010	6,294	6,202	4,883	4,848	4,292	4,490	3,891	3,195	2,595	2,577	2,378	2,140	2,012	2,097
Alm+Sps	62,553	61,441	62,339	64,599	68,708	69,945	64,895	62,235	62,432	61,039	61,807	57,233	61,714	65,918	63,941	64,460	65,735	67,377	67,744	69,226	68,772	70,047	69,578	71,132
Grs+And	30,870	32,842	32,822	30,454	26,550	24,851	30,582	32,896	32,245	32,877	31,898	36,530	33,330	29,193	31,710	30,997	30,314	29,379	29,619	28,107	28,806	27,753	28,357	26,685

Table 5.11 continue

sample no	M98-99/2 (Belevi)										M98-99/2 (Belevi)													
analyse no	m1-23 c	m1-24	m1-25	m1-26	m1-27	m1-28	m1-29	m1-30	m1-31	m1-32 r	m1-61 r	m1-62	m1-63	m1-64	m1-65	m1-66	m1-67	m1-68 c	m1-69	m1-70	m1-71	m1-72	m1-73	m1-74
SiO2	36,98	37,26	37,12	37,25	37,00	37,13	37,16	37,28	37,88	37,86	36,89	37,37	37,35	37,31	37,24	36,95	37,14	36,74	37,11	37,14	36,98	37,16	36,93	37,32
TiO2	0,15	0,17	0,12	0,08	0,15	0,09	0,09	0,06	0,15	0,06	0,07	0,10	0,08	0,16	0,19	0,05	0,16	0,21	0,14	0,15	0,18	0,11	0,07	0,05
Al2O3	20,39	20,61	20,73	20,64	20,57	20,53	20,58	20,60	21,08	21,03	20,80	20,76	20,56	20,47	20,49	20,22	20,37	20,38	20,18	20,56	20,35	20,49	20,56	20,46
FeO	20,26	20,80	21,74	23,99	25,95	28,01	28,89	26,26	25,49	26,48	27,84	28,66	29,20	24,68	22,72	21,70	20,47	20,07	20,93	22,04	23,63	25,56	29,92	29,76
MnO	11,62	11,06	10,19	7,71	4,65	2,19	0,36	0,42	0,49	0,40	0,35	0,93	0,65	4,83	8,08	10,27	10,27	10,90	10,06	9,08	6,85	4,09	0,58	0,37
MgO	0,53	0,53	0,63	0,69	0,85	0,95	1,06	1,48	1,54	1,66	1,63	1,30	1,12	0,77	0,62	0,62	0,54	0,59	0,60	0,61	0,66	0,75	1,13	1,20
CaO	9,36	9,92	10,00	9,88	10,43	10,57	11,15	12,74	13,17	12,34	11,62	11,03	10,85	11,26	10,52	9,66	10,50	10,58	10,26	10,40	10,78	11,47	10,28	9,92
Na2O	0,02	0,00	0,05	0,06	0,03	0,03	0,01	0,06	0,06	0,01	0,06	0,02	0,03	0,03	0,00	0,04	0,02	0,04	0,00	0,04	0,00	0,00	0,00	0,06
K2O	0,01	0,00	0,00	0,00	0,00	0,02	0,00	0,00	0,00	0,01	0,01	0,01	0,01	0,02	0,00	0,00	0,00	0,00	0,00	0,02	0,00	0,01	0,00	0,00
Cr2O3	0,10	0,03	0,09	0,03	0,03	0,00	0,03	0,07	0,00	0,06	0,03	0,06	0,04	0,01	0,05	0,05	0,02	0,06	0,06	0,02	0,04	0,00	0,06	0,08
Total	99,41	100,38	100,67	100,32	99,66	99,51	99,34	98,97	99,86	99,91	99,29	100,24	99,89	99,54	99,92	99,57	99,49	99,57	99,33	100,06	99,47	99,64	99,53	99,21
normalized oxygens 24																								
Si	5,998	5,984	5,951	5,984	5,970	5,991	5,990	5,989	6,003	6,008	5,934	5,971	5,996	6,008	5,994	5,994	6,004	5,951	6,014	5,978	5,982	5,987	5,964	6,025
Ti	0,018	0,020	0,015	0,009	0,018	0,011	0,011	0,008	0,018	0,007	0,008	0,012	0,009	0,019	0,023	0,006	0,020	0,025	0,017	0,018	0,022	0,013	0,008	0,006
Al	3,898	3,902	3,918	3,908	3,912	3,904	3,910	3,901	3,937	3,933	3,944	3,910	3,890	3,885	3,888	3,866	3,882	3,891	3,855	3,901	3,880	3,891	3,914	3,894
Fe	2,748	2,794	2,915	3,223	3,501	3,779	3,894	3,528	3,378	3,513	3,745	3,829	3,919	3,323	3,058	2,944	2,767	2,718	2,836	2,966	3,196	3,444	4,041	4,018
Mn	1,596	1,504	1,384	1,049	0,635	0,299	0,050	0,057	0,066	0,054	0,047	0,126	0,088	0,659	1,102	1,411	1,406	1,495	1,381	1,238	0,938	0,558	0,079	0,050
Mg	0,128	0,127	0,151	0,164	0,205	0,227	0,255	0,355	0,365	0,393	0,391	0,311	0,268	0,185	0,150	0,150	0,131	0,142	0,144	0,147	0,160	0,179	0,273	0,288
Ca	1,626	1,707	1,718	1,700	1,803	1,827	1,926	2,193	2,236	2,098	2,002	1,888	1,866	1,943	1,814	1,679	1,819	1,836	1,781	1,793	1,868	1,980	1,779	1,716
Na	0,007	0,000	0,014	0,018	0,011	0,009	0,003	0,019	0,017	0,004	0,018	0,007	0,010	0,010	0,000	0,013	0,006	0,013	0,000	0,013	0,000	0,000	0,000	0,020
K	0,001	0,000	0,000	0,000	0,000	0,003	0,000	0,000	0,000	0,002	0,002	0,002	0,002	0,003	0,000	0,000	0,000	0,000	0,000	0,003	0,000	0,002	0,000	0,000
Cr	0,012	0,004	0,011	0,003	0,004	0,000	0,003	0,009	0,000	0,007	0,003	0,008	0,005	0,001	0,006	0,007	0,002	0,008	0,007	0,003	0,005	0,000	0,008	0,010
Total	16,020	16,038	16,065	16,056	16,055	16,052	16,039	16,049	16,019	16,011	16,091	16,056	16,049	16,035	16,029	16,062	16,034	16,072	16,029	16,058	16,047	16,055	16,058	16,016
Mg	0,128	0,127	0,151	0,164	0,205	0,227	0,255	0,355	0,365	0,393	0,391	0,311	0,268	0,185	0,150	0,150	0,131	0,142	0,144	0,147	0,160	0,179	0,273	0,288
Mn	1,596	1,504	1,384	1,049	0,635	0,299	0,050	0,057	0,066	0,054	0,047	0,126	0,088	0,659	1,102	1,411	1,406	1,495	1,381	1,238	0,938	0,558	0,079	0,050
Ca	1,626	1,707	1,718	1,700	1,803	1,827	1,926	2,193	2,236	2,098	2,002	1,888	1,866	1,943	1,814	1,679	1,819	1,836	1,781	1,793	1,868	1,980	1,779	1,716
FeII	2,649	2,662	2,747	3,086	3,357	3,646	3,769	3,396	3,333	3,456	3,560	3,676	3,778	3,214	2,935	2,761	2,645	2,527	2,694	2,822	3,034	3,283	3,869	3,946
Total X	6,000	6,000	6,000	6,000	6,000	6,000	6,000	6,000	6,000	6,000	6,000	6,000	6,000	6,000	6,000	6,000	6,000	6,000	6,000	6,000	6,000	6,000	6,000	6,000
rest Fe	0,099	0,132	0,167	0,136	0,145	0,133	0,125	0,132	0,044	0,058	0,185	0,153	0,141	0,109	0,123	0,183	0,123	0,192	0,143	0,145	0,163	0,161	0,171	0,072
Si	5,998	5,984	5,951	5,984	5,970	5,991	5,990	5,989	6,003	6,008	5,934	5,971	5,996	6,008	5,994	5,994	6,004	5,951	6,014	5,978	5,982	5,987	5,964	6,025
Aliv	0,002	0,016	0,049	0,016	0,030	0,009	0,010	0,011	0,000	0,000	0,066	0,029	0,004	0,000	0,006	0,006	0,000	0,049	0,000	0,022	0,018	0,013	0,036	0,000
Total Z	6,000	6,000	6,000	6,000	6,000	6,000	6,000	6,000	6,003	6,008	6,000	6,000	6,000	6,008	6,000	6,000	6,004	6,000	6,014	6,000	6,000	6,000	6,000	6,025
Alvi	3,896	3,886	3,869	3,893	3,882	3,895	3,901	3,890	3,937	3,933	3,878	3,881	3,886	3,885	3,882	3,860	3,882	3,842	3,855	3,879	3,863	3,879	3,878	3,894
Cr	0,012	0,004	0,011	0,003	0,004	0,000	0,003	0,009	0,000	0,007	0,003	0,008	0,005	0,001	0,006	0,007	0,002	0,008	0,007	0,003	0,005	0,000	0,008	0,010
Ti	0,018	0,020	0,015	0,009	0,018	0,011	0,011	0,008	0,018	0,007	0,008	0,012	0,009	0,019	0,023	0,006	0,020	0,025	0,017	0,018	0,022	0,013	0,008	0,006
FeIII	0,099	0,132	0,167	0,136	0,145	0,133	0,125	0,132	0,044	0,058	0,185	0,153	0,141	0,109	0,123	0,183	0,123	0,192	0,143	0,145	0,163	0,161	0,171	0,072
Total Y	4,025	4,042	4,062	4,042	4,049	4,039	4,040	4,039	4,000	4,005	4,074	4,054	4,041	4,015	4,035	4,057	4,026	4,067	4,022	4,044	4,053	4,053	4,066	3,981
Alm(%)	44,152	44,366	45,792	51,439	55,945	60,770	62,824	56,596	55,556	57,596	59,333	61,263	62,967	53,570	48,910	46,010	44,077	42,114	44,899	47,031	50,560	54,718	64,488	65,771
Prp(%)	2,139	2,111	2,521	2,738	3,415	3,792	4,257	5,910	6,078	6,543	6,509	5,176	4,466	3,076	2,495	2,494	2,177	2,366	2,395	2,451	2,660	2,982	4,550	4,793
Sps(%)	26,602	25,074	23,060	17,483	10,591	4,988	0,826	0,948	1,103	0,898	0,783	2,093	1,468	10,978	18,359	23,516	23,436	24,921	23,014	20,629	15,642	9,302	1,318	0,839
Grs(%)	26,238	27,352	27,265	27,296	28,816	29,364	30,985	35,202	36,683	34,337	31,767	30,127	29,902	31,331	29,089	26,626	29,221	28,905	28,457	28,667	29,677	31,583	28,277	27,969
And(%)	0,786	1,069	1,282	1,020	1,205	1,087	1,081	1,264	0,580	0,562	1,582	1,281	1,161	1,034	1,099	1,306	1,073	1,633	1,180	1,202	1,419	1,415	1,311	0,556
Uva(%)	0,083	0,028	0,080	0,024	0,028	0,000	0,027	0,079	0,000	0,064	0,026	0,060	0,036	0,010	0,048	0,048	0,015	0,062	0,055	0,020	0,042	0,000	0,058	0,072
Prp	2,139	2,111	2,521	2,738	3,415	3,792	4,257	5,910	6,078	6,543	6,509	5,176	4,466	3,076	2,495	2,494	2,177	2,366	2,395	2,451	2,660	2,982	4,550	4,793
Alm+Sps	70,754	69,441	68,852	68,922	66,536	65,757	63,650	57,544	56,659	58,494	60,116	63,356	64,435	64,549	67,269	69,526	67,513	67,035	67,913	67,660	66,202	64,020	65,805	66,610
Grs+And	27,024	28,421	28,547	28,316	30,021	30,451	32,066	36,466	37,263	34,899	33,349	31,408	31,062	32,365	30,188	27,932	30,295	30,538	29,636	29,869	31,096	32,998	29,587	28,525

Table 5.11 continue

sample no	M98-99/2 (Belevi)		
analyse no	m1-75	m1-76	m1-77 r
SiO2	33,47	37,81	37,40
TiO2	0,13	0,04	0,07
Al2O3	18,45	20,60	20,69
FeO	24,81	25,78	26,21
MnO	0,32	0,39	0,50
MgO	1,50	1,75	1,84
CaO	10,56	12,72	12,31
Na2O	0,11	0,00	0,02
K2O	0,02	0,02	0,01
Cr2O3	0,02	0,06	0,09
Total	89,38	99,17	99,13
normalized oxygens 24			
Si	5,974	6,037	5,989
Ti	0,017	0,005	0,008
Al	3,882	3,877	3,905
Fe	3,703	3,442	3,509
Mn	0,049	0,052	0,068
Mg	0,399	0,416	0,439
Ca	2,019	2,176	2,112
Na	0,037	0,000	0,005
K	0,005	0,005	0,002
Cr	0,002	0,007	0,011
Total	16,085	16,011	16,038
Mg	0,399	0,416	0,439
Mn	0,049	0,052	0,068
Ca	2,019	2,176	2,112
FeII	3,533	3,356	3,381
Total X	6,000	6,000	6,000
rest Fe	0,170	0,086	0,129
Si	5,974	6,037	5,989
Aliv	0,026	0,000	0,011
Total Z	6,000	6,037	6,000
Alvi	3,856	3,877	3,894
Cr	0,002	0,007	0,011
Ti	0,017	0,005	0,008
FeIII	0,170	0,086	0,129
Total Y	4,046	3,976	4,041
Alm(%)	58,883	55,926	56,345
Prp(%)	6,647	6,941	7,319
Sps(%)	0,814	0,868	1,139
Grs(%)	32,082	35,365	33,912
And(%)	1,555	0,837	1,190
Uva(%)	0,020	0,063	0,094
Prp	6,647	6,941	7,319
Alm+Sps	59,696	56,794	57,485
Grs+And	33,637	36,202	35,103

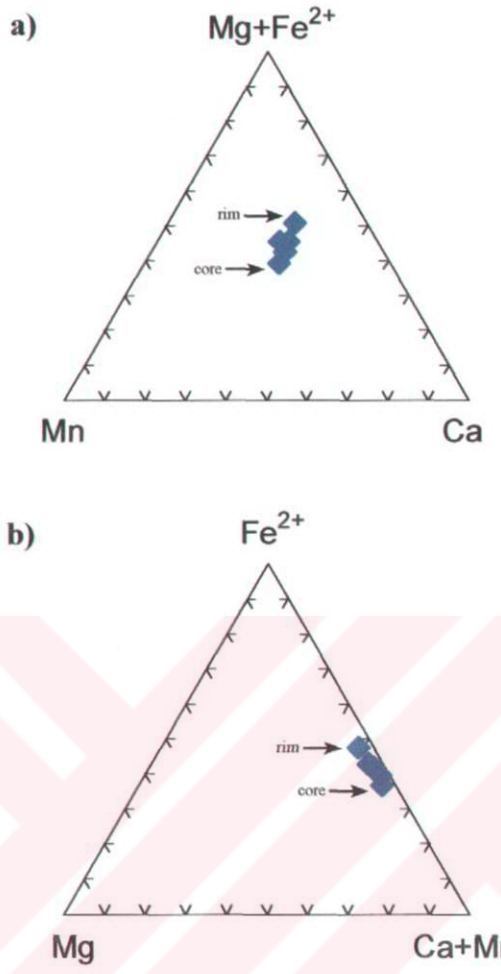


Figure 5.38 Ternary atomic proportions of Alm+Prp-Sps-Grs (a) and Alm-Prp-Grs+Sps (b) for a garnet grain from garnet-amphibolite sample (M97-149/10) in metaolistostrome unit.

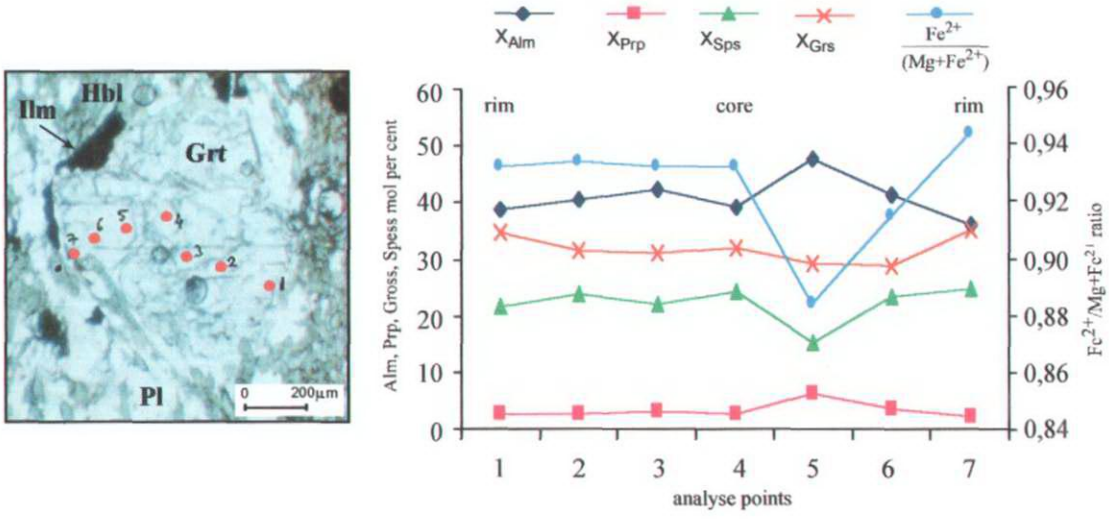


Figure 5.39 Garnet photomicrograph in plane polarized light and composition of selected garnet grain in M97-149/10. Traverse is from rim to rim.

garnet (Figure 5.42b). This zone probably represents the peak conditions of blueschist stage. Zoning maps of five elements and the profiles of end-members are given in Figure 5.42b and Figure 5.42c,d, respectively. The garnet shows almost symmetric zoning patterns. Normal growth zoning, characterized by a bell-shaped Mn profile and by increase Mg and decrease $Fe^{2+}/(Fe^{2+}+Mg)$ profiles towards rim, is observed in core and mantle section of the garnet. X_{Grs} increases in very small rate along core and mantle. Transition from core to mantle is pronounced in X_{Alm} and X_{Sps} (Figure 5.42b,c,d). Decrease of profile slopes commonly defines this transition. Profiles in the rim demonstrate retrograde garnet growth zoning. Except for X_{Grs} and X_{Prp}, inverse X_{Alm} and X_{Sps} profiles are observed in rim (Figure 5.42c).

The core section of garnet is inclusion-free forms the richest part of garnet in terms of X_{Sps}. Mantle and rim have got minimum X_{Sps} content. This can not be explained by diffusional effects. Minimum X_{Sps} and maximum X_{Alm} contents in mantle can be expressed by garnet growth connected with forming of different reaction assemblages from core. The boundary between core and mantle is not smooth, but represented by a cloudy zone (Figure 5.42a). This irregular boundary can be observed in the garnet-Mn map too (Figure 5.42b). This wavy rim represents garnet-consuming reactions. Tiny and bluish coloured zoisite inclusions that are in equilibrium with omphacite in eclogites exist in the mantle. Zoisite inclusions occur mostly in mantle part of garnet (10-32). But, there is no zoisite in the mineral assemblage of matrix. Prominent Fe-enrichment is limited to the mantle (Figure 5.42b). The Fe-rich section, named mantle, demonstrates an increase in (especially) pressure together with heating. The boundary between mantle and rim is not texturally sharp and clear (Figure 5.42a). Increasing X_{Grs} and X_{Prp} and decreasing X_{Alm} in the rim are usually indicative of growth during heating at lower pressures relative to the mantle.

Cation totals per formula unit range from 16.011 to 16.091 in second garnet grain (**61-77**) from sample **M98-99/2** (Table 5.11). These values are close to the ideal stoichiometric value of 16.00. Si (5.934 – 6.037), octahedrally coordinated aluminium (3.842 – 3.894), Ti (0.005 – 0.025) and Cr (0.00- 0.011) atoms per

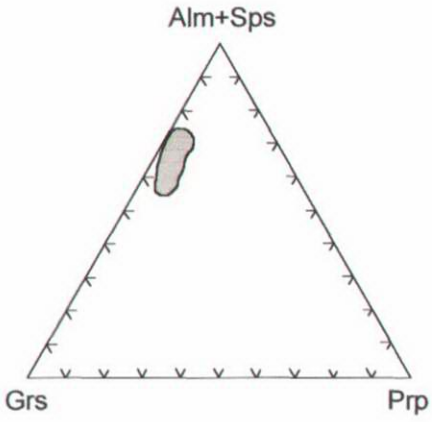


Figure 5.40 In almandine+spessartine - grossular - pyrope ternary diagram, location of selected garnet grains from metaolistostrome matrix.

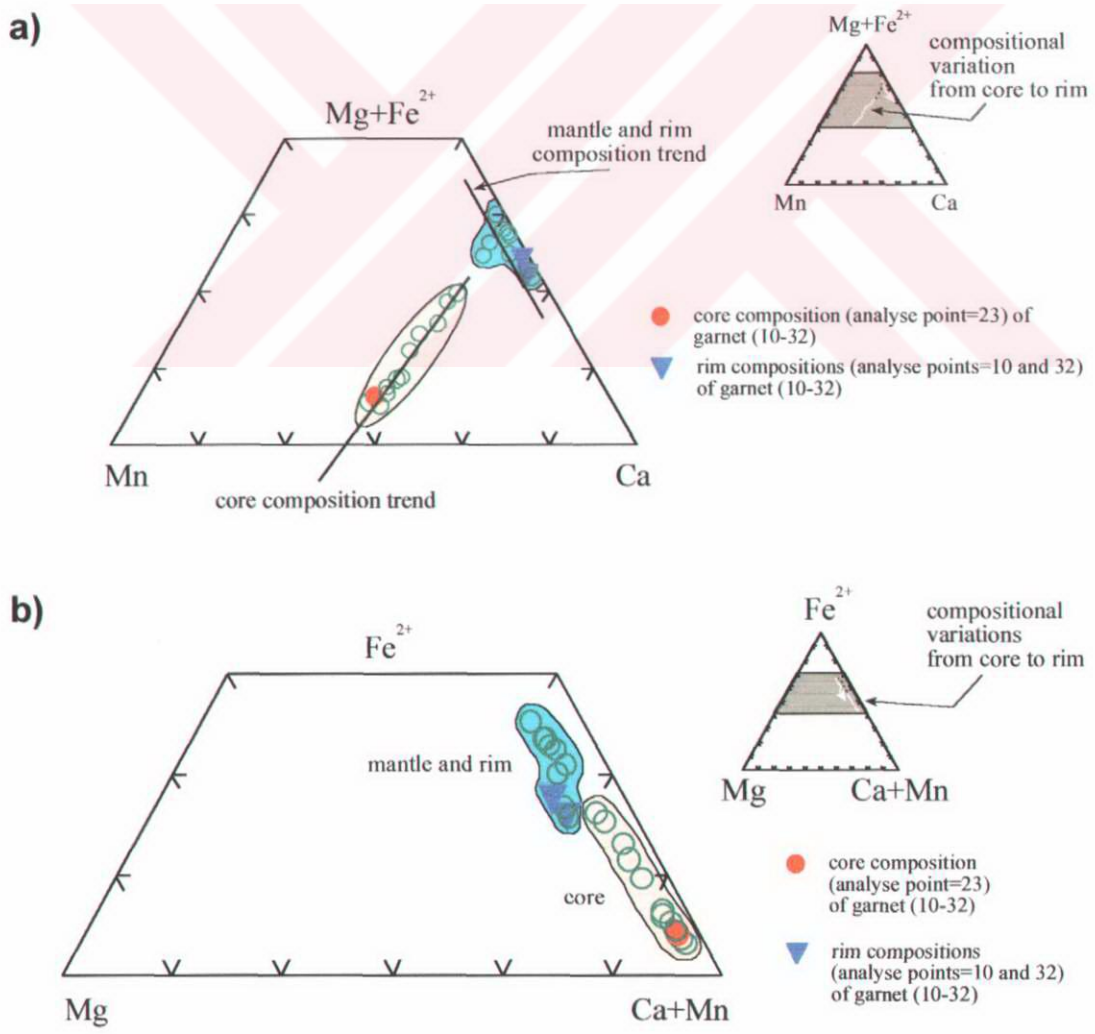


Figure 5.41 Ternary atomic proportions of Alm+Prp-Sps-Grs (a) and Alm-Prp-Grs+Sps (b) for garnet (10-32) from garnet-phengite schist (M98-99/2).

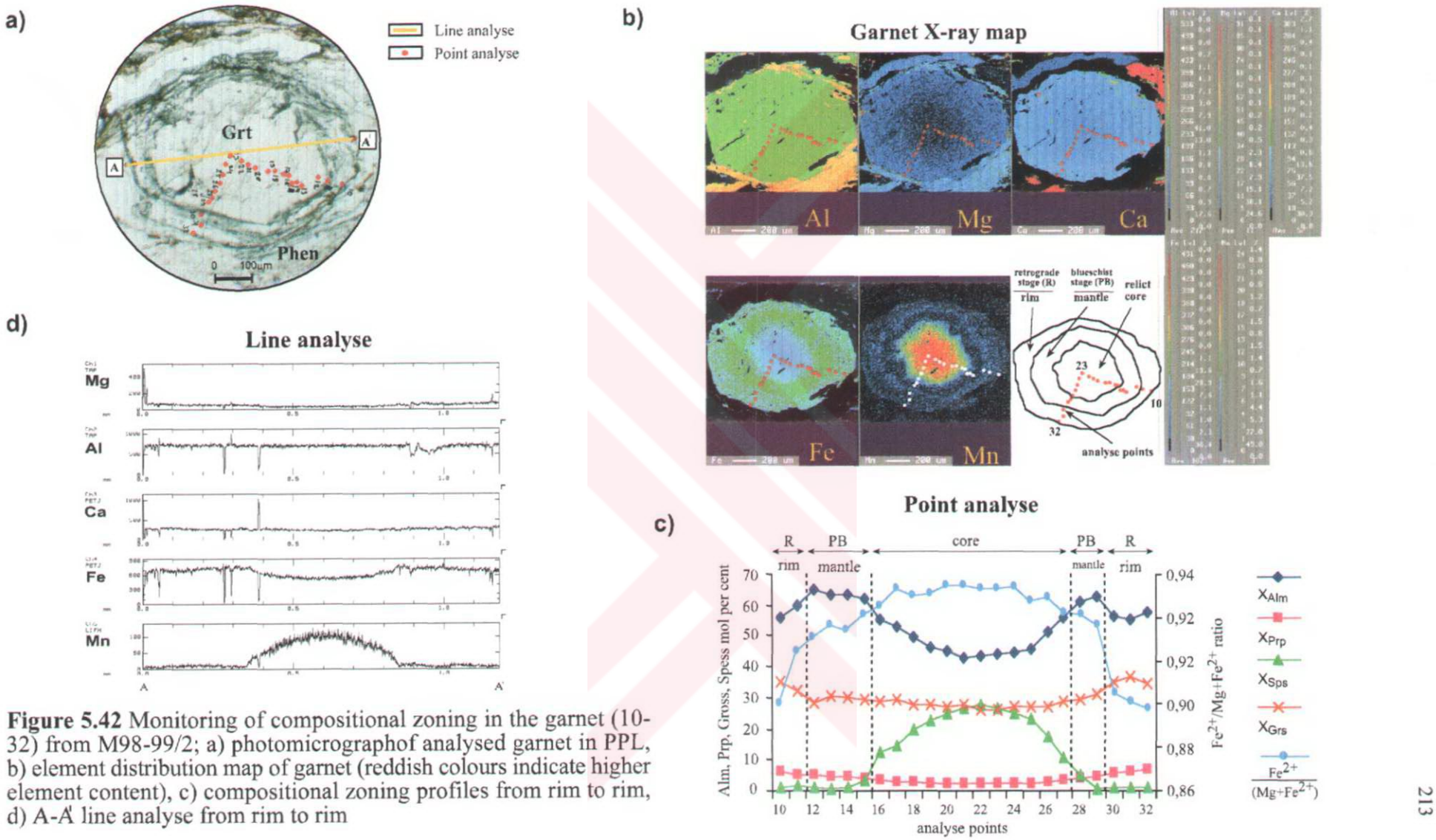


Figure 5.42 Monitoring of compositional zoning in the garnet (10-32) from M98-99/2; a) photomicrographof analysed garnet in PPL, b) element distribution map of garnet (reddish colours indicate higher element content), c) compositional zoning profiles from rim to rim, d) A-A' line analyse from rim to rim

garnet formula unit are observed in these ranges. Al(VI) averages 3.875 per 24 oxygens. The amount of ferric iron ranges from 0.072 to 0.192. The proportions of Ca, Fe^{2+}, Mg and Mn for this garnet are illustrated in Figure 5.43. According to this diagram, core (relict core) and mantle (overgrowth) – rim compositions are quite different. Core and mantle compositional trends are almost perpendicular each other. This shows that core and mantle growth occured in different reaction assemblages. Garnet which is composed of average 69 percent pyralspite and 31 percent ugrandite series is rich-in almandine (average 54 mol%) (Figure 5.43). Core and rim compositions of the garnet are "Alm_{43} Prp_2 Grs_{29} Sps_{26}" and "Alm_{57} Prp_8 Grs_{34} Sps_1", respectively. Average compositions belonging to core, mantle and rim are given in Table 5.12. Compositional discontinuity (gap) between core and mantle is exist (Figure 5.43a-5.43b). The core shows a composition trend almost parallel to $Mg+Fe^{2+}$ - Mn edge of triangle while mantle and rim compositions concentrate near to $Mg+Fe^{2+}$ - Ca edge (Figure 5.43a).

Table 5.12 Average end-member compositions of the garnet (61-77) belonging to core, mantle and rim.

	Average compositions
Core	Alm_{48} Prp_3 Sps_{19} Grs_{30}
Mantle	Alm_{65} Prp_5 Sps_1 Grs_{29}
Rim	Alm_{59} Prp_7 Sps_1 Grs_{33}

Garnet (**61-77**) that is 1310 microns in diameter can be described as a subhedral crystal shape with badly formed crystal faces. This garnet shows optical zonation in core, mantle and rim sections (Figure 5.44a). The mantle and rim are belong to a blueschist stage (PB) and retrograde stage (R), respectively, while the core section named as relict core. The chemistry and zonation structure of the garnet are illustrated by line and point analyses (Figure 5.44b,c). The core section of the garnet is inclusion-free. X_{Alm} content in the core increases regularly towards the mantle boundary, balanced by a decrease in X_{Sps}. The characteristic bell-shaped curve of X_{Sps} is restricted to the core. X_{Grs} irregularly and X_{Prp} gradually increase towards the

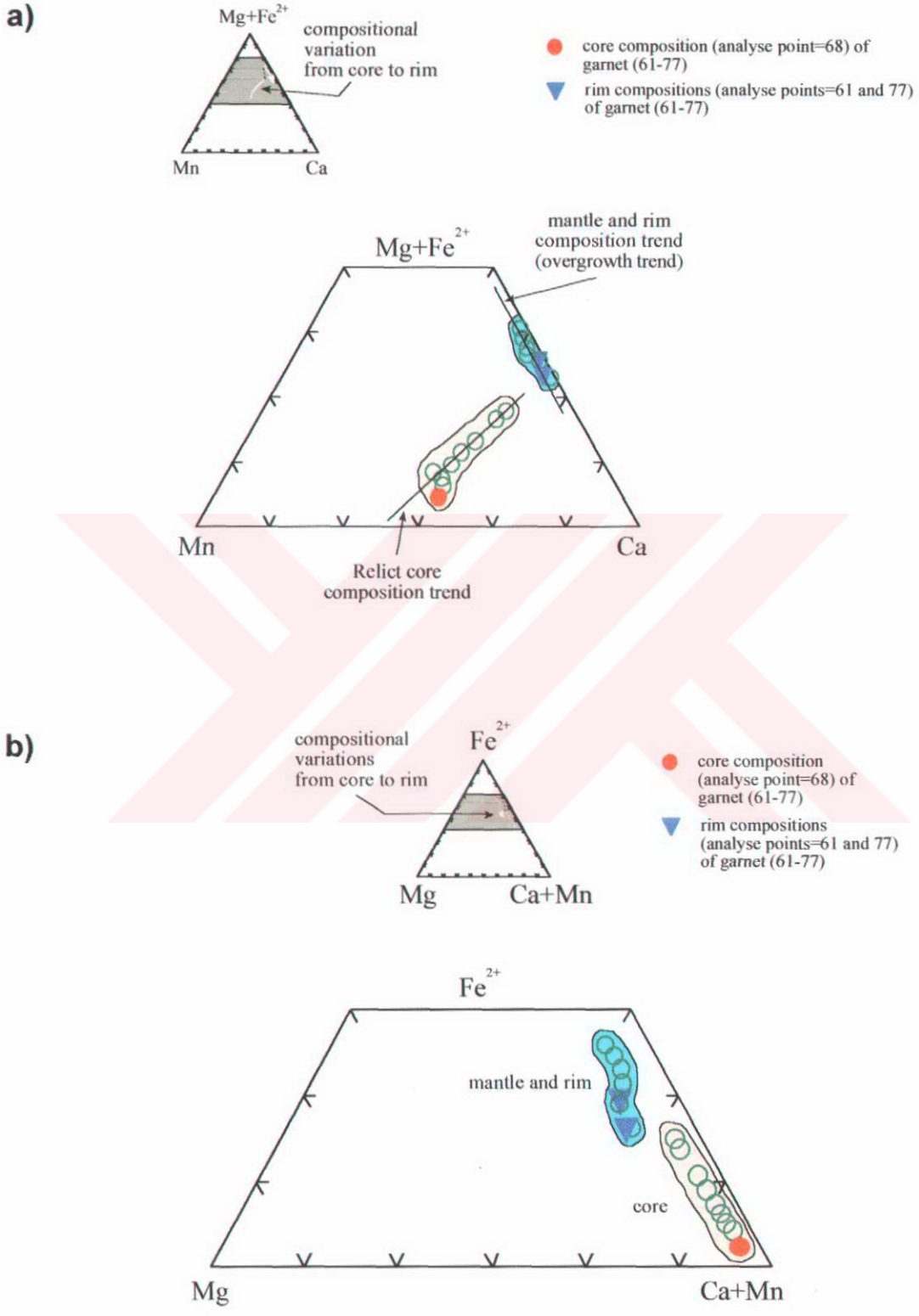


Figure 5.43 Ternary atomic proportions of Alm+Prp-Sps-Grs (a) and Alm-Prp-Grs+Sps (b) for garnet (61-77) from garnet-phengite schist (M98-99/2).

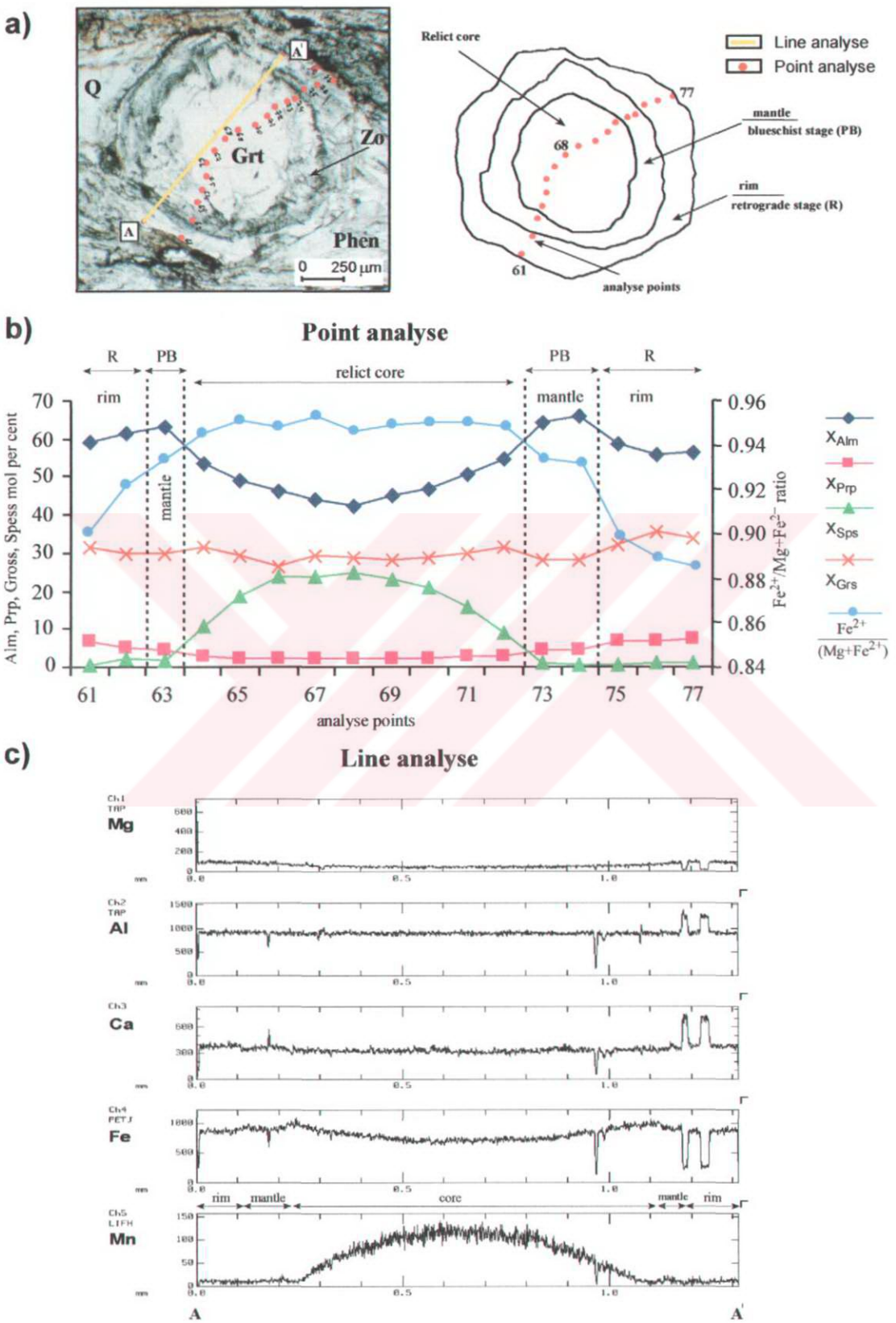


Figure 5.44 Compositional zoning in the garnet (61-77) from M98-99/2; a) microphoto of analysed garnet in PPL, b) element zoning profiles from rim to rim , c) A-A' line analyse from rim to rim.

limit of the core. This may display heating from core to rim. $Fe^{2+}/(Fe^{2+}+Mg)$ ratio is almost flat in the core except close to mantle boundary. This shows that there is no important change in metamorphic grade during core growth. The core – mantle boundary can be seen optically. Prominent differences in the evolution of the element profiles are recognized between core and mantle. When compared with the core, especially X_{Alm} and X_{Prp} increase, while X_{Grs}, X_{Sps} and $Fe^{2+}/(Fe^{2+}+Mg)$ ratios decrease in the mantle. These trends are interpreted as effect of increasing pressure. Small, bluish coloured zoisite inclusions also exist in the mantle. This also supports the increase in pressure. The boundary between mantle and rim is more pronounced than that of mantle and core. The rim is characterized by the tiny and cloudy inclusions (graphite ?). The mantle – rim boundary is rounded by a corrosion stage. Consuming reactions are probably related with decompression. Increasing of X_{Grs} and X_{Prp} contents and decreasing of X_{Alm} may be indicative of the retrograde garnet growth. Partial increase in X_{Sps} and decrease in $Fe^{2+}/(Fe^{2+}+Mg)$ ratio are additional evidence for garnet growth during the decompression.

Sample two: In selected garnet grain (**36-46**) from sample **94-30**, cation proportions based on one formula unit of garnet appear a somewhat high: the range of total cations is 16.058 - 16.095 with an averages of 16.077 which is close to the ideal stoichiometric value of 16.00 (Table 5.11). Minor amounts of Al are assigned to tetrahedral sites, averaging 0.061 based on one formula unit; Al(VI) averages 3.873 in lower of the ideal value 4.00. Alkalis, Cr and Ti are present in insignificant proportions. The amounts of ferric iron ranges from 0.129 to 0.219. Andradite content of the garnet is not high. Therefore, compositional variation of this garnet may be shown in quaternary solid solution system composed of almandine, pyrope, grossular and spessartine. Core and rim composition of analysed garnet (94-30) is given in Figure 5.45. This garnet that belongs to pyralspite series is rich in almandine. Core and rim compositions of the garnet are "Alm_{68} Prp_5 Grs_{25} Sps_2" and "Alm_{62} Prp_6 Grs_{31} Sps_1", respectively.

The garnet (**36-46**) that is 1430 microns in diameter is anhedral with badly developed crystal faces (Figure 5.46a). Two zones; a core with intense zoisite

inclusions (blueschist stage-PB) and tiny-cloudy inclusion-rich rim (retrograde stage-R), are optically distinguished in this garnet. Chemical zonation of garnet (36-46) is given in Figure 5.46b-5.46c. Patterns in Figure 5.46b are similar to mantle and rim garnet growths of garnet (61-77) in M98-99/2 (Figure 5.44b). Mantle and rim were interpreted as a prograde (PB) and retrograde (R) garnet growths in Figure 5.44b, respectively. The same is valid for garnet (36-46) in sample 94-30.

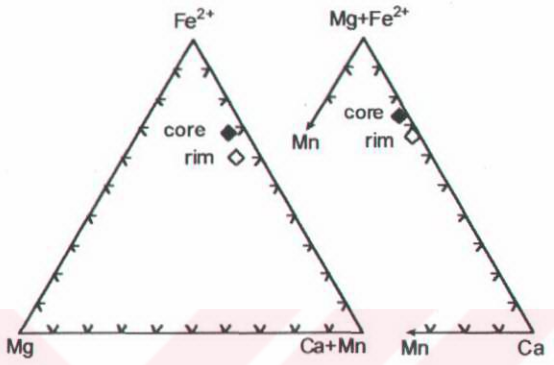


Figure 5.45 Ternary atomic proportions of Alm - Prp - Gross + Spess and of Alm + Prp - Spess - Gross for garnet (36-46) from 94-30.

5.4.1.5. Garnets in marble-schist series

Two samples were chosen from Akkoyunlu-**M97-36** (northwest of Tire) and Akyurt-**M99-52/5** (northeasth of Ortaklar). The general mineral assemblage of these two samples is "garnet – biotite - white mica – chlorite – plagioclase - quartz". Garnet analyses are given in Table 5.13. The end-members of the garnet can be given as follows: almandine 57 – 71 mol%, pyrope 3 – 4 mol%, grossular 22 – 27 mol%, spessartine 1 – 12 mol% and andradite 0 – 0.5 mol%. In the pyrope – (almandine + spessartine) – grossular ternary diagram (Figure 5.47), garnet compositions plot close to almandine + spessartine corner.

Sample one: Cation sums of the garnet (**1-9**) from sample **M97-36** range from 15.990 to 16.028 (Table 5.13). A minor amount of aluminium is assigned to tetrahedral sites with an average value of 0.004 based on one formula unit. Whereas the average value of Al(VI) is 3.942. The rest of this site is filled by Fe^{3+}, Cr and Ti.

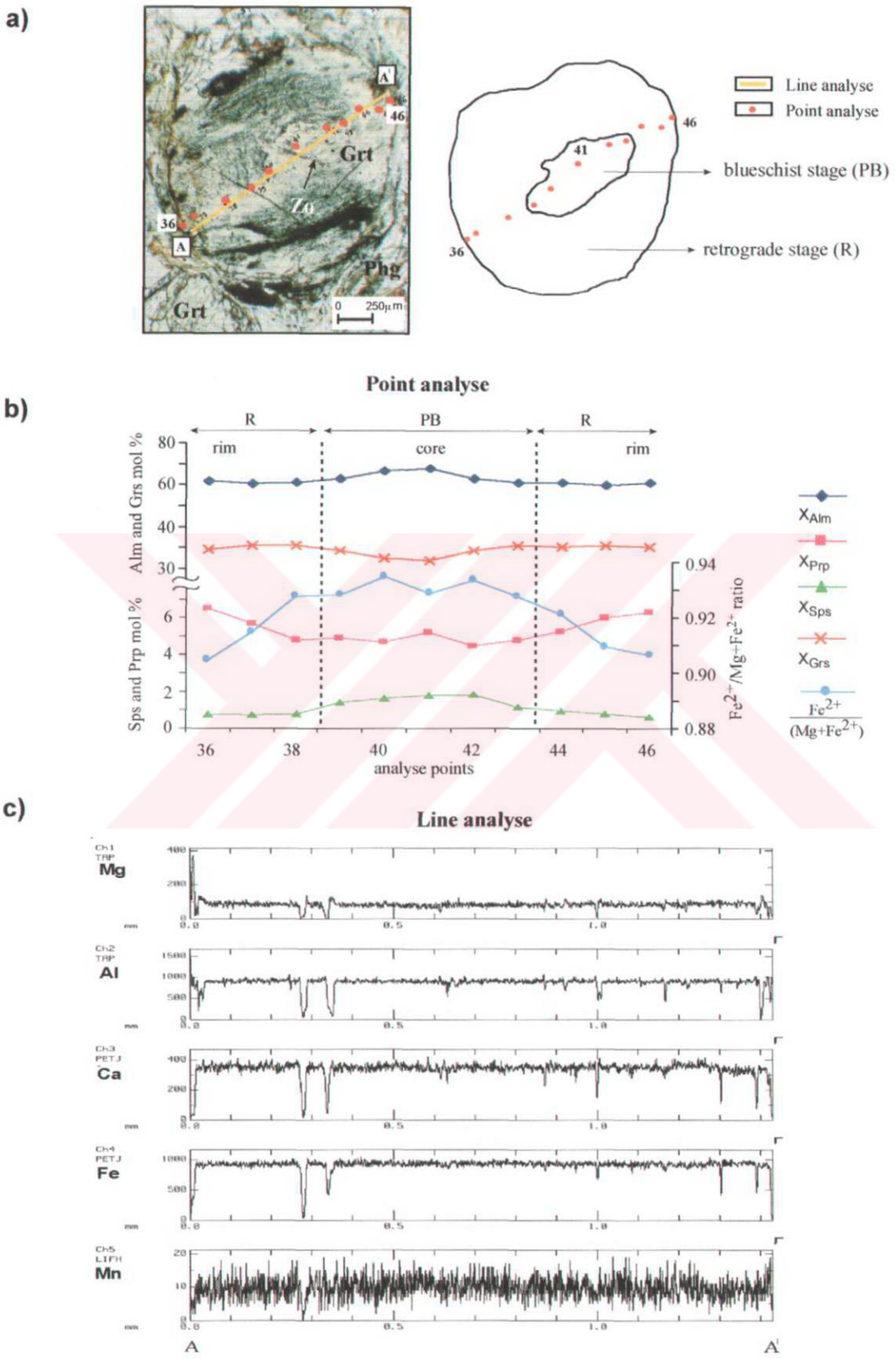


Figure 5.46 Compositional zoning in the garnet (36-46) from sample 94-30; a) microphoto of analysed garnet in PPL, b) element zoning profiles from rim to rim , c) A-A' line analyse from rim to rim.

Table 5.13 Representative garnet analyses from the Marble-schist series in Tire (Akkoyunlu) and Tire (Akyurt) (r: rim, c: core).

sample no	M97-36 (Akkoyunlu)									M99-52/5 (Akyurt)							
analyse no	m17-1 r	m17-2	m17-3	m17-4	m17-5 c	m17-6	m17-7	m17-8	m17-9 r	m18-12r	m18-13	m18-14	m18-15	m18-16	m18-17	m18-18	m18-19r
SiO2	37,67	37,74	37,84	37,64	37,49	37,89	37,74	37,93	37,63	37,83	37,61	37,98	37,86	37,81	37,73	37,59	37,70
TiO2	0,09	0,18	0,14	0,18	0,12	0,10	0,05	0,06	0,09	0,10	0,09	0,09	0,17	0,14	0,11	0,07	0,03
Al2O3	21,16	21,02	20,83	20,85	21,10	21,18	21,13	21,02	20,97	21,13	21,16	20,97	20,89	20,80	20,99	20,88	21,28
FeO	30,62	28,74	28,01	26,48	26,97	26,70	29,55	32,29	30,24	29,23	28,52	27,02	26,27	26,13	27,79	29,05	29,00
MnO	0,96	2,77	3,80	5,55	5,67	5,14	2,27	0,89	0,76	2,35	3,67	5,26	6,39	6,22	5,18	3,55	2,59
MgO	1,14	0,98	0,91	0,84	0,92	0,86	0,92	1,10	1,11	1,10	1,07	0,93	0,90	0,87	0,94	1,14	1,15
CaO	9,32	9,35	9,06	9,25	8,53	9,27	9,08	7,94	9,74	9,19	8,47	8,72	8,86	8,65	8,30	8,32	8,83
Na2O	0,08	0,02	0,08	0,02	0,04	0,02	0,03	0,00	0,00	0,00	0,01	0,11	0,07	0,08	0,03	0,00	0,04
K2O	0,00	0,00	0,00	0,01	0,01	0,00	0,00	0,00	0,00	0,00	0,00	0,00	0,00	0,00	0,00	0,00	0,00
Cr2O3	0,06	0,09	0,05	0,07	0,00	0,01	0,06	0,05	0,02	0,05	0,03	0,07	0,03	0,07	0,06	0,01	0,12
Total	101,09	100,89	100,72	100,88	100,84	101,17	100,83	101,29	100,55	100,98	100,62	101,15	101,43	100,76	101,13	100,61	100,73
normalized oxygens 24																	
Si	5,982	6,002	6,032	6,002	5,984	6,011	6,009	6,025	6,001	6,007	6,000	6,031	6,009	6,032	6,007	6,009	5,998
Ti	0,010	0,022	0,017	0,021	0,014	0,012	0,006	0,007	0,010	0,011	0,010	0,011	0,020	0,017	0,013	0,008	0,004
Al	3,961	3,941	3,914	3,919	3,970	3,960	3,965	3,936	3,942	3,955	3,979	3,925	3,908	3,912	3,939	3,935	3,990
Fe	4,066	3,822	3,734	3,531	3,600	3,542	3,934	4,289	4,032	3,881	3,805	3,588	3,486	3,486	3,700	3,883	3,858
Mn	0,128	0,373	0,513	0,749	0,766	0,691	0,306	0,120	0,103	0,316	0,496	0,707	0,859	0,840	0,698	0,481	0,349
Mg	0,270	0,232	0,215	0,200	0,218	0,203	0,219	0,261	0,263	0,261	0,254	0,221	0,212	0,206	0,223	0,271	0,271
Ca	1,586	1,593	1,547	1,580	1,459	1,575	1,549	1,351	1,664	1,563	1,448	1,483	1,506	1,478	1,416	1,425	1,505
Na	0,024	0,007	0,024	0,006	0,013	0,005	0,009	0,000	0,000	0,000	0,003	0,032	0,020	0,023	0,010	0,000	0,012
K	0,000	0,000	0,000	0,001	0,002	0,000	0,000	0,000	0,000	0,000	0,000	0,000	0,000	0,000	0,000	0,000	0,000
Cr	0,007	0,011	0,007	0,008	0,000	0,001	0,007	0,007	0,002	0,006	0,004	0,009	0,004	0,008	0,007	0,001	0,015
Total	16,028	15,993	15,996	16,009	16,025	15,998	15,996	15,990	16,015	15,995	15,996	15,999	16,021	15,995	16,005	16,013	15,987
Mg	0,270	0,232	0,215	0,200	0,218	0,203	0,219	0,261	0,263	0,261	0,254	0,221	0,212	0,206	0,223	0,271	0,271
Mn	0,128	0,373	0,513	0,749	0,766	0,691	0,306	0,120	0,103	0,316	0,496	0,707	0,859	0,840	0,698	0,481	0,349
Ca	1,586	1,593	1,547	1,580	1,459	1,575	1,549	1,351	1,664	1,563	1,448	1,483	1,506	1,478	1,416	1,425	1,505
FeII	4,016	3,802	3,724	3,470	3,557	3,531	3,927	4,268	3,970	3,860	3,802	3,588	3,423	3,475	3,663	3,823	3,858
Total X	6,000	6,000	6,000	6,000	6,000	6,000	6,000	6,000	6,000	6,000	6,000	5,999	6,000	6,000	6,000	6,000	5,983
rest Fe	0,050	0,021	0,009	0,060	0,042	0,010	0,007	0,021	0,062	0,021	0,003	0,000	0,064	0,011	0,037	0,060	0,000
Si	5,982	6,002	6,032	6,002	5,984	6,011	6,009	6,025	6,001	6,007	6,000	6,031	6,009	6,032	6,007	6,009	5,998
Aliv	0,018	0,000	0,000	0,000	0,016	0,000	0,000	0,000	0,000	0,000	0,000	0,000	0,000	0,000	0,000	0,000	0,002
Total Z	6,000	6,002	6,032	6,002	6,000	6,011	6,009	6,025	6,001	6,007	6,000	6,031	6,009	6,032	6,007	6,009	6,000
Alvi	3,943	3,941	3,914	3,919	3,954	3,960	3,965	3,936	3,942	3,955	3,979	3,925	3,908	3,912	3,939	3,935	3,988
Cr	0,007	0,011	0,007	0,008	0,000	0,001	0,007	0,007	0,002	0,006	0,004	0,009	0,004	0,008	0,007	0,001	0,015
Ti	0,010	0,022	0,017	0,021	0,014	0,012	0,006	0,007	0,010	0,011	0,010	0,011	0,020	0,017	0,013	0,008	0,004
FeIII	0,050	0,021	0,009	0,060	0,042	0,010	0,007	0,021	0,062	0,021	0,003	0,000	0,064	0,011	0,037	0,060	0,000
Total Y	4,011	3,994	3,947	4,008	4,010	3,984	3,986	3,971	4,016	3,994	3,996	3,945	3,996	3,947	3,996	4,005	4,007
Alm(%)	66,934	63,361	62,075	57,841	59,288	58,858	65,443	71,125	66,170	64,330	63,370	59,804	57,045	57,916	61,048	63,716	64,477
Prp(%)	4,497	3,868	3,588	3,331	3,628	3,377	3,643	4,352	4,377	4,347	4,237	3,677	3,532	3,436	3,717	4,523	4,538
Sps(%)	2,141	6,219	8,550	12,492	12,774	11,509	5,101	2,002	1,720	5,267	8,265	11,791	14,315	14,007	11,640	8,011	5,832
Grs(%)	25,982	26,198	25,573	25,748	23,969	26,103	25,681	22,319	27,218	25,801	24,029	24,605	24,554	24,417	23,260	23,334	25,036
And(%)	0,397	0,281	0,170	0,534	0,341	0,146	0,084	0,164	0,499	0,213	0,077	0,068	0,527	0,172	0,293	0,407	0,023
Uva(%)	0,049	0,074	0,044	0,054	0,000	0,007	0,048	0,038	0,016	0,042	0,023	0,054	0,027	0,051	0,042	0,008	0,093
Prp	4,497	3,868	3,588	3,331	3,628	3,377	3,643	4,352	4,377	4,347	4,237	3,677	3,532	3,436	3,717	4,523	4,538
Alm+Sps	69,075	69,580	70,625	70,333	72,062	70,367	70,544	73,128	67,890	69,597	71,635	71,596	71,360	71,923	72,688	71,727	70,310
Grs+And	26,379	26,479	25,743	26,282	24,310	26,249	25,765	22,482	27,718	26,014	24,106	24,673	25,081	24,590	23,552	23,741	25,060

The andradite content of the garnet ranges from 0.084 mol% to 0.584 mol% and is negligible. Fe^{2+} / Mg / Ca / Mn ratios for the garnet are given in Figure 5.48. According to Figure 5.48, the garnet is a calcium-, mangenese- and magnesium-bearing almandine. Garnet which is composed of average 74 percent pyralspite and 26 percent ugrandite series is rich-in almandine (average 63 mol%) and grossular (average 25 mol%). Core and rim compositions of the garnet are "Alm_{60} Prp_3 Grs_{24} Sps_{13}" and "Alm_{68} Prp_4 Grs_{26} Sps_2", respectively.

Garnet (**1-9**) which is 850 microns in diameter has a subhedral crystal form. The garnet does not display textural zonation. A broad bell- shaped X_{Sps} profile and slight increasing of X_{Alm} and X_{Prp} content from core to rim mark the growth zoning (Figure 5.49b,c). In addition, $Fe^{2+}/(Fe^{2+}+Mg)$ pattern also supports this idea. Growth occurred probably in an blueschist stage (PB). Maximum X_{Sps} and minimum X_{Alm} – X_{Prp} contents of the garnet are observed in the core. This may represent relatively low-temperature conditions when compared to the rim. Increase of X_{Alm} and decrease of X_{Sps} are observed at the core – rim boundary. X_{Alm} , X_{Grs} and X_{Sps}. express increasing in pressure and temperature in the core of the garnet (Figure 5.49b). According to the end-member profiles, the core section of the garnet represents a prograde growth. Whereas, garnet growth in the rim should not have occurred during the retrograde stage (R). Difference between peak and minimum values of end-members are not big. All end-members profiles show a distribution near to the rim. X_{Alm} and X_{Grs} patterns display reversals in the rim. The reversals and flat profiles may be related with post-growth diffusion effects.

Sample two: Cation totals per formula unit range from 15.987 to 16.021 in garnet crystal (**12-19**) from sample **M99-52/5** (Table 5.13). These values are close to the ideal stoichiometric value of 16.00. Si (5.998 – 6.032), octahedrally coordinated aluminium (3.908 – 3.988), Ti (0.004 – 0.020) and Cr (0.001- 0.015) atoms per garnet formula unit are observed in these ranges. Al(VI) averages 3.943 per 24 oxygens. The amount of ferric iron ranges from 0.0 to 0.064. The proportions of Ca, Fe^{2+}, Mg and Mn for this garnet are illustrated in Figure 5.50. Garnet which is composed of average 75 percent pyralspite and 25 percent ugrandite series is rich in

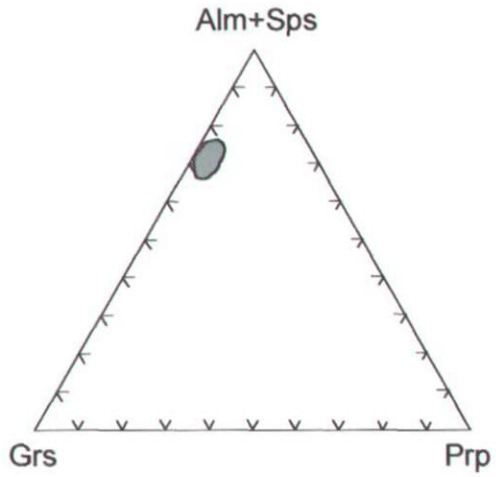


Figure 5.47 In almandine+spessartine - grossular - pyrope ternary diagram, location of selected garnet grains from garnet-mica schist belonging to marble-schist series.

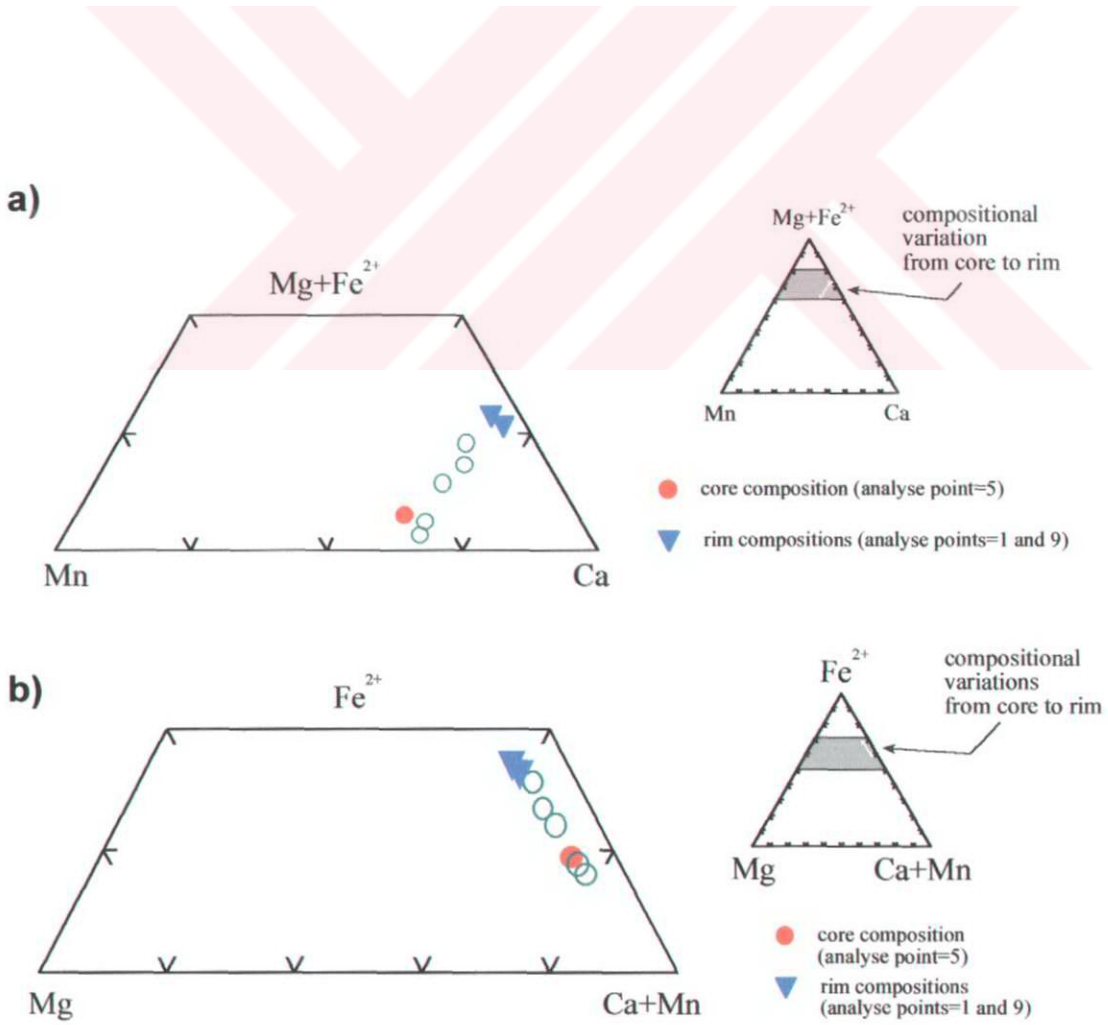
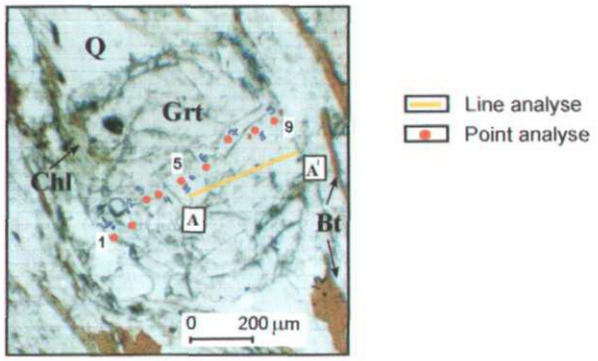
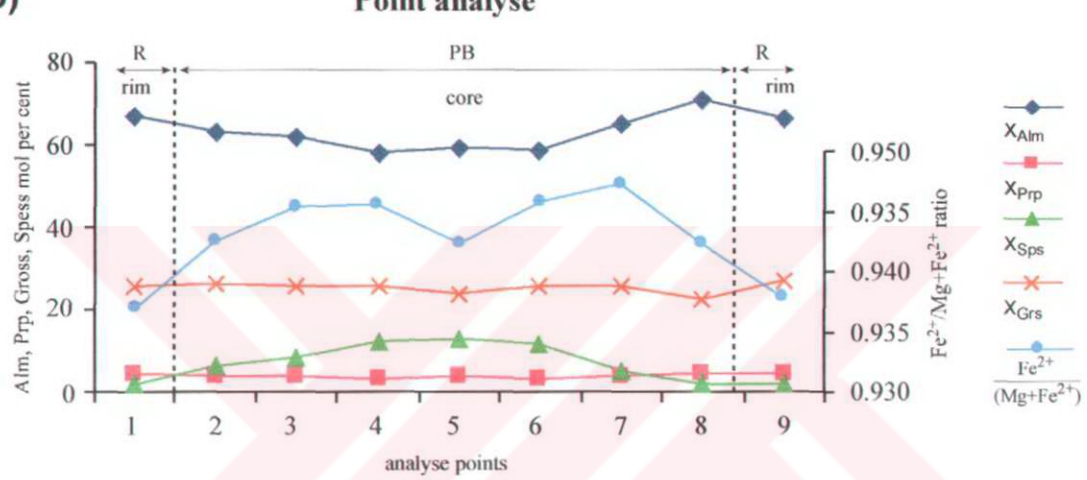


Figure 5.48 Ternary atomic proportions of Alm+Prp-Sps-Grs (a) and Alm-Prp-Grs+Sps (b) for garnet (1-9) from garnet-mica schist (M97-36).

a)



b)



c)

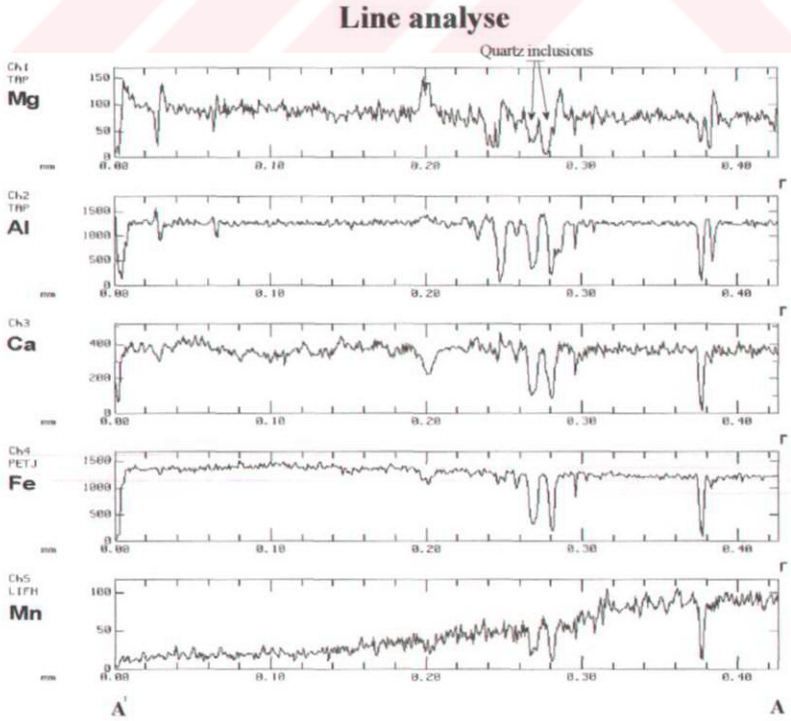


Figure 5.49 Compositional zoning in the garnet from sample M97-36; a) microphoto of analysed garnet in PPL, b) element zoning profiles from rim to rim , c) A-A' line analyse from rim to rim.

almandine (average 61 mol%) (Figure 48). Core and rim compositions of the garnet are "Alm58 Prp3 Grs25 Sps14" and "Alm65 Prp4 Grs26 Sps5 ", respectively.

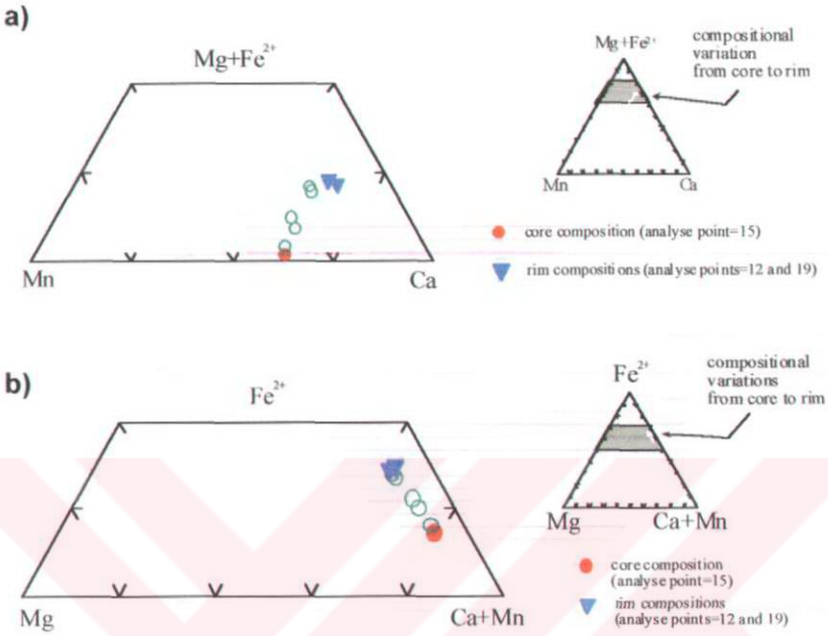
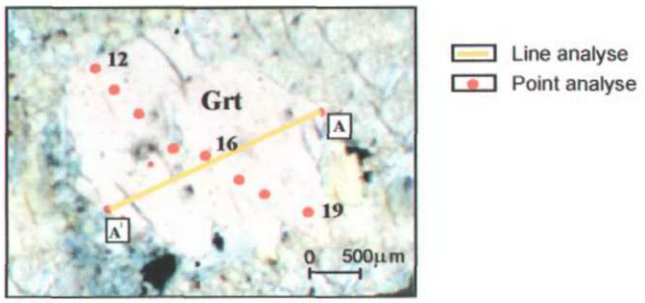


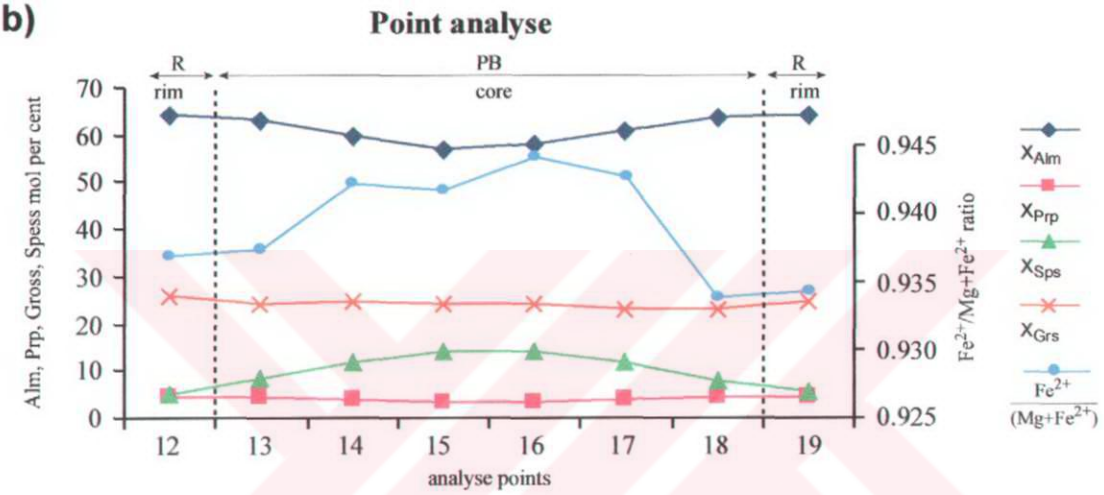
Figure 5.50 Ternary atomic proportions of Alm+Prp-Sps-Grs (a) and Alm-Prp-Grs+Sps (b) for garnet (12-19) from garnet-mica schist (M99-52/5).

The garnet grain which is 2620 microns in diameter has a sub-euhedral crystal form and does not show textural zoning (Figure 5.51a). Chemical zonation in garnet is given in Figure 49b,c. Zoning patterns in Figure 5.51b show the rimward decrease of X_{Sps} and $Fe^{2+}/(Fe^{2+}+Mg)$, and the slightly increase of X_{Alm} and X_{Prp}. This is a typical composition trend of growth zoning. Minimum X_{Prp} and X_{Alm}, and maximum $Fe^{2+}/(Fe^{2+}+Mg)$ ratio and X_{Sps} contents exist in the core. X_{Sps} is substituted by X_{Alm} and small amounts of X_{Prp}. X_{Grs} value displays a slight decrease near the core – rim boundary. Whereas, X_{Prp} reaches its maximum level in the same section. These pattern are probably related to increasing pressure and temperature (blueschist stage – PB) conditions (Loomis and Nimick, 1982). All end-member patterns show a flat increase from core to rim (Figure 5.51b,c). The rim which is marked by flat patterns

a)



b)



c)

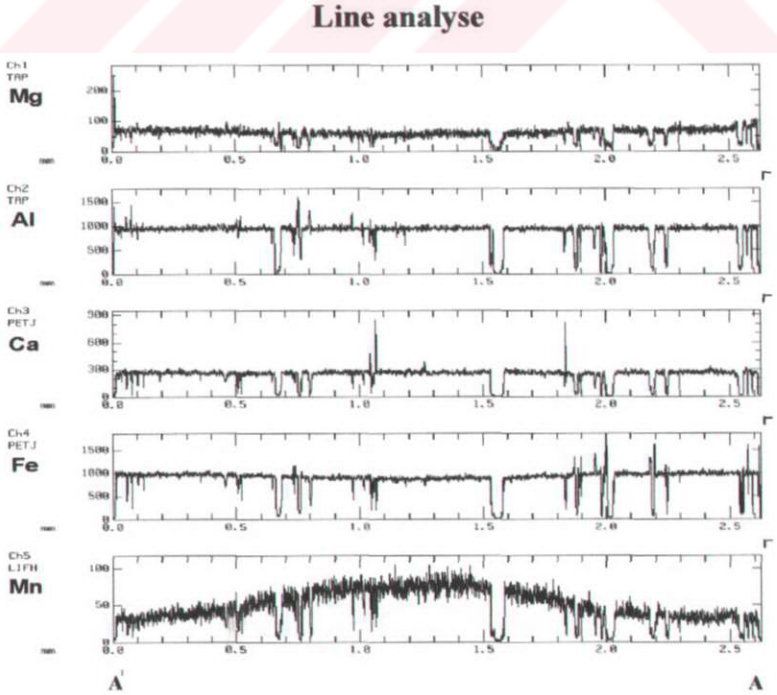


Figure 5.51 Compositional zoning in the garnet (12-19) from M99-52/5; a) microphoto of analysed garnet in PPL, b) element zoning profiles from rim to rim , c) A-A' line analyse from rim to rim.

may be a modified part of an epidote-blueschist stage-garnet by diffusional effects during a retrograde stage (R).

5.5. Micas

Micas will be treated in two groups; trioctahedral and dioctahedral. The general formula of the mica group minerals is $IM_{2-3}\square_{1-0}T_4O_{10}(OH)_2$, where I (K, Na, Ca) represents the interlayer site, M (Al, Cr, Fe^{3+},Ti, Fe^{2+}, Mg, Mn) the octahedral sites, $\square$ (vacancy) and T (Si, Al) the tetrahedral sites (Rieder et al. 1998). The octahedral sheet can be made up in two ways: either dominantly of divalent cations such as Mg and Fe, in which case all three sites are filled (*trioctahedral mica*), or else dominantly trivalent cations such as Al, in which case one of three sites is left vacant (*dioctahedral mica*). Important rock-forming micas are the trioctahedral phlogopite – biotite series and the dioctahedral "white" micas: muscovite, paragonite and margarite. Both muscovite and paragonite can contain Mg and Fe(2+) in substitution for Al(3+) in their octahedral sites. This substitution is accompanied by a coupled substitution of Si for Al in the T-sites, which yields white micas with Si:Al T-site ratios greater than 3:1. This substitution is called the phengite substitution ($MgSiAl_2$) which is favoured by high pressure and low temperature.

5.5.1. Dioctahedral micas

Dioctahedral micas occur in eclogite blocks (95-70/4), the matrix of metaolistostrome (94-30 and M98-99/2) and garnet-mica schists (M97-36 and M99-52/5) belonging to the marble-schist series. Representative white mica (dioctahedral mica) analyses from metaolistostrome unit and marble-schist series are given in Table 5.14 and 5.15, respectively.

5.5.1.1. White mica in eclogite block

Silica content in white micas range from 3.345 – 3.480 (average = 3.410) cations per formula unit (p.f.u). According to Figure 5.52 a – b – c - d, the white micas are

Table 5.14 Representative dioctahedral mica analyses from the Metaolistostrome unit.

	95-70/4 (eclogite block)														94-30 (metaolistostrome matrix)									
	rim			rim				rim		rim	rim		rim		rim			rim	rim					rim
	m3-64	m3-65	m3-66	m3-67	m3-90	m3-91	m3-112	m3-117	m3-118	m3-119	m3-120	m3-121	m3-122	m3-124	1A	2A	3A	4A	94-30-11	94-30-12	94-30-13	94-30-14	94-30-15	
SiO2	50,89	50,5	51,38	51,65	51,73	51,59	51,06	49,1	49,13	50,05	49,91	49,98	49,2	51,26	49,11	49,33	48,65	48,61	49,03	49,03	48,66	48,52	48,31	
TiO2	0,141	0,145	0,12	0,048	0,053	0,138	0,086	0,279	0,302	0,292	0,201	0,285	0,33	0,084	0,401	0,218	0,272	0,348	0,173	0,144	0,259	0,24	0,076	
Al2O3	26,08	26,07	25,42	25,69	25,81	25,67	25,47	27,78	27,75	28	27,19	27,39	28,24	25,93	27,55	27,23	26,98	27,46	26,95	26,61	27,31	27,59	26,85	
FeO	2,2	2,22	2,12	2,22	2,21	2,07	2,22	2,09	2,03	2,02	2,04	2,08	1,88	2,06	2,57	2,64	2,57	2,62	2,23	2,17	2,41	2,48	2,23	
MnO	0,018	0,058	0,054	0,023	0,053	0,05	0,018	0,044	0	0	0,02	0,021	0	0,064	0,019	0	0,031	0,009	0,013	0	0	0,022	0	
MgO	3,67	3,77	3,9	4	3,69	3,81	3,92	3,04	2,97	3,09	3,24	3,12	2,99	3,76	2,86	2,92	2,71	2,78	3,23	3,25	2,99	2,86	3,03	
CaO	0,03	0,03	0	0	0,01	0	0,01	0,03	0	0	0	0,02	0,07	0	0,01	0	0	0,04	0,017	0	0	0	0	
Na2O	0,32	0,3	0,167	0,204	0,204	0,222	0,22	0,698	0,649	0,633	0,38	0,536	0,7	0,231	0,544	0,515	0,394	0,457	0,355	0,394	0,437	0,527	0,331	
K2O	10,67	10,46	10,34	10,53	10,22	10,43	10,36	9,63	9,97	9,96	10,21	9,79	9,63	10,32	9,65	9,52	9,71	9,54	9,82	9,98	9,82	9,67	9,88	
Total	94,02	93,59	93,56	94,37	93,98	94,02	93,41	92,69	92,84	94,06	93,25	93,28	93,07	93,72	92,714	92,373	91,317	91,864	91,818	91,579	91,886	91,91	90,707	
normalized to 22 oxygen																								
Si	6,886	6,865	6,966	6,948	6,969	6,959	6,941	6,713	6,718	6,743	6,793	6,787	6,692	6,932	6,725	6,772	6,765	6,717	6,772	6,796	6,726	6,704	6,760	
Ti	0,014	0,015	0,012	0,005	0,005	0,014	0,009	0,029	0,031	0,030	0,021	0,029	0,034	0,009	0,041	0,023	0,028	0,036	0,018	0,015	0,027	0,025	0,008	
Al	4,160	4,178	4,062	4,073	4,099	4,082	4,081	4,477	4,473	4,446	4,362	4,384	4,527	4,133	4,447	4,406	4,423	4,473	4,388	4,347	4,450	4,494	4,429	
Fe	0,249	0,252	0,240	0,250	0,249	0,233	0,252	0,239	0,232	0,228	0,232	0,236	0,214	0,233	0,294	0,303	0,299	0,303	0,258	0,251	0,279	0,287	0,261	
Mn	0,002	0,007	0,006	0,003	0,006	0,006	0,002	0,005	0,000	0,000	0,002	0,002	0,000	0,007	0,002	0,000	0,004	0,001	0,002	0,000	0,000	0,003	0,000	
Mg	0,740	0,764	0,788	0,802	0,741	0,766	0,794	0,620	0,605	0,620	0,657	0,631	0,606	0,758	0,584	0,597	0,562	0,573	0,665	0,671	0,616	0,589	0,632	
Ca	0,004	0,004	0,000	0,000	0,001	0,000	0,001	0,004	0,000	0,000	0,000	0,003	0,010	0,000	0,001	0,000	0,000	0,006	0,003	0,000	0,000	0,000	0,000	
Na	0,084	0,079	0,044	0,053	0,053	0,058	0,058	0,185	0,172	0,165	0,100	0,141	0,185	0,061	0,144	0,137	0,106	0,122	0,095	0,106	0,117	0,141	0,090	
K	1,842	1,814	1,788	1,807	1,756	1,795	1,797	1,680	1,739	1,712	1,773	1,696	1,671	1,780	1,686	1,667	1,722	1,682	1,730	1,764	1,732	1,704	1,764	
Total	13,982	13,978	13,907	13,941	13,881	13,913	13,936	13,952	13,970	13,943	13,941	13,910	13,938	13,913	13,925	13,905	13,909	13,912	13,929	13,951	13,946	13,947	13,944	
Si/2	3,443	3,433	3,483	3,474	3,485	3,480	3,471	3,357	3,359	3,371	3,397	3,394	3,346	3,466	3,363	3,386	3,383	3,359	3,386	3,398	3,363	3,352	3,380	
Ti/2	0,007	0,007	0,006	0,002	0,003	0,007	0,004	0,014	0,016	0,015	0,010	0,015	0,017	0,004	0,021	0,011	0,014	0,018	0,009	0,008	0,013	0,012	0,004	
Al/2	2,080	2,089	2,031	2,037	2,049	2,041	2,041	2,239	2,236	2,223	2,181	2,192	2,264	2,067	2,223	2,203	2,211	2,236	2,194	2,174	2,225	2,247	2,214	
Fe/2	0,124	0,126	0,120	0,125	0,124	0,117	0,126	0,119	0,116	0,114	0,116	0,118	0,107	0,116	0,147	0,152	0,149	0,151	0,129	0,126	0,139	0,143	0,130	
Mn/2	0,001	0,003	0,003	0,001	0,003	0,003	0,001	0,003	0,000	0,000	0,001	0,001	0,000	0,004	0,001	0,000	0,002	0,001	0,001	0,000	0,000	0,001	0,000	
Mg/2	0,370	0,382	0,394	0,401	0,370	0,383	0,397	0,310	0,303	0,310	0,329	0,316	0,303	0,379	0,292	0,299	0,281	0,286	0,332	0,336	0,308	0,295	0,316	
Ca/2	0,002	0,002	0,000	0,000	0,001	0,000	0,001	0,002	0,000	0,000	0,000	0,001	0,005	0,000	0,001	0,000	0,000	0,003	0,001	0,000	0,000	0,000	0,000	
Na/2	0,042	0,040	0,022	0,027	0,027	0,029	0,029	0,093	0,086	0,083	0,050	0,071	0,092	0,030	0,072	0,069	0,053	0,061	0,048	0,053	0,059	0,071	0,045	
K/2	0,921	0,907	0,894	0,903	0,878	0,897	0,898	0,840	0,869	0,856	0,886	0,848	0,835	0,890	0,843	0,833	0,861	0,841	0,865	0,882	0,866	0,852	0,882	
T1: Si	2,000	2,000	2,000	2,000	2,000	2,000	2,000	2,000	2,000	2,000	2,000	2,000	2,000	2,000	2,000	2,000	2,000	2,000	2,000	2,000	2,000	2,000	2,000	
T2: Si	1,443	1,433	1,483	1,474	1,485	1,480	1,471	1,357	1,359	1,371	1,397	1,394	1,346	1,466	1,363	1,386	1,383	1,359	1,386	1,398	1,363	1,352	1,380	
T2: Al	0,557	0,567	0,517	0,526	0,515	0,520	0,529	0,643	0,641	0,629	0,603	0,606	0,654	0,534	0,637	0,614	0,617	0,641	0,614	0,602	0,637	0,648	0,620	
Total T2	2,000	2,000	2,000	2,000	2,000	2,000	2,000	2,000	2,000	2,000	2,000	2,000	2,000	2,000	2,000	2,000	2,000	2,000	2,000	2,000	2,000	2,000	2,000	
Ti	0,007	0,007	0,006	0,002	0,003	0,007	0,004	0,014	0,016	0,015	0,010	0,015	0,017	0,004	0,021	0,011	0,014	0,018	0,009	0,008	0,013	0,012	0,004	
Mn	0,001	0,003	0,003	0,001	0,003	0,003	0,001	0,003	0,000	0,000	0,001	0,001	0,000	0,004	0,001	0,000	0,002	0,001	0,001	0,000	0,000	0,001	0,000	
M2: Al	1,523	1,521	1,514	1,511	1,534	1,520	1,511	1,595	1,595	1,594	1,578	1,586	1,610	1,533	1,586	1,589	1,594	1,595	1,580	1,571	1,588	1,599	1,595	
M2: Mg	0,370	0,382	0,394	0,401	0,370	0,383	0,397	0,310	0,303	0,310	0,329	0,316	0,303	0,379	0,292	0,299	0,281	0,286	0,332	0,336	0,308	0,295	0,316	
M2: Fe	0,098	0,086	0,083	0,085	0,090	0,087	0,086	0,078	0,086	0,081	0,082	0,083	0,070	0,080	0,100	0,101	0,109	0,100	0,078	0,085	0,090	0,093	0,085	
rest Fe	0,026	0,040	0,037	0,040	0,035	0,030	0,040	0,041	0,030	0,033	0,034	0,035	0,036	0,036	0,047	0,050	0,040	0,051	0,051	0,040	0,049	0,051	0,045	
Total M2	2,000	2,000	2,000	2,000	2,000	2,000	2,000	2,000	2,000	2,000	2,000	2,000	2,000	2,000	2,000	2,000	2,000	2,000	2,000	2,000	2,000	2,000	2,000	
M1: Al	0,000	0,000	0,000	0,000	0,000	0,000	0,000	0,000	0,000	0,000	0,000	0,000	0,000	0,000	0,000	0,000	0,000	0,000	0,000	0,000	0,000	0,000	0,000	
M1: Mg	0,000	0,000	0,000	0,000	0,000	0,000	0,000	0,000	0,000	0,000	0,000	0,000	0,000	0,000	0,000	0,000	0,000	0,000	0,000	0,000	0,000	0,000	0,000	
M1: Fe	0,026	0,040	0,037	0,040	0,035	0,030	0,040	0,041	0,030	0,033	0,034	0,035	0,036	0,036	0,047	0,050	0,040	0,051	0,051	0,040	0,049	0,051	0,045	
Vacanz.	0,974	0,960	0,963	0,960	0,965	0,970	0,960	0,959	0,970	0,967	0,966	0,965	0,964	0,964	0,953	0,950	0,960	0,949	0,949	0,960	0,951	0,949	0,955	
Total M1	1,000	1,000	1,000	1,000	1,000	1,000	1,000	1,000	1,000	1,000	1,000	1,000	1,000	1,000	1,000	1,000	1,000	1,000	1,000	1,000	1,000	1,000	1,000	
A: K	0,921	0,907	0,894	0,903	0,878	0,897	0,898	0,840	0,869	0,856	0,886	0,848	0,835	0,890	0,843	0,833	0,861	0,841	0,865	0,882	0,866	0,852	0,882	
A: Na	0,042	0,040	0,022	0,027	0,027	0,029	0,029	0,093	0,086	0,083	0,050	0,071	0,092	0,030	0,072	0,069	0,053	0,061	0,048	0,053	0,059	0,071	0,045	
A: Ca	0,002	0,002	0,000	0,000	0,001	0,000	0,001	0,002	0,000	0,000	0,000	0,001	0,005	0,000	0,001	0,000	0,000	0,003	0,001	0,000	0,000	0,000	0,000	
Total A	0,965	0,949	0,916	0,930	0,906	0,926	0,928	0,934	0,956	0,938	0,936	0,920	0,933	0,920	0,916	0,902	0,914	0,905	0,914	0,935	0,924	0,923	0,927	
X(Ms)	0,557	0,567	0,517	0,526	0,515	0,520	0,529	0,643	0,641	0,629	0,603	0,606	0,654	0,534	0,637	0,614	0,617	0,641	0,614	0,602	0,637	0,648	0,620	
X(Cel)	0,332	0,325	0,370	0,361	0,363	0,368	0,357	0,257	0,259	0,272	0,293	0,286	0,256	0,356	0,241	0,256	0,250	0,235	0,278	0,289	0,250	0,237	0,269	
X(Fe-Cel)	0,112	0,107	0,113	0,113	0,122	0,112	0,113	0,099	0,100	0,100	0,104	0,107	0,090	0,110	0,122	0,130	0,133	0,124	0,108	0,108	0,113	0,115	0,111	
Ms mol%	66,268	67,268	68,268	69,268	70,268	71,268	72,268	73,268	74,268	75,268	76,268	77,268	78,268	79,268	80,268	81,268	82,268	83,268	84,268	85,268	86,268	87,268	88,268	
Pa mol%	3,020	2,916	1,616	1,940	1,983	2,118	2,126	7,314	6,624	6,423	3,833	5,512	7,392	2,244	5,792	5,482	4,201	4,995	3,758	4,050	4,647	5,657	3,510	
Cel mol%	30,712	30,196	32,564	32,155	32,647	32,411	32,006	26,290	26,416	27,075	28,404	28,239	25,699	31,790	26,608	27,842	27,678	26,393	27,846	28,457	26,640	26,048	27,349	
Fe/(Fe+Mg)	0,252	0,248	0,234	0,237	0,252	0,234	0,241	0,278	0,277	0,268	0,261	0,272	0,261	0,235	0,335	0,337	0,347	0,346	0,279	0,273	0,311	0,327	0,292	

Table 5.14 continue

	94-30 (metaolistostrome matrix)										M98-99/2 (metaolistostrome matrix)												
	rim				rim	rim				rim	rim				rim	rim		rim					
	94-30-20	94-30-21	94-30-22	94-30-23	94-30-24	94-30-31	94-30-32	94-30-33	94-30-34	94-30-35	m1-1	m1-2	m1-3	m1-4	m1-5	m1-6	m1-7	m1-8	m1-9	m1-33	m1-35	m1-39	m1-40
SiO2	48,57	48,59	49,1	48,56	48,64	49,05	48,81	48,64	49,54	49,25	48,750	48,170	48,080	48,01	48,38	48,82	48,95	48,92	49,21	49,34	49,37	48,82	49,19
TiO2	0,319	0,351	0,326	0,314	0,366	0,172	0,157	0,089	0,113	0,155	0,241	0,265	0,254	0,283	0,229	0,223	0,224	0,266	0,214	0,181	0,183	0,265	0,223
Al2O3	27,77	27,52	27,63	27,63	27,61	27,12	26,62	26,75	26,74	27,18	26,550	27,510	27,390	27,61	27,36	27,18	27,4	27,74	27,14	26,56	27,7	27,75	26,92
FeO	2,53	2,66	2,62	2,41	2,56	2,59	2,29	2,27	2,34	2,41	2,370	2,010	2,080	2,21	2,11	2,11	1,91	2,07	2,13	2,16	2,14	2,02	2,05
MnO	0,01	0,018	0,016	0,034	0	0,012	0	0,028	0,027	0,01	0,019	0,007	0,052	0	0,024	0	0,016	0	0,009	0,03	0,01	0	0
MgO	2,83	2,86	2,83	2,86	2,83	2,94	3,01	3,17	3,14	3,08	3,070	2,910	2,840	2,86	2,87	2,84	2,83	2,9	2,89	3,18	2,89	2,85	3,05
CaO	0	0	0	0	0	0	0	0,01	0,017	0,01	0,000	0,000	0,000	0,018	0	0,019	0	0	0	0	0,018	0	0
Na2O	0,684	0,63	0,644	0,655	0,693	0,327	0,286	0,315	0,308	0,314	0,366	0,499	0,457	0,637	0,549	0,506	0,509	0,483	0,54	0,356	0,521	0,553	0,594
K2O	9,42	9,28	9,35	9,12	9,41	9,83	9,67	9,76	9,51	9,73	9,330	9,280	9,220	9,29	9,11	9,12	9,23	9,16	9,12	9,4	9,35	9,19	9,09
Total	92,134	91,909	92,527	91,583	92,11	92,041	90,843	91,033	91,735	92,14	90,810	90,734	90,434	91,003	90,677	90,867	91,07	91,6	91,335	91,207	92,21	91,529	91,151
normalized to 22 oxygen																							
Si	6,690	6,706	6,728	6,710	6,701	6,767	6,806	6,777	6,830	6,775	6,802	6,715	6,724	6,688	6,741	6,782	6,778	6,741	6,802	6,834	6,764	6,736	6,808
Ti	0,033	0,036	0,034	0,033	0,038	0,018	0,016	0,009	0,012	0,016	0,025	0,028	0,027	0,030	0,024	0,023	0,023	0,028	0,022	0,019	0,019	0,027	0,023
Al	4,508	4,477	4,463	4,501	4,484	4,411	4,375	4,393	4,346	4,407	4,366	4,521	4,515	4,533	4,494	4,451	4,472	4,506	4,422	4,337	4,473	4,513	4,392
Fe	0,291	0,307	0,301	0,278	0,295	0,299	0,267	0,264	0,270	0,277	0,276	0,234	0,243	0,257	0,246	0,245	0,221	0,239	0,246	0,250	0,245	0,233	0,237
Mn	0,001	0,002	0,002	0,004	0,000	0,001	0,000	0,003	0,003	0,001	0,002	0,001	0,006	0,000	0,003	0,000	0,002	0,000	0,001	0,004	0,001	0,000	0,000
Mg	0,581	0,588	0,578	0,589	0,581	0,605	0,626	0,658	0,645	0,632	0,638	0,605	0,592	0,594	0,596	0,588	0,584	0,596	0,595	0,657	0,590	0,586	0,629
Ca	0,000	0,000	0,000	0,000	0,000	0,000	0,000	0,001	0,003	0,001	0,000	0,000	0,000	0,003	0,000	0,003	0,000	0,000	0,000	0,000	0,003	0,000	0,000
Na	0,183	0,169	0,171	0,175	0,185	0,087	0,077	0,085	0,082	0,084	0,099	0,135	0,124	0,172	0,148	0,136	0,137	0,129	0,145	0,096	0,138	0,148	0,159
K	1,655	1,634	1,634	1,608	1,654	1,730	1,720	1,735	1,672	1,707	1,660	1,650	1,645	1,651	1,619	1,616	1,630	1,610	1,608	1,661	1,634	1,618	1,605
Total	13,942	13,920	13,910	13,898	13,938	13,918	13,888	13,927	13,863	13,901	13,870	13,889	13,876	13,927	13,871	13,845	13,847	13,848	13,841	13,857	13,867	13,862	13,854
Si/2	3,345	3,353	3,364	3,355	3,351	3,384	3,403	3,389	3,415	3,388	3,401	3,358	3,362	3,344	3,371	3,391	3,389	3,371	3,401	3,417	3,382	3,368	3,404
Ti/2	0,017	0,018	0,017	0,016	0,019	0,009	0,008	0,005	0,006	0,008	0,013	0,014	0,013	0,015	0,012	0,012	0,012	0,014	0,011	0,009	0,009	0,014	0,012
Al/2	2,254	2,239	2,231	2,250	2,242	2,205	2,188	2,197	2,173	2,204	2,183	2,260	2,258	2,267	2,247	2,225	2,236	2,253	2,211	2,168	2,237	2,257	2,196
Fe/2	0,146	0,153	0,151	0,139	0,147	0,149	0,134	0,132	0,135	0,139	0,138	0,117	0,122	0,129	0,123	0,123	0,111	0,119	0,123	0,125	0,123	0,117	0,119
Mn/2	0,001	0,001	0,001	0,002	0,000	0,001	0,000	0,002	0,002	0,001	0,001	0,000	0,003	0,000	0,001	0,000	0,001	0,000	0,001	0,002	0,001	0,000	0,000
Mg/2	0,290	0,294	0,289	0,295	0,291	0,302	0,313	0,329	0,323	0,316	0,319	0,302	0,296	0,297	0,298	0,294	0,292	0,298	0,298	0,328	0,295	0,293	0,315
Ca/2	0,000	0,000	0,000	0,000	0,000	0,000	0,000	0,001	0,001	0,001	0,000	0,000	0,000	0,001	0,000	0,001	0,000	0,000	0,000	0,000	0,001	0,000	0,000
Na/2	0,091	0,084	0,086	0,088	0,093	0,044	0,039	0,043	0,041	0,042	0,049	0,067	0,062	0,086	0,074	0,068	0,068	0,065	0,072	0,048	0,069	0,074	0,080
K/2	0,827	0,817	0,817	0,804	0,827	0,865	0,860	0,867	0,836	0,854	0,830	0,825	0,822	0,825	0,810	0,808	0,815	0,805	0,804	0,830	0,817	0,809	0,802
T1: Si	2,000	2,000	2,000	2,000	2,000	2,000	2,000	2,000	2,000	2,000	2,000	2,000	2,000	2,000	2,000	2,000	2,000	2,000	2,000	2,000	2,000	2,000	2,000
T2: Si	1,345	1,353	1,364	1,355	1,351	1,384	1,403	1,389	1,415	1,388	1,401	1,358	1,362	1,344	1,371	1,391	1,389	1,371	1,401	1,417	1,382	1,368	1,404
T2: Al	0,655	0,647	0,636	0,645	0,649	0,616	0,597	0,611	0,585	0,612	0,599	0,642	0,638	0,656	0,629	0,609	0,611	0,629	0,599	0,583	0,618	0,632	0,596
Total T2	2,000	2,000	2,000	2,000	2,000	2,000	2,000	2,000	2,000	2,000	2,000	2,000	2,000	2,000	2,000	2,000	2,000	2,000	2,000	2,000	2,000	2,000	2,000
Ti	0,017	0,018	0,017	0,016	0,019	0,009	0,008	0,005	0,006	0,008	0,013	0,014	0,013	0,015	0,012	0,012	0,012	0,014	0,011	0,009	0,009	0,014	0,012
Mn	0,001	0,001	0,001	0,002	0,000	0,001	0,000	0,002	0,002	0,001	0,001	0,000	0,003	0,000	0,001	0,000	0,001	0,000	0,001	0,002	0,001	0,000	0,000
M2: Al	1,599	1,592	1,595	1,605	1,593	1,589	1,591	1,585	1,588	1,591	1,584	1,618	1,620	1,611	1,618	1,617	1,625	1,624	1,612	1,586	1,618	1,625	1,600
M2: Mg	0,290	0,294	0,289	0,295	0,291	0,302	0,313	0,329	0,323	0,316	0,319	0,302	0,296	0,297	0,298	0,294	0,292	0,298	0,298	0,328	0,295	0,293	0,315
M2: Fe	0,093	0,095	0,098	0,082	0,098	0,099	0,088	0,079	0,082	0,084	0,083	0,065	0,068	0,078	0,071	0,078	0,071	0,065	0,079	0,075	0,077	0,068	0,074
rest Fe	0,052	0,059	0,052	0,058	0,050	0,050	0,045	0,053	0,053	0,054	0,055	0,052	0,054	0,051	0,052	0,045	0,040	0,054	0,044	0,050	0,046	0,048	0,045
Total M2	2,000	2,000	2,000	2,000	2,000	2,000	2,000	2,000	2,000	2,000	2,000	2,000	2,000	2,000	2,000	2,000	2,000	2,000	2,000	2,000	2,000	2,000	2,000
M1: Al	0,000	0,000	0,000	0,000	0,000	0,000	0,000	0,000	0,000	0,000	0,000	0,000	0,000	0,000	0,000	0,000	0,000	0,000	0,000	0,000	0,000	0,000	0,000
M1: Mg	0,000	0,000	0,000	0,000	0,000	0,000	0,000	0,000	0,000	0,000	0,000	0,000	0,000	0,000	0,000	0,000	0,000	0,000	0,000	0,000	0,000	0,000	0,000
M1: Fe	0,052	0,059	0,052	0,058	0,050	0,050	0,045	0,053	0,053	0,054	0,055	0,052	0,054	0,051	0,052	0,045	0,040	0,054	0,044	0,050	0,046	0,048	0,045
Vacanc.	0,948	0,941	0,948	0,942	0,950	0,950	0,955	0,947	0,947	0,946	0,945	0,948	0,946	0,949	0,948	0,955	0,960	0,946	0,956	0,950	0,954	0,952	0,955
Total M1	1,000	1,000	1,000	1,000	1,000	1,000	1,000	1,000	1,000	1,000	1,000	1,000	1,000	1,000	1,000	1,000	1,000	1,000	1,000	1,000	1,000	1,000	1,000
A: K	0,827	0,817	0,817	0,804	0,827	0,865	0,860	0,867	0,836	0,854	0,830	0,825	0,822	0,825	0,810	0,808	0,815	0,805	0,804	0,830	0,817	0,809	0,802
A: Na	0,091	0,084	0,086	0,088	0,093	0,044	0,039	0,043	0,041	0,042	0,049	0,067	0,062	0,086	0,074	0,068	0,068	0,065	0,072	0,048	0,069	0,074	0,080
A: Ca	0,000	0,000	0,000	0,000	0,000	0,000	0,000	0,001	0,001	0,001	0,000	0,000	0,000	0,001	0,000	0,000	0,000	0,000	0,000	0,000	0,001	0,000	0,000
Total A	0,919	0,901	0,903	0,892	0,919	0,909	0,899	0,911	0,879	0,896	0,880	0,893	0,884	0,913	0,884	0,878	0,883	0,870	0,876	0,878	0,887	0,883	0,882
X(Ms)	0,655	0,647	0,636	0,645	0,649	0,616	0,597	0,611	0,585	0,612	0,599	0,642	0,638	0,656	0,629	0,609	0,611	0,629	0,599	0,583	0,618	0,632	0,596
X(Cel)	0,230	0,232	0,239	0,241	0,233	0,257	0,283	0,277	0,293	0,269	0,280	0,258	0,257	0,240	0,262	0,276	0,282	0,265	0,284	0,302	0,270	0,263	0,294
X(Fe-Cel)	0,115	0,121	0,125	0,114	0,118	0,127	0,121	0,111	0,122	0,118	0,121	0,100	0,103	0,104	0,108	0,115	0,107	0,106	0,117	0,115	0,112	0,105	0,111
Ms mol%	66,971	66,988	66,375	66,328	66,583	68,790	68,203	68,652	67,354	68,701	67,372	68,087	68,277	67,391	66,834	66,291	66,437	67,547	65,487	66,720	66,718	66,964	64,779
Pa mol%	7,391	6,912	6,948	7,262	7,432	3,478	3,066	3,367	3,315	3,370	4,017	5,564	5,143	7,023	6,121	5,390	5,568	5,413	5,893	3,840	5,650	6,124	6,433
Cel mol%	25,638	26,101	26,677	26,211	25,965	27,732	28,732	27,981	29,331	27,929	28,611	26,349	26,580	25,586	27,044	28,120	27,995	27,040	28,620	29,440	27,632	26,912	28,787
Fe/(Fe+Mg)	0,334	0,343	0,343	0,321	0,337	0,331	0,299	0,287	0,295	0,305	0,302	0,279	0,291	0,302	0,292	0,294	0,275	0,286	0,293	0,276	0,294	0,285	0,274

Table 5.14 continue

	M98-99/2			
	m1-41	m1-78	m1-80	m1-95
SiO2	49,51	49,09	49,14	49,13
TiO2	0,167	0,23	0,256	0,253
Al2O3	27	27,17	26,86	26,72
FeO	1,98	2,35	2,32	2,14
MnO	0,013	0	0,067	0
MgO	2,78	3,11	3,07	2,96
CaO	0,013	0	0	0
Na2O	0,476	0,529	0,424	0,573
K2O	8,91	9,28	9,47	9,4
Total	91,02	91,838	91,639	91,233
normalized to 22 oxygen				
Si	6,845	6,767	6,792	6,813
Ti	0,028	0,024	0,027	0,026
Al	4,400	4,415	4,376	4,368
Fe	0,229	0,271	0,268	0,248
Mn	0,002	0,000	0,008	0,000
Mg	0,573	0,639	0,632	0,612
Ca	0,002	0,000	0,000	0,000
Na	0,128	0,141	0,114	0,154
K	1,571	1,632	1,670	1,663
Total	13,777	13,888	13,885	13,885
Si/2	3,422	3,383	3,396	3,407
Ti/2	0,014	0,012	0,013	0,013
Al/2	2,200	2,207	2,188	2,184
Fe/2	0,114	0,135	0,134	0,124
Mn/2	0,001	0,000	0,004	0,000
Mg/2	0,286	0,319	0,316	0,306
Ca/2	0,001	0,000	0,000	0,000
Na/2	0,064	0,071	0,057	0,077
K/2	0,786	0,816	0,835	0,831
T1: Si	2,000	2,000	2,000	2,000
T2: Si	1,422	1,383	1,396	1,407
T2: Al	0,578	0,617	0,604	0,593
Total T2	2,000	2,000	2,000	2,000
Ti	0,014	0,012	0,013	0,013
Mn	0,001	0,000	0,004	0,000
M2: Al	1,622	1,591	1,584	1,591
M2: Mg	0,286	0,319	0,316	0,306
M2: Fe	0,076	0,078	0,083	0,090
rest Fe	0,038	0,058	0,051	0,034
Total M2	2,000	2,000	2,000	2,000
M1: Al	0,000	0,000	0,000	0,000
M1: Mg	0,000	0,000	0,000	0,000
M1: Fe	0,038	0,058	0,051	0,034
Vacanc.	0,962	0,942	0,949	0,966
Total M1	1,000	1,000	1,000	1,000
A: K	0,786	0,816	0,835	0,831
A: Na	0,064	0,071	0,057	0,077
A: Ca	0,001	0,000	0,000	0,000
Total A	0,850	0,887	0,892	0,908
X(Ms)	0,578	0,617	0,604	0,593
X(Cel)	0,302	0,269	0,278	0,289
X(Fe-Cel)	0,121	0,114	0,118	0,117
Ms mol%	65,022	66,520	67,079	65,059
Pa mol%	5,279	5,763	4,564	6,027
Cel mol%	29,699	27,717	28,356	28,913
Fe/(Fe+Mg)	0,286	0,298	0,298	0,289

phengitic. Average value of paragonite mol% (=100*Na/(Na+K)), muscovite mol% (=100*K/(Na+K)) and celadonite mol% (=100*(Si-3)) in phengite are 4, 67 and 29, respectively (Figure 5.52c). Phengite compositions can be described by a solid solution of muscovite, Al-celadonite, AlFe-celadonite, annite and phlogopite. Activities of phlogopite and annite end members in the analysed phengite flakes is zero. Maximum X_{Cel} (=(1-(4-Si))*(Mg/(Mg+Fe))) and $X_{Fe\text{-}Cel}$ (=(1-(4-Si))*(Fe/(Fe+Mg))) content of phengites are 0.303 and 0.132 (Table 5.14). Analysed phengites are richer in X_{Cel} relative to $X_{Fe\text{-}Cel}$. There is no meaningful zonation in individual phengite flakes from rim to rim (Table 5.14). Phengite analyses from different flakes display a general trend in which is related to Tschermak substitution (Figure 5.52a-d). Tschermak substitution ($R^{2+}_{-1}Si_{-1}Al_2$) can be named as inverse phengite substitution. R^{2+} is Mg and Fe. This substitution is clearer between different flakes showing same schistosity (see below).

$(K_{0.87}Na_{0.02})\ (Al_{1.54}Mg_{0.37}Fe_{0.09}Ti_{0.00})\ (Si_{3.48}Al_{0.52})\ O_{10}\ (OH)_2$ (analyse no: m3-90 (table 5.14)

+0.06 -0.06 -0.01 -0.13 +0.13

$(K_{0.84}Na_{0.09})\ (Al_{1.60}Mg_{0.31}Fe_{0.08}Ti_{0.01})\ (Si_{3.35}Al_{0.65})\ O_{10}\ (OH)_2$ (analyse no: m3-117 (table 5.14)

Tschermak substitution reflects the impact of retrograde metamorphism on phengites which were produced during high-pressure metamorphism.

5.5.1.2. White mica from matrix of the Metaolistostrome

Silica contents in white micas of two samples (94-30 and M98-99/2) from phengite-garnet schist (matrix of metaolistostrome) range from 3.309 to 3.422 (average = 3.378) cations per formula unit (Table 5.14). White micas, similar to eclogite blocks, are phengitic (Figure 5.52a-b-c-d). Phengites show Tschermak substitution towards muscovite. But this substitution is weaker compared micas from eclogite block (Figure 5.52a-d). Phengitic white micas have a low Na/(Na+K) ratio and high Si content (Figure 5.52b). Average values of paragonite, muscovite and celadonite mol% in phengite are 5, 67 and 28, respectively (Figure 5.52c).

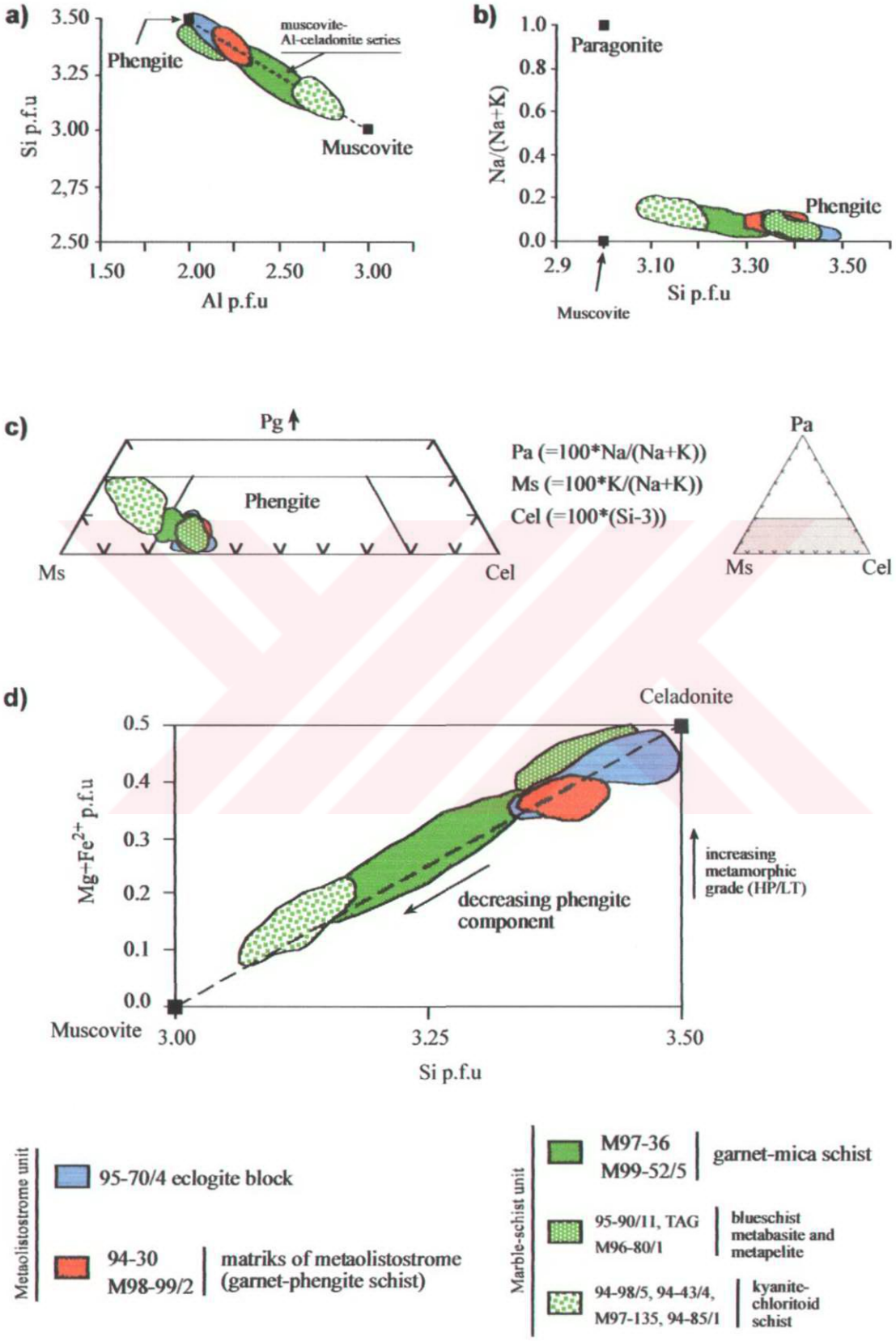


Figure 5.52 Phengite compositions from the Metaolistostrome and the Marble-schist units shown in term of **a)** Si p.f.u. vs Al p.f.u; **b)** Na/(Na+K) vs Si p.f.u; **c)** Ms-Pa-Cel triangle and **d)** Si vs (Fe^{2+}+Mg) per formula unit (p.f.u). The ideal celadonite muscovite substitution line is also shown by dotted line in (d).

Enrichment of Mg and Fe in octahedral site and Si in tetrahedral site which are related with phengite substitution are illustrated in Figure 5.52d. In this diagram, all white mica analyses display phengitic compositions which are rich-in celadonite. These data are consistent with phengites from eclogite block. Although the great majority of phengites display no zonation, some flakes exhibit distinct zonation (Figure 5.53). Phengite rims are less siliceous than their cores. Si (p.f.u) and X_{Cel} display decrease from core to rim. Whereas, X_{Ms} (= 4-Si), Na and T2Al increase rimward. This zonation pattern represents the Tschermak substitution which results from the retrograde metamorphism under medium pressure / medium to high temperature conditions. X_{Cel} content decreases with increasing T2Al and decreasing Si and Mg. This zoning profile characterizes a decrease of pressure (Evans and Patrick, 1987). Increasing of Ti and Na marks the increase of temperature.

5.5.1.3. White mica in the Marble-schist series

Most micas belonging to the Marble-schist series, i.e garnet-mica schist, kyanite-chloritoid schist and blueschist metabasite, are trioctahedral. White mica analyses from *garnet-mica schist* (M97-36 (Tire) / M99-52/5 (Akyurt)), *kyanite-chloritoid schist* (94-43/4 (Selçuk) / 94-85/1 (Şirince), M97-135 (Dilek Peninsula) / 94-98/5 (Dilek Peninsula) / 95-41/2 (Dilek Peninsula)) and *blueschist metapelite- metabasite* (M96-80/1 (Dilek Peninsula) / TAG (Dilek Peninsula) / 95-90/11 (Dilek Peninsula)) are given in Table 5.15. Si contents of white micas from garnet-mica schist, kyanite-chloritoid schist and blueschist metabasites range from 3.146 – 3.342, 3.073 – 3.207 and 3.345 – 3.443 cations per formula unit, respectively. 3.284 is the average Si value of marble-schist series. White micas in marble-schist series are rich-in muscovite (average 70.8 mol%) and celadonite (average 21.4 mol%) and their paragonite contents does not exceed 17 mol% (Figure 5.52a,b). White micas in the marble-schist series display a continuous evolution between phengite and muscovite (Figure 5.52a). The white micas in blueschist metabasites from the marble-schist series have high celadonite end-member relative to those from garnet-mica schists. Si:Al T-site ratios in garnet-mica schists are greater than 3 (average 4.41). This value suggests that white micas in garnet-mica schists are phengitic in composition. Due to

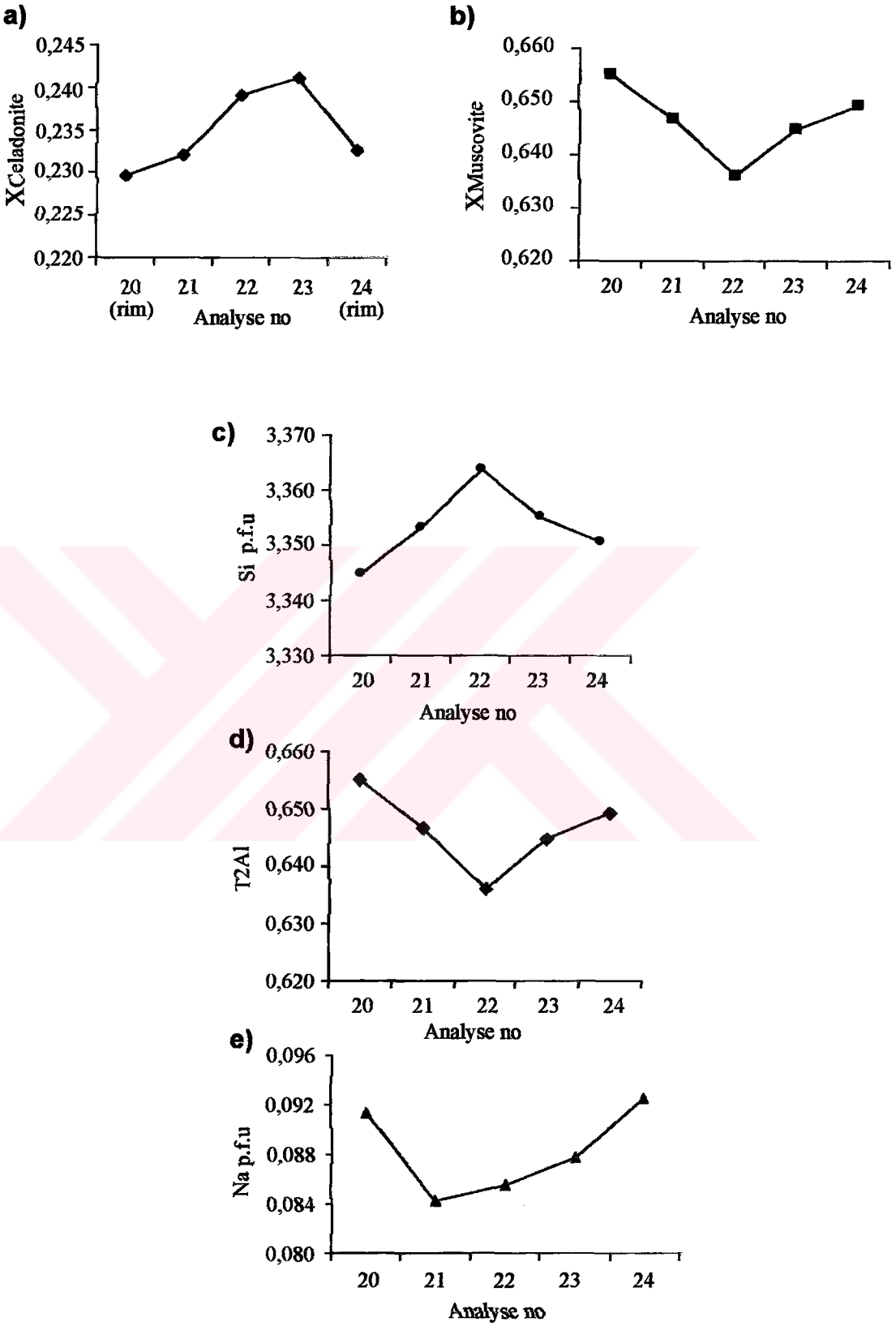


Figure 5.53 Compositional variation (Si, Na, T2Al, X_{Cel} and X_{Ms}) of individual phengite flake in 94-30. The length of analyse line is 245 microns. Analyse are made from rim to rim.

Table 5.15 Representative dioctahedral mica analyses from the Marble-schist series.

	M97-36			M99-52/5			94-98/5					94-43/4					94-85/1		M97-135	
	Garnet-mica schist						Kyanite-chloritoid schist													
	m17-35	m17-37	m17-38	m18-38	m18-39	m18-40	1	2	3	4	5	1	2	3	4	5	1	2	1	2
SiO2	48,27	48,71	48,52	49,53	48,05	46,51	47,02	46,38	46,45	46,48	45,90	45,54	46,75	49,42	46,15	45,72	49,36	45,72	48,50	49,72
TiO2	0,45	0,36	0,41	0,24	0,40	0,39	0,00	0,21	0,18	0,05	0,23	0,18	0,05	0,15	0,13	0,11	0,24	0,16	0,08	0,02
Al2O3	30,67	30,23	30,33	28,53	30,96	33,50	32,79	33,77	32,73	32,86	34,06	34,00	34,56	34,46	35,25	35,39	36,59	33,86	35,65	36,18
FeO	1,68	1,97	2,73	2,73	2,27	1,71	2,98	2,98	2,66	2,69	2,53	2,55	2,44	2,37	2,22	1,97	2,39	2,12	2,53	2,16
MnO	0,00	0,00	0,00	0,04	0,01	0,02	0,03	0,00	0,00	0,06	0,00	0,00	0,00	0,00	0,04	0,00	0,06	0,00	0,00	0,00
MgO	2,08	2,29	2,36	2,88	2,11	1,11	1,23	0,84	1,13	1,00	0,68	0,66	0,77	0,98	0,47	0,37	0,59	0,67	0,73	0,65
CaO	0,10	0,04	0,03	0,00	0,00	0,00	0,01	0,00	0,00	0,00	0,00	0,04	0,01	0,01	0,03	0,03	0,01	0,00	0,00	0,03
Na2O	0,47	0,49	0,80	0,48	0,70	0,97	0,79	1,07	0,89	1,14	1,10	1,16	0,96	1,17	1,31	1,38	1,24	1,19	0,98	0,95
K2O	9,68	9,15	9,20	9,49	9,43	9,00	9,99	9,88	10,06	9,58	9,73	9,64	10,10	9,56	9,49	9,30	9,11	8,59	9,88	9,03
Total	93,51	93,24	94,43	93,98	93,94	93,24	94,83	95,14	94,08	93,85	94,23	93,74	95,64	98,12	95,08	94,28	99,58	92,31	98,35	98,73
normalized to 22 oxygen																				
Si	6,527	6,581	6,518	6,685	6,478	6,292	6,327	6,227	6,299	6,307	6,204	6,189	6,224	6,370	6,163	6,145	6,251	6,249	6,254	6,326
Ti	0,046	0,037	0,041	0,025	0,041	0,040	0,000	0,021	0,018	0,005	0,023	0,018	0,005	0,014	0,013	0,011	0,023	0,016	0,008	0,002
Al	4,888	4,814	4,803	4,539	4,920	5,342	5,201	5,343	5,232	5,256	5,427	5,446	5,424	5,236	5,549	5,606	5,462	5,455	5,419	5,425
Fe	0,190	0,223	0,307	0,308	0,256	0,193	0,336	0,335	0,301	0,305	0,286	0,290	0,272	0,256	0,247	0,222	0,253	0,242	0,273	0,230
Mn	0,000	0,000	0,000	0,005	0,001	0,002	0,004	0,000	0,000	0,007	0,000	0,000	0,000	0,000	0,004	0,000	0,007	0,000	0,000	0,000
Mg	0,419	0,461	0,473	0,579	0,424	0,224	0,246	0,168	0,228	0,201	0,137	0,133	0,153	0,188	0,093	0,074	0,112	0,137	0,139	0,123
Ca	0,015	0,006	0,004	0,000	0,000	0,000	0,001	0,001	0,000	0,000	0,000	0,005	0,002	0,002	0,004	0,004	0,001	0,000	0,000	0,005
Na	0,124	0,127	0,209	0,126	0,182	0,254	0,205	0,279	0,234	0,301	0,288	0,305	0,247	0,292	0,338	0,360	0,304	0,315	0,244	0,234
K	1,670	1,577	1,577	1,634	1,622	1,553	1,714	1,692	1,740	1,658	1,677	1,671	1,715	1,572	1,617	1,594	1,472	1,497	1,625	1,466
Total	13,880	13,827	13,932	13,901	13,923	13,901	14,033	14,066	14,054	14,039	14,042	14,057	14,040	13,929	14,027	14,017	13,883	13,912	13,963	13,810
Si/2	3,263	3,291	3,259	3,343	3,239	3,146	3,163	3,113	3,150	3,154	3,102	3,095	3,112	3,185	3,081	3,073	3,125	3,125	3,127	3,163
Ti/2	0,023	0,018	0,021	0,012	0,020	0,020	0,000	0,011	0,009	0,002	0,011	0,009	0,002	0,007	0,006	0,006	0,011	0,008	0,004	0,001
Al/2	2,444	2,407	2,401	2,269	2,460	2,671	2,600	2,672	2,616	2,628	2,713	2,723	2,712	2,618	2,774	2,803	2,731	2,728	2,710	2,713
Fe/2	0,095	0,111	0,153	0,154	0,128	0,097	0,168	0,167	0,151	0,153	0,143	0,145	0,136	0,128	0,124	0,111	0,126	0,121	0,136	0,115
Mn/2	0,000	0,000	0,000	0,002	0,001	0,001	0,002	0,000	0,000	0,003	0,000	0,000	0,000	0,000	0,002	0,000	0,003	0,000	0,000	0,000
Mg/2	0,210	0,231	0,236	0,290	0,212	0,112	0,123	0,084	0,114	0,101	0,068	0,067	0,076	0,094	0,047	0,037	0,056	0,069	0,070	0,061
Ca/2	0,008	0,003	0,002	0,000	0,000	0,000	0,000	0,000	0,000	0,000	0,000	0,003	0,001	0,001	0,002	0,002	0,001	0,000	0,000	0,002
Na/2	0,062	0,064	0,105	0,063	0,091	0,127	0,103	0,139	0,117	0,150	0,144	0,152	0,123	0,146	0,169	0,180	0,152	0,157	0,122	0,117
K/2	0,835	0,788	0,788	0,817	0,811	0,777	0,857	0,846	0,870	0,829	0,838	0,835	0,857	0,786	0,808	0,797	0,736	0,749	0,813	0,733
T1: Si	2,000	2,000	2,000	2,000	2,000	2,000	2,000	2,000	2,000	2,000	2,000	2,000	2,000	2,000	2,000	2,000	2,000	2,000	2,000	2,000
T2: Si	1,263	1,291	1,259	1,343	1,239	1,146	1,163	1,113	1,150	1,154	1,102	1,095	1,112	1,185	1,081	1,073	1,125	1,125	1,127	1,163
T2: Al	0,737	0,709	0,741	0,657	0,761	0,854	0,837	0,887	0,850	0,846	0,898	0,905	0,888	0,815	0,919	0,927	0,875	0,875	0,873	0,837
Total T2	2,000	2,000	2,000	2,000	2,000	2,000	2,000	2,000	2,000	2,000	2,000	2,000	2,000	2,000	2,000	2,000	2,000	2,000	2,000	2,000
Ti	0,023	0,018	0,021	0,012	0,020	0,020	0,000	0,011	0,009	0,002	0,011	0,009	0,002	0,007	0,006	0,006	0,011	0,008	0,004	0,001
Mn	0,000	0,000	0,000	0,002	0,001	0,001	0,002	0,000	0,000	0,003	0,000	0,000	0,000	0,000	0,002	0,000	0,003	0,000	0,000	0,000
M2: Al	1,708	1,698	1,660	1,612	1,699	1,817	1,764	1,785	1,766	1,781	1,816	1,818	1,824	1,803	1,856	1,876	1,856	1,852	1,837	1,876
M2: Mg	0,210	0,231	0,236	0,290	0,212	0,112	0,123	0,084	0,114	0,101	0,068	0,067	0,076	0,094	0,047	0,037	0,056	0,069	0,070	0,061
M2: Fe	0,060	0,053	0,083	0,084	0,068	0,050	0,111	0,120	0,111	0,112	0,105	0,107	0,097	0,096	0,089	0,081	0,073	0,071	0,090	0,062
rest Fe	0,035	0,058	0,071	0,070	0,060	0,047	0,056	0,047	0,040	0,041	0,038	0,038	0,039	0,032	0,035	0,029	0,053	0,050	0,047	0,053
Total M2	2,000	2,000	2,000	2,000	2,000	2,000	2,000	2,000	2,000	2,000	2,000	2,000	2,000	2,000	2,000	2,000	2,000	2,000	2,000	2,000
M1: Al	0,000	0,000	0,000	0,000	0,000	0,000	0,000	0,000	0,000	0,000	0,000	0,000	0,000	0,000	0,000	0,000	0,000	0,000	0,000	0,000
M1: Mg	0,000	0,000	0,000	0,000	0,000	0,000	0,000	0,000	0,000	0,000	0,000	0,000	0,000	0,000	0,000	0,000	0,000	0,000	0,000	0,000
M1: Fe	0,035	0,058	0,071	0,070	0,060	0,047	0,056	0,047	0,040	0,041	0,038	0,038	0,039	0,032	0,035	0,029	0,053	0,050	0,047	0,053
Vacanz.	0,965	0,942	0,929	0,930	0,940	0,953	0,944	0,953	0,960	0,959	0,962	0,962	0,961	0,968	0,965	0,971	0,947	0,950	0,953	0,947
Total M1	1,000	1,000	1,000	1,000	1,000	1,000	1,000	1,000	1,000	1,000	1,000	1,000	1,000	1,000	1,000	1,000	1,000	1,000	1,000	1,000
A: K	0,835	0,788	0,788	0,817	0,811	0,777	0,857	0,846	0,870	0,829	0,838	0,835	0,857	0,786	0,808	0,797	0,736	0,749	0,813	0,733
A: Na	0,062	0,064	0,105	0,063	0,091	0,127	0,103	0,139	0,117	0,150	0,144	0,152	0,123	0,146	0,169	0,180	0,152	0,157	0,122	0,117
A: Ca	0,008	0,003	0,002	0,000	0,000	0,000	0,000	0,000	0,000	0,000	0,000	0,003	0,001	0,001	0,002	0,002	0,001	0,000	0,000	0,002
Total A	0,904	0,855	0,895	0,880	0,902	0,904	0,960	0,986	0,987	0,979	0,982	0,990	0,981	0,933	0,979	0,979	0,889	0,906	0,935	0,852
X(Ms)	0,737	0,709	0,741	0,657	0,761	0,854	0,837	0,887	0,850	0,846	0,898	0,905	0,888	0,815	0,919	0,927	0,875	0,875	0,873	0,837
X(Cel)	0,181	0,196	0,157	0,224	0,149	0,078	0,069	0,038	0,065	0,061	0,033	0,030	0,040	0,078	0,022	0,018	0,038	0,043	0,043	0,057
X(Fe-Cel)	0,082	0,095	0,102	0,119	0,090	0,068	0,094	0,076	0,085	0,092	0,069	0,065	0,072	0,107	0,059	0,055	0,087	0,080	0,084	0,106
Ms mol%	73,664	71,695	70,111	69,147	72,580	74,979	76,782	77,095	76,670	73,379	77,436	77,265	78,615	71,170	76,496	76,055	73,650	73,464	77,140	74,127
Pa mol%	5,482	5,787	9,312	5,338	8,130	12,282	9,182	12,713	10,309	13,311	13,298	14,084	11,312	13,202	15,984	17,170	15,208	15,447	11,592	11,851
Cel mol%	20,854	22,517	20,578	25,516	19,290	12,740	14,036	10,192	13,021	13,310	9,266	8,650	10,072	15,628	7,520	6,776	11,143	11,089	11,268	14,023
Fe/(Fe+Mg)	0,312	0,326	0,394	0,347	0,376	0,463	0,577	0,665	0,569	0,602	0,677	0,685	0,640	0,576	0,727	0,750	0,694	0,638	0,662	0,652

Table 5.15 continue

	M96-80/1 (Blueschist metabasite)												TAG (Blueschist metabasite)							95-90/11 (Blue. Metaba.)			
	rim		rim						rim			rim	rim		rim	rim			rim				
	m6-4	m6-5	m6-6	m6-7	m6-8	m6-9	m6-10	m6-18	m6-20	m6-21	m6-22	m6-23	m9-30	m9-31	m9-32	m9-42	m9-43	m9-44	m9-45	m14-1	m14-2	m14-4	m14-5
SiO2	48,16	48,81	48,26	48,58	49,00	49,00	48,65	48,31	48,91	48,92	48,63	48,36	49,13	48,82	49,52	49,52	49,47	49,26	49,33	49,59	49,42	49,32	49,16
TiO2	0,19	0,19	0,21	0,14	0,13	0,17	0,18	0,25	0,13	0,19	0,11	0,28	0,30	0,24	0,19	0,21	0,14	0,18	0,34	0,12	0,25	0,13	0,15
Al2O3	23,77	24,37	24,18	23,85	24,26	24,41	23,55	24,20	24,54	24,61	23,68	24,18	26,51	26,52	26,31	25,97	26,32	25,84	25,96	26,95	27,44	27,01	26,71
FeO	4,87	4,39	4,71	5,33	4,39	5,47	5,76	5,72	4,81	4,93	5,68	5,88	5,49	5,44	5,07	5,37	5,33	5,37	5,58	3,98	4,13	3,87	4,22
MnO	0,02	0,02	0,01	0,03	0,01	0,00	0,01	0,02	0,00	0,00	0,00	0,04	0,00	0,00	0,02	0,03	0,01	0,00	0,03	0,02	0,03	0,00	0,03
MgO	3,29	3,45	3,52	3,40	3,54	3,34	3,36	3,28	3,39	3,41	3,32	3,22	2,72	2,71	2,90	3,07	3,10	2,96	2,88	2,88	2,65	2,95	2,77
CaO	0,15	0,04	0,02	0,02	0,04	0,09	0,04	0,06	0,04	0,02	0,05	0,06	0,00	0,00	0,00	0,00	0,00	0,00	0,01	0,01	0,00	0,02	0,04
Na2O	0,38	0,35	0,35	0,24	0,27	0,30	0,23	0,25	0,39	0,33	0,24	0,29	0,55	0,60	0,60	0,46	0,46	0,44	0,45	0,70	0,64	0,75	0,76
K2O	9,39	9,79	9,81	9,77	9,92	9,54	10,15	9,81	9,64	9,63	9,38	10,15	10,25	10,15	10,21	10,44	10,38	10,01	10,41	10,11	10,22	10,17	9,86
Total	90,23	91,46	91,07	91,36	91,65	92,37	92,04	91,97	91,87	92,11	91,29	92,47	94,97	94,59	94,85	95,06	95,25	94,07	95,05	94,43	94,85	94,44	93,87
normalized to 22 oxygen																							
Si	6,874	6,864	6,832	6,869	6,880	6,847	6,870	6,811	6,852	6,841	6,885	6,800	6,701	6,691	6,746	6,747	6,725	6,765	6,735	6,743	6,699	6,720	6,738
Ti	0,020	0,020	0,022	0,015	0,014	0,018	0,019	0,027	0,014	0,020	0,012	0,030	0,031	0,025	0,019	0,021	0,014	0,019	0,035	0,012	0,025	0,013	0,015
Al	3,999	4,040	4,035	3,975	4,015	4,021	3,920	4,022	4,052	4,056	3,952	4,007	4,262	4,284	4,224	4,171	4,217	4,183	4,178	4,320	4,385	4,338	4,315
Fe	0,581	0,516	0,558	0,630	0,515	0,639	0,680	0,674	0,563	0,576	0,672	0,691	0,626	0,623	0,577	0,612	0,606	0,617	0,637	0,453	0,468	0,441	0,484
Mn	0,003	0,002	0,001	0,003	0,001	0,000	0,001	0,003	0,000	0,000	0,000	0,005	0,000	0,000	0,002	0,003	0,001	0,000	0,003	0,003	0,004	0,000	0,003
Mg	0,700	0,723	0,743	0,717	0,741	0,696	0,707	0,689	0,708	0,711	0,701	0,675	0,553	0,554	0,589	0,623	0,628	0,606	0,586	0,584	0,535	0,599	0,566
Ca	0,023	0,006	0,003	0,003	0,006	0,013	0,006	0,009	0,006	0,003	0,008	0,009	0,000	0,000	0,000	0,000	0,000	0,000	0,001	0,002	0,000	0,002	0,005
Na	0,104	0,094	0,096	0,065	0,074	0,082	0,063	0,068	0,105	0,088	0,066	0,080	0,145	0,159	0,158	0,121	0,122	0,118	0,118	0,184	0,167	0,198	0,201
K	1,710	1,756	1,772	1,762	1,777	1,700	1,828	1,764	1,723	1,718	1,730	1,820	1,783	1,774	1,774	1,815	1,800	1,754	1,813	1,754	1,767	1,768	1,724
Total	14,013	14,022	14,062	14,042	14,024	14,016	14,096	14,067	14,022	14,014	14,023	14,117	14,101	14,109	14,089	14,114	14,113	14,051	14,107	14,054	14,050	14,080	14,052
Si/2	3,437	3,432	3,416	3,435	3,440	3,424	3,435	3,406	3,426	3,420	3,443	3,400	3,350	3,345	3,373	3,374	3,362	3,382	3,367	3,372	3,350	3,360	3,369
Ti/2	0,010	0,010	0,011	0,007	0,007	0,009	0,010	0,013	0,007	0,010	0,006	0,015	0,016	0,012	0,010	0,011	0,007	0,009	0,018	0,006	0,013	0,007	0,008
Al/2	1,999	2,020	2,018	1,988	2,008	2,010	1,960	2,011	2,026	2,028	1,976	2,004	2,131	2,142	2,112	2,085	2,109	2,091	2,089	2,160	2,192	2,169	2,158
Fe/2	0,291	0,258	0,279	0,315	0,258	0,320	0,340	0,337	0,282	0,288	0,336	0,346	0,313	0,312	0,289	0,306	0,303	0,308	0,319	0,226	0,234	0,220	0,242
Mn/2	0,001	0,001	0,001	0,003	0,001	0,000	0,001	0,001	0,000	0,000	0,000	0,002	0,000	0,000	0,001	0,002	0,001	0,000	0,002	0,001	0,002	0,000	0,002
Mg/2	0,350	0,362	0,371	0,358	0,370	0,348	0,354	0,345	0,354	0,355	0,350	0,337	0,276	0,277	0,294	0,312	0,314	0,303	0,293	0,292	0,268	0,300	0,283
Ca/2	0,011	0,003	0,002	0,002	0,003	0,007	0,003	0,005	0,003	0,001	0,004	0,005	0,000	0,000	0,000	0,000	0,000	0,000	0,001	0,001	0,000	0,001	0,003
Na/2	0,052	0,047	0,048	0,032	0,037	0,041	0,031	0,034	0,052	0,044	0,033	0,040	0,072	0,079	0,079	0,060	0,061	0,059	0,059	0,092	0,083	0,099	0,101
K/2	0,855	0,878	0,886	0,881	0,888	0,850	0,914	0,882	0,861	0,859	0,865	0,910	0,892	0,887	0,887	0,907	0,900	0,877	0,906	0,877	0,884	0,884	0,862
T1: Si	2,000	2,000	2,000	2,000	2,000	2,000	2,000	2,000	2,000	2,000	2,000	2,000	2,000	2,000	2,000	2,000	2,000	2,000	2,000	2,000	2,000	2,000	2,000
T2: Si	1,437	1,432	1,416	1,435	1,440	1,424	1,435	1,406	1,426	1,420	1,443	1,400	1,350	1,345	1,373	1,374	1,362	1,382	1,367	1,372	1,350	1,360	1,369
T2: Al	0,563	0,568	0,584	0,565	0,560	0,576	0,565	0,594	0,574	0,580	0,557	0,600	0,650	0,655	0,627	0,626	0,638	0,618	0,633	0,628	0,650	0,640	0,631
Total T2	2,000	2,000	2,000	2,000	2,000	2,000	2,000	2,000	2,000	2,000	2,000	2,000	2,000	2,000	2,000	2,000	2,000	2,000	2,000	2,000	2,000	2,000	2,000
Ti	0,010	0,010	0,011	0,007	0,007	0,009	0,010	0,013	0,007	0,010	0,006	0,015	0,016	0,012	0,010	0,011	0,007	0,009	0,018	0,006	0,013	0,007	0,008
Mn	0,001	0,001	0,001	0,003	0,001	0,000	0,001	0,001	0,000	0,000	0,000	0,002	0,000	0,000	0,001	0,002	0,001	0,000	0,002	0,001	0,002	0,000	0,002
M2: Al	1,436	1,452	1,434	1,422	1,448	1,434	1,395	1,416	1,452	1,449	1,419	1,403	1,481	1,487	1,485	1,459	1,471	1,474	1,456	1,532	1,542	1,529	1,527
M2: Mg	0,350	0,362	0,371	0,358	0,370	0,348	0,354	0,345	0,354	0,355	0,350	0,337	0,276	0,277	0,294	0,312	0,314	0,303	0,293	0,292	0,268	0,300	0,283
M2: Fe	0,202	0,176	0,183	0,209	0,174	0,210	0,241	0,224	0,187	0,186	0,225	0,242	0,227	0,224	0,210	0,217	0,207	0,214	0,231	0,169	0,176	0,164	0,181
rest Fe	0,088	0,083	0,096	0,106	0,083	0,110	0,099	0,113	0,094	0,102	0,111	0,104	0,087	0,088	0,079	0,089	0,096	0,095	0,087	0,057	0,058	0,056	0,061
Total M2	2,000	2,000	2,000	2,000	2,000	2,000	2,000	2,000	2,000	2,000	2,000	2,000	2,000	2,000	2,000	2,000	2,000	2,000	2,000	2,000	2,000	2,000	2,000
M1: Al	0,000	0,000	0,000	0,000	0,000	0,000	0,000	0,000	0,000	0,000	0,000	0,000	0,000	0,000	0,000	0,000	0,000	0,000	0,000	0,000	0,000	0,000	0,000
M1: Mg	0,000	0,000	0,000	0,000	0,000	0,000	0,000	0,000	0,000	0,000	0,000	0,000	0,000	0,000	0,000	0,000	0,000	0,000	0,000	0,000	0,000	0,000	0,000
M1: Fe	0,088	0,083	0,096	0,106	0,083	0,110	0,099	0,113	0,094	0,102	0,111	0,104	0,087	0,088	0,079	0,089	0,096	0,095	0,087	0,057	0,058	0,056	0,061
Vacanz.	0,912	0,917	0,904	0,894	0,917	0,890	0,901	0,887	0,906	0,898	0,889	0,896	0,913	0,912	0,921	0,911	0,904	0,905	0,913	0,943	0,942	0,944	0,939
Total M1	1,000	1,000	1,000	1,000	1,000	1,000	1,000	1,000	1,000	1,000	1,000	1,000	1,000	1,000	1,000	1,000	1,000	1,000	1,000	1,000	1,000	1,000	1,000
A: K	0,855	0,878	0,886	0,881	0,888	0,850	0,914	0,882	0,861	0,859	0,865	0,910	0,892	0,887	0,887	0,907	0,900	0,877	0,906	0,877	0,884	0,884	0,862
A: Na	0,052	0,047	0,048	0,032	0,037	0,041	0,031	0,034	0,052	0,044	0,033	0,040	0,072	0,079	0,079	0,060	0,061	0,059	0,059	0,092	0,083	0,099	0,101
A: Ca	0,011	0,003	0,002	0,002	0,003	0,007	0,003	0,005	0,003	0,001	0,004	0,005	0,000	0,000	0,000	0,000	0,000	0,000	0,001	0,001	0,000	0,001	0,003
Total A	0,918	0,928	0,935	0,915	0,929	0,898	0,949	0,920	0,917	0,905	0,902	0,955	0,964	0,966	0,966	0,968	0,961	0,936	0,966	0,970	0,967	0,984	0,965
X(Ms)	0,563	0,568	0,584	0,565	0,560	0,576	0,565	0,594	0,574	0,580	0,557	0,600	0,650	0,655	0,627	0,626	0,638	0,618	0,633	0,628	0,650	0,640	0,631
X(Cel)	0,239	0,252	0,238	0,231	0,260	0,221	0,222	0,205	0,237	0,232	0,226	0,197	0,164	0,162	0,188	0,189	0,184	0,190	0,176	0,209	0,187	0,207	0,199
X(Fe-Cel)	0,198	0,180	0,178	0,203	0,181	0,203	0,213	0,201	0,189	0,188	0,217	0,202	0,186	0,183	0,185	0,185	0,178	0,193	0,191	0,162	0,163	0,153	0,170
Ms mol%	65,596	66,272	66,991	67,232	66,648	67,004	67,357	37,800	66,124	66,960	66,787	68,438	68,494	68,233	66,900	68,249	68,751	67,776	68,651	65,977	67,701	66,120	65,407
Pa mol%	4,003	3,560	3,622	2,468	2,788	3,245	2,320	33,345	4,014	3,445	2,532	3,003	5,555	6,100	5,945	4,590	4,651	4,559	4,480	6,923	6,393	7,401	7,642
Cel mol%	30,401	30,168	29,387	30,300	30,564	29,751	30,323	28,855	29,862	29,595	30,681	28,559	25,951	25,663	27,155	27,201	26,598	27,665	26,869	27,100	25,906	26,479	26,951
Fe/(Fe+Mg)	0,454	0,417	0,429	0,468	0,410	0,479	0,490	0,495	0,443	0,448	0,490	0,506	0,531	0,530	0,495	0,495	0,491	0,504	0,521	0,437	0,466	0,424	0,461

quite low X_{Cel} contents of white micas from kyanite-chloritoid schists, they close to the muscovite composition (Figure 5.52a). The muscovite- Al-celadonite series is due to by Tschermak (phengite => muscovite) or inverse Tschermak (muscovite => phengite) substitution. Tschermak substitution between phengite and muscovite is especially marked in garnet-mica schists (Figure 5.52a). Example of this substitution is given below.

$(K_{0.81}Na_{0.06})\ (Al_{1.61}Mg_{0.29}Fe_{0.09}Ti_{0.01})\ (Si_{3.34}Al_{0.66})\ O_{10}\ (OH)_2$ (analyse no: m18-38 (table 5.14)

+0.21 -0.18 -0.04 -0.19 +0.19

$(K_{0.77}Na_{0.12})\ (Al_{1.82}Mg_{0.11}Fe_{0.05}Ti_{0.02})\ (Si_{3.15}Al_{0.85})\ O_{10}\ (OH)_2$ (analyse no: 18-40 (table 5.14)

Except for blueschist metabasites and metapelites that contain glaucophane, white micas in marble-schist series indicate a slight enrichment in Na which is connected to a decrease of Si (Figure 5.52b). In the muscovite (Ms) - paragonite (Pa) – celadonite (Cel) triangle diagram, white micas belonging to marble-schist series are phengitic (blueschist metabasites and metapelites), intermediate (garnet-mica schist) and muscovitic (kyanite-chloritoid schist) (Figure 5.52c). In Figure 5.52d, the dashed line represents the ideal tschermaks substitution between the end members muscovite and celadonite. This plot indicates a decrease of phengite component with Tschermaks substitution (Figure 5.52d). Celadonite content of phengites in kyanite-chloritoid schists is quite low. They have a composition close to the muscovite end member. Due to effective Tschermak substitution, garnet-mica schists display a broad phengitic composition range. White micas from blueschist metabasites and metapelites in marble-schist series show the highest celadonite content (Figure 5.52d). In addition, phengites in these rocks do not display a zoning profile.

5.5.2. Trioctahedral micas

Trioctahedral micas exist in blueschist metabasite blocks (M98-52/2) from the metaolistostrome unit and the garnet-mica schists (M97-36 and M99-52/5), blueschist metabasite (TAG), Kyanite-chloritoid schist (M98-135/1, 94-43/4 and 94-

85/1) and chloritoid phyllite (95-41/2) from the marble-schist series. Representative trioctahedral mica (biotite and chlorite) analyses are listed in Table 5.16 and 5.17.

5.5.2.1. Trioctahedral micas in the Metaolistostrome unit

Biotites: Trioctahedral micas from M98-52/2 (blueschist metabasite block) display Fe/(Fe+Mg) values between 0.334 and 0.387, and Ti and Al^{VI} (Al in M site) contents in range of 0.065 – 0.100 and 0.197 – 0.214, on the basis of 22 (O) (Table 5.16). Biotites show decrease in Fe / Fe + Mg ratio with increasing metamorphic grade (Okay 1989). The most of trioctahedral micas from M98-52/2 plot on the biotite – phlogopite (name for composition near the Mg-rich end-member) tie line. Two analyses fall into biotite field. In Figure 5.54, trioctahedral micas from M98-52/2 are poorer in Fe / Fe + Mg ratio and Al^{IV} when compared to marble-schist series.

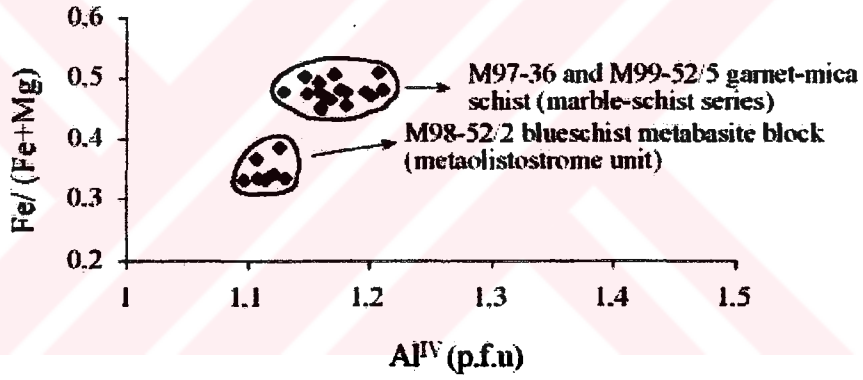


Figure 5.54 Compositional difference of biotites from the Metaolistostrome unit and the Marble-schist series (Tosch and Lugmair, 1990).

Trioctahedral mica analyses (M98-52/2) plotted into a diagram showing the variations in mica compositions plot close to phlogopite – annite composition rather than eastonite (Figure 5.55). In addition, white mica compositions from metaolistostrom and marble – schist units are also given in Figure 5.55. Maximum phlogopite content of the analysed trioctahedral micas is 0.666. Average annite and phlogopite contents are 0.349 and 0.651, respectively. Neither phlogopite $[KMg_3(AlSi_3)O_{10}(OH)_2]$ nor annite $[KFe_3(AlSi_3)O_{10}(OH)_2]$ has Al in M sites but, in

Table 5.16 Represantative trioctahedral mica analyses from blueschist metabasite block (M98-52/2) and garnet-mica schist (M97-36 and M99-52/5).

	M98-52/2							M97-36								M99-52/5								
	m11-1	m11-36	m11-2	m11-37	m11-3	m11-23	m11-24	m17-10	m17-11	m17-12	m17-13	m17-26	m17-28	m17-29	m17-30	m18-2	m18-25	m18-26	m18-29	m18-31	m18-30	m18-33	m18-32	m18-27
SiO2	38,83	38,44	38,86	39,17	38,83	38,52	38,48	36,83	37,18	36,79	36,56	37,51	37,72	37,72	37,48	37,39	36,91	37,2	37,62	37,03	37,47	37,6	37,09	37,59
TiO2	1,207	1,269	1,348	1,175	1,178	1,615	1,78	1,438	1,492	1,43	1,462	1,361	1,448	1,445	1,449	1,344	1,33	1,199	1,625	1,71	1,631	1,7	1,468	1,635
Al2O3	15,27	15,25	15,07	14,99	15,05	14,87	15,02	18,1	17,92	17,7	17,75	17,22	17,68	17,53	17,88	17,94	17,89	17,67	17,91	18,66	18,41	18,12	17,8	17,81
FeO	14,45	14,09	14	14,07	14,17	14,97	15,86	18,08	18,03	18,05	19,29	17,35	17,64	17,06	17,25	18,09	18,47	18,16	16,65	16,75	17,42	17,13	16,91	17,14
MnO	0,462	0,537	0,527	0,544	0,545	0,645	0,715	0,083	0,113	0,05	0,111	0,031	0,077	0,018	0,12	0,039	0,141	0,101	0,043	0,08	0,098	0,058	0,097	0,076
MgO	15,56	15,58	15,64	15,69	15,64	14,37	14,07	10,91	11,3	11,03	10,33	11,77	11,28	11,65	11,42	9,94	10,05	10,37	10,19	10,08	10,66	10,45	10,75	10,58
CaO	0,028	0	0	0,022	0,038	0,089	0	0,036	0,025	0,044	0	0,048	0,053	0,04	0,029	0,043	0,076	0,092	0,187	0,019	0,06	0,097	0,064	0,054
Na2O	0,091	0,037	0,096	0,09	0,051	0,05	0,061	0,177	0,096	0,101	0,049	0,152	0,187	0,12	0,089	0,115	0,047	0,081	0,115	0,075	0,071	0,024	0,091	0,047
K2O	9,56	9,51	9,68	9,49	9,35	9,42	9,66	9,08	8,98	8,79	8,84	8,52	8,93	8,87	9,05	8,61	8,37	8,76	8,35	8,38	8,75	8,84	8,72	8,74
Summe	95,55	94,81	95,31	95,29	94,96	94,58	95,68	94,798	95,167	94,049	94,392	94,025	95,043	94,465	94,794	93,564	93,349	93,679	92,763	92,857	94,635	94,054	93,051	93,732
normalized to 22 oxygens																								
Si	5,758	5,741	5,772	5,807	5,783	5,789	5,749	5,577	5,597	5,607	5,585	5,682	5,667	5,681	5,640	5,707	5,660	5,686	5,742	5,651	5,639	5,685	5,674	5,704
Ti	0,135	0,143	0,151	0,131	0,132	0,182	0,200	0,164	0,169	0,164	0,168	0,155	0,164	0,164	0,164	0,154	0,153	0,138	0,187	0,196	0,185	0,193	0,169	0,187
Al	2,669	2,685	2,638	2,620	2,642	2,634	2,645	3,231	3,180	3,180	3,196	3,075	3,131	3,112	3,172	3,227	3,234	3,183	3,222	3,357	3,266	3,229	3,209	3,186
Fe	1,792	1,760	1,739	1,744	1,765	1,881	1,981	2,289	2,269	2,300	2,464	2,198	2,216	2,149	2,171	2,309	2,368	2,321	2,125	2,137	2,192	2,166	2,163	2,175
Mn	0,058	0,068	0,066	0,068	0,069	0,082	0,090	0,011	0,014	0,006	0,014	0,004	0,010	0,002	0,015	0,005	0,018	0,013	0,006	0,010	0,012	0,007	0,013	0,010
Mg	3,439	3,468	3,462	3,467	3,472	3,219	3,133	2,462	2,535	2,505	2,352	2,658	2,526	2,615	2,561	2,261	2,297	2,362	2,318	2,293	2,391	2,355	2,451	2,393
Ca	0,004	0,000	0,000	0,003	0,006	0,014	0,000	0,006	0,004	0,007	0,000	0,008	0,009	0,006	0,005	0,007	0,012	0,015	0,031	0,003	0,010	0,016	0,010	0,009
Na	0,026	0,011	0,028	0,026	0,015	0,015	0,018	0,052	0,028	0,030	0,015	0,045	0,054	0,035	0,026	0,034	0,014	0,024	0,034	0,022	0,021	0,007	0,027	0,014
K	1,808	1,812	1,834	1,795	1,776	1,806	1,841	1,754	1,724	1,709	1,723	1,646	1,711	1,704	1,737	1,676	1,637	1,708	1,626	1,631	1,680	1,705	1,701	1,692
Sum	15,690	15,686	15,689	15,662	15,659	15,622	15,658	15,546	15,521	15,509	15,517	15,471	15,487	15,469	15,491	15,381	15,395	15,451	15,290	15,301	15,394	15,363	15,417	15,369
Si/2	2,879	2,870	2,886	2,904	2,892	2,894	2,875	2,789	2,798	2,803	2,793	2,841	2,833	2,841	2,820	2,853	2,830	2,843	2,871	2,826	2,819	2,842	2,837	2,852
Ti/2	0,067	0,071	0,075	0,065	0,066	0,091	0,100	0,082	0,084	0,082	0,084	0,078	0,082	0,082	0,082	0,077	0,077	0,069	0,093	0,098	0,092	0,097	0,084	0,093
Al/2	1,335	1,342	1,319	1,310	1,321	1,317	1,323	1,615	1,590	1,590	1,598	1,537	1,565	1,556	1,586	1,614	1,617	1,592	1,611	1,678	1,633	1,615	1,605	1,593
Fe/2	0,896	0,880	0,869	0,872	0,882	0,941	0,991	1,145	1,135	1,150	1,232	1,099	1,108	1,074	1,085	1,154	1,184	1,160	1,063	1,069	1,096	1,083	1,081	1,087
Mn/2	0,029	0,034	0,033	0,034	0,034	0,041	0,045	0,005	0,007	0,003	0,007	0,002	0,005	0,001	0,008	0,003	0,009	0,007	0,003	0,005	0,006	0,004	0,006	0,005
Mg/2	1,720	1,734	1,731	1,734	1,736	1,609	1,567	1,231	1,268	1,253	1,176	1,329	1,263	1,308	1,281	1,131	1,149	1,181	1,159	1,146	1,195	1,177	1,225	1,196
Ca/2	0,002	0,000	0,000	0,002	0,003	0,007	0,000	0,003	0,002	0,004	0,000	0,004	0,004	0,003	0,002	0,004	0,006	0,008	0,015	0,002	0,005	0,008	0,005	0,004
Na/2	0,013	0,005	0,014	0,013	0,007	0,007	0,009	0,026	0,014	0,015	0,007	0,022	0,027	0,018	0,013	0,017	0,007	0,012	0,017	0,011	0,010	0,004	0,013	0,007
K/2	0,904	0,906	0,917	0,897	0,888	0,903	0,920	0,877	0,862	0,854	0,861	0,823	0,856	0,852	0,869	0,838	0,819	0,854	0,813	0,816	0,840	0,852	0,851	0,846
T1: Si	2,000	2,000	2,000	2,000	2,000	2,000	2,000	2,000	2,000	2,000	2,000	2,000	2,000	2,000	2,000	2,000	2,000	2,000	2,000	2,000	2,000	2,000	2,000	2,000
T2: Si	0,879	0,870	0,886	0,904	0,892	0,894	0,875	0,789	0,798	0,803	0,793	0,841	0,833	0,841	0,820	0,853	0,830	0,843	0,871	0,826	0,819	0,842	0,837	0,852
T2: Al	1,121	1,130	1,114	1,096	1,108	1,106	1,125	1,211	1,202	1,197	1,207	1,159	1,167	1,159	1,180	1,147	1,170	1,157	1,129	1,174	1,181	1,158	1,163	1,148
Sum T2	2,000	2,000	2,000	2,000	2,000	2,000	2,000	2,000	2,000	2,000	2,000	2,000	2,000	2,000	2,000	2,000	2,000	2,000	2,000	2,000	2,000	2,000	2,000	2,000
Ti	0,067	0,071	0,075	0,065	0,066	0,091	0,100	0,082	0,084	0,082	0,084	0,078	0,082	0,082	0,082	0,077	0,077	0,069	0,093	0,098	0,092	0,097	0,084	0,093
Mn	0,029	0,034	0,033	0,034	0,034	0,041	0,045	0,005	0,007	0,003	0,007	0,002	0,005	0,001	0,008	0,003	0,009	0,007	0,003	0,005	0,006	0,004	0,006	0,005
M2: Al	0,214	0,213	0,205	0,214	0,213	0,211	0,197	0,404	0,388	0,393	0,391	0,379	0,399	0,397	0,406	0,467	0,447	0,435	0,482	0,304	0,452	0,457	0,441	0,445
rest Al	0,000	0,000	0,000	0,000	0,000	0,000	0,000	0,000	0,000	0,000	0,000	0,000	0,000	0,000	0,000	0,000	0,000	0,000	0,000	0,000	0,000	0,000	0,000	0,000
M2: Mg	0,860	0,867	0,866	0,867	0,868	0,805	0,783	0,616	0,634	0,626	0,588	0,664	0,631	0,654	0,640	0,565	0,574	0,591	0,580	0,573	0,598	0,589	0,613	0,598
rest Mg	0,860	0,867	0,866	0,867	0,868	0,805	0,783	0,616	0,634	0,626	0,588	0,664	0,631	0,654	0,640	0,565	0,574	0,591	0,580	0,573	0,598	0,589	0,613	0,598
M2: Fe	0,830	0,815	0,821	0,820	0,819	0,852	0,874	0,893	0,886	0,895	0,930	0,877	0,883	0,867	0,864	0,888	0,893	0,899	0,842	0,820	0,852	0,854	0,855	0,858
rest Fe	0,066	0,065	0,048	0,052	0,063	0,089	0,116	0,252	0,248	0,255	0,302	0,221	0,225	0,208	0,221	0,266	0,291	0,261	0,220	0,249	0,244	0,229	0,226	0,229
Sum M2	2,000	2,000	2,000	2,000	2,000	2,000	2,000	2,000	2,000	2,000	2,000	2,000	2,000	2,000	2,000	2,000	2,000	2,000	2,000	2,000	2,000	2,000	2,000	2,000
M1: Al	0,000	0,000	0,000	0,000	0,000	0,000	0,000	0,000	0,000	0,000	0,000	0,000	0,000	0,000	0,000	0,000	0,000	0,000	0,000	0,000	0,000	0,000	0,000	0,000
M1: Mg	0,860	0,867	0,866	0,867	0,868	0,805	0,783	0,616	0,634	0,626	0,588	0,664	0,631	0,654	0,640	0,565	0,574	0,591	0,580	0,573	0,598	0,589	0,613	0,598
M1: Fe	0,066	0,065	0,048	0,052	0,063	0,089	0,116	0,252	0,248	0,255	0,302	0,221	0,225	0,208	0,221	0,266	0,291	0,261	0,220	0,249	0,244	0,229	0,226	0,229
Vacanc.	0,075	0,068	0,086	0,081	0,069	0,106	0,100	0,133	0,118	0,119	0,110	0,114	0,144	0,138	0,138	0,168	0,134	0,148	0,200	0,178	0,158	0,182	0,161	0,173
Sum M1	1,000	1,000	1,000	1,000	1,000	1,000	1,000	1,000	1,000	1,000	1,000	1,000	1,000	1,000	1,000	1,000	1,000	1,000	1,000	1,000	1,000	1,000	1,000	1,000
A: K	0,904	0,906	0,917	0,897	0,888	0,903	0,920	0,877	0,862	0,854	0,861	0,823	0,856	0,852	0,869	0,838	0,819	0,854	0,813	0,816	0,840	0,852	0,851	0,846
A: Na	0,013	0,005	0,014	0,013	0,007	0,007	0,009	0,026	0,014	0,015	0,007	0,022	0,027	0,018	0,013	0,017	0,007	0,012	0,017	0,011	0,010	0,004	0,013	0,007
A: Ca	0,002	0,000	0,000	0,002	0,003	0,007	0,000	0,003	0,002	0,004	0,000	0,004	0,004	0,003	0,002	0,004	0,006	0,008	0,015	0,002	0,005	0,008	0,005	0,004
ms (activity)	0,001	0,001	0,001	0,001	0,001	0,001	0,001	0,005	0,004	0,004	0,003	0,003	0,005	0,005	0,005	0,008	0,005	0,006	0,009	0,009	0,007	0,008	0,006	0,007
cel (activity)	0,002	0,002	0,003	0,003	0,002	0,003	0,003	0,005	0,004	0,004	0,003	0,004	0,005	0,005	0,005	0,007	0,005	0,006	0,009	0,007	0,006	0,007	0,006	0,007
pa (activity)	0,000	0,000	0,000	0,000	0,000	0,000	0,000	0,000	0,000	0,000	0,000	0,000	0,000	0,000	0,000	0,000	0,000	0,000	0,000	0,000	0,000	0,000	0,000	0,000
phl (activity)	0,142	0,145	0,147	0,145	0,143	0,116	0,109	0,049	0,053	0,050	0,042	0,059	0,052	0,058	0,053	0,037	0,038	0,043	0,039	0,037	0,043	0,042	0,048	0,044
east (activity)	0,045	0,046	0,044	0,043	0,044	0,038	0,035	0,049	0,049	0,047	0,042	0,046	0,046	0,049	0,050	0,041	0,041	0,043	0,042	0,047	0,047	0,045	0,048	0,044
ann (activity)	0,010	0,010	0,007	0,008	0,009	0,014	0,020	0,042	0,040	0,042	0,054	0,034	0,036	0,032	0,035	0,043	0,046	0,044	0,031	0,033	0,036	0,035	0,034	0,035
phl (endmember)	0,657	0,663	0,666	0,665	0,663	0,631	0,613	0,518	0,528	0,521	0,488	0,547	0,533	0,549	0,541	0,495	0,492	0,504	0,522	0,518	0,522	0,521	0,531	0,524
ann (endmember)	0,343	0,337	0,334	0,335	0,337	0,369	0,387	0,482	0,472	0,479	0,512	0,453	0,467	0,451	0,459	0,505	0,508	0,496	0,478	0,482	0,478	0,479	0,469	0,476

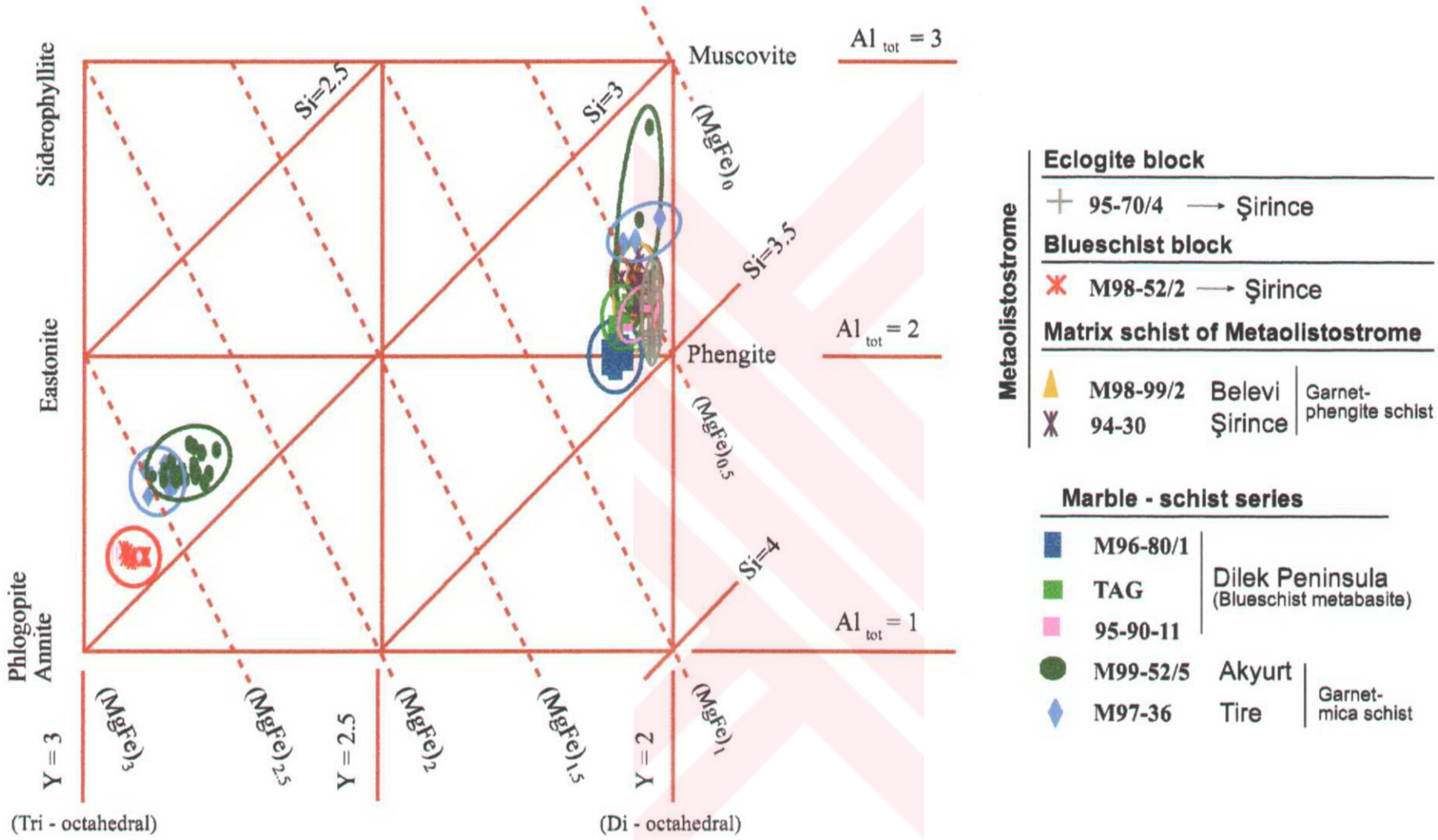


Figure 5.55 Principal variations in mica compositions showing for each the number of octahedral sites filled (di-octahedral, 2; tri-octahedral ,3), and Si Al and M^{2+} atoms per formula unit (Deer et al. 1992).

most natural biotites, there is appreciable substitution of Al for (Mg,Fe) balanced by Al for Si in tetrahedral sites (Tschermak substitution – Mg_{-1} Si_1 Al_2). An average composition of biotite which is the product of this substitution is given below:

$$(K_{0.90}\ Na_{0.01})\ (Al_{0.21}\ Mg_{1.70}\ Fe_{0.91}\ Ti_{0.08})\ (Si_{2.89}\ Al_{1.11})\ O_{10}\ (OH)_2$$

The major substitutions in biotite (Fe/Mg ratio, Al content) tend to reflect rock composition rather than metamorphic grade (Figure 5.54). But Ti content increases with increasing metamorphic grade.

Chlorites: Selected micropyrobe analyses from sample M98-52/2 are presented in Table 5.17. The mineral formulae were calculated of the basis of 14 oxygens (water-free) with total iron as FeO. The cation sums of chlorites are close to the ideal value of 10.0 indicating that ferric iron does not play essential role. They show rather constant Si-contents of 2.7 – 2.8 p.f.u.. Mg< — >Fe substitution occurs over a very wide range and natural tri-octahedral chlorites can as a first approximation be expressed as binary between (Mg_5Al) $(Si_3Al)O_{10}(OH)_8$ clinochlore and (Fe_5Al) $(Si_3Al)O_{10}(OH)_8$ daphnite end-members. Average X_{Mg} (=Mg/(Mg+Fe+Mn) value of chlorites from M98-52/2 is 0.70. Clinochlore end-members of these chlorites is richer relative to daphnite.

5.5.2.2. Trioctahedral mica in the Marble-schist series

The general features of trioctahedral micas in garnet-mica schist, kyanite-chloritoid schist and chloritoid phyllites are given below.

5.5.2.2.1. Trioctahedral mica in garnet-mica schists

Biotite: Analysed trioctahedral micas from sample M97-36 and M99-52/5 show Fe/(Fe+Mg) values between 0.451 and 0.511, and Ti and Al^{VI} (Al in M site) contents in range of 0.069 – 0.098 and 0.379 – 0.504, on the basis of 22 (O) (Table 5.16). Trioctahedral mica analyses are rich in Fe / Fe + Mg ratio and Al^{IV} p.f.u (Figure 52) and change between annite-phlogopite and eastonite composition in range (Figure 5.55). Maximum annite content of analysed trioctahedral micas is 0.512. Average

Table 5.17 Representative chlorite analyses from the Metaolistostrome unit (M98-85/2) and the Marble-schist series.

	metaolistostrome unit		marble-schist series																			
	Blue. metaba.		Blueschist metabasite						Garnet-mica schist			Chloritoid phyllite			Kyanite-chloritoid schist							
	M98-52/2		TAG						M97-36			95-41/2			M97-135/1				94-43/4		94-85/1	
	m11-17	m11-21	m9-6	m9-17	m9-18	m9-19	m9-48	m9-50	1	2	3	1	2	3	1	2	3	4	1	2	1	2
SiO2	27,64	27,79	27,91	28,36	27,45	27,31	27,13	26,90	24,77	26,18	25,89	23,20	22,70	23,58	26,99	27,27	27,20	27,58	27,87	26,96	26,70	25,67
TiO2	0,05	0,01	0,00	0,05	0,07	0,06	0,04	0,06	0,08	0,09	0,08	0,00	0,14	0,09	0,00	0,09	0,00	0,08	0,00	0,09	0,08	0,03
Al2O3	19,89	20,22	18,62	18,12	19,08	18,99	19,00	19,41	22,07	21,80	21,72	21,03	21,10	22,08	24,41	24,75	24,41	24,14	22,88	22,83	23,24	24,50
FeO	15,59	17,00	21,48	21,35	22,12	22,37	21,62	22,23	24,74	21,92	21,92	30,78	29,58	32,30	6,90	7,43	7,47	7,40	8,24	9,38	9,77	10,29
MnO	0,87	0,92	0,12	0,12	0,13	0,08	0,06	0,05	0,12	0,08	0,14	0,15	0,20	0,19	0,95	0,90	0,84	0,85	0,85	0,95	1,20	1,04
MgO	23,16	21,95	19,77	19,08	19,39	19,25	19,34	19,09	14,84	17,86	17,94	9,99	10,52	9,16	24,55	24,37	23,98	23,96	23,73	22,65	23,08	22,68
CaO	0,00	0,01	0,02	0,41	0,05	0,07	0,01	0,03	0,07	0,00	0,02	0,00	0,00	0,00	0,01	0,01	0,04	0,04	0,00	0,01	0,00	0,00
Na2O	0,00	0,04	0,00	0,03	0,07	0,02	0,00	0,00	0,02	0,00	0,02	0,04	0,06	0,02	0,02	0,01	0,00	0,04	0,01	0,04	0,02	0,01
K2O	0,00	0,01	0,00	0,00	0,01	0,00	0,01	0,03	0,17	0,02	0,00	0,00	0,01	0,00	0,01	0,00	0,02	0,01	0,00	0,00	0,01	0,00
Total	87,20	87,95	87,99	87,53	88,40	88,21	87,27	87,82	86,88	87,96	87,73	85,19	84,30	87,42	83,84	84,83	83,96	84,10	83,56	82,91	84,10	84,22
based on 14 oxygens																						
Si	2,788	2,797	2,867	2,926	2,818	2,814	2,816	2,782	2,631	2,694	2,674	2,611	2,572	2,596	2,692	2,693	2,714	2,745	2,803	2,757	2,704	2,604
Ti	0,004	0,001	0,000	0,004	0,006	0,005	0,003	0,005	0,006	0,007	0,006	0,000	0,012	0,007	0,000	0,007	0,000	0,006	0,000	0,007	0,006	0,002
Al	2,364	2,399	2,255	2,204	2,309	2,307	2,324	2,367	2,764	2,644	2,645	2,790	2,818	2,865	2,871	2,882	2,871	2,832	2,713	2,752	2,775	2,930
Fe	1,315	1,431	1,845	1,842	1,899	1,928	1,876	1,923	2,198	1,886	1,893	2,897	2,802	2,973	0,576	0,614	0,623	0,616	0,693	0,802	0,828	0,873
Mn	0,074	0,078	0,011	0,010	0,012	0,007	0,005	0,005	0,011	0,007	0,013	0,014	0,019	0,017	0,080	0,075	0,071	0,072	0,072	0,082	0,103	0,089
Mg	3,481	3,292	3,027	2,934	2,967	2,957	2,992	2,943	2,350	2,739	2,762	1,677	1,777	1,503	3,650	3,587	3,566	3,555	3,558	3,454	3,485	3,429
Ca	0,000	0,001	0,002	0,045	0,005	0,007	0,002	0,004	0,007	0,000	0,002	0,000	0,000	0,000	0,001	0,001	0,005	0,004	0,000	0,001	0,000	0,000
Na	0,000	0,008	0,000	0,005	0,013	0,005	0,000	0,000	0,005	0,000	0,004	0,008	0,012	0,004	0,004	0,002	0,000	0,008	0,001	0,008	0,005	0,002
K	0,000	0,001	0,000	0,000	0,001	0,000	0,001	0,004	0,023	0,003	0,000	0,000	0,001	0,000	0,002	0,000	0,002	0,002	0,000	0,000	0,001	0,000
Total	10,026	10,007	10,006	9,971	10,029	10,030	10,019	10,032	9,994	9,979	9,999	9,998	10,013	9,966	9,875	9,860	9,852	9,839	9,840	9,864	9,905	9,929
XMg	0,715	0,686	0,620	0,613	0,608	0,604	0,614	0,604	0,515	0,591	0,592	0,365	0,386	0,335	0,848	0,839	0,837	0,838	0,823	0,796	0,789	0,781
Al(IV)	1,212	1,203	1,133	1,074	1,182	1,186	1,184	1,218	1,369	1,306	1,326	1,389	1,428	1,404	1,308	1,307	1,286	1,255	1,197	1,243	1,296	1,396
Al(VI)	1,152	1,195	1,121	1,130	1,127	1,121	1,140	1,149	1,395	1,337	1,319	1,401	1,391	1,461	1,563	1,575	1,585	1,577	1,517	1,509	1,479	1,534

annite and phlogopite content are 0.479 and 0.521, respectively. Average biotite composition from garnet-mica schists is given below:

$$(K_{0.85}\ Na_{0.01})\ (Al_{0.43}\ Mg_{1.22}\ Fe_{1.12}\ Ti_{0.09})\ (Si_{2.83}\ Al_{1.17})\ O_{10}\ (OH)_2$$

Average Ti (p.f.u) in garnet-mica schist is higher as 0.01 as than blueschist metabasite block in metaolistostrome unit. This may be related with metamorphic grade or bulk rock chemistry.

Chlorite: Selected micropyrobe analyses from sample M97-36 are given in Table 5.17. The cation sums of micropyrobe analyses are close to the ideal value of 10.0. Average value of cation sums is 9.99. Si-contents are between 2.6 – 2.7 p.f.u.. Average X_{Mg} value of chlorites from M97-36 is 0.56. Clinochlore end-member of chlorite is slightly richer.

5.5.2.2.2. Trioctahedral mica in kyanite-chloritoid schists

Trioctahedral mica type in kyanite-chloritoid schists (M98-135/1-Dilek Peninsula, 94-43/4-Selçuk, 94-85/1-Şirince) is chlorite. Average of cation sums is 9.87. They show rather constant Si-contents of 2.6 – 2.8 p.f.u. On the contrary, X_{Mg} values decrease from Dilek peninsula (0.85) to Şirince (0.78). Chlorites in kyanite-chloritoid schists are rich in Mg and are clinochlore in composition.

5.5.2.2.3. Trioctahedral mica in chloritoid phyllites

Chloritoid phyllites (95-41/2) are exposed in western part of Dilek Peninsula. X_{Mg} contents of chlorites are extremely low in contrast to kyanite-chloritoid schists. Maximum X_{Mg} ratio in chlorites is 0.386. This low ratio may be related to bulk-rock chemistry. Daphnite composition in these chlorites is more dominant.

5.6. Chloritoids

Structural formula of chloritoids have been calculated (Table 5.18) on the basis of 12 oxygens (water-free). Most of resulting Si exceeds ideal value of 2.0 p.f.u. The

Table 5.18 Representative chloritoid analyses from the Marble-schist series.

sample	Dilek Peninsula								Kusadasi				Selcuk			Sirince								
	95-41/2			M97-135/1					94-24/1				94-43/4			94-85/1								
	rim	core	core	rim	←		→	core	core	rim	inclusion	core	core	rim	core	rim	←							→ core
SiO2	22,20	23,96	23,84	25,09	25,20	24,91	25,11	24,69	25,24	26,27	25,18	25,20	25,32	25,13	25,06	25,01	24,52	25,12	25,52	23,93	24,86	25,30	25,17	25,15
TiO2	0,08	0,00	0,03	0,06	0,09	0,00	0,17	0,15	0,08	0,00	0,03	0,00	0,00	0,00	0,00	0,00	0,12	0,00	0,40	0,06	0,09	0,09	0,03	0,06
Al2O3	39,33	40,51	40,76	41,13	41,01	40,75	41,03	40,41	41,68	37,41	41,92	42,00	41,48	41,04	41,10	41,83	41,46	42,17	42,03	39,46	40,62	41,25	41,04	41,25
FeO	24,95	24,49	23,71	11,51	12,16	12,91	12,95	13,33	10,82	10,41	9,67	11,16	12,79	12,99	12,81	12,57	12,46	11,78	11,86	10,40	13,19	13,07	13,40	13,36
MnO	0,56	0,44	0,58	5,91	3,48	3,68	4,00	4,82	5,79	7,44	6,73	4,45	3,02	3,50	3,09	5,53	5,60	4,12	3,94	3,63	4,65	5,01	5,31	5,67
MgO	1,78	1,81	1,91	7,33	8,60	8,00	7,72	7,05	8,36	5,60	8,17	8,57	8,22	8,13	8,19	6,72	6,74	8,02	7,98	7,08	7,26	6,94	6,73	6,65
CaO	0,00	0,00	0,00	0,01	0,01	0,00	0,00	0,00	0,00	0,01	0,00	0,00	0,00	0,00	0,00	0,01	0,01	0,00	0,00	0,00	0,00	0,00	0,01	0,00
Na2O	0,03	0,05	0,01	0,04	0,04	0,00	0,02	0,02	0,01	0,00	0,00	0,01	0,03	0,00	0,00	0,00	0,00	0,02	0,00	0,06	0,03	0,00	0,03	0,02
K2O	0,01	0,02	0,01	0,02	0,00	0,01	0,01	0,00	0,00	0,00	0,02	0,00	0,00	0,00	0,00	0,01	0,00	0,00	0,01	0,00	0,01	0,00	0,00	0,01
Total	88,93	91,27	90,85	91,10	90,59	90,26	91,00	90,46	91,97	87,13	91,72	91,39	90,86	90,78	90,25	91,68	90,92	91,23	91,73	84,62	90,71	91,66	91,70	92,18
based on 12 oxygens																								
Si	1,894	2,017	2,009	2,033	2,036	2,023	2,034	2,019	2,005	2,337	2,005	2,006	2,042	2,029	2,033	2,014	1,986	2,009	2,051	2,086	2,025	2,047	2,038	2,025
Ti	0,005	0,000	0,002	0,004	0,006	0,000	0,010	0,009	0,005	0,000	0,002	0,000	0,000	0,000	0,000	0,000	0,007	0,000	0,024	0,004	0,006	0,006	0,002	0,004
Al	3,954	4,018	4,047	3,928	3,905	3,901	3,917	3,896	3,902	3,923	3,933	3,941	3,943	3,905	3,929	3,970	3,958	3,976	3,980	4,054	3,899	3,934	3,917	3,915
Fe3+	0,046	0,000	0,000	0,072	0,095	0,099	0,083	0,104	0,098	0,077	0,067	0,059	0,057	0,095	0,071	0,030	0,042	0,024	0,020	0,000	0,101	0,066	0,083	0,085
Fe2+	1,734	1,723	1,671	0,709	0,726	0,778	0,794	0,807	0,620	0,697	0,577	0,684	0,805	0,782	0,798	0,816	0,802	0,764	0,777	0,758	0,798	0,819	0,824	0,815
Mn	0,040	0,032	0,041	0,406	0,238	0,253	0,274	0,334	0,389	0,561	0,454	0,300	0,206	0,239	0,212	0,377	0,384	0,279	0,268	0,268	0,321	0,343	0,364	0,387
Mg	0,114	0,113	0,120	0,440	0,515	0,483	0,463	0,428	0,494	0,356	0,484	0,508	0,491	0,488	0,493	0,403	0,407	0,478	0,473	0,454	0,439	0,416	0,404	0,397
Ca	0,000	0,000	0,000	0,001	0,001	0,000	0,000	0,000	0,000	0,001	0,000	0,000	0,000	0,000	0,000	0,001	0,001	0,000	0,000	0,000	0,000	0,000	0,001	0,000
Na	0,005	0,008	0,002	0,006	0,006	0,000	0,003	0,003	0,001	0,000	0,000	0,002	0,005	0,000	0,000	0,000	0,000	0,003	0,000	0,010	0,005	0,000	0,004	0,004
K	0,001	0,002	0,001	0,002	0,000	0,001	0,001	0,000	0,000	0,000	0,002	0,000	0,000	0,000	0,000	0,001	0,000	0,000	0,001	0,000	0,001	0,000	0,000	0,001
Al VI	2,102	1,983	1,990	1,963	1,958	1,977	1,956	1,972	1,990	1,663	1,994	1,994	1,958	1,971	1,967	1,986	2,006	1,991	1,925	1,910	1,970	1,947	1,960	1,971
Al IV	1,852	2,035	2,058	1,966	1,946	1,924	1,961	1,924	1,912	2,260	1,939	1,947	1,984	1,934	1,961	1,983	1,952	1,985	2,055	2,144	1,930	1,987	1,957	1,944
XMg	0,06	0,06	0,07	0,28	0,35	0,32	0,30	0,27	0,33	0,22	0,32	0,34	0,33	0,32	0,33	0,25	0,26	0,31	0,31	0,31	0,28	0,26	0,25	0,25

XMg = Mg / (Mg+Mn+Fe2+)

main substitution in chloritoid is Mn (Fe^{2+}) Mg_{-1} (Figure 5.56). To a lesser extent, the substitution Al_1 Fe^{3+} occurs. Chloritoid porphyroblasts in 94-85/1 and M97-135/1 from kyanite-chloritoid schists are compositionaly zoned with higher Mn and Fe^{2+} contents in cores and higher Mg content in the inner rims (Figure 5.56).

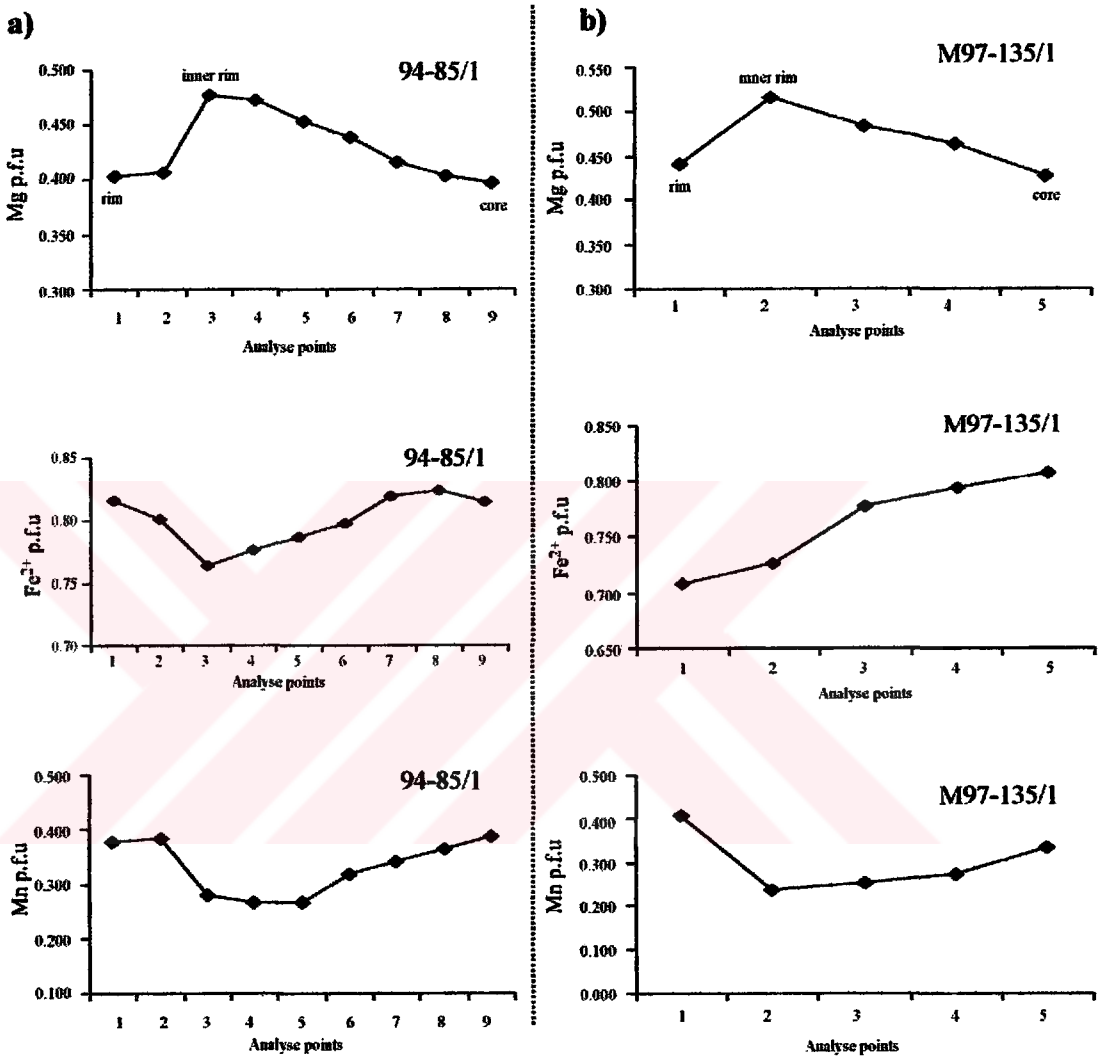


Figure 5.56 Fe^{2+}, Mg and Mn p.f.u variation in chloritoids from kyanite-chloritoid schist (94-85/1(a); M97-135/1 (b)).

Mn pattern shows mirror image of Mg pattern. Mn tends to concentrate in the core of garnet and chloritoid porphyroblasts relative to other minerals during early stages of

crystallization. In samples 94-85/1 and M97-135/1, Mg (p.f.u) is close to 0.40 – 0.42 in the core, increasing to about 0.48 – 0.51 (inner rim) and then decreasing to about 0.40 – 0.44 on the rim, respectively (Figure 5.56).In sample M97-135/1, Fe^{2+} p.f.u value almost gradually decreases from core to rim. Whereas, in sample 94-85/1, Fe^{2+} p.f.u decreases from core to inner rim and then steeply increases rimward (Figure 5.56). Fe^{2+} and Mn are enriched relative to Mg in the cores of the chloritoids, reflecting the prograde metamorphism. Chloritoids tend to become richer in Mg with increasing metamorphic grade. As stated by Chopin and Schreyer (1983), Mg-rich chloritoids are characteristic minerals in high-pressure metamorphic pelites. The most Mg-rich chloritoid (X_{Mg} = 0.35) stem from kyanite-chloritoid schist north of Tuzburgaz (Dilek Peninsula). Maximum X_{Mg} ratios obtained from kyanite-chloritoid schists in Kuşadası, Selçuk and Şirince are 0.34, 0.33 and 0.32, respectively (Table 5.18). A decrease of X_{Mg} ratio of chloritoids from west (Dilek Peninsula) to east (Şirince) may be interpreted to be the result of the increasing effects of retrograde overprint from west to east.

5.7. Epidotes

Composition of epidote group minerals from metaolistostrome unit, i.e eclogite, omphacite-epidotite, blueschist metabasite and omphacite metagabbro blocks, and marble-schist series (blueschist metabasite) are reported in Table 5.19. All iron is considered to be ferric. Based on 12.5 oxygens, cation totals range from 7.755 to 8.012. Average value is 7.979 which is in good agreement with the ideal value of 8.00. Examination of the analytical data shows that potassium and sodium may be present in considerably small in amounts (Na_2O and K_2O average just, in turn, 0.021and 0.007 weight percent in samples in which they were detected). Weight percent averages for TiO_2, Cr_2O_3 and MnO are 0.121, 0.074 and 0.224, respectively. These oxides exhibit reasonably small variations. But, variation of MgO content is pronounced from core to rim. In 95-70/4, the difference of Mg (p.f.u) value between core (0.006) and analyse point number 4 (0.016) is not so high. But, Mg (p.f.u) steeply increases towards rim (0.318) (Figure 5.58a4). Compositional variations within the epidote group are related mainly to the substitution Al <—> Fe^{3+}. All

Table 5.19 Representative epidote and zoisite analyses from the Metalistostrome and the Marble-schist series

	Metaolistostrome unit																						
	Eclogite																						
	95-70-4											M96-31		M97-34/2				M98-45C			SE-1		
	ep	ep	ep	ep	ep	ep	ep	ep	ep	zo	zo	ep	ep	ep	ep	ep	zo	ep	zo	zo	ep	ep	ep
	core	→					rim	inc	inc	core	rim	core	core	core	core	rim	core	core	core	core	inc	inc	
	m3-1	m3-2	m3-3	m3-4	m3-5	m3-6	m3-7	m3-49	m3-50	m3-62	m3-63	m5-31	m5-36	m7-11	m7-68	m7-69	m7-71	m4-32	m4-33	m4-79	m8-136	m8-177	m8-178
SiO2	38,48	38,86	38,64	38,75	39,50	42,29	44,91	38,34	38,56	38,75	38,65	37,86	38,37	37,84	37,74	37,44	38,08	38,75	38,52	37,90	38,30	38,24	37,83
TiO2	0,19	0,18	0,10	0,15	0,11	0,11	0,14	0,15	0,12	0,16	0,11	0,00	0,16	0,08	0,15	0,01	0,08	0,21	0,19	0,56	0,06	0,06	0,07
Al2O3	26,80	26,73	26,78	26,60	25,40	21,74	18,50	27,14	27,28	27,72	26,94	25,03	27,07	23,58	24,64	23,55	24,07	26,22	26,05	26,85	24,92	25,32	24,28
Fe2O3	6,65	7,13	7,27	7,24	7,41	7,50	6,85	7,68	7,16	6,70	7,38	9,98	7,48	11,84	10,14	10,73	10,98	8,71	8,62	6,57	9,96	8,55	10,90
MnO	0,21	0,25	0,29	0,24	0,24	0,19	0,21	0,35	0,31	0,06	0,20	0,23	0,15	0,45	0,22	0,39	0,49	0,31	0,27	0,18	0,63	0,42	0,38
MgO	0,05	0,05	0,09	0,14	0,55	1,85	2,62	0,03	0,06	0,07	0,04	0,00	0,06	0,03	0,05	0,04	0,03	0,10	0,11	0,10	0,03	0,03	0,05
CaO	23,21	23,35	23,56	23,29	22,32	20,26	17,60	23,65	24,04	23,89	23,85	23,88	23,93	23,35	23,31	23,14	23,41	23,36	23,34	23,72	23,42	22,40	23,01
Na2O	0,00	0,00	0,02	0,00	0,05	0,09	0,12	0,04	0,00	0,00	0,00	0,00	0,00	0,02	0,00	0,00	0,00	0,00	0,05	0,02	0,02	0,00	0,01
K2O	0,03	0,01	0,00	0,00	0,00	0,02	0,01	0,00	0,01	0,01	0,01	0,00	0,00	0,00	0,00	0,00	0,00	0,02	0,00	0,00	0,00	0,00	0,00
Cr2O3	0,05	0,07	0,01	0,02	0,01	0,07	0,05	0,10	0,03	0,03	0,06	0,07	0,05	0,10	0,04	0,03	0,09	0,15	0,14	0,32	0,04	0,12	0,00
Total	95,66	96,63	96,76	96,42	95,59	94,12	91,02	97,48	97,58	97,39	97,23	97,05	97,27	97,28	96,28	95,34	97,23	97,83	97,28	96,23	97,38	95,14	96,52
based on 12.5 oxygens																							
Si4+	3,057	3,061	3,045	3,060	3,137	3,381	3,658	3,007	3,017	3,025	3,033	3,012	3,013	3,024	3,024	3,041	3,034	3,034	3,035	3,005	3,035	3,072	3,030
Ti4+	0,012	0,011	0,006	0,009	0,006	0,006	0,009	0,009	0,007	0,009	0,006	0,000	0,010	0,005	0,009	0,001	0,005	0,013	0,011	0,033	0,004	0,004	0,004
Al3+	2,510	2,482	2,488	2,476	2,378	2,049	1,776	2,509	2,516	2,551	2,492	2,348	2,505	2,221	2,327	2,255	2,260	2,420	2,419	2,510	2,328	2,398	2,292
Fe3+	0,398	0,423	0,431	0,430	0,443	0,451	0,420	0,453	0,422	0,394	0,436	0,598	0,442	0,712	0,611	0,656	0,658	0,513	0,511	0,392	0,594	0,517	0,657
Mn2+	0,014	0,017	0,019	0,016	0,016	0,013	0,015	0,023	0,021	0,004	0,013	0,015	0,010	0,030	0,015	0,027	0,033	0,020	0,018	0,012	0,042	0,029	0,025
Mg2+	0,006	0,006	0,011	0,016	0,065	0,220	0,318	0,004	0,007	0,008	0,004	0,000	0,007	0,003	0,006	0,005	0,004	0,011	0,012	0,012	0,004	0,004	0,006
Ca2+	1,976	1,971	1,989	1,970	1,899	1,735	1,536	1,988	2,015	1,998	2,006	2,036	2,013	1,999	2,001	2,014	1,998	1,960	1,970	2,015	1,988	1,928	1,974
Na1+	0,000	0,000	0,003	0,000	0,007	0,014	0,019	0,006	0,000	0,000	0,000	0,000	0,000	0,003	0,000	0,000	0,000	0,000	0,007	0,004	0,003	0,000	0,001
K1+	0,003	0,001	0,000	0,000	0,000	0,002	0,001	0,000	0,001	0,001	0,001	0,000	0,000	0,000	0,000	0,000	0,000	0,002	0,000	0,000	0,000	0,000	0,000
Cr3+	0,003	0,004	0,000	0,001	0,001	0,005	0,003	0,006	0,002	0,002	0,003	0,004	0,003	0,006	0,002	0,002	0,005	0,009	0,009	0,020	0,002	0,008	0,000
Total	7,977	7,974	7,992	7,978	7,953	7,876	7,754	8,005	8,007	7,993	7,995	8,013	8,003	8,003	7,995	8,000	7,998	7,983	7,992	8,004	7,999	7,960	7,990
Si	3,057	3,061	3,045	3,060	3,137	3,381	3,658	3,007	3,017	3,025	3,033	3,012	3,013	3,024	3,024	3,041	3,034	3,034	3,035	3,005	3,035	3,072	3,030
Al(IV)	0,000	0,000	0,000	0,000	0,000	0,000	0,000	0,000	0,000	0,000	0,000	0,000	0,000	0,000	0,000	0,000	0,000	0,000	0,000	0,000	0,000	0,000	0,000
X total	3,057	3,061	3,045	3,060	3,137	3,381	3,658	3,007	3,017	3,025	3,033	3,012	3,013	3,024	3,024	3,041	3,034	3,034	3,035	3,005	3,035	3,072	3,030
Al(VI)	2,510	2,482	2,488	2,476	2,378	2,049	1,776	2,509	2,516	2,551	2,492	2,348	2,505	2,221	2,327	2,255	2,260	2,420	2,419	2,510	2,328	2,398	2,292
FeIII	0,398	0,423	0,431	0,430	0,443	0,451	0,420	0,453	0,422	0,394	0,436	0,598	0,442	0,712	0,611	0,656	0,658	0,513	0,511	0,392	0,594	0,517	0,657
Ti	0,012	0,011	0,006	0,009	0,006	0,006	0,009	0,009	0,007	0,009	0,006	0,000	0,010	0,005	0,009	0,001	0,005	0,013	0,011	0,033	0,004	0,004	0,004
Y total	2,919	2,915	2,925	2,915	2,827	2,506	2,205	2,972	2,944	2,954	2,934	2,945	2,957	2,938	2,947	2,912	2,924	2,946	2,941	2,935	2,925	2,919	2,953
Mg	0,006	0,006	0,011	0,016	0,065	0,220	0,318	0,004	0,007	0,008	0,004	0,000	0,007	0,003	0,006	0,005	0,004	0,011	0,012	0,012	0,004	0,004	0,006
Mn	0,014	0,017	0,019	0,016	0,016	0,013	0,015	0,023	0,021	0,004	0,013	0,015	0,010	0,030	0,015	0,027	0,033	0,020	0,018	0,012	0,042	0,029	0,025
Ca	1,976	1,971	1,989	1,970	1,899	1,735	1,536	1,988	2,015	1,998	2,006	2,036	2,013	1,999	2,001	2,014	1,998	1,960	1,970	2,015	1,988	1,928	1,974
Z total	1,995	1,993	2,019	2,002	1,981	1,968	1,869	2,015	2,043	2,010	2,023	2,051	2,030	2,033	2,022	2,046	2,035	1,991	2,000	2,040	2,034	1,961	2,006
%Pistachite	13,674	14,550	14,770	14,803	15,699	18,048	19,118	15,300	14,350	13,367	14,885	20,289	14,994	24,273	20,805	22,532	22,553	17,496	17,440	13,510	20,328	17,733	22,275

ep: epidote
zo: zoisite
inc: inclusion in garnet
%Pistachite=100*Fe(3+)/(Fe(3+)+Al(VI))

Table 5.19 continue

	Metaolistostrome unit																									
	Eclogite		Omphacite epidotite								Blueschist metabasite								Ompacite metagabbro							**
	M99-5/4		M98-163/2		M97-151/3						93-55/5				M98-52/2				91-16						95-90/11	*
	zo	zo	ep	ep	ep	ep	ep	zo	zo	zo	ep	ep	ep	ep	ep	ep	ep	ep	zo	zo	ep	ep	ep	ep	ep	
	core	rim	rim	rim	core →		rim	core	core	core	core	rim	core	rim	corona	corona	core	rim	core	core	core →		rim	core		
	m19-26	m19-27	m12-11	m12-48	m16-1	m16-2	m16-3	m16-32	m16-4	m16-33	m10-40	m10-41	m10-70	m10-74	m11-46	m11-47	m11-50	m11-51	m15-33	m15-34	m15-44	m15-45	m15-46	m14-33		
SiO2	38,94	38,80	38,39	38,77	38,77	38,77	38,99	39,16	39,11	39,12	38,41	38,15	38,32	40,90	38,02	37,90	38,04	37,74	39,14	38,81	38,90	38,87	39,00	38,40		
TiO2	0,27	0,13	0,06	0,07	0,06	0,01	0,15	0,11	0,05	0,16	0,24	0,11	0,15	0,02	0,06	0,08	0,06	0,05	0,17	0,25	0,16	0,01	0,11	0,00		
Al2O3	28,65	27,95	24,37	24,42	26,03	26,77	27,48	27,47	27,73	28,08	26,31	25,11	26,51	18,83	23,32	21,51	22,54	22,11	28,28	27,82	26,55	27,67	28,24	23,38		
Fe2O3	4,91	5,82	10,50	10,85	8,78	7,94	7,29	7,12	6,73	6,60	8,29	9,74	7,78	12,46	12,22	13,62	12,84	13,75	6,20	5,98	7,57	6,01	6,17	11,73		
MnO	0,13	0,25	0,14	0,15	0,30	0,61	0,60	0,32	0,27	0,24	0,63	0,39	0,59	0,48	0,42	0,80	0,83	0,45	0,20	0,13	0,18	0,10	0,17	0,02		
MgO	0,04	0,11	0,02	0,04	0,07	0,10	0,06	0,06	0,08	0,07	0,06	0,00	0,03	3,04	0,03	0,01	0,01	0,02	0,13	0,09	0,08	0,06	0,14	0,05		
CaO	23,66	23,23	23,09	23,48	23,55	23,14	23,28	23,92	23,62	23,75	23,16	23,12	22,87	20,26	22,76	22,44	22,31	22,60	23,42	23,43	23,08	23,69	23,84	23,39		
Na2O	0,05	0,02	0,00	0,02	0,00	0,05	0,00	0,00	0,03	0,02	0,00	0,02	0,00	0,19	0,00	0,01	0,02	0,00	0,02	0,08	0,02	0,00	0,00	0,03		
K2O	0,01	0,00	0,00	0,00	0,01	0,02	0,02	0,00	0,00	0,00	0,02	0,02	0,02	0,03	0,00	0,03	0,02	0,00	0,00	0,00	0,00	0,00	0,00	0,02		
Cr2O3	0,00	0,06	0,05	0,08	0,04	0,18	0,08	0,06	0,03	0,07	0,30	0,05	0,25	0,08	0,05	0,00	0,04	0,03	0,16	0,05	0,07	0,09	0,07	0,00		
Total	96,66	96,37	96,62	97,89	97,61	97,59	97,94	98,23	97,66	98,11	97,41	96,70	94,29	96,28	96,88	96,40	96,72	96,75	97,72	96,64	96,61	96,50	97,74	97,02		
based on 12.5 oxygens																										
Si4+	3,041	3,047	3,061	3,057	3,044	3,038	3,034	3,037	3,044	3,029	3,022	3,037	3,041	3,034	3,046	3,075	3,064	3,047	3,035	3,044	3,065	3,053	3,027	3,066		
Ti4+	0,016	0,008	0,004	0,004	0,003	0,001	0,008	0,007	0,003	0,009	0,014	0,006	0,011	0,009	0,004	0,005	0,004	0,003	0,010	0,015	0,010	0,001	0,006	0,000		
Al3+	2,638	2,588	2,291	2,270	2,409	2,472	2,520	2,512	2,544	2,563	2,440	2,356	2,454	2,474	2,203	2,057	2,140	2,104	2,585	2,572	2,466	2,562	2,584	2,200		
Fe3+	0,289	0,344	0,630	0,644	0,519	0,468	0,427	0,416	0,394	0,385	0,491	0,583	0,461	0,464	0,737	0,831	0,778	0,835	0,362	0,353	0,449	0,355	0,360	0,705		
Mn2+	0,009	0,017	0,009	0,010	0,020	0,041	0,039	0,021	0,018	0,016	0,042	0,026	0,028	0,039	0,028	0,055	0,057	0,031	0,013	0,009	0,012	0,007	0,011	0,002		
Mg2+	0,004	0,012	0,002	0,005	0,008	0,011	0,007	0,007	0,010	0,008	0,007	0,000	0,004	0,004	0,004	0,001	0,001	0,003	0,015	0,011	0,010	0,007	0,016	0,006		
Ca2+	1,980	1,955	1,973	1,984	1,981	1,943	1,941	1,988	1,969	1,971	1,953	1,972	1,960	1,940	1,954	1,951	1,925	1,955	1,946	1,969	1,949	1,994	1,982	2,001		
Na1+	0,007	0,004	0,000	0,004	0,000	0,007	0,000	0,000	0,004	0,003	0,000	0,003	0,000	0,000	0,000	0,002	0,003	0,000	0,002	0,012	0,003	0,000	0,000	0,004		
K1+	0,001	0,000	0,000	0,000	0,001	0,002	0,002	0,000	0,000	0,000	0,002	0,002	0,000	0,002	0,000	0,003	0,002	0,000	0,000	0,000	0,000	0,000	0,000	0,002		
Cr3+	0,000	0,003	0,003	0,005	0,002	0,011	0,005	0,004	0,002	0,004	0,018	0,003	0,022	0,016	0,003	0,000	0,003	0,002	0,010	0,003	0,004	0,005	0,004	0,000		
Total	7,984	7,977	7,973	7,983	7,988	7,994	7,983	7,991	7,988	7,988	7,989	7,989	7,980	7,981	7,979	7,980	7,977	7,979	7,978	7,987	7,967	7,984	7,991	7,985		
Si	3,041	3,047	3,061	3,057	3,044	3,038	3,034	3,037	3,044	3,029	3,022	3,037	3,034	3,278	3,046	3,075	3,064	3,047	3,035	3,044	3,065	3,053	3,027	3,066		
Al(IV)	0,000	0,000	0,000	0,000	0,000	0,000	0,000	0,000	0,000	0,000	0,000	0,000	0,000	0,000	0,000	0,000	0,000	0,000	0,000	0,000	0,000	0,000	0,000	0,000		
X total	3,041	3,047	3,061	3,057	3,044	3,038	3,034	3,037	3,044	3,029	3,022	3,037	3,034	3,278	3,046	3,075	3,064	3,047	3,035	3,044	3,065	3,053	3,027	3,066		
Al(VI)	2,638	2,588	2,291	2,270	2,409	2,472	2,520	2,512	2,544	2,563	2,440	2,356	2,474	1,779	2,203	2,057	2,140	2,104	2,585	2,572	2,466	2,562	2,584	2,200		
FeIII	0,289	0,344	0,630	0,644	0,519	0,468	0,427	0,416	0,394	0,385	0,491	0,583	0,464	0,752	0,737	0,831	0,778	0,835	0,362	0,353	0,449	0,355	0,360	0,705		
Ti	0,016	0,008	0,004	0,004	0,003	0,001	0,008	0,007	0,003	0,009	0,014	0,006	0,009	0,001	0,004	0,005	0,004	0,003	0,010	0,015	0,010	0,001	0,006	0,000		
Y total	2,942	2,939	2,924	2,918	2,931	2,941	2,956	2,934	2,941	2,957	2,946	2,946	2,947	2,532	2,943	2,893	2,922	2,943	2,957	2,940	2,925	2,918	2,950	2,905		
Mg	0,004	0,012	0,002	0,005	0,008	0,011	0,007	0,007	0,010	0,008	0,007	0,000	0,004	0,363	0,004	0,001	0,001	0,003	0,015	0,011	0,010	0,007	0,016	0,006		
Mn	0,009	0,017	0,009	0,010	0,020	0,041	0,039	0,021	0,018	0,016	0,042	0,026	0,039	0,033	0,028	0,055	0,057	0,031	0,013	0,009	0,012	0,007	0,011	0,002		
Ca	1,980	1,955	1,973	1,984	1,981	1,943	1,941	1,988	1,969	1,971	1,953	1,972	1,940	1,740	1,954	1,951	1,925	1,955	1,946	1,969	1,949	1,994	1,982	2,001		
Z total	1,993	1,984	1,984	1,998	2,009	1,995	1,987	2,016	1,997	1,995	2,001	1,998	1,983	2,136	1,986	2,007	1,983	1,988	1,974	1,988	1,971	2,008	2,010	2,008		
%Pistachit	9,861	11,733	21,571	22,096	17,717	15,920	14,482	14,197	13,415	13,047	16,746	19,847	15,778	29,697	25,066	28,785	26,667	28,418	12,277	12,066	15,398	12,177	12,240	24,258		

ep: epidote
zo: zoisite
inc: inclusion in garnet
%Pistachite=100*Fe(3+)/(Fe(3+)+Al(VI))

* Blueschist metabasite in marble-schist series
* * Marble-schist series

aluminium is 6-fold coordinated in the analysed epidote group minerals. Ferric iron and aluminium exhibit a reciprocal concentration relationship as shown in Figure 5.57. The general trend parallel to the line $\Sigma(Al+Fe)^{3+}$ =3.0 indicates that these minerals are essentially binary pistachite (Ps) – Zoisite (Zo) solid solutions (Ernst, 1976). The only major chemical variation appears in terms of ferric iron and aluminium contents. The overall range in composition of epidote groups minerals in the present study is Ps_{10-30}. Pistachite range in eclogite, omphacite-epidotite, blueschist metabasite and omphacite metagabbros are, in turn, 10-24, 13-22, 16-30 and 12-15, respectively. Epidotes in omphacite metagabbros show a composition which is closer to the zoisite end-member and tend to be enriched in Al^{VI} relative to Fe^{3+}. Whereas blueschist metabasites display more pistachitic compositions. Eclogites and omphacite-epidotites indicate intermediate compositions between zoisite (clinozoisite) and pistachite (Figure 5.57).

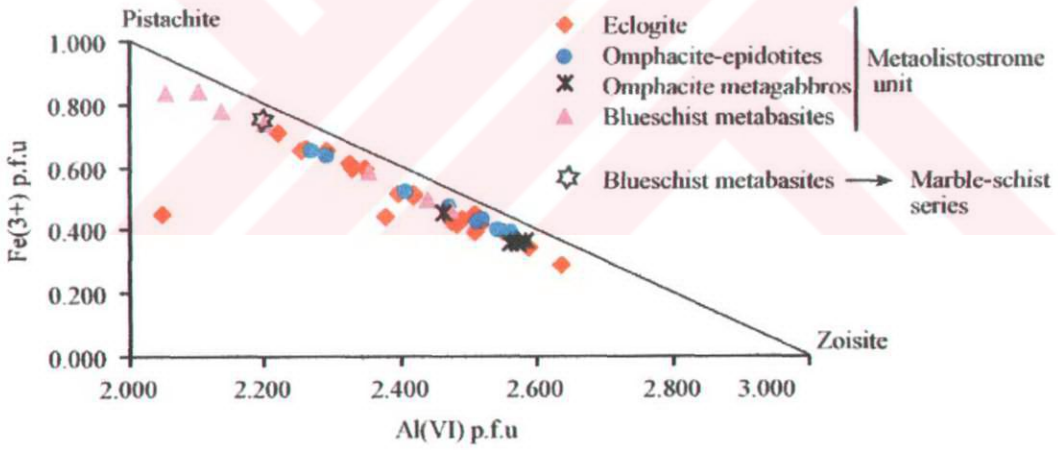


Figure 5.57 Al(VI) vs. Fe(3+) plot for epidotes from the Metaolistostrome unit and the Marble-schist series.

Some epidote grains show optical zoning by interference colours (Figure 5.58a1), usually as a distinct core and rim. In Figure 5.58, three zoned epidote grains were analysed from eclogite (95-70/4), omphacite-epidotite (M97-151/3) and omphacite metagabbro (91-16). Photomicrograph under crossed polars and element patterns of this zoned epidote (95-70/4) are given in Figure 5.58a1, a2, a3, a4. Chemical zoning of the grain ranges from Ps_{13} (core) to Ps_{19} (rim) in 95-70/4. This grain exhibit

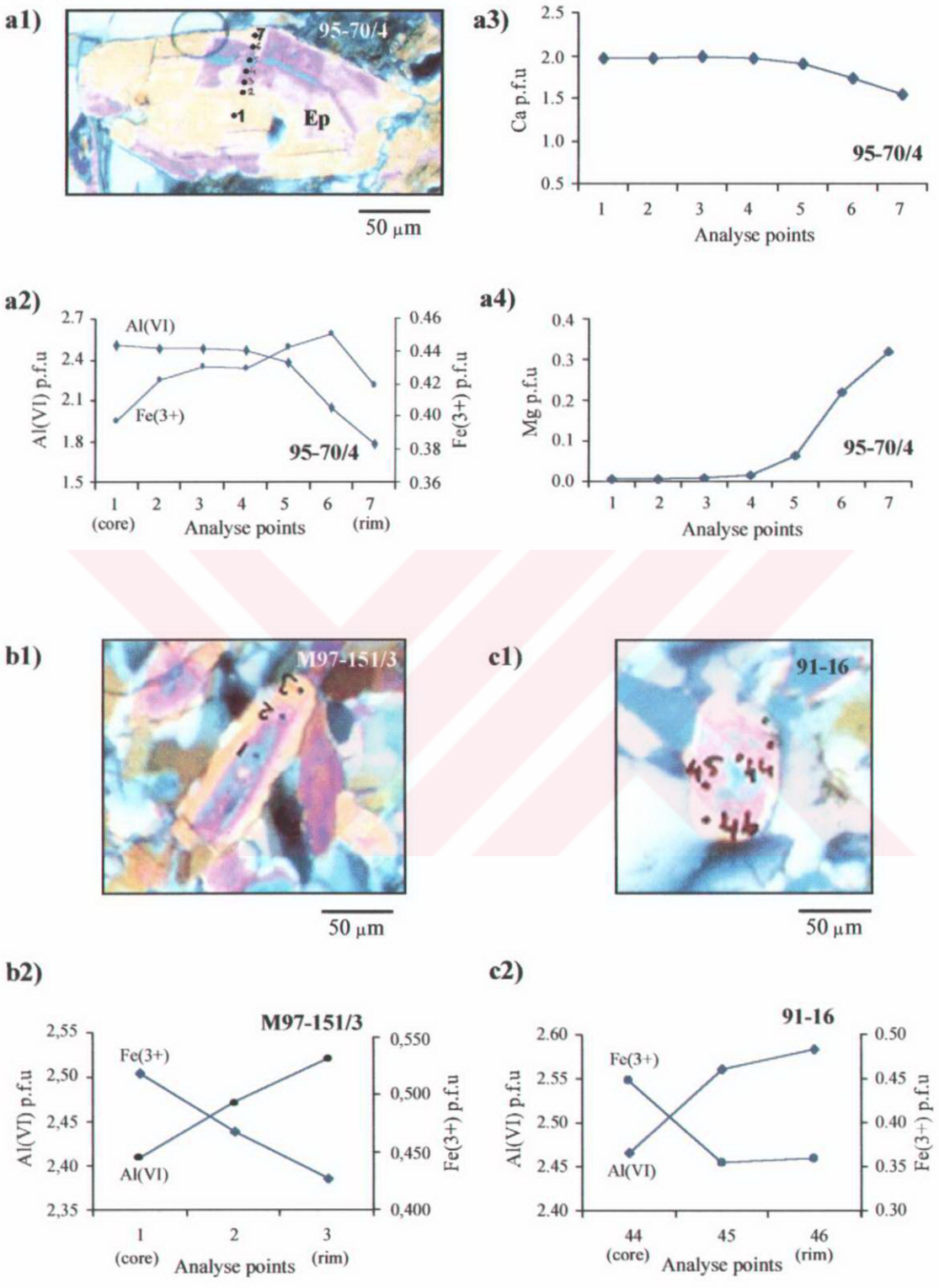


Figure 5.58 Compositional variations, normal zoning (95-70/4) and reverse zoning (M97-151/3 and 91-16) in different epidote grains from core to rim.

distinct Fe^{3+} - Mg enrichment and Al^{VI} – Ca depletion of the rims (Figure 5.58a2, a3, a4), whereas M97-151/3 and 91-16 possess a margin strongly depleted in ferric iron relative to core (Figure 5.58b2 – 5.58c2). In blueschist metabasites (95-55/5 and M98-52/2), normal zoning profile which is represented by Al^{IV}- rich core and Fe^{3+} rich rim is observed. Fe^{3+}/Al^{VI} ratio with decreasing pressure increases in epidotes that have normal zoning (Figure 5.58a2). The inverted zoning of epidote (for example, Fe^{3+}-rich cores, Al^{VI} rich rims) is not so common among the analysed epidote grains. Generally analysed epidotes have normal zoning. Zoning from high to low iron-rich epidote is usually ascribed to crystallization of aluminium-rich zones at higher metamorphic temperatures (Deer et al. 1992). Epidotes with an aluminium-rich core and iron-rich margin (normal zoning) may be correlated with an initial prograde metamorphism that was followed subsequently by a retrograde event (Deer et al. 1992).

5.8. Plagioclase

30 selected analyses of plagioclase from the Metaolistostrome unit (eclogite, bluschist metabasite, omphacite-epidotite, omphacite metagabbro, garnet-amphibolite blocks and metaolistostrome matrix) and the Marble-schist series (blueschist metabasites and garnet-mica schist) are presented in Table 5.20. Based on 32 oxygens, cation totals range between 15.824 – 16.037 with an average of 15.912. Minor elements are present in negligible amounts. Averages per formula unit are Ti, Cr and Mg = 0.00; Fe^{2+}= 0.006 and Mn= 0.001. Ca and K ranges are 0.000 – 0.383 and 0.000- 0.004 respectively. 30 analysed plagioclase are extremely albitic, except for M97-149/10 (m2-22), with an average composition of $Ab_{97.50}$ $An_{2..35}$ $Or_{0.15}$ in metaolistostrome unit and $Ab_{99.09}$ $An_{0.76}$ $Or_{0.15}$ in marble-schist series. There is no obvious chemical distinction in albites. Sodic plagioclase has been encountered only as a secondary mineral associated with omphacite and amphibole breakdown. Albite–rich plagioclase in the eclogites formed during retrogression of omphacite. Plagioclase, especially in blueschist in metabasites, are nearly pure albites.

Table 5.20 Representative plagioclase analyses from the Metaolistostrome unit and the Marble-schist series

	Metaolistostrome unit																					
	Eclogite									Blueschist metabasite				Omphacite-epidotite					Omp. me	Garnet amphibolite		Metaolist. matrix	
Sample no	95-21/10		SE-1	M98-45C	M96-31		M97-34/2		M99-5/4	95-55/5		M98-52/2		M96-92/4	M97-151/3		M98-163/2		91-16	M97-149/10		M98-99/2	
Analyse no	m20-18	m20-17	m19-176	m4-75	m4-85	m4-86	m7-21	m7-14	m19-8	m10-12	m10-64	m11-4	m11-76	m13-1	m16-19	m16-20	m12-6	m12-23	m15-30	m2-22	m2-35	m1-1a	m1-23a
SiO2	68,23	67,82	67,87	67,87	68,08	67,33	67,75	67,42	67,57	68,24	68,95	68,67	68,61	68,62	68,41	67,27	68,69	68,49	68,64	61,74	66,89	68,59	68,35
TiO2	0,00	0,00	0,00	0,00	0,00	0,00	0,00	0,00	0,00	0,00	0,00	0,02	0,00	0,00	0,00	0,00	0,01	0,01	0,00	0,00	0,01	0,00	0,00
Al2O3	19,33	19,37	19,49	19,05	19,41	19,48	18,77	19,54	19,23	19,34	18,93	19,23	19,18	19,45	19,17	19,89	19,50	19,07	19,18	22,44	19,14	19,30	19,84
FeO	0,04	0,08	0,12	0,13	0,13	0,08	0,18	0,06	0,06	0,05	0,00	0,09	0,21	0,03	0,14	0,09	0,10	0,04	0,05	0,07	0,09	0,23	0,07
MnO	0,01	0,00	0,00	0,02	0,05	0,00	0,02	0,00	0,00	0,01	0,03	0,01	0,00	0,02	0,00	0,03	0,00	0,00	0,00	0,04	0,02	0,04	0,06
MgO	0,00	0,00	0,00	0,00	0,00	0,00	0,01	0,00	0,00	0,00	0,01	0,00	0,00	0,00	0,00	0,00	0,04	0,00	0,01	0,00	0,00	0,01	0,00
CaO	0,15	0,29	0,09	0,09	0,43	0,78	0,29	0,77	0,14	0,18	0,01	0,11	0,11	0,17	0,16	0,97	0,45	0,07	0,11	4,00	0,11	0,08	0,14
Na2O	12,12	11,89	12,09	12,18	11,94	12,12	12,03	11,89	12,07	12,12	12,20	12,11	12,09	12,07	12,17	11,38	12,08	12,21	11,84	9,90	12,34	12,43	11,43
K2O	0,03	0,00	0,06	0,00	0,02	0,04	0,04	0,05	0,01	0,04	0,04	0,06	0,07	0,02	0,00	0,01	0,02	0,04	0,01	0,07	0,04	0,03	0,03
Cr2O3	0,02	0,00	0,00	0,02	0,01	0,07	0,00	0,04	0,00	0,00	0,04	0,01	0,02	0,02	0,00	0,05	0,00	0,01	0,01	0,00	0,00	0,00	0,00
Total	99,94	99,45	99,71	99,36	100,07	99,91	99,09	99,77	99,08	99,97	100,21	100,32	100,30	100,40	100,05	99,69	100,90	99,94	99,86	98,26	98,64	100,71	99,92
Number of ions on the basis of 32 oxygens																							
Si4+	11,889	11,890	11,850	11,889	11,866	11,729	11,913	11,779	11,870	11,886	11,986	11,929	11,926	11,912	11,908	11,805	11,868	11,931	11,999	11,039	11,772	11,846	11,971
Ti4+	0,000	0,000	0,000	0,000	0,000	0,000	0,000	0,000	0,000	0,000	0,000	0,003	0,000	0,000	0,000	0,000	0,001	0,001	0,000	0,000	0,001	0,000	0,000
Al3+	2,978	3,002	3,009	2,950	2,991	3,000	2,918	3,018	2,987	2,978	2,909	2,954	2,948	2,985	2,950	3,086	2,979	2,937	2,964	3,547	2,978	2,947	3,072
Fe2+	0,003	0,005	0,009	0,009	0,009	0,006	0,013	0,004	0,004	0,004	0,000	0,007	0,015	0,002	0,010	0,007	0,007	0,003	0,004	0,005	0,007	0,017	0,005
Mn2+	0,001	0,000	0,000	0,001	0,003	0,000	0,001	0,000	0,000	0,001	0,002	0,001	0,000	0,001	0,000	0,002	0,000	0,000	0,000	0,003	0,002	0,003	0,004
Mg2+	0,000	0,000	0,000	0,000	0,000	0,000	0,001	0,000	0,000	0,000	0,001	0,000	0,000	0,000	0,000	0,000	0,005	0,000	0,001	0,000	0,000	0,002	0,000
Ca2+	0,014	0,027	0,008	0,008	0,040	0,073	0,027	0,072	0,013	0,017	0,001	0,010	0,011	0,016	0,015	0,091	0,042	0,006	0,010	0,383	0,010	0,008	0,013
Na1+	1,024	1,010	1,023	1,034	1,009	1,023	1,025	1,007	1,028	1,023	1,028	1,020	1,019	1,016	1,027	0,968	1,012	1,031	1,003	0,858	1,053	1,041	0,970
K1+	0,002	0,000	0,003	0,000	0,001	0,002	0,002	0,003	0,001	0,002	0,002	0,004	0,004	0,001	0,000	0,001	0,001	0,002	0,001	0,004	0,002	0,001	0,002
Cr3+	0,002	0,000	0,000	0,002	0,001	0,008	0,000	0,004	0,000	0,000	0,004	0,001	0,002	0,002	0,000	0,005	0,000	0,001	0,001	0,000	0,000	0,000	0,000
Total	15,913	15,934	15,902	15,894	15,921	15,842	15,902	15,887	15,902	15,911	15,934	15,928	15,924	15,934	15,911	15,964	15,914	15,913	15,984	15,840	15,824	15,863	16,037
Ab	98,46154	97,40	98,91	99,21	96,09	93,17	97,21	93,07	98,66	98,22	99,68	98,67	98,62	98,31	98,54	91,35	95,92	99,21	98,89	68,90	98,85	99,14	98,50
An	1,346154	2,60	0,80	0,79	3,82	6,63	2,59	6,66	1,25	1,59	0,09	0,99	1,03	1,57	1,46	8,59	3,96	0,60	1,03	30,77	0,93	0,73	1,33
Or	0,192308	0,00	0,30	0,00	0,09	0,21	0,20	0,27	0,10	0,19	0,23	0,34	0,35	0,13	0,00	0,06	0,12	0,19	0,07	0,33	0,22	0,13	0,17

Omp. me: omphacite metagabbro

Table 5.20 contiuned

	Marble-schist series						
	Blueschist metabasite					Garnet-mica schist	
Sample no	95-90/11		TAG			M97-36	
Analayse no	m14-29	m14-63	m9-21	m9-22	m9-23	m17-34	m17-36
SiO2	69,13	67,88	68,67	68,85	68,79	67,83	68,82
TiO2	0,01	0,04	0,04	0,01	0,01	0,00	0,00
Al2O3	19,29	18,73	19,29	19,24	19,24	19,20	19,15
FeO	0,02	0,17	0,06	0,02	0,06	0,05	0,04
MnO	0,02	0,00	0,00	0,00	0,00	0,02	0,00
MgO	0,02	0,00	0,00	0,00	0,00	0,01	0,01
CaO	0,04	0,19	0,04	0,02	0,05	0,21	0,04
Na2O	12,35	12,20	12,23	12,21	12,12	11,92	12,41
K2O	0,02	0,07	0,01	0,01	0,02	0,05	0,02
Cr2O3	0,00	0,03	0,06	0,04	0,05	0,00	0,00
Total	100,91	99,30	100,40	100,40	100,33	99,29	100,49
Number of ions on the basis of 32 oxygens							
Si4+	11,923	11,898	11,911	11,943	11,949	11,907	11,909
Ti4+	0,002	0,005	0,005	0,001	0,001	0,000	0,000
Al3+	2,941	2,903	2,958	2,951	2,955	2,980	2,930
Fe2+	0,001	0,012	0,004	0,001	0,004	0,004	0,003
Mn2+	0,002	0,000	0,000	0,000	0,000	0,001	0,000
Mg2+	0,003	0,000	0,000	0,000	0,000	0,001	0,002
Ca2+	0,004	0,018	0,004	0,002	0,005	0,020	0,003
Na1+	1,032	1,037	1,028	1,027	1,020	1,014	1,041
K1+	0,001	0,004	0,000	0,001	0,001	0,003	0,001
Cr3+	0,000	0,003	0,006	0,004	0,005	0,000	0,000
Total	15,909	15,879	15,918	15,930	15,941	15,930	15,889
Ab	99,52	97,93	99,58	99,74	99,47	97,84	99,58
An	0,38	1,69	0,38	0,18	0,45	1,91	0,31
Or	0,10	0,38	0,04	0,08	0,08	0,25	0,11

CHAPTER SIX

P-T ESTIMATIONS

6.1. Introduction

Pressure and temperature (P-T) conditions were estimated for two groups of rocks: the Marble-schist series and the Metaolistostrome unit. Average metamorphic conditions and P-T loops of these rock groups are given below.

6.2. Marble-schist series

This series, which is composed of various kinds of metapelites, metabasites and marbles, was investigated in Dilek Peninsula and Selçuk-Tire areas.

6.2.1. Dilek Peninsula

Metapelites intercalated with metabasites which contain Na-amphibole (crossite) and phengite (maximum Si=3.37 p.f.u), are generally made up of chloritoid (maximum X_{Mg}=0.35), kyanite, phengite (maximum Si^{4+}=3.44 p.f.u), chlorite and quartz. In addition, meta-bauxite lenses in marbles include diaspore but no corundum. Glaucophane exists in both metapelites and metabasites in Dilek Peninsula. It is associated with albite, but no Na-pyroxene. This evidence indicates the elevated, but not very high, pressure of metamorphism. The possible pressure range, defined by the lower stability limit of albite (Holland 1979) and the uppermost

breakdown limit of glaucophane (Ernst 1979), is relatively wide. The occurrence of chloritoid relatively rich-in Mg end-member (X_{Mg}=0.35), and kyanite in the assemblage is another indicator for high pressure (Seidel 1981; Chopin and Schreyer 1983).

In Dilek Peninsula, upper and lower temperature limits of high-pressure metamorphism are given by equilibrium curves of diaspore = corundum + H_2O (Haas 1972) and pyrophyllite = kyanite +quartz + H2O (Haas and Holdaway 1973), respectively (Figure 6.1). Moreover, the equilibrium curve of lawsonite = margarite + zoisite + H_2O (Heinrich & Althaus, 1980) is also used to estimate the temperature range of epidote-blueschist facies matamorphism in Dilek Peninsula. Si^{4+} content of white mica in metapelites is higher than that of metabasites. Therefore, maximum Si^{4+} content of phengite (3.44 p.f.u) in metapelites is accepted for minimum pressure limit. The Si^{4+} isopleths after Masonne and Schreyer (1989) are given in Figure 6.1. Colombi (1989) calibration based on the Ti content of amphiboles is used for temperature estimation of glaucophane bearing metapelites. According to Colombi (1989), core of crossite gives 445°C for peak temperature of epidote-blueschist facies metamorphism. This temperature value is consistent with univariant reaction curves diaspore = corundum + H_2O, lawsonite = margarite + zoisite + H_2O and phrophyllite = kyanite + quartz + H_2O (Figure 6.1). Temperatures obtained by Colombi (1989) calibration also coincide with the mineral assemblages. The combination of peak temperature (445°C) with Si isopleth (Si=3.44) gives minimum pressure at about 11 kbar for epidote-blueschist facies metamorphism (Figure 6.1). Because of the lacking of biotite and K-feldspar in the mineral assemblage of metabasites, 11 kbar represents minimum pressure. The pressure estimation from glaucophane-bearing metabasites which are intercalated with metapelites, is lower than that of metapelites. The core of crossites which are rimmed by barroisite, give 450°C based on Colombi (1989) calibration. Whereas, intermediate zone between core and rim gives an average temperature of about 460°C. The slight increase of temperature in intermediate zone may be represented by the low Si^{4+} content of phengites in metabasite (sample 95-90/11). The combination of Si^{4+}= 3.37 isopleth of phengite

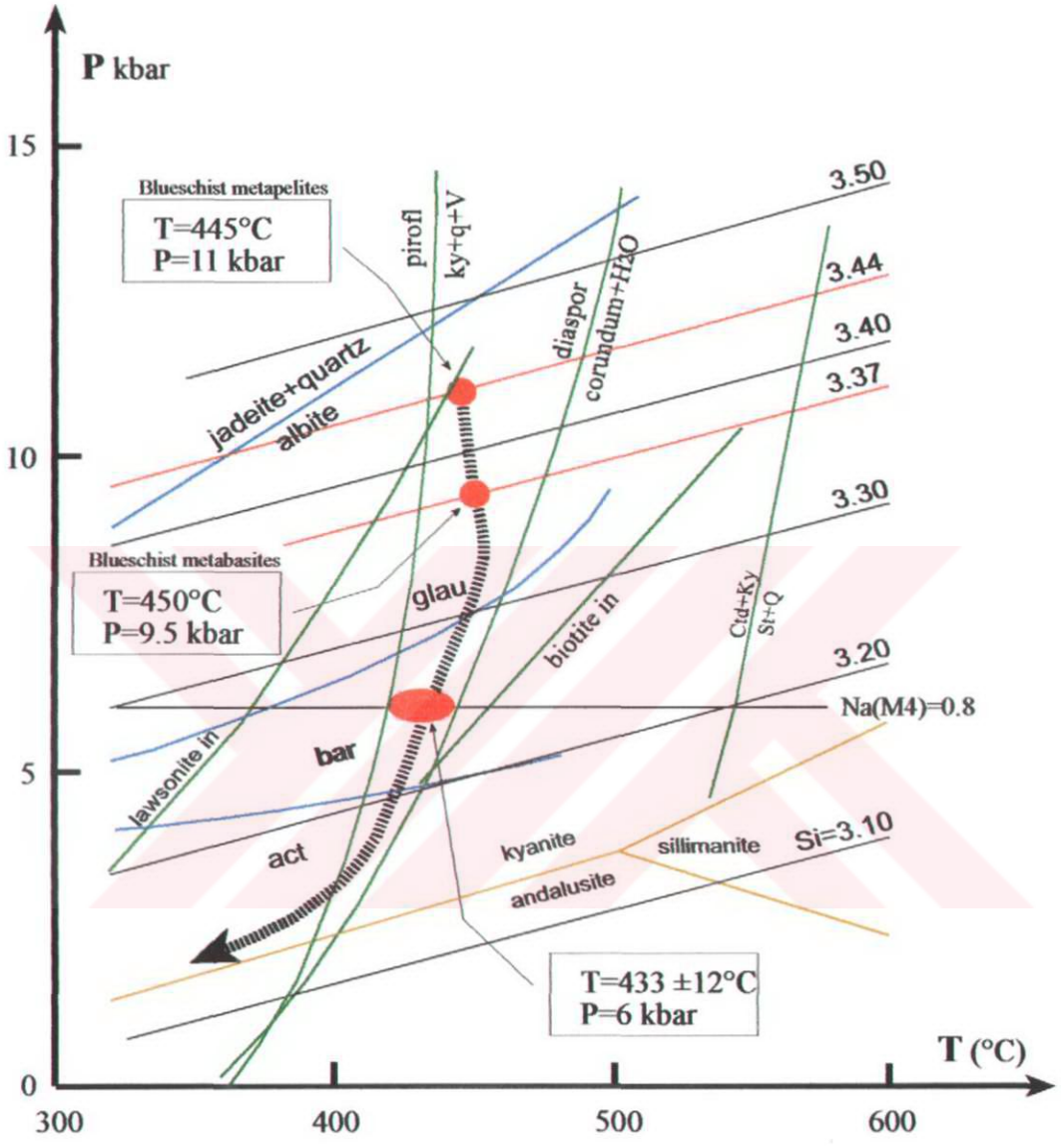


Figure 6.1 P-T conditions and apparent P-T path for blueschist metabasite and metapelites from Dilek Peninsula. Data sources: jadeite + quartz = albite (Holland, 1980); chloritoid + kyanite = staurolite + quartz reaction after Bhaskar Rao & Johannes (1979); stability fields of Al silicates after Holdaway (1971); diaspore = corundum + H2O (Haas, 1971); pyrophyllite = kyanite + quartz+ vapour (Haas & Holdaway, 1973); stability field of barroisitic amphibole (Ernst 1979); upper stability limit of lawsonite + albite (Heinrich & Althaus, 1980); Na(M4) line after Brown (1977); biotite-in curve from Piccardo et al.(1979); Si^{4+} in phengite are after Massonne & Schreyer (1989).

with temperature obtained from core composition of crossite gives at about 9.5 kbar. This pressure value is 1.5 kbar lower than metapelites. Samos Island of Cycladic Complex is situated two km west of Dilek Peninsula. These two regions display great similarities in terms of rock succession and high-pressure assemblage (Candan et al., 1997). In the eastern part of Samos, the temperature was estimated 440°C for assumed 12 kbar (Okrusch et al., 1985) during the high-pressure event. 11 kbar and 445°C estimates for peak pressure and temperature of epidote-blueschist facies metamorphism in Dilek Peninsula is consistent with the maximum temperature at about 470°C for diaspore/corundum isograde after Haas (1972). The absence of corundum in meta-bauxite overlying the blueschist metabasite reveals that this equilibrium curve of the reaction was not crossed. Therefore, the maximum temperature during epidote-blueschist facies in Dilek peninsula prevealed below 470°C and is consistent with Samos Island.

Epidote-blueschist facies metamorphism is overprinted by retrograde metamorphism under greenschist facies conditions. In Dilek Peninsula, upper and lower temperature limits of greenschist facies overprint are defined by equilibrium curves of diaspore = corundum + H_2O and phrophyllite = kyanite + quartz + H_2O, respectively. Retrogressive transition from epidote-blueschist to greenschist facies in Dilek Peninsula is represented by crossite-barroisite transformation. The presence of Na-Ca amphibole (barroisite) rims around Na amphibole (crossite-glacophane) indicates that P-T conditions changed from the sodic to Na-Ca amphibole stability fields. Barroisites in sample 95-90/11 give an average pressure of 6 kbar in Na_{M4} vs Al^{VI} diagram of Brown (1976) (Figure 6.2). In Figure 6.1, kyanite and diaspore equilibrium curves are crossed by Na_{M4}=0.8 line representing 6 kbar. Crossing points of kyanite and diaspore equilibrium curves by Na_{M4}=0.8 line give maximum (445°C) and minimum (420°C) temperature range of peak temperature of greenschist facies metamorphism. Average temperature is 433 ±12 °C. According to Si^{4+} and Mg contents, distribution of phengites from metapelites in Dilek Peninsula are given in Figure 6.3. In this diagram, two groups of phengite are distinguished. Minimum and maximum Si^{4+} p.f.u contents of phengites with high Si^{4+} and Mg content formed

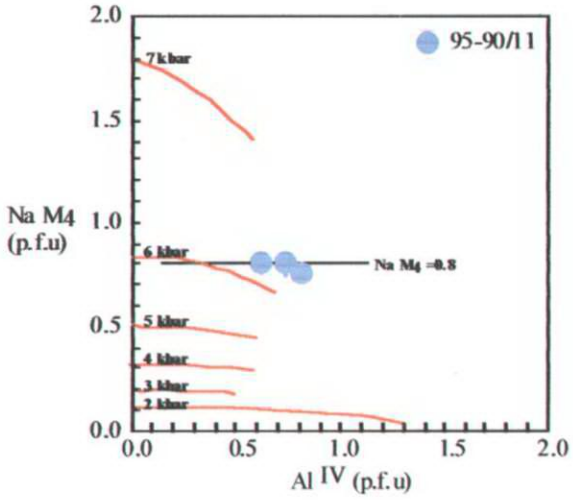


Figure 6.2 The relationship between the pressure of retrograde metamorphism and NaM4 content of barrosites in Dilek Peninsula (Brown 1976).

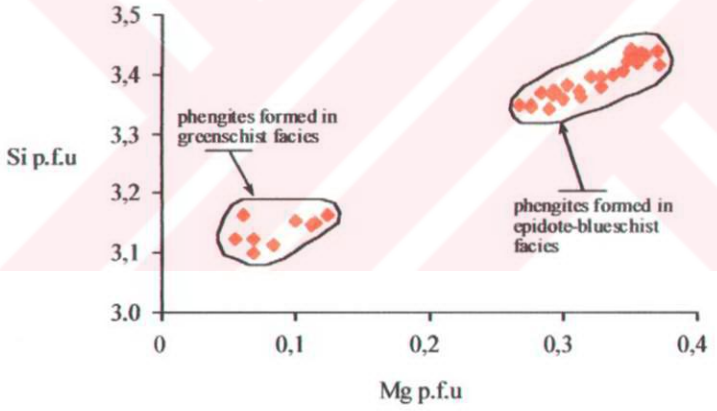


Figure 6.3 Phengite compositions generated under greenschist and epidote-blueschist facies conditions from metapelites in Dilek Peninsula.

during the epidote-blueschist facies conditions are 3.34 and 3.44, respectively. In Figure 6.1, Si^{4+} isopleths corresponding to these values occur in glaucophane stability field of Ernst (1979). Therefore, it is interpreted that phengites which have high Si and Mg content were formed during epidote-blueschist facies metamorphism. The second group of phengite has lower Si and Mg content. Maximum and minimum Si^{4+} contents are in range of 3.16 and 3.10 p.f.u. This phengite group is emerged in actinolite stability field of Ernst (1979) (Figure 6.1). Phengites with Si^{4+} contents

between 3.16 and 3.10 p.f.u were formed during greenschist facies metamorphism. But there is no phengite generation coexisting with barroisite. Therefore, these phengites in actinolite stability field do not give peak pressure conditions for greenschist facies. These Si^{4+} isopleths and the existence of phyrophyllite as the breakdown product of kyanite can be used to determine the direction of clockwise P-T loop.

Pressure and temperature conditions for Dilek Peninsula can be summarized as follows: i) high pressure metamorphism in Dilek Peninsula prevailed under epidote-blueschist facies condition with pressure and temperature conditions at about 11 kbar / 445°C; ii) retrograde overprint under greenschist facies condition occurred at pressure 6 kbar and temperature around 433±12°C (Figure 6.1).

6.2.2. Selçuk – Tire area

The Marble-schist series are also exposed in Selçuk and Tire areas, apart from Dilek Peninsula. In these areas, mineral assemblages of metapelites are different from Dilek Peninsula. Metapelites with no sodic and sodic-calcic amphiboles are dominated by biotite and garnet. Si^{4+} content of phengites in two samples from the Marble-schist series changes from 3.34 to 3.14 p.f.u. The range of Si^{4+} contents in phengite is lower than on the Dilek Peninsula. In addition, garnets have been effected by retrograde diffusion. Both areas have very probably a common high-pressure history. The fact that both areas have been influenced in different way by greenschist facies. Therefore, the peak P-T conditions during the epidote-blueschist facies metamorphism of the Marble-schist series in Selçuk – Tire area are mostly obliterated by the greenschist overprint when compared with the P-T path of Dilek Peninsula (Figure 6.1 and Figure 6.4). According to Green and Hellman (1982) phengite-garnet geothermometer, temperature estimations from different stages of the overprint using sample M99-52/5 are given in Table 6.1 and Figure 6.4. Pressures are estimated by the combination of the phengite Si^{4+} isopleths of Massonne & Schreyer (1989) and Green and Hellman (1982) geothermometer.

Table 6.1 Temperature estimations obtained by representative garnet-phengite (matrix) pairs after Green and Hellman (1982) geothermometer from sample M99-52/5 (garnet and phengite analyses are given in Table 5.13 and Table 5.15, respectively). Pressure estimations are based on Si^{4+} content in phengite after Massonne and Schreyer (1989).

Mineral pairs	Analyse no	Si p.f.u in Phen.	Fe / Fe + Mg	Mg	KD	P estimations (kbar)	T estimations (°C)
phengite	38 (core)	3.34	0.34	0.58	31	8.6	453±10
garnet	16 (core)	-	0.944	0.206			
phengite	39 (mantle)	3.24	0.37	0.42	26	6	456±10
garnet	14 (mantle)	-	0.942	0.221			
phengite	40 (rim)	3.14	0.46	0.22	17	4	487±10
garnet	12 (rim)	-	0.936	0.261			

Decrease in Si^{4+} (p.f.u) content and increase in Fe/Fe+Mg ratio of phengite represent decrease in pressure. In addition, gradual increase of Mg (p.f.u) in garnet from core to rim indicates increase in temperature (Table 6.1). Temperature estimation obtained from sample M99-52/5 show that core and mantle-rim of garnet are formed under epidote-blueschist and greenschist facies conditions, respectively. In addition, phengites which have Si content below the celadonite + chlorite = muscovite + phlogopite + quartz + H_2O curve (Bucher and Frey, 1994) are assumed to have been formed under greenschist facies condition. Biotites which are partly altered by chlorite are not in equilibrium with garnet rim. Therefore, the garnet-biotite thermometer (Bhattacharya et al. 1992) gives unrealistically low temperatures. There are no big differences of temperature estimations between core and mantle of garnet-phengite pairs based on Green and Hellman (1982) calibration. It reveals that the Transformation from epidote-blueschist to greenschist facies occurred under isothermal decompression conditions. However a slight increasing of temperature in garnet-phengite schists of the Marble-schist series is observed in late stages of greenschist facies overprint in Selçuk-Tire area (Figure 6.4). This case is represented by low Si (3.14) content in phengites and low Fe /Fe + Mg ratio in garnet rim (Table 6.1). In addition, the existence of plagioclase (An_{29}) supports an increasing of

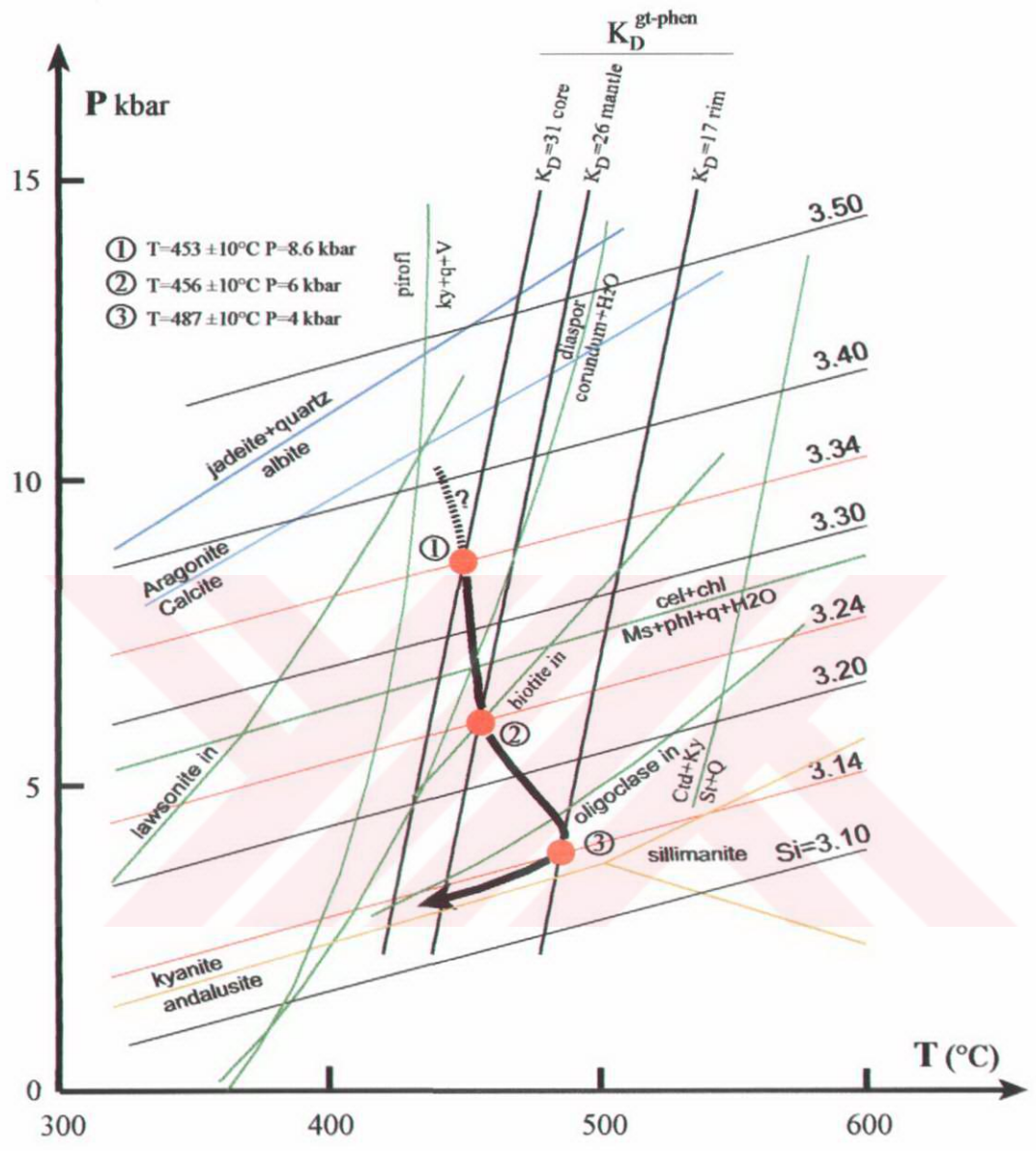


Figure 6.4 PT- diagram showing the metamorphic evolution of the marble - schist series in Selçuk - Tire area, based on data from Table 6.1. Curves; K_D between garnet and phengite with Green & Hellman's (1987) calibration; jadeite + quartz stability after Holland (1980); stability limit of aragonite after Johannes & Puhan (1971); chloritoid + kyanite = staurolite + quartz reaction after Bhaskar Rao & Johannes (1979); oligoclase-in (Maruyama et al. 1983); biotite-in Piccardo et al.(1979); celadonite + chlorite = muscovite + phlogopite + quartz + H_2O (Bucher and Frey, 1994); Lawsonite + albite = zoisite + paragonite + quartz + H_2O reaction (lawsonite in) after Heinrich and Althaus (1980); stability fields of Al silicates after Holdaway (1971); diaspore = corundum + H2O (Haas, 1971); pyrophyllite = kyanite + quartz + vapour (Haas & Holdaway, 1973). Si isopleths are from Massonne and Schreyer (1989). Abbreviations: K_D, Fe/Mg distribution coefficents in garnet-phengite pairs: gt, garnet: phen, phengite.

temperature. The point which is represented by garnet (rim) – phengite (rim, Si^{4+}=3.14) in Figure 6.4 also occurs below the oligoclase-in curve. After an increase in temperature, the P-T path follows almost parallel to stability line of kyanite (Figure 6.4).

6.3. Metaolistostrome unit

The Metaolistostrome unit is mainly made up of metapelitic matrix and high-pressure blocks. P-T conditions of individual high-pressure blocks and matrix are estimated, and the results are compared with each other.

6.3.1. Matrix of the Metaolistostrome

P-T conditions of the matrix of the Metaolistostrome are estimated from two samples (M98-99/2 and 94-30). Garnet – phengite geothermometer after Krogh and Raheim (1978) which is not suggested for pelites was not used. The garnet – phengite geothermometer, calibrated by Green and Hellman (1982), was used to determine P-T conditions of this unit. Temperature estimations were made according to Ca < %2 and mg ~67 type of this calibration. All Fe in phengite was assumed Fe^{2+} because no reasonable Fe^{3+} calculation is possible from stoichiometric considerations (Carswell et al., 1997). Because of this assumption, the calculated temperatures should be the maximum temperature values (Green & Hellman 1982). In addition, this thermometer was combined with the phengite barometer of Massonne and Schreyer (1989). Phengites generally do not show regular zonation in M98-99/2 and 94-30. But, some phengite flakes rarely display an increasing in Si^{4+} (p.f.u) contents from core (3.36) to mantle (3.42) and than decrease towards the rim (3.25). These changes in Si^{4+} from core to rim can be interpreted as prograde and retrograde zonation, respectively. These two zonations exist in M98-99/2. Whereas, only retrograde zonation is observed in 94-30. In Figure 6.5, K_D curves 1, 2, 3 and 4 represent the distribution of Fe and Mg between phengite and garnet pairs. 1, 2, 3 and 4 belong to samples M98-99/2 and 94-30, respectively. Si isopleths are after Massonne and Schreyer (1989) (Table 6.2 and Figure 6.5). Peak pressure and

temperature are ~10.6 kbar and 452 – 457 °C for epidote – blueschist facies (curve 1) (Figure 6.5). The decompression path shown in Figure 6.5 is based on the changes in garnet – phengite composition from mantle in M98-99/2 and core in 94-30 to rim (Table 6.2). Peak pressure and temperature of retrograde metamorphism under greenschist facies conditions are estimated as ~6.8 kbar and 488 – 492 °C, respectively. These values which are obtained from different samples in the same unit are quite close to each other (Table 6.2). The P-T path in Figure 6.5 shows that the temperature was increasing during the uplift of this unit.

Table 6.2 Garnet – phengite Fe / Mg exchange geothermometry for the matrix of the Metaolistostrome.

Sample	Pairs Grt Phen	Phengite	Garnet	K_D	P (kbar)*	T (°C) **
M98-99/2	mantle-core curve no 1	Fe: 0.114 Mg: 0.286 Si: 3.42	Fe: 4.01 Mg: 0.28	32	~ 10.6	452
	rim-rim curve no 2	Fe: 0.112 Mg: 0.223 Si: 3.25	Fe: 3.74 Mg: 0.39	19	~ 6.8	492
94-30	core-core curve no 3	Fe: 0.135 Mg: 0.323 Si: 3.42	Fe: 4.24 Mg: 0.31	32	~ 10.6	457
	rim-rim curve no 4	Fe: 0.104 Mg: 0.207 Si: 3.25	Fe: 3.83 Mg: 0.39	19	~ 6.8	488

* pressure calibration after Massonne & Schreyer (1989)

** temperature calibration after Green & Hellman (1982)

6.3.2. Eclogite blocks

P-T estimations belonging to eclogite blocks in the matrix of the Metaolistostrome unit were made from four different blocks in the Selçuk area. The representative samples of these blocks are M99-5/4, M98-45C, SE-1 and 95-21/10. Temperature ranges of high-pressure / low temperature metamorphism were calculated by the distribution of Fe^{2+} and Mg between garnet and omphacite based on Ellis and Green (1979) calibration. Temperature ranges and K_D values obtained from representative garnet (core-mantle-rim) and omphacite (core) pairs are given in Table 6.3 and Figure 6.6. Representative garnet and omphacite analyses, which are used in temperature estimations, are given in Table 5.8 and Table 5.6, respectively.

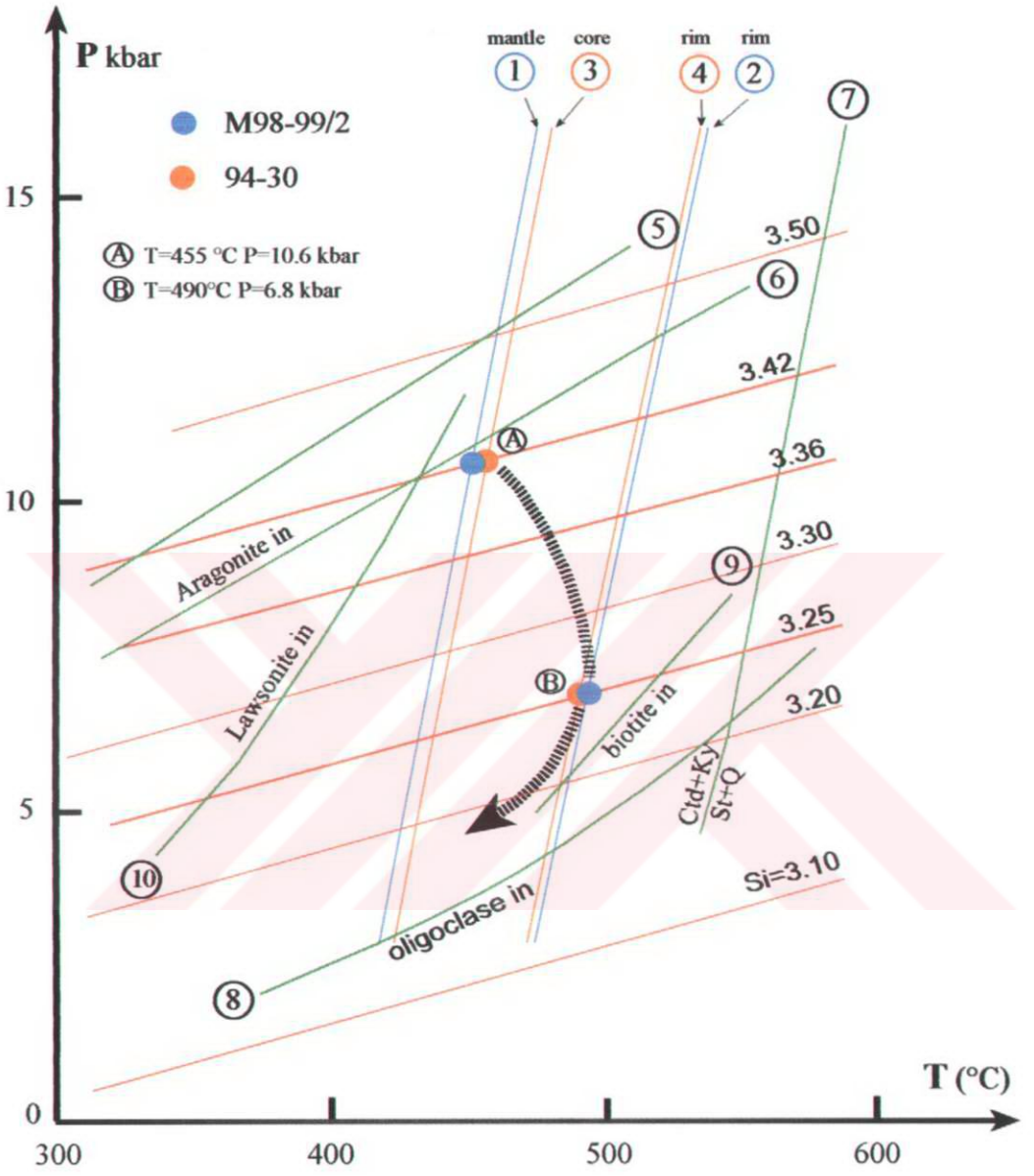


Figure 6.5 PT -diagram showing the metamorphic evolution of the matrix of the Metaolistostrome, based on data from Table 6.2. Curves 1 to 4 represent the K_D values of garnet and phengite after Green & Hellman's (1987) calibration; (5): jadeite + quartz stability (Holland, 1980); (6): Stability limit of aragonite (Johannes & Puhan, 1971); (7): Chloritoid + kyanite = staurolite + quartz reaction after Bhaskar Rao & Johannes (1979); (8): Oligoclase-in (Maruyama et al. 1983); (9): Biotite-in Piccardo et al.(1979); (10): Lawsonite + albite = zoisite + paragonite + quartz + H2O reaction after Heinrich and Althaus (1980). Si isopleths are after Massonne and Schreyer (1989).

Table 6.3 Temperature estimates obtained from Ellis & Green (1979) garnet clinopyroxene Fe/Mg exchange thermometry for eclogite blocks

Sample	Pairs Grn - omp	analyse no of garnet*	Analyse no of omphacite*	K_D	Maximum X_{Jd} mol %	Temperature range (°C)	Average temperature (°C)
M99-5/4	Rim-core	10	1	32	49	500	~493
	Core-core	13		38		485	
M98-45C	Rim-core	5	53	39	44	473	~467
	Core-core	12		55		460	
SE-1	Rim-core	35	126	40	32	523	~515
	Core-core	43		39		506	
95-21/10	Rim-core	1	21	41	36	550	~479
	Mantle-core	3		48		482	
	Core-core	14		87		408	

* representative garnet and omphacite analyses are given in Table 5.8 and Table 5.6, respectively

Except for 95-21/10, the maximum temperature ranges for high-pressure metamorphism are estimated based on garnet (core-rim) and omphacite (core) pairs. Omphacites do not show regular zonation, although the cores of omphacite crystals generally have maximum jadeite content. Temperature ranges obtained by Ellis and Green (1979) geothermometer, change from 467 to 515 °C. Jadeite isopleths are calculated by Holland (1980) calibration. Equilibrium conditions have been estimated by combination of the Ellis and Green (1979) Fe^{2+}/Mg exchange geothermometer, with the jadeite content of omphacite (low albite = Jadeite + quartz, Holland, 1979). Jadeite isopleths and average temperature for HP/LT metamorphism belonging to each sample, give a minimum pressure range between 11.3 ±0.5 and 11.9 ±0.5 kbar (Table 6.4 and Figure 6.6). Sodic plagioclase in eclogite samples is of secondary origin and is related to the breakdown of omphacite during retrogressive decompression. Sodic plagioclase in eclogite samples is not pure albite and has 0.8-1.37 mol % anorthite content. The existance of sodic plagioclase in eclogite parageneses indicates that the pressures, calculated by the geobarometer of Holland (1980), are minimum pressures for HP/LT metamorphism (Carswell and Harley 1990).

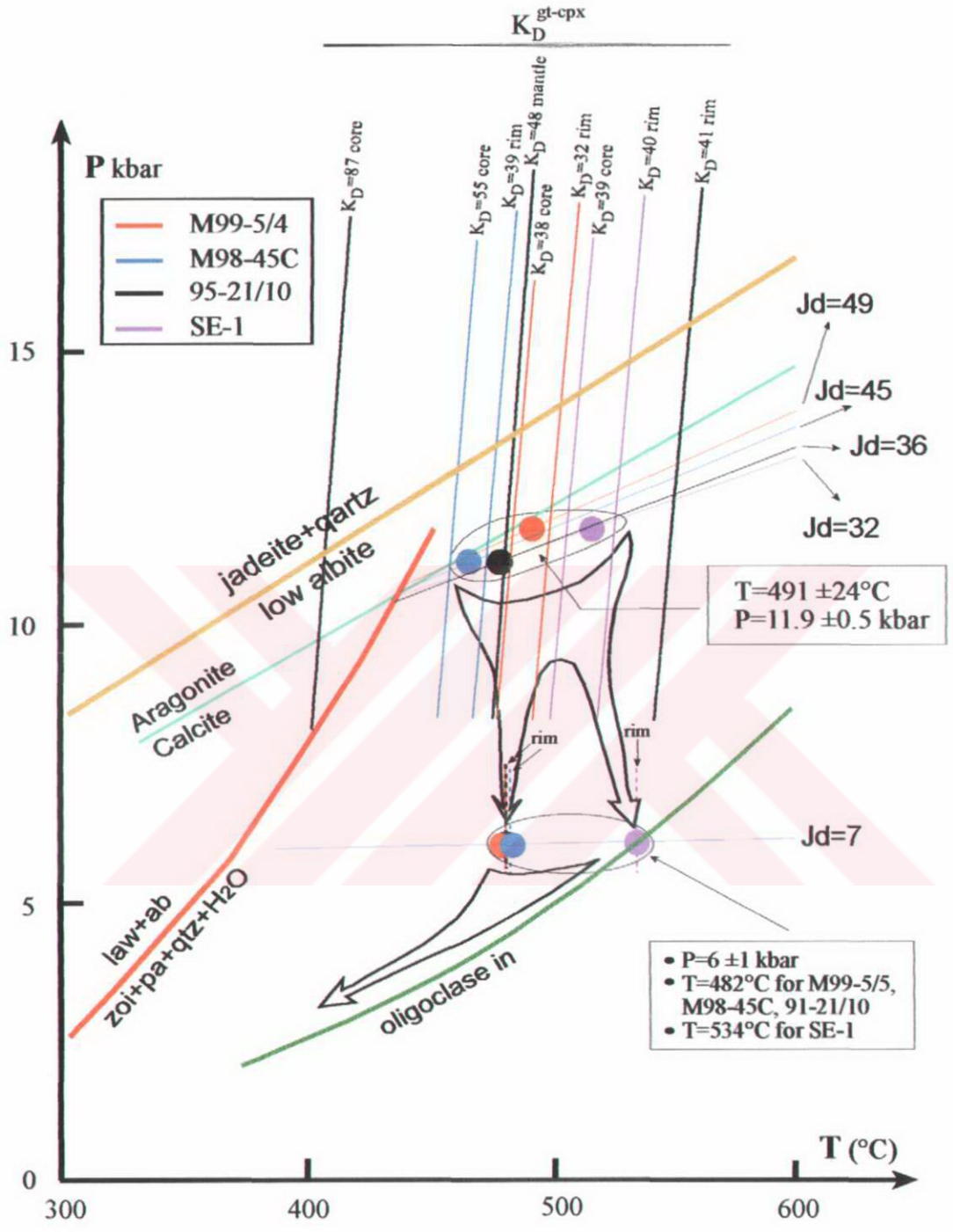


Figure 6.6 P-T estimations of prograde and retrograde eclogite crystallization. Dotted lines indicate temperature limits of each samples obtained after Graham and Powell (1984) geothermometry for retrograde metamorphism (Table 6.5). Jadeite isopeths are calculated from the data of Powell and Holland (1985). Lawsonite + albite = zoisite + paragonite+ quartz + H2O reaction curve, stability limit of aragonite and oligoclase-in curves are from Heinrich and Althaus (1980), Johannes and Puhan (1971) and Maruyama et al. (1983), respectively. Abbreviations: K_D, Fe/Mg distribution coefficents in garnet-clinopyroxene pairs: Jd, jadeite: gt, garnet: cpx, clinopyroxene.

Table 6.4 Pressure estimations obtained from eclogite blocks by Holland (1980) calibration for high-pressure metamorphism.

Sample	Omphacite*	Plagioclase*	Temperature (°C)	Estimated pressure (kbar)
SE-1	Omphacite analyse no: 126 Jd=32 mol%	Plagioclase analyse no=5 An=0.8 mol%	493	11.9 ±0.5
M99-5/4	Omphacite analyse no: 1 Jd=49 mol%	Plagioclase analyse no=8 An=1.26 mol%	467	11.9 ±0.5
M98-45C	Omphacite analyse no: 53 Jd=45 mol%	Plagioclase analyse no=5 An=0.8 mol%	515	11.3 ±0.5
95-21/10	Omphacite analyse no: 21 Jd=36 mol%	Plagioclase analyse no=5 An=1.37 mol%	479	11.9 ±0.5

*Representative omphacite and plagioclase analyses are given in table 5.5 and table 5.20, respectively.

High-pressure assemblages are retrograted by greenschist overprint. The temperature range of this overprint was estimated by Graham and Powell (1984) calibration from eclogite samples. Representative garnet (rim) and amphibole (rim) pairs give temperature value changing from 481 to 534 °C (Table 6.5).

Table 6.5 Temperature estimations obtained from eclogite blocks after Graham and Powell (1984) calibration for retrograde metamorphism

Sample	Garnet*	Amphibole*	K_D	Temperature (°C)
M99-5/4	Analyse no:10 (rim)	Analyse no:21 (rim)	16	481
M98-45C	Analyse no:5 (rim)	Analyse no:34 (rim)	15	483
SE-1	Analyse no:35 (rim)	Analyse no:160 (rim)	17	534
95-21/10	Analyse no:24 (rim)	Analyse no:4 (rim)	28	481

*Representative garnet and amphibole analyses are given in table5.8 and table 5.3, respectively.

The analyses of garnet cores and amphibole rims are used to obtain the maximum K_D values for retrograde metamorphism. The rims of zoned garnet and amphibole crystals are assumed to represent equilibrium partitioning. Except for sample SE-1, temperature range obtained from garnet (rim) and amphibole (rim) is quite narrow and changes between 481 and 483 °C (Table 6.5). According to Graham and Powell (1984) calibration, temperature values of sample SE-1 are 534 °C for garnet (rim) – amphibole (rim) (Table 6.5). Although the pressure value is quite similar, the temperature values of sample SE-1 are relatively different and higher compared to the other eclogite samples.

The minimum jadeite content in omphacites ranges between 15 and 17 mol%, except for sample M98-45C. Jd=15 and 17 isopleths at 480-490 °C give pressure about 9 kbar after Holland (1980) calibration. This value most probably represents an intermediate stage of retrograde overprint. Sodic plagioclases which are the breakdown product of omphacite, have quite low anorthite content (max 3.4 mol%). In sample M98-45C, minimum jadeite content of omphacite and maximum anorthite content of plagioclase are 7.2 and 3.4 mol%, respectively. This gives a minimum pressure 6.1 ±0.5 kbar after Holland (1980) calibration (Figure 6.6). This value is consistent with the pressure value (~6.5 kbar) obtained from the matrix of the metaolistostrome for retrograde metamorphism. The consistency of P-T estimations reveals that matrix and blocks experienced a common retrograde overprint. Therefore, a maximum pressure interval of retrograde metamorphism for all other eclogite blocks may be assumed as 6 ±1 kbar.

6.3.3. Omphacite metagabbro and omphacite-epidotite blocks

P-T conditions of three omphacite-epidotite samples from Torbalı (M98-163/2),-Selçuk (M97-151/3), Söke (M96-92/4) and one omphacite-metagabbro from Selçuk (91-16) were estimated. Because of the absence of garnet, it is difficult to estimate the temperature of high-pressure metamorphism. In the omphacite-metagabbro sample (91-16), amphiboles are in textural in equilibrium with omphacites. These amphiboles (m15-1, m15-2, m15-3, m15-31, m15-50 and m15-57 in Table 5.4)

which plot into the high-pressure field in Figure 5.11, give an average temperature value of 531 °C using Colombi (1989) geothermometry based on Ti-content of amphiboles. According to Spear (1980) calibration, representative pairs of Na-Ca amphibole (m15-50) and plagioclase (m15-30 in Table 5.20) which has maximum albite content plot near the curve of 490 ±20 °C (Figure 6.7). Temperatures values between 553 and 570 °C which are not realistic for omphacite metagabbros have been obtained by the model of Holland and Blunndy (1994) at 12 kbar. An average temperature value of about 510 ±20 °C after Colombi (1989) and Spear (1980) calibrations can be accepted for peak temperatures for the high-pressure metamorphism. This average temperature is used for the geobarometeric calibration of Holland (1980), based on the jadeite + quartz = albite (low) reaction. Maximum jadeite content of omphacite (m15-55 in Table 5.7) is 47 mol % in omphacite-metagabbro sample (91-16). Jd_{47} isopleth was calculated by Holland (1980) calibration and plagioclase which has maximum albite content (m15-30 in Table 5.20). According to this isopleth, minimum pressure is of about 12.2 ±0.5 kbar at 510°C (Figure 6.8).

Pressure and temperature conditions of retrograde metamorphism are estimated by Holland (1980) and Colombi (1989) calibrations, respectively. Re-equilibrated amphiboles (m15-29, m15-36 and m15-48 in Table 5.4) from sample 91-16 indicate an average 488 ±10 °C after the calibration of Colombi (1989). The temperatures deduced after Holland and Blunndy (1994) are unrealistically high. The average temperature obtained by this calibration, is 597 °C. Minimum jadeite content of omphacites (m15-23 in Table 5.7) in sample 91-16 is 8 mol%. The combination of Holland (1980) calibration and plagioclase with maximum anorthite content (m15-47 in Table 5.20) give 6.8 ±0.5 kbar for 488 °C. The pairs of amphibole rim (m15-36) and plagioclase (m15-47) with maximum anorthite content ($An_{5.27}$) give about 7 kbar for 476 °C after Plyusnina (1982) calibration (Figure 6.9) and about 490 ±20 °C at 6.8 kbar after Spear (1980) calibration (Figure 6.7).

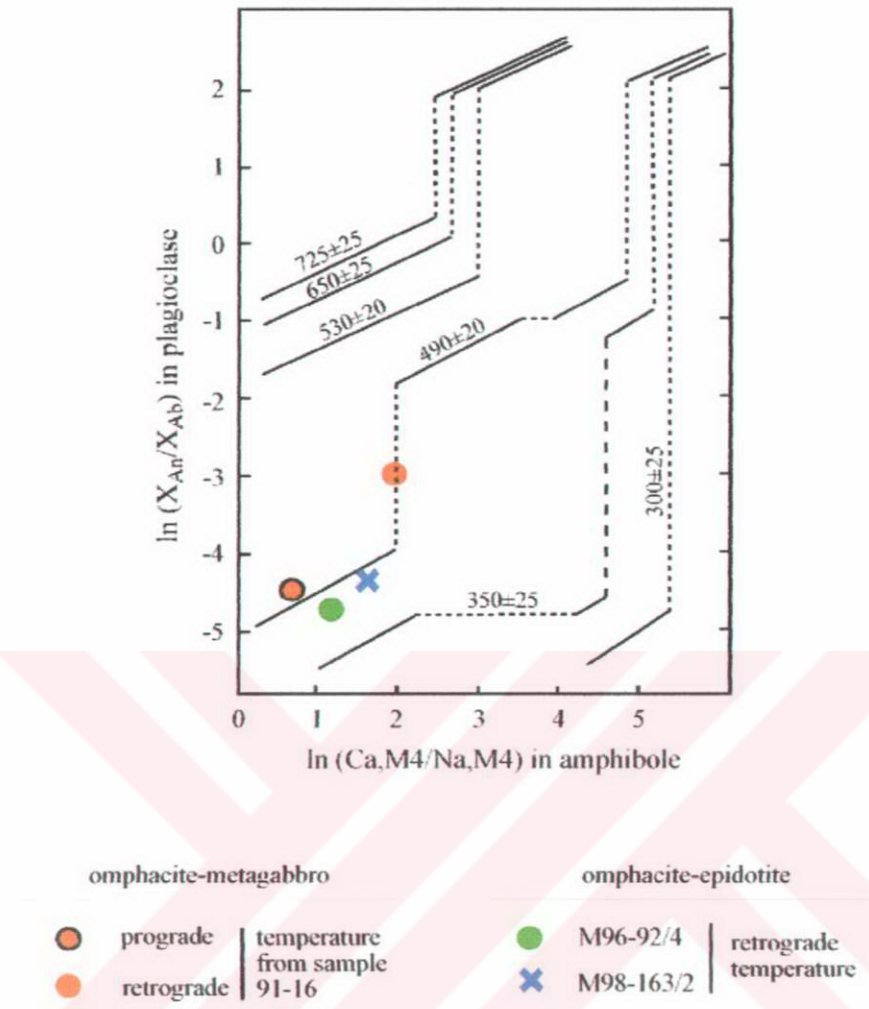


Figure 6.7 Spear (1980) geothermometer based on plagioclase-amphibole exchange equilibria. Amphibole and plagioclase analyses are given in Table 5.4 and Table 5.20, respectively.

Because of the absence of garnet, the estimation of temperature conditions is difficult in omphacite-epidotites which mainly have a mineral assemblage of omphacite – plagioclase (albite) – amphibole – epidote. The only pair of minerals (albite and high-pressure amphibole?) that could be used as a thermometer (Holland and Blunndy, 1994) must be excluded since this thermometer gives unrealistic results for temperature conditions of high-pressure metamorphism. Therefore, 500 °C which is the average of peak temperatures obtained from omphacite-metagabbro and eclogite samples was used for geobarometric estimations. Pressure was calculated

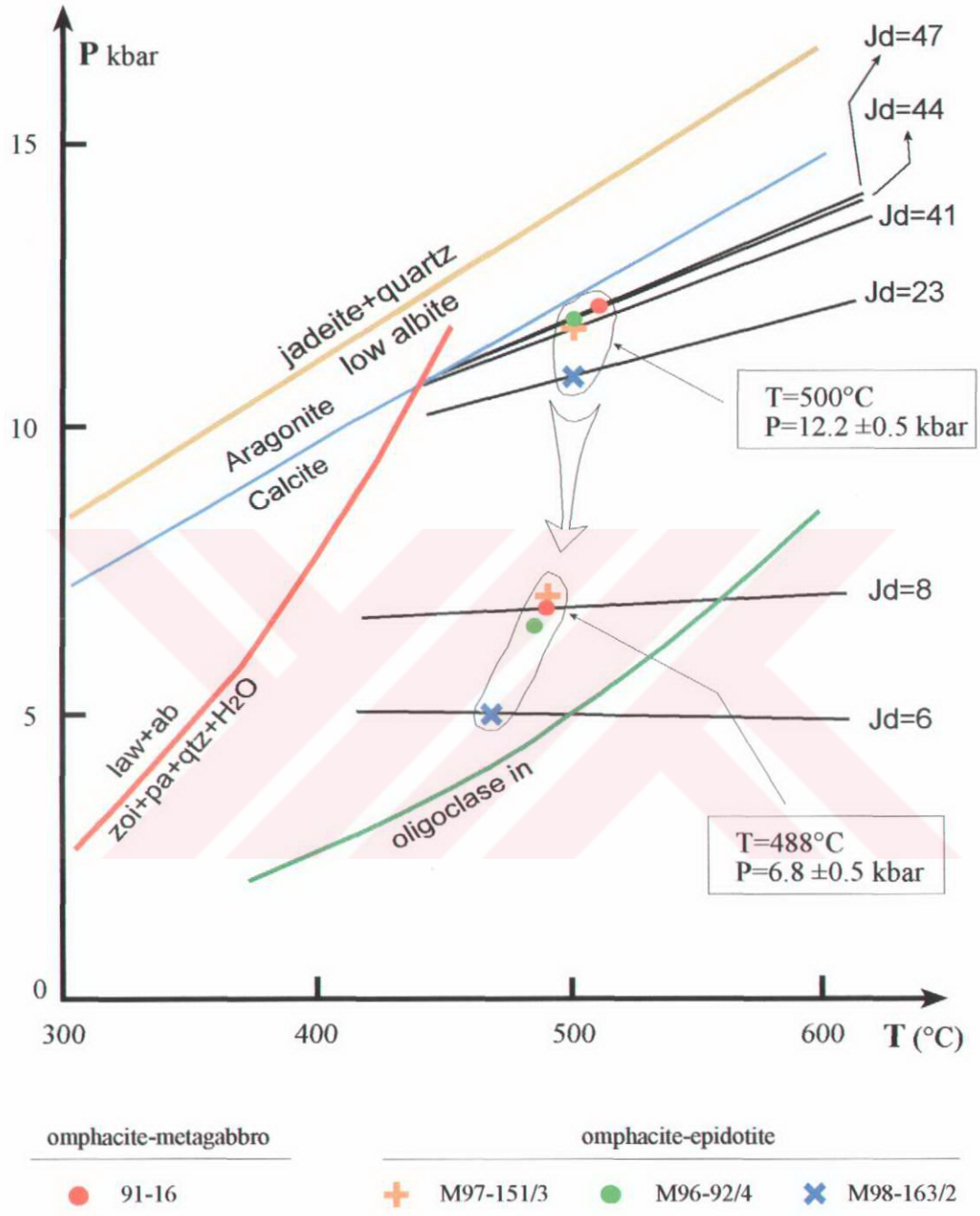


Figure 6.8 P-T path of the omphacite-metagabbro and omphacite-epidotites based on various geothermobarometric calibrations. Jadeite isopeths are calculated by the data of Powell and Holland (1985). Lawsonite + albite = zoisite + paragonite+ quartz + H2O reaction curve, stability limit of aragonite and oligoclase-in curves are after Heinrich and Althaus (1980), Johannes and Puhan (1971) and Maruyama et al. (1983), respectively.

with the jadeite + quartz = low albite barometer of Holland (1980) (Table 6.6).

Table 6.6 Pressure estimations obtained from omphacite-epidotites using Holland (1980) calibration.

	Omphacite*		Plagioclase**			
Sample	Analyse no	Max. jd mol%	Analyse no	Max. An mol%	Temperature(°C)	Estimated pressure (kbar) (Holland, 1980)
M97-151/3	m16-24	41	m16-19	1.45	500	11.8 ±0.5
M96-92/4	m13-32	44	m13-1	0.79	500	11.88 ±0.5
M98-163/2	m12-15	23	m12-23	0.60	500	10.8 ±0.5

* representative omphacite analyses are given in table5. 4
** representative plagioclase analyses are given in table 5.20

Maximum Jd content of omphacites is 23 mol% in M98-163/2. In general, the low jadeite content of omphacites is regarded to represent an intermediate stage of the retrograde overprint, but this may not be always true. If the basic rocks were not buried deep, the jadeite content of omphacite could be low. In addition, the existence of amphiboles belonging to the pre-eclogitic stage which has not been completely replaced by omphacite in this sample, shows that this block was not burried to depth for a complete transformation from amphibole to omphacite. The fact that plagioclase in the original basic igneous rock has higher anorthite component is another possibility to explain the lower jadeite content of omphacite in sample M98-163/2. This lower jadeite content leads to estimate a slightly lower pressure (10.8 ±0.5 kbar) in this sample. The pressure of 11.8 ±0.5 kbar calculated from two omphacite-epidotite samples can be assumed as the minimum pressure for high-pressure metamorphism (Table 6.6 and Figure 6.8).

P-T estimations of retrograde metamorphism are based on Plyusnina (1982), Holland (1980), Brown (1977), Colombi (1989) and Spear (1980) calibrations for omphacite-epidotites (M98-163/2, M97-151/3 and M96-92/4) (Table 6.7).

Sample M98-163/2: Amphibole analyse (m12-4) gives temperatures ranging between 470 and 474 °C after Colombi (1989), based on Ti content of amphibole, and Plyusnina (1982) calibrations (Figure 6.9). The temperature of about 490 ±20 °C was calculated by the amphibole-plagioclase (Spear, 1980) thermometer (Figure 6.7). Pressure estimations are based on Holland (1980) and Brown (1977) calibrations (Figure 6.10). These calibrations give pressures ranging between 5 and 6 kbar (Table 6.7).

Sample M97-151/3: Plyusnina (1982) which is based on Ca mol% in plagioclase, and total Al in amphibole and Colombi (1989) calibrations were used for temperature estimation in this sample. Plyusnina (1982) and Colombi (1989) give 493 and 486 °C for the retrograde overprint, respectively (Table 6.7 and Figure 6.9). The pressure is also established after Plyusnina (1982) as 5 kbar (Table 6.7, Figure 6.8 and 6.9). Due to the absence of an equilibrium assemblage (omphacite and albite), estimated pressure values after Holland (1980) geobarometry are quite high. On the other hand, Spear (1980) and Brown (1977) calibrations give unrealistic P-T estimations. Therefore, these calibrations were not used for the calculations.

Sample M96-92/4: the amphiboles in this sample give a similar range of temperatures with an average of: 485 °C after the calibration of Colombi (1989), and less than 490 ±20 °C after the calibration of Spear (1980) (Table 6.7). Pressure is estimated 7 kbar using Brown (1977) calibration (Table 6.10 and Figure 6.10).

It can be concluded based on different geothermobarometric calibrations that the average of P-T values of omphacite-metagabbro and omphacite epidotites for high-pressure metamorphism can be assumed as minimum 12.2 kbar at 510 ±10 °C and minimum 11.8 kbar at 500 ±20 °C, respectively. The geothermobarometric calculations from the retrograde phases in these rocks suggests that retrograde overprint developed at 6 ±1 kbar pressure and 480 ±10 °C temperature.

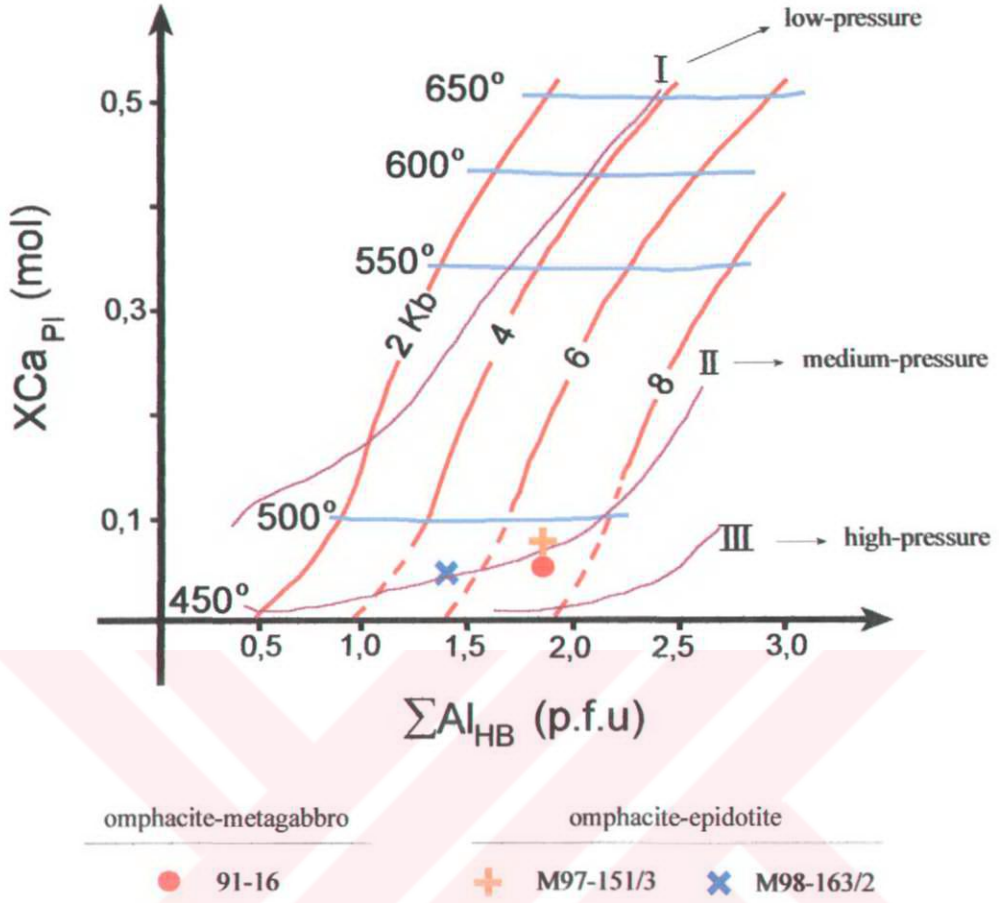


Figure 6.9 Pressure and temperature estimations of retrograde overprint in omphacite-metagabbro and omphacite - epidotites after Plyusnina (1982) calibration.

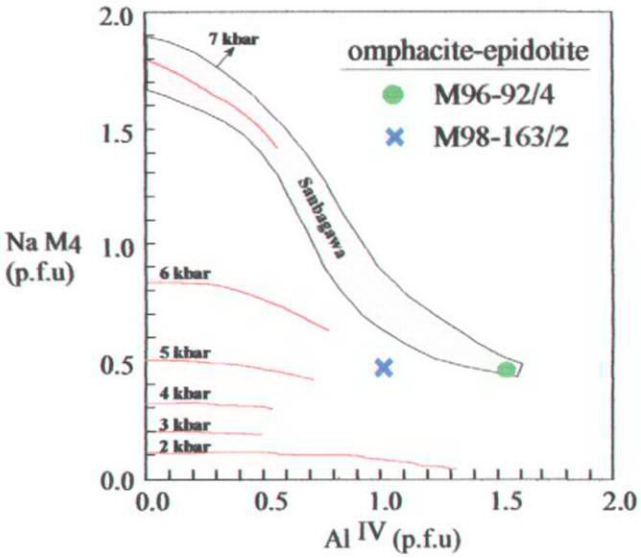


Figure 6.10 The relationship between pressure and Na_{M4} content of amphiboles in omphacite-epidotite samples. Shaded area represents amphiboles which was formed in 7 kbar from Sanbagawa (Brown 1976).

Table 6.7 Estimation of P-T condition obtained from omphacite-epidotite samples for retrograde overprint based on different calibrations.

Sample	P and T estimation	Pressure estimation		Temperature estimation	
	Plyusnina (1982)	Holland (1980)	Brown (1977)	Colombi (1989)	Spear (1980)
M98-163/2 (omphacite-epidotite)	Amphibole analyse no: m12-4 Plagioclase Analyse no: m12-6 (An_4) P=5 kbar T=470 °C (Figure 6.9)	Clinopyroxene analyse no: m12-38 (Jd_6) Plagioclase Analyse no: m12-6 (An_4) P=5 kbar at T=475 °C	Amphibole analyse no: m12-41 P=6 ±1 kbar (Figure 6.10)	Amphibole analyse no: m12-4 T=474 °C	Amphibole Analyse no: m12-12 Plagioclase Analyse no: m12-43 T= below 490 ±20 °C (Figure 6.7)
M97-151/3 (omphacite-epidotite)	Amphibole analyse no: m16-22 Plagioclase Analyse no: m16-20 ($An_{8.6}$) P=7 kbar T=493 °C (Figure 6.9)	Disequilibrium No results	Unrealistic results	Amphibole analyse no: m16-22 T=486 °C	Unrealistic results
M96-92/4 (omphacite-epidotite)	Unrealistic results	Disequilibrium No results	Amphibole analyse no: m13-14 P=7 kbar (Figure 6.10)	Amphibole analyse no: m13-14 T=485 °C	Amphibole Analyse no: m13-14 Plagioclase Analyse no: m13-2 T= below 490 ±20 °C (Figure 6.7)

Representative amphibole, clinopyroxene and plagioclase analyses are given in table 5.4, table 5.7 and table 5.20, respectively

6.3.4. Blueschist metabasite blocks

P-T conditions were estimated from two different blocks for blueschist metabasites in Şirince (M98-52/2) and Çamlık (94-55/5) areas. The temperature range of high-pressure / low temperature metamorphism is calculated by Colombi (1989) calibration, based on Ti content in amphibole, and the distribution of Fe^{2+} and Mg between garnet and amphibole pairs after Graham and Powell (1984) (Table 6.8). The Graham and Powell (1984) calibration gives an average temperature of 458 – 459 °C. Similarly, the temperatures calculated by Colombi (1989) calibration range between 454 and 457 °C. The difference between both calibrations is all 5 °C. The average temperature of 457 °C for blueschist metabasites can be assumed as peak temperature of HP/LT metamorphism. On the other hand, it is difficult to estimate the pressure conditions in blueschist metabasites due to lack of appropriate mineral assemblages for the geobarometric calibrations. Therefore, geobarometer after Brown 1977 based on Al-in-sodic amphibole are used to estimate pressure conditions. According to Brown (1977) calibration, Na, Na-Ca and Ca amphiboles from the blueschist metabasites are plotted onto the Brown (1977) diagram (Figure 6.11). Although, the sodic amphiboles with maximum NaM4 content are selected from two samples, this geobarometer gives relatively low-pressure values for peak pressure of blueschist metabasites (Table 6.9).

The point representing the peak temperature at about 457 °C after Green and Hellman (1982) and minimum pressure at about 7 kbar after Brown (1977) is plotted into barroisite stability field of Ernst (1979) diagram in Figure 6.12. Whereas, the Na-amphiboles used for the pressure estimation, are crossite in composition. According to Ernst (1979) diagram, glaucophane stability field begins at about 7.8 kbar for 457 °C (Figure 6.12). When the stability fields of Na-amphibole on this diagram are considered it can be concluded that Na-amphiboles in blueschist metabasites should have been formed in higher pressure than 7.8 kbar. The possible upper pressure range can be restricted by the jadeite (pure) + quartz = low albite reaction curve (Holland 1980) and the uppermost breakdown limit of glaucophane

Table 6.8 Temperature estimations for HP/LT metamorphism for blueschist metabasites after Graham and Powell (1984) and Colombi (1989) geothermometric calibrations. Representative garnet and amphibole analyses are given in Table 5.9 and Table 5.1, respectively.

Sample no	Graham and Powell (1984)				Colombi (1989)	
	Analyse no	K_D	T °C	Average tempareture	Analyse no	T °C
M98-52/2	Garnet (core) -11 / Amphibole (core) - 60	18.6	448	459	Amphibole (rim) - 60	459
	Garnet (rim) - 5 / Amphibole (core) - 60	12.8	470			
94-55/5	Garnet (core) -31 / Amphibole (core) - 48	22	456	458	Amphibole (rim) - 48	454
	Garnet (rim) - 37 / Amphibole (core) - 48	18.8	461			

(Ernst 1979). Maximum pressure limit of blueschist metabasites is 12.8 kbar (Figure 6.12). K_D curves (1-2-3-4) of Green and Powell (1984) calibration and upper stability curves of low albite and barroisite defines a polygon, shaded area in Figure 6.12. A pressure range between 7.8 and 12.8 kbar with an average value of about 10 kbar for 457 °C can be postulated for the blueschist (Figure 6.12).

The temperature of retrograde overprint under greenschist facies conditions is calculated after Bhattacharye et al., (1992) garnet – biotite Fe/Mg exchange thermometry. Due to the absence of biotite in mineral assemblage of 94-55/5, this calibration is only applies to sample M98-52/2. The existence of Na-amphibole inclusions in the core of garnet suggests that the garnet core crystallized during the epidote – blueschist facies metamorphism. Therefore, a garnet rim which was in-

equilibrium with biotite during the greenschist facies overprint is used with the Bhattacharye et al., (1992) calibration to estimate the peak temperature for greenschist facies metamorphism (Table 6.10).

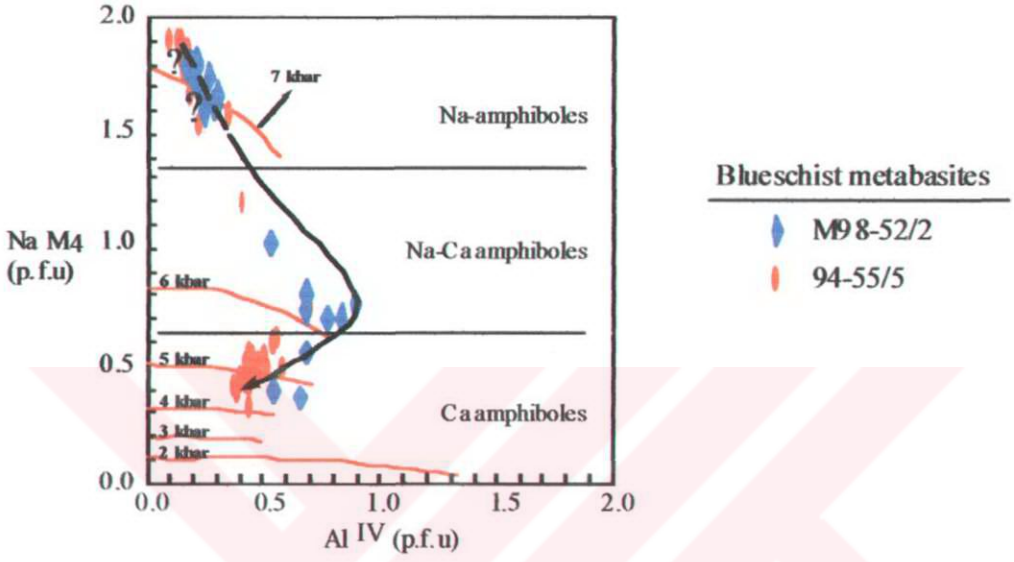


Figure 6.11 The relationship between pressure and Na_{M4} vs Al^{IV} diagram after Brown (1977) from blueschist metabasites in the Metaolistostrome unit. The line indicates the transformation path from Na-to Ca-amphibole. Although there is an consistence between the change of the amphibole composition and replacement textures representing the decreasing pressure, the Na-amphiboles give relatively low pressure values at about 7 kbar.

Table 6.9 Pressure estimations for blueschist metabasites based on Brown (1977) geobarometry. Representative amphibole analyses are given in Table 5.1.

Sample	Amphibole analyse no	NaM4	Al^{IV}	Pressure estimation (Kbar)
M98-52/2	69	1.796	0.173	~7
94-55/5	2	1.903	0.146	~7

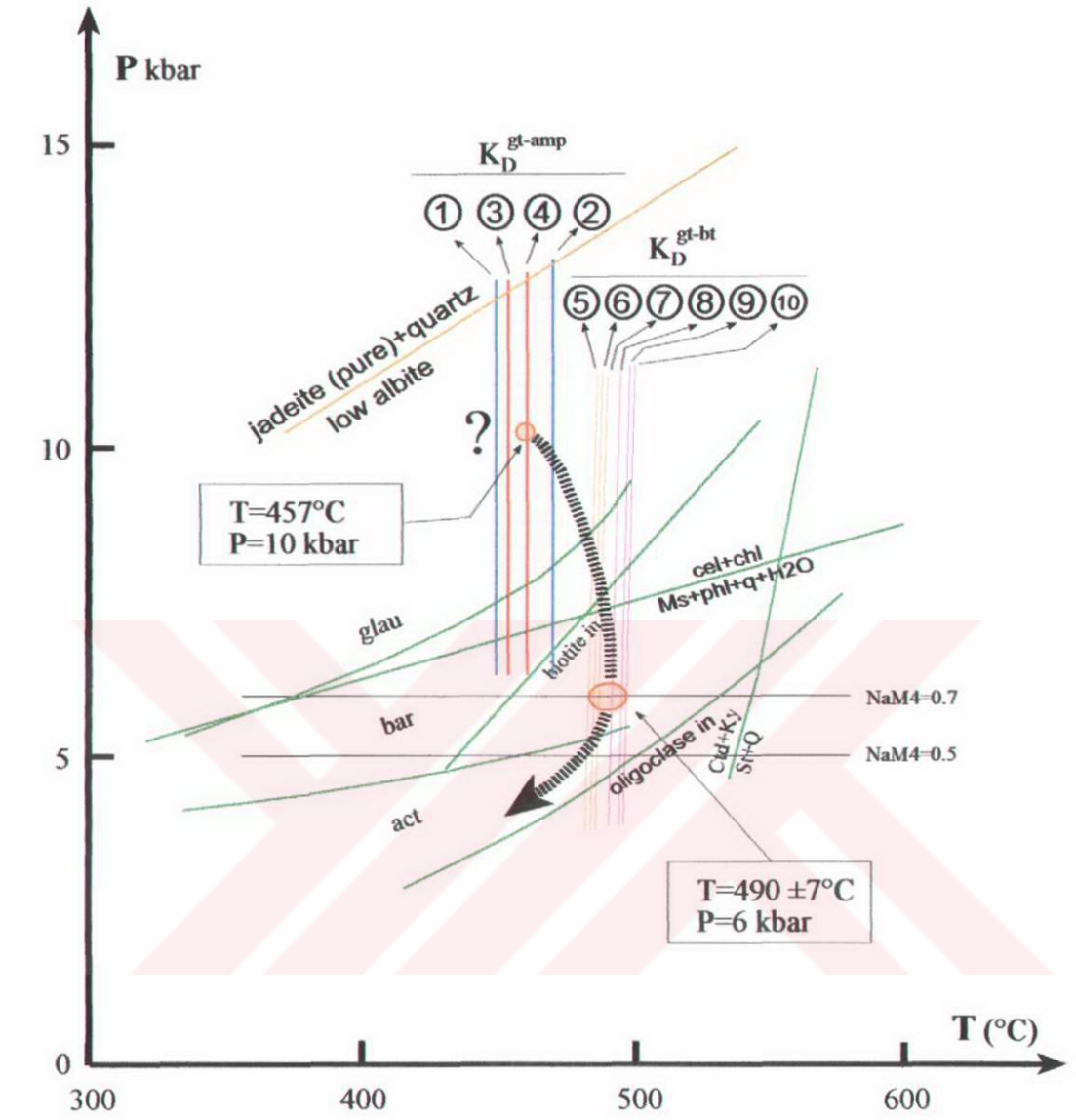


Table 6.8

M98-52/2	①	grt (core)-amp (core), KD=18.6
	②	grt (rim)-amp (core), KD=12.8
94-55/5	③	grt (core)-amp (core), KD=22
	④	grt (rim)-amp (core), KD=18.8

M98-52/2 (Table 6.10)

⑤ grt (rim)-bt (core), KD=11.2	⑧ grt (rim)-bt (core), KD=11.9
⑥ grt (rim)-bt (mantle), KD=11.1	⑨ grt (rim)-bt (mantle), KD=11.8
⑦ grt (rim)-bt (rim), KD=10.8	⑩ grt (rim)-bt (rim), KD=11.5

Figure 6.12 The possible P-T path of blueschist metabasites in the Metaolistostrome unit based on the data from Table 6.8 and 6.10. Curves; (1)- (4) K_D between garnet and amphibole after Green & Powell's (1984) calibration; (5)- (10) K_D between garnet and biotite with Bhattacharya el al., (1992) calibration; jadeite + quartz stability (Holland, 1980); chloritoid + kyanite = staurolite + quartz reaction after Bhaskar Rao & Johannes, 1979); oligoclase-in (Maruyama et al. 1983); Na_{M4} lines after Brown (1977); biotite-in after Piccardo et al.(1979); celadonite + chlorite = muscovite + phlogopite + quartz + H_2O reaction after Bucher and Frey (1994). Abbreviations: K_D, Fe/Mg distribution coefficents in garnet-biotite and garnet-amphibole pairs: gt, garnet; bt, biotite; amp, amphibole; glau, glaukofan; bar, barroisite; act, actinolite.

Table 6.10 Peak temperature estimations for greenschist facies overprint on blueschist metabasites (P=6 kbar). Representative garnet and biotite analyses from sample M98-52/2 are given in Table 5.9 and Table 5.16, respectively. Grt: garnet, Bt: biotite.

	Grt rim	Bt core	Grt rim	Grt rim	Bt mantle	Grt rim	Grt rim	Bt rim	Grt rim
Analyse no	5	2	15	5	56	15	5	1	15
K_D	11.2		11.9	11.1		11.8	10.8		11.5
T (°C)	492		483	493		484	496		487
Average T (°C)	**488**			**489**			**492**		

As seen in Table 6.10, the temperature estimations for peak conditions of greenschist facies overprint can be given at about 490 ±7 °C for an assumed 6 kbar pressure. There is a slight increase in temperature deduced from core (average 488 °C) to rim (average 492 °C) of biotite. Although Brown's (1977) calibration gives erroneous results in high pressures, it yields concordant values in low pressure conditions. Amphibole path in Figure 6.11 gives maximum value of Al^{IV} (=0.898 p.f.u) approximately at 6 kbar (Na_{M4}=0.7). Brown (1977) suggests that the amphiboles become richer in Al^{IV} with increasing temperature of regional metamorphism. For greenschist facies overprint, 6 kbar pressure can be postulated as pressure at the calculated temperature of about 490 °C. After that peak pressure and temperature condition, a decrease in pressure (Na_{M4}=0.5) which is associated with cooling occurs during the greenschist facies metamorphism (Figure 6.11).

In summary; Dilek Peninsula and Selçuk – Tire areas have been subjected to the subduction related HP/LT metamorphism under epidote-blueschist facies conditions (P=11 kbar T= 445 °C and P= 8.6 T= 453°C respectively) (Figure 6.13). PT-path of the matrix of the Metaolistostrome unit begins from boundary between epidote-blueschist and greenschist facies (Figure 6.13). The peak P-T conditions for the matrix of the Metaolistostrome unit were estimated at about T=455 °C and P=10.6 kbar representing epidote-blueschist facies conditions. P-T estimations obtained from

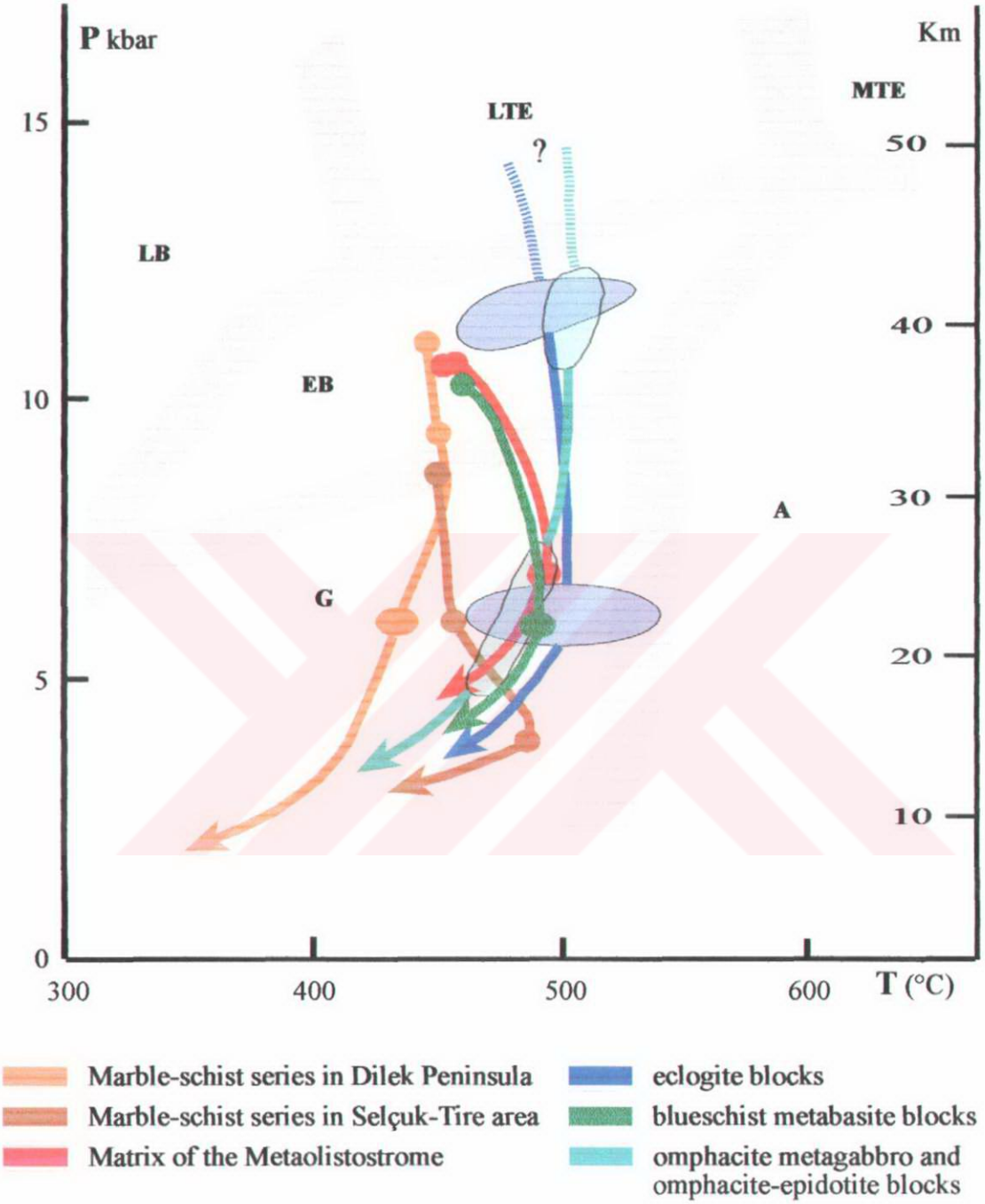


Figure 6.13 Comparative P-T paths from the Marble-schist series and the Metaolistostrome unit (blocks and matrix). Stability fields of metamorphic facies are after Carswell (1990). Abbreviations: LTE, low-temperature eclogite; MTE, medium-temperature eclogite; LB, lawsonite blueschist; EB, epidote blueschist; G, greenschist; A, amphibolite facies.

blocks in the matrix of the Metaolistostrome unit for prograde metamorphism are given below;

Eclogite blocks P=11.9 ±0.5 kbar T=491 ±24 °C

Omphacite metagabbro and omphacite-epidotite blocks P=12.2 ±0.5 kbar T=500 °C

Blueschist metabasite blocks P=10 kbar T=457 °C

The prograde metamorphism in epidote-blueschist facies conditions is retrograded by the greenschist facies overprint. P-T estimations for greenschist facies overprint under the decompression with slightly increase of temperature in some rock groups are given below;

Marble-schist series in Dilek Peninsula P=6 kbar T=433 ±12 °C

Marble-schist series in Selçuk-Tire area P=4 kbar T=487 ±10 °C

The matrix of the Metaolistostrome P=6.8 kbar T=490 °C

Eclogite blocks P=6 ±1 kbar T=482 °C

Omphacite metagabbro and omphacite-epidotite blocks P=6.8 ±0.5 kbar T=488 °C

Blueschist metabasite blocks P=6 kbar T=490 ±7 °C

CHAPTER SEVEN

DISCUSSION

This chapter can be divided into three titles as lithostratigraphic correlation of Mesozoic-Early Tertiary rock series of the Menderes Massif and Cycladic Complex (Samos and Syros Islands, P-T evolution and the ages of HP/LT metamorphism and following greenschist overprint in Menderes Massif and Cycladic Complex and tectono-metamorphic evolution of the western part of the Menderes Massif

Lithostratigraphic correlation of Mesozoic-Early Tertiary rock series of the Menderes Massif and Cycladic Complex (Samos and Syros Islands): Menderes Massif, mainly made up of the Pan-African basement and its Paleozoic-Early Tertiary sequence, can be described as a complex nappe pile mostly modified by the Alpin deformation (Partzsch et al., 1998; Candan et al., 1999). In Dilek Peninsula, Selçuk, Torbalı, Tire and Gölmarmara areas, the lowest parts of the Menderes Metamorphics consist of Paleozoic micaschist, black metaquartzite, phyllite and marble intercalation. This detrital sequence is overlain by Lower Triassic – Upper Cretaceous series. The contact relationship between Paleozoic sequence and the overlying Lower Triassic – Upper Cretaceous sequence is still controversial. The Mesozoic sequence starts with mica schists / garnet-mica schist with marble, metaquartzite, phyllite, mafic volcanic rocks, quartz metaconglomerate and carbonate metaconglomerate intercalations. Especially in the Dilek Peninsula, lense-shaped mafic volcanic rocks contain relict Na-amphibole. Quartz metaconglomerates which are completely made up of quartzite pebbles, are recognized in several

localities on Dilek Peninsula, Selçuk and Kuşadası (Figure 3.1, 3.11 and 3.17). The coexistence of mafic volcanic rocks and metaconglomerates with mafic material in their matrix can be interpreated to present an intraplate extension setting in Menderes Massif during the Lower Triassic time. The micaschists pass gradually upward into the thick massive platform-type neritic carbonates (Milas Formation) with a transition zone represented by marble - schist intercalation. In addition, Late Triassic primary yellowish dolomites are characteristics for this transition zone. Late Triassic to Liassic age was suggested by Dürr (1975), Dürr et al., (1978) and Konak et al., (1987) for lowermost level of this sequence. This platform sequence contains metabauxite lenses and horizons. Jurassic (Konak et al., 1987) or Cretaceous (Dürr 1975; Özer 1998) ages have been proposed for these metabauxite horizons. In the Dilek Peninsula, metabauxites are dominated by diaspore and chloritoid. The retrograde overprint of blueschist metabasites under greenschist facies conditions is well consistent with the corundum – diaspore isograde in the Dilek Peninsula and blueschist relics are restricted to the low-temperature site of diaspore-corundum transition. Poorly-preserved upper Cretaceous rudist fossils occur uppermost level of platform marbles. Rudist fossils are stratigraphically above the metabauxites (Dürr 1975; Konak et al., 1987; Özer 1998).

The Cycladic Complex is exposed as a series of small islands in the centre of the Aegean Sea. In Cyclades, the Pre-Alpidic basement is overlain by a Mesozoic sequence consisting of neritic carbonates and pelitic sediments and subordinately acidic and basic volcanites. The island of Syros and Samos are parts of the Cycladic blueschist belt. The island of Samos is situated two kilometers to the NW of Dilek Peninsula. The crystalline series of the Samos form a piles of nappes (Figure 7.1) (Papanikolaou, 1979; Okrush et al., 1985; Ring et al., 1999a) including the Kalithea nappe, the Ampelos nappe and the Kerketea unit. The Ampelos nappe, which contains widespread blueschist relics, glaucophane metagabbro, glaucophanite and omphacite rocks (Mposkos and Perdikatsis, 1984; Okrush et al., 1985; Chen 1992), is made up of three tectonic units: Vourliotes, Ampelos and Aghios. The Vourliotes unit which is exposed in the eastern part of Samos, consists of marbles and metapelites-with minor ultramafic and mafic intercalations (Figure 7.1) (Okrusch et

al., 1985). This isoclinally folded succession (Chen, 1992) with widespread blueschist relicts is typified by the presence of metaclastic quartzitic phyllites with the striking assemblage of kyanite-chloritoid. The quartz metaconglomerates in the Dilek Peninsula, Kuşadası, Selçuk and along the southern flank of Menderes Massif may be correlated with the quartzitic phyllites occurring on Samos Island, Vourliotes unit, in terms of its stratigraphical position and mineralogical composition (Okrush et al., 1985; Chen 1992; Candan et al., 1997; Oberhaensli et al., 1998). In Vourliotes unit, kyanite – chloritoid ± Mg-carpholite assemblage is reported by Okrusch et al., (1985). In the southern flank of the Menderes Massif, the occurrence of Fe-Mg-carpholite-kyanite HP assemblage (Rimmele et al., 2002) in quartz metacoglomerate supports the continuation of this quartzitic phyllites and quartz metaconglomerates not only in Dilek Peninsula but also along the southern flank of The Menderes Massif (Figure 7.2). The marbles in the eastern part of the island contain lenses of metabauxite with diaspore and chloritoid (Mposkos, 1978; Papanikolaou, 1979). Papanikolaou (1979) recognized traces of rudist fossils, suggesting an upper Cretaceous age for the metabauxite-bearing marbles. Candan (1997, 1999), Oberhaensli et al., (1998), Ring et al., (1999a, 1999b) emphasize the resemblance of the Vourliotes unit which contains common Na-amphiboles relicts, and the Dilek Peninsula (Figure 7.2). According to Ring et al., (1999b) the Cycladic blueschist unit on Samos Island consists of three high-pressure nappes, which are made up of from top to bottom: (1) the Selçuk nappe (Metaolistostrome unit), (2) the Ampelos nappe (Permocarboniferous to Mesozoic passive margin sequence), and (3) the Agios Nikolaos nappe (Carboniferous basement). Candan et al., (1997); Oberhaensli et al., (1998) and Ring et al., (1999b) argued that the Selçuk nappe (Metaolistostrome unit) can be correlated with the ophiolitic melanges exposing on Syros and Tinos islands. In these islands, rock unit with similar lithologies and tectonic position is exposed (Candan et al., 1997; Oberhaensli et al.,1998; Ring et al., 1999b). The Vourliotes unit of the Ampelos nappe, which can be used to correlate the Cyclades and the Marble-schist series in Menderes Massif, consist of quartzite, metapelite and metabasite which are overlain by marble with metabauxite. These data also support that the Mesozoic to Early Tertiary sequence of the Menderes Massif is in lateral continuation of the Alpine units of the Cycladic Complex.

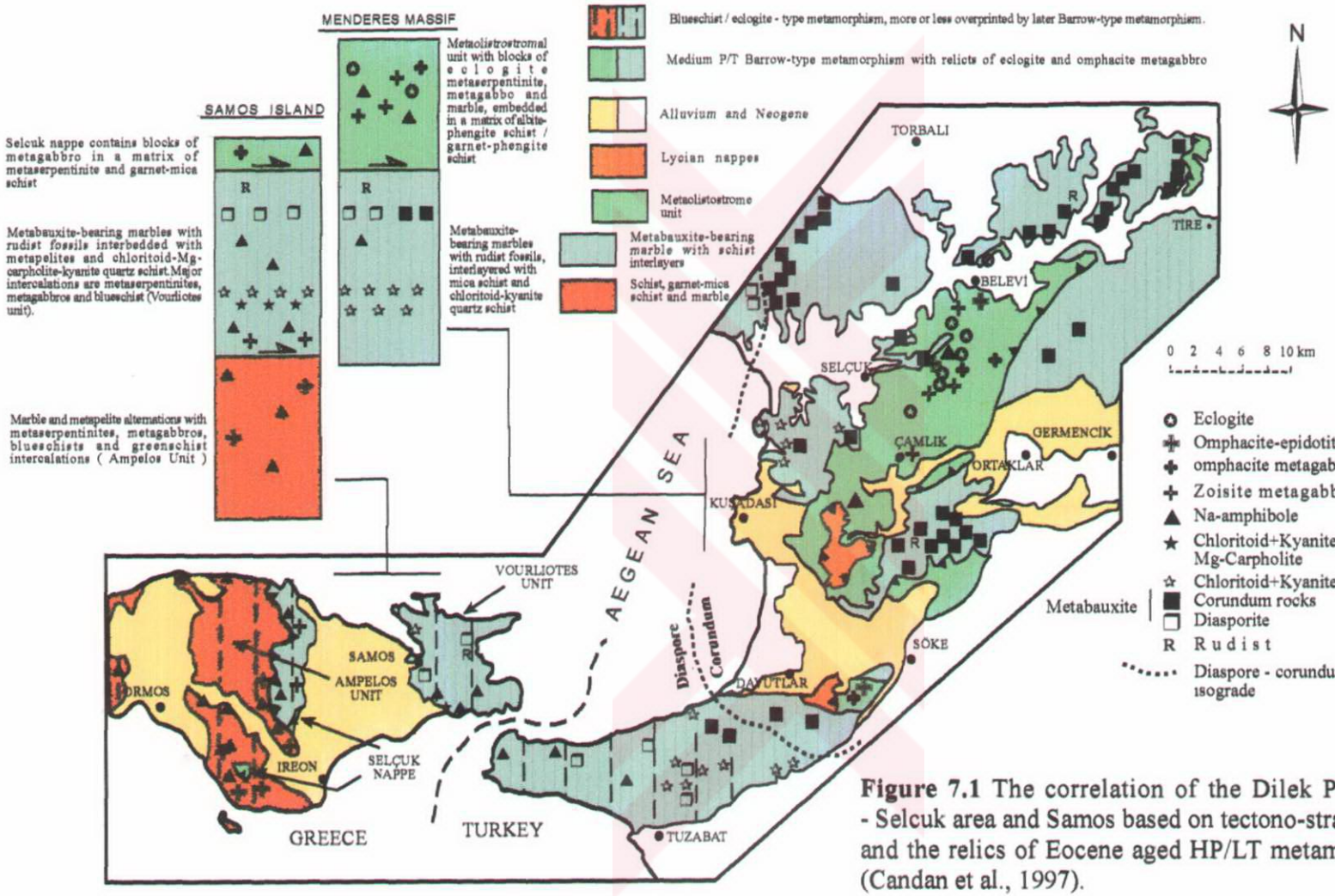


Figure 7.1 The correlation of the Dilek Peninsula - Selcuk area and Samos based on tectono-stratigraphy and the relics of Eocene aged HP/LT metamorphism (Candan et al., 1997).

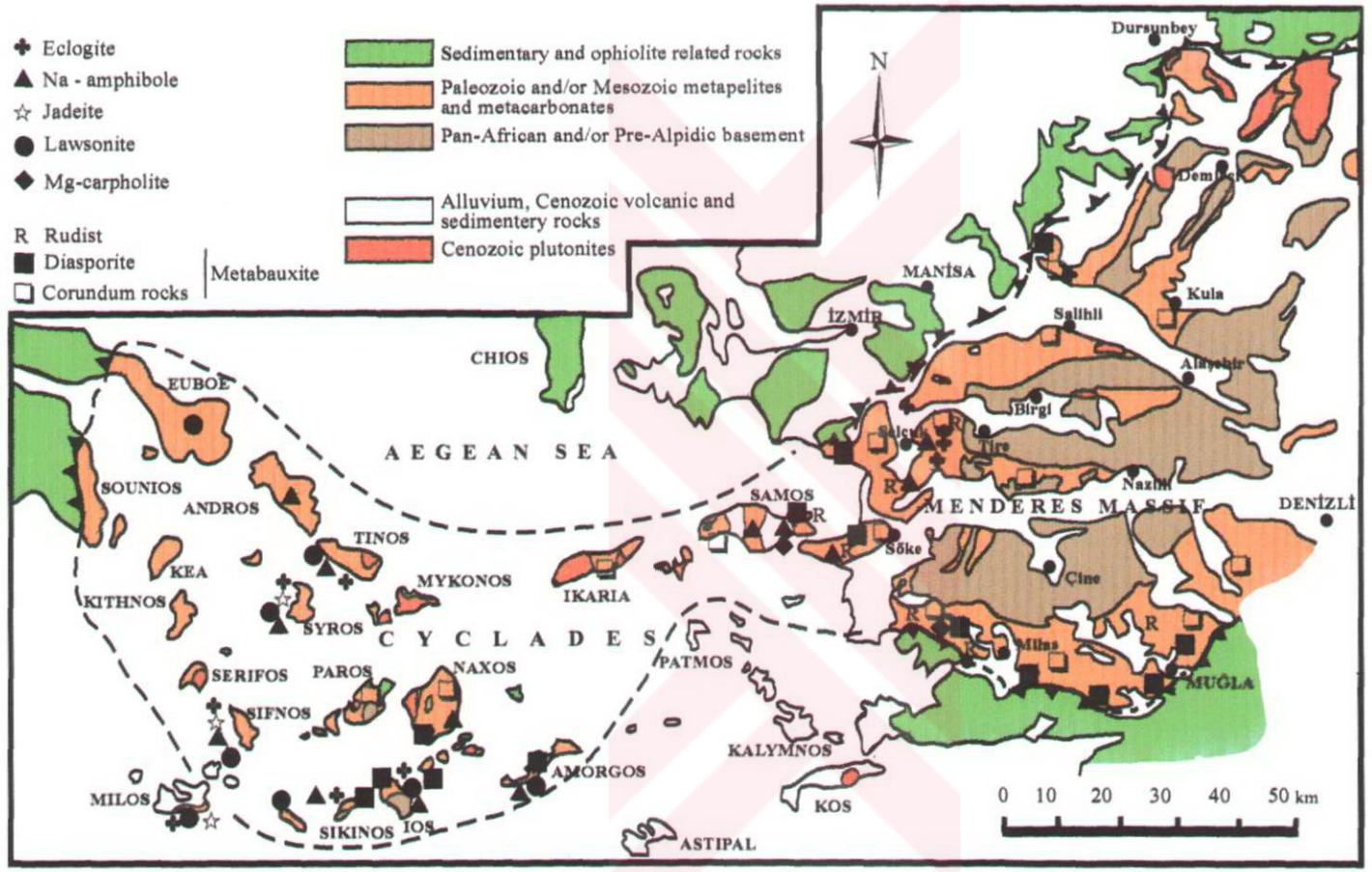


Figure 7.2 Correlation of the Menderes Massif with the Cycladic Complex in terms of the main units and relic high-pressure rocks The localities are after Önay (1949); Okrusch & Bröker (1990); Candan et al., (1997); Candan et al., (1999) and Özer (1998).

In Syros, the succession of schists and marble forms the lower part of the Ermoupolis unit (Bonneau et al., 1980; Maluski et al., 1987). This succession was subjected to repetition by thrusting (Dixon & Ridley, 1984). On Syros island, the marble-schist succession is tectonically overlain by a metamorphosed olistostrome unit with high-pressure blocks (Dixon, 1969; Ridley and Dixon 1984).

The Metaolistostrome unit which is named as Selçuk Formation by Erdoğan and Güngör (1992), exposes in the west and northwest part of the Menderes Massif. The Metaolistostrome unit crops out in southwest of Söke, Selçuk, east of Torbalı, west of Tire and southwest of Gölmarmara (Candan & Kun 1989; Erdoğan & Güngör 1992; Candan et al., 1997, 1999; Güngör 1998, Çetinkaplan et al., 2000a, 2000b; Gessner et al., 2000). The Metaolistostrome unit is regarded as stratigraphically uppermost unit of the Menderes Massif by Erdoğan & Güngör (1992) and Güngör (1998). These authors advocate that the contact between the Marble-schist series and the Metaolistostrome unit is gradational. However our evidence supports that, platform type marbles are tectonically overlain by the Metaolistostrome unit. The evidence about the tectonic character of this contact are given below:

1) In the southern flank of Menderes Massif, the metabauxite and rudist-bearing platform type marble which is named as Milas Formation, grades into thin-bedded, red, pelagic marbles (Kızılağaç Formation) (Dürr, 1975). Whereas Kızılagaç Formation which represents gradual foundering of the platform owing to the obducted oceanic crust onto the platform, is absent between platform marbles with rudist fossils and the Metaolistostrome unit in Selçuk and Tire areas.
2) In Torbalı area, the Metaolistostrome unit rests directly upon the probably Paleozoic aged sequence which is composed of black metaquarzite, black phyllite and mica schist.
3) In Gölmarmara area, the Metaolistostrome unit is directly underlain by the sequence which is composed of garnet-mica schist, mica schist, yellowish-brown metaquartzite and thin marble layers.
4) In Selçuk and Söke areas, metaserpentinite blocks in some localities occur directly on the platform type marble.

5) A jump in the metamorphic grade of the matrix of the Metaolistostrome unit and schist of the Marble-schist series can be recognized in the field. Garnet is present in all the places in the matrix of the Metaolistostrome unit. Whereas, the first garnet occurrence in the Marble-schist series is observed in Akyurt and Hasançavuşlar areas.

The best outcrops of the Metaolistostrome unit which is made up of blocks and matrix, are exposed between Selçuk and Ortaklar. Furthermore, the same unit is also observed in Söke, Torbalı, Tire and Gölmarmara as small tectonic slices. The blocks of the Metaolistostrome unit are embedded in a matrix which consists of garnet-phengite schist and albite-phengite schist. Eclogite, omphacite metagabbro, omphacite-epidotite, zoisite metagabbro, Ti-metagabbro, metabasite (with or without Na-amphibole relict), metaserpentinite and marble form the main block types of the Metaolistostrome unit. Eclogites which are recognized around Selçuk, west of Hasançavuşlar village and Gölmarmara, are observed as tectonic inclusion in metaserpentinite or individual blocks in matrix. Eclogites are partly retrograded to the garnet amphibolites along the margins by the greenschist overprint. Zoisite metagabbro blocks occur as isolated blocks are derived from strongly deformed parts of omphacite metagabbros. The low strain Ca-amphibole augens appear in zoisite metagabbros. The common occurrence of the similar zoisite metagabbro blocks which are exposed in metamorphosed olistostrome of Syros, have been emphasized by Ridley and Dixon (1984). These rocks are named as gneissic metabasites by these authors. Ti-metagabbro blocks are common especially in Selçuk-Ortaklar area. Ti-metagabbros are remarkably rich in Fe and Ti (TiO_2 = 2.33 – 5.24 wt %). The main Ti-phases are ilmenite and dominantly sphene. Ilmenite is relict igneous phase and is often replaced or rimmed partly by sphene. Metabasite blocks are quite common in the Metaolistostrome unit. The existance of gneissic metabasites which is named as metabasite in Metaolistostrome unit (Menderes Massif), have been argued by Ridley (1984) in Syros. Metabasites are subjected to epidote-blueschist facies metamorphism. The relict Na-amphibole bearing metabasite blocks occur NE of Şirince (Figure 3.17) and N of Kirazlı (Figure 3.32). Metaserpentinites and marbles form the most common block types in the Metaolistostrome unit. Metabauxite-

bearing marble blocks are derived from underlying thick marble sequence. In Samos island, the Metaolistostrome unit which is called as Selçuk nappe by Ring et al (1999a), contains block of metagabbro in a matrix of serpentinite and garnet-mica schist. In the northern part of Syros island, the marble-schist succession is overlain by an association of glaucophane rocks, metagabbros, ultramafics, and eclogites forming big blocks enclosed in a matrix of serpentinites, chlorite-schist and metatuffites. (Dixon 1969; Dixon & Ridley, 1987; Höpfer 1989). This association in Syros is regarded as a separate tectonic unit forming a metamorphosed olistostrome or ophiolitic melange (Okrusch & Bröcker, 1990). The Metaolistostrome unit in Menderes Massif displays great similarity to metamorphosed olistostrome in Syros and Samos in terms of the characteristic high-pressure blocks and tectonic position (Dixon 1969, Ridley and Dixon 1984, Candan et al., 1997).

P-T evolution and the ages of HP/LT metamorphism and following greenschist overprint in Menderes Massif and Cycladic Complex: Quartz metaconglomerates from Dilek Peninsula, Selçuk and Kuşadası are probably Lower Triassic in age and contain typical kyanite – chloritoid (max. X_{Mg}=0.35) – phengite assemblage in their phyllitic matrix. Si contents of white micas from kyanite – chloritoid – phengite schist, blueschist metabasites, mica schist and garnet-mica schists in the Marble-schist series display a continuous evolution between phengite and muscovite. Maximum Si and X_{Mg} content of phengite and chloritoids, respectively, decrease from Dilek Peninsula to Tire. This is related with increase of greenschist overprint from west to east. Almandine-rich garnets of the Marble-schist series in the Menderes Massif, display compositional and structural zoning. These garnets do not contain inclusion-free relict cores like the garnets in the matrix of the Metaolistostrome unit. The other important feature, difference between peak and minimum values of end-members in garnet is not so big, due to partly flattened end-member profiles with greenschist overprint. A broad bell-shaped growth zoning in the core and the reversals of end-member profiles in the rim which are related with post-growth diffusional effects, are typical features for the Marble-schist series garnet. End-member profiles show normal growth zoning as defined by Hollister (1966). Garnet growth occurred during the epidote-blueschist stage. This stage is

mainly characterized by minimum X_{Sps} and X_{Grs} values and maximum X_{Alm} value. P-T conditions at about 8.6 kbar and 453 ±10 °C given in Figure 6.4 probably reflects initial conditions of the greenschist facies overprint. The peak P-T conditions during the epidote-blueschist facies metamorphism of the Marble-schist series in Selçuk-Tire area is mostly obliterated by greenschist overprint when compared with P-T path of the Dilek Peninsula. The retrograde stage (P=4 kbar T=487 ±10 °C) is defined by flat or reversal profiles. Profiles showing normal growth zoning demonstrate resetting by diffusion-controlled retrogressive effects. The intensity of diffusion decreases away from the rims of garnet.

HP/LT metamorphism in Dilek Peninsula is represented by "Na-amphibole + phengite" assemblage in blueschist metabasite and metapelites, and "Kyanite – chloritoid - phengite" assemblage in quartz metaconglomerates. In Dilek Peninsula, epidote-blueschist facies metamorphism (P=11 kbar T=445 °C) was subsequently followed by the greenschist-facies overprint (P=6 kbar T=433 ±12 °C) under isothermal decompression conditions. Candan et al., (1977) estimated that pressure and temperature are minimum 10 kbar and less than 470 °C for epidote-blueschist facies metamorphism in Dilek Peninsula. These values are consistent with the results obtained by this study. The preservation of blueschist assemblages reveals the absence of thermal relaxation, on the contrary, presence of isothermal decompression during rapid uplift and exhumation of these rocks. In this area, retrograde processes during exhumation occurred under isothermal decompression conditions. The Marble-schist series rocks in Selçuk – Tire area have suffered the same HP/LT metamorphism. Some P-T estimations supporting the increasing of the temperature during the greenschist-facies overprint are identified. This is also verified by the highly retrogression of the blueschist facies assemblages in this area (Figure 6.13). Increase of temperature during the incipient stage of the transformation from epidote-blueschist to greenschist facies is very limited (P=6 kbar T=456 ±10 °C). Therefore, for this part of PT-path, exhumation process can be accepted to have been developed under the isothermal decompression conditions; i.e, tectonic denudation rather than isostatic uplift and erosion of whole-crust system (England & Richardson, 1977). However, P-T estimations for the Selçuk – Tire domain reveal a thermal relaxation

and heating during last stage of the retrograde overprint (P=4 kbar T=487 ±10 °C). Decrease in pressure which is accompanied by increasing of temperature during greenschist overprint might be explained by isostatic uplift and erosion.

The Marble-schist series rocks are overlain by the Metaolistostrome unit. The matrix of the Metaolistostrome unit is composed of garnet-phengite schist and albite-phengite schist. Si^{+4} contents of white micas in the matrix range from 3.31 to 3.42 (average 3.37) cations per formula unit. White micas which have a low Na / (Na+K) ratio and high Si content, display phengitic compositions. The rims of phengitic white micas have lesser Si^{+4} p.f.u. than their cores. This zonation pattern represents the Tschermak substitution which results from the retrograde metamorphism. Low Si contents of phengites in the Marble-schist series supports the existance of tectonic contact between the Marble-schist series and the Metaolistostrome unit. Garnets with high almandine content in garnet-phengite schist display compositional zoning consisting of relict core, mantle (blueschist stage) and rim (retrograde stage). Prograde growth and retrograde zoning patterns are observed in core – mantle and rim, respectively. The evidence about metamorphism forming inclusion-free relict core before blueschist stage are not determined. The relict core has been subjected to the resorbtion which is represented by irregular grain boundary of the core. This suggests changing in P-T conditions and in reaction assemblage. This is clearly visible in ternary atomic proportion diagram of Alm+Prp-Sps-Grs end-members (Figure 5.41 and 5.43) and end-member zoning profiles in mantle of garnet (Figure 5.42 and 5.44). Blueschist stage is represented by mantle part of garnet. Bluish zoisite inclusions which are always in equilibrium with blueschist mineral assemblage, occur in this part. On the contrary, there is no zoisite in the mineral assemblage of matrix. Prominent Fe-enrichment which demonstrates an increase in pressure, is limited to the mantle. The estimated P-T condition from mantle is 10.6 kbar and 455 °C. In general, the mantle-rim boundary is not texturally sharp and clear. Increasing XGrs and X_{Prp} and decreasing X_{Alm} in the rim are indicative of growth during heating at lower pressure relative to the mantle (P=6.8 kbar T=490 °C)

Pressure difference at the rims of garnets in matrix of the Metaolistostrome unit and the Marble-schist series shows that these two main units have been affected in different intensity from greenschist overprint and have been juxtaposed in late stage of greenschist overprint (Figure 6.13). In addition, this is another evidence about tectonic contact between the Marble-schist series and the Metaolistostrome unit.

High-pressure blocks with well-preserved high-pressure mineral assemblage in matrix of the Metaolistostrome unit are eclogite, omphacite-epidotite, omphacite metagabbro and blueschist metabasites. Eclogite blocks in the Metaolistostrome unit can be classified as ophiolitic or Alpine type HP/LT eclogites (Figure 5.12). Maximum jadeite content of clinopyroxenes which are omphacite in composition, in eclogite is 49 mol %. Garnet crystals in eclogite can be divided into mainly three parts as a core, mantle and rim. Normal growth zoning which is characterized by bell-shaped X_{Sps} profile and by increase in X_{Prp} and X_{Alm} and decreasing $Fe^{2+}/Fe^{2+}+Mg$ ratio towards the rims are observed in cores and mantles of garnet crystals. These profiles are most probably formed during prograde eclogite stage (PE). This stage in some garnets can be divided into three episodes as a PE1, PE2 and PE3. These episodes are characterized as below;

PE1 (core): almost flat X_{Alm}, X_{prp} and X_{Grs} profiles

PE2 (mantle): increase of X_{Alm} and X_{Grs} values

PE3 (mantle): minimum $Fe^{2+}/Fe^{2+}+Mg$ ratio and maximum X_{Prp} value

Diffusional retrograde zoning (R) is observed at the rims. This zoning causes reversed profiles of end-members in the outermost a few ten microns. Eclogites in the Metaolistostrome unit do not contain any prograde and/or retrograde mineral assemblages characterizing the blueschist facies conditions such as Na-amphibole, lawsonite etc.,. Blocks which have eclogite facies mineralogy were most probably formed under low-temperature eclogite facies conditions. The rocks which are formed in eclogite facies conditions, subjected to re-equilibration in greenschist facies conditions during the retrograde overprint. Therefore, obtained pressure values may not plot into low-temperature eclogite field (Figure 6.13). In P-T estimations for eclogites, the garnet core does not give maximum P-T conditions which are obtained from near to garnet rim due to retrograde effects. This causes lower P-T estimations.

P-T estimation which is obtained from the eclogite blocks for eclogite stage is P= 11.9 ±0.5 kbar T= 491 ±24 °C. Retrograde overprint in greenschist facies conditions occurred P= 6 ±1 kbar T= 482 °C in condition. This shows that exhumation processes occurred in approximately isothermal decompression conditions (Figure 6.6).

Maximum jadeite content of clinopyroxenes which are omphacite in composition, in omphacite-epidotite and omphacite metagabbros are 44 and 45 mol %, respectively. P-T estimation for eclogite stage and greenschist overprint of this blocks are P= 12.2 ±0.5 kbar T= 500 °C and P= 6.8 ±0.5 kbar T= 488 °C, respectively. Omphacite metagabbro and omphacite-epidotite blocks are also observed in epidote-blueschist facies field (Figure 6.13). But, there is no evidence that omphacite metagabbro and omphacite-epidotites are formed by epidote-blueschist facies metamorphism. The mentioned blocks should have been undergone to HP/LT metamorphism in low-temperature eclogite facies conditions. Their mineralogy also reflects eclogite-facies assemblage. However, obtained pressures using Holland (1980) calibration are slightly lower than low-temperature eclogite facies. This can be explained by the changing of the composition of the phases during the retrograde overprint. P-T path of blocks indicate that retrograde processes during exhumation occurred while the rocks decompressed isothermally or with cooling.

In blueschist metabasites, epidote-blueschist facies metamorphism is represented by Na-amphiboles (glaucophane and crossite). Na –and Na-Ca amphibole relicts in Şirince area are commonly observed as inclusion in garnet porphyroblast. In matrix of metabasites, rare Na-amphiboles are, in turns, rimmed towards rimward by barroisite and actinolite representing a continuous retrograde transformation in greenschist facies (Figure 6.13). The effects of retrograde overprint in garnet are represented by the development of albite, epidote and chlorite along the rims. Garnet crystals in Na-amphibole bearing metabasites with normal growth zoning which is characterized by bell-shaped X_{Sps} profile and by increasing X_{Prp} and X_{Alm}, and decreasing Fe^{2+}/Fe^{2+}+Mg ratio towards the rims are observed in core and mantle of

garnet crystal. These profiles are most probably formed during prograde blueschist stage (PB). Some garnet crystals from blueschist metabasites include Na-amphibole inclusions in core and mantle sections of the crystal. Growth zoning profiles at the rim are re-constructed by limited diffusional retrograde effects. The reason of that reversal of the profiles is observed at the rims. Diffusional modification of the profiles is restricted to range in 30-40 microns from rim to core. In Na-amphibole bearing metabasite blocks, P-T condition which is postulated for epidote-blueschist facies metamorphism, is P= 10 kbar T= 457 °C. The pressure and Temperature estimations for greenschist facies overprint can be given P= 6 kbar T= 490 ±7 °C. Blueschist metabasite blocks in the matrix of the Metaolistostrome unit show approximately same P-T path with the matrix of the Metaolistostrome unit (Figure 6.13). The P-T conditions associated with the exhumation path of these rocks in the Metaolistostrome unit are broadly constrained by the existence of barroisite, hornblende and biotite. The retrograde mineral assemblage indicates that the uplift path involved decompression with slight the Metaolistostrome unit have experienced a common P-T history (Figure 6.13).

Two-fold Tertiary metamorphism in Cyclades has been studied by several authors. This complex underwent a high-pressure metamorphism in Eocene time and was effected by a Oligocene/Miocene medium pressure overprint under greenschist facies conditions (Okrush and Bröcker, 1990). HP rocks of the Cyclades are dominated by the formation of Eocene blueschist and eclogite facies rocks which are best preserved in the islands of Sifnos, Syros and Tinos (Dürr et al., 1978; Altherr et al., 1979). The exhumation of HP rocks during the late Oligocene to Early Miocene caused some retrograde effects on the assemblages of Eocene high-pressure metamorphism (Altherr et al., 1979; Schliestedt et al., 1987). Except in Naxos island, the retrograde overprint in Cycladic Complex was carried out under greenschist facies conditions (Jansen & Schuiling, 1976; Buick & Holland, 1987). The P-T conditions of high-pressure metamorphism in Samos are estimated as 400-470 °C, 10-14 kbar for Selçuk nappe and 420-490 °C, 11-13 kbar for Amphelos nappe by Ring et al., (1999). Chen et al., (1995) estimated about 6-7 kbar and 450-490 °C for Barrovian-type overprint in Samos Island. In Sifnos, blueschist assemblages formed

at 460 ±30 °C, 15 ±3 kbar, were partly replaced by greenschist assemblages at 400-480 °C and 4-7 kbar conditions (Schliestedt & Matthews, 1987). The high-pressure assemblages in Syros conform the transition from the epidote-blueschist to eclogite facies with temperatures of about 450-500 °C and pressure in the range between 12 and 20 kbar (Okrush & Brõcker, 1990). Blueschist event in Tinos Island is characterized by P=12-20 kbar, T=450-500 °C and is followed by a subsequent greenschist facies overprint at somewhat lower temperatures and at pressures of 4-7 kbar (Bröcker 1990). The P-T condition of metamorphism in Ios are estimated as 9-11 kbar and 350 to 400 °C for epidote-blueschist facies and 5-7 kbar and 380-420 °C for greenschist facies overprint (Van Der Maar & Jansen, 1983). Eocene high-pressure/low-temperature metamorphism in Naxos is carried out under blueschist facies conditions (9 kbar and 400-500 °C) (Lister et al.,1984). Retrograde overprint in Naxos locally reached up to high amphibolite facies conditions (P=5-7 kbar T=700 °C) (Lister et al.,1984). P-T estimations obtained from western part of Menderes Massif display similarities with those of Sifnos and Syros and Samos Islands supporting the common HP/LT evolution of these two crystalline complexes. Some slight differences in P-T values may be related with different burial depth of slices.

Cycladic blueschist belt comprises rock sequences with different exhumation-related P-T paths (Figure 7.3). Rock sequences exposed in **Sifnos, Syros** and **Tinos** islands and to the west of the NE – SW trending island chain show isothermal or cooling decompression paths, whereas rocks exposed east of this chain have broad clockwise P-T loop with significant heating (Avigad et al. 1992).

It is also remarkable that rocks which have suffered heating, have emerged from shallower structural levels (Avigad et al. 1992). The peak pressure condition during the HP/LT metamorphism is at about 10 kbar in Naxos (Jansen and Schuling, 1976) and Ios (Van deer Maar and Jansen, 1983) islands corresponding to the shallower burial depth with respect to Tinos, Syros and Sifnos islands. Pressure for HP/LT metamorphism from matrix of the Metaolistostrome unit in Selçuk (Menderes Massif) is estimated at about 10.6 kbar. This value reveals that, the Metaolistostrome unit in Selçuk was not buried to the same great depth similar to Syros and Sifnos.

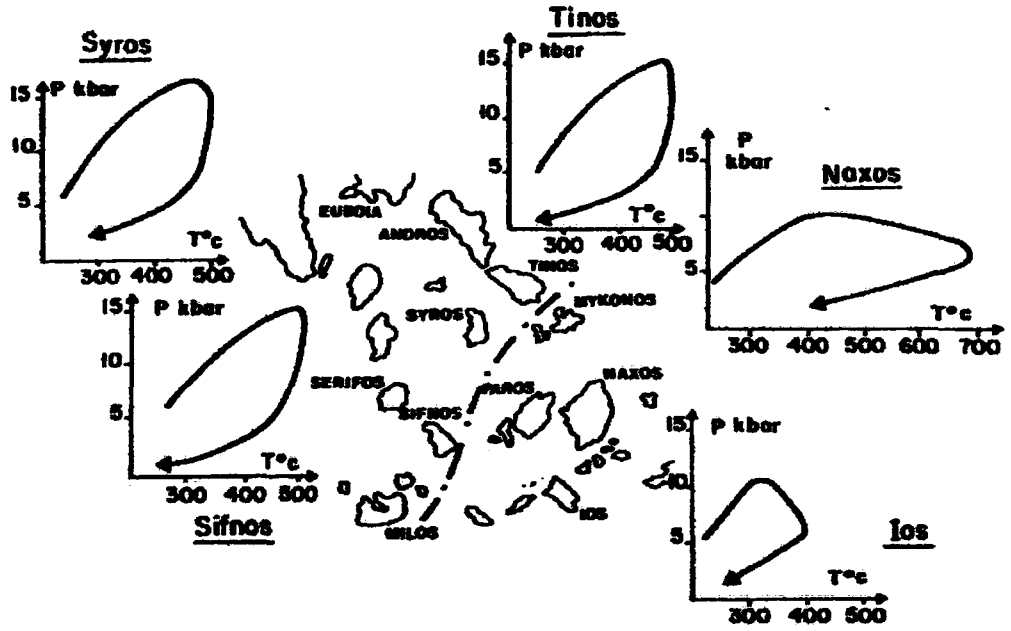


Figure 7.3 P-T paths obtained for Eocene high-pressure metamorphism in the Cyclades. The rocks exposed in the north-west part of the Cyclades have isothermal/cooling decompression paths whereas in the eastern part of the complex show broad clockwise P-T paths with significant heating (Avigad et al. 1992).

$^{40}Ar/^{39}Ar$ – cooling ages of phengites from blueschists of Dilek Peninsula yielded Eocene age (40Ma) (Oberhaensli et al., 1998). This is only one age obtained for HP/LT metamorphism from Triassic-Early Tertiary sequence of Menderes Massif. In Cyclades, age data for high-pressure metamorphism display a coherent pattern overall the Cycladic Complex. The age of high-pressure metamorphism and the following cooling in shelf / basement unit underlying the ophiolitic melange of Syros is placed into the Eocene (53-40 Ma) and 40-35 Ma by $^{40}Ar/^{39}Ar$ method, respectively (Altherr et al., 1979; Maluski et al., 1987 and Bröcker et al., 1993). High-pressure metamorphism in continental passive margin sediments in Cyclades is usually bracketed into the Eocene (53-40 Ma) (Gessner et al., 2001). Ring et al., (1999) is interpreated the age of the peak conditions of high-pressure metamorphism older than 50 Ma in islands of Sifnos, Naxos, Ios Syros, Tinos and Ikaria. Ring et al., (1999) suggests that cooling during decompression in these islands occurred between

35 and 40 Ma. These age data are consistent with $^{40}Ar/^{39}Ar$ – cooling ages of phengites from blueschists in Dilek Peninsula. On the other hand, Gessner et al., (2001) reported that $^{40}Ar/^{39}Ar$ ages at about 37-40 Ma of Ring et al., (unpublished data) from Samos Island can be interpreted to represent the phengite crystallization during a high-pressure deformation event which post-date the peak conditions of high-pressure metamorphism. Considering these interpretations, the phengite cooling age (40 Ma) from Dilek Peninsula suggests that the peak of epidote-blueschist facies metamorphism in Menderes Massif might be older than 40 Ma. Although there are very limited age determinations from subduction-related high-pressure metamorphism under epidote-blueschist facies conditions in the northwest part of the Menderes Massif, these preliminary results are well consistent with the general age interval of Cycladic Complex for HP/LT metamorphism. Based on geochronological data, stratigraphical similarities and petrological evidence, Lower Triassic – Upper Cretaceous sequence of Menderes Massif can be envisaged to be the eastward lateral continuation of the Cycladic blueschist unit of Samos Island as well as Cycladic Complex.

Okay (2001) interpreted that Lower Triassic to Upper Cretaceous the Marble-schist series and the Metaolistostrome unit in the western part of Menderes Massif are an isolated tectonic slices of the Cycladic Complex restricted only to the NW part of Menderes Massif. This interpretation is not supported by new HP evidence which have been already obtained from the southern flank of Menderes Massif. On Bodrum Peninsula, a widespread distribution of " Fe-Mg-carpholite + chloritoid + quartz" paragenesis at the base of Lycian Nappes, located at the top of Menderes Massif, was reported by Oberhaensli et al., (2001). This assemblage implies minimum pressure 6-8 kbar and maximum temperature about 400°C, suggesting a low grade HP/LT metamorphism (Oberhaensli et al., 2001). The HP/LT rocks with carpholite have not been found only in Lycian nappes which is outside of the Menderes Massif, but also, in the southern flank of Menderes Massif (Selimiye). Fe-Mg-carpholite-Kyanite assemblage in Lower Triassic metaconglomerates which can be obviously correlated in terms of their stratigraphical position with the carpholite-kyanite-chloritoid bearing-quartz metaconglomerates recognized in Samos island (Okrusch et al., 1985;

Chen 1992, 1995), recently nave been recognized by Rimmele et al., (2002). In addition, Mn-rich carpholite from west of Yatağan and blue amphiboles from Çal (Denizli) and northeast of Milas supports that Lower Triassic to Upper Cretaceous series exposed along the southern flank of the Menderes Massif underwent HP/LT metamorphism. This result is important in terms of distribution of the effects of the Eocene HP/LT metamorphism in Menderes Massif. This HP/LT metamorphism showing a broad distribution in the massif, can not be restricted only to the western part of Menderes Massif (Dilek Peninsula, Selçuk, Tire and Gölmarmara (Akhisar)). As a conclusion, the cover series of the Menderes Massif has been effected by Eocene HP/LT metamorphism with different overprint history. This reveals the common metamorphic history of Menderes Massif and Cycladic complex.

HP/LT facies metamorphism is subsequently followed by re-equilibration during decompression under greenschist facies conditions in western part of Menderes Massif. In Cyclades, decompression occurred dominantly under greenschist facies conditions, was dated at about 18-25 Ma (Altherr et al., 1982; Wijbrans and McDougall, 1988; Wijbrans et al., 1990; Bröcker et al., 1993; Bröcker & Enders 1999). There is no age determination from the greenschist equivalents of the epidote-blueschist series of Triassic-Early Tertiary sequence of Menderes Massif. There are some mica ages representing greenschist to amphibolite facies metamorphism at about 36 ±2 (Lips et al., 2000) and 35 ±5 Ma (Satır & Friederichsen 1986). But these age determinations are obtained from Pan-African and Paleozoic series of Menderes Massif. No evidence have been reported from Menderes Massif until today, whether the Pan-African and Paleozoic series of the Menderes Massif were also buried to the same depth and suffered Eocene HP/LT metamorphism. Exhumation of the rocks which have undergone epidote-blueschist facies metamorphism, at 38 km depth needs a time of 38 Ma and 19 Ma for 0.1 and 0.2 cm/yr uplift rate, respectively. Based on this uplift rates and the age of HP/LT metamorphism in Cycladic Complex (53-40 Ma), phengite –cooling age (40Ma) for epidote-blueschist facies of Lower Triassic-Upper Cretaceous series from Menderes Massif and 36 ±2 and 35 ±5 Ma mica ages (Lips et al., 2000; Satır & Friederichsen 1986) for greenschist facies metamorphism of Pan-African and Paleozoic series, may

be used as an evidence for tectonic contact relationship between these two main sequence. It can be suggested that Pan-African / Paleozoic units and Lower Triassic to Upper Cretaceous series of the Menderes Massif have experienced different tectono-metamorphic evolution during the Eocene time and tectonically juxtaposed after the HP/LT metamorphism.

As a conclusion, it can be suggested that the western part of Menderes Massif, Selçuk – Torbalı – Gölmarmara – Dilek Peninsula underwent progressive regional epidote-blueschist facies metamorphism which is subsequently followed by re-equilibration during decompression under greenschist facies condition. Although the greenschist overprint has not been dated yet, Eocene age from HP/LT series from western part of Menderes Massif which is well consistent with ages that were obtained for HP/LT metamorphism in the Cycladic Complex, support the common tectono-metamorphic evolution of these two crystalline complex.

Tectono-metamorphic evolution of the western part of the Menderes Massif: The Anatolide-Tauride platform was bounded by the northern and southern branches of the Neo-Tethyan ocean during the Early Triassic and Early Cretaceous (Şengör & Yılmaz 1981). In the western Anatolia, Anatolide-Tauride platform is made up of several tectonic units e.i, Tavşanlı zone, Afyon zone, Menderes Massif and Lycian nappes. These main tectonic units which are especially characterized by similar stratigraphies, have been organized during the continues tectonic processes which are related with closure of northern branch of Neo-Tethys ocean by the process of intra-oceanic subduction, obduction of oceanic lithosphere, accretion and continental collusion (Okay et al., 1996, 2001; Candan et al., 2002). The most important evidence for evolution of the northern margin of Anatolide-Tauride platform is represented by ophiolite obduction and foundering of platform (Şengör & Yılmaz 1981; Okay 1996, 2001; Göncüoğlu et al., 2000; Candan et al., 2002). These events are characterized by pelagic carbonate sedimentation and followed by deposition of flysch-type clastic sediments with carbonate and ophiolite blocks representing the propagation of the obducted ophiolites. The occurrence of HP/LT metamorphism under dominantly blueschist facies conditions in the main tectonic zones of the

Anatolides (Okay et al., 1996; Oberhaensli et al., 2001; Candan et al., 1997, 2002) display the subduction and following collusion processes of the Neotethys ocean during Albian-Eocene time. HP/LT metamorphism recognized in the western part of Menderes Massif which is one of the main tectonic units of Anatolides, can be attributed to this continues processes starting with closure of Neo-Tethyan ocean.

The sequence in the northwest part of Menderes Massif consists of two tectonic units; 1) Lower Triassic to Upper Cretaceous passive continental margin sediments with blueschist relicts and 2) the Metaolistostrome unit, probably Paleocene (?) in age, with blueschist and eclogite relicts (Candan et al., 1997;Candan & Çetinkaplan 2000; Çetinkaplan et al., 2000). The metamorphic evolution of the western part of Menderes Massif can be divided into three stages;

1) Foundering of Anatolide-Tauride platform related with obduction of oceanic crust and deposition of olistostromes on the main tectonic zones of the Anatolides: intra-oceanic subduction of Neo-Tethyan ocean and following ophiolite obduction caused to foundering of Anatolide-Tauride platform (Okay et al., 1996; Şengör & Yılmaz 1981). In Tavşanlı zone occurring in the northernmost margin of Anatolide-Tauride platform, this event begins with sedimentation of pelagic carbonates on the neritic carbonate during the Cenomanian. Candan et al., (2002) and Okay et al., (2001) suggests that related to the consumption of Neo-Tethyan ocean, the main tectonic zones of Anatolide-Tauride platform display a continues southward younging in terms of deposition of the sediments, tectonic and metamorphic events. In Afyon zone which has equivalent rocks of Menderes Massif, the transition from neritic to pelagic carbonate deposition occurred in Lower Maastrichtian time (Göncüoğlu et al., 1992). The olistostrome unit overlying the pelagic carbonates in Afyon zone deposited in Upper Maastrichtian – Lower Paleocene time interval (Göncüoğlu et al., 1992). In Menderes Massif, the foundering is represented by Late-Campanian – Late Maastrichtian aged red pelagic carbonates which conformably overlay the rudist-bearing platform type carbonates (Özer 1999). In the subsequent stage, pelagic carbonates are overlain by an olistostrome with carbonate and ophiolite blocks. The age of this blocky unit which is deposited in front of the obducted ophiolite slab, is

dated as Middle Paleocene in Milas and Lower-Middle Eocene in Çal (Denizli) (Özer et al., 2001). This shows that deposition of pelagic carbonate and olistostrome in main tectonic zones of Anatolide-Tauride platform is a continues process, from north to south which is directly related with the consumption of Neo-Tethyan ocean (Candan et al., 2002). In contrast to the southern flank of Menderes Massif, red pelagic carbonates in western part of Menderes Massif have not been recognized until today. This can be explained by the tectonic contact between platform type marble and olistostrome and missing some units during the exhumation.

2) Subduction of the Anatolide – Tauride platform and HP/LT evolution of the Triassic to Early Tertiary sequence of the Menderes Massif: The initiation of the closure of the Neo-Tethyan ocean related with intra-oceanic subduction has been assumed as Albian (Şengör & Yılmaz 1981; Okay et al., 1998). Obduction of the oceanic lithosphere, foundering of the Anatolide-Tauride platform, subduction of the northernmost passive continental margin sediments, Tavşanlı zone, of Anatolide-Tauride platform started Albian time and lasted until the Late Eocene time as a continues southward younging process. In the present, the main tectonic zones from north to south can be characterized by the imbricated metamorphosed thrust sheets which have been formed with subsequent tectonic development during subduction of Anatolite-Tauride platform (Candan et al., 2002). In this process, Mesozoic – Early Tertiary sequence of the Menderes Massif was buried to a depth at about 38 km, and has been underwent HP/LT metamorphism after the following stages of the HP/LT metamorphism of the main tectonic units of the Anatolides; Tavşanlı zone, Lycian nappes and Afyon zone (Candan et al., 2002). Passive continental margin sediments and olistostrome in western part of Menderes Massif underwent progressive epidote-blueschist facies metamorphism related with this northward-directed subduction during Middle-Late Eocene time ($^{40}Ar/^{39}Ar$ phengite cooling age, Oberhaensli et al., 1998).

Although platform sequence and the matrix of overlying olistostrome in the Menderes Massif have been subjected to epidote-blueschist facies metamorphism. The olistostrome contains numerous eclogite, omphacite-epidotite and omphacite

metagabbro blocks. The blocks representing mineral assemblages of two different metamorphism i.e; eclogite and blueschist, coexist in the Metaolistostrome unit. This can be explained by two ways: **a)** the protoliths of the eclogite - omphacite metagabbro – omphacite epidotite blocks which are closely related with ultrabasic rocks, are joined into olistostrome as passive blocks in front of the advancing ophiolite nappe in Paleocene (Figure 7.4a). During the Paleocene, while olistostrome deposition was continuing in the Menderes Massif, Afyon Zone was subjected to HP/LT metamorphism (Figure 7.4b). In the Eocene, Mesozoic-Early Tertiary series of the Menderes Massif have been buried to different depths. Some parts of this series buried to greater depths, were suffered to eclogite facies metamorphism. Whereas the rest of this series, which was relatively shallower in depth (38 km), have been undergone to epidote-blueschist metamorphism (Figure 7.4b). During the exhumation process, some of the deeply buried parts of the series may be emplaced into the olistostrome in the shallower depths as tectonic slices. No evidence about the effects of the Tertiary HP/LT metamorphism on Paleozoic and Pan-African series of the Menderes Massif have been recognized yet. This can be explained that Paleozoic and Pan-African series should have not been subducted to the same depths with Mesozoic-Early Tertiary series of the Menderes Massif during the Eocene time (Figure 7.4b). According to the mineral assemblage of the Triassic leucocratic granites intruded into the Pan-African series, 20 km depth for the burial of the Pan-African basement and overlying Paleozoic series of the Menderes Massif can be assumed (Koralay 2001). This Eocene MP/MT metamorphism can be attributed to the burden of the overlying Lycian nappes and peridotite slab. During the Oligocene time, HP series of the Mesozoic-Early Tertiary sequence raised to the shallower depths along a major tectonic zone and juxtaposed with the Paleozoic and Pan-African series of the Menderes Massif. The Rb/Sr muscovite ages from both of the Pan-African gneisses and Triassic leucocratic granites between 29.8 – 26.2 Ma (Koralay et al., 1998), can be interpreted as the time of the retrograde overprint of the Pan-African and overlying Mesozoic-Early Tertiary HP series (Figure 7.4c). The common presence of the Early Miocene lacustrine sediments on the Menderes Massif (Yılmaz et al., 2000) that the uplift and exhumation of the Menderes Massif occurred before Early Miocene time (Figure 7.4d). **b)** the eclogite - omphacite metagabbro –

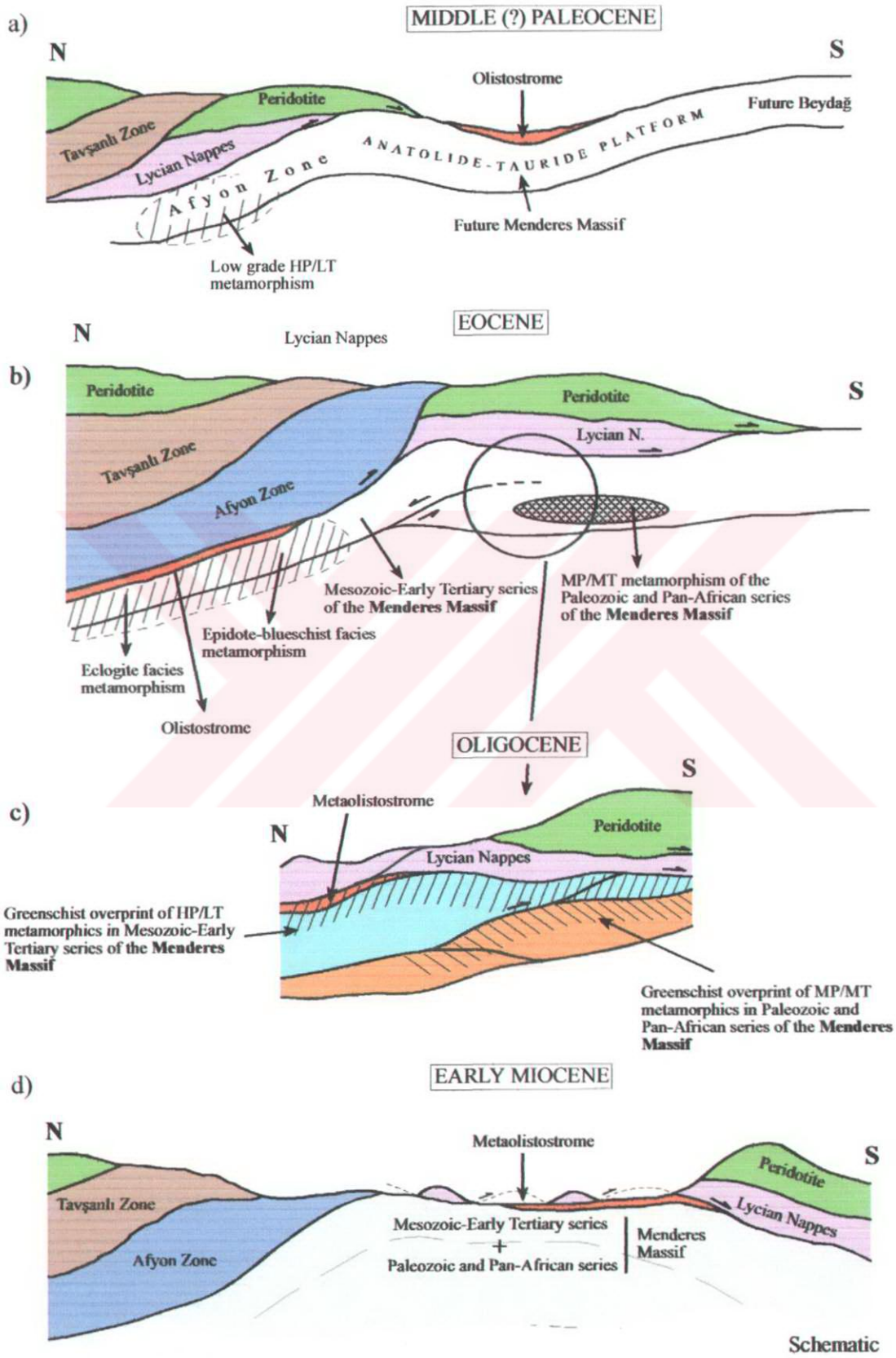


Figure 7.4. Schematic representation of the tectonic evolution of the Eocene HP/LT series of the Menderes Massif.

omphacite epidotite blocks are joined into olistostrome as metamorphosed passive blocks in front of the advancing ophiolite nappes in Paleocene and subducted to 38 km depth with surrounding olistostrome. In this depth, olistostrome have been subjected to epidote-blueschist facies metamorphism in the Eocene time. During the exhumation, blocks and matrix of the olistostrome was affected by greenschist overprint. However, this tectonic model is not consistent well with the general characteristics of the tectonic zones of the Anatolides occurring of the northern part of the Menderes Massif. The existence of the eclogite, omphacite metagabbro and omphacite epidotite have not been reported from the Lycian nappes and Afyon Zone. On the other hand, the eclogite occurrence is extremely rare in Tavşanlı Zone. On the contrary to the common occurrence of the eclogites in metaolistostrome of the Menderes Massif, only one occurrence have been detected in Sivrihisar region (Kulaksız 1981). In addition, the eclogites in Sivrihisar, Tavşanlı zone, are characterized by the presence of glaucophane. Furthermore, during the Paleocene time Tavşanlı Zone is situated quite far away from the Menderes Massif and separated by the exhumed Lycian nappes and overlying peridotite slab. According to this paleogeographical position, the transportation of the eclogites from Tavşanlı Zone seems as a very low possibility.

3) The possible exhumation models of the Triassic-Early Tertiary sequence of the western part of Menderes Massif: In Tavşanlı zone occurring in northernmost margin of Anatolide-Tauride platform, blueschist exhumation is attributed to a combination of detachment in the upper crust and buoyancy of subducted continental lithosphere and progressive shallowing of the subduction zone by Okay et al., (1998). However, this exhumation model for Tavşanlı zone can not explain the HP/LT metamorphism of the Lycian nappes, Afyon zone and Menderes Massif. In the same area, Sherlock et al., (1999) suggested that the preservation of blueschists is related with synchronous subduction and exhumation by the underplated cold continental crustal material. Oberhaensli et al., (2001) suggest two exhumation models for preservation of Fe-Mg carpholite occurrences at the base of Lycian nappes;

- A simple-shear related exhumation and nappe-transport model that resulted in cool retrograde P-T path (Ruppel et al., 1988). Simple shear produces retrograde P-T path

with simultaneous cooling and uplift on the set of exhumation. This model is same with that of Sherlock et al., (1999).

- Pure shear related exhumation: This model produces retrograde P-T paths where isothermal decompression is more important than cooling (Ruppel et al., 1988). Oberhaensli et al., (2001) emphasizes that simple shear model for exhumation and nappe transport is of major importance and result in cool retrograde paths. This model may be suitable for preservation of Fe-Me carpholite (low grade HP/LT metamorphism) close to major shear zones at the base of Lycian nappe stack. But, P-T paths obtained from Triassic-Early Tertiary sequence in the western part of Menderes Massif (Figure 6.13) display isothermal decompression conditions during the exhumation. In this area, mineral assemblages related to HP/LT metamorphism are partly preserved from greenschist overprint, except for Tire area. This may be explained by pure shear related exhumation model of Ruppel et al., (1988). This model contains retrograde P-T path in isothermal decompression conditions, rapid tectonic transport, preservation of HP/LT assemblages and intense deformation. These features also exist in detachment zones which are dominant mechanism for exhumation of high-pressure metamorphic assemblages in Aegean region (Jolivet et al., 1994; Avigad et al., 1997).

CHAPTER EIGHT

CONCLUSIONS

1) In Dilek Peninsula, Selçuk, Torbalı, Tire and Gölmarmara areas, the lowest part of Menderes Metamorphics consists of Paleozoic detrital and carbonate rocks are overlain by Lower Triassic – Upper Cretaceous sequence. This sequence is mainly composed of, in ascending order, mica schist / garnet-mica schist with marble, metaquartzite, phyllite, mafic volcanic rock and metaconglomerate intercalations, and metabauxite-bearing marble. Lower Triassic-Upper Cretaceous series is tectonically overlain by the Metaolistostrome unit. Lycian Nappes occur as small klippen lying on top of the Metaolistostrome unit.
2) HP/LT metamorphism under epidote-blueschist facies conditions is represented by blueschist metabasite / metapelites and kyanite-chloritoid-phengite assemblage in Lower Triassic-Upper Cretaceous passive continental margin series.
3) HP/LT metamorphism in the Metaolistostrome unit is characterized by blocks which have been subjected to eclogite and epidote-blueschist facies metamorphisms. Eclogite facies metamorphism is represented by eclogite, omphacite epidotite and omphacite metagabbro blocks. Whereas, blueschist metabasite blocks and phengite-bearing matrix of metaolistostrome display the epidote-blueschist facies conditions.
4) Eclogite and related blocks should have been incorporated into the Metaolistostrome unit as tectonic slices during the exhumation.

5) Garnets in the Metaolistostrome unit and the Marble-schist series commonly display normal growth zoning. Increase in pressure is demonstrated by prominent Fe-enrichment and minimum Mn content of garnet.
6) P-T conditions of subducted related epidote-blueschist facies metamorphism is about 11 kbar and 450 °C. Following greenschist overprint occurred under 6 kbar pressure and 480-490 °C temperature conditions.
7) The preservation of blueschist assemblages reveals the presence of approximately isothermal decompression during rapid uplift and exhumation of HP/LT rocks.
8) Western part of Menderes Massif, Dilek Peninsula-Selçuk-Torbalı-Tire-Akhisar (Gölmarmara), underwent progressive epidote-blueschist metamorphism in Eocene time which is subsequently followed by re-equilibration during isothermal decompression under greenschist facies conditions.
9) Eocene HP/LT metamorphism in Menderes Massif is a result of continues process which is directly related with the consumption of Neo-Tethyan ocean.
10) Geological, petrological, mineralogical and stratigraphical similarities of Eocene HP/LT rocks of Menderes Massif with Samos Island as well as Cycladic Complex reveal the common tectono-metamorphic evolution of two crystalline complex during the Eocene time.

REFERENCES

Altherr, R., Schliestedt, M., Okrusch, M., Seidel, E., Kreuzer, H., Harre, W., Lenz, H., Wendt, I. & Wagner, G.A., (1979) Geochronology of high-pressure rocks on Sifnos (Cyclades, Greece). Contrib. Mineral . Petrol., 70, 245-255.

Anderson. D.E. & Olimpio, J.C. (1977) Progressive homogenization of metamorphic garnets, South Morar, Scotland: Evidence for volume diffusion. Canadian Mineralogist. 15, 205-216.

Andriessen, P.A.M., Boelrijk, N.A.I.M., Hebeda, E.H., Priem, H.N.A., Verdurmen, E.A.Th. & Verschure, R.H., (1979) Dating the events of metamorphism and granitic magmatism in the Alpine Orogen of Naxos (Cyclades, Greece). Contrib. Mineral. Petrol., 69, 215-225.

Atherton , M.P & W.M. Edmunds (1966) An electron microprobe study of some zoned garnets from metamorphic rocks. Earth planet Sci. Lett., I, 185-193.

Avigad, D. & Garfunkel, Z., (1991) Low-angle faults above and below a blueschist belt-Tinos Island, Cyclades, Greece. Terra Nova, 1, 182-187.

Avigad, D. , Matthews, A., Evans, B., & Garfunkel, Z., (1992) Cooling during the exhumation of a blueschist terrane: Sifnos (Cyclades), Greece. Eur. J. Mineral, 4, 619-634.

Avigad, D., Garfunkel, Z., Jolivet, L., & Azanon, J.M. (1997) Back arc extention and denudation of Mediterranean eclogites. Tectonics, 16: 924-941.

Bahaskar Rao, B., & Johannes, W., (1979) Further data on stability of staurolite + quartz and related assemblages. Neues Jahrb. Mineral. Monatsh., p.437-447.

Başarır, E., (1970) Bafa Gölü doğusunda kalan Menderes Masifi güney kanadının petrografisi ve jeolojisi . Ege Üniversitesi, Fen. Fak. Yayınları., no.102 İzmir/Turkey.

Bethune, P. de, D. Laduron & J. Bocquet (1975) Diffusion processes in resorbed garnets. Contrib. Mineral. Petrol., 50, 197-204.

Bhattacharya, A., Mohanty, L., Maji, A., & Sen, S.K. (1992) Non-ideal mixing in the phlogopite-alline binary: contrasts from experimental data on Mg-Fe partitioning and a formulation of the biotite-garnet geothermometry. Contrib. Min. Petr. 111, 87-93.

Biermann, C., (1981) (100) deformation twins in naturally deformed amphiboles. Nature, 292, 821-823.

Blatt, H. & Tracy, R. (1999) Petrology igneous, sedimentary and metamorphic. Second ed. Third printing. W.H. Fremann & Company, 529p.

Bonneau, M., Blake, M.C., Geyssant, J., Kienast, J.R., Lepvrier, C., Maluski, H., Papanikolaou, D. (1980) Sur la signification des rochers metamorphiques (schistes blues) des Cyclades (Hellenides, Greece). L'example de I'ile de Syros. C.R. Acad. Sci., Paris, D, 290, 1463-1466.

Bozkurt, E., & Oberhaensli, R., (2001) Menderes Massif (Western Turkey): structural, metamorphic and magmatic evolution –a sythesis. Int. J. Earth Sci. 89, 679-708.

Brinkman, R., (1967) Die südflanke des Menderes-Massivs bei milas, Bodrum und Ören. Scient. Rep. Fac. Sci. Ege Univ. 43, 3-12.

Brown, E.H. (1976) The crossite content of Ca-amphiboles as a guide to pressure of metamorphism. Journal of Petrology, v.18, part 1, pp. 53-72.

Brown, E.H. (1977) The crossite content of Ca-amphiboles as a guide to pressure of metamorphism. Journal of Petrology. 18, 53-72.

Bröcker, M., (1990) Blueschist-to-greenschist transition in metabasites from Tinos Island, Cyclades, Greece: Compositional control or fluid infiltration. Lithos, 25:25-39.

Bröcker, M., & Enders, M., (1999) U-Pb zircon geochronology of unusual eclogite-facies rocks from Syros and Tinos (Cyclades, Greece). Geological Magazine 136, 111-118.

Bröcker, M., Kreuzer, H., Matthews, A., & Okrush, M. (1993) $^{40}Ar/^{39}Ar$ and oxygen isotope studies of polymetamorphism from Tinos Island, Cycladic blueschist belt, Greece. Journal of Metamorphic Geology, 11, 223-240.

Bucher , K., & Frey, M.,(Eds). (1994) Petrogenesis of metamorphic rocks. Springer – Verlag, p.318.

Buick, I.S. & Holland, T.J.B. (1987) Structural and thermal evolution of the migmatitic core and its schist envelope on Naxos, Greek Cyclades. Terra cognita, 7, 170.

Candan, O., (1995) Menderes Masifi'nde kalıntı granulit fasiyesi metamorfizması (in Turkish with English Abstract). Turkish J. Earth Sci 4: 35-55.

Candan, O., & Çetinkaplan, M., (2001) Menderes Masifi'nde eklojit/epidot-mavişist metamorfizmaları ve Kikladik Kompleksle korelasyonu. YDABÇAG-494 nolu TÜBİTAK projesi, p.188.

Candan, O., Çetinkaplan, M., Oberhaensli, R. & Rimmele, G., (2002) Fe-Mg Carpholite – pyrophyllite – chloritoid – bearing Triassic metapelites from Afyon Zone; Turkey: First evidence for Alpine low-grade, high-P / low-T metamorphism. 1st International Symposium of Faculty of Mines (İTÜ) on Earth Sciences and Engineering. p. 107.

Candan, O. & Dora., O.Ö, (1998) Menderes Masifi'nde granulit, eklojit ve mavi şist kalıntıları: Pan-Afrikan ve Tersiyer metamorfik evrimine bir yaklaşım. Türkiye Jeoloji Bült 41 (1), 1-35

Candan, O., Dora, O.Ö, Dürr, S.T. & Oberhaensli, R., (1994) Erster Nachweis von Granulit-und Eklogit-Relicten im Menderes Massiv / Türkei. Gaattinger. Abr. Geol. Palaont. 5.Symposium TSK 217-220, 2 Abb.

Candan, O., Dora, O.Ö., Oberhaensli, R., Oelsner, F. & Dürr, S., (1997) Blueschist relicts in the Mesozoic cover series of the Menderes Massif and correlations with Samos Island, Clclades. Schweiz. Mineral Petrogr. Mitt. 77, 95-99.

Candan, O., Dora, O.Ö, Oberhaensli, R., Çetinkaplan, M., Oelsner, F. & Dürr, S., (1998) Menderes Masifi'nde iki farklı yüksek basınç metamorfizması: Pan-Afrikan ve Tersiyer olaylar. 51. Türkiye Jeoloji Kurultayı (Abstracts), Ankara, 52.

Candan, O., Dora, O.Ö, Oberhaensli, R., Çetinkaplan, M., Partzsch, J., & Dürr, S., (1999) Tertiary high-pressure/low temperature metamorphism in the northwest part of the Menderes Massif and correlation with the Cycladic Compex, Greece. Geological Bulletin of Turkey, Vol.41, No.1, 1-14.

Candan, O., & Kun, N., (1989) Menderes Masifi'nin batısında paleomelanj kuşağının varlığı. TPJD Bült., 1/3, 237-251.

Carswell, A.D. (1990) Eclogite facies rocks. Blackie, 396 p.

Carswell, D.A. & Harley, S.L. (1990) Mineral barometry and thermometry. In Carswell ,D.A.(Ed.), Eclogite facies rocks. Chapman and Hall. 396p.

Carswell, D.A., O'Brien, P:J., Wilson, R.N., Zhai, M. (1997) Thermobarometry of phengite bearing eclogites in Dabie mountains of central China. J. Metamorphic Geol., 75, 239-252.

Chen, G., (1992) Evolution of the high- and medium- pressure metamorphic rocks on the island of Samos, Greece. Ph.D. Thesis. Julius-Maximilians University, Würzburg, 170 p.

Chen, G., Okrush, M., & Sauerschell, W., (1995) Polymetamorphic evolution of high-pressure rocks of Samos, Greece. IESCA Proc, pp 359-365.

Chopin, C. & Schreyer, W. (1983) Magnesiocarpholite and magnesiochloritoid: two index minerals of pelitic blueschist and their preliminary phase relations in the model system MgO-Al_2O_3-SiO_2-H_2O. Am J. Sci., 283-A, 72-96.

Coleman, R.G., Lee, D.E., Beatty, L.B., & Brannock, W.W. (1965) Eclogites and eclogites: Their differences and similarities. Geol. Soc. Am. Bull. 76: 483-508.

Crawford, M.L. (1974) Calcium zoning in almandine: a model based on plagioclase equilibria. In The Feldspars. Manchester University Press, 629-644.

Çağlayan, M.A., Öztürk, E.M., Öztürk, Z., Sav, H., & Akat, U., (1980) Menderes Masifi güneyine ait bulgular ve yapısal yorum (in Turkish with English Abstract). Geol. Eng. Turkey 10, 9-19.

Çetinkaplan, M., 1995, Geochemical mineralogical and petrographical investigation of the eclogites in southern part of Tire area, Ödemiş - Kiraz Submassif of Menderes Massif. Unpublished Master Theses, D.E.U. Graduate School of Nature and Applied sciences, 92pp.

Çetinkaplan, M., Oberhaensli, R., & Candan, O., (2000a) Eclogite and blueschist relics in the Mesozoic cover series of the Menderes Massif: a Tertiary subduction-related high-pressure metamorphism. 53. Türkiye Jeoloji Kurultayı (Abstracts), Ankara, 311.

Çetinkaplan, M., Oberhaensli, R., & Candan, O., (2000b) Tertiary high-pressure / low temperature metamorphism in the Mesozoic-Early Tertiary series of the Menderes Massif and correlation with the Cycladic Complex, Greece. In: O.Ö. Dora, İ. Özgenç, H. Sözbilir (Ed), IESCA 2000-Abstracts, İzmir, 140.

Deer, W.A. Howie, R.A. & Zussman, J (1992) The rock forming minerals. 2nd Edition. Longman Scientific, 696p.

Dixon, J.E., (1969) The metamorphic rocks of Syros, Greece. Unpubl. Ph.D. thesis, University of Cambridge.

Dixon, J.E. & Ridley, J.R., (1984) Syros. In Helgeson, H.C. (ed), Chemical transport in metasomatic processes, 489-501, Reidel Publising Company.

Dodson, M.H. (1976) Kinetic processes and thermal history of slowly cooling solids. Nature, 259, 551-553.

Dora, O.Ö, Kun, N. & Candan, O., (1990) Metamorphic history and geotectonic evolution of the Menderes Massif. In: M.Y. Savaşçın, A.H. Eronat (Ed), Proceedings of International Earth Sciences Congress on Aegean Regions, İzmir, 2, 102-115.

Dora, O.Ö., Candan, O., Oberhaensli, R., & Dürr, St. (1995) New evidence on the geotectonic evolution of the Menderes Massif. In: Ö Pişkin, M Ergün, MY Savaşçın, G Tarcan (Ed), Proceedings of International Earth Sciences Colliquim on the Aegean Region, İzmir, 1, 53-72.

Draper, G. & Bonne, R. (1981) Denudation rates, thermal evolution, and preservation of blueschist terrains. J. Geol., 89: 601-613.

Dürr, St., (1975) Uber Alter und geotektonische Stellung des Menderes Kristallins / SW -Anatolien und seine Equivalente in der Mittleren Aegean. Unpublished Habilitation thesis, University of Marburg, 107 p.

Dürr, S., Alther, R., Keller, J., Okrush, M., & Seidel, E., (1978) The median Aegean crystalline belt: Stratigraphy, structure, metamorphism, magmatism. Closs, H.,

Roeder, D.R., Schmidt, E., (Eds), Alps, Apennines, Hellenides. Schweizerbart, Stuttgart, 445-477.

Draper, G.R, & Bone, R. (1981) Denudation rates, thermal evolution and preservation of blueschist terrains. J. Geol., 89, 601-613.

Edmunds, W. M. & Atherton, M.P. (1971) Polymetamorphic evolution of garnet in the Fanad aureole, Donegal, Eire. Lithos 4, 148-161.

Ellis, D.J. & Green, D.H. (1979) An experimental study of the effect of Ca upon garnet-clinopyroxene Fe-Mg exchange equilibria. Contrib. Mineral. Petrol., 71, 13-22.

England, P.C. & Richardson, S.W. (1977) The incluence of erosion upon the mineral facies of rocks from different metamorphic environment. J. Geol. Soc. Lond., 134, 201-213.

England, P.C. & Thompson, A.B. (1984) Temperature-pressure-time paths of regional metamorphism. I: heat transfer during the evolution of regions of thickened continental crust. J. Petrol., 25, 894-928.

Erdoğan , B., & Güngör, T., (1992) Stratigraphy and tectonic evolution of the northern margin of the Menderes Massif, Turkish Association of Petroleum Geologist Bulletin. 4/1, 9-34.

Ernst, W.G. (1976) Mineral chemistry of eclogites and related rocks from the Voltri group, Western Liguria, Italy. Schweiz. Mineral. Petrogr. Mitt. 56, 293-343.

Ernst, W.G. (1979) Coexisting sodic and calcic amphiboles from high-pressure metamorphic belts and the stability of barroisitic amphibole. Miner. Mag. 43, 269-278.

Ernst, W.G. & Dal Piaz, G.V. (1978) Mineral parageneses of eclogitic rocks and related mafic schists of the Piemonte ophiolite nappe, Breuil-St. Jacques area, Italian Western Alps. American Mineralogist, 63, 621-640.

Essene, E.J. & Fyfe, W.S. (1967) Omphacite in Californian metamorphic rocks. Contrib. Mineral. Petrol., 15, 1-23.

Evans, B.W. (1966) Microprobe study of zoning in eclogite garnets. Geol. Soc. Am. Spec. paper, 87,54.

Evans, B.W & Patrick, B.E (1987) Phengite-3T high-pressure metamorphosed granitic orthogheisses, Seward Peninsula, Alaska. Canadian Mineralogist, 25, 141-158.

Florance, F.P. & Spear, F.S. (1991) Effects of diffusional modification of garnet growth zoning on P-T path calculations. Contrib. Mineral. Petrol., 107, 487-500.

Gapais, D., & White, S.H. (1982) Ductile shear bands in a naturally deformed quartzite. Text. Microstruct 5,1-17.

Gessner, K., Piazolo, S., Güngör, T., Ring, U., Kröner, A., & Passchier C.W. (2000) Tectonic significance of deformation patterns in granitoid rocks of the Menderes Nappes, Anatolide belt, southwest Turkey. Int. J. Earth Sci., 89, 766-780.

Gessner, K., Ring, U., Passchier, C.W. & Güngör, T., (2001a) How to resist subduction: evidence for large-scale out-of-sequence thrusting during Eocene collision in western Turkey. Journal of the Geolocical Society, 158, 769-784.

Göncüoğlu, M.C., Özcan, A. Turhan, N. & Işık, A. (1992) Stratigraphy of the Kütahya region. ISGB-92 Guide Book, 3-8.

Göncüoğlu, M.C., Turhan, N., Şentürk, K., Özcan, A., Uysal, Ş., & Yalınız, M.K., (2000) A geotraverse across northwestern Turkey: tectonic units of the central Sakarya region and their tectonic evolution. In: Bozkurt E, Winchester, J.A. Piper J.D.A (Ed) Tectonics and magmatism in Turkey and the surrounding area. Geol. Soc. Lond. Spec. Publ. 173, 139-161.

Graham, C.M., & Powell, R., (1984) A garnet-hornblende geothermometer: calibration testing and application to the Pelona schist, Southern California. J. Metam. Geol. 2, 13-31.

Green, D.H., & Hellman, P.L., (1982) Fe-Mg partitioning between coexesting garnet and phengite at high pressure, and comments on a garnet-phengite geothermometer. Lithos, 15, 253-266.

Gutnic, M., Monod, O., Poisson, A. & Dumont, J.F., (1979) Geologie des Taurides Occidentales (Turquie). Mem Soc Geol France 137, 1-40.

Güngör.,T. (1998) Stratigrahpy and tectonic evolution of the Menderes Massif in the Söke-Selçuk region. PhD thesis. Unpublished. D.E.U. 147 p.

Haas, H. (1971) Equilibria in the system Al_2O_3-SiO_2-H_2O involving the stability limits of diaspore and pyrophyllite and thermodynamic data of these minerals. PhD thesis.

Haas, H., (1972) Equilibria in the system Al_2O_3-SiO_2-H_2O involving the stability limits of diaspore and pyrophyllite, and metamorphic data on these minerals. American Minereralogist., 57, 1375-1385.

Haas, H., & Holdaway, M.J. (1973) Equilibria in the system Al_2O_3-SiO_2-H_2O involving the stability limits of pyrophyllite and thermodynamic data of pyrophyllite. Am. J. Sci. 273, 449-456.

Hecht, J., (1984) Geological map of Greece 1:50.000 Syros island. Inst. Geol. Mineral Exploration, Athens.

Heinrich, W. & Althaus, E. (1980) Die obere Stabilitaetsgranze von lawsonite plus albite bzw. Jadeite. Fortschr: Miner., 58 Beih. 1, 49-50.

Hetzel, R & Reischmann, T., (1996) Intrusion age of Pan - African augen gneisses in the southern Menderes Massif and the age of cooling after Alpine ductile extensional deformation. Geol. Mag., 133 , 565 - 572.

Holdaway, M.J. (1971) Stability of andalusite and the aluminum silicate phase diagram. Am. J. Sci. 271, 97-131.

Holland, T., & Blundy, J. (1994) Non-ideal interactions in calcic amphiboles and their bearing on amphibole-plagioclase thermometry. Contrib. Min. Petr. 116: 433-447.

Hollister, L.S (1966) Garnet zoning: an interpreation based on the Rayleigh – fractionation model. Science 154: 1647-1651.

Holland, T.J.B. (1979) Experimental determination of the reaction paragonite= jadeite+kyanite+H2O and internal consistent thermodynamic data for part of the system Na_2O-Al_2O_3-SiO_2-H_2O, with application to eclogites and blueschists. Contrib Mineral. Petrol., 68, 293-301.

Holland, T.J.B. (1980) The reaction albite=jadeite+quartz determined experimentally in the range 600-1200 °C. Amer. Mineral., 65, 129-134.

Höpfer, N. (1989) Petrologie der metagabbros und eclogite von Syros (Kykladen, Griechland). Diploma thesis, Universitat Bonn, 128 pp.

Humpries, S.E. (1984) The mobility of the rare earth elements in the crust. In: Henderson P. (ed.), Rare earth element geochemistry. Elsevier, Amsterdam, pp. 315-341.

Jacobshagen, V. (1986) Geologie von Griechenland. Berlin: Gebrüder Borntraeger.

Jansen, J.B.H. & Schuling, R.D. (1976) Metamorphism on Naxos: Petrology and geothermal gradients. American Journal of Science., 276, 1225-1253.

Johannes, W. & Puhan, D. (1971) The calcite-aragonite transition, reinvistegated. Contrib Mineral. Petrol., 31, 28-38.

Jolivet, L., Brun, J-P., Gautier, P., Lallemant, S., and Patriat, M. (1994) 3D-kinematics of extension in the Aegean region from the early Miocene to the present, in sights from the ductile crust. Bull. Soc. geol. France, 165, 195-200.

Jolivet, L., Goffe, P., Monie, C., Patriat, Truffet-Luxey. M. & Bonneau, M. (1996) Miocene detachment in Crete and exhumation P-T-t paths of high-pressure metamorphic rocks. Tectonics, 15, 1129-1153.

Konak, N., Akdeniz, N. & Öztürk, E.M., 1987, Geoylogy of the south of Menderes Massif, I.G.C.P. project no:5, Giude book, Correlation of Variscan and pre-Variscan events of the alpine-mediterranean mountain belt, Field Meeting, Turkey, 42-53.

Konak, N., Akmakoğlu, A., Elibol, E, Havzoğlu, T., Hepşen, N., Karamanderesi, Ü.H., Keskin, H., Sarıkaya, H., Sav, H. & Yusufoğlu, H., (1994) Menderes Masifi'nin orta kesimlerindeki bindirmeli yapıların gelişimi. 47. Türkiye Jeoloji Kurultayı Bildiri özleri, p.34.

Koralay, E. (2001) Geology, geochemistry and geochronology of granitic gneisses and leucocratic orthogneisses at the eastern part of Ödemiş-Kiraz submassif, Menderes Massif: Pan-African and Triassic magmativ activity. Ph.D. thesis (unpublished). D.E.U, 191 p.

Koralay, E., Satır, M. & Dora, O.Ö. (1998) Geochronologic evidence of Triassic and Precambrian magmatism in the Menderes Massif, west Turkey. III. International Turkish Geology Symposium (Abstracts), Ankara, 285 .

Kretz, R. (1973) Kinetics of the crystallization of garnet at two localities near Yellowknife. Can. Mineral. 12, 1-120.

Krogh, E.J. & Raheim, A. (1978) Temperature and pressure dependence of Fe-Mg partitioning between garnet ahd phengite with particular reference to eclogites. Contrib. Mineral. Petrol., 66, 75-80.

Kryza, R., Muszynski, A., & Vielzeuf, D. (1990) Glaucophane-bearing assemblage overprinted by greenschist-facies metamorphism in the Variscan Kaczawa complex, Sudetes, Poland. J. metamorphic Geol., 8, 345-355.

Kulaksız, S., (1981) Geology of the region of northwest of Sivrihisar (in Turkish). Yerbilimleri, 8, 103-124.

Laird, J. & Albee, A. L., (1981) Pressure, temperature, and time indicators in mafic schist: Their aplication to reconstructing the polymekamorphic history of Vermont. American Journal of Science, 281, 127-175.

Leake, B.E., Winchell, H., Binns, A., Kato, A., Gottardi, G., Fonteilles, E., Hilmy, E., Neuvonen, K., & Kirsh, H.J. (1978) Nomenclature of amphiboles. Mineralogical Magazine, vol 42, pp 553-563.

Linthout, K & Westra, L. (1968) Compositional zoning in almandine rich garnets and its relation to the metamorphic history of their host rocks. Konink. Nederl. Akad. Wetensch. Proc., Ser. B, 71, 297-312.

Lips, A.L.W, Cassard, D. Sözbilir, H. Yılmaz, H., (2001) Multistage exhumation of the Menderes Massif, western Anatolia (Turkey). Int. J. Earth Sci. 89, 781-792.

Lister, G.S., Banga, G., & Feenstra, A., (1984) Metamorphic core complexes of Cordilleran type in the Cyclades, Aegean Sea, Greece. Geology, v.12, p.221-225.

Lister, G.S., Banga, G. & Feenstra, A. (1984) Metamorphic core complexes of Cordilleran type in the Cyclades, Aegean Sea, Greece. Geology, 12: 221-225.

Loomis, T. P. (1975) Reaction zoning of garnet. Contrib. Mineral. Petrol., 52, 285-306.

Loomis, T.P. & Nimick, F.B. (1982) Equilibrium in MnFeMg aluminous pelitic compositions and the equilibrium growth of garnet. Canadian Mineralogist, 20, 393-410.

Maluski, H., Bonneau, M, & Kienast, J.R. (1987) Dating the metamorphic events in the Cycladic area: $^{39}Ar/^{40}Ar$ data from metamorphic rocks of the island of Syros (Greece). Bulletin de la Societe geologique de France, 8, 833-842.

Maruyama. S., Suzuki. K., & Liou, J.G., (1983) Greenschist-amphibolite transition equilibria at low pressures: Journal of Petrology, 24, 583-604.

Massonne, H.J. & Schreyer, W. (1989) Stability fied of high-pressuri assemblage talc+phengite and two new phengite barometers. Eur. J. Mineral, 1, 391-410.

Mengel, F. & Rivers, T., (1990) Decompression reactions and P-T conditions in high-grade rocks, Northern Labrodor: P-T-t paths from individual samples and implications for Early Proterozoic tectonic evolution. Journal of Petrology, 32, 139-167.

Morimoto, N., Fabries, J., Ferguson, A.K., Ginzburg, I.V., Ross, M., Seifert, F.A., & Zussman, J.Z. (1988) Nomenclature of pyroxenes. Amer. Min. v.73, p 1123-1133.

Möller, C. (1998) Decompressed eclogites in the Sveconorwegian (-Grenvillian) orogen of SW Sweden: petrology and tectonic implications. J. metamorphic Geol., 16, 641-656.

Mposkos, E., (1978) Diasporite – und Schmirgelvorkommen der Insel Samos (Griechenland). 4th internat. Congr. 2, 614-631.

Mposkos, E. & Perdikatsis, V., (1984) Petrology of glaucophane metagabbros and related rocks from Samos. Aegean Island (Greece). N.Jb. Min. Abh. 149, 1, 43-63.

Müller, G. & Schneider, A. (1971) Chemistry and genesis of garnets in metamorphic rocks. Contrib Mineral. Petrol., 31, 178-200.

Nitsch, K.H. (1974) Neue Erkenntnisse zur stabilitat von Lawsonit. Fortschr. Miner., 51, Beiheft 1, 34-35.

Oberhaensli, R ., Candan, O., Dora,O.Ö & Dürr, St., (1997) Eclogites within the Menderes crystalline complex / western Turkey /Anatolia. Lithos , 41, 135-150.

Oberhaensli, R., Monie, P., Candan, O., Warkus, F., Partzsch, J.H., & Dora, O.Ö., (1998) The age of blueschist metamorphism in The Mesozoic cover series of the Menderes Massif. Schweiz. Mineral. Petrogr. Mitt., 78, 309-316.

Oberhaensli, R., Partzsch, J., Candan, O., & Çetinkaplan, M., (2001) First occurrence of Fe-Mg-carpholite documenting a high-pressure metamorphism in

metasediments of the Lycian Nappes, SW Turkey. Int. J. Earth Sci. 89: 867-873.

Oelsner, F., Candan, O., & Oberhaensli, R., 1997, New evidence for the time of the high grade metamorphism in the Menderes Massif, SW-Turkey. Geologische Vereinigung, Zürich.1p

Okay, A.İ., (1989) An exotic/blueschist slice in a Barrovian-style metamorphic terrain, Alanya nappes, southern Turkey. Journal of Petrology., 30, 107-132.

Okay, A.I. (2001) Stratigraphic and metamorphic inversions in the central Menderes Massif: a new structural model. Int. J. Earth Sci. 89: 709-727.

Okay, A.I., Harris, N.B.W., & Kelley, S.P., (1998) Exhumation of blueschists along a tethyan suture in northwest Turkey. Tectonophysics, 285, 275-299.

Okay, A.I., Satır, M., Maluski, H., Siyako, M., Monie, P., Metzger, R., & Akyüz, S., (1996) Paleo- and Neo- Tethyan events in northwest Turkey: geological and geochrononical constrains. In: Yin, A., Harrison, M. (eds), Tectonics of Asia. Cambridge University Press, Cambridge, pp. 420-441.

Okay, A.I., Tanseli, İ., & Tüysüz, O., (2001) Obduction, subduction and collision as reflected in the Upper Cretaceaous-Lower Eocene sedimentary record of western Turkey. Geol. Mag. 138 (2), pp. 117-142.

Okrusch, M., Richter, P. & Katsikatsos, G., (1985) High pressure rocks of Samos, Greece. In: The geological evolution of Eastern Mediterrenean Geol. Soc. London. Spec. Pub. 17, (ed.) Dixon and Robertson., 529-536.

Okrush, M., & Brocker, M., (1990) Eclogites associated with high grade blueschist in the Cyclades archipellago. Greece: A review. Eur. J. Mineral., 2, 451-478.

Önay, T.S., (1949) Über die smirgelgesteine SW-Anatoliens. Schweiz. Min Petr. Mitt. 29: 359-484.

Özer, S., (1993) Upper Cretaceous rudists from the Menderes Massif. 6th. Cong. of the Geol. Soc. of Greece Bull. XXVIII, 3, 55-73.

Özer, S., (1998) Rudist bearing upper Cretaceous metamorphic sequences of the Menderes Massif (Western Turkey). Geobios Mem. Spec.22, 235-249

Özer, S., (1999) Description of the genus Distefanella Parona (Rudist, Bivalvia) in the Cenomainan of western Turkey. Rev. Geol. Mediterr 26, 67-77.

Özer, S. & İrtem, O., (1982) Işıklar-Altındağ (Bornova-İzmir) alanı Üst Kreatase kireçtaşlarının jeolojik konumu, stratigrafisi ve fasiyes özellikleri. Bulletin of the Geological Society of Turkey, 25, 41-47.

Özer, S., Sözbilir, H., Özkar-Tansel, İ., Toker, V., & Sarı, B., (2001) Stratigraphy of Upper Creataceous-Paleocene sequences in the southern Menderes Massif (W. Turkey). Int. J. Earth Sci. 89: 852-866,

Papanikolaou, D.J., (1979) Unites tectoniques et phases de deformation dans I'ıle de Samos, Mer Egee, Greece. Bull. Soc. Geol. France, XIX, 6, 745-752.

Papanikolaou, D.J., & Demirtaşlı, E., (1987) Geological correlation between the Alpine Segments of the Hellenides-Balkanides and Taurides-Pontides. Flügel, Sassi and Grecula (Ed), 7., Pre-Variscan and Variscan events in the Alpine-Mediterranean mountain belts. 387-396.

Partzsch, J., Oberhaensli, R., Candan, O. & Warkus, F., (1998) The evolution of the Central Menderes Massif, West Turkey: A complex nappe pile recording 1.0 Ga of geological history.Freiberger Forschungsheft, C.471, 166-168.

Passchier, C.W., & Trouw, R.A.J (Ed) (1996) Microtectonics. Springer, 289p.

Petrakakis, K., (1986) Metamorphism of high-grade gneisses from the Moldanubian zone, Austria, with particular reference to the garnets. Journal of metamorphic Geol., 4, 323-344.

Piccardo, G.B., Messiga, B., & Mazzucotelli, A., (1979) Chemical petrology and geodynamic evolution of the ophiolitic metavolcanites (prasinites) from the voltri massif, piemontese ophiolite nappe (Vestern Liguria, Italy). Ofioliti, 4, 373-402.

Pierdzig, S. (1989) Kartierung, Geologie und petrographie des südteils von Syros (Kykladen, Griechenland). Diploma thesis, Universitat Bonn.

Plyusnina, L.P. (1982) Geothermometry and geobarometry of plagioclase-hornblende-bearing assemblages. Contrib Mineral Petrol, 80, 140-146.

Powell, R. & Holland, T.J.B. (1985) An internally consistent dataset with uncertainties and correlations: 3 Applications to geobarometry, worked examples and a computer program. Journal of Metamorphic Geol. 6, 173-204.

Raase, P., (1974) Al and Ti contents of hornblende, indicators of pressure and temperature of regional metamorphism. Contrib. Mineral. Petrol. 45: 231-236.

Ridley, J. & Dixon, J.E., (1984) Reaction pathways during the progress deformation of a blueschist metabasite: the role of chemical disequilibrium and restricted range equilibrium. Journal of metamorphic Geol. 2, 115-128.

Rieder, M. Cavazzını, G. D'yakonov, Y.S. Frank-Kamenetskıı, V.A. Gottardi, G. Guggenheim, S. Kdval, P.V. Müller, G. Neiva, A.M.R. Radoslovich, E.W. Robert, J-L. Sassi, F.P. Takeda, H. Weiss, Z. & Wones, D.R (1998) Nomenclature of the micas. American Mineralogist, IMA mica report, Final.

Rimmele, G., Oberhaensli, R., Goffe, B., Jolivet, L., Candan, O. & Çetinkaplan, M., (2002) High pressure rocks from the southern Menderes Massif and the Lycian nappes: implication for tectonic evolution of southwest Turkey. 1st International Symposium of Faculty of Mines (İTÜ) on Earth sciences and Engineering. p. 108.

Ring, U., S. Laws. & M, Bernetb., (1999a) Structural analysis of a complex nappe sequence and late orogenic basins from the Aegean ısland of Samos Greece. J. Struct. Geol., 21, 1575-1601.

Ring, U., Gessner, K., Güngör, T., & Passchier, C.W. (1999b) The Menderes Massif of western Turkey and the Cycladic Massif in the Aegean-do they really correlate ? Geological Society of London, 156, 3-6.

Ruppel, C., Royden, L., & Hodges, K.V., (1988) Thermal modeling of extentional tectonics: application to pressure-temperature-time histories of metamorphic rocks. Tectonics, 7, 947-957.

Satır, M., & Friedrichsen, H., (1986) The origin and evolution of the Menderes Massif, W-Turkey: Rubidium/Strontium and oxygen isotope study. Geol. Rundsch., 75, 703-714.

Schliestedt, M., Altherr, R. & Mathews, A. (1987) Evolution of the Cycladic Crystalline complex: Petrology, isotope geochemistry and geochronology. In: (ed., H.C. Helgeson) Chemical Transport in Metosomatic Processes, NATO ASI Series, 218 C, 389-428, D. Reidel, Dordrecht.

Schliestedt, M., & Matthews, A. (1987) Transformation of blueschist to greenschist facies rocks as a consequence of fluid infiltration, Sifnos (Cyclades), Greece. Contrib. Mineral Petrol., 97, 237-250.

Schuiling, R.D., (1962) On petrology, age and structure of the Menderes migmatite complex (SW -Turkey). Bull. Mineral. Res. Explor. Inst. Turkey., 58, 71-84.

Seewald, J.S. & Seyfried, W.E. (1990) The effect of temperature on metal mobility in subseafloor hydrothermal systems: constraints from basalt alteration experiments. Earth Planet. Sci. Lett., 101, 388-403.

Seidel, E., (1981) Fe-Mg verteilung in koexistierenden karpholiten und chloritoiden. Fortschr. Mineral. 59, Beiheft 1. 180-181.

Sherlock, S., Kelley, S.P., Inger, S., Harris, N., & Okay, A.İ. (1999) 40Ar/39Ar and Rb-Sr geochronology of high-pressure metamorphism and exhumation history of the Tavşanlı zone, NW Turkey. Contrib. Mineral. Petrol., 137, 46-58.

Smulikowski, K. (1972) Classification of eclogites and allied rocks. Krystalinikum, 9, 107-130.

Spear, F.S. (1980) NaSi-CaAl exchange equilibrium between plagioclase and amphiboles. An ampirical model. Contrib. Mineral. Petrol. 72, 33-41.

Sun, S.S., & Mc Donough, W.F., (1989) Chemical and isotopic systematics of oceanic basalts: implication for the mantle composition and processes. In: Saunders A.D. & Norry M.J. (eds.), Magmatism in ocean basins. Geol. Soc. London. Spec. Pub. 42, 313-345.

Şengör, A.M.C., Satır, M., & Akkök, R., (1984b) Timing of tectonic events in the Menderes Massif, western Turkey: implication for tectonic evolution and evidence for Pan-African basement in Turkey. Tectonics 3, 693-707.

Şengör, A.M.C., & Yılmaz, Y. (1981) Tethyan evolution of Turkey: a plate tectonic approach. Tectonophysics, 75,181-241.

Tosch , S. & Lugmair, G.W., (1990) Earth Planet Sci Lett. 99, 230-249.

Van der Maar, P.A. & Jansen, J.B.H. (1983) The geology of the polymetamorphic complex of Ios, Cyclades, Greece and its significance for the Cycladic Massif. Geol. Rundschau. 72, 283-299.

Wijbrans, J.R., & McDougall, I., (1988) Metamorphic evolution of the Attic-Cycladic metamorphic belt on Naxos (Cyclades, Greece). Journal of Metamorphic Geol., 6, 571-594.

Wijbrans, J.R, Schliestedt, M., & York, D., (1990) Single grain argon laser probeadating of phengites from the blueschist to greenschist transition on sifnos (Cyclades, Greece). Contrib. Mineral. Petrol.,104, 582-593.

White, S.H., (1979b) Large strain deformation: report on a tectonic studies group discussion meeting held at imperial College, London; introduction. Journal of Struct. Geol. 4, 333-339.

Yalçın, Ü. (1987) Petrologie und geochemie der Metabauxite SW-Anatoliens. PhD Thesis, Univ Bochum.

Yardley , B.W.D. (1977) An emprical study of diffusion in garnet. American Mineralogist, 62, 793-800.

Yılmaz, Y., Genç, C., Gürer, F., Bozcu, M., Yılmaz, M., Karacık, Z., Altunkaynak, Ş. & Elmas, A., (2000) When did the western Anatolian grabens begin to develop ? In: Bozkurt, E., Winchester, J.A & Piper, J.D (eds.), Tectonics and magmatism in Turkey and the surrounding area. Geological Society Special publication No.173, 353-384.

T.C. YÜKSEKÖĞRETİM KURULU
DOKÜMANTASYON MERKEZİ